frontiers | Research Topics

Intermediate filaments structure, function and clinical significance

Edited by
Yaming Jiu, Fang Cheng, Dolores Pérez-Sala and Ming Guo

Published in
Frontiers in Cell and Developmental Biology

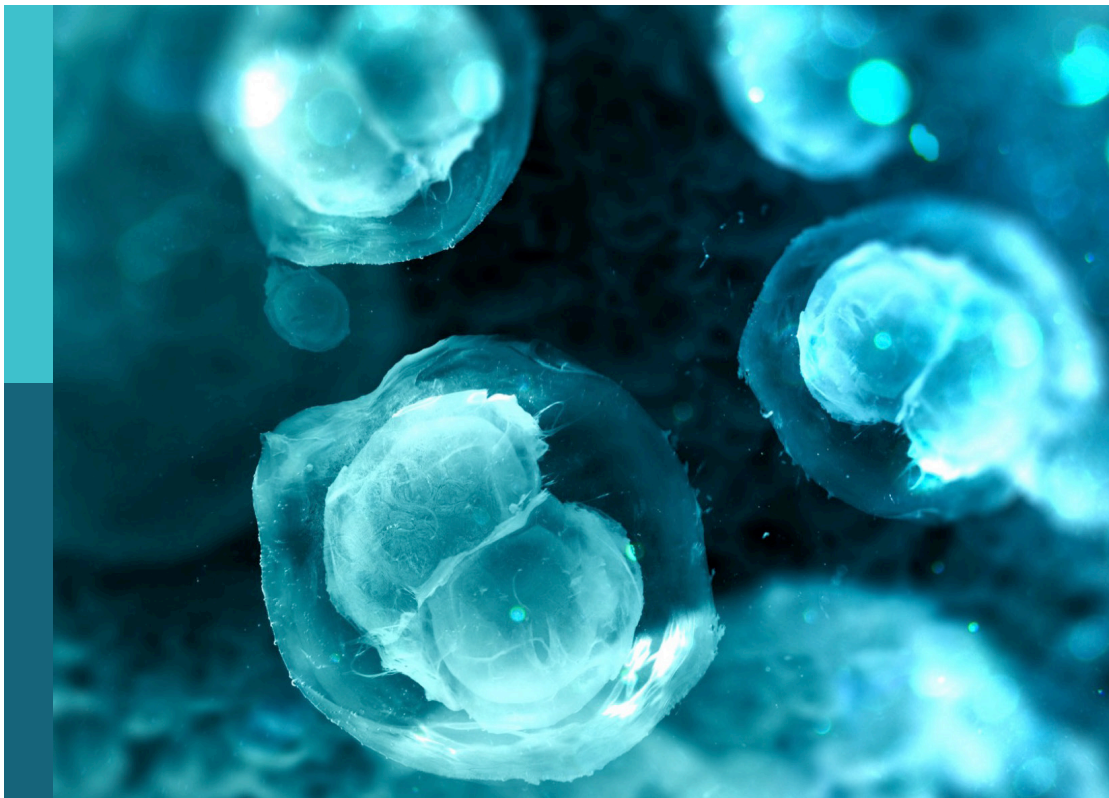

ISSN 1664-8714
ISBN 978-2-83251-046-9
DOI 10.3389/978-2-83251-046-9

About Frontiers

Frontiers is more than just an open access publisher of scholarly articles: it is a pioneering approach to the world of academia, radically improving the way scholarly research is managed. The grand vision of Frontiers is a world where all people have an equal opportunity to seek, share and generate knowledge. Frontiers provides immediate and permanent online open access to all its publications, but this alone is not enough to realize our grand goals.

Frontiers journal series

The Frontiers journal series is a multi-tier and interdisciplinary set of open-access, online journals, promising a paradigm shift from the current review, selection and dissemination processes in academic publishing. All Frontiers journals are driven by researchers for researchers; therefore, they constitute a service to the scholarly community. At the same time, the *Frontiers journal series* operates on a revolutionary invention, the tiered publishing system, initially addressing specific communities of scholars, and gradually climbing up to broader public understanding, thus serving the interests of the lay society, too.

Dedication to quality

Each Frontiers article is a landmark of the highest quality, thanks to genuinely collaborative interactions between authors and review editors, who include some of the world's best academicians. Research must be certified by peers before entering a stream of knowledge that may eventually reach the public - and shape society; therefore, Frontiers only applies the most rigorous and unbiased reviews. Frontiers revolutionizes research publishing by freely delivering the most outstanding research, evaluated with no bias from both the academic and social point of view. By applying the most advanced information technologies, Frontiers is catapulting scholarly publishing into a new generation.

What are Frontiers Research Topics?

Frontiers Research Topics are very popular trademarks of the *Frontiers journals series*: they are collections of at least ten articles, all centered on a particular subject. With their unique mix of varied contributions from Original Research to Review Articles, Frontiers Research Topics unify the most influential researchers, the latest key findings and historical advances in a hot research area.

Find out more on how to host your own Frontiers Research Topic or contribute to one as an author by contacting the Frontiers editorial office: frontiersin.org/about/contact

Intermediate filaments structure, function and clinical significance

Topic editors

Yaming Jiu — Institut Pasteur of Shanghai, Chinese Academy of Sciences (CAS), China

Fang Cheng — Sun Yat-sen University, China

Dolores Pérez-Sala — Spanish National Research Council (CSIC), Spain

Ming Guo — Massachusetts Institute of Technology, United States

Citation

Jiu, Y., Cheng, F., Pérez-Sala, D., Guo, M., eds. (2022). *Intermediate filaments structure, function and clinical significance*. Lausanne: Frontiers Media SA.

doi: 10.3389/978-2-83251-046-9

Table of contents

05 Editorial: Intermediate filaments structure, function, and clinical significance
Dolores Pérez-Sala and Ming Guo

08 Desmin Modulates Muscle Cell Adhesion and Migration
Coralie Hakibilen, Florence Delort, Marie-Thérèse Daher, Pierre Joanne, Eva Cabet, Olivier Cardoso, Fany Bourgois-Rocha, Cuixia Tian, Eloy Rivas, Marcos Madruga, Ana Ferreiro, Alain Lilienbaum, Patrick Vicart, Onnik Agbulut, Sylvie Hénon and Sabrina Batonnet-Pichon

28 Impact of Vimentin on Regulation of Cell Signaling and Matrix Remodeling
Zofia Ostrowska-Podhorodecka, Isabel Ding, Masoud Norouzi and Christopher A. McCulloch

43 Vimentin Suppresses Inflammation and Tumorigenesis in the Mouse Intestine
Linglu Wang, Ponnuswamy Mohanasundaram, Michelle Lindström, Muhammad Nadeem Asghar, Giulia Sultana, Julia O. Misiorek, Yaming Jiu, Hongbo Chen, Zhi Chen, Diana M. Toivola, Fang Cheng and John E. Eriksson

56 Intermediate Filaments in Cellular Mechanoresponsiveness: Mediating Cytoskeletal Crosstalk From Membrane to Nucleus and Back
Anne-Betty Ndiaye, Gijsje H. Koenderink and Michal Shemesh

65 Pathophysiological Role of Vimentin Intermediate Filaments in Lung Diseases
Ranu Surolia and Veena B. Antony

82 Vimentin Tail Segments Are Differentially Exposed at Distinct Cellular Locations and in Response to Stress
Irene Lois-Bermejo, Patricia González-Jiménez, Sofia Duarte, María A. Pajares and Dolores Pérez-Sala

100 Extracellular vimentin is expressed at the rear of activated macrophage-like cells: Potential role in enhancement of migration and phagocytosis
Divyendu Goud Thalla, Ashish Chand Rajwar, Annalena Maria Laurent, Johanna Elisabeth Becher, Lucina Kainka and Franziska Lautenschläger

111 A heterozygous p.S143P mutation in *LMNA* associates with proteasome dysfunction and enhanced autophagy-mediated degradation of mutant lamins A and C
Gun West, Minttu Turunen, Anna Aalto, Laura Virtanen, Song-Ping Li, Tiina Heliö, Annika Meinander and Pekka Taimen

126 Effects of mutant lamins on nucleo-cytoskeletal coupling in *Drosophila* models of *LMNA* muscular dystrophy
Nicholas M. Shaw, Jose L. Rios-Monterrosa, Gregory R. Fedorchak, Margaret R. Ketterer, Gary S. Coombs, Jan Lammerding and Lori L. Wallrath

144 Expression of vimentin alters cell mechanics, cell-cell adhesion, and gene expression profiles suggesting the induction of a hybrid EMT in human mammary epithelial cells
Suganya Sivagurunathan, Amir Vahabikashi, Haiqian Yang, Jun Zhang, Kelly Vazquez, Dhivyaa Rajasundaram, Yuliya Politanska, Hiam Abdala-Valencia, Jacob Notbohm, Ming Guo, Stephen A. Adam and Robert D. Goldman

160 Cortical tension regulates desmosomal morphogenesis
Marcin Moch, Jana Schieren and Rudolf E. Leube

frontiers | Frontiers in Cell and Developmental Biology

TYPE Editorial
PUBLISHED 30 November 2022
DOI 10.3389/fcell.2022.1103110

OPEN ACCESS

EDITED AND REVIEWED BY
Philipp Kaldis,
Lund University, Sweden

*CORRESPONDENCE
Dolores Pérez-Sala,
dperezsala@cib.csic.es

SPECIALTY SECTION
This article was submitted to Cell Growth and Division, a section of the journal Frontiers in Cell and Developmental Biology

RECEIVED 19 November 2022
ACCEPTED 23 November 2022
PUBLISHED 30 November 2022

CITATION
Pérez-Sala D and Guo M (2022), Editorial: Intermediate filaments structure, function, and clinical significance.
Front. Cell Dev. Biol. 10:1103110.
doi: 10.3389/fcell.2022.1103110

Editorial: Intermediate filaments structure, function, and clinical significance

Dolores Pérez-Sala[1]* and Ming Guo[2]

[1]Department of Structural and Chemical Biology, Centro de Investigaciones Biológicas Margarita Salas, CSIC, Madrid, Spain, [2]Department of Mechanical Engineering, Physics of Living Systems Center, Center for Multi-Cellular Engineered Living Systems, Massachusetts Institute of Technology, Cambridge, MA, United States

KEYWORDS

Vimentin, desmin, lamin, mechanosensing, cytoskeletal interplay, intermediate filaments in pathophysiology, epithelial–mesenchymal transition (EMT), extracellular vimentin

Editorial on the Research Topic
Intermediate filaments structure, function, and clinical significance

The cytoskeleton is a highly complex network formed by three main types of structures, namely, microtubules, actin microfilaments and intermediate filaments (IF). Cytoskeletal structures can be viewed as macromolecular machines implementing cell dynamics, making possible a plethora of processes including intracellular transport, contractility, migration and division. In this complex and dynamic mesh, IF are not merely structural scaffolds giving support to cellular organelles. Instead, they function as integrators of cytoskeletal networks and link mechanical and chemical cues to signal transduction, regulation of cell morphology and proliferation, organelle homeostasis and gene transcription, among other essential cellular processes (Etienne-Manneville, 2018; Vahabikashi et al., 2022).

In contrast to actin and tubulin, coded by a low number of genes, IF proteins are the products of over 60 different genes, and their versatility provides structures specific for certain subcellular compartments, as in the case of nuclear lamins, or cell-type-specific flavors, with proteins "tailored" for expression in mesenchymal cells (vimentin), muscle cells (desmin), neurons (neurofilaments) or astrocytes (glial fibrillary acidic protein) (Eriksson et al., 2009).

As IF mediate critical cellular functions, their disruption by mutation or environmental factors leads to disease, as in aging syndromes (lamins), cardiac and skeletal muscle myopathies (desmin), skin diseases (keratins), neurodegenerative disease (GFAP), or cancer progression, fibrosis and infection (vimentin) (Eriksson et al., 2009).

Articles collected in the *Intermediate filaments structure, function, and clinical significance* Topic include cutting-edge original research reports, state-of-the-art review articles covering the essentials of the field, and trends and perspectives towards the key open questions in IF biology and biophysics.

As IFs are key integrators of cellular structures, several articles deal with their crosstalk with other cytoskeletal components. Cellular mechanoresponsiveness, the process by which cells sense and adapt to mechanical changes, was traditionally considered an actin-orchestrated process. Nevertheless, it is becoming clear that mechanosensitivity requires the close interplay between the three cytoskeletal filament systems, with IF playing a central role (Ndiaye et al.) Mechanical stability is particularly important in epithelia. The article by Moch et al., illustrates the crosstalk between adherens junction-associated actomyosin cytoskeleton and the desmosome-anchored keratin IFs in regulating epithelial mechanics. They show how cortical tension affects the complex desmosome structure, modulating desmosome formation and protein composition, thus evidencing a novel desmosomal mechanoresponsive pathway which senses alterations in force balance.

Alterations in cell-cell adhesion and cell mechanics are key during epithelial-mesenchymal transition (EMT), the process by which cancerous epithelial cells acquire tumorigenic potential with increased migratory and invasive capacities leading to metastasis. The type III IF protein vimentin is a marker and player of this process (Battaglia et al., 2018; Ridge et al., 2022), but the molecular mechanisms involved are largely unknown. Sivagurunathan et al., show that vimentin induction in an epithelial cell line alters keratin networks and disrupts desmosomes, reducing intercellular forces and stiffness. At the same time, vimentin activates transcription of genes involved in cell locomotion, thus creating the perfect scenario for increased cell migration and therefore, tumorigenic potential. Importantly, vimentin also influences cell migration by controlling extracellular matrix remodeling and interactions. The review by Ostrowska-Podhorodecka et al., provides an expert view of the multiple roles of vimentin in this process. Vimentin controls collagen deposition and extracellular matrix structure. Moreover, it interacts with adhesion receptors such as integrins, regulating the growth, maturation and strength of integrin-dependent adhesions, thus affecting cell migration through connective tissues. Importantly, the work by Hakibilen et al., identifies a novel role for desmin, a muscle-specific type III IF protein highly homologous to vimentin, in cell-matrix adhesion, which is critical for strength transmission, satellite cell migration and muscle regeneration. In this case, desmin appears to promote cell adhesion and limit migration. This work suggests a potential involvement of adhesion and migration defects in the pathogenesis of desminopathies, which could lead to novel therapeutic approaches. Therefore, the role of vimentin and other type III IFs in cell adhesion and migration in physiology and pathophysiology can be highly complex and potentially dependent on the cell type and the host tissue. In two models of intestinal inflammation and tumorigenesis (Wang et al.), vimentin appears to play a protective role, since vimentin-null (*Vim*−/−) mice challenged with dextran sodium sulfate display higher generation of reactive oxygen and nitrogen species and worse colitis than the wild type mice, and develop more and larger tumors in the tumorigenesis model. Conversely, vimentin plays a key role in lung diseases, not only during EMT occurring in lung cancer, but in infectious diseases and in lung fibrosis (Ridge et al., 2022). The review by Surolia and Antony provides a deep analysis of the roles of vimentin in lung pathophysiology, covering processes from lung injury and acute respiratory syndrome, to respiratory infections, both viral and bacterial, as well as chronic lung diseases, such as fibrosis and chronic obstructive pulmonary disease. This clinically-oriented review also examines the therapeutic strategies targeting vimentin, including anti-vimentin compounds and antibodies, that could be relevant for lung disease.

The multifaceted roles of vimentin are supported by its great versatility. Vimentin is a hub for multiple posttranslational modifications that finely tune its assembly mode, cellular localization and interactions (Viedma-Poyatos et al., 2020; Griesser et al., 2021). Therefore, the diverse vimentin proteoforms can perform amazingly different functions. The structure of vimentin is not fully understood, and multiple approaches have been employed to characterize it, both *in vitro* and in cells. Most advances have improved our comprehension of the central alpha-helical domain (rod) and the N-terminal domain (head) of the protein (Eldirany et al., 2021). However, the disposition of the intrinsically disordered C-terminal domain (tail), involved in cytoskeletal crosstalk, remains unsolved. Based on epitope accessibility analyses, Lois-Bermejo et al., propose that at least two different conformations of vimentin tail coexist in cells, with a "packed" conformation predominant in perinuclear filaments and stress-induced bundles, and a "loose or extended" conformation mainly present in peripheral filaments, which could arise by tail phosphorylation, and potentially influence vimentin assembly and interactions. Besides its presence in long cytoplasmic filaments, vimentin can exist in small particles at the migration front of cells, and even appear at the cell surface or in the extracellular medium in various non-filamentous forms. Indeed, extracellular vimentin can act as a ligand for various agents, including pathogens, and vimentin present in exosomes influences cell migration (Ramos et al., 2020). Thalla et al., observe extracellular vimentin on the "back" of activated macrophage-like cells as small fragments forming agglomerates on the cell surface. This polarized release of vimentin appears to enhance migration and phagocytic activity of these cells, raising new exciting avenues for the study of the involvement of vimentin in immune cells functions.

Nuclear IF, the lamins, are key for nuclear integrity and gene transcription, and mutations in the corresponding genes cause the diseases known as laminopathies, characterized by severe clinical manifestations, either organ-selective or systemic, as in the premature aging syndromes (Worman

and Bonne, 2007). Lamins line the inner nuclear membrane and play key roles in integration of signals and transmission of forces between the cytoplasm and the nucleus. Shaw et al., investigate how disease-causing *LMNA* mutations alter nucleo-cytoskeletal coupling in a *Drosophila* model of muscular dystrophy. They identify lamin residues important for connecting the nucleus to the cytoskeleton, unveiling that specific mutations cause different defects in subcellular mechanics, with potentially distinct pathogenic implications. In addition, the mutant proteins themselves can exert deleterious effects in cells, as a consequence, among other factors, of impaired protein degradation. Indeed, West et al., show that a mutation in the *LMNA* gene causes the mutant proteins to overload and impair the ubiquitin proteasome system. Under these conditions, compensatory enhanced autophagy or restoration of protein degradation, achieved by a chemical chaperone, help maintaining the levels of mutant proteins, and therefore cell homeostasis. Consequently, the authors propose the protein degradation machinery as a therapeutic target in laminopathies associated with proteostasis defects.

In summary, the articles contained in this Topic highlight the complex biological and pathophysiological roles of IF, reinforcing their importance as central players in cell and tissue homeostasis, as well as their promise as therapeutic targets.

Author contributions

All authors listed have made a substantial, direct, and intellectual contribution to the work and approved it for publication.

Funding

Work at the authors' laboratories is supported by grants from "la Caixa" Foundation, Grant Agreement LCF/PR/HR21/52410002, EJP RD COFUND-EJP N° 825575 "Alexander", Agencia Estatal de Investigación, MICINN and ERDF Grants N°: RTI 2018-097624-B-I00 and PID2021-126827OB-I00 to DP-S, and NIH 1R01 GM140108 awarded to MG.

Acknowledgments

The authors are grateful to all authors, reviewers and editors who have participated in this Research Topic for their excellent contributions.

Conflict of interest

The authors declare that the research was conducted in the absence of any commercial or financial relationships that could be construed as a potential conflict of interest.

Publisher's note

References

Battaglia, R. A., Delic, S., Herrmann, H., and Snider, N. T. (2018). Vimentin on the move: New developments in cell migration. *F1000Res.* 7, F1000 Faculty Rev-1796. doi:10.12688/f1000research.15967.1

Eldirany, S. A., Lomakin, I. B., Ho, M., and Bunick, C. G. (2021). Recent insight into intermediate filament structure. *Curr. Opin. Cell Biol.* 68, 132–143. doi:10.1016/j.ceb.2020.10.001

Eriksson, J. E., Dechat, T., Grin, B., Helfand, B., Mendez, M., Pallari, H. M., et al. (2009). Introducing intermediate filaments: From discovery to disease. *J. Clin. Invest.* 119, 1763–1771. doi:10.1172/JCI38339

Etienne-Manneville, S. (2018). Cytoplasmic intermediate filaments in cell biology. *Annu. Rev. Cell Dev. Biol.* 34, 1–28. doi:10.1146/annurev-cellbio-100617-062534

Griesser, E., Vemula, V., Mónico, A., Pérez-Sala, D., and Fedorova, M. (2021). Dynamic posttranslational modifications of cytoskeletal proteins unveil hot spots under nitroxidative stress. *Redox Biol.* 44, 102014. doi:10.1016/j.redox.2021.102014

Ramos, I., Stamatakis, K., Oeste, C. L., and Perez-Sala, D. (2020). Vimentin as a multifaceted player and potential therapeutic target in viral infections. *Int. J. Mol. Sci.* 21, 4675. doi:10.3390/ijms21134675

Ridge, K. M., Eriksson, J. E., Pekny, M., and Goldman, R. D. (2022). Roles of vimentin in health and disease. *Genes Dev.* 36, 391–407. doi:10.1101/gad.349358.122

Vahabikashi, A., Adam, S. A., Medalia, O., and Goldman, R. D. (2022). Nuclear lamins: Structure and function in mechanobiology. *Apl. Bioeng.* 6, 011503. doi:10.1063/5.0082656

Viedma-Poyatos, A., Pajares, M. A., and Pérez-Sala, D. (2020). Type III intermediate filaments as targets and effectors of electrophiles and oxidants. *Redox Biol.* 36, 101582. doi:10.1016/j.redox.2020.101582

Worman, H. J., and Bonne, G. (2007). Laminopathies": A wide spectrum of human diseases. *Exp. Cell Res.* 313, 2121–2133. doi:10.1016/j.yexcr.2007.03.028

frontiers in Cell and Developmental Biology

ORIGINAL RESEARCH
published: 08 March 2022
doi: 10.3389/fcell.2022.783724

Desmin Modulates Muscle Cell Adhesion and Migration

*Coralie Hakibilen[1], Florence Delort[1], Marie-Thérèse Daher[1], Pierre Joanne[2], Eva Cabet[1], Olivier Cardoso[3], Fany Bourgois-Rocha[1], Cuixia Tian[4], Eloy Rivas[5], Marcos Madruga[6], Ana Ferreiro[1,7], Alain Lilienbaum[1], Patrick Vicart[1], Onnik Agbulut[2], Sylvie Hénon[3] and Sabrina Batonnet-Pichon[1]**

[1]Université de Paris, BFA, UMR 8251, CNRS, Paris, France, [2]Sorbonne Université, Institut de Biologie Paris-Seine (IBPS), CNRS UMR 8256, INSERM ERL U1164, Biological Adaptation and Ageing, Paris, France, [3]Université de Paris, MSC, UMR 7067, CNRS, Paris, France, [4]Department of Neurology, Cincinnati Children's Hospital Medical Center, College of Medicine, University of Cincinnati, Cincinnati, OH, United States, [5]Servicio de Anatomia Patologica, Hospital Universitario Virgen Del Rocio, Sevilla, Spain, [6]Unidad de Neurologia Pediatrica, Hospital Universitario Virgen Del Rocio, Sevilla, Spain, [7]APHP, Centre de Référence Maladies Neuromusculaires Nord/Est/Ile-de-France, Groupe Hospitalier Pitié-Salpêtrière, Paris, France

Cellular adhesion and migration are key functions that are disrupted in numerous diseases. We report that desmin, a type-III muscle-specific intermediate filament, is a novel cell adhesion regulator. Expression of p.R406W mutant desmin, identified in patients with desmin-related myopathy, modified focal adhesion area and expression of adhesion-signaling genes in myogenic C2C12 cells. Satellite cells extracted from desmin-knock-out (DesKO) and desmin-knock-in-p.R405W (DesKI-R405W) mice were less adhesive and migrated faster than those from wild-type mice. Moreover, we observed mislocalized and aggregated vinculin, a key component of cell adhesion, in DesKO and DesKI-R405W muscles. Vinculin expression was also increased in desmin-related myopathy patient muscles. Together, our results establish a novel role for desmin in cell-matrix adhesion, an essential process for strength transmission, satellite cell migration and muscle regeneration. Our study links the patho-physiological mechanisms of desminopathies to adhesion/migration defects, and may lead to new cellular targets for novel therapeutic approaches.

Keywords: desmin, vinculin, focal adhesion, migration, myopathies, intermediate filaments

OPEN ACCESS

Edited by:
Dolores Pérez-Sala, Spanish National Research Council (CSIC), Spain

Reviewed by:
Cecile Leduc, UMR7592 Institut Jacques Monod (IJM), France
Paris Alexander Skourides, University of Cyprus, Cyprus

****Correspondence:***
Sabrina Batonnet-Pichon
sabrina.pichon@u-paris.fr
orcid.org/0000-0003-0544-1086

Specialty section:
This article was submitted to Cell Growth and Division, a section of the journal Frontiers in Cell and Developmental Biology

Received: *26 September 2021*
Accepted: *09 February 2022*
Published: *08 March 2022*

Citation:
Hakibilen C, Delort F, Daher M-T Joanne P, Cabet E, Cardoso O, Bourgois-Rocha F, Tian C, Rivas E, Madruga M, Ferreiro A, Lilienbaum A, Vicart P, Agbulut O, Hénon S and Batonnet-Pichon S (2022) Desmin Modulates Muscle Cell Adhesion and Migration. Front. Cell Dev. Biol. 10:783724. doi: 10.3389/fcell.2022.783724

INTRODUCTION

The cytoskeleton orchestrates many essential cell processes such as cellular division, mechanosensing, adhesion and motility. These functions derive from the three main structural networks: microfilaments (actin filaments), microtubules and intermediate filaments (IFs). Most studies focus on the role of microfilament or microtubule networks in cell adhesion and migration. However, new insights indicate an important role of the IF family in various cell types such as myoblasts (Etienne-Manneville, 2018; Agnetti et al., 2021; Kural Mangit et al., 2021).

The cell-specific IF network is often pictured as an integrator of microfilaments and microtubules via a complex set of cross-bridging proteins (Seifert et al., 1992). In all tissues, IFs form transcellular

Abbreviations: BSA, bovine serum albumin; Cy3-, 5-, Cyanine Dyes 3-, 5-; DMEM, Dulbecco's Modified Eagle's Medium; ECL, enhanced chemiluminescence; EGFP, enhanced green fluorescent protein; FA, focal adhesions; FBS, fetal bovine serum; GAPDH, glyceraldhyde-3-phosphate dehydrogenase; IF, intermediate filament; PBS, phosphate buffered saline; SDS–PAGE, sodium dodecyl sulfate–polyacrylamide gel electrophoresis; TIRFM, total internal reflection fluorescence microscope.

networks in direct interaction with specific cell–cell or cell–matrix junctions called desmosomes and hemidesmosomes (Troyanovsky et al., 1993; Mogensen et al., 1998). IFs contribute mainly to cell shape maintenance and cellular organelle anchoring and are involved in cell strength, adhesion and cohesion. IF are also important in cell division (Duarte et al., 2019) and resistance to stress (Etienne-Manneville, 2018). IFs seem to mediate key cell functions (i.e., cell adhesion and migration, organelle shaping and positioning) by providing cellular signposts through post-translational modifications (Omary et al., 2006; Pallari and Eriksson, 2007; Hyder et al., 2008).

Unlike microfilaments and microtubules, IFs are not polarized. IFs share a basic structure with a common tripartite organization characterized by a central alpha-helical coiled-coil-forming domain and non-alpha-helical "head" and "tail" domains of variable lengths and sequences (Strelkov et al., 2003). IFs self-assemble into filaments of ~10-nm diameter (Herrmann et al., 1996). Yet, IF proteins exhibit tissue-specific expression: vimentin in cells derived from mesenchymal cells as fibroblasts or endothelial cells, desmin in muscle and cytokeratin generally in epithelial cells (Toivola et al., 2005). Keratin IFs have an important role in adhesion and cell–cell interactions through their association with hemidesmosomes and desmosomes (Osmani and Labouesse, 2015; Seltmann et al., 2015).

In vitro, cell adhesion and, in part, cell migration are controlled by integrins and focal adhesion (FA) formation. Among the 24 pairs of integrins described in vertebrates (Luo et al., 2007), α5β1 and α7β1 are the main pairs expressed in skeletal muscle cells. α5β1 and α7β1, respectively, function in adhesion to fibronectin and laminin, two essential components of the muscle extracellular matrix. FAs also involve vinculin, a 120-kDa cytoskeletal protein and major component of cell–cell and cell–extracellular matrix adhesion junctions (Bays and DeMali, 2017). In mature FAs, vinculin is crucial in the "molecular clutch" that mediates transmission of force from cytoplasmic F-actin to membrane-bound integrins. In adult striated muscle, FA complexes (called costameres) mediate connections between fibers and extracellular matrix (Pardo et al., 1983), thereby providing a substrate for assembly and maintenance of the muscle during mechanical constraints (contraction/relaxation) (Sparrow and Schöck, 2009; García-Pelagio et al., 2011). Costameres formed *in vitro* involve integrins and vinculin, but muscle cells also express an isoform of vinculin containing an additional 68-amino-acid insert within the tail domain, called metavinculin (Bays and DeMali, 2017). Expression of metavinculin depends on the differentiation state and increases with myogenesis (Saga et al., 1985).

Integrins are also increasingly linked to IFs as well. For instance, keratins could stabilize hemidesmosomes by regulating integrin turnover in keratinocytes (Seltmann et al., 2015). Similarly, in fibroblasts, vimentin, a type III IF that shares high homology with desmin, plays key roles in adhesion and migration by regulating integrin functions (Ivaska et al., 2007; Kim et al., 2016). The coalescence of vimentin IFs at mature FAs is required for endoplasmic spreading (Lynch et al., 2013). Finally synemin, a desmin-associated type VI IF, can interact with vinculin, metavinculin, talin and zyxin, thereby linking the heteropolymeric IFs to adhesion-type junctions within striated muscle cells, suggesting that it plays an important role in cytoskeleton component assembly and morphogenesis (Paulin et al., 2020; Russell, 2020).

The muscle-specific IF is desmin. During skeletal muscle differentiation, desmin progressively replaces vimentin and is commonly used as a differentiation marker. Importantly, to date more than 70 mutations in the desmin gene have been causally linked to rare neuromuscular diseases called desminopathies, associated either with abnormal desmin expression linked to muscle protein aggregation (Goldfarb et al., 1998; Dagvadorj et al., 2004; Fidziańska et al., 2005; Mavroidis et al., 2008; Pica et al., 2008; Fichna et al., 2014; Clemen et al., 2015), or with a total lack of desmin [4 families described, (Carmignac et al., 2009; Henderson et al., 2013)]. In both cases, muscles are disorganized, which triggers at least late skeletal muscle weakness. A well-established mouse model of desmin disruption (DesKO) demonstrated the importance of desmin in maintaining muscle integrity and function. DesKO mice are viable and fertile, but develop progressive myopathy associated with regeneration defects (Agbulut et al., 2001), loss of costamere anchorage and muscle fatigability (Li et al., 1996; Li et al., 1997; Joanne et al., 2021). We generated a new mouse knock-in model of a specific desmin missense mutation, p.R405W, corresponding to p.R406W in humans, which partially mimics the patient phenotype with desmin aggregates present in myofibrils (Batonnet-Pichon et al., 2017; Herrmann et al., 2020). Currently, there is no established link between desmin and skeletal muscle cell adhesion.

Using these two mouse models, we focused here on the potential link between desmin and cell adhesion and migration in undifferentiated muscle cells as well as in mature muscle. To do so, we developed stable cell lines under the desmin promoter to determine the impact of the p.R406W mutation on genome-wide expression. We then followed adhesion in C2C12 myoblasts overexpressing p.R405W mutant desmin, using vinculin as a well-established marker of adhesion. We then extracted satellite cells from KO or R405W KI mouse models and investigated the functional adhesion of shear-stressed satellite cells and their non-directed migration properties. Finally, we examined the expression level and localization of vinculin in muscle from patients with desminopathies and adult controls. Our findings reveal novel roles for desmin in muscle cell adhesion and migration, with important implications for clinical pathology.

MATERIALS AND METHODS

Mouse Models

Generation and characterization of desmin knock-out mice (DesKO) were previously described (Li et al., 1996). DesKO mouse genotype was confirmed by polymerase chain reaction using primers 5′ TTGGGGTCGCTGCGGTCTAGCC 3′, 5′ GGT CGTCTATCAGGTTGTCACG 3′ and 5′ GATCGATCTCGC CATACAGCGC 3′. For DesKI-R405W mice, genotypes were

determined with primers 5′ CTGGAGGAGGAGATCCGACA 3′ and 5′ GGCCCTCGTTAATTTTCTGC 3′.

All animal experiments were conducted with respect to animal health and well-being, and all procedures were approved by our institutional ethics committee (authorization CEB-16-2016).

Cell Lines, Culture and Electroporation

C2C12 cells (ATCC) were grown in DMEM (Dulbecco's Modified Eagle's Medium, Life Technologies) supplemented with 10% fetal bovine serum (FBS, PAA Laboratories) and 1% penicillin/streptomycin (Life Technologies). pEGFP constructs (Charrier et al., 2016; Charrier et al., 2018) were electroporated into C2C12 cells using a Gene Pulser II (BioRad, Hercules, CA). Briefly, cells were trypsinized (Trypsin-EDTA, Life Technologies) for 5 min at 37°C and resuspended in complete DMEM medium at 2×10^6 cells/ml. Then, 400 µl of the cell suspension were introduced in a 0.4-cm gap Gene Pulser Cuvette (BioRad) and submitted to 250 V, 1 mF for 25 ms. After electroporation, cells were plated on fibronectin-coated glass coverslips for 24 h before TIRFM microscopy.

For stable expression, we first replaced the pcDNA3 CMV promoter with the murine 4 kb desmin promoter, which contains all essential sites to induce expression in skeletal and cardiac muscle cells. Then 5′-Myc-tagged complete human *desmin* wild-type cDNA was subcloned. This plasmid also contains the puromycin resistance gene for selection. Mutated plasmid carrying the R406W mutation was then obtained using the Quick Change-XL site-directed mutagenesis kit (Stratagene), following the manufacturer's instructions. All plasmids were sequenced (Eurofins, MWG). Stable C2C12 cells expressing WT or R406W mutant desmin were generated after nucleofection of these plasmids with Amaxa nucleofector (Lonza, Basel, Switzerland) according to the manufacturer's instructions. Subsequently, puromycin (Euromedex, 1 µg/ml) selection was applied for 1 week. Proliferation selections yielded around thirty clones for each construct. Clones were chosen based on Myc-desmin expression as well as their proliferation and differentiation abilities.

Satellite cells were extracted from two gasctrocnemius and two plantaris muscles of 1-month-old DesKI-R405W (Batonnet-Pichon et al., 2017; Herrmann et al., 2020) and DesKO mice (Li et al., 1996). Our protocol was adapted from previous studies (Ohanna et al., 2005). Briefly, muscles were incubated 4 × 10 min in DMEM/F12 + Glutamax solution (Life Technologies) containing 1.5 mg/ml protease XIV (Sigma-Aldrich, Saint-Louis) and 1/500 primocin (InvivoGen) at 37°C under regular agitation. Following each incubation, tubes were centrifuged at 400 g for 30 s at room temperature. The first floating cells were eliminated, and the three other fractions containing satellite cells were diluted in 20% FBS medium and sieved with a 40-µm filter. Filtrate containing satellite cells was centrifuged for 5 min at 1,400 g at room temperature. Cells were then incubated in DMEM/F12 + Glutamax containing 20% FBS, 2% Ultroser (Pall Life Science, Portsmouth, United Kingdom), 8.6 ng/ml FGF2 (Life Technologies), 1/100 N2 (Life Technologies) and 1/500 primocin and seeded onto 6-well plates coated with 1/20 Matrigel (Corning, NY, United States) at 100 cells/cm^2. After activation and proliferation, satellite cells were maintained in T150 flasks at 1,000 cells/cm^2 on plastic covered with 1/20 Matrigel. For analysis, cells were seeded at the adapted concentration on fibronectin or laminin.

Western Blotting

A total of 30 µg of muscle or cell extracts were loaded per well on a 10% acrylamide gel for SDS-PAGE. After migration, proteins were transferred onto nitrocellulose membranes (0.45 µm, Macherey Nagel), which were saturated 1 h with 5% non-fat milk in 0.5% Tween/PBS solution. Membranes were incubated with primary antibodies 1 h at room temperature or overnight at 4°C. Monoclonal mouse anti-vinculin (1/15,000, #V9264, Sigma-Aldrich), polyclonal rabbit anti-desmin (1/1,000, #C3956, Sigma-Aldrich), monoclonal rabbit anti-vimentin (1/2,500, #ab92547, abcam) and polyclonal rabbit anti-GAPDH (1/2,500, #G9545, Sigma-Aldrich) were used.

Isotype-specific anti-mouse or anti-rabbit secondary antibodies coupled with horseradish peroxidase (1/10,000, #31430 or #31460, Pierce, Thermo Scientific) were detected following incubation with Clarity Western ECL (BioRad) and visualized with a CCD camera (FUJI Las 4000 or Ai600, GE Healthcare).

Gene Microarray Analyses

Total RNAs from the C2C12 skeletal myoblasts were purified using standard RNA extraction protocols (NucleoSpin RNA II, Macherey-Nagel). RNA concentration and integrity were determined using a Bioanalyzer 2100 (Agilent Technologies). Cy3-or Cy5-labeled cRNA was made using the Agilent Low RNA Input Linear Amp Kit (Agilent Technologies) following the manufacturer's instructions, which employs a linear amplification method with T7 polymerase. Yields of cRNA and the dye-incorporation rate were measured with an ND-1000 Spectrophotometer (NanoDrop Technologies). Non-transfected control C2C12 cRNAs were labeled with Cy3 and experimental samples expressing wild-type or R406W mutant desmin C2C12 cRNAs were labeled with Cy5. The paired labeled Cy3/Cy5 cRNAs (825 ng) were mixed and hybridized overnight (17 h, 65°C) to Agilent Whole Mouse Genome Oligo Microarrays 4 × 44 K (Agilent Technologies). Fluorescence signals of the hybridized Agilent Oligo Microarrays were detected using Agilent's DNA microarray scanner (Agilent Technologies) and analyzed using Agilent Feature Extraction Software and the Rosetta Resolver gene expression data analysis system (Rosetta Biosoftware). To highlight the most relevant pathways and genes, bioinformatics analyses were achieved. Gene ontology analysis and functional annotation of differentially expressed genes were performed using the DAVID web tool (https://david.ncifcrf.gov/summary.jsp). Gene annotations of Biological Process, Cellular Component and Molecular Function, together with annotations from the KEGG pathway database, were used, and only gene ontology terms that presented at least five genes in common with our gene expression matrix were considered in the analysis. Each *p*-value was directly calculated by the software.

Cell Immunofluorescence

Cells were fixed with 2% paraformaldehyde (Santa Cruz Biotechnologies, Dallas, TX, United States) for 15 min at room temperature, then permeabilized with 0.5% Triton X-100 (Sigma-Aldrich) for 10 min and blocked with 4% BSA (Sigma-Aldrich). They were incubated with mouse monoclonal anti-vinculin primary antibody (1/150, Sigma-Aldrich) or mouse monoclonal anti-desmin antibody (1/100, DAKO, D33) for 1 h at room temperature. After three washes with PBS, cells were incubated 45 min with isotype-specific anti-mouse secondary antibody labeled with Alexa-488 (Molecular Probes) or anti-rabbit secondary antibody labeled with Alexa-568 (Molecular Probes). DNA was stained with Hoechst 33258 (1 µg/ml, Sigma-Aldrich) during secondary antibody incubation. Finally, cells were washed in PBS and mounted in Fluoromount medium (Interchim). Images were acquired by confocal microscopy (LSM700 Zeiss) at the imaging facility of the Functional and Adaptive Biology (BFA) unit.

TIRFM

Electroporated cells were plated on fibronectin-coated glass coverslips 24 h before TIRF microscopy (Ti-Eclipse, NIKON). Cells were fixed and vinculin was immunostained as described above with anti-vinculin (1/150, Sigma-Aldrich) and then secondary antibody Alexa-568. The TIRFM system and image acquisition are controlled by MetaMorph software (Version 7.6, Molecular Device). The 25 × 25-mm glass coverslips were installed in a microscopy chamber and cells were covered with 50 µl of 1× PBS. The parameters of the TIRFM angle were previously determined on C2C12 cells. Cells of interest (carrying the desmin:GFP fusion) were identified by epifluorescence at 488-nm. Area and adhesion patches were analyzed using a macro developed by O. Cardoso (MSC Paris University, **Supplementary Figure S1**). Briefly, quantification was based on pixel binarization from a thresholding function in the ImageJ software. Area and patch number were then determined by the particle analysis function of the software.

Adhesion Under Shear Stress

Satellite cells were plated 24 h before the experiment in a fibronectin-coated channel of an Ibitreat micro-slide VI 0.4 (Ibidi). DMEM/F12 + Glutamax (Life Technologies) supplemented with 4 mM EDTA (Sigma-Aldrich) was injected with a pump syringe (Standard Infusion Only PHD ULTRA™ Syringe Pumps, Harvard Apparatus, France) in the chamber slide at 218 ml/h as previously described (Modulevsky et al., 2012). Images of adhesive cells were taken every 15 s for 24 min with an Olympus IX83 microscope. Cells at each time point were counted with Fiji Cell Counter software with at least 80 cells per condition.

Cellular Migration

Satellite cells were plated on fibronectin or laminin-coated 96-well plates 24 h before the experiment and medium was renewed 2 h before the start. Cells were placed at 37°C under 5% CO_2 in a microscope enclosure. Bright field images were taken every 7 min for each position. Cell migration was followed with the Fiji Manual Tracking plugin. Cell persistence quantifies the ability of a cell to maintain its direction of motion. It is the ratio between its distance to origin at the end of the trajectory over the total distance travelled. Mean speed and persistence for each cell were calculated with Excel software. For each condition, at least 250 cells were counted.

Preparation of Quadriceps and Soleus Muscles

Quadriceps and/or soleus muscles were removed from mice at 1, 3, 5 and 12 months of age after euthanizing by cervical dislocation. For immunohistochemical analysis, muscles were embedded in tragacanth gum (Fisher Scientific) and frozen by plunging in isopentane precooled with liquid nitrogen for at least 1 min. For western blotting, muscles were directly frozen in liquid nitrogen in microtubes, pulverized in a cryogenic mortar (Dominique Dutscher) and resuspended in RIPA buffer [50 mM Tris, 150 mM NaCl, 1% NP40, 5 mM EDTA, 1 mM NA_3VO_4, 10 mM NaF, 1 mM PMSF and anti-protease (Sigma-Aldrich)].

Muscle Sections and Immunofluorescence Staining

Serial sections of 7-µm thickness were sliced using a CM1950 cryostat (Leica), recovered on Superfrost Plus microscope slides (Thermo Scientific) and stored at −80°C. Muscle sections were kept at room temperature for 15 min before staining. Endogenous fluorescence was prevented by treatment with 50 mM NH_4Cl for 30 min. Sections were permeabilized in 0.5% Triton X100/PBS for 10 min, blocked in 4% bovine serum albumin (BSA, Sigma-Aldrich)/PBS and incubated with mouse monoclonal anti-vinculin (Sigma-Aldrich) or rabbit polyclonal anti-laminin (1/100, #L9393, Sigma-Aldrich) primary antibodies for 1 h at room temperature. Primary antibodies were detected by incubating sections with suitable secondary antibodies for 45 min. DNA was stained with 1 µg/ml Hoechst 33258 (Sigma-Aldrich) during secondary antibody incubation. Muscles were washed in PBS and mounted in Fluoromount medium (Interchim, San Diego, CA, United States). All images were captured using a digital camera mounted to a confocal laser scanning microscope (LSM700 ZEISS) at the imaging facility of the BFA unit.

Patients and Human Biopsies

All patients presented a homozygous mutation in the *desmin* gene. The four patients were from Spain, United States (USA) and France. The control was from France. There were two biopsies from the same Spanish patients at 1 and 3 years old. The patient from the USA was a young girl deceased at around age of 20 (article in preparation). The French patients were previously presented (Carmignac et al., 2009). Muscle samples from all family members were obtained after informed consent for medical publications and presentations, in agreement with local ethics committees.

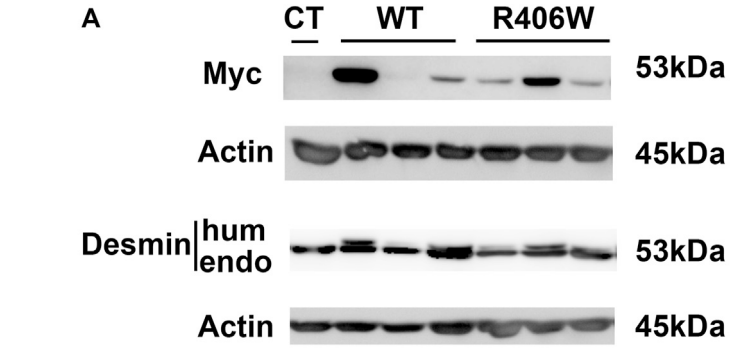

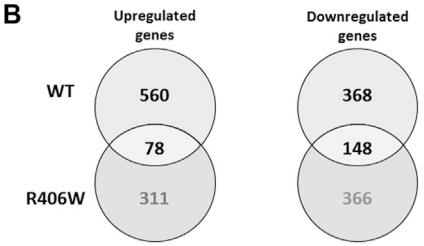

Top 5 Clusters of Upregulated genes	Top 5 Clusters of Downregulated genes
Cell adhesion (22) ($4{,}8.10^{-4}$)	Extracellular region (125) ($7{,}1.10^{-31}$)
Clathrin-coated vesicle (7) ($4{,}2.10^{-3}$)	Muscle contraction (17) ($3{,}9.10^{-12}$)
Cell differentiation (37) ($2{,}0.10^{-2}$)	Sarcomer (15) ($4{,}3.10^{-11}$)
Intermediate filament (5) ($9{,}4.10^{-2}$)	Myofibril (15) ($2{,}0.10^{-10}$)
NA	Cell adhesion (37) ($1{,}9.10^{-9}$)

C

Top 5 of upregulated genes of the cell adhesion cluster	Fold Change	P-value
catenin (cadherin associated protein), alpha-like 1	2,00997	$8.53554.10^{-6}$
mannan-binding lectin serine peptidase 2	2,0755	0.00544
protocadherin 9	15,04775	$7.05313.10^{-12}$
selectin, platelet	2,79664	$9.90042.10^{-20}$
cadherin 10	2,08627	0.00104

Top 5 of downregulated genes of the cell adhesion cluster	Fold change	P-value
cadherin 15	-5,36823	$1.25178.10^{-15}$
transglutaminase 2, c polypeptide	-4,28279	$3.92231.10^{-11}$
protocadherin beta 20	-2,29136	$2.63510.10^{-7}$
protocadherin beta 21	-2,01354	$6.59937.10^{-6}$
perp, tp53 apoptosis effector	-3,5212	$3.03033.10^{-6}$

FIGURE 1 | Human desmin expression and DNA chip analysis in stable cell lines. **(A)** The amounts of endogenous and human (Myc tagged) desmin in WT and p.R406W expressing clones were compared by Western blot. Actin was used as a loading control. **(B)** Genes that were upregulated or downregulated in C2C12 cells expressing R406W desmin or WT desmin were compared (right) and clustered using gene ontology enrichment analysis (left). The number of hits and *p*-values are respectively shown in brackets **(C)** Examples of up-regulated (right) or down-regulated (left) genes from the clusters determined in **(B)**.

All human biopsies were frozen in nitrogen liquid and conserved at −80°C. Frozen biopsy samples were lysed following the same protocol as for mouse muscle: the lysis step was followed by a 2-h incubation with rotation at 4°C.

Statistical Analysis

For microarray analysis, to identify differentially expressed genes with a fold change ≥2, one-way ANOVA was performed using a threshold p-value ≤ 0.01. For other statistical analyses, non-parametric statistical tests were carried out using GraphPadPrism software or R free software. A non-parametric ad hoc "nparcomp" test was performed for FA area comparison. Histograms were generated using GraphPadPrism software and a Mann-Whitney test was used for immunodetection results. A Kruskall-Wallis test followed by a Dunnet multiple comparisons post-test was used for the migration experiment. A Friedman test followed by a Dunnet multiple comparisons post-test was applied to the percentages of detachment from the shear stress experiment. Differences were considered significant at $p < 0.05$. All error bars correspond to the standard deviation (SD).

RESULTS

R406W Mutant Desmin Overexpression Induces Modifications of Adhesion Pathways

To investigate the impact of desmin mutations on genome-wide expression, we first generated murine C2C12 myoblast cell lines stably expressing human wild-type or R406W desmin under the 4 Kb human desmin promoter. To distinguish between exogenous and endogenous desmin, a c-Myc tag was introduced at the 5′ end of the desmin cDNA. We selected three clones for each construct (WT or p.R406W) and monitored desmin expression by western blot. Myc-desmin was detected both in wild-type and R406W desmin expressing cells, but presented various expression levels, probably due to the location of the inserted transgene (**Figure 1A**). Interestingly, two bands corresponding to endogenous (mouse, lower band) and exogenous (human, higher band) desmin were revealed with anti-desmin specific antibodies, allowing us to quantify the ratio

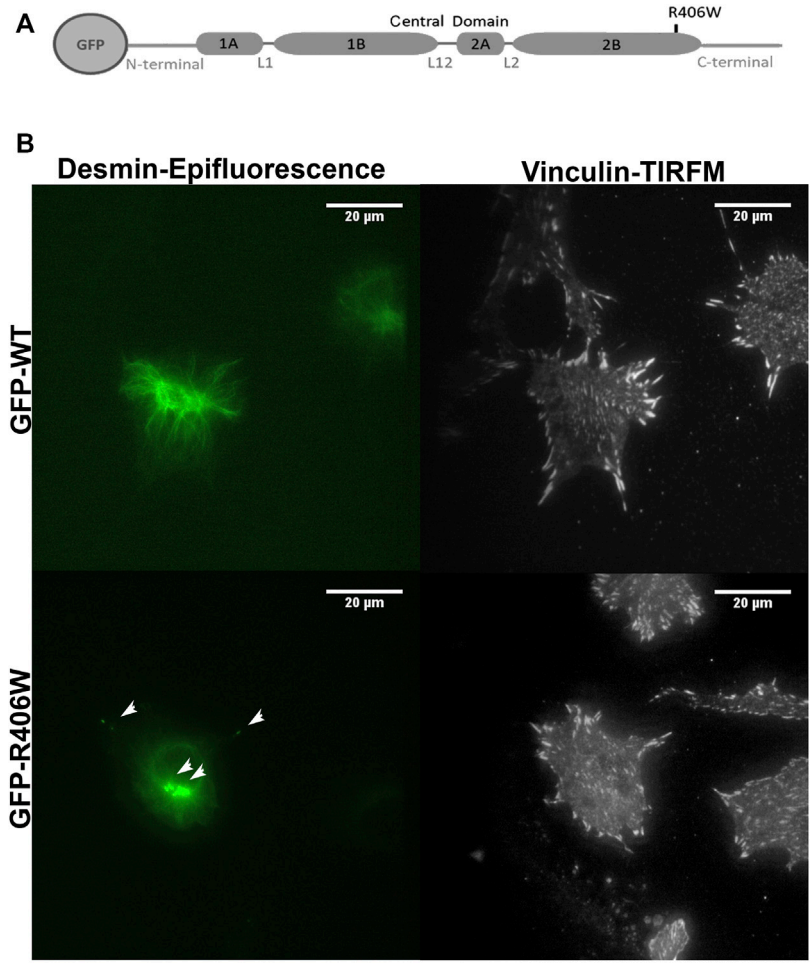

FIGURE 2 | Desmin and vinculin morphology in C2C12 cells. **(A)** Representation of WT or R406W mutant desmin fused to GFP at the N-terminus. **(B)** GFP-WT desmin or GFP-R406W desmin were electroporated into C2C12 myoblasts. Vinculin was stained in red with Alexa-568. Epifluorescence images were taken 24 h after transfection. The p.R406W expressing cells show intracytoplasmic aggregates of desmin, unlike those expressing wild-type desmin. The cells were observed using a ×60 immersion objective. The scale bar corresponds to 20 µm.

between the two forms. As previously reported (Delort et al., 2019), endogenous desmin was always more highly expressed than exogenous desmin (**Figure 1A**, the ratio of exogenous/endogenous varies from 0.1 to 0.7), corresponding to moderate desmin overexpression close to the pathophysiological conditions observed in patients.

We next performed transcriptomic profiling of C2C12 cells stably expressing wild-type and R406W desmin (using each clone expressing the same level of Myc-desmin WT or R406W with ratio exogenous/endogenous desmin around 0.5) in comparison to non-transfected C2C12 cells with Agilent Whole Mouse Genome Oligo Microarrays. In cells expressing wild-type desmin, 638 genes were up- and 516 genes were down-regulated compared to non-transfected cells, whereas in p.R406W-expressing cells, 389 genes were up and 514 genes were downregulated (**Figure 1B**, right). To identify specifically up and downregulated genes in mutant-expressing cells, we removed all mutually modified genes in our analysis. After this step, we specifically identified 311 genes that were up and 366 genes that were downregulated in p.R406W-expressing cells (**Figure 1B**, right).

The most relevant pathways and genes were identified by bioinformatic analyses. The top Gene Ontology categories included muscle contraction, myofibril, cell differentiation and interestingly, cell adhesion. The biological process of cell adhesion was found in both up-regulated and down-regulated clusters, indicating a strong perturbation of this function specifically in C2C12 cells expressing R406W desmin. Among these differentially expressed genes, we identified 37 down (p = 1.9e-9) and 22 upregulated (p = 4.8e-4) genes related to cell adhesion (see **Figure 1B**, left; **Supplementary Table S1** for complete list), including genes of IF family (**Supplementary Table S1, S2**) and genes involved in cadherin or catenin related pathways (**Figure 1C**).

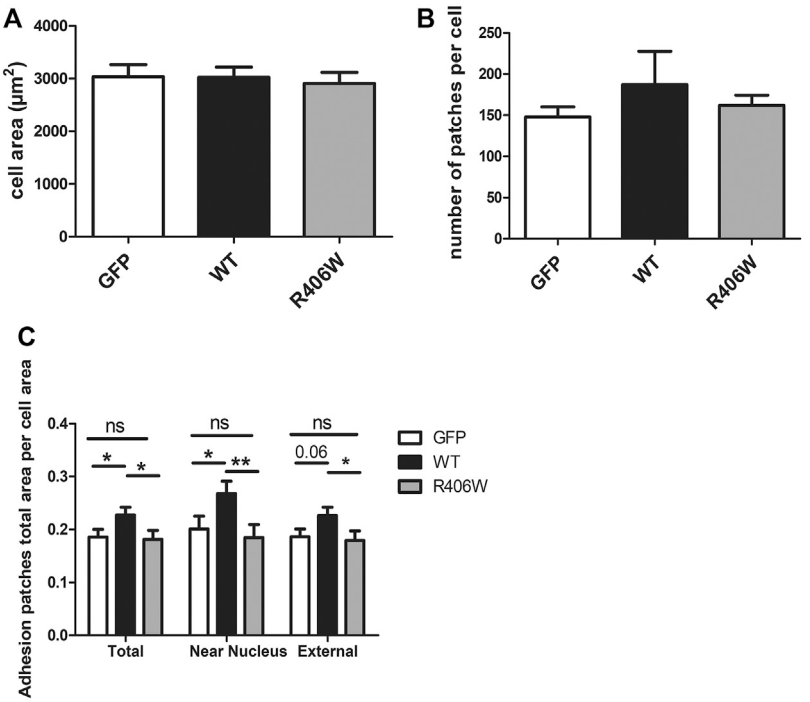

FIGURE 3 | Effect of desmin mutation on the total area of focal adhesions in C2C12 cells. **(A)** Average area of cells electroporated with GFP, GFP-WT desmin or GFP-R406W desmin. **(B)** Average vinculin patch number per cell counted for the three cell lines and **(C)** Average total vinculin patch area per cell area for the three cell lines, for the entire cells ("Total"), for the region of the cells located under the nucleus ("Near nucleus") and for the cell minus this nuclear zone ("External"). Kruskal-Wallis tests were performed. *$p < 0.05$, **$p < 0.01$. The measurements were performed with a home-designed ImageJ macro described in the *Materials and Methods* section and **Supplementary Figure S1**. These results represent the average of n > 40 cells per condition from three independent experiments.

Overexpression of Desmin Modulates Focal Adhesion Area in Electroporated C2C12 Cells

To further explore the impact of desmin in the adhesion process, we focused on FAs. We electroporated murine C2C12 undifferentiated myoblasts carrying N-ter-GFP fused human WT desmin or R406W mutant desmin cDNA (**Figure 2A**). We first checked that the two constructs have similar expression levels (**Supplementary Figure S2**) and then analyzed the organization of the desmin network using epifluorescence and TIRFM (**Figure 2B**, the two analyses were performed on the same cells). Cells electroporated with wild-type desmin cDNA exhibit a well-organized desmin network, whereas cells electroporated with R406W desmin cDNA displayed aggregates near the nucleus and in the cytoplasm as expected (**Figure 2B**, arrowheads).

To determine the impact of WT or mutated desmin overexpression on cell adhesion, we stained vinculin, an established marker of FA complexes (**Figure 2B**). As the number and area of vinculin patches reflect the formation and regulation of FAs, we first analyzed these parameters. In addition, we measured the total cell surface. Cells electroporated with GFP alone were used as a control (**Figure 3**).

None of the overexpressed forms of desmin resulted in a change in total cell area (**Figure 3A**) or in the number of FA patches per cell (**Figure 3B**). However, the total area of the patches, normalized by the cell area, was 22% larger for cells overexpressing WT desmin compared to that of cells expressing GFP alone (**Figure 3C**). Moreover, this effect was more pronounced in the central region of the cells, near the nucleus (33% increase), and less in the periphery (21% increase), where the effect of GFP-desWT expression was just beyond significance. On the contrary, such an increase was not observed with the expression of desR406W, suggesting a loss of function regarding FA modulation. The same results were obtained when staining paxillin instead of vinculin (data not shown).

DesKO and DesKI Satellite Cells Exhibit Decreased Adhesive Properties on Fibronectin Substrate Under Hydrodynamic Flow

To avoid overexpression of desmin, and to be closer to physiological conditions, we used satellite cells extracted from a knock-out mouse model of desmin and a homozygous knock-in mouse model carrying the p.R405W mutation (murine homologue of the human p.R406W mutation), respectively named DesKO (Li et al., 1996) and DesKI-R405W (Batonnet-Pichon et al., 2017; Herrmann et al., 2020). We first confirmed the absence of desmin expression in DesKO satellite cells (**Figures 4A,B**). Second, we followed

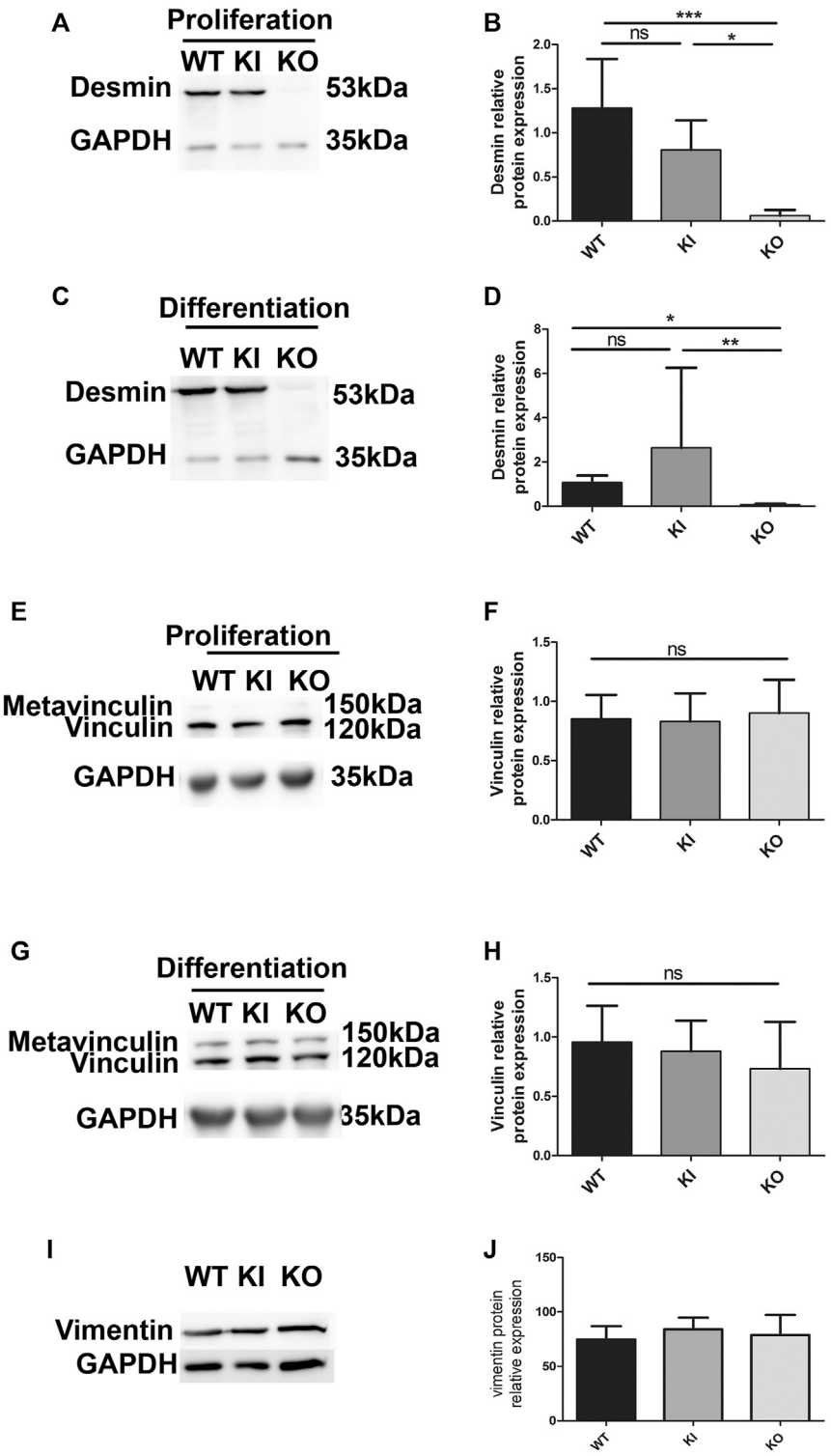

FIGURE 4 | Relative protein expression of desmin, vinculin and vimentin in proliferating and differentiating satellite cells. Relative protein expression of desmin in proliferating **(A,B)** and differentiating **(C,D)** satellite cells was quantified by immunodetection and normalized by GAPDH protein expression. Each histogram represents the average of two lines per condition (3 for DesKI) and three independent experiments. The relative protein expression of vinculin was measured in proliferating **(E,F)** and differentiating **(G,H)** satellite cells by Western blot and normalized to the expression of GAPDH. The relative protein expression of vimentin was measured in proliferating **(I,J)** satellite cells by Western blot and normalized to the expression of GAPDH. Non-parametric Kruskal-Wallis tests were performed on the samples with: n.s, not significant; $^{*}p < 0.05$; $^{**}p < 0.01$ and $^{***}p < 0.001$.

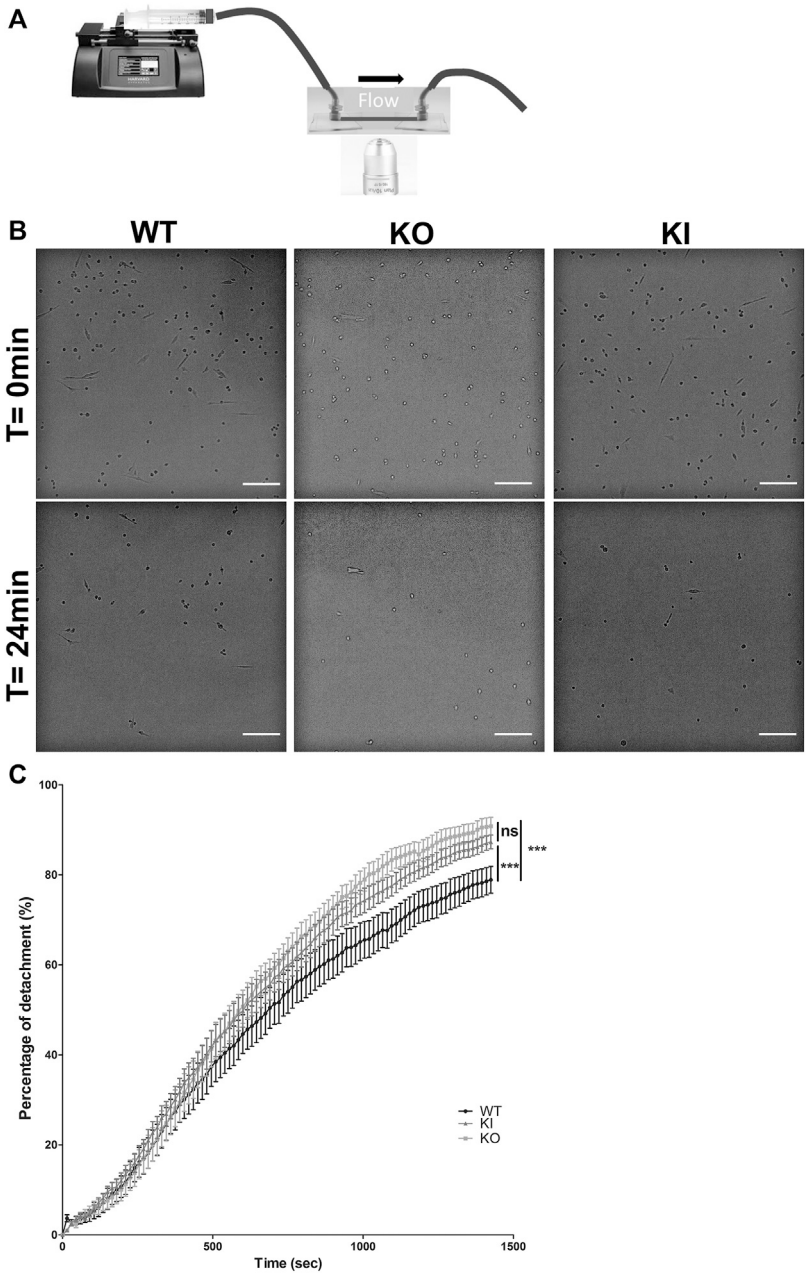

FIGURE 5 | Detachment of satellite cells during the application of a shear flow. **(A)** A syringe-pump delivered a constant flow of medium through tubing on cells seeded on Ibidi slides. Images were acquired every 15 s during the experiment. **(B)** Satellite cells detached over time. After 24 min, the remaining cells were counted. More WT satellite cells remained adhered to the substrate than DesKO and DesKI-R405W satellite cells. Images were taken on an inverted microscope using a ×10 objective. Scale bar = 200 µm. **(C)** The number of cells remaining adhered to the substrate were counted to measure the percentage of detachment over time. A significant difference in detachment was measured between the WT satellite cells and the DesKO and DesKI-R405W mutant satellite cells. A non-parametric Friedman test was used: ***$p < 0.001$. The error bars correspond to the SD. The experiment was repeated 3 times with two independent satellites cells lines extracted from two mice each for WT and KO genotype and three independent satellites cells lines extracted from three mice for KI genotype.

desmin levels in proliferating (**Figures 4A,B**) and differentiating (**Figures 4C,D**) DesKI-R405W cells. As expected, desmin expression increases during differentiation. However, contrary to muscle (Herrmann et al., 2020), satellite cells had a similar amount of mutated or WT desmin, even during differentiation (**Figures 4A–D**).

Since modifications of the FA areas were observed in C2C12 myoblasts overexpressing desmin, we checked whether vinculin expression could be altered in satellite cells. Vinculin expression remained unchanged in all cell types and conditions (**Figures 4E–H**), as well as vimentin (**Figures 4I,J**), which is co-expressed with desmin in prolifating muscle cell.

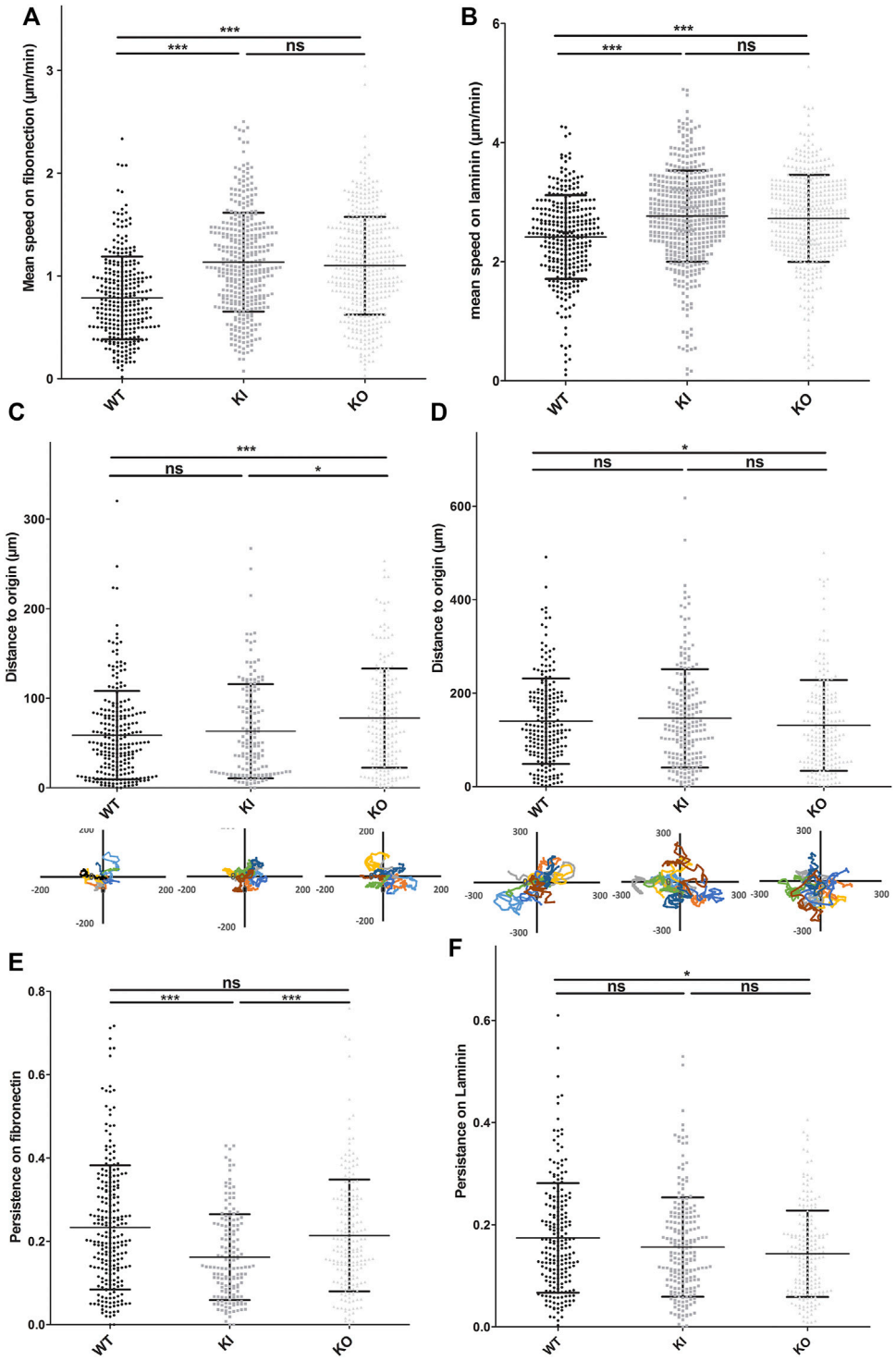

FIGURE 6 | DesKO and DesKI-R405W cells move faster on fibronectin and laminin substrates. Cells were seeded on culture wells coated with fibronectin **(A,C,E)** or laminin **(B,D,F)**. Pictures were taken every 7 min. Cells were tracked by hand using ImageJ software and its manual tracking plugin. Each average represents two different cell extractions for each mice genotype, and experiments were repeated 3 times. with $n > 150$ cells and the error bars represent the SD. **(A,B)** The mean speed of each cell line is represented. The distance to the origin on fibronectin **(C)** and laminin **(D)** was calculated from the coordinates obtained during the migration follow-up with ImageJ software. WT DesKO and DesKI-R405W cell migration way was calculated with Excel software from a representative sample of eight cells per genotype. Cell persistence on fibronectin **(E)** and laminin **(F)** was calculated by their distance from the origin and their total migration distance. A Kruskal-Wallis test was performed, and the error bars correspond to the SD: n.s, not significant; $*p < 0.05$; $***p < 0.001$

To determine whether desmin could have a role in cellular adhesion, we performed functional analysis under shear stress in DesKO or DesKI-R405W contexts. Satellite cells were seeded on fibronectin-coated Ibitreat microslides and a constant flow was applied with a home-made setup (**Figure 5A**). After 24 min of shear stress, satellite cells were almost completely peeled off (**Figure 5B**). However, more WT cells seemed to be left attached than DesKI-R405W or DesKO cells. To confirm this qualitative observation, we determined the detachment rate by counting cells manually on each image (**Figure 5C**). From 0 to 500 s, all three cell types presented similar behaviors. In contrast, from 500 s, DesKO and DesKI-R405W satellite cells peeled off more significantly than the WT cells. Indeed, from 1,000 s, homozygous mutant cells (DesKO and DesKI-R405W) had a detachment rate 10% higher than that of WT cells. Finally, at the end of the experiment (24 min), 78.9% of the WT cells were detached from the substrate (**Figure 5C**) compared to 90.8% and 87.3% respectively of DesKO and DesKI-R405W cells. Altogether, this suggests that homozygous DesKO and DesKI-R405W satellite cells are less adhesive than WT cells on fibronectin.

DesKO and DesKI-R405W Satellite Cells Exhibit Higher Migration Speed

Satellite cells can migrate into mature muscle in regenerative conditions and in culture on different substrates. Migration and adhesion are related and interdependent processes. Thus, to determine whether desmin mutation can also affect cell migration, we used time-lapse to follow the non-directed motion of satellite cells on the two main substrates expressed in muscle: fibronectin and laminin. First we confirmed, as described *in vitro* (Siegel et al., 2009), that satellite cells present a higher migration rate on laminin than on fibronectin-coated surfaces (**Supplementary Figure S3**). Second, we compared WT to homozygous DesKO and DesKI-R405W cells on each type of substrate. On fibronectin, the average velocities of homozygous DesKO (1.1 μm min^{-1}) and DesKI (1.13 μm min^{-1}) cells were significantly higher (around 58%) than those of WT cells (0.79 μm min^{-1}) (**Figure 6A**). No significant difference was observed between the two mutant cells.

Satellite cells migrated faster on laminin, with mean migration rates of 2.41, 2.73, and 2.76 μm min^{-1}, respectively for WT, DesKO and DesKI-R405W cells (**Figure 6B**, **Supplementary Videos S1/WT, S2/KI and S3/KO**). Thus, DesKO and DesKI-R405W mutant satellite cells migrate about 15% faster than WT cells on laminin.

Together, these results suggest that desmin is involved in migration, and desmin modifications (loss or non-sense mutation) alter cell migratory properties.

The ability of cells to migrate in a directional way can be represented by cell persistence (see *Materials and Methods*). On fibronectin, the average persistence of WT, DesKO and DesKI-R405W cells was 0.23, 0.21 and 0.16, respectively (**Figure 6E**). Thus, DesKI-R405W cells had a 24% decrease in persistence compared to WT cells, suggesting less directionality. However, although DesKO cells migrated faster than WT cells on fibronectin, their directionalities were similar (**Figure 6C**).

On laminin, WT, DesKO, and DesKI-R405W cells had similar persistence (0.17, 0.14 and 0.16, respectively, less than 12% difference, **Figure 6F**).

Vinculin Expression and Localization Are Altered in DesKO and DesKI-R405W Muscle

Finally, to confirm a link between desmin and markers of adhesion, we analyzed vinculin expression in mature muscle. In mouse models of desminopathies, as in patients, not all muscles are affected in the same way. In mice, the soleus, a slow posture muscle, is one of the muscles presenting the most pathological defects. Thus, we performed expression analysis on the soleus from DesKO and DesKI-R405W mice at ages presenting a well-established phenotype, with either a strong decrease in weight (DesKO, DesKI-R405W) or around the time of death for DesKI-R405W mice (Batonnet-Pichon et al., 2017; Herrmann et al., 2020).

The soleus of one-year-old DesKO mice had a 2.5-fold increase in vinculin expression compared to WT mice (**Figures 7A,B**). The same augmentation was also observed in the quadriceps of DesKO mice, in an age-dependent manner, without any changes in metavinculin quantity (**Supplementary Figure S4**). In the same way, the vinculin level was also increased in the soleus from 3-month-old DesKI-R405W mice compared to WT mice (**Figures 7C,D**). Furthermore, this increase was associated with a rise in the desmin level at this age (**Figures 7E,F**). Similar alterations of vinculin and desmin expression were found in the quadriceps muscles of 3-month-old DesKI-R405W mice (**Supplementary Figure S5**).

To determine if this higher expression level is associated with altered localization of vinculin in mature muscle, we performed immunostaining on soleus muscles. First, as expected, desmin labeling was detected in muscle sections from WT but not DesKO mice (**Supplementary Figure S6A**). Second, soleus from 5-month-old WT mice showed a well-localized laminin layer around the muscle fibers (**Figure 8A**). In addition, vinculin was observed at the membrane, with homogeneous staining all around the fiber periphery. In contrast, in the soleus of homozygous DesKO mice, the muscle fibers appeared disorganized, with varying size and an increased interfiber space, suggesting dystrophy and fibrosis as previously described (Li et al., 1997; Agbulut et al., 2001). Moreover, the vinculin immunostaining along the sarcolemma presented some heterogeneity in DesKO mice, with more intense areas at the membrane (white arrows, **Figure 8A**). In addition, some vinculin was surprisingly located inside the fibers (white arrows, **Figure 8A**), which was never observed in WT mouse muscles.

Fibers in the soleus of 1-year-old DesKO mice appeared more affected than those of 5-month-old DesKO mice. In addition to internalized nuclei (red arrows, **Figure 8B**), more

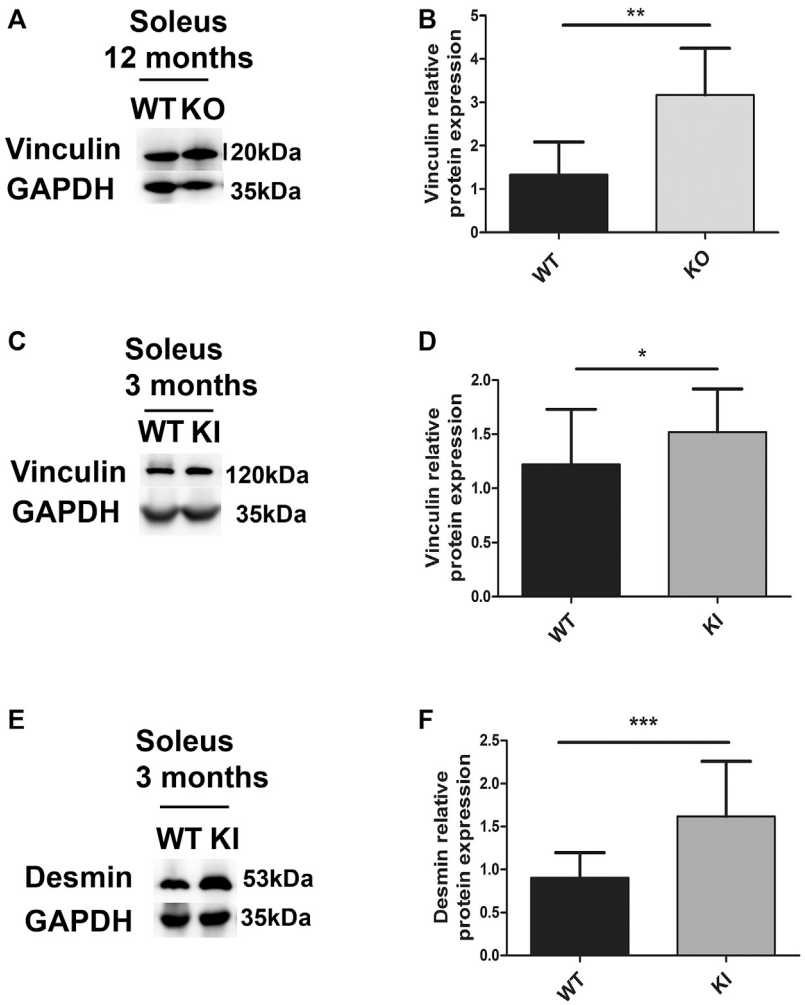

FIGURE 7 | Relative vinculin and desmin protein expression in DesKO and DesKI-R405W mouse soleus. The amount of vinculin was measured in the soleus of mutant DesKO **(A,B)** and DesKI-R405W mice **(C,D)**. The amount of desmin was measured in the soleus of mutant DesKI-R405W mice **(E,F)**. Each histogram represents the average relative protein expression of four independent GAPDH-standardized Western blot experiments for 7 WT mice and 7 DesKO mice or 6 WT and 5 DesKI-R405W mice. A Mann-Whitney non-parametric test was performed, with $*p < 0.05$; $**p < 0.01$; $***p < 0.001$. Error bars represent the SD.

fibers presented very variable size and shape, a sign of muscular dystrophy. Laminin labeling also showed an even greater increase in matrix space, possibly due to fibrosis. Interestingly, intrafibrillar accumulations of vinculin were more abundant (white arrows, **Figure 8B**). As in the 5-month-old muscles, vinculin staining was much more diffuse and heterogeneous along the membranes. The same characteristics were also observed in homozygous DesKO mouse diaphragms at 1 year of age (**Supplementary Figure S6B**).

In parallel, we analyzed vinculin localization in the soleus from 3-month-old DesKI-R405W mice (**Figure 8C**). Laminin staining revealed that fibers of homozygous DesKI-R405W mice were smaller than those of WT mice, suggesting muscle atrophy, as recently described (Herrmann et al., 2020). DesKO mouse muscle exhibit thickening of the matrix space between the fibers. Again, DesKI mice had more accumulations of the vinculin staining area (white arrows in **Figure 8C**) at the plasma membrane than WT mice. However, contrary to DesKO mice, no vinculin accumulation was detected inside the fibers of DesKI mice.

Together, these results suggest that vinculin increase is associated with mislocalization in adult muscle in both models.

Vinculin Expression is Also Altered in Patients With Desminopathies Associated With a Total Lack of Desmin

To see if vinculin expression modifications were also found in muscles of patients with pathological conditions, we obtained protein extracts from biopsies of patients carrying mutations leading to a total lack of desmin expression (**Figure 9A**). Indeed, the absence of desmin in patient tissue was associated with increased vinculin in the muscles (**Figure 9**). In contrast, the amount of actin was not disturbed (**Figure 9**).

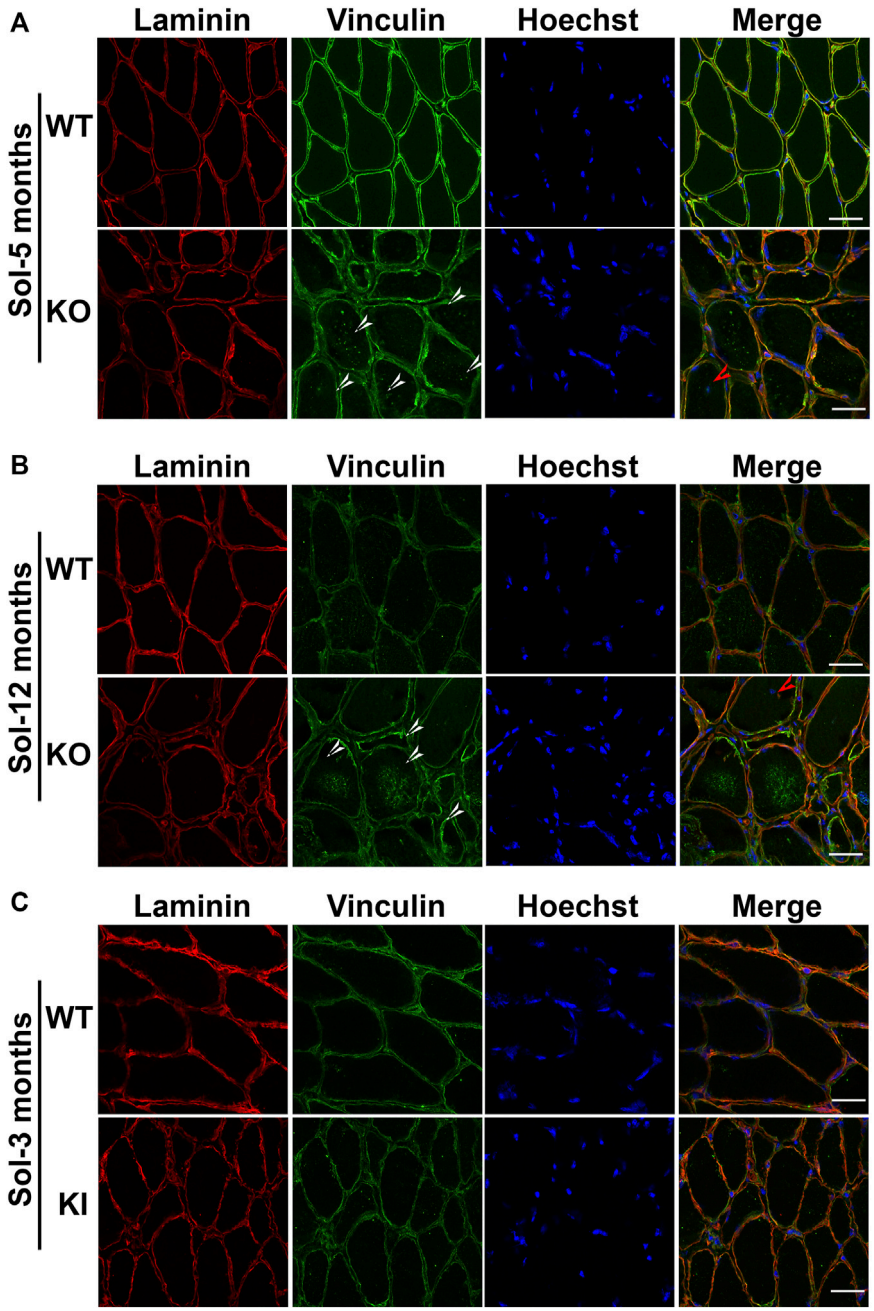

FIGURE 8 | Localization of vinculin in the soleus of DesKO and DesKI-R405W mice. Microscopic images of soleus cross sections from DesKO mice at 5 months **(A)** and 1 year of age **(B)** and DesKI-R405W 3-month-old mice **(C)**. Vinculin accumulations in and around the fibers are shown by the white arrows and central nuclei by red arrows. Laminin was stained in red, vinculin in green and nuclei in blue. Images were taken with a ×40 objective, and the scale bar corresponds to 30 μm.

DISCUSSION

Desmin Regulates Various Signaling Pathways Including Adhesion

Desmin is well known as a specific IF essential for muscle integrity and function. However, desminopathies highlight other potential important roles of desmin. To investigate pathways associated with desmin expression, we performed a wide analysis of gene expression in stable C2C12 cells overexpressing WT or p.R406W desmin. As expected, we observed modifications in several genes encoding proteins which are able to co-polymerize with desmin (Hol and Capetanaki, 2017) and sarcomeres or are involved in contraction linked to specific desmin location at the Z-disk.

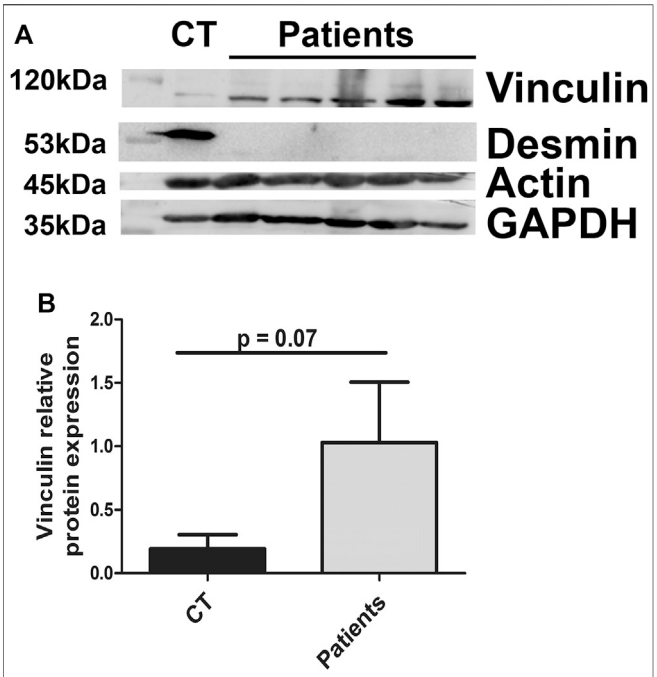

FIGURE 9 | Vinculin relative protein expression in patient muscle biopsies. The amounts of vinculin, actin, and desmin were measured in muscle biopsies from controls (CT) or patients carrying homozygous mutations in the desmin gene. GAPDH was used as a loading control.

Surprisingly, desmin network perturbation also led to alterations of gene expression associated with adhesion signaling. Specific cell adhesion molecules were upregulated, potentially leading to perturbation of cell adhesion properties (anchoring, moving and interactions with extracellular matrix). All these functions are essential for muscle, particularly during regeneration or force generation. Further, these processes are altered in DesKO mice (Agbulut et al., 2001). Taken together, our results highlight for the first time a potential new role of desmin in cell adhesion.

Overexpression of Desmin Modulates Focal Adhesion Area in Electroporated C2C12 Cells

As cell interactions with the ECM are essential for adhesion, we first focused our study on the link between desmin IFs and FAs, the main adhesive cell complexes, in adherent undifferentiated C2C12 myoblasts. Overexpression of wild-type desmin in C2C12 myoblasts increases the total area of adhesion patches containing vinculin without increasing their number. These results suggest a gain of function for myoblasts enriched in wild-type desmin. Moreover the increase is more pronounced for the adhesion patches located at the center of the cells, suggesting that desmin could play a role in the maintenance of the focal adhesions. Yet, electroporation of p.R406W desmin does not modify the total area of adhesion patches, indicating a loss of function of mutated desmin. Similar results have been found by our lab concerning the role of desmin in the rigidity of the cells, with a higher rigidity of C2C12 cells overexpressing WT desmin but not of cells overexpressing p.E413K mutated desmin (Charrier et al., 2018). Thus, desmin could play a role in the development and/or maintenance of FAs, with this function lost in the presence of the mutation. In endothelial cells, vimentin participates in the maturation of FAs to allow better adhesion of cells subjected to hemodynamic stress (Tsuruta and Jones, 2003). Desmin and vimentin share a large homology (80%) and both proteins are expressed in myoblasts. However, overexpression of WT or mutated desmin does not modify the vimentin network (Charrier et al., 2016), nor expression (**Figures 4I,J**).

Thus, desmin could have the same role in FA regulation in undifferentiated myoblasts as vimentin in other cells. However, desmin seems to play at least a role in FA regulation, since the number of patches per cell is not affected by desmin mutation. Interestingly, FA size closely correlates with the local forces that cells develop on their substrates (Balaban et al., 2001). The present study, along with our previous findings regarding p.E413K desmin, a mutation which is associated with impaired contractility (Charrier et al., 2016), suggest that desmin mutation could impair the forces that myoblasts develop against their substrates by interfering with modulation of FAs.

It would also be interesting to compare the composition of FAs for cells overexpressing WT desmin vs. p.R406W mutated desmin, in particular regarding integrins or proteins associated with FA maturation. However, myoblasts are specific muscle cells and unfortunately the proteins tested (such as beta1 and alpha7 integrins, or Zyxin) did not provide sufficiently specific immunostaining to perform TIRFM experiments.

The p.R406W mutation is localized at the end of the 2B domain in the TYRKLLEGEE consensus domain that could have a role in maintaining structure and interactions with important proteins to modulate FAs. In particular, desmin interacts and co-polymerizes with synemin, a type VI intermediate filament also expressed in muscle. Synemin is also linked to FAs in muscle (Sun et al., 2008a; Sun et al., 2008b). However, synemin is totally excluded from aggregates of p.E401K, p.R406W, and p.E413K mutants overexpressed in C2C12 cells (Chourbagi et al., 2011). Thus, the effect of the p.R406W mutation on FA maturation could be due to a lack of or decreased interaction with synemin. Moreover, synemin presents altered localization and expression in the soleus in DesKO (Rodríguez et al., 2018) and DesKI-R349P (Clemen et al., 2015) mice, reinforcing the potential link between desmin network perturbation and the observed vinculin defects.

Furthermore, desmin interacts with several proteins in costameres, such as plectin, or syncoilin. These proteins are themselves linked to the dystrophin-glycoprotein complex, which is a specific adhesion complex complementary to FAs observed in muscle (Ervasti, 2003). Immunostaining of soleus muscles from 1-year-old DesKO mice showed some fibers presenting dystrophin accumulations at the membrane. Thus, desmin could affect not only FA regulation but also the other adhesion complexes

through its various protein interactions, leading to costamere weakness.

DesKO and DesKI Satellite Cells Exhibit Decreased Adhesive Properties on Fibronectin Substrate Under Hydrodynamic Flow

As FAs are involved in the strength of adhesive bonds between cells and the ECM, we decided to measure the strength of cell adhesion under shear stress, elicited by a flow with a fixed and constant speed. We have previously seen that desmin p.R406W presents a loss of function compared to WT desmin. Our results show that satellite cells lacking desmin or expressing p.R405W desmin detach more rapidly than WT cells. This suggests that these cells adhere less to the substrate, i.e., fibronectin, compared to control cells. These results are consistent with the TIRFM data obtained on C2C12 myoblasts, suggesting a loss of function of the R406W mutated desmin with respect to AF regulation.[1] Alteration of FA maturation could lead to a decrease in their adhesive strength which would be characterized by lower resistance during shear-stress, increasing the rate of detachment. Moreover, DesKO satellite cells demonstrate that desmin absence leads to the same phenotype as the p.R405W mutation in satellite cells. This confirms the loss of function observed in the mutant compared to WT. In adhesion patches, integrins are considered essential contributors to the interaction with the substrate. Further, α5 integrin is crucial in muscle functions. Mice lacking this integrin chain have muscular dystrophies (Taverna et al., 1998). Moreover, keratin type I/II IFs can regulate integrin turnover (Seltmann et al., 2015). Thus, it is possible that desmin modifies FA adhesion, especially integrin clustering, directly or via its interaction with other IFs such as synemin or keratin.

DesKO and DesKI-R405W Satellite Cells Exhibit Faster Migration

FAs assemble and disassemble in a dynamic fashion when cells are moving (Webb et al., 2002). We thus analyzed the migration of WT satellite cells or homozygous DesKO and DesKI-R405W cells. We chose to use fibronectin and laminin, the two main components of the extracellular matrix of skeletal muscle (Gillies and Lieber, 2011), which are essential during the muscle regeneration process (Repesh et al., 1982; Gulati et al., 1983; Lukjanenko et al., 2016), when satellite cells are activated. In particular, satellite cells synthetize fibronectin during their activation (Bentzinger et al., 2012), reinforcing the hypothesis that fibronectin is the primordial substrate for their adhesion and laminin is more important as a substrate for migration. As expected, satellite cells migrated faster on laminin than on fibronectin regardless of the genotype of the cells (WT, DesKO or DesKI-R405W) (Siegel et al., 2009). Homozygous DesKI-R405W and DesKO satellite cells migrated faster than WT cells on both fibronectin and laminin.

As migration is in part linked to the adhesion process, the difference in migration speed observed in mutant cells (DesKO and DesKI-R405W) could be due to decreased interaction with the matrix. Indeed, changes in the cell-laminin and cell-fibronectin interactions of the DesKO and DesKI-R405W satellite cells would explain their faster movement. This hypothesis aligns with our previous observations showing alterations in vinculin patch size in cells overexpressing desmin p.R406W and decreased adhesion of DesKI-R405W and DesKO satellite cells to fibronectin. However contratry to FA regulation, desmin seems to have opposite effect on migration than vimentin. Indeed, vimentin KO cells exhibits slower migration rate (Eckes et al., 2000) and overexpression of vimentin lead to increase migration speed (Mendez et al., 2010). Moreover vimentin is considered as an epithelio-mesenchymal transition (EMT) marker and facilitates invasion of mesenchymal cells by controlling the dynamics and distribution of FAs (Mendez et al., 2010; Menko et al., 2014; De Pascalis et al., 2018). In contrast keratin 6 KO cells lead to a decrease of migration rate by modulating FA pathways (Wong and Coulombe, 2003; Rotty and Coulombe, 2012; Wang et al., 2018). Desmin (type III IF) is closer to vimentin (type III IF) than to keratins (type I and II IF), suggesting at first sight a more similar role. However, in muscle, desmin is upregulated during differentiation and vimentin decreased suggesting specific role of desmin in this tissue. Moreover, we did not see modification of vimentin expression level in desKO or desKI satellite cells (**Figures 3I,J**), that could suggest a compensation leading to the increase of migration rate. Thus regarding FA modulation or migration, vimentin and desmin could have some distinct roles by interacting with specific partners. Finally in the microarray, vimentin or synemin gene does not appear to be regulated, whereas keratin one seems to be modulated (**Supplementary Table S2**). Depending on the cell type, IFs have different effects on cell migration that may be explained by the difference in IF proteins or integrin expression patterns. Keratin 18 and 19 are known to be expressed in mature muscle and could be associated with desmin (Muriel et al., 2020). Moreover Keratin 16 overexpression has already been demonstrated linked to increase cell migration in cancer (Yuanhua et al., 2019)**.** Altogether, keratins in association with desmin would be a potential pathway to explore. However we did not succeed in identifying keratins expression in undifferentiated myoblasts and satellite cells, maybe their expression level is too low to be detected or antibody conditions need to be adapted. Indeed these keratins have been described in mature muscle with an mRNA level at least 1,000 times lower than that of desmin (Muriel et al., 2020). Desmin expression is low in satelitte cells or undifferentiated myoblasts and increases during differentiation and it could be the same for keratins. Thus some optimization is needed to confirm the potential role of keratins in future work. Altogether, keratins in association with desmin would be a potential pathway to explore in future work.

We also studied the persistence of the satellite cells. No difference was observed between the cell genotypes on laminin. However, on fibronectin, the DesKO satellite cells presented decreased persistence compared to WT and DesKI-R405W cells.

[1]Note that TIRFM experiments could unfortunately not be reproduced on satellite cells, due to their poor attachment to the glass coverslips, a necessary experimental condition for TIRFM.

Interestingly, vimentin knock-out also leads to downregulation of persistence during wound healing experiments (Eckes et al., 2000). Thus, desmin seems to have a similar function in myoblasts to that of vimentin in other cell types. It is therefore consistent that desmin invalidation could affect cell persistence. Moreover, vimentin expression is not increased upon desmin KO (Capetanaki et al., 1997; Li et al., 1997). Thus, vimentin cannot compensate for the loss of skeletal-muscle-specific desmin.

The difference between the two types of mutant cells (DesKO and DesKI-R405W) could be due their differential effects on the interactions of desmin and its partner. The mutation localized at the end of the 2B domain could potentially alter some interactions (as with synemin) but not others, whereas the absence of desmin modifies its entire interactome. In fact, phenotypes of DesKI-R405W mice are not totally similar those of DesKO mice, even if they share some similarities, suggesting a mutant-specific effect.

It is difficult to extrapolate the adhesive properties and migration of satellite cells to mature muscle. Indeed, *in vivo*, faster migration speed would allow satellite cells to reach the injury site to regenerate the tissue more rapidly. However, if satellite cells continue migrating for too long, this could impair their ability to fuse with the fibers to restore the muscle, especially with the decrease of cell-matrix adhesion. Indeed, defects in regeneration, particularly a delay in fiber maturation, are described in DesKO mice (Agbulut et al., 2001). This would be consistent with defective satellite cell adhesion. Moreover, in the case of DesKO, the directionality seems to also be affected. This could therefore lead to an error or delay in addressing satellite cells to the location of the injury that could partly explain the observed regeneration defects in DesKO mice.

Vinculin Expression and Localization Are Altered in DesKO and DesKI-R405W Muscle

We further quantified the expression of vinculin in mature skeletal muscle. In our model, desmin expression is increased by around two fold in the quadriceps and soleus muscle of 3-month-old homozygous DesKI-R405W mice compared to WT mice (Herrmann et al., 2020). Vinculin expression increased in an age-dependent manner in DesKO mice (quadriceps and soleus). This increase also occurred in the soleus of 3-month-old DesKI-R405W mice. At first, this alteration seems to contradict previous results obtained *in vitro* showing a decrease in the area of cellular FAs associated with weaker adhesion of satellite cells, which also does not present modifications of vinculin expression. However, the amount of vinculin increases during aging, especially in cardiac cells (DeLeon-Pennell and Lindsey, 2015). In addition, vinculin can regulate cell stiffness due to its ability to form adhesion patches (Auernheimer and Goldmann, 2014). Thus, overexpression of vinculin could lead to increased muscle rigidity. This increase could also be a compensation effect against, in part, costamere fragility which could rise over time due to the progressive degradation of muscle fibers. Indeed, at least in the DesKO model, focal disorganizations inside the muscle have been described and could induce costamere fragility (Li et al., 1996). In response to this alteration, muscle fibers would overexpress vinculin and maybe some other costamere proteins to try to maintain adhesion.

In parallel, we determined the localization of vinculin in DesKO or DesKI-R405W fibers. In normal muscle, vinculin is located at the costamere, at the interface between the membrane and endomysium; yet, vinculin shows an increased expression level as well as mislocalization with peripheral accumulation for both models and intramyofibrillar accumulation in DesKO muscles. These vinculin intrafibrillar deposits seem to worsen over time according to our observations in 1-year-old soleus. Vinculin accumulations were

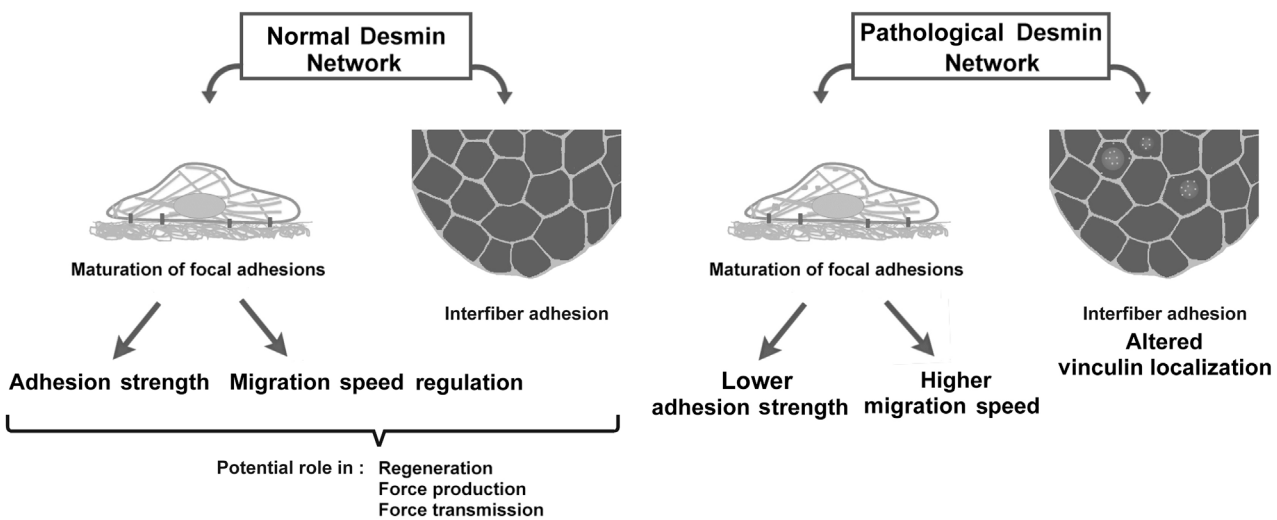

FIGURE 10 | Schematic representation of desmin roles in adhesion and migration and the potential consequences on muscle.

found only at the periphery and not inside the fibers in DesKI-R405W mouse muscles. This may be partly explained by the fact that mice die at the age of 3 months. Indeed, the muscular injury may not have been fully developed yet. However, as the accumulations are inside DesKO fibers, they therefore are totally independent of desmin aggregation (as found in DesKI-R405W). Moreover, we know that the desmin-rich aggregates found in patients with desminopathies are composed of several proteins captured during their formation. Laser microdissection of aggregates followed by proteomic analysis performed in five patients with different mutations in the desmin gene did not demonstrate the presence of vinculin in these formations (Maerkens et al., 2013). Finally, preliminary results from muscle biopsies of patients with mutations leading to desmin invalidation also show an increase in vinculin. These results suggest that the disturbed localization of vinculin is not due to the presence of aggregates in the fibers but rather to the disorganization of the desmin network itself.

In sum, these results suggest that disruption in the desmin network could lead to alteration of muscle fiber adhesion. Physiologically, the decrease in adhesion between fibers and extracellular matrix as well as vinculin mislocalization and the defects of satellite cell adhesion and migration could lead to reduced force transmission produced by muscles. Indeed, disorganization of sarcomeres due to the lack or presence of desmin aggregates generates a defect in force production (Li et al., 1997; Anderson et al., 2002) that causes the muscle weakness observed in patients. However, force transmission is not only longitudinal to the tendon (Sharafi and Blemker, 2011), but also lateral from costameres to the endomysium (Zhang and Gao, 2014). Thus, reduced force production and altered force transmission would generate significant muscle weakness in patients. In addition, the adhesion and migration defects observed in satellite cells could lead to decreased muscle regeneration and efficiency.

CONCLUSION

This study demonstrates that disruption of desmin leads to defects in skeletal muscle cell adhesion and migration (**Figure 10**). This new role of desmin opens avenues of investigation into the physiology and pathology of desminopathies, potentially leading to the identification of new therapeutic targets for these currently incurable diseases.

DATA AVAILABILITY STATEMENT

The datasets presented in this study can be found in online repositories. The names of the repository/repositories and accession number(s) can be found below: Gene Expression Omnibus, GSE185589.

ETHICS STATEMENT

Ethical review and approval was not required for the study on human participants in accordance with the local legislation and institutional requirements. Written informed consent to participate in this study was provided by the participants' legal guardian/next of kin. The animal study was reviewed and approved by Buffon Ethics Commitee, authorization CEB-16-2016.

AUTHOR CONTRIBUTIONS

CH, FD, OA, SH, and SB-P designed the research, performed experiments, analyzed data, and wrote the paper. PJ and FB-R performed experiments. PV and M-TD critically read and corrected the paper. AL and EC extracted muscles from DesKI-R405 mice, analyzed data, and critically read the paper. OC developed the macro for ImageJ software. CT, AF, ER, and MM kindly provided muscle biopsies from DesKO patients and reviewed and edited the paper.

FUNDING

CH, FB-R, M-TD, FD, AL, EC, PV, AF, OC, SH, and SB-P were supported by Université de Paris and the French National Center for Scientific Research (CNRS). This work was supported by the Association Française Contre les Myopathies (AFM) (grant numbers 18358, 20802, 22142 and 22956).

ACKNOWLEDGMENTS

We thank Z. Li for the DesKO mice. We acknowledge the "plateforme d'Hébergement et d'expérimentation animale Buffon" for the DesKO- and DesKI-R405W mice. Confocal images were acquired at the imaging facility of the BFA unit. We are grateful to C. Tourrel-Cuzin of the "Plateau imagerie cellulaire et cytométrie PIC2" for technical help and access to TIRFM. We thank the ImagoSeine core facility of the Institut Jacques Monod, member of IBiSA and France-BioImaging (ANR-10-INBS-04) infrastructures for videomicroscopy experiments.

SUPPLEMENTARY MATERIAL

The Supplementary Material for this article can be found online at: https://www.frontiersin.org/articles/10.3389/fcell.2022.783724/full#supplementary-material

Supplementary Figure 1 | Method for measuring focal adhesion area. **(A)** Observation of vinculin by TIRFM allows visualization of adhesion patches. Epifluorescence and TIRFM images were taken with the ×40 objective. Scale bar = 10 µm. **(B)** ImageJ software was used to measure the area of adhesion. The four steps used for image processing are listed.

Supplementary Figure 2 | Relative amount of transfected desmin compared to endogenous in electroporated C2C12 cells. The amount of GFP-WT and GFP-R406W desmin was measured in C2C12 cells, 24 h after electroporation. Endogenous and exogenous (GFP-constructs) was detected by anti-desmin antibody. Each histogram represents the average relative protein expression of four independent experiments

normalized by electroporation rate. Measured on >100 cells. The error bars represent the SD.

Supplementary Figure 3 | Mean migration rates of satellite cells according to the substrate. Mean migration rates of WT **(A)**, DesKO **(B)** and DesKI-R405W **(C)** cells are plotted against the substrate on which they are adhered. Each point represents the average speed of a cell and the error bars represent the standard deviation. A non-parametric Mann-Whitney test was performed: $^{***}p < 0.001$.

Supplementary Figure 4 | Relative vinculin protein expression in DesKO mouse quadriceps. The amounts of vinculin **(B,E,H)** and metavinculin **(C,F,I)** were measured in quadriceps of mutant DesKO mice at 3 months **(A–C)**, 5 months **(D–F)** and 1 year **(G–I)** of age. Each histogram represents the average relative protein expression of four independent GAPDH-standardized experiments for more than 5 WT mice and five DesKO mice (3 months: 8 WT and 6 DesKO; 5 months: 6 WT and 6 DesKO; 1 year: 6 WT and 5 DesKO). A non-parametric Mann-Whitney test was performed on the samples. All conditions are not significant with $^{*}p < 0.05$; $^{**}p < 0.01$; $^{***}p < 0.001$. The error bars represent the SD.

Supplementary Figure 5 | Relative vinculin and desmin protein expression in 3-month-old DesKI-R405W mouse quadriceps. The amount of desmin **(A,B)** and vinculin **(C,D)** was measured in quadriceps of DesKI-R405W mice at 3 months. Each histogram represents the average relative protein expression of three independent GAPDH-standardized experiments from 5 WT and 2 DesKI-R405W mice. Vinculin (120 kDa) and desmin (53 KDa) are revealed on the same gel than GAPDH (35 KDa), which are consequently presented twice on the panel **(A, C)**. A non-parametric Mann-Whitney test was performed on the samples with $^{**}p < 0.01$; $^{***}p < 0.001$. The error bars represent the SD.

Supplementary Figure 6 | Protein localization in muscles of 1-year-old DesKO mice. Microscopic images of cross sections of the soleus **(A)** and diaphragm **(B)**. **(A)** Desmin (green) is found on the edges of the fibers as well as inside the fibers of WT mice (white arrows). No desmin labeling is found in homozygous DesKO individuals. Laminin is stained in red, nuclei are in blue. **(B)** Vinculin (green) accumulations and a thickening of vinculin labeling at the fiber membrane are shown by white arrows. Laminin is marked in red, and nuclei in blue. The confocal images were taken with a ×40 objective and the scale bar corresponds to 30 µm.

REFERENCES

Agbulut, O., Li, Z., Périé, S., Ludosky, M.-A., Paulin, D., Cartaud, J., et al. (2001). Lack of Desmin Results in Abortive Muscle Regeneration and Modifications in Synaptic Structure. *Cell Motil. Cytoskeleton* 49, 51–66. doi:10.1002/cm.1020

Agnetti, G., Herrmann, H., and Cohen, S. (2021). New Roles for Desmin in the Maintenance of Muscle Homeostasis. *FEBS J.* doi:10.1111/febs.15864

Anderson, J., Joumaa, V., Stevens, L., Neagoe, C., Li, Z., Mounier, Y., et al. (2002). Passive Stiffness Changes in Soleus Muscles from Desmin Knockout Mice Are Not Due to Titin Modifications. *Pflugers Arch.* 444, 771–776. doi:10.1007/s00424-002-0875-0

Auernheimer, V., and Goldmann, W. H. (2014). Vinculin E29R Mutation Changes Cellular Mechanics. *Biochem. Biophys. Res. Commun.* 452, 661–664. doi:10.1016/j.bbrc.2014.08.133

Balaban, N. Q., Schwarz, U. S., Riveline, D., Goichberg, P., Tzur, G., Sabanay, I., et al. (2001). Force and Focal Adhesion Assembly: a Close Relationship Studied Using Elastic Micropatterned Substrates. *Nat. Cel Biol.* 3, 466–472. doi:10.1038/35074532

Batonnet-Pichon, S., Behin, A., Cabet, E., Delort, F., Vicart, P., and Lilienbaum, A. (2017). Myofibrillar Myopathies: New Perspectives from Animal Models to Potential Therapeutic Approaches. *J. Neuromuscul. Dis.* 4, 1–15. doi:10.3233/JND-160203

Bays, J. L., and DeMali, K. A. (2017). Vinculin in Cell-Cell and Cell-Matrix Adhesions. *Cell. Mol. Life Sci.* 74, 2999–3009. doi:10.1007/s00018-017-2511-3

Bentzinger, C. F., Wang, Y. X., and Rudnicki, M. A. (2012). Building Muscle: Molecular Regulation of Myogenesis. *Cold Spring Harbor. Perspect. Biol.* 4, a008342. doi:10.1101/cshperspect.a008342

Capetanaki, Y., Milner, D. J., and Weitzer, G. (1997). Desmin in Muscle Formation and Maintenance: Knockouts and Consequences. *Cell Struct. Funct.* 22, 103–116. doi:10.1247/csf.22.103

Carmignac, V., Sharma, S., Arbogast, S., Fischer, D., Serreri, C., Serria, M., et al. (2009). G.O.7 A Homozygous Desmin Deletion Causes an Emery-Dreifuss like Recessive Myopathy with Desmin Depletion. *Neuromuscul. Disord.* 19, 600. doi:10.1016/j.nmd.2009.06.179

Charrier, E. E., Asnacios, A., Milloud, R., De Mets, R., Balland, M., Delort, F., et al. (2016). Desmin Mutation in the C-Terminal Domain Impairs Traction Force Generation in Myoblasts. *Biophys. J.* 110, 470–480. doi:10.1016/j.bpj.2015.11.3518

Charrier, E. E., Montel, L., Asnacios, A., Delort, F., Vicart, P., Gallet, F., et al. (2018). The Desmin Network Is a Determinant of the Cytoplasmic Stiffness of Myoblasts. *Biol. Cel* 110, 77–90. doi:10.1111/boc.201700040

Chourbagi, O., Bruston, F., Carinci, M., Xue, Z., Vicart, P., Paulin, D., et al. (2011). Desmin Mutations in the Terminal Consensus Motif Prevent Synemin-Desmin Heteropolymer Filament Assembly. *Exp. Cel Res.* 317, 886–897. doi:10.1016/j.yexcr.2011.01.013

Clemen, C. S., Stöckigt, F., Strucksberg, K.-H., Chevessier, F., Winter, L., Schütz, J., et al. (2015). The Toxic Effect of R350P Mutant Desmin in Striated Muscle of Man and Mouse. *Acta Neuropathol.* 129, 297–315. doi:10.1007/s00401-014-1363-2

Dagvadorj, A., Olivé, M., Urtizberea, J.-A., Halle, M., Shatunov, A., Bönnemann, C., et al. (2004). A Series of West European Patients with Severe Cardiac and Skeletal Myopathy Associated with a De Novo R406W Mutation in Desmin. *J. Neurol.* 251, 143–149. doi:10.1007/s00415-004-0289-3

De Pascalis, C., Pérez-González, C., Seetharaman, S., Boëda, B., Vianay, B., Burute, M., et al. (2018). Intermediate Filaments Control Collective Migration by Restricting Traction Forces and Sustaining Cell-Cell Contacts. *J. Cell Biol.* 217, 3031–3044. doi:10.1083/jcb.201801162

DeLeon-Pennell, K. Y., and Lindsey, M. L. (2015). Cardiac Aging: Send in the Vinculin Reinforcements. *Sci. Transl. Med.* 7, 292fs26. doi:10.1126/scitranslmed.aab3391

Delort, F., Segard, B.-D., Hakibilen, C., Bourgois-Rocha, F., Cabet, E., Vicart, P., et al. (2019). Alterations of Redox Dynamics and Desmin post-translational Modifications in Skeletal Muscle Models of Desminopathies. *Exp. Cel Res.* 383, 111539. doi:10.1016/j.yexcr.2019.111539

Duarte, S., Viedma-Poyatos, Á., Navarro-Carrasco, E., Martínez, A. E., Pajares, M. A., and Pérez-Sala, D. (2019). Vimentin Filaments Interact with the Actin Cortex in Mitosis Allowing normal Cell Division. *Nat. Commun.* 10, 4200. doi:10.1038/s41467-019-12029-4

Eckes, B., Colucci-Guyon, E., Smola, H., Nodder, S., Babinet, C., Krieg, T., et al. (2000). Impaired Wound Healing in Embryonic and Adult Mice Lacking Vimentin. *J. Cel Sci.* 113 (Pt 13), 2455–2462. doi:10.1242/jcs.113.13.2455

Ervasti, J. M. (2003). Costameres: the Achilles' Heel of Herculean Muscle. *J. Biol. Chem.* 278, 13591–13594. doi:10.1074/jbc.R200021200

Etienne-Manneville, S. (2018). Cytoplasmic Intermediate Filaments in Cell Biology. *Annu. Rev. Cel Dev. Biol.* 34, 1–28. doi:10.1146/annurev-cellbio-100617-062534

Fichna, J. P., Karolczak, J., Potulska-Chromik, A., Miszta, P., Berdynski, M., Sikorska, A., et al. (2014). Two Desmin Gene Mutations Associated with Myofibrillar Myopathies in Polish Families. *PLoS One* 9, e115470. doi:10.1371/journal.pone.0115470

Fidziańska, A., Kotowicz, J., Sadowska, M., Goudeau, B., Walczak, E., Vicart, P., et al. (2005). A Novel Desmin R355P Mutation Causes Cardiac and Skeletal Myopathy. *Neuromuscul. Disord.* 15, 525–531. doi:10.1016/j.nmd.2005.05.006

García-Pelagio, K. P., Bloch, R. J., Ortega, A., and González-Serratos, H. (2011). Biomechanics of the Sarcolemma and Costameres in Single Skeletal Muscle Fibers from normal and Dystrophin-Null Mice. *J. Muscle Res. Cel Motil.* 31, 323–336. doi:10.1007/s10974-011-9238-9

Gillies, A. R., and Lieber, R. L. (2011). Structure and Function of the Skeletal Muscle Extracellular Matrix. *Muscle Nerve* 44, 318–331. doi:10.1002/mus.22094

Goldfarb, L. G., Park, K.-Y., Cervenáková, L., Gorokhova, S., Lee, H.-S., Vasconcelos, O., et al. (1998). Missense Mutations in Desmin Associated with Familial Cardiac and Skeletal Myopathy. *Nat. Genet.* 19, 402–403. doi:10.1038/1300

Gulati, A. K., Zalewski, A. A., and Reddi, A. H. (1983). An Immunofluorescent Study of the Distribution of Fibronectin and Laminin during Limb Regeneration in the Adult Newt. *Develop. Biol.* 96, 355–365. doi:10.1016/0012-1606(83)90173-2

Henderson, M., De Waele, L., Hudson, J., Eagle, M., Sewry, C., Marsh, J., et al. (2013). Recessive Desmin-Null Muscular Dystrophy with central Nuclei and Mitochondrial Abnormalities. *Acta Neuropathol.* 125, 917–919. doi:10.1007/s00401-013-1113-x

Herrmann, H., Häner, M., Brettel, M., Müller, S. A., Goldie, K. N., Fedtke, B., et al. (1996). Structure and Assembly Properties of the Intermediate Filament Protein

Vimentin: The Role of its Head, Rod and Tail Domains. *J. Mol. Biol.* 264, 933–953. doi:10.1006/jmbi.1996.0688

Herrmann, H., Cabet, E., Chevalier, N. R., Moosmann, J., Schultheis, D., Haas, J., et al. (2020). Dual Functional States of R406W-Desmin Assembly Complexes Cause Cardiomyopathy with Severe Intercalated Disc Derangement in Humans and in Knock-In Mice. *Circulation* 142, 2155–2171. doi:10.1161/CIRCULATIONAHA.120.050218

Hol, E. M., and Capetanaki, Y. (2017). Type III Intermediate Filaments Desmin, Glial Fibrillary Acidic Protein (GFAP), Vimentin, and Peripherin. *Cold Spring Harb. Perspect. Biol.* 9, a021642. doi:10.1101/cshperspect.a021642

Hyder, C. L., Pallari, H.-M., Kochin, V., and Eriksson, J. E. (2008). Providing Cellular Signposts - Post-translational Modifications of Intermediate Filaments. *Nucl. Dyn. Cytoskelet. Signal.* 582, 2140–2148. doi:10.1016/j.febslet.2008.04.064

Ivaska, J., Pallari, H.-M., Nevo, J., and Eriksson, J. E. (2007). Novel Functions of Vimentin in Cell Adhesion, Migration, and Signaling. *Exp. Cel Res.* 313, 2050–2062. doi:10.1016/j.yexcr.2007.03.040

Joanne, P., Hovhannisyan, Y., Bencze, M., Daher, M.-T., Parlakian, A., Toutirais, G., et al. (2021). Absence of Desmin Results in Impaired Adaptive Response to Mechanical Overloading of Skeletal Muscle. *Front. Cel Dev. Biol.* 9, 662133. doi:10.3389/fcell.2021.662133

Kim, J., Jang, J., Yang, C., Kim, E. J., Jung, H., and Kim, C. (2016). Vimentin Filament Controls Integrin α5β1-mediated Cell Adhesion by Binding to Integrin through its Ser38 Residue. *FEBS Lett.* 590, 3517–3525. doi:10.1002/1873-3468.12430

Kural Mangit, E., Boustanabadimaralan Düz, N., and Dĩnçer, P. (2021). A Cytoplasmic Escapee: Desmin Is Going Nuclear. *Turk J. Biol.* 45, 711–719. doi:10.3906/biy-2107-54

Li, Z., Colucci-Guyon, E., Pinçon-Raymond, M., Mericskay, M., Pournin, S., Paulin, D., et al. (1996). Cardiovascular Lesions and Skeletal Myopathy in Mice Lacking Desmin. *Develop. Biol.* 175, 362–366. doi:10.1006/dbio.1996.0122

Li, Z., Mericskay, M., Agbulut, O., Butler-Browne, G., Carlsson, L., Thornell, L.-E., et al. (1997). Desmin Is Essential for the Tensile Strength and Integrity of Myofibrils but Not for Myogenic Commitment, Differentiation, and Fusion of Skeletal Muscle. *J. Cel Biol.* 139, 129–144. doi:10.1083/jcb.139.1.129

Lukjanenko, L., Jung, M. J., Hegde, N., Perruisseau-Carrier, C., Migliavacca, E., Rozo, M., et al. (2016). Loss of Fibronectin from the Aged Stem Cell Niche Affects the Regenerative Capacity of Skeletal Muscle in Mice. *Nat. Med.* 22, 897–905. doi:10.1038/nm.4126

Luo, B.-H., Carman, C. V., and Springer, T. A. (2007). Structural Basis of Integrin Regulation and Signaling. *Annu. Rev. Immunol.* 25, 619–647. doi:10.1146/annurev.immunol.25.022106.141618

Lynch, C. D., Lazar, A. M., Iskratsch, T., Zhang, X., and Sheetz, M. P. (2013). Endoplasmic Spreading Requires Coalescence of Vimentin Intermediate Filaments at Force-Bearing Adhesions. *MBoC* 24, 21–30. doi:10.1091/mbc.E12-05-0377

Maerkens, A., Kley, R. A., Olivé, M., Theis, V., van der Ven, P. F. M., Reimann, J., et al. (2013). Differential Proteomic Analysis of Abnormal Intramyoplasmic Aggregates in Desminopathy. *J. Proteomics* 90, 14–27. doi:10.1016/j.jprot.2013.04.026

Mavroidis, M., Panagopoulou, P., Kostavasili, I., Weisleder, N., and Capetanaki, Y. (2008). A Missense Mutation in Desmin Tail Domain Linked to Human Dilated Cardiomyopathy Promotes Cleavage of the Head Domain and Abolishes its Z-disc Localization. *FASEB J.* 22, 3318–3327. doi:10.1096/fj.07-088724

Mendez, M. G., Kojima, S. I., and Goldman, R. D. (2010). Vimentin Induces Changes in Cell Shape, Motility, and Adhesion during the Epithelial to Mesenchymal Transition. *FASEB J.* 24, 1838–1851. doi:10.1096/fj.09-151639

Menko, A. S., Bleaken, B. M., Libowitz, A. A., Zhang, L., Stepp, M. A., and Walker, J. L. (2014). A Central Role for Vimentin in Regulating Repair Function During Healing of the Lens Epithelium. *Mol. Biol. Cell* 25, 776–790. doi:10.1091/mbc.E12-12-0900

Modulevsky, D. J., Tremblay, D., Gullekson, C., Bukoresthliev, N. V., and Pelling, A. E. (2012). The Physical Interaction of Myoblasts with the Microenvironment during Remodeling of the Cytoarchitecture. *PLoS ONE* 7, e45329. doi:10.1371/journal.pone.0045329

Mogensen, M. M., Henderson, C. G., Mackie, J. B., Lane, E. B., Garrod, D. R., and Tucker, J. B. (1998). Keratin Filament Deployment and Cytoskeletal Networking in a Sensory Epithelium that Vibrates during Hearing. *Cel Motil. Cytoskeleton* 41, 138–153. doi:10.1002/(SICI)1097-0169(1998)41:2<138::AID-CM5>3.0.CO;2-A

Muriel, J. M., O'Neill, A., Kerr, J. P., Kleinhans-Welte, E., Lovering, R. M., and Bloch, R. J. (2020). Keratin 18 is an Integral Part of the Intermediate Filament Network in Murine Skeletal Muscle. *Am. J. Physiol. Cell Physiol.* 318, C215–C224. doi:10.1152/ajpcell.00279.2019

Ohanna, M., Sobering, A. K., Lapointe, T., Lorenzo, L., Praud, C., Petroulakis, E., et al. (2005). Atrophy of S6K1−/− Skeletal Muscle Cells Reveals Distinct mTOR Effectors for Cell Cycle and Size Control. *Nat. Cel Biol.* 7, 286–294. doi:10.1038/ncb1231

Omary, M. B., Ku, N.-O., Tao, G.-Z., Toivola, D. M., and Liao, J. (2006). 'Heads and Tails' of Intermediate Filament Phosphorylation: Multiple Sites and Functional Insights. *Trends Biochem. Sci.* 31, 383–394. doi:10.1016/j.tibs.2006.05.008

Osmani, N., and Labouesse, M. (2015). Remodeling of Keratin-Coupled Cell Adhesion Complexes. *Curr. Opin. Cel Biol.* 32, 30–38. doi:10.1016/j.ceb.2014.10.004

Pallari, H.-M., and Eriksson, J. E. (2007). Intermediate Filaments as Signaling Platforms. *Sci. STKE* 2006, pe53. doi:10.1126/stke.3662006pe53

Pardo, J. V., Siliciano, J. D., and Craig, S. W. (1983). A Vinculin-Containing Cortical Lattice in Skeletal Muscle: Transverse Lattice Elements ("costameres") Mark Sites of Attachment between Myofibrils and Sarcolemma. *Proc. Natl. Acad. Sci.* 80, 1008–1012. doi:10.1073/pnas.80.4.1008

Paulin, D., Hovhannisyan, Y., Kasakyan, S., Agbulut, O., Li, Z., and Xue, Z. (2020). Synemin-related Skeletal and Cardiac Myopathies: an Overview of Pathogenic Variants. *Am. J. Physiol. Cell Physiol.* 318, C709–C718. doi:10.1152/ajpcell.00485.2019

Pica, E. C., Kathirvel, P., Pramono, Z. A. D., Lai, P.-S., and Yee, W.-C. (2008). Characterization of a Novel S13F Desmin Mutation Associated with Desmin Myopathy and Heart Block in a Chinese Family. *Neuromuscul. Disord.* 18, 178–182. doi:10.1016/j.nmd.2007.09.011

Repesh, L. A., Fitzgerald, T. J., and Furcht, L. T. (1982). Changes in the Distribution of Fibronectin during Limb Regeneration in Newts Using Immunocytochemistry. *Differentiation* 22, 125–131. doi:10.1111/j.1432-0436.1982.tb01236.x

Rodríguez, M. A., Liu, J.-X., Parkkonen, K., Li, Z., and Pedrosa Domellöf, F. (2018). The Cytoskeleton in the Extraocular Muscles of Desmin Knockout Mice. *Invest. Ophthalmol. Vis. Sci.* 59, 4847–4855. doi:10.1167/iovs.18-24508

Rotty, J. D., and Coulombe, P. A. (2012). A Wound-Induced Keratin Inhibits Src Activity During Keratinocyte Migration and Tissue Repair. *J. Cell Biol.* 197, 381–389. doi:10.1083/jcb.201107078

Russell, M. A. (2020). Synemin Redefined: Multiple Binding Partners Results in Multifunctionality. *Front. Cel Dev. Biol.* 8, 159. doi:10.3389/fcell.2020.00159

Saga, S., Hamaguchi, M., Hoshino, M., and Kojima, K. (1985). Expression of Meta-Vinculin Associated with Differentiation of Chicken Embryonal Muscle Cells. *Exp. Cel Res.* 156, 45–56. doi:10.1016/0014-4827(85)90260-5

Seifert, G. J., Lawson, D., and Wiche, G. (1992). Immunolocalization of the Intermediate Filament-Associated Protein Plectin at Focal Contacts and Actin Stress Fibers. *Eur. J. Cel Biol.* 59, 138–147.

Seltmann, K., Cheng, F., Wiche, G., Eriksson, J. E., and Magin, T. M. (2015). Keratins Stabilize Hemidesmosomes through Regulation of β4-Integrin Turnover. *J. Invest. Dermatol.* 135, 1609–1620. doi:10.1038/jid.2015.46

Sharafi, B., and Blemker, S. S. (2011). A Mathematical Model of Force Transmission from Intrafascicularly Terminating Muscle Fibers. *J. Biomech.* 44, 2031–2039. doi:10.1016/j.jbiomech.2011.04.038

Siegel, A. L., Atchison, K., Fisher, K. E., Davis, G. E., and Cornelison, D. D. W. (2009). 3D Timelapse Analysis of Muscle Satellite Cell Motility. *Stem Cell Dayt. Ohio* 27, 2527–2538. doi:10.1002/stem.178

Sparrow, J. C., and Schöck, F. (2009). The Initial Steps of Myofibril Assembly: Integrins Pave the Way. *Nat. Rev. Mol. Cel Biol.* 10, 293–298. doi:10.1038/nrm2634

Strelkov, S. V., Herrmann, H., and Aebi, U. (2003). Molecular Architecture of Intermediate Filaments. *BioEssays* 25, 243–251. doi:10.1002/bies.10246

Sun, N., Critchley, D. R., Paulin, D., Li, Z., and Robson, R. M. (2008a). Human α-synemin Interacts Directly with Vinculin and Metavinculin. *Biochem. J.* 409, 657–667. doi:10.1042/BJ20071188

Sun, N., Critchley, D. R., Paulin, D., Li, Z., and Robson, R. M. (2008b). Identification of a Repeated Domain within Mammalian α-synemin that Interacts Directly with Talin. *Exp. Cel Res.* 314, 1839–1849. doi:10.1016/j.yexcr.2008.01.034

Taverna, D., Disatnik, M.-H., Rayburn, H., Bronson, R. T., Yang, J., Rando, T. A., et al. (1998). Dystrophic Muscle in Mice Chimeric for Expression of α5 Integrin. *J. Cel Biol.* 143, 849–859. doi:10.1083/jcb.143.3.849

Toivola, D. M., Tao, G.-Z., Habtezion, A., Liao, J., and Omary, M. B. (2005). Cellular Integrity Plus: Organelle-Related and Protein-Targeting Functions of Intermediate Filaments. *Trends Cel Biol.* 15, 608–617. doi:10.1016/j.tcb.2005.09.004

Troyanovsky, S. M., Eshkind, L. G., Troyanovsky, R. B., Leube, R. E., and Franke, W. W. (1993). Contributions of Cytoplasmic Domains of Desmosomal Cadherins to Desmosome Assembly and Intermediate Filament anchorage. *Cell* 72, 561–574. doi:10.1016/0092-8674(93)90075-2

Tsuruta, D., and Jones, J. C. R. (2003). The Vimentin Cytoskeleton Regulates Focal Contact Size and Adhesion of Endothelial Cells Subjected to Shear Stress. *J. Cel Sci.* 116, 4977–4984. doi:10.1242/jcs.00823

Wang, F., Chen, S., Liu, H. B., Parent, C. A., and Coulombe, P. A. (2018). Keratin 6 Regulates Collective Keratinocyte Migration by Altering Cell–Cell and Cell–Matrix Adhesion. *J. Cell Biol.* 217, 4314–4330. doi:10.1083/jcb.201712130

Webb, D. J., Parsons, J. T., and Horwitz, A. F. (2002). Adhesion Assembly, Disassembly and Turnover in Migrating Cells - over and over and over Again. *Nat. Cel Biol.* 4, E97–E100. doi:10.1038/ncb0402-e97

Wong, P., and Coulombe, P. A. (2003). Loss of Keratin 6 (K6) Proteins Reveals a Function for Intermediate Filaments During Wound Repair. *J. Cell Biol.* 163, 327–337. doi:10.1083/jcb.200305032

Yuanhua, L., Pudong, Q., Wei, Z., Yuan, W., Delin, L., Yan, Z., et al. (2019). TFAP2A Induced KRT16 as an Oncogene in Lung Adenocarcinoma via EMT. *Int. J. Biol. Sci.* 15, 1419–1428. doi:10.7150/ijbs.34076

Zhang, C., and Gao, Y. (2014). The Role of Transmembrane Proteins on Force Transmission in Skeletal Muscle. *J. Biomech.* 47, 3232–3236. doi:10.1016/j.jbiomech.2014.07.014

Conflict of Interest: The authors declare that the research was conducted in the absence of any commercial or financial relationships that could be construed as a potential conflict of interest.

Publisher's Note: All claims expressed in this article are solely those of the authors and do not necessarily represent those of their affiliated organizations or those of the publisher, the editors and the reviewers. Any product that may be evaluated in this article, or claim that may be made by its manufacturer, is not guaranteed or endorsed by the publisher.

frontiers in Cell and Developmental Biology

REVIEW
published: 11 March 2022
doi: 10.3389/fcell.2022.869069

Impact of Vimentin on Regulation of Cell Signaling and Matrix Remodeling

Zofia Ostrowska-Podhorodecka, Isabel Ding, Masoud Norouzi and Christopher A. McCulloch*

Faculty of Dentistry, University of Toronto, Toronto, ON, Canada

Vimentin expression contributes to cellular mechanoprotection and is a widely recognized marker of fibroblasts and of epithelial-mesenchymal transition. But it is not understood how vimentin affects signaling that controls cell migration and extracellular matrix (ECM) remodeling. Recent data indicate that vimentin controls collagen deposition and ECM structure by regulating contractile force application to the ECM and through post-transcriptional regulation of ECM related genes. Binding of cells to the ECM promotes the association of vimentin with cytoplasmic domains of adhesion receptors such as integrins. After initial adhesion, cell-generated, myosin-dependent forces and signals that impact vimentin structure can affect cell migration. Post-translational modifications of vimentin determine its adaptor functions, including binding to cell adhesion proteins like paxillin and talin. Accordingly, vimentin regulates the growth, maturation and adhesive strength of integrin-dependent adhesions, which enables cells to tune their attachment to collagen, regulate the formation of cell extensions and control cell migration through connective tissues. Thus, vimentin tunes signaling cascades that regulate cell migration and ECM remodeling. Here we consider how specific properties of vimentin serve to control cell attachment to the underlying ECM and to regulate mesenchymal cell migration and remodeling of the ECM by resident fibroblasts.

Keywords: EMT, vimentin, PTM, cell migration, cell adhesion

OPEN ACCESS

Edited by:
Dolores Pérez-Sala, Spanish National Research Council (CSIC), Spain

Reviewed by:
Ranu Surolia, University of Alabama at Birmingham, United States
Inmaculada Navarro-Lérida, Autonomous University of Madrid, Spain

****Correspondence:***
Zofia Ostrowska-Podhorodecka zofia.ostrowska.podhorodecka@utoronto.ca

Specialty section:
This article was submitted to Cell Growth and Division, a section of the journal Frontiers in Cell and Developmental Biology

Received: *03 February 2022*
Accepted: *25 February 2022*
Published: *11 March 2022*

Citation:
Ostrowska-Podhorodecka Z, Ding I, Norouzi M and McCulloch CA (2022) Impact of Vimentin on Regulation of Cell Signaling and Matrix Remodeling. Front. Cell Dev. Biol. 10:869069. doi: 10.3389/fcell.2022.869069

INTRODUCTION

Phenotypic regulation in many cell types is influenced by their interactions with the extracellular matrix (ECM), a major structural component of many organs and soft connective tissues that is comprised mainly of fibrillar collagens (Begum et al., 2017; Liu et al., 2018; Rada et al., 2018), glycoproteins such as fibronectin (Kendall and Feghali-Bostwick, 2014; Li C.-L. et al., 2017; Yu et al., 2018) and vitronectin (Braam et al., 2008; Hurt et al., 2010) and a broad repertoire of proteoglycans (Teng et al., 2012; Sun et al., 2017; Cao et al., 2018) and polysaccharides (An and Brodsky, 2016). In many organs the ECM is a highly dynamic structure and, in some tissues, ECM proteins like collagen undergo surprisingly rapid physiological turnover (Sodek, 1977). Remodeling involves deposition, degradation, and modifications of the ECM by resident cells and secreted enzymes (Kim et al., 2011; Lu et al., 2011; Lu et al., 2012; Lee et al., 2019; Nallanthighal et al., 2019). ECM remodeling plays a central role in tissue and organ health and is

Abbreviations: VIF, Vimentin intermediate filaments; EMT, epithelial-mesenchymal transition; ECM, extracellular matrix; PTM, post-translational modifications; FA, focal adhesion; ECV, extracellular vimentin.

intimately involved in the migration of cells that occurs in developmental processes, wound healing and cancer metastasis.

The physical reorganization of fibrillar proteins that accompanies the migration of fibroblasts through the ECM is a central feature of collagen remodeling (Feng et al., 2014), which is crucial for the maintenance of tissue health in many organs (Cox and Erler, 2011). After an injury or chronic infection, tissues often exhibit a short-term wound healing response that is intended to create a new and functionally appropriate ECM that then enables restoration of tissue structure (Walker et al., 2018). The mechanical properties of ECM, such as the stiffness of collagen fibrils or of the underlying substrate to which cells are attached, play crucial roles in processes such as epithelial-mesenchymal transition (EMT) and cell differentiation (Engler et al., 2006; Saha et al., 2008; Santiago et al., 2010). Epithelial-mesenchymal transition (EMT) is a potentially reversible process by which epithelial cells transdifferentiate into highly motile cells with mesenchymal cell phenotypes. During EMT, epithelial cells undergo modifications that affect the structure of intercellular junctions and of adhesion complexes with the ECM that affect ECM remodeling. Modifications associated with EMT also include the disaggregation of epithelial cells from one another and the underlying basement membrane. Subsequently, new transcriptional programs are activated that promote the acquisition of mesenchymal characteristics in affected cells (Thiery and Sleeman, 2006; Thiery et al., 2009; Nieto et al., 2016).

As described in the Human Protein Atlas database (Atlas, 2021), vimentin intermediate filaments (VIFs) are expressed in a wide variety of tissues including skin, kidney, and lung (Schaffeld et al., 2001; Mendez et al., 2010; Lowery et al., 2015; Uhlen et al., 2015). Vimentin is a 54 kDa, 466 amino acid Type III intermediate filament (UniProtKB-P08670). Vimentin exhibits a tripartite structure consisting of a central α-helical "rod" domain, flanked by intrinsically disordered amino-terminal "head" and carboxy-terminal "Tail" domains (Strelkov et al., 2001). In physiological conditions, vimentin spontaneously assembles into 10 nm diameter filaments (Herrmann and Aebi, 1998). Filament assembly is initiated from elementary, parallel coiled-coil α-helical dimeric building blocks, which self-associate in a half-staggered, anti-parallel manner to yield tetramers (Chernyatina et al., 2015). Subsequently, lateral association of 8 tetrameric subunits results in unit-length filaments, which longitudinally extend to form mature vimentin filaments (Herrmann and Aebi, 1998), which is considered in more detail in earlier reviews (Danielsson et al., 2018) (Ostrowska-Podhorodecka and McCulloch, 2021).

The recent uptick of interest in vimentin originates in part from the growing appreciation of its diverse roles in a broad range of cellular functions that affect tissue and organ structure. Notably, alterations of vimentin expression are linked to diseases including lung and liver fibrosis and several types of cancer (Li F. J. et al., 2017; Battaglia et al., 2018; Strouhalova et al., 2020), all of which involve cell migration and ECM remodeling. In addition to these discrete pathological conditions, vimentin expression is crucial for effective wound healing and tissue regeneration. Higher vimentin expression is associated with enhanced cell motility, adhesion to the ECM and collagen deposition (dos Santos et al., 2015; Cheng et al., 2016). Indeed, the importance of vimentin is now widely recognized in cellular functions ranging from motility to signal transduction (Mendez et al., 2010; Lowery et al., 2015). In contrast, the lack of vimentin in vimentin knockout mice resulted in the loss of cell morphology and reduced cell adhesion, as well as impairment in the directional migration of fibroblasts. In addition, at the tissue level, vimentin deficiency reduced the capacity for wound-healing (Blanchoin et al., 2014; Danielsson et al., 2018). For more detailed information on this topic, see reviews of vimentin functions in matrix adhesion (Danielsson et al., 2018; Ostrowska-Podhorodecka and McCulloch, 2021).

Expression of vimentin in epithelial cells during EMT is associated with the adoption of a more mesenchymal cell shape, increased focal adhesion formation and enhanced cell motility (Lepekhin et al., 2001; Mendez et al., 2010; Ostrowska-Podhorodecka et al., 2021). Conversely, diminished vimentin expression in mesenchymal cells is associated with reduced motility and the adoption of an epithelial cell like shape (Mendez et al., 2010; Ostrowska-Podhorodecka et al., 2021). While it has been suggested that vimentin expression affects ECM remodeling and cell migration through the ECM (Mendez et al., 2010; Nieto et al., 2016; Cheng and Eriksson, 2017; Patteson et al., 2019; Ding et al., 2020; Ostrowska-Podhorodecka et al., 2021), the definitive roles played by vimentin in regulating ECM structure (Menko et al., 2014; Walker et al., 2018), autophagy (Su et al., 2019), mRNA processing (Challa and Stefanovic, 2011) and transcriptional regulation (Deng et al., 2013) remain elusive. Through its integration of environmental signals, vimentin seems to adjust the dynamics and structures of the microtubule and actomyosin networks, which are crucial for generating the forces needed for cell migration (Battaglia et al., 2018). As the regulatory functions of vimentin in cell migration and ECM remodeling are not well-understood, we consider a potential role for vimentin in integrating signaling, matrix remodeling and migration.

CELLULAR LOCALIZATION OF VIMENTIN INTERMEDIATE FILAMENTS

For many years VIFs were considered as very stable cytoskeletal structures whose principal functions provided resistance to mechanical stress (Kim and Coulombe, 2007) and participation in mechanotransduction (Gregor et al., 2014). More recent evidence indicates that the vimentin network exhibits a broad array of properties that support essential cellular functions (Duarte et al., 2019; Patteson et al., 2019; Strouhalova et al., 2020). In this context, vimentin is localized to discrete cytoplasmic and membrane compartments (**Figure 1**) in mesenchymal cells (Mendez et al., 2010), fibroblasts (Mendez et al., 2010; Helfand et al., 2011; Ding et al., 2020), astrocytes (Lepekhin et al., 2001), epithelial cells (Vuoriluoto et al., 2011), cells in lymphoid tissues (Otsuki et al., 2011), glandular cells (Peuhu et al., 2017), and various cancer cell types (Vuoriluoto et al., 2011; Havel et al., 2015; Rawla et al., 2019; Kuppe et al.,

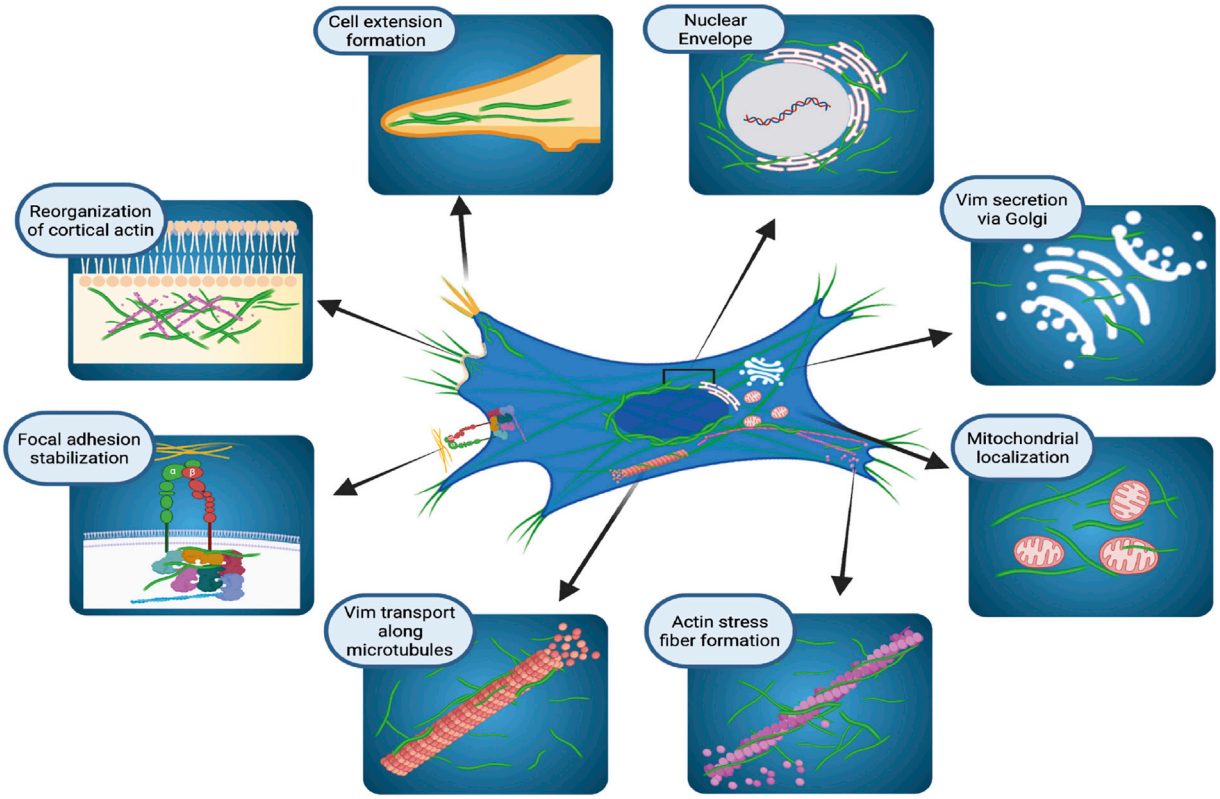

FIGURE 1 | Cellular localization and functions of vimentin intermediate filaments. Schematic illustration of how vimentin controls several, diverse cellular functions in organelle anchoring, cytoskeletal plasticity, focal adhesion regulation, and cell migration. Figure created with BioRender.com.

2021; Thalla et al., 2021). In the cell body, vimentin is predominantly perinuclear (Dupin et al., 2011) where it protects DNA from mechanical damage (Patteson et al., 2019), but vimentin also co-localizes with the endoplasmic reticulum (Lee et al., 2020) and contributes to the positioning of mitochondria and Golgi apparatus in the cytosol (Gao and Sztul, 2001; Lowery et al., 2015), indicating that vimentin may play a broader role in cell regulation than previously recognized.

The presence of VIFs in the cell periphery during mitosis is associated with the organization of cortical actin filament arrays, suggesting that vimentin filaments may help to strengthen the cortex during cell division (Duarte et al., 2019). Electron microscopy and live-cell imaging of cultured cells shows that vimentin filaments undergo continuous and relatively dynamic changes of assembly and localisation to produce a broad repertoire of VIF structures (Herrmann et al., 1996; Noding et al., 2014; Lowery et al., 2015; Strouhalova et al., 2020). These structures range from flexible, extended polymerized networks to non-filamentous structures that are observed in particles of various sizes (Chou et al., 1990; Robert et al., 2015; Premchandar et al., 2016). In cultured fibroblasts, VIFs are rather homogenously distributed throughout the cytoplasm. But fibroblasts exhibit a perinuclear location of VIF after treatment with agents that affect vimentin filament organization, such as withaferin A (Ding et al., 2020) or the p21 kinase inhibitor, IPA3 (Ostrowska-Podhorodecka et al., 2021). The dynamic assembly and disassembly of VIFs helps cells to adapt to heat-shock or oxidative stress (Perez-Sala et al., 2015; Robert et al., 2015; Duarte et al., 2019). The rapid and reversible remodeling of VIFs relies on the exchange of subunits and on post-translational modifications, which we consider later in this review.

ROLE OF VIMENTIN AS AN EFFECTOR AND A TARGET OF POST-TRANSCRIPTIONAL GENE REGULATION IN ECM BIOLOGY

Vimentin may regulate ECM remodeling through its impact on post-transcriptional gene regulation, which in turn impacts the synthesis and degradation of ECM proteins. One of the regulatory processes affected by vimentin is the spatial regulation of RNA expression and its interaction with ribonucleoprotein (RNP) complexes (**Figure 2**). Ultrastructural *in situ* hybridization experiments demonstrate that ~29% of total cytoplasmic poly (A) mRNAs co-localize with vimentin filaments (Bassell et al., 1994). More direct evidence of vimentin's involvement in post-transcriptional gene regulation arises from its interaction with type I collagen mRNAs (Zhang and Stefanovic, 2016). Specifically, RNA co-purification and *in situ* hybridization experiments demonstrate a tripartite assembly between the 5′

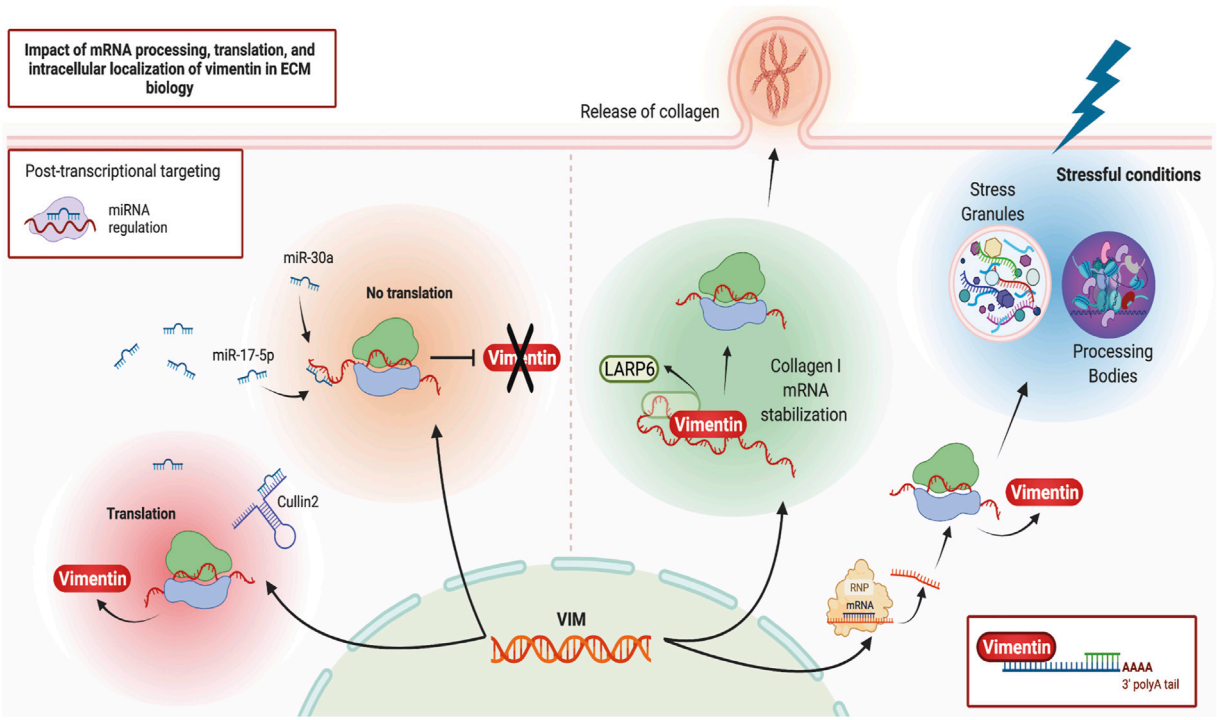

FIGURE 2 | Vimentin and post-transcriptional gene regulation. Schematic illustration of various post-transcriptional regulatory pathways that can impact or be impacted by vimentin. Figure created with BioRender.com.

untranslated region stem-loop (5′ SL) domain of collagen mRNAs, La ribonucleoprotein domain family member 6 (LARP6) protein, and vimentin filaments (Cai et al., 2010; Challa and Stefanovic, 2011). In this instance, vimentin regulates collagen synthesis by sequestering LARP6-bound collagen mRNAs. During wound healing or in fibrotic lesions, when demand for type I collagen is increased (Cheng and Eriksson, 2017), these mRNAs are made available for translation (Challa and Stefanovic, 2011). In addition to collagen mRNA, vimentin can specifically bind and post-transcriptionally regulate several other genes, including binding to the 5′ UTR and repression of the mu opioid receptor mRNA in Mouse neuroblastoma cell lines (Song et al., 2013), binding to the 3′ UTR and stabilisation of the alkaline phosphatase mRNA in human primary osteoblasts (Schmidt et al., 2015), and binding to the 3′ UTR and stabilisation of the tissue factor (TF) mRNA in human breast cancer cells through blocking miR-dependent negative regulation of TF mRNA (Francart et al., 2020). Currently, collagen is the only ECM component whose mRNA is post-transcriptionally regulated by vimentin.

More recently, proximity-based assays have shed light on vimentin's involvement in cellular differentiation, homeostasis, and stress response through its association with RNA-binding proteins, misfolded aggregates, Stress Granules and Processing Bodies (Lin et al., 2016; Pattabiraman et al., 2020). These processes are of particular importance for cells subjected to repeated mechanical or inflammatory stressors. Stress Granules and Processing Bodies are cytoplasmic compartments comprised of translationally repressed mRNAs, post-transcriptional regulatory factors, and other RNA binding proteins. These membrane-less organelles form part of the cellular response to a broad range of stressful conditions such as starvation and protein misfolding. For example, these responses prioritize the translation of stress response mRNAs and targeting the mRNAs codifying misfolded proteins for degradation (Luo et al., 2018; Marcelo et al., 2021). Accordingly, during differentiation and under stressful conditions, vimentin protects cells and their progeny by spatially segregating misfolded proteins, Stress Granules and other cytoplasmic RNP complexes. Vimentin directs their asymmetric partitioning during mitosis so that undesirable metabolites accumulate in one daughter cell while the other daughter cell remains healthy (Ogrodnik et al., 2014; Pattabiraman et al., 2020). The precise mechanisms and extent of vimentin's involvement in cellular differentiation, stress response and the resultant modifications of ECM remodeling through post-transcriptional gene regulation are not understood in depth but almost certainly will provide useful avenues for future research in IF biology.

Vimentin is one of the main mediators of EMT and metastasis in a variety of cancers (Satelli and Li, 2011; Strouhalova et al., 2020) and is itself a target of post-transcriptional gene regulation. One well-studied pathway that affects vimentin expression at the transcript level is through MicroRNAs (miRNAs) (Guo et al., 2014), which are ~22 nucleotide-long non-coding RNAs that bind to the 3′ untranslated region (UTR) of target mRNAs and

mark them for translational repression (Bartel, 2004). For instance, through direct interaction with the 3' UTR of vimentin mRNA and its subsequent downregulation, miR-30a supresses the invasive phenotypes of breast cancer cell lines (Cheng et al., 2012) while miR-17-5p inhibits the metastasis of colorectal cancer in liver tissues (Kim et al., 2020). Conversely, in an alternative mechanism, a non-coding RNA "sponge" known as Cullin2 circular RNA (or circ-10720) regulates vimentin expression by sequestering vimentin-targeting miRNAs, thus promoting EMT (Meng et al., 2018). Therefore, vimentin mRNA is a target of post-transcriptional regulatory events that impact the abundance of vimentin protein. Vimentin protein also contributes to post-transcriptional regulation of other mRNAs, especially during cell differentiation and environmental stress. Obtaining a more detailed understanding of these post-transcriptional regulatory networks could impact future translational research as these networks could provide potential targets for drug development.

VISCOELASTIC PROPERTIES OF VIMENTIN ENHANCE CELL RESISTANCE TO DEFORMATION

The migration of cells through soft connective tissues depends in part on their ability to remodel the ECM through synthesis and degradation. Migration in turn is reliant on the ability of cells to attach to ECM proteins and to navigate through pores in the ECM, which, depending on their size, may require cell deformation. The deformability of a cell and its ability to return to its original shape are affected by the viscoelastic properties of cells and their constituents (Moeendarbary et al., 2013; van Bodegraven and Etienne-Manneville, 2021). VIFs exhibit distinct viscoelastic properties that are not typically exhibited by other filamentous biopolymers such as actin filaments (Shah et al., 1998). This unique trait confers distinct rheological properties upon vimentin filaments. As a result, vimentin not only enhances cell integrity after exposure to shear force, but also provides flexibility in cells recovering from membrane deformation. The fine tuning of membrane stiffness by vimentin may contribute to a wide array of biological functions including cell migration, division, cell adhesion to substrates, autophagy, and signal transduction (Wang and Stamenovic, 2002; Vakhrusheva et al., 2019).

Cell migration through ECMs like collagen networks often provokes nuclear rupture, which is related to constriction and deformation of the nuclear membrane as cells traverse pores in the ECM. VIFs form intricate networks such as the nuclear cage that extends from the perinuclear region to the sub-cortex. In these networks, vimentin filaments function as elastic springs, dissipating tensile forces when migrating cells squeeze through constricting pores. These properties of vimentin can prevent extensive fluctuations of nuclear shape (Block et al., 2018). In addition, vimentin may interact with nucleases to buffer DNA damage (Irianto et al., 2016). In view of these findings, vimentin may play a crucial role in maintaining the precision of signaling by safeguarding DNA integrity, which is observed in cells subjected to migration-induced nuclear deformation (Patteson et al., 2019). Taken together, VIF expression contributes to cell viability by limiting organellar deformation during mechanical stress and by facilitating the recovery of cell and organellar shape.

POST-TRANSLATIONAL MODIFICATIONS OF VIMENTIN AFFECT MIGRATION AND THE ECM

Post-translational modifications (PTMs) are implicated in the spatiotemporal regulation of vimentin expression and organization of the VIF network, which consequently impacts the stability of the underlying cytoskeleton and remodelling of the ECM (Kalyanasundaram et al., 2021). Currently it is not straightforward to dissect the repertoire of signaling pathways associated with each vimentin PTM because of the sheer redundancy and complexity of the system and its multiple components (**Figure 3**). Moreover, modifications to single amino acids in vimentin may yield opposite downstream effects compared with modifications to multiple residues because of altered binding of interacting proteins and the resultant generation of downstream signals. One of the most carefully studied PTMs of vimentin is phosphorylation, which can promote VIF disassembly into squiggles, as seen in migrating cells (Yang et al., 2019). Phosphorylation is one of the cardinal features of signaling processes that are contemporaneously stimulated by other PTMs (Snider and Omary, 2014). The phosphorylation and dephosphorylation of vimentin have been reviewed previously. Shi et al., 2016 provide a comprehensive analysis of the effect of vimentin phosphorylation on cell motility. Accordingly, we focus here on separate vimentin PTMs that are associated with cell migration and/or ECM remodeling.

Proteolysis

Vimentin, like other intracellular proteins, is prone to caspase-mediated proteolytic cleavage. Phosphorylation protects vimentin from caspase-mediated proteolysis (Tripathi and Kulkarni, 2021), which occurs at vimentin D85 (via caspase 3 and caspase 7) and D259 (via caspase 6) to generate pro-apoptotic N-terminal fragments (Byun et al., 2001). AKT1 activation induces migration of sarcoma cells through an interaction with the vimentin head region, resulting in S39 phosphorylation and protection from caspase-induced proteolysis of vimentin (Zhu et al., 2011), thereby providing an example of the central position of vimentin in signaling systems that affect cell migration.

Ubiquitination

Proteasome-dependent degradation of vimentin by ubiquitination promotes the collapse of vimentin network architecture, triggering major cytoskeletal rearrangements. Specific ubiquitination sites are not well studied and recorded. Vimentin can be ubiquitinated at K97, K120, K129, K139, K143, K168, K188, K223, K236, K282, K294, K313, K334, K373, K439, and K445 (Database, 2022). Substrate proteins are linked to ubiquitin *via* distinct ubiquitin lysine residues (K6, K11, K27,

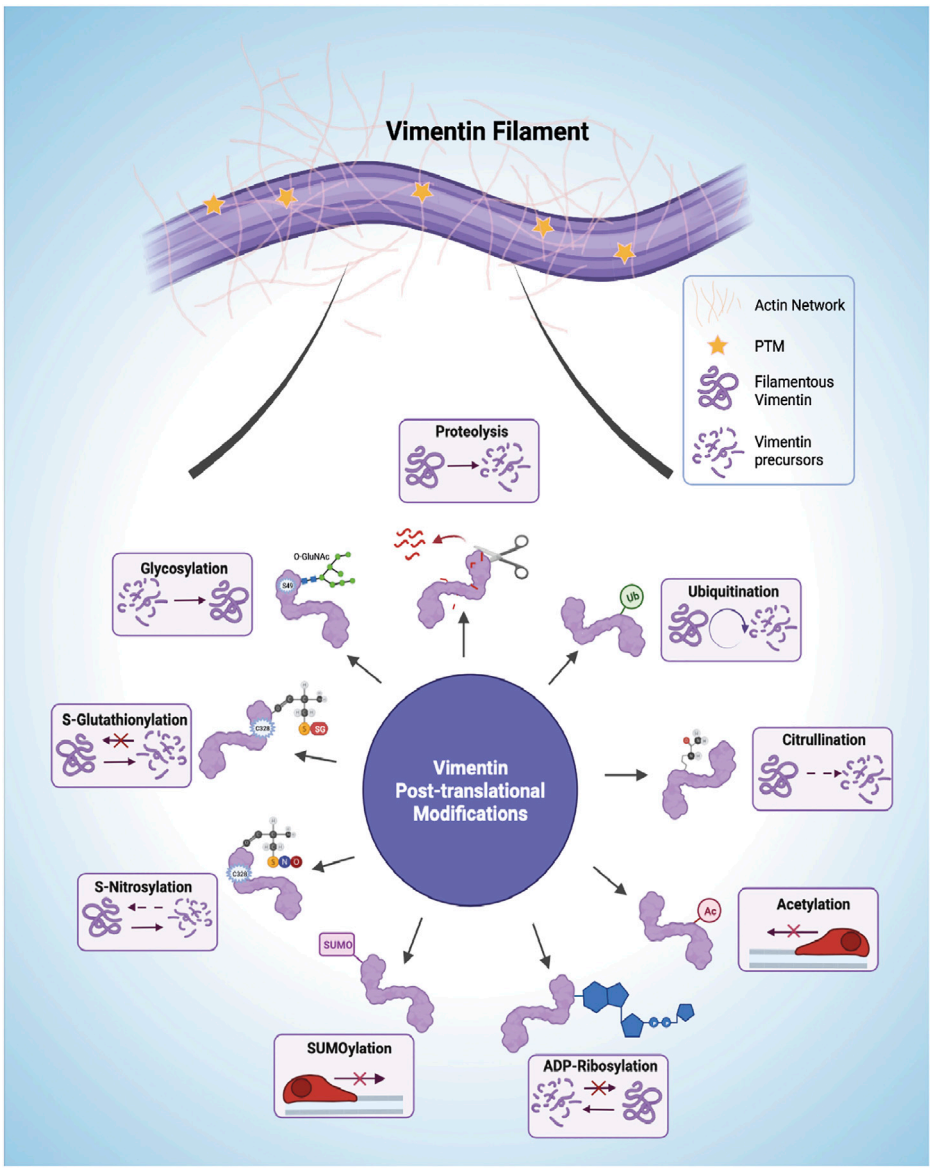

FIGURE 3 | Post-translational modifications (PTMs) of vimentin intermediate filaments (VIFs). VIFs undergo multiple PTMs, including proteolysis, ubiquitination, citrullination, acetylation, ADP-Ribosylation, SUMOylation (SUMO), S-Nitrosylation, S-Glutathionylation, and glycosylation. The horizontal arrows presented in the acetylation and SUMOylation panel shows decreased cell mobility. Figure created with BioRender.com.

K29, K33, K48, and K63) (Technology, 2022). Beclin 1, a critical regulator of autophagy, increases cell migration by interacting with vimentin to affect its K48-linked ubiquitination. The K48-linked polyubiquitin chains mainly target proteins for proteasomal degradation (Manohar et al., 2019). Beclin 1 also interacts with ubiquitin-specific peptidase 14, a key de-ubiquitinase of vimentin (Cheng et al., 2019). Thus, autophagy processes mediated through ubiquitination, which impact vimentin filament integrity, affecting cell migration. Moreover, vimentin ubiquitination is balanced by deubiquitination in selected systems. For instance, in human gastric cancer cell lines, the deubiquitinating enzyme USP14 directly interacts with vimentin and stabilizes it through deubiquitination (Zhu et al., 2017). This report also shows that miR320, as a tumor suppressor, is upstream of U14 and vimentin. It downregulates vimentin directly by targeting its 3′UTR, or indirectly by inhibiting the USP14 deubiquitination pathway (Zhu et al., 2017).

Citrullination

The search for causative mechanisms in rheumatic diseases and fibrosis, which involves extensive and often dysregulated ECM remodeling, has generated considerable interest in citrullinated vimentin, which involves the conversion of arginine residues to citrulline by the enzyme, peptidyl arginine deiminase (PAD) (Pruitt et al., 2014). Vimentin is a substrate for PAD2 that citrullinates residues in the non-α-helical head domain, which

contains about 9% arginine residues (Inagaki et al., 1989; Hsu et al., 2014). A vimentin peptide with citrullinated R176, which is found in coil 1B of vimentin, was identified in a vimentin pool secreted from lung macrophages and characterized by tandem MS2 (Li et al., 2021). Vimentin can also be citrullinated at several arginine residues in the tail domain. For example, R440 and R450 are citrullinated in reactive astrocytes in brain tissues of scrapie-infected mice (Jang et al., 2020). Citrullination impairs vimentin filament assembly, which enhances the formation of soluble precursors that are transported extracellularly (Inagaki et al., 1989) and that subsequently elicit autoimmune responses in joints affected by rheumatoid arthritis (Musaelyan et al., 2018) and in liver fibrosis (Vassiliadis et al., 2012). Citrullinated vimentin is increased after cell injury and is strongly expressed in the leading edge of repair-modulating leader cells, which stimulates their migration and differentiation into myofibroblasts (Walker et al., 2018). These leader cells display invasive potential that facilitates three-dimensional migration (Bleaken et al., 2016) and contribute to alterations of ECM structure.

Acetylation

The acetylation of vimentin and other EMT-related proteins affects the migratory capacity and the metastatic properties of various types of cancer cells (Boggs et al., 2015). Acetylation mainly targets vimentin at lysine residues, including K294, K313, K334, K373, and K439 (Yang et al., 2019). Hyperacetylation is generally associated with decreased cell motility through enhancement of vimentin filament stability and the formation of EMT-related protein complexes (Yang et al., 2019). In contrast, deacetylation of K120 of vimentin reduces metastasis in hepatocellular carcinoma, suggesting that acetyl-modified K120 regulates cell migration, possibly through upregulation of Snail and downregulation of E-cadherin, processes that ultimately enhance EMT (Guo et al., 2018).

ADP-Ribosylation

ADP-ribosylation is exhibited by certain pathogenic bacterial species and involves the attachment of ADP-ribose to host proteins through the formation of an O-glycosidic bond by pathogen-derived enzymes (Palazzo et al., 2018). Vimentin in mammalian cells is a target of *Streptococcus pyogenes* (Icenogle et al., 2012), which involves the secretion of the exotoxin, ADP-ribosyltransferase and is followed by sharp reductions of host cell migration, alterations of ECM structure and increased spreading of the pathogen (Coye and Collins, 2004).

SUMOylation

The conjugation of small, ubiquitin-like modifier (SUMO) protein to lysine residues of acceptor proteins like vimentin can impact cell migration through poorly defined mechanisms (Wang et al., 2010). PIAS1 mediates SUMOylation of vimentin (K439, K445) in the C-terminus, which disrupts filament disassembly (Li et al., 2020). This modification increases vimentin solubility by inducing hyperphosphorylation of the vimentin N-terminus and retards cell migration, suggesting that vimentin filament assembly is required for efficient cell migration.

S-Nitrosylation

Reactive nitric oxide transfers nitrosyl moieties from donor to acceptor proteins, a process that involves nitric oxide synthase and modifies C328 of vimentin in response to mechanotransduction through the Akt pathway (Huang et al., 2009) and in stress sensing (Perez-Sala et al., 2015). The presence of thiol modifications seems to retard the longitudinal assembly of vimentin filaments without inhibiting the formation of more mature filaments (Kaus-Drobek et al., 2020) and leads to altered ECM remodeling. As altered network rearrangements, filament stabilization, and bundling are linked to cysteine modifications of vimentin structure (Viedma-Poyatos et al., 2020), it will be important to define how these modifications contribute to altered cell migration (Kaschula et al., 2019) and potentially, ECM remodeling.

S-Glutathionylation

Modifications of vimentin C328 protect against electrophilic and oxidative stress by preserving the flexibility of VIFs (Perez-Sala et al., 2015). But unlike S-nitrosylation, S-glutathiolylation completely blocks the maturation of unit length filaments to mature filaments (Kaus-Drobek et al., 2020), indicating that this process is an efficient molecular switch that contributes to the assembly of the vimentin network, thereby affecting cell-mediated remodeling of the ECM.

Glycosylation

This vimentin PTM is mediated by the addition of O-linked β-N-acetylglucosamine (O-GlcNAc) on serine and threonine residues mediated by O-GlcNAc transferase and O-GlcNAcase (Hanover et al., 2010; Hart et al., 2011; Hart, 2014). Glycosylation of vimentin is restricted to the head domain of mature filaments (i.e., not ULFs) at residues T33, S34, S39, and S49, which impacts the formation of homo-oligomeric complexes between adjacent filaments (Tarbet et al., 2018). In particular, glycosylation of S34 and S39 promotes the assembly of VIFs while S49 eliminates crosslinking of adjacent filaments; these processes contribute to the alterations of normal filament morphology. In mammalian cells, site-specific glycosylation of vimentin is required for the cytoskeletal modifications involved in cell migration (Tarbet et al., 2018).

ROLE OF VIMENTIN IN TRACTIONAL FORCE GENERATION AND ECM CONTRACTION

As described in the discussion of PTMs above, some of the mechanisms by which vimentin regulate cell migration through ECM are now being defined. As vimentin interacts with actin filaments and microtubules to affect their structure and function (Mendez et al., 2010; Hookway et al., 2015), these interactions are also likely to regulate cell motility and the

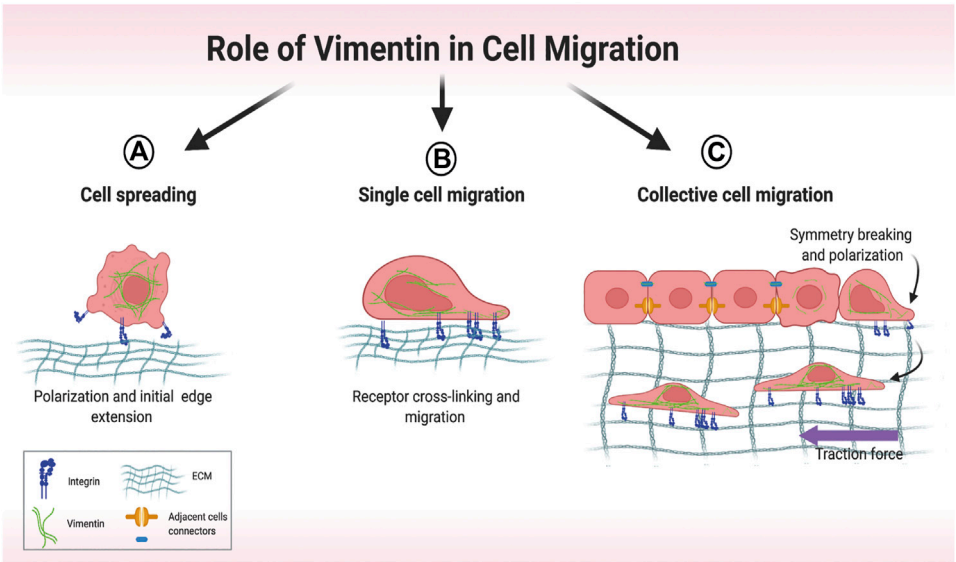

FIGURE 4 | Overview of different modes of cell migration. **(A)** Early stages of cell spreading. Cell attachment to the extracellular matrix (ECM) involves initial cell polarization and edge extension. **(B)** Single-cell migration relies on vimentin-dependent cross-linking of collagen receptors. **(C)** In collective migration, cells are tightly connected, which restricts migration. Symmetry-breaking events lead to cell polarization and directed migration. Motile cells at the front exert attractive forces on their neighbors, which then coordinate their movement. Created with BioRender.com.

ability of migrating cells to remodel the ECM (Battaglia et al., 2018). Many types of cell migration rely on the formation and extension of relatively short (< 2 μm) membrane protrusions like filopodia, which then coalesce and contribute to the generation of lamellipodia and invadopodia (Lorenz et al., 2004; Yamaguchi et al., 2005; Baldassarre et al., 2006; Gardel et al., 2010). These protrusive regions of the cell are filled with highly polarized arrays of actin filaments situated in the cortex that enable the formation of longer (>10 μm) cell extensions. Cortical actin filaments are mechanically integrated with collagen fibrils by integrin receptors during early phases of cell migration and in collagen contraction (Grinnell et al., 2006; Ostrowska-Podhorodecka et al., 2021). In these processes, vimentin facilitates and supports cell extension formation through direct associations with actin filaments (Esue et al., 2006; Battaglia et al., 2018) or indirectly through interactions with proteins such as CARMIL2 (Lanier et al., 2015; Battaglia et al., 2018).

Vimentin is essential for the elongation of invadopodia (Yoneyama et al., 2014), and promotes lamellipodia growth and the formation and stabilization of long cytoplasmic extensions (Ding et al., 2020; Ostrowska-Podhorodecka et al., 2021). Moreover, vimentin colocalizes with non-muscle myosin II (Menko et al., 2014) and regulates the contractility of actomyosin bundles through the guanine exchange factor H1 and RhoA, which affect cell migration (Jiu et al., 2017) and tractional remodeling of the ECM. In fibroblasts, mechanosensitive actin stress fibers (Skau et al., 2018) along with vimentin filaments insert into ECM adhesions and regulate the mechanical integrity of cells and tissues (Costigliola et al., 2017).

IMPACT OF VIMENTIN ON SINGLE CELL AND COLLECTIVE CELL MIGRATION

Arising from its involvement in several discrete cellular processes, VIF networks orchestrate cell spreading (**Figure 4A**) (Ostrowska-Podhorodecka and McCulloch, 2021), single cell migration (**Figure 4B**) (Patteson et al., 2019) and collective migration (**Figure 4C**) (De Pascalis et al., 2018). In cell spreading, the expansion of cell area on an unoccupied surface initiates adhesive interactions that enable cells to migrate (Janmey et al., 2021), which requires the formation of cell protrusions stabilized by VIFs (Ostrowska-Podhorodecka et al., 2021). Cell migration is strongly influenced by the nature of the local microenvironment. In two-dimensional single cell migration, cells spread within a single plane, which is guided by vimentin filaments (Ding et al., 2020). Vimentin mediates the transition of mesenchymal leader cells to a myofibroblast phenotype in the single cell migration of EMT (Walker et al., 2018). VIFs are also prominent elements of reparative cells at the wound edge and are associated with accelerated wound closure (Helfand et al., 2011; Menko et al., 2014).

At higher resolution, long (>4 μm) vimentin filaments serve as a load-bearing scaffolds to distribute traction stress during single cell migration (Costigliola et al., 2017). As wound closure involves the generation of contractile forces that can affect the structure of actin cytoskeletons, the vimentin network serves to diminish cell deformation (Janmey et al., 1991) and preserve cell integrity. Reduced vimentin expression in human mesenchymal stem cells is associated with increased deformation of the cell body after stretching (Sharma et al., 2018). Overexpression of vimentin in ameboid cancer cells contributes to cell resilience by limiting

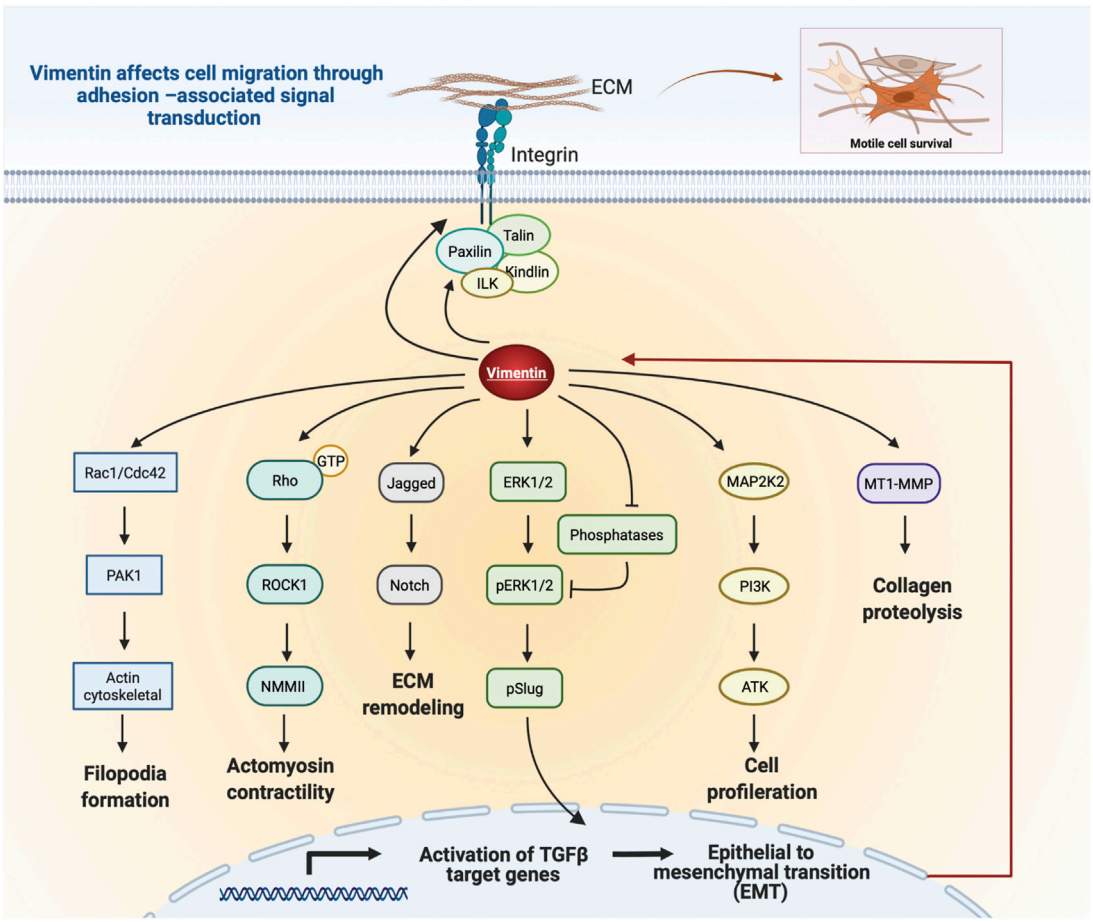

FIGURE 5 | Schematic illustration of vimentin-dependent regulation of migratory signaling transduction. Vimentin coordinates filopodia formation by controlling actin filaments assembly via Rac1/Cdc42 and PAK1 pathways. Vimentin-dependent Rho/ROCK1 signalling transduction controls cell contractility and migration. Vimentin impacts Notch signaling by binding to Jagged1. Regulation of Slug phosphorylation and activity by Vim-ERK cooperation. Vimentin protects ERK from dephosphorylation and thus supports its activity and Slug phosphorylation. Vimentin coordinates cell proliferation by downregulation of the PI3K/AKT signalling cascade. Vimentin induces ECM remodeling by MT1-MMP-dependent collagen proteolysis. Vimentin filaments mediate integrin mechanotransduction and control the assembly of focal adhesions. Figure was created with BioRender.com.

deformations in response to fast contractions (Lavenus et al., 2020), indicating that cell type-specific expression levels of vimentin endow cells with a broad range of mechanical properties.

Collective cell migration is promoted by the elevation of traction forces in the migrating cell monolayer and by the preservation of intercellular contacts (**Figure 4C**) (De Pascalis et al., 2018), which also serve to coordinate cell movement through dense connective tissue (Messica et al., 2017). In smooth muscle cells, VIFs are involved in the formation of intercellular junctions by associating with linker proteins such as plakoglobin and desmoplakin, which in turn connect with the cytoplasmic tails of cadherins (Delva et al., 2009; Tang et al., 2019). At the same time vimentin associates with actin filaments to facilitate intracellular and intercellular mechanical force transmission, which is required for cell motility (Tang, 2008).

Vimentin promotes collective cell migration by restricting actin flow, aligning tractional stress (Jiu et al., 2015; Costigliola et al., 2017; Battaglia et al., 2018) and supporting lateral cell–cell contacts (Mayor and Etienne-Manneville, 2016; Battaglia et al., 2018). In the collective cell migration that is seen in certain wound healing sites, reduced vimentin expression (along with nestin) diminishes the abundance of actin stress fibers parallel to the wound and promotes stress fiber formation perpendicular to the wound; these changes impact retrograde actin flow and the ability of cells to translocate (De Pascalis et al., 2018). In epithelial cells that express vimentin, VIFs are a component of junctional complexes that couple VE-cadherin to actin filaments, the IF cytoskeleton (Kowalczyk et al., 1998) and to FAs (Tsuruta and Jones, 2003; Kreis et al., 2005; Terriac et al., 2017), where VIFs bind to integrin-enriched matrix adhesions (Ivaska et al., 2007).

In highly motile epithelial cells, VIFs often co-distribute with keratin, the IF type first expressed in embryogenesis (Franz et al., 1983). In collective cell migration, co-expressed keratin and vimentin filaments exhibit spatially-distinct arrays (Osborn et al., 1980), which are necessary for preserving cytoplasmic

viscoelasticity and for coupling through integrins to the ECM and to neighboring cells (Bilandzic et al., 2019; Yoon and Leube, 2019).

IMPACT OF VIMENTIN ON SIGNALING PATHWAYS THAT AFFECT CELL MIGRATION AND ECM

Vimentin expression accelerates cell migration through paxillin-dependent regulation of Cdc42 activation, which leads to PAK1-dependent vimentin phosphorylation and filament assembly (Ostrowska-Podhorodecka et al., 2021). Thus, vimentin can regulate cell migration through its physical properties and by activating downstream signaling pathways that regulate cell movement (**Figure 5**). Further, vimentin affects Notch signaling in response to hemodynamic stress in the arterial wall. As a result of increased shear stress, phosphorylation of vimentin S38 initiates interactions between vimentin and Jagged1, which strengthens the Notch activation potential and adversely affects arterial wall remodeling and the ECM (van Engeland et al., 2019). Moreover, loss of vimentin in hepatic stellate cells decreases the phosphorylation of extracellular-signal regulated kinase (ERK) and AKT signaling, indicating a role for vimentin in controlling migration of hepatic stellate cells via the ERK/AKT and Rho pathways (Wang et al., 2019). Further, vimentin plays a role in wound healing through its regulation of TGF-β1 and Slug signalling, which are of central importance for ECM synthesis and remodeling and which manifest as the effect of vimentin depletion on suppression of the TGF-Slug–EMT pathway in fibroblasts (Cheng et al., 2016; Cheng and Eriksson, 2017). Taken together, these studies suggest an unexpected signaling role for vimentin in ECM structure and cell migration.

ROLE OF VIMENTIN IN REGULATING INTEGRIN-DEPENDENT CELL MIGRATION

Cells organize their migratory activities partly through tightly controlled protein-protein interactions in cell adhesions to the ECM. Integrins are transmembrane receptors expressed by many cells and are obligate heterodimers comprised of α and β subunits. The β subunit contains a large extracellular domain, a transmembrane domain and a cytoplasmic domain, while the α subunit forms a similar structure, but contains different motifs within its extracellular domain (Takada et al., 2007). The interaction of different α and β extracellular domains and their ability to bind to specific sequences, contribute to the ligand specificity exhibited by integrins. Intracellular signals that affect the cytoplasmic face of α and β subunits promotes allosteric modifications of integrins that affect their binding to extracellular ECM ligands. In this context, vimentin spatially localises to cell-matrix adhesions in various cell types (Danielsson et al., 2018) where vimentin filaments directly interact with β1 integrin (Kreis et al., 2005) and β3 integrin tails (Vohnoutka et al., 2019). Vimentin thus plays an essential role in the assembly and function of FA complexes.

Vimentin incorporates into nascent focal complexes and mature adhesions in a structure-dependent manner. While small vimentin oligomers (e.g., unit length filaments) are abundant in nascent adhesions, mature adhesions exhibit fully organized vimentin filaments (Terriac et al., 2017). In fibroblasts, vimentin deletion results in the limitation of the size of β1 integrin-rich focal adhesion through the inhibition of paxillin enrichment in adhesion sites (Terriac et al., 2017; Ostrowska-Podhorodecka et al., 2021). Further, vimentin is required for β1 integrin trafficking to the leading edge of migrating prostate cancer cells (Hafeez et al., 2011). Through its interactions with focal adhesion proteins like talin, the cytoplasmic domain of the β integrin subunit can interact with the actomyosin contractile machinery (Calderwood et al., 2013; Zacharchenko et al., 2016; Wang et al., 2019). In this context, vimentin plays an important role in the turnover of FAs and in the formation and release of integrin endocytic vesicles. Further, vimentin may regulate collagen remodeling through a functional link between β1 integrin and the membrane-bound collagenase, MT1-MMP (Galvez et al., 2002; Kwak et al., 2012). Vimentin complexes with the cytoplasmic tail of MT1-MMP and is necessary for MT1-MMP translocation to the plasma membrane (Kwak et al., 2012). Thus, vimentin influences the subcellular localization and activity of MT1-MMP, which through its interactions with the β1 and αvβ3 integrins, facilitates collective cell migration through collagen matrices (Galvez et al., 2002).

As vimentin can also be detected on the surface of cells (extracellular vimentin-ECV) and in the ECM after its release from activated macrophages (Mor-Vaknin et al., 2003; Frescas et al., 2017), there has been increasing interest in ECV and its potential effects on cell migration, particularly through modifications of the interactions of cell with the ECM through integrins. While ECV enhances axonal growth in injured mouse spinal cord (Shigyo and Tohda, 2016), the impact of ECV on cell motility and the ECM is not defined. Recent data indicate that ECV facilitates adherence of vimentin-negative MCF-7 cells to their underlying substrate. Further, gap closure and Transwell migration assays show that the migration rates of MCF-7 and MCF-10a cells are increased after treatment with ECV (100 ng/ml) (Thalla et al., 2021). The very limited data on the impact of ECV on cell migration and ECM suggest productive avenues for future research.

CONCLUSION AND FUTURE PERSPECTIVES: A ROLE FOR VIMENTIN AS A REGULATOR OF CELL-MATRIX ADHESIONS AND MATRIX REMODELING

In the context of ECM remodeling and cell migration, we considered how vimentin helps cells to sense, integrate, and respond to microenvironmental information. Vimentin can directly interact with focal adhesions and regulate cellular

processes and discrete signaling pathways. These events in turn affect cell migration and ECM remodeling by spatially and temporally integrating arrays of external and internal signals. Cell-specific levels of vimentin expression, PTMs, and direct and indirect interactions with other cytoskeletal components, control the mechanical properties of cells during migration and ECM remodeling. It appears that the extraordinarily broad array of PTMs of vimentin and its structure in response to extracellular and intracellular mechanical signals are crucial for cell and tissue integrity (Costigliola et al., 2017; Messica et al., 2017; van Bodegraven and Etienne-Manneville, 2021). Expression of VIF may thus control the mechanical properties of the cells and modify their ability to remodel collagen by its incorporation as an adaptor protein in the β1 integrin adhesive machinery (Terriac et al., 2017; Ostrowska-Podhorodecka et al., 2021). Further studies on vimentin's role in regulating cell signaling and matrix remodeling could advance our understanding of the pathology of vimentin-dependent changes in ECM remodeling, which contribute to the fibrosis associated with chronic inflammation. Further, a deeper knowledge of vimentin-dependent signaling systems in wound healing and tissue regeneration could provide new avenues for identifying drug targets for fibrosis and wound care.

AUTHOR CONTRIBUTIONS

All authors contributed to the acquisition of information, to the writing and the revising of the text, and to the content and design of figures; CM provided supervision and funding.

FUNDING

This work was Supported by a Canadian Institutes of Health Research (CIHR) grant (MOP 503020) and by a Canada Research Chair Tier 1 (CM). Figures were created with BioRender.com.

REFERENCES

An, B., and Brodsky, B. (2016). Collagen Binding to OSCAR: the Odd Couple. *Blood* 127, 521–522. doi:10.1182/blood-2015-12-682476

Atlas, T. H. P. (2021). Tissue Expressions of VIM [Online]. Available: https://www.proteinatlas.org/ENSG00000026025-VIM/tissue.

Baldassarre, M., Ayala, I., Beznoussenko, G., Giacchetti, G., Machesky, L. M., Luini, A., et al. (2006). Actin Dynamics at Sites of Extracellular Matrix Degradation. *Eur. J. Cell Biol.* 85, 1217–1231. doi:10.1016/j.ejcb.2006.08.003

Bartel, D. P. (2004). MicroRNAs. *Cell* 116, 281–297. doi:10.1016/s0092-8674(04)00045-5

Bassell, G. J., Powers, C. M., Taneja, K. L., and Singer, R. H. (1994). Single mRNAs Visualized by Ultrastructural *In Situ* Hybridization Are Principally Localized at Actin Filament Intersections in Fibroblasts. *J. Cell Biol* 126, 863–876. doi:10.1083/jcb.126.4.863

Battaglia, R. A., Delic, S., Herrmann, H., and Snider, N. T. (2018). Vimentin on the Move: New Developments in Cell Migration. *F1000Res* 7, F1000. doi:10.12688/f1000research.15967.1

Begum, A., Ewachiw, T., Jung, C., Huang, A., Norberg, K. J., Marchionni, L., et al. (2017). The Extracellular Matrix and Focal Adhesion Kinase Signaling Regulate Cancer Stem Cell Function in Pancreatic Ductal Adenocarcinoma. *PLoS One* 12, e0180181. doi:10.1371/journal.pone.0180181

Bilandzic, M., Rainczuk, A., Green, E., Fairweather, N., Jobling, T. W., Plebanski, M., et al. (2019). Keratin-14 (KRT14) Positive Leader Cells Mediate Mesothelial Clearance and Invasion by Ovarian Cancer Cells. *Cancers (Basel)* 11, 1. doi:10.3390/cancers11091228

Blanchoin, L., Boujemaa-Paterski, R., Sykes, C., and Plastino, J. (2014). Actin Dynamics, Architecture, and Mechanics in Cell Motility. *Physiol. Rev.* 94, 235–263. doi:10.1152/physrev.00018.2013

Bleaken, B. M., Menko, A. S., and Walker, J. L. (2016). Cells Activated for Wound Repair Have the Potential to Direct Collective Invasion of an Epithelium. *MBoC* 27, 451–465. doi:10.1091/mbc.e15-09-0615

Block, J., Witt, H., Candelli, A., Danes, J. C., Peterman, E. J. G., Wuite, G. J. L., et al. (2018). Viscoelastic Properties of Vimentin Originate from Nonequilibrium Conformational Changes. *Sci. Adv.* 4, eaat1161. doi:10.1126/sciadv.aat1161

Boggs, A. E., Vitolo, M. I., Whipple, R. A., Charpentier, M. S., Goloubeva, O. G., Ioffe, O. B., et al. (2015). α-Tubulin Acetylation Elevated in Metastatic and Basal-like Breast Cancer Cells Promotes Microtentacle Formation, Adhesion, and Invasive Migration. *Cancer Res.* 75, 203–215. doi:10.1158/0008-5472.can-13-3563

Braam, S. R., Zeinstra, L., Litjens, S., Ward-Van Oostwaard, D., Van Den Brink, S., Van Laake, L., et al. (2008). Recombinant Vitronectin Is a Functionally Defined Substrate that Supports Human Embryonic Stem Cell Self-Renewal via αVβ5 Integrin. *Stem Cells* 26, 2257–2265. doi:10.1634/stemcells.2008-0291

Byun, Y., Chen, F., Chang, R., Trivedi, M., Green, K. J., and Cryns, V. L. (2001). Caspase Cleavage of Vimentin Disrupts Intermediate Filaments and Promotes Apoptosis. *Cell Death Differ* 8, 443–450. doi:10.1038/sj.cdd.4400840

Cai, L., Fritz, D., Stefanovic, L., and Stefanovic, B. (2010). Nonmuscle Myosin-dependent Synthesis of Type I Collagen. *J. Mol. Biol.* 401, 564–578. doi:10.1016/j.jmb.2010.06.057

Calderwood, D. A., Campbell, I. D., and Critchley, D. R. (2013). Talins and Kindlins: Partners in Integrin-Mediated Adhesion. *Nat. Rev. Mol. Cell. Biol.* 14, 503–517.

Cao, J., Ma, J., Sun, L., Li, J., Qin, T., Zhou, C., et al. (2018). Targeting Glypican-4 Overcomes 5-FU Resistance and Attenuates Stem Cell-like Properties via Suppression of Wnt/β-catenin Pathway in Pancreatic Cancer Cells. *J. Cell Biochem* 119, 9498–9512. doi:10.1002/jcb.27266

Challa, A. A., and Stefanovic, B. (2011). A Novel Role of Vimentin Filaments: Binding and Stabilization of Collagen mRNAs. *Mol. Cell Biol* 31, 3773–3789. doi:10.1128/mcb.05263-11

Cheng, C.-W., Wang, H.-W., Chang, C.-W., Chu, H.-W., Chen, C.-Y., Yu, J.-C., et al. (2012). MicroRNA-30a Inhibits Cell Migration and Invasion by Downregulating Vimentin Expression and Is a Potential Prognostic Marker in Breast Cancer. *Breast Cancer Res. Treat.* 134, 1081–1093. doi:10.1007/s10549-012-2034-4

Cheng, F., and Eriksson, J. E. (2017). Intermediate Filaments and the Regulation of Cell Motility during Regeneration and Wound Healing. *Cold Spring Harb Perspect. Biol.* 9, 1. doi:10.1101/cshperspect.a022046

Cheng, F., Shen, Y., Mohanasundaram, P., Lindström, M., Ivaska, J., Ny, T., et al. (2016). Vimentin Coordinates Fibroblast Proliferation and Keratinocyte Differentiation in Wound Healing via TGF-β-Slug Signaling. *Proc. Natl. Acad. Sci. USA* 113, E4320–E4327. doi:10.1073/pnas.1519197113

Cheng, Z., Xin, H., and Han, T. (2019). BECN1 Promotes the Migration of NSCLC Cells through Regulating the Ubiquitination of Vimentin. *Cell Adh Migr* 13, 249–259. doi:10.1080/19336918.2019.1638690

Chernyatina, A. A., Guzenko, D., and Strelkov, S. V. (2015). Intermediate Filament Structure: the Bottom-Up Approach. *Curr. Opin. Cell Biol.* 32, 65–72. doi:10.1016/j.ceb.2014.12.007

Chou, Y.-H., Bischoff, J. R., Beach, D., and Goldman, R. D. (1990). Intermediate Filament Reorganization during Mitosis Is Mediated by P34cdc2 Phosphorylation of Vimentin. *Cell* 62, 1063–1071. doi:10.1016/0092-8674(90)90384-q

Costigliola, N., Ding, L., Burckhardt, C. J., Han, S. J., Gutierrez, E., Mota, A., et al. (2017). Vimentin Fibers orient Traction Stress. *Proc. Natl. Acad. Sci. USA* 114, 5195–5200. doi:10.1073/pnas.1614610114

Cox, T. R., and Erler, J. T. (2011). Remodeling and Homeostasis of the Extracellular Matrix: Implications for Fibrotic Diseases and Cancer. *Dis. Model. Mech.* 4, 165–178.

Coye, L. H., and Collins, C. M. (2004). Identification of SpyA, a Novel ADP-Ribosyltransferase of Streptococcus Pyogenes. *Mol. Microbiol.* 54, 89–98. doi:10.1111/j.1365-2958.2004.04262.x

Danielsson, F., Peterson, M. K., Caldeira Araujo, H., Lautenschlager, F., and Gad, A. K. B. (2018). Vimentin Diversity in Health and Disease. *Cells* 7, 1. doi:10.3390/cells7100147

Database, G. T. H. G. (2022). *VIM Gene - Vimentin*. Israel: Weizmann Institute of Science.

De Pascalis, C., Pérez-González, C., Seetharaman, S., Boëda, B., Vianay, B., Burute, M., et al. (2018). Intermediate Filaments Control Collective Migration by Restricting Traction Forces and Sustaining Cell-Cell Contacts. *J. Cell Biol* 217, 3031–3044. doi:10.1083/jcb.201801162

Delva, E., Tucker, D. K., and Kowalczyk, A. P. (2009). The Desmosome. *Cold Spring Harbor Perspect. Biol.* 1, a002543. doi:10.1101/cshperspect.a002543

Deng, Z., Du, W. W., Fang, L., Shan, S. W., Qian, J., Lin, J., et al. (2013). The Intermediate Filament Vimentin Mediates microRNA miR-378 Function in Cellular Self-Renewal by Regulating the Expression of the Sox2 Transcription Factor. *J. Biol. Chem.* 288, 319–331. doi:10.1074/jbc.m112.418830

Ding, I., Ostrowska-Podhorodecka, Z., Lee, W., Liu, R. S. C., Carneiro, K., Janmey, P. A., et al. (2020). Cooperative Roles of PAK1 and Filamin A in Regulation of Vimentin Assembly and Cell Extension Formation. *Biochim. Biophys. Acta (Bba) - Mol. Cell Res.* 1867, 118739. doi:10.1016/j.bbamcr.2020.118739

dos Santos, G., Rogel, M. R., Baker, M. A., Troken, J. R., Urich, D., Morales-Nebreda, L., et al. (2015). Vimentin Regulates Activation of the NLRP3 Inflammasome. *Nat. Commun.* 6, 6574. doi:10.1038/ncomms7574

Duarte, S., Viedma-Poyatos, Á., Navarro-Carrasco, E., Martínez, A. E., Pajares, M. A., and Pérez-Sala, D. (2019). Vimentin Filaments Interact with the Actin Cortex in Mitosis Allowing normal Cell Division. *Nat. Commun.* 10, 4200. doi:10.1038/s41467-019-12029-4

Dupin, I., Sakamoto, Y., and Etienne-Manneville, S. (2011). Cytoplasmic Intermediate Filaments Mediate Actin-Driven Positioning of the Nucleus. *J. Cell Sci* 124, 865–872. doi:10.1242/jcs.076356

Engler, A. J., Sen, S., Sweeney, H. L., and Discher, D. E. (2006). Matrix Elasticity Directs Stem Cell Lineage Specification. *Cell* 126, 677–689. doi:10.1016/j.cell.2006.06.044

Esue, O., Carson, A. A., Tseng, Y., and Wirtz, D. (2006). A Direct Interaction between Actin and Vimentin Filaments Mediated by the Tail Domain of Vimentin. *J. Biol. Chem.* 281, 30393–30399. doi:10.1074/jbc.m605452200

Feng, Z., Wagatsuma, Y., Kikuchi, M., Kosawada, T., Nakamura, T., Sato, D., et al. (2014). The Mechanisms of Fibroblast-Mediated Compaction of Collagen Gels and the Mechanical Niche Around Individual Fibroblasts. *Biomaterials* 35, 8078–8091.

Francart, M.-E., Vanwynsberghe, A. M., Lambert, J., Bourcy, M., Genna, A., Ancel, J., et al. (2020). Vimentin Prevents a miR-dependent Negative Regulation of Tissue Factor mRNA during Epithelial-Mesenchymal Transitions and Facilitates Early Metastasis. *Oncogene* 39, 3680–3692. doi:10.1038/s41388-020-1244-1

Franz, J. K., Gall, L., Williams, M. A., Picheral, B., and Franke, W. W. (1983). Intermediate-size Filaments in a Germ Cell: Expression of Cytokeratins in Oocytes and Eggs of the Frog Xenopus. *Proc. Natl. Acad. Sci.* 80, 6254–6258. doi:10.1073/pnas.80.20.6254

Frescas, D., Roux, C. M., Aygun-Sunar, S., Gleiberman, A. S., Krasnov, P., Kurnasov, O. V., et al. (2017). Senescent Cells Expose and Secrete an Oxidized Form of Membrane-Bound Vimentin as Revealed by a Natural Polyreactive Antibody. *Proc. Natl. Acad. Sci. USA* 114, E1668–E1677. doi:10.1073/pnas.1614661114

Gálvez, B. G., Matías-Román, S., Yáñez-Mó, M., Sánchez-Madrid, F., and Arroyo, A. G. (2002). ECM Regulates MT1-MMP Localization with Beta1 or Alphavbeta3 Integrins at Distinct Cell Compartments Modulating its Internalization and Activity on Human Endothelial Cells. *J. Cell Biol* 159, 509–521. doi:10.1083/jcb.200205026

Gao, Y.-s., and Sztul, E. (2001). A Novel Interaction of the Golgi Complex with the Vimentin Intermediate Filament Cytoskeleton. *J. Cell Biol* 152, 877–894. doi:10.1083/jcb.152.5.877

Gardel, M. L., Schneider, I. C., Aratyn-Schaus, Y., and Waterman, C. M. (2010). Mechanical Integration of Actin and Adhesion Dynamics in Cell Migration. *Annu. Rev. Cell Dev. Biol.* 26, 315–333. doi:10.1146/annurev.cellbio.011209.122036

Gregor, M., Osmanagic-Myers, S., Burgstaller, G., Wolfram, M., Fischer, I., Walko, G., et al. (2014). Mechanosensing through Focal Adhesion-anchored Intermediate Filaments. *FASEB j.* 28, 715–729. doi:10.1096/fj.13-231829

Grinnell, F., Rocha, L. B., Iucu, C., Rhee, S., and Jiang, H. (2006). Nested Collagen Matrices: a New Model to Study Migration of Human Fibroblast Populations in Three Dimensions. *Exp. Cell Res* 312, 86–94. doi:10.1016/j.yexcr.2005.10.001

Guo, D., Song, X., Guo, T., Gu, S., Chang, X., Su, T., et al. (2018). Vimentin Acetylation Is Involved in SIRT5-Mediated Hepatocellular Carcinoma Migration. *Am. J. Cancer Res.* 8, 2453–2466.

Guo, F., Parker Kerrigan, B. C., Yang, D., Hu, L., Shmulevich, I., Sood, A. K., et al. (2014). Post-transcriptional Regulatory Network of Epithelial-To-Mesenchymal and Mesenchymal-To-Epithelial Transitions. *J. Hematol. Oncol.* 7, 19. doi:10.1186/1756-8722-7-19

Hafeez, B. B., Zhong, W., Weichert, J., Dreckschmidt, N. E., Jamal, M. S., and Verma, A. K. (2011). Genetic Ablation of PKC Epsilon Inhibits Prostate Cancer Development and Metastasis in Transgenic Mouse Model of Prostate Adenocarcinoma. *Cancer Res.* 71, 2318–2327. doi:10.1158/0008-5472.can-10-4170

Hanover, J. A., Krause, M. W., and Love, D. C. (2010). The Hexosamine Signaling Pathway: O-GlcNAc Cycling in Feast or Famine. *Biochim. Biophys. Acta (Bba) - Gen. Subjects* 1800, 80–95. doi:10.1016/j.bbagen.2009.07.017

Hart, G. W., Slawson, C., Ramirez-Correa, G., and Lagerlof, O. (2011). Cross Talk between O-GlcNAcylation and Phosphorylation: Roles in Signaling, Transcription, and Chronic Disease. *Annu. Rev. Biochem.* 80, 825–858. doi:10.1146/annurev-biochem-060608-102511

Hart, G. W. (2014). Three Decades of Research on O-GlcNAcylation Â€" A Major Nutrient Sensor that Regulates Signaling, Transcription and Cellular Metabolism. *Front. Endocrinol.* 5, 183. doi:10.3389/fendo.2014.00183

Havel, L. S., Kline, E. R., Salgueiro, A. M., and Marcus, A. I. (2015). Vimentin Regulates Lung Cancer Cell Adhesion through a VAV2-Rac1 Pathway to Control Focal Adhesion Kinase Activity. *Oncogene* 34, 1979–1990. doi:10.1038/onc.2014.123

Helfand, B. T., Mendez, M. G., Murthy, S. N. P., Shumaker, D. K., Grin, B., Mahammad, S., et al. (2011). Vimentin Organization Modulates the Formation of Lamellipodia. *MBoC* 22, 1274–1289. doi:10.1091/mbc.e10-08-0699

Herrmann, H., and Aebi, U. (1998). Structure, Assembly, and Dynamics of Intermediate Filaments. *Subcell Biochem.* 31, 319–362.

Herrmann, H., Häner, M., Brettel, M., Müller, S. A., Goldie, K. N., Fedtke, B., et al. (1996). Structure and Assembly Properties of the Intermediate Filament Protein Vimentin: the Role of its Head, Rod and Tail Domains. *J. Mol. Biol.* 264, 933–953. doi:10.1006/jmbi.1996.0688

Hookway, C., Ding, L., Davidson, M. W., Rappoport, J. Z., Danuser, G., and Gelfand, V. I. (2015). Microtubule-dependent Transport and Dynamics of Vimentin Intermediate Filaments. *MBoC* 26, 1675–1686. doi:10.1091/mbc.e14-09-1398

Hsu, P.-C., Liao, Y.-F., Lin, C.-L., Lin, W.-H., Liu, G.-Y., and Hung, H.-C. (2014). Vimentin Is Involved in Peptidylarginine Deiminase 2-induced Apoptosis of Activated Jurkat Cells. *Mol. Cell* 37, 426–434. doi:10.14348/molcells.2014.2359

Huang, B., Chen, S. C., and Wang, D. L. (2009). Shear Flow Increases S-Nitrosylation of Proteins in Endothelial Cells. *Cardiovasc. Res.* 83, 536–546. doi:10.1093/cvr/cvp154

Hurt, E. M., Chan, K., Duhagon Serrat, M. A., Thomas, S. B., Veenstra, T. D., and Farrar, W. L. (2010). Identification of Vitronectin as an Extrinsic Inducer of Cancer Stem Cell Differentiation and Tumor Formation. *Stem Cells* 28, 390–398. doi:10.1002/stem.271

Icenogle, L. M., Hengel, S. M., Coye, L. H., Streifel, A., Collins, C. M., Goodlett, D. R., et al. (2012). Molecular and Biological Characterization of Streptococcal SpyA-Mediated ADP-Ribosylation of Intermediate Filament Protein Vimentin. *J. Biol. Chem.* 287, 21481–21491. doi:10.1074/jbc.m112.370791

Inagaki, M., Takahara, H., Nishi, Y., Sugawara, K., and Sato, C. (1989). Ca2+-dependent Deimination-Induced Disassembly of Intermediate Filaments Involves Specific Modification of the Amino-Terminal Head Domain. *J. Biol. Chem.* 264, 18119–18127. doi:10.1016/s0021-9258(19)84685-9

Irianto, J., Pfeifer, C. R., Bennett, R. R., Xia, Y., Ivanovska, I. L., Liu, A. J., et al. (2016). Nuclear Constriction Segregates mobile Nuclear Proteins Away from Chromatin. *MBoC* 27, 4011–4020. doi:10.1091/mbc.e16-06-0428

Ivaska, J., Pallari, H.-M., Nevo, J., and Eriksson, J. E. (2007). Novel Functions of Vimentin in Cell Adhesion, Migration, and Signaling. *Exp. Cell Res.* 313, 2050–2062. doi:10.1016/j.yexcr.2007.03.040

Jang, B., Kim, M. J., Lee, Y. J., Ishigami, A., Kim, Y. S., and Choi, E. K. (2020). Vimentin Citrullination Probed by a Novel Monoclonal Antibody Serves as a Specific Indicator for Reactive Astrocytes in Neurodegeneration. *Neuropathol. Appl. Neurobiol.* 46, 751–769. doi:10.1111/nan.12620

Janmey, P. A., Euteneuer, U., Traub, P., and Schliwa, M. (1991). Viscoelastic Properties of Vimentin Compared with Other Filamentous Biopolymer Networks. *J. Cell Biol.* 113, 155–160. doi:10.1083/jcb.113.1.155

Janmey, P. A., Hinz, B., and Mcculloch, C. A. (2021). Physics and Physiology of Cell Spreading in Two and Three Dimensions. *Physiology* 36, 382–391. doi:10.1152/physiol.00020.2021

Jiu, Y., Peränen, J., Schaible, N., Cheng, F., Eriksson, J. E., Krishnan, R., et al. (2017). Vimentin Intermediate Filaments Control Actin Stress Fiber Assembly through GEF-H1 and RhoA. *J. Cell Sci* 130, 892–902. doi:10.1242/jcs.196881

Jiu, Y., Lehtimäki, J., Tojkander, S., Cheng, F., Jäälinoja, H., Liu, X., et al. (2015). Bidirectional Interplay between Vimentin Intermediate Filaments and Contractile Actin Stress Fibers. *Cell Rep.* 11, 1511–1518. doi:10.1016/j.celrep.2015.05.008

Kalyanasundaram, A., Li, N., Gardner, M. L., Artiga, E. J., Hansen, B. J., Webb, A., et al. (2021). Fibroblast-Specific Proteotranscriptomes Reveal Distinct Fibrotic Signatures of Human Sinoatrial Node in Nonfailing and Failing Hearts. *Circulation* 144, 126–143. doi:10.1161/circulationaha.120.051583

Kaschula, C. H., Tuveri, R., Ngarande, E., Dzobo, K., Barnett, C., Kusza, D. A., et al. (2019). The Garlic Compound Ajoene Covalently Binds Vimentin, Disrupts the Vimentin Network and Exerts Anti-metastatic Activity in Cancer Cells. *BMC Cancer* 19, 248. doi:10.1186/s12885-019-5388-8

Kaus-Drobek, M., Mücke, N., Szczepanowski, R. H., Wedig, T., Czarnocki-Cieciura, M., Polakowska, M., et al. (2020). Vimentin S-Glutathionylation at Cys328 Inhibits Filament Elongation and Induces Severing of Mature Filaments *In Vitro*. *FEBS J.* 287, 5304–5322. doi:10.1111/febs.15321

Kendall, R. T., and Feghali-Bostwick, C. A. (2014). Fibroblasts in Fibrosis: Novel Roles and Mediators. *Front. Pharmacol.* 5, 123. doi:10.3389/fphar.2014.00123

Kim, S.-H., Turnbull, J., and Guimond, S. (2011). Extracellular Matrix and Cell Signalling: the Dynamic Cooperation of Integrin, Proteoglycan and Growth Factor Receptor. *J. Endocrinol.* 209, 139–151. doi:10.1530/joe-10-0377

Kim, S., and Coulombe, P. A. (2007). Intermediate Filament Scaffolds Fulfill Mechanical, Organizational, and Signaling Functions in the Cytoplasm. *Genes Dev.* 21, 1581–1597. doi:10.1101/gad.1552107

Kim, T. W., Lee, Y. S., Yun, N. H., Shin, C. H., Hong, H. K., Kim, H. H., et al. (2020). Correction: MicroRNA-17-5p Regulates EMT by Targeting Vimentin in Colorectal Cancer. *Br. J. Cancer* 123, 1204. doi:10.1038/s41416-020-1027-z

Kowalczyk, A. P., Navarro, P., Dejana, E., Bornslaeger, E. A., Green, K. J., Kopp, D. S., et al. (1998). VE-cadherin and Desmoplakin Are Assembled into Dermal Microvascular Endothelial Intercellular Junctions: a Pivotal Role for Plakoglobin in the Recruitment of Desmoplakin to Intercellular Junctions. *J. Cell Sci* 111 (Pt 20), 3045–3057. doi:10.1242/jcs.111.20.3045

Kreis, S., Schonfeld, H., Melchior, C., Steiner, B., and Kieffer, N. (2005). The Intermediate Filament Protein Vimentin Binds Specifically to a Recombinant Integrin ?2/?1 Cytoplasmic Tail Complex and Co-localizes with Native ?2/?1 in Endothelial Cell Focal Adhesions. *Exp. Cell Res.* 305, 110–121. doi:10.1016/j.yexcr.2004.12.023

Kuppe, C., Ibrahim, M. M., Kranz, J., Zhang, X., Ziegler, S., Perales-Patón, J., et al. (2021). Decoding Myofibroblast Origins in Human Kidney Fibrosis. *Nature* 589, 281–286. doi:10.1038/s41586-020-2941-1

Kwak, H.-I., Kang, H., Dave, J. M., Mendoza, E. A., Su, S.-C., Maxwell, S. A., et al. (2012). Calpain-mediated Vimentin Cleavage Occurs Upstream of MT1-MMP Membrane Translocation to Facilitate Endothelial Sprout Initiation. *Angiogenesis* 15, 287–303. doi:10.1007/s10456-012-9262-4

Lanier, M. H., Kim, T., and Cooper, J. A. (2015). CARMIL2 Is a Novel Molecular Connection between Vimentin and Actin Essential for Cell Migration and Invadopodia Formation. *MBoC* 26, 4577–4588. doi:10.1091/mbc.e15-08-0552

Lavenus, S. B., Tudor, S. M., Ullo, M. F., Vosatka, K. W., and Logue, J. S. (2020). A Flexible Network of Vimentin Intermediate Filaments Promotes Migration of Amoeboid Cancer Cells through Confined Environments. *J. Biol. Chem.* 295, 6700–6709. doi:10.1074/jbc.ra119.011537

Lee, J. E., Cathey, P. I., Wu, H., Parker, R., and Voeltz, G. K. (2020). Endoplasmic Reticulum Contact Sites Regulate the Dynamics of Membraneless Organelles. *Science* 367, 1. doi:10.1126/science.aay7108

Lee, Y. H., Seo, E. K., and Lee, S. T. (2019). Skullcapflavone II Inhibits Degradation of Type I Collagen by Suppressing MMP-1 Transcription in Human Skin Fibroblasts. *Int. J. Mol. Sci.* 20, 1. doi:10.3390/ijms20112734

Lepekhin, E. A., Eliasson, C., Berthold, C. H., Berezin, V., Bock, E., and Pekny, M. (2001). Intermediate Filaments Regulate Astrocyte Motility. *J. Neurochem.* 79, 617–625. doi:10.1046/j.1471-4159.2001.00595.x

Li, C.-L., Yang, D., Cao, X., Wang, F., Hong, D.-Y., Wang, J., et al. (2017a). Fibronectin Induces Epithelial-Mesenchymal Transition in Human Breast Cancer MCF-7 Cells via Activation of Calpain. *Oncol. Lett.* 13, 3889–3895. doi:10.3892/ol.2017.5896

Li, C., Mcmanus, F. P., Plutoni, C., Pascariu, C. M., Nelson, T., Alberici Delsin, L. E., et al. (2020). Quantitative SUMO Proteomics Identifies PIAS1 Substrates Involved in Cell Migration and Motility. *Nat. Commun.* 11, 834. doi:10.1038/s41467-020-14581-w

Li, F. J., Surolia, R., Li, H., Wang, Z., Liu, G., Kulkarni, T., et al. (2021). Citrullinated Vimentin Mediates Development and Progression of Lung Fibrosis. *Sci. Transl Med.* 13, 1. doi:10.1126/scitranslmed.aba2927

Li, F. J., Surolia, R., Li, H., Wang, Z., Kulkarni, T., Liu, G., et al. (2017b). Autoimmunity to Vimentin Is Associated with Outcomes of Patients with Idiopathic Pulmonary Fibrosis. *J.I.* 199, 1596–1605. doi:10.4049/jimmunol.1700473

Lin, Y., Mori, E., Kato, M., Xiang, S., Wu, L., Kwon, I., et al. (2016). Toxic PR Poly-Dipeptides Encoded by the C9orf72 Repeat Expansion Target LC Domain Polymers. *Cell* 167, 789–802. doi:10.1016/j.cell.2016.10.003

Liu, B., Xu, T., Xu, X., Cui, Y., and Xing, X. (2018). Biglycan Promotes the Chemotherapy Resistance of colon Cancer by Activating NF-Kb Signal Transduction. *Mol. Cell Biochem* 449, 285–294. doi:10.1007/s11010-018-3365-1

Lorenz, M., Yamaguchi, H., Wang, Y., Singer, R. H., and Condeelis, J. (2004). Imaging Sites of N-Wasp Activity in Lamellipodia and Invadopodia of Carcinoma Cells. *Curr. Biol.* 14, 697–703. doi:10.1016/j.cub.2004.04.008

Lowery, J., Kuczmarski, E. R., Herrmann, H., and Goldman, R. D. (2015). Intermediate Filaments Play a Pivotal Role in Regulating Cell Architecture and Function. *J. Biol. Chem.* 290, 17145–17153. doi:10.1074/jbc.r115.640359

Lu, P., Takai, K., Weaver, V. M., and Werb, Z. (2011). Extracellular Matrix Degradation and Remodeling in Development and Disease. *Cold Spring Harb Perspect. Biol.* 3, 1. doi:10.1101/cshperspect.a005058

Lu, P., Weaver, V. M., and Werb, Z. (2012). The Extracellular Matrix: a Dynamic Niche in Cancer Progression. *J. Cell Biol* 196, 395–406. doi:10.1083/jcb.201102147

Luo, Y., Na, Z., and Slavoff, S. A. (2018). P-bodies: Composition, Properties, and Functions. *Biochemistry* 57, 2424–2431. doi:10.1021/acs.biochem.7b01162

Manohar, S., Jacob, S., Wang, J., Wiechecki, K. A., Koh, H. W. L., Simões, V., et al. (2019). Polyubiquitin Chains Linked by Lysine Residue 48 (K48) Selectively Target Oxidized ProteinsIn Vivo. *Antioxid. Redox Signaling* 31, 1133–1149. doi:10.1089/ars.2019.7826

Marcelo, A., Koppenol, R., De Almeida, L. P., Matos, C. A., and Nóbrega, C. (2021). Stress Granules, RNA-Binding Proteins and Polyglutamine Diseases: Too Much Aggregation? *Cell Death Dis* 12, 592. doi:10.1038/s41419-021-03873-8

Mayor, R., and Etienne-Manneville, S. (2016). The Front and Rear of Collective Cell Migration. *Nat. Rev. Mol. Cell Biol* 17, 97–109. doi:10.1038/nrm.2015.14

Mendez, M. G., Kojima, S. I., and Goldman, R. D. (2010). Vimentin Induces Changes in Cell Shape, Motility, and Adhesion during the Epithelial to Mesenchymal Transition. *FASEB j.* 24, 1838–1851. doi:10.1096/fj.09-151639

Meng, J., Chen, S., Han, J.-X., Qian, B., Wang, X.-R., Zhong, W.-L., et al. (2018). Twist1 Regulates Vimentin through Cul2 Circular RNA to Promote EMT in Hepatocellular Carcinoma. *Cancer Res.* 78, 4150–4162. doi:10.1158/0008-5472.can-17-3009

Menko, A. S., Bleaken, B. M., Libowitz, A. A., Zhang, L., Stepp, M. A., and Walker, J. L. (2014). A central Role for Vimentin in Regulating Repair Function during Healing of the Lens Epithelium. *MBoC* 25, 776–790. doi:10.1091/mbc.e12-12-0900

Messica, Y., Laser-Azogui, A., Volberg, T., Elisha, Y., Lysakovskaia, K., Eils, R., et al. (2017). The Role of Vimentin in Regulating Cell Invasive Migration in Dense Cultures of Breast Carcinoma Cells. *Nano Lett.* 17, 6941–6948. doi:10.1021/acs.nanolett.7b03358

Moeendarbary, E., Valon, L., Fritzsche, M., Harris, A. R., Moulding, D. A., Thrasher, A. J., et al. (2013). The Cytoplasm of Living Cells Behaves as a Poroelastic Material. *Nat. Mater* 12, 253–261. doi:10.1038/nmat3517

Mor-Vaknin, N., Punturieri, A., Sitwala, K., and Markovitz, D. M. (2003). Vimentin Is Secreted by Activated Macrophages. *Nat. Cell Biol* 5, 59–63. doi:10.1038/ncb898

Musaelyan, A., Lapin, S., Nazarov, V., Tkachenko, O., Gilburd, B., Mazing, A., et al. (2018). Vimentin as Antigenic Target in Autoimmunity: A Comprehensive Review. *Autoimmun. Rev.* 17, 926–934. doi:10.1016/j.autrev.2018.04.004

Nallanthighal, S., Heiserman, J. P., and Cheon, D.-J. (2019). The Role of the Extracellular Matrix in Cancer Stemness. *Front. Cell Dev. Biol.* 7, 86. doi:10.3389/fcell.2019.00086

Nieto, M. A., Huang, R. Y.-J., Jackson, R. A., and Thiery, J. P. (2016). Emt: 2016. *Cell* 166, 21–45. doi:10.1016/j.cell.2016.06.028

Nöding, B., Herrmann, H., and Köster, S. (2014). Direct Observation of Subunit Exchange along Mature Vimentin Intermediate Filaments. *Biophysical J.* 107, 2923–2931. doi:10.1016/j.bpj.2014.09.050

Ogrodnik, M., Salmonowicz, H., Brown, R., Turkowska, J., redniawa, W., Pattabiraman, S., et al. (2014). Dynamic JUNQ Inclusion Bodies Are Asymmetrically Inherited in Mammalian Cell Lines through the Asymmetric Partitioning of Vimentin. *Proc. Natl. Acad. Sci.* 111, 8049–8054. doi:10.1073/pnas.1324035111

Osborn, M., Franke, W., and Weber, K. (1980). Direct Demonstration of the Presence of Two Immunologically Distinct Intermediate-Sized Filament Systems in the Same Cell by Double Immunofluorescence Microscopy. *Exp. Cell Res.* 125, 37–46. doi:10.1016/0014-4827(80)90186-x

Ostrowska-Podhorodecka, Z., Ding, I., Lee, W., Tanic, J., Abbasi, S., Arora, P. D., et al. (2021). Vimentin Tunes Cell Migration on Collagen by Controlling β1 Integrin Activation and Clustering. *J. Cell Sci* 134, 1. doi:10.1242/jcs.254359

Ostrowska-Podhorodecka, Z., and Mcculloch, C. A. (2021). Vimentin Regulates the Assembly and Function of Matrix Adhesions. *Wound Repair Regen.* 29, 602–612. doi:10.1111/wrr.12920

Otsuki, S., Inokuchi, M., Enjoji, M., Ishikawa, T., Takagi, Y., Kato, K., et al. (2011). Vimentin Expression Is Associated with Decreased Survival in Gastric Cancer. *Oncol. Rep.* 25, 1235–1242. doi:10.3892/or.2011.1185

Palazzo, L., Leidecker, O., Prokhorova, E., Dauben, H., Matic, I., and Ahel, I. (2018). Serine Is the Major Residue for ADP-Ribosylation upon DNA Damage. *Elife* 7, 1. doi:10.7554/eLife.34334

Pattabiraman, S., Azad, G. K., Amen, T., Brielle, S., Park, J. E., Sze, S. K., et al. (2020). Vimentin Protects Differentiating Stem Cells from Stress. *Sci. Rep.* 10, 19525. doi:10.1038/s41598-020-76076-4

Patteson, A. E., Pogoda, K., Byfield, F. J., Mandal, K., Ostrowska-Podhorodecka, Z., Charrier, E. E., et al. (2019). Loss of Vimentin Enhances Cell Motility through Small Confining Spaces. *Small* 15, e1903180. doi:10.1002/smll.201903180

Pérez-Sala, D., Oeste, C. L., Martínez, A. E., Carrasco, M. J., Garzón, B., and Cañada, F. J. (2015). Vimentin Filament Organization and Stress Sensing Depend on its Single Cysteine Residue and Zinc Binding. *Nat. Commun.* 6, 7287. doi:10.1038/ncomms8287

Peuhu, E., Virtakoivu, R., Mai, A., Wärri, A., and Ivaska, J. (2017). Epithelial Vimentin Plays a Functional Role in Mammary Gland Development. *Development* 144, 4103–4113. doi:10.1242/dev.154229

Premchandar, A., Mücke, N., Poznański, J., Wedig, T., Kaus-Drobek, M., Herrmann, H., et al. (2016). Structural Dynamics of the Vimentin Coiled-Coil Contact Regions Involved in Filament Assembly as Revealed by Hydrogen-Deuterium Exchange. *J. Biol. Chem.* 291, 24931–24950. doi:10.1074/jbc.m116.748145

Pruitt, K. D., Brown, G. R., Hiatt, S. M., Thibaud-Nissen, F., Astashyn, A., Ermolaeva, O., et al. (2014). RefSeq: an Update on Mammalian Reference Sequences. *Nucl. Acids Res.* 42, D756–D763. doi:10.1093/nar/gkt1114

Rada, M., Nallanthighal, S., Cha, J., Ryan, K., Sage, J., Eldred, C., et al. (2018). Inhibitor of Apoptosis Proteins (IAPs) Mediate Collagen Type XI Alpha 1-driven Cisplatin Resistance in Ovarian Cancer. *Oncogene* 37, 4809–4820. doi:10.1038/s41388-018-0297-x

Rawla, P., Sunkara, T., and Barsouk, A. (2019). Epidemiology of Colorectal Cancer: Incidence, Mortality, Survival, and Risk Factors. *pg* 14, 89–103. doi:10.5114/pg.2018.81072

Robert, A., Rossow, M. J., Hookway, C., Adam, S. A., and Gelfand, V. I. (2015). Vimentin Filament Precursors Exchange Subunits in an ATP-dependent Manner. *Proc. Natl. Acad. Sci. USA* 112, E3505–E3514. doi:10.1073/pnas.1505303112

Saha, K., Keung, A. J., Irwin, E. F., Li, Y., Little, L., Schaffer, D. V., et al. (2008). Substrate Modulus Directs Neural Stem Cell Behavior. *Biophysical J.* 95, 4426–4438. doi:10.1529/biophysj.108.132217

Santiago, J.-J., Dangerfield, A. L., Rattan, S. G., Bathe, K. L., Cunnington, R. H., Raizman, J. E., et al. (2010). Cardiac Fibroblast to Myofibroblast Differentiation *In Vivo* and *In Vitro*: Expression of Focal Adhesion Components in Neonatal and Adult Rat Ventricular Myofibroblasts. *Dev. Dyn.* 239, 1573–1584. doi:10.1002/dvdy.22280

Satelli, A., and Li, S. (2011). Vimentin in Cancer and its Potential as a Molecular Target for Cancer Therapy. *Cell. Mol. Life Sci.* 68, 3033–3046. doi:10.1007/s00018-011-0735-1

Schaffeld, M., Herrmann, H., Schultess, J., and Markl, J. (2001). Vimentin and Desmin of a Cartilaginous Fish, the Shark *Scyliorhinus stellaris*: Sequence, Expression Patterns and *In Vitro* Assembly. *Eur. J. Cell Biol.* 80, 692–702. doi:10.1078/0171-9335-00206

Schmidt, Y., Biniossek, M., Stark, G. B., Finkenzeller, G., and Simunovic, F. (2015). Osteoblastic Alkaline Phosphatase mRNA Is Stabilized by Binding to Vimentin Intermediary Filaments. *Biol. Chem.* 396, 253–260. doi:10.1515/hsz-2014-0274

Shah, J. V., Wang, L. Z., Traub, P., and Janmey, P. A. (1998). Interaction of Vimentin with Actin and Phospholipids. *Biol. Bull.* 194, 402–405. doi:10.2307/1543125

Sharma, P., Bolten, Z. T., Wagner, D. R., and Hsieh, A. H. (2018). Correction to: Deformability of Human Mesenchymal Stem Cells Is Dependent on Vimentin Intermediate Filaments. *Ann. Biomed. Eng.* 46, 375–376. doi:10.1007/s10439-017-1975-5

Shi, A. M., Tao, Z. Q., Li, R., Wang, Y. Q., Wang, X., and Zhao, J. (2016). Vimentin and Post-Translational Modifications in Cell Motility During Cancer - a Review. *Eur. Rev. Med. Pharmacol. Sci.* 20, 2603–2606.

Shigyo, M., and Tohda, C. (2016). Extracellular Vimentin Is a Novel Axonal Growth Facilitator for Functional Recovery in Spinal Cord-Injured Mice. *Sci. Rep.* 6, 28293. doi:10.1038/srep28293

Skau, C. T., Plotnikov, S. V., Doyle, A. D., and Waterman, C. M. (2018). Retraction for Skau et al., Inverted formin 2 in focal adhesions promotes dorsal stress fiber and fibrillar adhesion formation to drive extracellular matrix assembly. *Proc. Natl. Acad. Sci. U S A.* 115, E2900. doi:10.1073/pnas.1803125115

Snider, N. T., and Omary, M. B. (2014). Post-translational Modifications of Intermediate Filament Proteins: Mechanisms and Functions. *Nat. Rev. Mol. Cell Biol* 15, 163–177. doi:10.1038/nrm3753

Sodek, J. (1977). A Comparison of the Rates of Synthesis and Turnover of Collagen and Non-collagen Proteins in Adult Rat Periodontal Tissues and Skin Using a Microassay. *Arch. Oral Biol.* 22, 655–665. doi:10.1016/0003-9969(77)90095-4

Song, K. Y., Choi, H. S., Law, P.-Y., Wei, L.-N., and Loh, H. H. (2013). Vimentin Interacts with the 5′-untranslated Region of Mouse Mu Opioid Receptor (MOR) and Is Required for post-transcriptional Regulation. *Rna Biol.* 10, 256–266. doi:10.4161/rna.23022

Strelkov, S. V., Herrmann, H., Geisler, N., Lustig, A., Ivaninskii, S., Zimbelmann, R., et al. (2001). Divide-and-conquer Crystallographic Approach towards an Atomic Structure of Intermediate Filaments. *J. Mol. Biol.* 306, 773–781. doi:10.1006/jmbi.2001.4442

Strouhalova, K., Přechová, M., Gandalovičová, A., Brábek, J., Gregor, M., and Rosel, D. (2020). Vimentin Intermediate Filaments as Potential Target for Cancer Treatment. *Cancers (Basel)* 12, 1. doi:10.3390/cancers12010184

Su, L.-X., Pan, P., Wang, X.-T., Long, Y., Liu, D.-W., and Zhou, X. (2019). Vimentin Modulates Apoptosis and Inflammatory Cytokine Release by a Human Monocytic Cell Line (THP-1) in Response to Lipopolysaccharides *In Vitro*. *Chin. Med. J. (Engl)* 132, 1336–1343. doi:10.1097/cm9.0000000000000187

Sun, B., Huang, Z., Wang, B., Yu, Y., Lin, S., Luo, L., et al. (2017). Significance of Glypican-3 (GPC3) Expression in Hepatocellular Cancer Diagnosis. *Med. Sci. Monit.* 23, 850–855. doi:10.12659/msm.899198

Sutoh Yoneyama, M., Hatakeyama, S., Habuchi, T., Inoue, T., Nakamura, T., Funyu, T., et al. (2014). Vimentin Intermediate Filament and Plectin Provide a

Scaffold for Invadopodia, Facilitating Cancer Cell Invasion and Extravasation for Metastasis. *Eur. J. Cell Biol.* 93, 157–169. doi:10.1016/j.ejcb.2014.03.002

Takada, Y., Ye, X., and Simon, S. (2007). The Integrins. *Genome Biol.* 8, 215. doi:10.1186/gb-2007-8-5-215

Tang, D. D., Liao, G., and Gerlach, B. D. (2019). Reorganization of the Vimentin Network in Smooth Muscle. *J. Eng. Sci. Med. Diagn. Ther.* 2, 0108011–0108015. doi:10.1115/1.4042313

Tang, D. D. (2008). Intermediate Filaments in Smooth Muscle. *Am. J. Physiology-Cell Physiol.* 294, C869–C878. doi:10.1152/ajpcell.00154.2007

Tarbet, H. J., Dolat, L., Smith, T. J., Condon, B. M., O'brien, E. T., 3rd, Valdivia, R. H., et al. (2018). Site-specific Glycosylation Regulates the Form and Function of the Intermediate Filament Cytoskeleton. *Elife* 7, 1. doi:10.7554/eLife.31807

Technology, C. S. (2022). K48-linkage Specific Polyubiquitin (D9D5) Rabbit mAb #8081 [Online]. Available: https://www.cellsignal.com/products/primary-antibodies/k48-linkage-specific-polyubiquitin-d9d5-rabbit-mab/8081.

Teng, Y. H.-F., Aquino, R. S., and Park, P. W. (2012). Molecular Functions of Syndecan-1 in Disease. *Matrix Biol.* 31, 3–16. doi:10.1016/j.matbio.2011.10.001

Terriac, E., Coceano, G., Mavajian, Z., Hageman, T. A., Christ, A. F., Testa, I., et al. (2017). Vimentin Levels and Serine 71 Phosphorylation in the Control of Cell-Matrix Adhesions, Migration Speed, and Shape of Transformed Human Fibroblasts. *Cells* 6, 1. doi:10.3390/cells6010002

Thalla, D. G., Jung, P., Bischoff, M., and Lautenschläger, F. (2021). Role of Extracellular Vimentin in Cancer-Cell Functionality and its Influence on Cell Monolayer Permeability Changes Induced by SARS-CoV-2 Receptor Binding Domain. *Int. J. Mol. Sci.* 22, 1. doi:10.3390/ijms22147469

Thiery, J. P., Acloque, H., Huang, R. Y. J., and Nieto, M. A. (2009). Epithelial-mesenchymal Transitions in Development and Disease. *Cell* 139, 871–890. doi:10.1016/j.cell.2009.11.007

Thiery, J. P., and Sleeman, J. P. (2006). Complex Networks Orchestrate Epithelial-Mesenchymal Transitions. *Nat. Rev. Mol. Cell Biol* 7, 131–142. doi:10.1038/nrm1835

Tsuruta, D., and Jones, J. C. R. (2003). The Vimentin Cytoskeleton Regulates Focal Contact Size and Adhesion of Endothelial Cells Subjected to Shear Stress. *J. Cell Sci* 116, 4977–4984. doi:10.1242/jcs.00823

Tripathi, D., and Kulkarni, S. (2021). Butein Induces Intrinsic Pathway of Apoptosis, Vimentin Proteolysis, and Inhibition of Cancer Stem Cell Population in a Human Papillary Thyroid Cancer Cell Line. *Toxicol In Vitro* 77, 105244

Uhlén, M., Fagerberg, L., Hallström, B. M., Lindskog, C., Oksvold, P., Mardinoglu, A., et al. (2015). Tissue-based Map of the Human Proteome. *Science* 347, 1260419. doi:10.1126/science.1260419

Vakhrusheva, A., Endzhievskaya, S., Zhuikov, V., Nekrasova, T., Parshina, E., Ovsiannikova, N., et al. (2019). The Role of Vimentin in Directional Migration of Rat Fibroblasts. *Cytoskeleton* 76, 467–476. doi:10.1002/cm.21572

van Bodegraven, E. J., and Etienne-Manneville, S. (2021). Intermediate Filaments from Tissue Integrity to Single Molecule Mechanics. *Cells* 10, 1. doi:10.3390/cells10081905

van Engeland, N. C. A., Suarez Rodriguez, F., Rivero-Müller, A., Ristori, T., Duran, C. L., Stassen, O. M. J. A., et al. (2019). Vimentin Regulates Notch Signaling Strength and Arterial Remodeling in Response to Hemodynamic Stress. *Sci. Rep.* 9, 12415. doi:10.1038/s41598-019-48218-w

Vassiliadis, E., Oliveira, C. P., Alvares-Da-Silva, M. R., Zhang, C., Carrilho, F. J., Stefano, J. T., et al. (2012). Circulating Levels of Citrullinated and MMP-Degraded Vimentin (VICM) in Liver Fibrosis Related Pathology. *Am. J. Transl Res.* 4, 403–414.

Viedma-Poyatos, Á., Pajares, M. A., and Pérez-Sala, D. (2020). Type III Intermediate Filaments as Targets and Effectors of Electrophiles and Oxidants. *Redox Biol.* 36, 101582. doi:10.1016/j.redox.2020.101582

Vohnoutka, R. B., Gulvady, A. C., Goreczny, G., Alpha, K., Handelman, S. K., Sexton, J. Z., et al. (2019). The Focal Adhesion Scaffold Protein Hic-5 Regulates Vimentin Organization in Fibroblasts. *MBoC* 30, 3037–3056. doi:10.1091/mbc.e19-08-0442

Vuoriluoto, K., Haugen, H., Kiviluoto, S., Mpindi, J.-P., Nevo, J., Gjerdrum, C., et al. (2011). Vimentin Regulates EMT Induction by Slug and Oncogenic H-Ras and Migration by Governing Axl Expression in Breast Cancer. *Oncogene* 30, 1436–1448. doi:10.1038/onc.2010.509

Walker, J. L., Bleaken, B. M., Romisher, A. R., Alnwibit, A. A., and Menko, A. S. (2018). In Wound Repair Vimentin Mediates the Transition of Mesenchymal Leader Cells to a Myofibroblast Phenotype. *MBoC* 29, 1555–1570. doi:10.1091/mbc.e17-06-0364

Wang, L., Zhang, J., Banerjee, S., Barnes, L., Sajja, V., Liu, Y., et al. (2010). Sumoylation of Vimentin354 Is Associated with PIAS3 Inhibition of Glioma Cell Migration. *Oncotarget* 1, 620–627. doi:10.18632/oncotarget.196

Wang, N., and Stamenovic, D. (2002). Mechanics of Vimentin Intermediate Filaments. *J. Muscle Res. Cell Motil* 23, 535–540. doi:10.1023/a:1023470709071

Wang, P. W., Wu, T. H., Lin, T. Y., Chen, M. H., Yeh, C. T., and Pan, T. L. (2019). Characterization of the Roles of Vimentin in Regulating the Proliferation and Migration of HSCs during Hepatic Fibrogenesis. *Cells* 8, 1. doi:10.3390/cells8101184

Wang, W. Y., Davidson, C. D., Lin, D., and Baker, B. M. (2019a). Actomyosin Contractility-Dependent Matrix Stretch and Recoil Induces Rapid Cell Migration. *Nat. Commun.* 10, 1186.

Yamaguchi, H., Lorenz, M., Kempiak, S., Sarmiento, C., Coniglio, S., Symons, M., et al. (2005). Molecular Mechanisms of Invadopodium Formation. *J. Cell Biol* 168, 441–452. doi:10.1083/jcb.200407076

Yang, C.-Y., Chang, P.-W., Hsu, W.-H., Chang, H.-C., Chen, C.-L., Lai, C.-C., et al. (2019). Src and SHP2 Coordinately Regulate the Dynamics and Organization of Vimentin Filaments during Cell Migration. *Oncogene* 38, 4075–4094. doi:10.1038/s41388-019-0705-x

Yoon, S., and Leube, R. E. (2019). Keratin Intermediate Filaments: Intermediaries of Epithelial Cell Migration. *Essays Biochem.* 63, 521–533. doi:10.1042/ebc20190017

Yu, Q., Xue, Y., Liu, J., Xi, Z., Li, Z., and Liu, Y. (2018). Fibronectin Promotes the Malignancy of Glioma Stem-like Cells via Modulation of Cell Adhesion, Differentiation, Proliferation and Chemoresistance. *Front. Mol. Neurosci.* 11, 130. doi:10.3389/fnmol.2018.00130

Zhang, Y., and Stefanovic, B. (2016). LARP6 Meets Collagen mRNA: Specific Regulation of Type I Collagen Expression. *Ijms* 17, 419. doi:10.3390/ijms17030419

Zacharchenko, T., Barsukov, I., Rigden, D. J., Bennett, D., and Mayans, O. (2016). Biophysical Analysis of the N-Terminal Domain from the Human Protein Phosphatase 1 Nuclear Targeting Subunit PNUTS Suggests an Extended Transcription Factor TFIIS-Like Fold. *Protein. J.* 35, 340–345.

Zhu, Q.-S., Rosenblatt, K., Huang, K.-L., Lahat, G., Brobey, R., Bolshakov, S., et al. (2011). Vimentin Is a Novel AKT1 Target Mediating Motility and Invasion. *Oncogene* 30, 457–470. doi:10.1038/onc.2010.421

Zhu, Y., Zhang, Y., Sui, Z., Zhang, Y., Liu, M., and Tang, H. (2017). USP14 De-ubiquitinates Vimentin and miR-320a Modulates USP14 and Vimentin to Contribute to Malignancy in Gastric Cancer Cells. *Oncotarget* 8, 48725–48736. doi:10.18632/oncotarget.10706

Conflict of Interest: The authors declare that the research was conducted in the absence of any commercial or financial relationships that could be construed as a potential conflict of interest.

Publisher's Note: All claims expressed in this article are solely those of the authors and do not necessarily represent those of their affiliated organizations, or those of the publisher, the editors, and the reviewers. Any product that may be evaluated in this article, or claim that may be made by its manufacturer, is not guaranteed or endorsed by the publisher.

frontiers in Cell and Developmental Biology

ORIGINAL RESEARCH
published: 25 March 2022
doi: 10.3389/fcell.2022.862237

Vimentin Suppresses Inflammation and Tumorigenesis in the Mouse Intestine

Linglu Wang[1], Ponnuswamy Mohanasundaram[2], Michelle Lindström[2], Muhammad Nadeem Asghar[2], Giulia Sultana[2], Julia O. Misiorek[2,3], Yaming Jiu[4,5], Hongbo Chen[1], Zhi Chen[6], Diana M. Toivola[2,7,8], Fang Cheng[1] and John E. Eriksson[2,8]**

[1]School of Pharmaceutical Sciences (Shenzhen), Shenzhen Campus of Sun Yat-sen University, Shenzhen, China, [2]Cell Biology, Biosciences, Faculty of Science and Engineering, Åbo Akademi University, Turku, Finland, [3]Department of Molecular Neurooncology, Institute of Bioorganic Chemistry Polish Academy of Sciences, Poznan, Poland, [4]Key Laboratory of Molecular Virology and Immunology, The Center for Microbes, Development and Health, Institut Pasteur of Shanghai, Chinese Academy of Sciences, Shanghai, China, [5]University of Chinese Academy of Sciences, Beijing, China, [6]Faculty of Biochemistry and Molecular Medicine, University of Oulu, Oulu, Finland, [7]Turku Center for Disease Modeling, University of Turku, Turku, Finland, [8]InFLAMES Research Flagship Center, Åbo Akademi University, Turku, Finland

OPEN ACCESS

Edited by:
Ming Guo, Massachusetts Institute of Technology, United States

Reviewed by:
Suganya Sivagurunathan, Northwestern University, United States
Yiwei Li, Huazhong University of Science and Technology, China

***Correspondence:**
Fang Cheng
chengf9@mail.sysu.edu.cn
John E. Eriksson
john.eriksson@abo.fi

Specialty section:
This article was submitted to Cell Growth and Division, a section of the journal Frontiers in Cell and Developmental Biology

Received: *25 January 2022*
Accepted: *22 February 2022*
Published: *25 March 2022*

Citation:
Wang L, Mohanasundaram P, Lindström M, Asghar MN, Sultana G, Misiorek JO, Jiu Y, Chen H, Chen Z, Toivola DM, Cheng F and Eriksson JE (2022) Vimentin Suppresses Inflammation and Tumorigenesis in the Mouse Intestine. Front. Cell Dev. Biol. 10:862237. doi: 10.3389/fcell.2022.862237

Vimentin has been implicated in wound healing, inflammation, and cancer, but its functional contribution to intestinal diseases is poorly understood. To study how vimentin is involved during tissue injury and repair of simple epithelium, we induced colonic epithelial cell damage in the vimentin null ($Vim^{-/-}$) mouse model. $Vim^{-/-}$ mice challenged with dextran sodium sulfate (DSS) had worse colitis manifestations than wild-type (WT) mice. $Vim^{-/-}$ colons also produced more reactive oxygen and nitrogen species, possibly contributing to the pathogenesis of gut inflammation and tumorigenesis than in WT mice. We subsequently describe that $CD11b^{+}$ macrophages served as the mainly cellular source of reactive oxygen species (ROS) production *via* vimentin-ROS-pSTAT3–interleukin-6 inflammatory pathways. Further, we demonstrated that $Vim^{-/-}$ mice did not develop colitis-associated cancer model upon DSS treatment spontaneously but increased tumor numbers and size in the distal colon in the azoxymethane/DSS model comparing with WT mice. Thus, vimentin has a crucial role in protection from colitis induction and tumorigenesis of the colon.

Keywords: vimentin, colon, dextran sodium sulfate, inflammation, tumorigenesis

INTRODUCTION

Abundant evidence reveals links between wound healing and cancerous tumor growth in a variety of common epithelial tumors (Dvorak, 1986) (Ben-Neriah and Karin, 2011). One good example is inflammatory bowel disease (IBD). Patients suffering from IBD with tissue damage and chronic mucosal inflammation are predisposed to the development of colorectal cancer (CRC), one of the most common malignancies in the world (Grivennikov et al., 2010a; Parent et al., 2010; Xie et al., 2020). Various cytokines and chemokines promote a localized inflammatory response upon intestinal injury and alter proliferation or survival of premalignant cells, thereby promoting oncogenesis (Newkirk et al., 2007).

Vimentin, the major type III intermediate filament protein prominently expressed throughout mesenchymal cell types, is strongly upregulated following injury to various tissues (Ivaska, 2011; Satelli and Li, 2011; Gan et al., 2016). Vimentin acts as a signal scaffold and functional determinants for many

signaling pathway involved in cell migration during wound repair (Chernoivanenko et al., 2013; Chung et al., 2013). Loss of vimentin leads to delayed wound healing due to impaired directional migration and contraction (Eckes et al., 1998; Eckes et al., 2000; Ivaska et al., 2007; Dave and Bayless, 2014). Vimentin in mesenchymal repair cells is associated with myosin IIB and modulates the collective migration of the lens epithelium in response to wounding (Menko et al., 2014). Induction of vimentin by the TGFβ1-Smad pathway in alveolar epithelial cells is a requisite for wound repair after lung injury (Rogel et al., 2011).

Vimentin has been indicated to modulate cell fate and cellular function of immunocytes. For instance, vimentin is cleaved by caspases in apoptotic neutrophils and is then found to be expressed on the surface of the apoptotic neutrophils (Lavastre et al., 2002). This may be a recognition signal of apoptotic neutrophils by phagocytes for the inflammatory resolution (Moisan and Girard, 2006). Pronounced reorganization of the vimentin network during circulating lymphocyte extravasation is a primary structural supporting source of lymphocytes, which limits mechanical deformation of the cells upon chemokine-induced polarization and stimulates cells migrating through size-limited endothelium pores (Brown et al., 2001). N-terminal phosphorylation and reorganization of vimentin by the PI3Kγ signaling pathway are necessary for chemokine-induced transmigration of leukocytes to the inflammation sites (Barberis et al., 2009).

The importance of vimentin in inflammation and the immune response became more evident from several studies on the vimentin knockout ($Vim^{-/-}$) mouse model. Although $Vim^{-/-}$ mice develop and reproduce without any devastating defects, it was found that they have leaky endothelial vessels and disrupted homing of lymphocytes (Nieminen et al., 2006). Interestingly, there is disturbed distribution of the adhesion molecules in both migrating and the receiving cells, such as integrins in the lymphocytes and intercellular cell adhesion molecule-1 and vascular cell adhesion molecule 1 in endothelial cells. The lack of vimentin either in lymphocytes or in endothelial cells severely impaired transcellular migration of lymphocytes through endothelial cell barriers (Nieminen et al., 2006).

Interestingly, vimentin may also participate in the pro-inflammatory responses required for elimination of bacterial infections, especially the production of reactive oxygen species (ROS) and nitric oxides species from macrophages upon epithelial injury of the gut (Mor-Vaknin et al., 2013; Mahesh et al., 2016). Recently, vimentin was found to directly interact with the inflammasome NLRP3 and regulate its activation in acute lung injury models. Loss of vimentin inhibits the activation of NLRP3 inflammasome signaling and cytokine production and thereby inhibits the pathophysiologic events upon injury, including lung inflammation, leaky endothelial, and alveolar epithelial barriers (Dos Santos et al., 2015; Zhou et al., 2020). However, different results in murine air pouch model suggested that vimentin is dispensable to establish an acute inflammatory response *in vivo*, indicating that the specificity of vimentin in regulation of inflammation is likely to be different *in vivo* different models (Moisan et al., 2007; Pan et al., 2021), probably due to complex crosstalk among microbiota, organic barriers, and immune system in the wound repair.

In our recent study, by integrating defined *in vitro* and *in vivo* models of epidermal wound healing, we found that vimentin IFs coordinate balanced signals regulating fibroblast proliferation and epithelial-to-mesenchymal transition, two significant cellular activities in wound repairing process. The absence of vimentin inhibited these cellular processes, causing a delayed wound re-epithelialization and chronic inflammation in the injured lesions (Cheng et al., 2016). Therefore, we are interested whether loss of vimentin induces chronic inflammation upon injury of other types of epitheliums, such as the intestine, and whether it would provide a permissive environment for tumor onset in the colon.

To test this hypothesis, we applied a well-known dextran sodium sulfate (DSS)–induced colitis model and an azoxymethane (AOM) plus DSS colitis-associated cancer (CAC) model to $Vim^{-/-}$ mice. We showed that the deletion of vimentin increases the level of ROS derived from macrophages *via* the vimentin-ROS-pSTAT3–interleukin-6 (IL-6) inflammatory pathways. Furthermore, $Vim^{-/-}$ mice have increased tumor size and number in the distal colon comparing with WT mice, which indicates that vimentin has a crucial role in colitis induction and tumorigenesis of the colon.

RESULTS

Increased Persistent Inflammation in Vimentin Null Mice During Chemical Intestinal Tissue Damage

First, we employed an intestine wound model to explore whether the delayed wound healing and prolonged inflammation phenotype that we observed during skin tissue damage with loss of vimentin (Cheng et al., 2016) can be recapitulated in a simple epithelium. In this chronic colitis model, 2.5% dextran sulfate sodium (DSS) is toxic to the colonic epithelial cells and induces tissue damage. After DSS-induced injury for 7 days, the mice are given 14 days of a water regimen to repair the colon epithelium, and this process is repeated to form three injury-healing cycles. In this model, following every round of wounding of the colon, the peak of disease (rectal bleeding, diarrhea, and weight loss) occurred during each healing period. Consistent with our hypothesis, $Vim^{-/-}$ mice subjected to DSS treatment exhibited a more dramatic weight loss, a higher rate of mortality, and increased blood in the stool (**Figures 1A–D**). In contrast, WT mice exposed to the same treatment had only mild weight loss, minor levels of blood in the stool, and no mortality (**Figures 1A–D**), indicating loss of vimentin inflames intestine upon injury. In line with these data, histologic images from colon sections of $Vim^{-/-}$ mice showed severe ulceration in gut mucosal lining, compared to WT (**Figure 1E**). Thus, these data support our hypothesis that endogenous vimentin is involved to a prompt colonic repair and to alleviate the injury-induced inflammation program.

Lack of Vimentin Increases ROS/RNS–NF-κB–IL-6 in the Colon Primarily by Macrophages

Previous work showed that vimentin modulates the production of ROS and nitrogen species (RNS), an important part of tissue

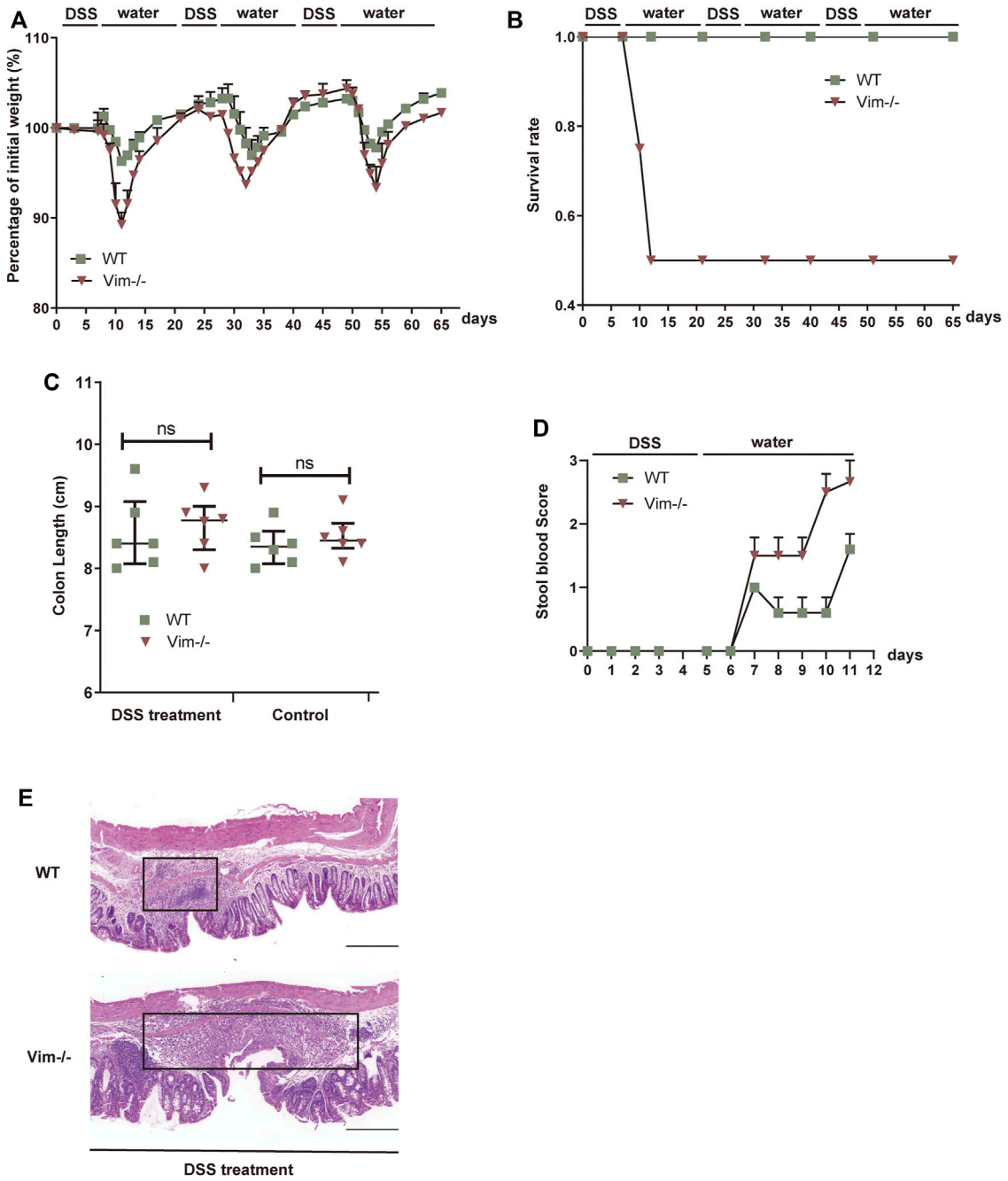

FIGURE 1 | Lack of vimentin promotes DSS-induced colitis. **(A–C)** Vimentin null ($Vim^{-/-}$) and wild-type (WT) mice were fed with 2.5% DSS or water for 7 consecutive days and then maintained with water for 14 days for three cycles. The mice were monitored for **(A)** body weight loss, **(B)** survival rate, and **(C)** total colon length after sacrificing at day 65. **(D)** $Vim^{-/-}$ and WT mice were fed with 2.5% DSS for 5 consecutive days, and stool blood scores from day 0 to day 11 were assigned as follows: 0, no blood; 1, positive hemoccult; 2, visible traces of blood; 3, gross rectal bleeding. **(E)** Representative pictures of Hematoxylin and Eosin staining of WT and $Vim^{-/-}$ mouse colon at day 65 upon 3× DSS induction or untreated ones (Control). Scale bar, 500 μm. Black box indicates the inflamed tissue area. n= 6, bars = mean ± SEM in all figure graphs; *, $p < 0.05$; **, $p < 0.01$; ***, $p < 0.001$.

damage and the inflammatory response (Tolstonog et al., 2001; Zhang et al., 2001). To address whether loss of vimentin could exacerbate the oxidative stress in the mouse colon upon DSS wounding, we used the chemiluminescent probe L-012, a ROS/RNS-sensing probe (Kielland et al., 2009; Asghar et al., 2014) for noninvasive imaging of ROS/RNS production in living mice. L-012 can be widely distributed and spatially and temporally emit light responding to inflammation sites. The L-012–indicating luminescence was later recorded by an ultrasensitive CCD camera (IVIS Spectrum, Xenogen, CA, USA). Strong

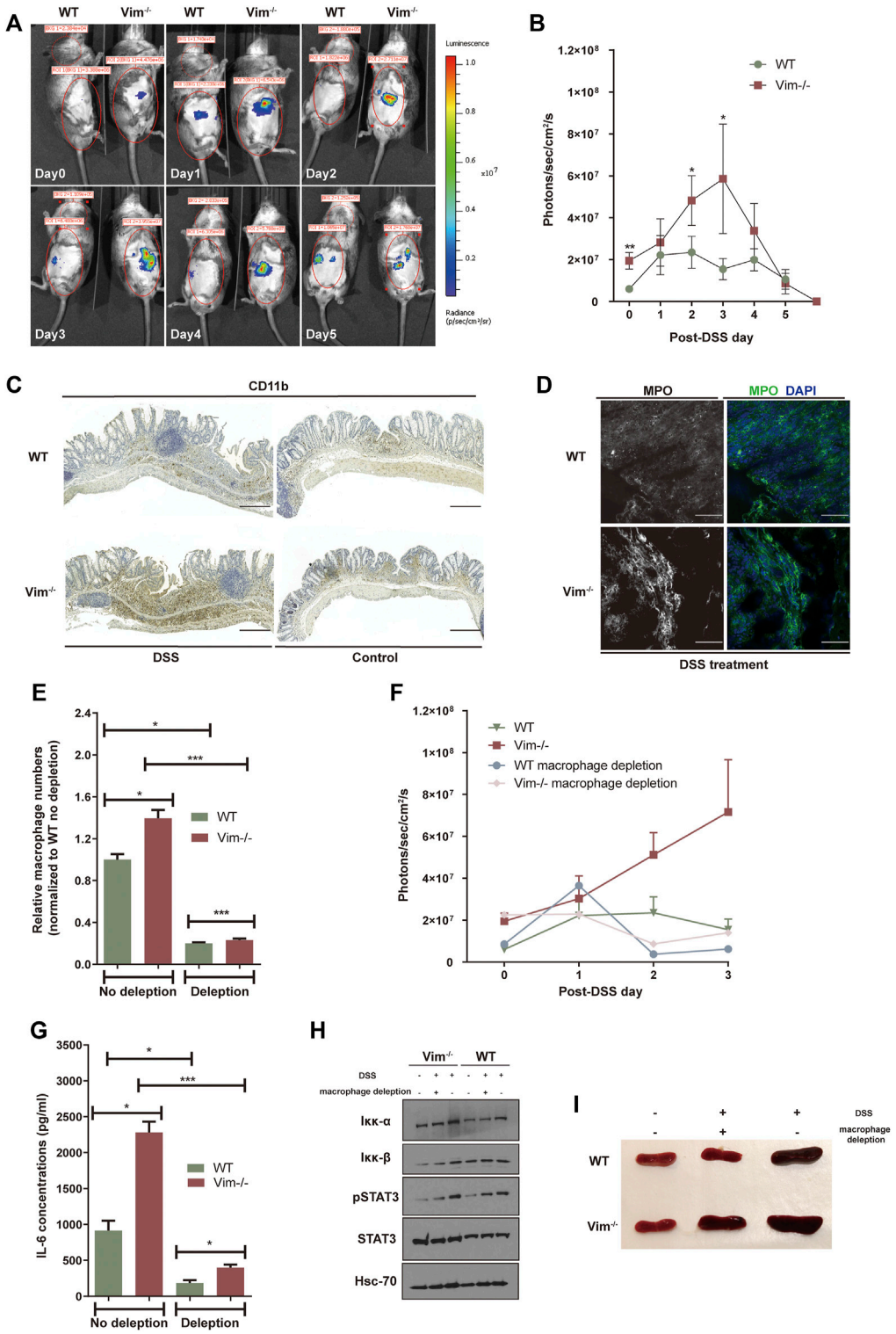

FIGURE 2 | Lack of vimentin increases ROS in the colon primarily by macrophages. **(A,B)** DSS (2.5%) were administered to Vim$^{-/-}$ and WT mice for 7 consecutive days from - day 1. Luminescent images **(A)** were taken from day 0 to day 5 upon DSS treatment after injection with L-012 and average luminescence values **(B)** were counted. Bars = mean ± SEM, n = 12. The pseudo colors represent photons/s cm^2 sr. time dependency of the L-012 luminescent signal. **(C,D)** DSS (2.5%) were administered to Vim$^{-/-}$ and WT mice for 7 consecutive days, followed by 8 days off water without DSS. Representative images and quantitation of **(C)** CD11b-labeling and **(D)** MPO-labeling of the colon samples on day 15 of the experiment. Scale bars, 500 µm. In panels B and D, bars = mean ± SEM, n = 6. **(E)** Peritoneal macrophage numbers in DSS-induced WT and Vim$^{-/-}$ mice upon depletion of macrophages in the circulation using clodronate liposomes or control liposomes. Bars = mean ± SEM, n = 3. **(F)** *In vivo* luminescence values in different timepoints of mice injected with L-012 upon DSS treatment and macrophage depletion. Bars = mean ± SEM, n = 3. **(G)** IL-6 concentration in the circulation of DSS-induced WT and Vim$^{-/-}$ mice upon macrophage depletion. Bars = mean ± SEM, n = 3. **(H)** Immunoblotting of Ikk-α, Ikk-β, pStat3, Stat-3, and Hsc-70 expression of total colon tissue lysates. **(I)** Representative spleen size of DSS-induced WT and Vim$^{-/-}$ mice.

luminescent signals observed from colon regions corresponded to inflammation in WT and $Vim^{-/-}$ colon regions, which peak on 3 days post 2.5% DSS oral administration (**Figures 2A,B**). However, $Vim^{-/-}$ mice were found to release higher levels of luminescence signals and thus to produce significantly more ROS/RNS than that WT mice in response to stimulation with DSS (**Figures 2A,B**). Thus, vimentin is crucial for regulating ROS/RNS upon DSS-induced tissue damage.

We next aimed to identify the cellular source of ROS and downstream inflammatory signaling in the colon. DSS is toxic to the epithelial cells in the crypts of the colonic mucosa and is commonly used to induce tissue damage *via* the mediation of inflammation (Wirtz et al., 2007). Therefore, upon DSS stimulation, ROS in the intestines may derive from macrophages and regional microflora (Formentini et al., 2017). Identified by anti-CD11b staining, we found that myeloid cells became detectable in colon sections of both WT and $Vim^{-/-}$ mice already 7 days after DSS induction, followed by the appearance of localized inflammatory cells in histology on day 15 (**Figure 2C**). Furthermore, we also observed more $CD11b^{+}$ monocytes or macrophages infiltrated in KO colon lamina propria (**Figure 2C**). Correspondingly, myeloperoxidase (MPO), an important enzyme with phagocytic lysis activity secreted by monocytes, exhibits strong cytoplasmic signals in $Vim^{-/-}$ colons compared to the WT group (**Figure 2D**). Thus, monocytes/macrophages were more abundant in the $Vim^{-/-}$ leukocyte population than in the WT population, and their overall contribution to phagocytic enzyme MPO production was greater (**Figure 2D**).

We next asked whether macrophages would be necessary for this inflammatory signaling. We found depletion of macrophage in the circulation using clodronate liposomes largely inhibited the peritoneal macrophages numbers in DSS-induced WT and $Vim^{-/-}$ mice to a similar level (**Figure 2E**). Interestingly, depletion of macrophages has significantly impaired the upregulation of ROS/RNS-dependent luminescent signal *in vivo* (**Figure 2F**), suggesting that macrophages are the major cell component generating ROS/RNS during DSS-induced inflammation.

As shown in **Figure 2F**, after macrophage depletion, the peak level of ROS/RNS was reduced, compared with the no-depletion control group in $Vim^{-/-}$ mice. These data suggest that the accumulation of ROS/RNS in the wound of $Vim^{-/-}$ mice after intestinal injury mainly results from the recruited macrophages. This was consistent with previous studies showing that monocytes lacking vimentin produce more superoxide and nitric oxide and thereby activate several intracellular signaling cascades that lead to proinflammatory genes activation (Mor-Vaknin et al., 2013).

Furthermore, it is likely that resident macrophages or macrophages transported to the inflammation site could be responsible to produce proinflammatory cytokines in these lesions. In line with this hypothesis, analysis of cytokine productions in circulation demonstrated a significantly reduced level of IL-6 concentration in $Vim^{-/-}$ and WT group upon macrophage depletion, although $Vim^{-/-}$ mice still maintains a relatively higher level of IL-6 concentration than WT group after macrophage depletion (**Figure 2G**). Consistently, immunoblot analysis of total colon tissue lysates revealed the substantial increase of STAT3 phosphorylation and NF-κB induction in DSS-treated WT and $Vim^{-/-}$ mice (**Figure 2H**). Furthermore, $Vim^{-/-}$ mice develop stronger splenomegaly than WT upon DSS induction, and we found that systemic depletion of macrophages prevented the development of splenomegaly in these mice (**Figure 2I**). Thus, enhanced cytokine secretion by macrophages, at least in part, induced $Vim^{-/-}$ mice from DSS-induced colitis.

Deletion of Vimentin Increases Colitis-Associated Tumor Incidence

To test whether the deletion of vimentin is prone to chronic injury-associated cancer, we introduced a AOM plus DSS colitis-associated colorectal model to resemble the pathology of human colitis-associated neoplasia (Tanaka et al., 2003; Becker et al., 2004). In this model, tumor initiation depends on metabolic activation of AOM, a colon-specific carcinogen (Neufert et al., 2007) and tumor development is promoted by DSS induced tissue damage and inflammation. To support our hypothesis, tumor development was strongly accelerated with significantly increased tumor number and size in $Vim^{-/-}$ mice comparing to their wild-type (WT) counterparts (**Figures 3A,B**). For up to 75 days of treatment (12 days after the last treatment cycle), very few neoplastic lesions were observed in the WT colons by histopathological examination. However, by the same time, low-grade dysplastic lesions were apparent the majority of $Vim^{-/-}$ mice and, correspondingly, in average tumor load, the diameters of all tumors in a given mouse (Yilmaz and Christofori, 2009) was significantly higher in $Vim^{-/-}$ mice (**Figures 3A,B**). The absence of vimentin had a stronger effect on tumor number and size 100 days upon the treatment (**Figure 3B**). By day 100, multifocal adenoma was seen in both $Vim^{-/-}$ and WT colons, encompassing epithelium areas with low- and high-grade flat dysplasia. Notably, tumor morphology was similar between $Vim^{-/-}$ and WT control mice (**Figure 3C**). Throughout the entire period, no invasive carcinoma (the cancerous glands penetrated the submucosa or desmoplastic reaction of the surrounding stroma) were detected in any WT or $Vim^{-/-}$ mouse. Gross assessment of the colon tumors by histopathological examination also revealed a more severe tumor score (**Figure 3D**) in $Vim^{-/-}$ mouse. Interestingly, in mice treated with AOM only, no tumors were observed in both WT and $Vim^{-/-}$ mice (**Supplementary Table S1**), suggesting that, in our mouse model, inclusion of a chemical carcinogen is not enough to switch the response toward a different course with pathological and molecular features commonly observed in sporadic human CAC. Besides, we found that consistent with the chronic colitis model, in the colitis-related cancer model, $Vim^{-/-}$ mice also exhibit more severe inflammatory symptoms (**Figures 3E–G**) than WT mice. Inflammatory cells, which often infiltrate tumors and preneoplastic lesions, produce a variety of cytokines and chemokines that propagate a localized inflammatory response (Pikarsky et al., 2004; Stojadinovic et al., 2008). We found that $CD11b^{+}$

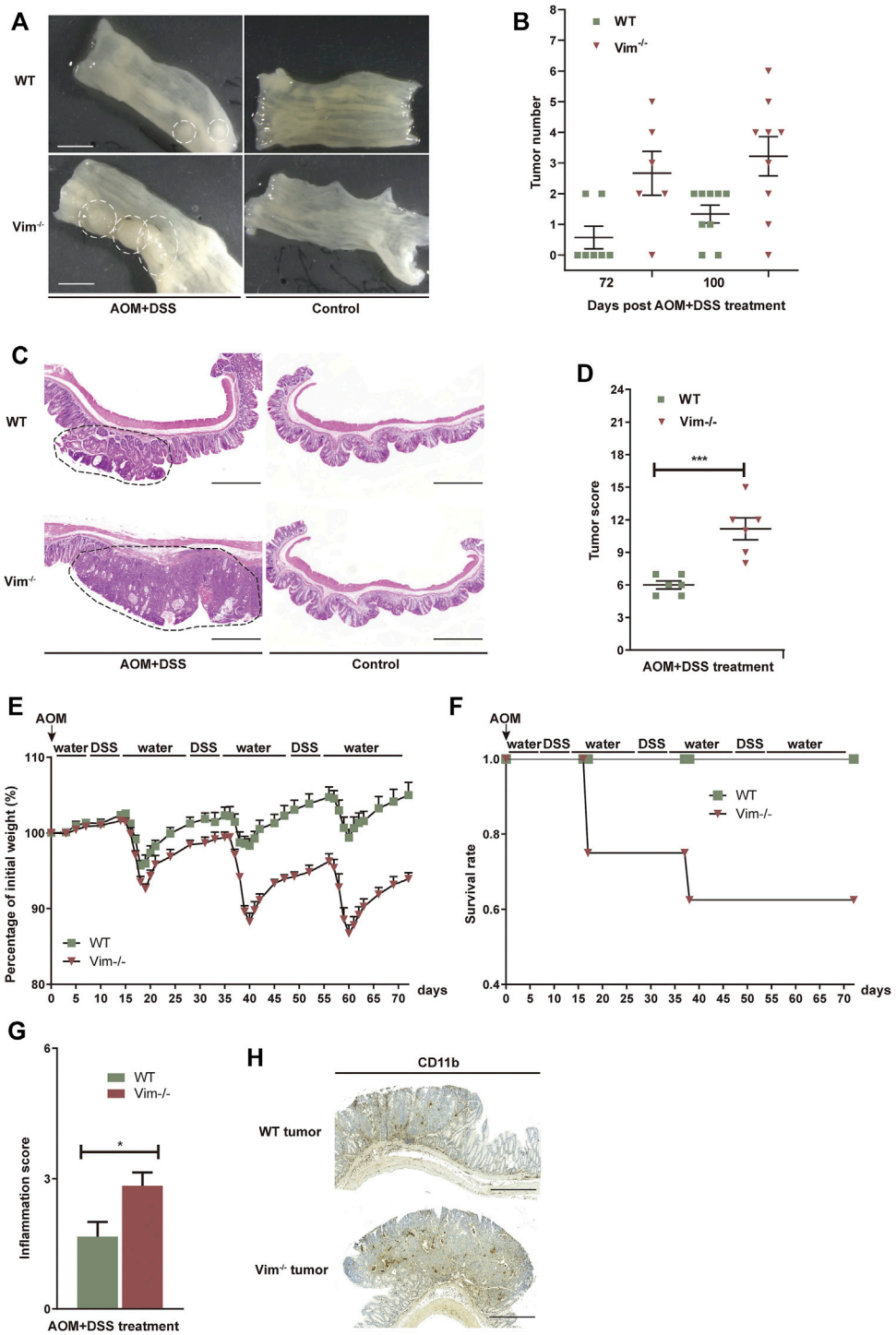

FIGURE 3 | Increased tumorigenesis in vimentin null mice in a colitis-associated colon cancer model. **(A)** Representative macroscopic view of WT and Vim$^{-/-}$ mouse colon on day 75 upon AOM + DSS induction. Scale bar, 1 mm. **(B)** Colitis-associated colorectal was induced *via* injection of AOM (7.5 mg/kg) and three cycles included 2% DSS feeding for 7 days and water for 14 days. The tumor numbers per mouse colon between WT and Vim$^{-/-}$ mice on day 75 and day 100 were recorded cumulatively from three independent experiments. Each dot represents one mouse. Lines indicate mean ± SEM. $n = 24$ **(C)** Representative pictures of Hematoxylin and Eosin staining of WT and Vim$^{-/-}$ mouse colon on day 100 upon AOM + DSS induction or untreated ones (Control). Scale bar, 500 μm. **(D)** Tumor score between WT and Vim$^{-/-}$ colons. $n = 6$. **(E,F)** Vim$^{-/-}$ and WT mice during AOM + DSS treatment in colitis-associated colon cancer model were monitored for body weight loss and the survival during the 72 days of treatment. **(G)** These mice from colitis-associated colon cancer model were sacrificed at day 72 and histological scores of colon tumor sections were determined on the basis of the colitis index. **(H)** Representative images and quantitation of CD11b-labeling of the colon tumor samples.

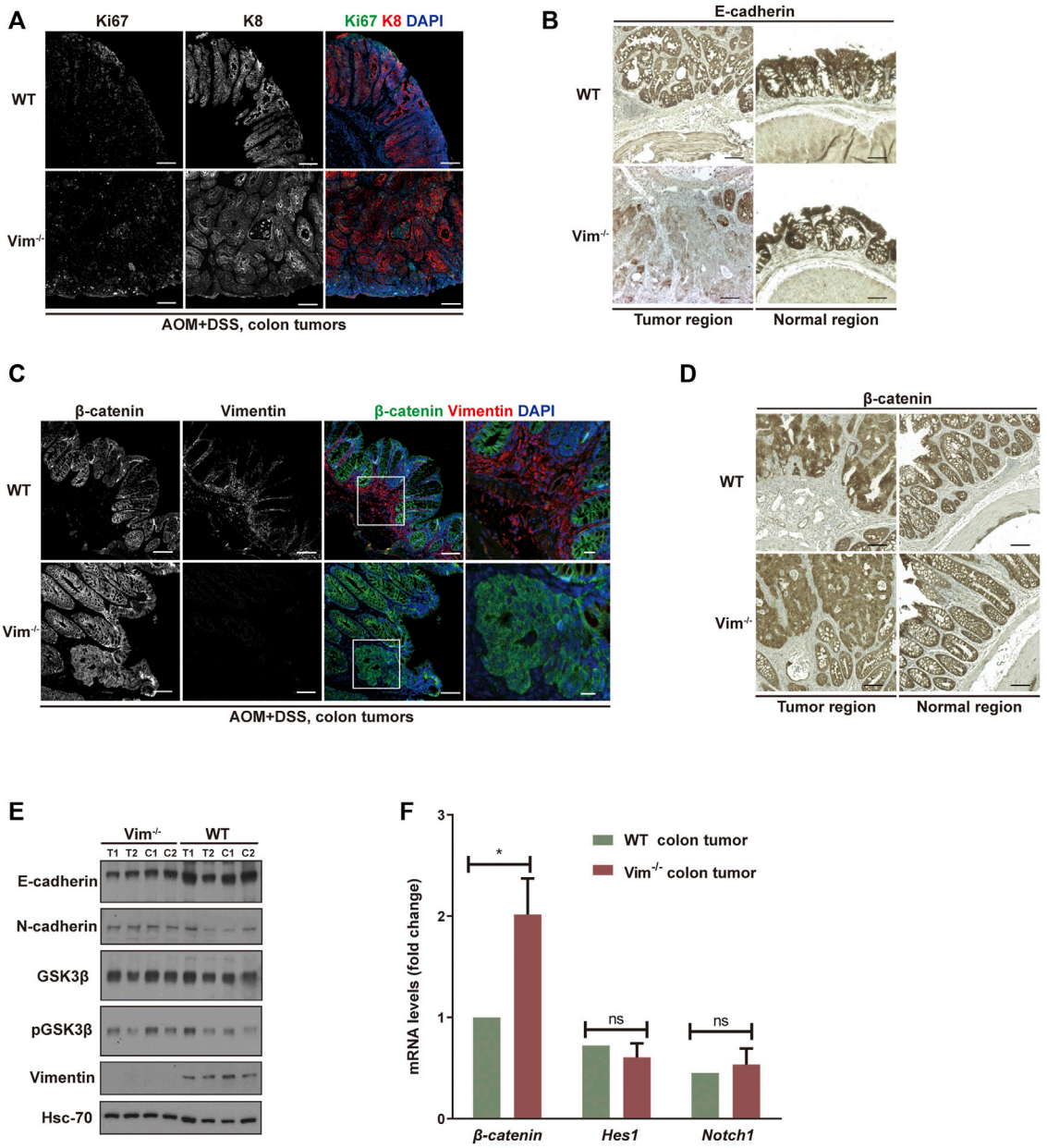

FIGURE 4 | Increased proliferation and tumor grade in Vim$^{-/-}$ cancer. **(A)** Representative confocal images indicated the expression of ki67 (in green), K8 (in red), and DAPI (in blue) in WT and Vim$^{-/-}$ colon tumors upon AOM and DSS treatment. **(B)** Representative pictures of tumors and their neighboring normal regions by immunohistochemical labeling of E-cadherin of WT and Vim$^{-/-}$ mouse colon upon AOM + DSS induction. **(C)** Representative confocal images of the expression of β-catenin (in green), vimentin (in red), and DAPI (in blue) in WT and Vim$^{-/-}$ colon tumors upon AOM and DSS treatment. **(D)** Representative pictures of tumors and their neighboring normal regions by immunohistochemical labeling of β-catenin of WT and Vim$^{-/-}$ mouse colon upon AOM + DSS induction. Scale bar (A–D), 200 μm. **(E)** Extracts (30 μg) from colon tumors of WT and Vim$^{-/-}$ mice were immunoblotted with anti–E-cadherin, anti–N-cadherin, anti–GSK-3β, anti–P-GSK-3β, or anti-vimentin. Hsc-70 blotted from the lysates to control for equal loading. **(F)** Quantitative real-time PCR (qRT-PCR) analysis of transcripts for β-catenin, Hes-1, and Notch-1 in WT and Vim$^{-/-}$ mouse colon tumors. Error bars = ± SEM; n =6; *, $p < 0.05$; ns, not significant.

macrophages were accumulated in tumor regions of WT and Vim$^{-/-}$ colon cancer samples (**Figure 3H**) similar to after DSS treatment in **Figure 2C**, suggesting that loss of vimentin not only may increase susceptibility to inflammation but also may greatly accelerate inflammation-associated colon cancer. Together, these data indicate that vimentin is a negative regulator for both tumor initiation and tumor growth in CAC. Vimentin deficiency leads to accelerated and

increased tumorigenesis in this colitis-associated colon cancer model.

Increased Proliferation and Tumor Grade in $Vim^{-/-}$ Cancer

We further assessed colon neoplasia lesions characterized by several features of incipient malignant disease, including irregular architecture/expansion of the colonic crypts, co-expression of epithelial and mesenchymal markers, and activation of β-catenin. We confirmed the loss of vimentin expression in $Vim^{-/-}$ colons *via* immunofluorescence and Western blotting analysis (**Figures 4C,E**). In addition, the analysis showed that the tumors come from the intestinal epithelium indicated by intact epithelial keratin 8 (K8) expressions in WT and $Vim^{-/-}$ tumor lesions in mice (**Figure 4A**). Proliferation marker Ki67 labeling suggests that the proliferation rate of tumor cells was higher in $Vim^{-/-}$ mice than WT mice (**Figure 4A**), but no obvious difference in basal crypt proliferation was revealed between control WT and $Vim^{-/-}$ mice. This was accompanied with the down-modulation of E-cadherin, a differentiation marker important for epithelium barrier function in $Vim^{-/-}$ tumors (**Figure 4B**). Parallel Western blotting analysis confirmed decreased E-cadherin and slight upregulation of N-cadherin in tumor regions of $Vim^{-/-}$ mice (**Figure 4E**). Wnt pathway activation is markedly frequent in human CAC, mostly involving early adenomatous polyposis coli mutations (Krieglstein et al., 2001). Notch pathway is another common signaling pathway involved in CAC development. Remarkably, regardless of genotype, nuclear and cytoplasmic β-catenin accumulation predominated in these tumors (**Figures 4C,D**), consistent with the frequent induction of β-catenin transcripts in $Vim^{-/-}$ tumors (**Figure 4F**), which is indicative of robust Wnt pathway activation. In contrast, in WT tumors, β-catenin was retained at the plasma membrane, suggesting a relative inactive Wnt pathway in these WT neoplasms. No obvious changes in Notch signaling were detected on the basis of the qPCR analysis of Notch1 and its target gene Hes1 between WT and $Vim^{-/-}$ tumors (**Figure 4F**). In sum, both histologically and molecularly, the DSS mouse model of IBD-associated cancer closely reproduces features frequently observed in its human counterpart, and there is an increased proliferation and tumor grade in $Vim^{-/-}$ cancer.

DISCUSSION

CRC is a multifactorial human disease that develops slowly over time as a result of inflammation and/or accumulation of mutations (Roper et al., 2013). We postulated upon our data that vimentin is a potent factor to participate in maintaining the homeostasis of cell and tissue and, in doing so, protect colonic epithelial tissues from inflammation and cancer and further may facilitate intestinal repair. The increased tumor burden of $Vim^{-/-}$ mice in the colitis-associated caner model is due to a delayed wound healing and the increased susceptibility to DSS-induced chronic colitis. This is in line with the stress-protective functions of intermediate filaments proteins particularly under regenerative conditions in many tissues (Toivola et al., 2010).

No tumors developed in the non-inflammatory AOM cancer model in $Vim^{-/-}$ mice, which is consistent with the earlier report that the absence of vimentin has no discernible effect on tumorigenesis in a teratocarcinoma model (Colucci-Guyon et al., 1994). Our data indicates that $Vim^{-/-}$ mice are more susceptible to DSS-induced colitis, and the chronic inflammation microenvironment may be a key tumor promoter. Vimentin has been reported to promote, to inhibit, or to have no effect in inflammation in different tissue injury models, indicating the context and model specificity of vimentin (Mor-Vaknin et al., 2003) (Mor-Vaknin et al., 2013) (Moisan et al., 2007) (Dos Santos et al., 2015). Furthermore, using the subcutaneous air pouch model in the back of mice, the $Vim^{-/-}$ mouse appears to have normal acute inflammatory response to lipopolysaccharide (LPS) or IL-21 stimulation (Moisan et al., 2007), indicating the specificity of vimentin regulation of inflammation in different *in vivo* models.

Vimentin was recently shown to be involved in the experimental murine colitis (Mor-Vaknin et al., 2013). However, their findings from earlier results suggest that vimentin secreted by activated human macrophages participates in the bacterial killing and the generation of oxidative metabolites (Mor-Vaknin et al., 2003). We found that, in the same experimental acute colitis model, $Vim^{-/-}$ mice are likely more capable to mediate bacterial killing by abundant production of ROS and nitric oxides from macrophages (Mor-Vaknin et al., 2013). In addition, increased ROS and other oxidative damage may stimulate gut inflammation and the development of IBDs, but these $Vim^{-/-}$ mice exhibited less gut inflammation and intestine disease (Mor-Vaknin et al., 2003). Therefore, we suspect that the complex crosstalk between microbiota, intestinal barrier, and immune system in the wound repair may vary from one laboratory from another (Peterson and Artis, 2014).

Inflammatory responses play decisive roles at different stages of tumor development. Many environmental causes of cancer and risk factors are associated with some form of chronic inflammation. Prolonged exposure of irritants in some organs, such as DSS in colon, prepares an inflammatory breeding ground for tumor development, since chronic inflammatory responses can promote tumor progression and metastatic spread, cause local immunosuppression, and further augment genomic instability (Grivennikov et al., 2010b). Our study demonstrated that vimentin knockout enhance inflammatory responses, such as the accumulation of ROS and the recruitment of $CD11b^{+}$ macrophages and monocytes in the colon. Brought with this enhancement, inflammation-induced mutagenesis and tumor suppression may occur in the injured colon, which benefit tumor initiation. Once initiated cells appear, the depletion of vimentin may break the balance of inflammation-associated protumorigenic and antitumorigenic effects, thus promoting the tumor growth. In this process, some signaling pathways intimately involved are activated, such as Wnt/GSK3β/β-catenin pathways. Our study showed a slight increase of GSK3β phosphorylation,

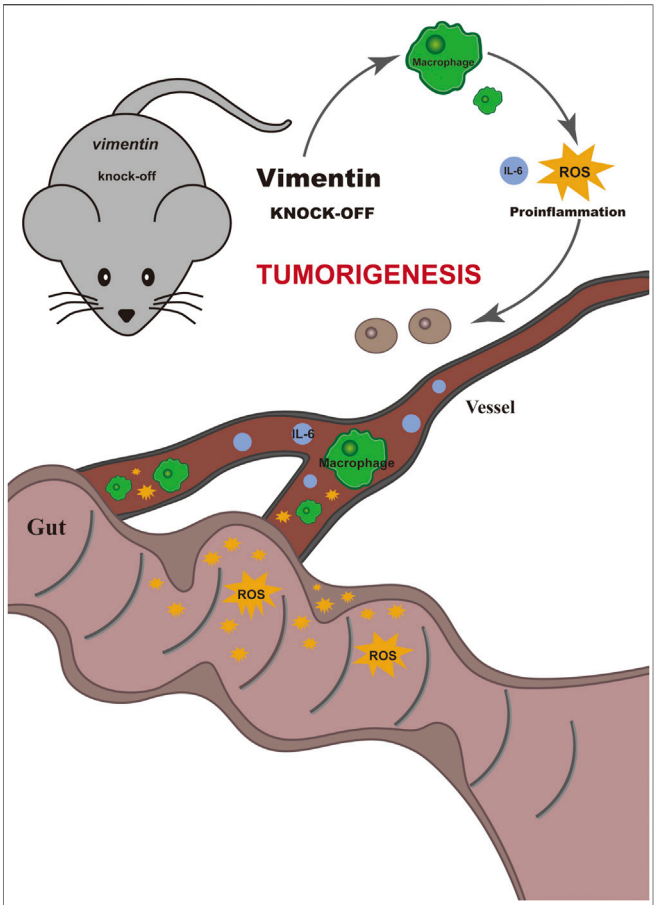

FIGURE 5 | Schematic illustrate the mechanism of vimentin protecting the intestinal epithelium from inflammation and promoting tumorigenesis. The loss of vimentin *in vivo* leads to susceptibility to develop colitis-associated colorectal cancer upon the combination of AOM carcinogen treatment and DSS inflammatory injury, whereas the deletion of vimentin alone does not predispose to colitis-associated colorectal cancer.

which inhibits GSK3β activity as a kinase and decreased the phosphorylation of its targeted protein, β-catenin, in the tumor of vimentin null mice. This reduced phosphorylation provided β-catenin from being ubiquitinated and regraded in proteasomes and further induced β-catenin accumulation. Other pathways including NF-κB and STAT3 signaling accelerated the transcription of β-catenin, thus resulting in a high level of β-catenin. The accumulation subsequently would induce epithelial mesenchymal transition and promote tumor invasion.

In summary, our data indicate that vimentin is a factor important for protecting the intestinal epithelium from inflammation and tumorigenesis promotion. We showed here that the loss of vimentin *in vivo* leads to susceptibility to develop colitis-associated CRC upon the combination of AOM carcinogen treatment and DSS inflammatory injury, whereas the deletion of vimentin alone does not predispose to colitis-associated CRC (**Figure 5**).

MATERIALS AND METHODS

Animals

All animals involved in studies are reported in accordance with the ARRIVE (Animal Research: Reporting of *In Vivo* Experiments) guidelines for reporting experiments involving animals (Kilkenny et al., 2010; McGrath et al., 2010). The specific pathogen–free mice are maintained at the Central animal Laboratory at University of Turku under permit 7284/04.10.03/2012 of the Ethical Committee for Animal Experiments of the University of Turku. Animal were kept under standard conditions during the whole experiments. Vimentin heterozygous mice with a mixed background of C57BL/6 and SVJ/129 were used to generate vimentin deficient homozygotes ($Vim^{-/-}$) and WT offspring (Colucci-Guyon et al., 1994). The genotypes of the mice were determined by PCR genotyping methods (Truett et al., 2000). Ten- to 12-week-old mice were used for the experiments. Mice in experiments including controls were cohoused littermates. Animal experiments were performed under the approved animal study protocols 2893/04.10.03/2011 and 2007-07005 by the State Provincial Office of South Finland and housed in Turku Central Animal facility, Finland.

Experimental Procedures and Animal Weight

For the AOM plus DSS colitis-associated colorectal model, briefly on day 0, mice were injected intraperitoneally (i.p.) with a single dose of AOM (7.5 mg/kg; Sigma) and then maintained on regular diet and water for 7 days. On day 7, mice were fed with 2% dextran sulfate sodium (DSS; TdB Consultancy; dissolved in water) for 7 days and maintained on autoclaved water for 14 days as a cycle. This 2% DSS-autoclaved water treatment cycle was conducted for two more times later (Wirtz et al., 2007).

For the AOM CRC model, the mice were injected i.p. once a week with AOM (7.5 mg/kg) for 4 weeks and sacrificed.

For the chronic colitis model, mice were fed with 2.5% DSS for 7 days and later maintained on autoclaved water for 14 days for two more times.

Mouse body weights were monitored daily during DSS treatment and weakly during water treatment. The clinical course of disease was followed by changes of body weight and monitoring for signs of rectal bleeding or diarrhea. At the end of the experiment, the mice were sacrificed, and samples from small intestine and colon (proximal colon and distal colon) were collected for further analysis as described below.

Tumor Scoring

Tumor scoring was analyzed with indicators as follows: mucosal ulceration; hyperplasia or colonic tumors; erosion, crypt loss, or abscess; colitis (inflammatory cells infiltration into the lamina propria mucosa); and edema. Severity scores ranged from 0 to 5 as follows: 0, within normal limits or absent; 1, minimal; 2, mild; 3, moderate; 4, marked; and 5, severe. Scores of every indicators were added together to get a total score as tumor scoring.

Sample Collection and Analysis

Mice were sacrificed using carbon dioxide inhalation and subsequent cervical dislocation. Colon was opened lengthwise and divided into 4 parts. The colon samples were imaged by a Leica M60 microscope (Leica, Mannheim, Germany) for polyp or tumor counting. Macroscopic tumors (adenomas, polyps, or colonic aberrant crypt foci) were counted and measured with a caliper.

Tissue samples were collected from distal colon and snap frozen in liquid nitrogen for RNA extraction (RNAlater, Ambion) or protein extraction.

Colon samples were fixed in 4% paraformaldehyde in phosphate-buffered saline (PBS, pH 7.4) for 24 h, transferred to 70% ethanol, and processed for paraffin embedding and histological analysis. Colon was also embedded with Optimal Cutting Temperature compound (Sakura Finetek) for immunofluorescence staining.

L-012 Probe Imaging

Mice were fed with 2.5% DSS for 7 consecutive days. At D1, mice were shaved and were imaged from D0 to D5. During bioluminescent, mice were narcotized with the anesthetic isoflurane (1.5–2.5%). The luminescent probe L-012 (Wako Chemical) was dissolved in sterile 0.9% NaCl to make the final working concentration of 50 mg/kg (Asghar et al., 2014). The imaging system used IVIS Spectrum (Xenogen, CA, USA).

Hematoxylin and Eosin Staining, Immunofluorescence and Immunohistochemistry

For Hematoxylin and Eosin staining and immunofluorescence, colon samples were embedded in paraffin. The paraffin embedded samples were sectioned in 5 μm and deparaffinized and rehydrated subsequently. Samples stained with Hematoxylin and Eosin staining were used for histology analysis. For immunofluorescence staining of the cells and tissue sections (Cheng et al., 2011), antigen of sectioned samples was retrieved with 0.1M citrate buffer in pH 6.0. Sectioned samples were later blocked with 5% goat serum and were incubated with primary antibodies overnight at 4°C. Then, sectioned samples were stained with secondary antibodies at room temperature for 3 h. Finally, DAPI staining was conducted for 10 min.

For immunochemistry staining of tissue sections, sectioned samples were stained and visualized by ABC staining system (Vector lab) and later counterstained with Mayers hematoxyline (Histolab). Isotype counterpart was served as negative controls.

Microscopic Image Acquisition and Quantification

All confocal images were acquired by Zeiss Zen software on a Zeiss LSM780 confocal laser scanning microscope (Carl Zeiss, Munich, Germany) with the following objectives: Plan-Apochromat 10× (NA of 0.45, air) and Plan-Apochromat 40× (NA of 1.30, oil). The following fluorochromes were used: Alexa Fluor 488 Dye (Invitrogen), Alexa Fluor 594 Dye (Invitrogen), and DAPI (Invitrogen). Immunohistochemistry images were taken with a Leica DC300F digital camera attached to a Leica DMLB microscope (Leica, Wetzlar, Germany). Images were viewed and adjusted with brightness and contrast by Adobe Photoshop software. Fluorescent images were processed and analyzed in a pipeline created in the BioimageXD framework (Kankaanpää et al., 2012). The pipeline detects the nuclei from the Hoechst channel and counts them. The cytoplasm of each cell was modeled with a 20-pixel ring around the nucleus. To quantify the invasion of neutrophils and macrophages in the colon tissues, sectioned samples embedded with paraffin from three different mice, and different time points per genotype were immunohistochemically stained for neutrophils (MPO) and macrophages (CD11b). Positively stained cells with distinct cellular borders and all cells presented within the sectioned samples were counted *via* a Zeiss Axiophot light microscope.

Macrophage Isolation, Purification and Depletion

Mice were sacrificed by spinal dislocation and injected with 5 ml of PBS. Peritoneal macrophages acquired from ascites extraction were then isolated and purified by the MagniSort™ Mouse F4/80 Positive Selection Kit (Invitrogen). For macrophages depletion, the mice received an i.p. injection of 300 μl of clodronate liposomes (LIPOSOMA), 1 day before the experiment. Empty liposomes were used in the no-depletion group. Samples were collected 3–7 days after DSS treatment.

ELISA Analysis

Peripheral blood serum samples were collected 3–7 days after DSS treatment, and IL-6 levels in the mouse serum were measured using an IL-6 ELISA kit (eBiosciences).

Tissue Preparation and Western Blot Analysis

Tissue lysates were prepared by homogenizing intestines in ice cold protein lysis buffer (20 mM Tris pH 7.5, 150 mM NaCl, 2 mM EDTA, 1% Triton-X100, 10% glycerol) using a Tissue Lyser II (QIAGEN; Hilden, Germany) for 12 cycles of 30 s at 30 Hz. Protein levels of tissue lysates were normalized by a BCA kit (Thermo Fisher Scientific) (Weigmann et al., 2007). After lysed in SDS-PAGE loading buffer and boiled at 95°C for 5 min, proteins were separated by SDS polyacrylamide electrophoresis using 10% gel at 120 V for 90 min, and separated proteins were transferred in to nitrocellulose membrane by doing wet transfer at 100 V for 30 min. Membranes were later blocked with 5% milk and incubated with primary antibody at 4°C for overnight with shaking. Then, membranes were incubated with secondary antibody at room temperature for 1 h with shaking and proteins were detected by Amersham ECL reagent (Cytiva).

Real-Time Quantitative PCR

Total RNA was extracted from colon tissue, tumors, colon biopsies, or cells using RNeasy mini kits (QIAGEN) or the FFPE Total RNA Isolation Kit (Invitrogen). cDNA was obtained by reverse-transcribing same amount of total RNA using the High-Capacity cDNA Reverse Transcription Kit (Applied Biosystems). The transcript levels of the genes were measured the SYBR Green PCR mix (Applied Biosystems) in an Applied Biosystems 7300 detection system (Bio-Rad). The quality of the quantitative PCR run was determined by standard curves and melting curve analysis. The data were normalized to the expression of a cellular housekeeping gene GAPDH. Primers sequences (forward and reverse) used in this study are listed in **Supplementary Table S2**.

Statistical Analysis

The results are expressed as the mean ± SEM. Comparisons between two groups were analyzed by two-tailed t tests. Comparisons between multiple groups were analyzed by one-wayANOVA. $p < 0.05$ was considered significant. Statistical differences were calculated with the two-tailed unpaired *t*-test, and differences were considered significant at $p \leq 0.05$. For statistical evaluation of qRT-PCR data, the values (logarithmic) were converted to ddCt values (linear log2 scale values), and *p*-values were calculated using one-tailed unpaired Student's t-test.

DATA AVAILABILITY STATEMENT

The original contributions presented in the study are included in the article/**Supplementary Material**, further inquiries can be directed to the corresponding authors.

ETHICS STATEMENT

The animal study was reviewed and approved by the Ethical Committee for Animal Experiments of the University of Turku.

AUTHOR CONTRIBUTIONS

LW, PM, ML, MA, GS, and JOM performed the experiment and data analysis. LW wrote the manuscript and prepared the figures. YJ, HC, ZC, and DT contributed to hypothesis formulation, manuscript revision, and result discussions. FC and JE led and participated in the whole process of the study.

FUNDING

This research was supported by Academy of Finland 315139/332582; Sigrid Juselius Foundation, ÅAU Center of Excellence of Cellular Mechanostasis, EuroCellNet COST Action (CA15214); InFLAMES Flagship Programme of the Academy of Finland (decision number: 337531); European Union Framework 7 International Reintegration Grant, Åbo Akademi University Center of Excellence on Cell Stress and Molecular Aging to DT, and Turku Doctoral Programme for Biomedical Sciences to JOM and MA, the National Natural Science Foundation of China (81702750, 81970145, and 82001698); the National Natural Science Foundation of China (81970145 and 82001698); Natural Science Foundation of Guangdong Province (2020A1515011465 and 2020A151501467, China); Science, Technology and Innovation Commission of Shenzhen Municipality (JCYJ20190807151609464, JCYJ20200109142605909, and JCYJ20210324120007020, China); Sun Yat-sen University (20ykzd17, China); International Collaboration of Science and Technology of Guangdong Province (2020A0505100031, China); Guangdong Provincial Key Laboratory of Digestive Cancer Research (No. 2021B1212040006, China).

ACKNOWLEDGMENTS

Imaging was performed at the Cell Imaging and Cytometry Core, Turku Bioscience Center, University of Turku, Åbo Akademi University and Biocenter Finland, and sample preparation for histology was done at the Turku Center for Disease Modeling histology service unit at University of Turku, Finland.

SUPPLEMENTARY MATERIAL

The Supplementary Material for this article can be found online at: https://www.frontiersin.org/articles/10.3389/fcell.2022.862237/full#supplementary-material

REFERENCES

Asghar, M. N., Emani, R., Alam, C., Helenius, T. O., Grönroos, T. J., Sareila, O., et al. (2014). *In Vivo* imaging of Reactive Oxygen and Nitrogen Species in Murine Colitis. *Inflamm. Bowel Dis.* 20, 1435–1447. doi:10.1097/mib.0000000000000118

Barberis, L., Pasquali, C., Bertschy-Meier, D., Cuccurullo, A., Costa, C., Ambrogio, C., et al. (2009). Leukocyte Transmigration Is Modulated by Chemokine-Mediated PI3Kγ-dependent Phosphorylation of Vimentin. *Eur. J. Immunol.* 39, 1136–1146. doi:10.1002/eji.200838884

Becker, C., Fantini, M. C., Schramm, C., Lehr, H. A., Wirtz, S., Nikolaev, A., et al. (2004). TGF-β Suppresses Tumor Progression in Colon Cancer by Inhibition of IL-6 Trans-signaling. *Immunity* 21, 491–501. doi:10.1016/j.immuni.2004.07.020

Ben-Neriah, Y., and Karin, M. (2011). Inflammation Meets Cancer, with NF-Kb as the Matchmaker. *Nat. Immunol.* 12, 715–723. doi:10.1038/ni.2060

Brown, M. J., Hallam, J. A., Colucci-Guyon, E., and Shaw, S. (2001). Rigidity of Circulating Lymphocytes Is Primarily Conferred by Vimentin Intermediate Filaments. *J. Immunol.* 166, 6640–6646. doi:10.4049/jimmunol.166.11.6640

Cheng, F., Pekkonen, P., Laurinavicius, S., Sugiyama, N., Henderson, S., Günther, T., et al. (2011). KSHV-initiated Notch Activation Leads to Membrane-Type-1 Matrix Metalloproteinase-dependent Lymphatic Endothelial-To-Mesenchymal Transition. *Cell Host & Microbe* 10, 577–590. doi:10.1016/j.chom.2011.10.011

Cheng, F., Shen, Y., Mohanasundaram, P., Lindström, M., Ivaska, J., Ny, T., et al. (2016). Vimentin Coordinates Fibroblast Proliferation and Keratinocyte Differentiation in Wound Healing via TGF-β-Slug Signaling. *Proc. Natl. Acad. Sci. USA* 113, E4320–E4327. doi:10.1073/pnas.1519197113

Chernoivanenko, I. S., Minin, A. A., and Minin, A. A. (2013). Role of Vimentin in Cell Migration. *Ontogenez* 44, 186–202. doi:10.7868/s0475145013030026

Chung, B.-M., Rotty, J. D., and Coulombe, P. A. (2013). Networking Galore: Intermediate Filaments and Cell Migration. *Curr. Opin. Cel Biol.* 25, 600–612. doi:10.1016/j.ceb.2013.06.008

Colucci-Guyon, E., Portier, M.-M., Dunia, I., Paulin, D., Pournin, S., and Babinet, C. (1994). Mice Lacking Vimentin Develop and Reproduce without an Obvious Phenotype. *Cell* 79, 679–694. doi:10.1016/0092-8674(94)90553-3

Dave, J. M., and Bayless, K. J. (2014). Vimentin as an Integral Regulator of Cell Adhesion and Endothelial Sprouting. *Microcirculation* 21, 333–344. doi:10.1111/micc.12111

Dos Santos, G., Rogel, M. R., Baker, M. A., Troken, J. R., Urich, D., Morales-Nebreda, L., et al. (2015). Vimentin Regulates Activation of the NLRP3 Inflammasome. *Nat. Commun.* 6, 6574. doi:10.1038/ncomms7574

Dvorak, H. F. (1986). Tumors: Wounds that Do Not Heal. Similarities between Tumor Stroma Generation and Wound Healing. *N. Engl. J. Med.* 315, 1650–1659. doi:10.1056/NEJM198612253152606

Eckes, B., Colucci-Guyon, E., Smola, H., Nodder, S., Babinet, C., Krieg, T., et al. (2000). Impaired Wound Healing in Embryonic and Adult Mice Lacking Vimentin. *J. Cel Sci.* 113, 2455–2462. doi:10.1242/jcs.113.13.2455

Eckes, B., Dogic, D., Colucci-Guyon, E., Wang, N., Maniotis, A., Ingber, D., et al. (1998). Impaired Mechanical Stability, Migration and Contractile Capacity in Vimentin-Deficient Fibroblasts. *J. Cel Sci* 111, 1897–1907. doi:10.1242/jcs.111.13.1897

Formentini, L., Santacatterina, F., Núñez de Arenas, C., Stamatakis, K., López-Martínez, D., Logan, A., et al. (2017). Mitochondrial ROS Production Protects the Intestine from Inflammation through Functional M2 Macrophage Polarization. *Cel Rep.* 19, 1202–1213. doi:10.1016/j.celrep.2017.04.036

Gan, Z., Ding, L., Burckhardt, C. J., Lowery, J., Zaritsky, A., Sitterley, K., et al. (2016). Vimentin Intermediate Filaments Template Microtubule Networks to Enhance Persistence in Cell Polarity and Directed Migration. *Cel Syst.* 3, 252–263.e8. doi:10.1016/j.cels.2016.08.007

Grivennikov, S. I., Greten, F. R., and Karin, M. (2010). Immunity, Inflammation, and Cancer. *Cell* 140, 883–899. doi:10.1016/j.cell.2010.01.025

Grivennikov, S. I., Greten, F. R., and Karin, M. (2010). Immunity, Inflammation, and Cancer. *Cell* 140, 883–899. doi:10.1016/j.cell.2010.01.025

Ivaska, J., Pallari, H.-M., Nevo, J., and Eriksson, J. E. (2007). Novel Functions of Vimentin in Cell Adhesion, Migration, and Signaling. *Exp. Cel Res.* 313, 2050–2062. doi:10.1016/j.yexcr.2007.03.040

Ivaska, J. (2011). Vimentin. *Small GTPases* 2, 51–53. doi:10.4161/sgtp.2.1.15114

Kankaanpää, P., Paavolainen, L., Tiitta, S., Karjalainen, M., Päivärinne, J., Nieminen, J., et al. (2012). BioImageXD: an Open, General-Purpose and High-Throughput Image-Processing Platform. *Nat. Methods* 9, 683–689. doi:10.1038/nmeth.2047

Kielland, A., Blom, T., Nandakumar, K. S., Holmdahl, R., Blomhoff, R., and Carlsen, H. (2009). *In Vivo* imaging of Reactive Oxygen and Nitrogen Species in Inflammation Using the Luminescent Probe L-012. *Free Radic. Biol. Med.* 47, 760–766. doi:10.1016/j.freeradbiomed.2009.06.013

Kilkenny, C., Browne, W., Cuthill, I. C., Emerson, M., and Altman, D. G. (2010). Animal Research: Reporting *In Vivo* Experiments: The ARRIVE Guidelines. *Br. J Pharmacol* 160, 1577–1579. doi:10.1111/j.1476-5381.2010.00872.x

Krieglstein, C. F., Cerwinka, W. H., Laroux, F. S., Salter, J. W., Russell, J. M., Schuermann, G., et al. (2001). Regulation of Murine Intestinal Inflammation by Reactive Metabolites of Oxygen and Nitrogen. *J. Exp. Med.* 194, 1207–1218. doi:10.1084/jem.194.9.1207

Lavastre, V., Pelletier, M., Saller, R., Hostanska, K., and Girard, D. (2002). Mechanisms Involved in Spontaneous andViscum albumAgglutinin-I-Induced Human Neutrophil Apoptosis:Viscum albumAgglutinin-I Accelerates the Loss of Antiapoptotic Mcl-1 Expression and the Degradation of Cytoskeletal Paxillin and Vimentin Proteins via Caspases. *J. Immunol.* 168, 1419–1427. doi:10.4049/jimmunol.168.3.1419

Mahesh, P. P., Retnakumar, R. J., and Mundayoor, S. (2016). Downregulation of Vimentin in Macrophages Infected with Live *Mycobacterium tuberculosis* Is Mediated by Reactive Oxygen Species. *Sci. Rep.* 6, 21526. doi:10.1038/srep21526

McGrath, J., Drummond, G., McLachlan, E., Kilkenny, C., and Wainwright, C. (2010). Guidelines for Reporting Experiments Involving Animals: the ARRIVE Guidelines. *Br. J Pharmacol* 160, 1573–1576. doi:10.1111/j.1476-5381.2010.00873.x

Menko, A. S., Bleaken, B. M., Libowitz, A. A., Zhang, L., Stepp, M. A., and Walker, J. L. (2014). A Central Role for Vimentin in Regulating Repair Function during Healing of the Lens Epithelium. *Mol. Biol. Cel.* doi:10.1091/mbc.e12-12-0900

Moisan, É., Chiasson, S., and Girard, D. (2007). The Intriguing normal Acute Inflammatory Response in Mice Lacking Vimentin. *Clin. Exp. Immunol.* 150, 158–168. doi:10.1111/j.1365-2249.2007.03460.x

Moisan, E., and Girard, D. (2006). Cell Surface Expression of Intermediate Filament Proteins Vimentin and Lamin B1in Human Neutrophil Spontaneous Apoptosis. *J. Leukoc. Biol.* 79, 489–498. doi:10.1189/jlb.0405190

Mor-Vaknin, N., Legendre, M., Yu, Y., Serezani, C. H., Garg, S. K., Jatzek, A., et al. (2013). Murine Colitis Is Mediated by Vimentin. *Sci. Rep.* 3, 1045. doi:10.1038/srep01045

Mor-Vaknin, N., Punturieri, A., Sitwala, K., and Markovitz, D. M. (2003). Vimentin Is Secreted by Activated Macrophages. *Nat. Cel Biol.* 5, 59–63. doi:10.1038/ncb898

Neufert, C., Becker, C., and Neurath, M. F. (2007). An Inducible Mouse Model of colon Carcinogenesis for the Analysis of Sporadic and Inflammation-Driven Tumor Progression. *Nat. Protoc.* 2, 1998–2004. doi:10.1038/nprot.2007.279

Newkirk, K. M., Parent, A. E., Fossey, S. L., Choi, C., Chandler, H. L., Rajala-Schultz, P. J., et al. (2007). Snai2 Expression Enhances Ultraviolet Radiation-Induced Skin Carcinogenesis. *Am. J. Pathol.* 171, 1629–1639. doi:10.2353/ajpath.2007.070221

Nieminen, M., Henttinen, T., Merinen, M., Marttila–Ichihara, F., Eriksson, J. E., and Jalkanen, S. (2006). Vimentin Function in Lymphocyte Adhesion and Transcellular Migration. *Nat. Cel Biol.* 8, 156–162. doi:10.1038/ncb1355

Pan, P., Su, L., Wang, X., Chai, W., Liu, D., Song, L., et al. (2021). Vimentin Regulation of Autophagy Activation in Lung Fibroblasts in Response to Lipopolysaccharide Exposure *In Vitro*. *Ann. Transl Med.* 9, 304. doi:10.21037/atm-20-5129

Parent, A. E., Newkirk, K. M., and Kusewitt, D. F. (2010). Slug (Snai2) Expression during Skin and Hair Follicle Development. *J. Invest. Dermatol.* 130, 1737–1739. doi:10.1038/jid.2010.22

Peterson, L. W., and Artis, D. (2014). Intestinal Epithelial Cells: Regulators of Barrier Function and Immune Homeostasis. *Nat. Rev. Immunol.* 14, 141–153. doi:10.1038/nri3608

Pikarsky, E., Porat, R. M., Stein, I., Abramovitch, R., Amit, S., Kasem, S., et al. (2004). NF-κB Functions as a Tumour Promoter in Inflammation-Associated Cancer. *Nature* 431, 461–466. doi:10.1038/nature02924

Rogel, M. R., Soni, P. N., Troken, J. R., Sitikov, A., Trejo, H. E., and Ridge, K. M. (2011). Vimentin Is Sufficient and Required for Wound Repair and Remodeling in Alveolar Epithelial Cells. *FASEB j.* 25, 3873–3883. doi:10.1096/fj.10-170795

Roper, J., and Hung, K. E. (2013). "Molecular Mechanisms of Colorectal Carcinogenesis," in *Molecular Pathogenesis of Colorectal Cancer*. Editor P. D. M. K. Haigis (New York, NY: Springer New York), 25–65. doi:10.1007/978-1-4614-8412-7_2

Satelli, A., and Li, S. (2011). Vimentin in Cancer and its Potential as a Molecular Target for Cancer Therapy. *Cell. Mol. Life Sci.* 68, 3033–3046. doi:10.1007/s00018-011-0735-1

Stojadinovic, O., Pastar, I., Vukelic, S., Mahoney, M. G., Brennan, D., Krzyzanowska, A., et al. (2008). Deregulation of Keratinocyte Differentiation and Activation: a Hallmark of Venous Ulcers. *J. Cel Mol Med* 12, 2675–2690. doi:10.1111/j.1582-4934.2008.00321.x

Tanaka, T., Kohno, H., Suzuki, R., Yamada, Y., Sugie, S., and Mori, H. (2003). A Novel Inflammation-Related Mouse colon Carcinogenesis Model Induced by Azoxymethane and Dextran Sodium Sulfate. *Cancer Sci.* 94, 965–973. doi:10.1111/j.1349-7006.2003.tb01386.x

Toivola, D. M., Strnad, P., Habtezion, A., and Omary, M. B. (2010). Intermediate Filaments Take the Heat as Stress Proteins. *Trends Cel Biol.* 20, 79–91. doi:10.1016/j.tcb.2009.11.004

Tolstonog, G. V., Shoeman, R. L., Traub, U., and Traub, P. (2001). Role of the Intermediate Filament Protein Vimentin in Delaying Senescence and in the Spontaneous Immortalization of Mouse Embryo Fibroblasts. *DNA Cel Biol.* 20, 509–529. doi:10.1089/104454901317094945

Truett, G. E., Heeger, P., Mynatt, R. L., Truett, A. A., Walker, J. A., and Warman, M. L. (2000). Preparation of PCR-Quality Mouse Genomic DNA with Hot Sodium Hydroxide and Tris (HotSHOT). *Biotechniques* 2952, 52–54. doi:10.2144/00291bm09

Weigmann, B., Tubbe, I., Seidel, D., Nicolaev, A., Becker, C., and Neurath, M. F. (2007). Isolation and Subsequent Analysis of Murine Lamina Propria Mononuclear Cells from Colonic Tissue. *Nat. Protoc.* 2, 2307–2311. doi:10.1038/nprot.2007.315

Wirtz, S., Neufert, C., Weigmann, B., and Neurath, M. F. (2007). Chemically Induced Mouse Models of Intestinal Inflammation. *Nat. Protoc.* 2, 541–546. doi:10.1038/nprot.2007.41

Xie, Y.-H., Chen, Y.-X., and Fang, J.-Y. (2020). Comprehensive Review of Targeted Therapy for Colorectal Cancer. *Sig Transduct Target. Ther.* 5, 22. doi:10.1038/s41392-020-0116-z

Yilmaz, M., and Christofori, G. (2009). EMT, the Cytoskeleton, and Cancer Cell Invasion. *Cancer Metastasis Rev.* 28, 15–33. doi:10.1007/s10555-008-9169-0

Zhang, J., Henrion, D., Ebrahimian, T., Benessiano, J., Colucci-Guyon, E., Langa, F., et al. (2001). Increased Contribution of L -Arginine-Nitric Oxide Pathway in Aorta of Mice Lacking the Gene for Vimentin. *J. Cardiovasc. Pharmacol.* 38, 552–560. doi:10.1097/00005344-200110000-00007

Zhou, H.-F., Ren, K., Zha, J.-H., Guo, Q., and Zhao, G.-J. (2020). Vimentin Promotes Endothelial Inflammation by Activating NLRP3. *Int. J. Cardiol.* 301, 155. doi:10.1016/j.ijcard.2019.09.024

Conflict of Interest: The authors declare that the research was conducted in the absence of any commercial or financial relationships that could be construed as a potential conflict of interest.

Publisher's Note: All claims expressed in this article are solely those of the authors and do not necessarily represent those of their affiliated organizations or those of the publisher, the editors, and the reviewers. Any product that may be evaluated in this article, or claim that may be made by its manufacturer, is not guaranteed or endorsed by the publisher.

frontiers | Frontiers in Cell and Developmental Biology

MINI REVIEW
published: 11 April 2022
doi: 10.3389/fcell.2022.882037

Intermediate Filaments in Cellular Mechanoresponsiveness: Mediating Cytoskeletal Crosstalk From Membrane to Nucleus and Back

Anne-Betty Ndiaye[†], *Gijsje H. Koenderink*[*†] *and Michal Shemesh*[*†]

Department of Bionanoscience, Kavli Institute of Nanoscience Delft, Delft University of Technology, Delft, Netherlands

OPEN ACCESS

Edited by:
Ming Guo, Massachusetts Institute of Technology, United States

Reviewed by:
Haiqian Yang, Massachusetts Institute of Technology, United States
Satish Kumar Gupta, Massachusetts Institute of Technology, United States

***Correspondence:**
Michal Shemesh
m.shemesh@tudelft.nl
Gijsje H. Koenderink
g.h.koenderink@tudelft.nl

[†]*These authors have contributed equally to this work*

Specialty section:
This article was submitted to Cell Growth and Division, a section of the journal Frontiers in Cell and Developmental Biology

Received: *23 February 2022*
Accepted: *24 March 2022*
Published: *11 April 2022*

Citation:
Ndiaye A-B, Koenderink GH and Shemesh M (2022) Intermediate Filaments in Cellular Mechanoresponsiveness: Mediating Cytoskeletal Crosstalk From Membrane to Nucleus and Back. Front. Cell Dev. Biol. 10:882037. doi: 10.3389/fcell.2022.882037

The mammalian cytoskeleton forms a mechanical continuum that spans across the cell, connecting the cell surface to the nucleus *via* transmembrane protein complexes in the plasma and nuclear membranes. It transmits extracellular forces to the cell interior, providing mechanical cues that influence cellular decisions, but also actively generates intracellular forces, enabling the cell to probe and remodel its tissue microenvironment. Cells adapt their gene expression profile and morphology to external cues provided by the matrix and adjacent cells as well as to cell-intrinsic changes in cytoplasmic and nuclear volume. The cytoskeleton is a complex filamentous network of three interpenetrating structural proteins: actin, microtubules, and intermediate filaments. Traditionally the actin cytoskeleton is considered the main contributor to mechanosensitivity. This view is now shifting owing to the mounting evidence that the three cytoskeletal filaments have interdependent functions due to cytoskeletal crosstalk, with intermediate filaments taking a central role. In this Mini Review we discuss how cytoskeletal crosstalk confers mechanosensitivity to cells and tissues, with a particular focus on the role of intermediate filaments. We propose a view of the cytoskeleton as a composite structure, in which cytoskeletal crosstalk regulates the local stability and organization of all three filament families at the sub-cellular scale, cytoskeletal mechanics at the cellular scale, and cell adaptation to external cues at the tissue scale.

Keywords: mechanobiology, migration, cytoskeleton, vimentin, keratin, actin, microtubules

INTRODUCTION

The cytoskeleton is a fascinating cellular machinery that performs multiple, to some extent contradictory, functions. It acts as a stable structural scaffold providing cells with a specific functional shape and protecting against external forces. Accordingly, genetic defects in cytoskeletal proteins are associated with mechanical defects in cells and tissues, which for instance result in kidney scarring (Feng et al., 2018), skin fragility (Haines and Lane 2012), and muscle failure (Adil et al., 2021). On the other hand, the cytoskeletal structures are also dynamic enough to enable cell migration, division and mechanosensitive response to the environment (Chaudhuri et al., 2020).

Although the cytoskeleton is highly dynamic at the subcellular (nm) scale, it nevertheless maintains structural integrity at the cell scale (microns) and at the tissue scale (up to millimeters). This disparity is most likely due to the composite nature of the cytoskeleton, based

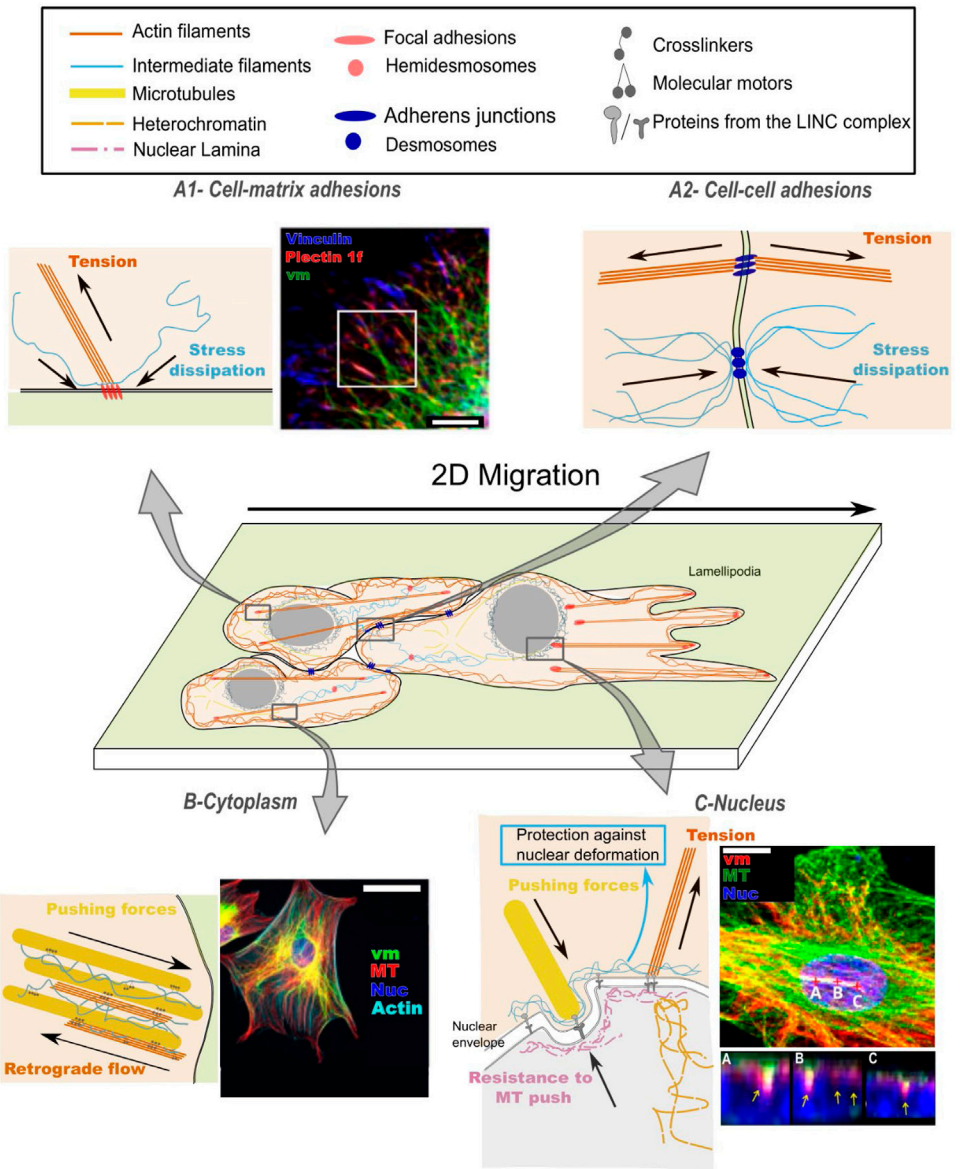

FIGURE 1 | Cytoskeletal crosstalk between intermediate filaments (IFs), actin filaments (AFs) and microtubules (MTs) contributes to mechanosensing: **(A)** at the cell surface: mechanical signals emerging from the matrix **(A1)** or from neighboring cells **(A2)**; **(B)** in the propagation of mechanical signals across the cell cytoplasm and **(C)** up to the cell nucleus. **(A1)** At cell-matrix adhesions, actin/vimentin crosstalk regulates focal adhesion turnover, which results in dissipation of local stresses. Fluorescence image from (Gregor et al., 2014) shows the intimate spatial relation between vimentin (vm), plectin and vinculin, orchestrating focal adhesion turnover; scale bar is 10 μm. **(A2)** At cell-cell adhesions, actin/intermediate filament crosstalk is activated upon tensile (pulling) forces and participates in the regulation of cellular prestress. **(B)** In the dense cytoplasm, mechanical forces are transmitted through all three cytoskeletal networks. The intermediate filament network affects the (de) polymerization rates of the other two networks, and the three networks co-align. Fluorescence image from (Vohnoutka et al., 2019) demonstrates the dense organization of vimentin, microtubules (MT) and actin. Vimentin spans from membrane sites to the nucleus (DAPI) and forms a cage surrounding the nucleus. Scale bar is 50 μm. **(C)** At the nucleus, forces are transmitted between the cytoskeleton and chromatin through LINC complexes, affecting nuclear shape and heterochromatin density, while intermediate filaments protect the nucleus from large deformations. Fluorescence image from (Feliksiak et al., 2020) shows microtubules and vimentin around the nucleus (DAPI); scale bar = 15 μm. Areas marked by A-B-C demonstrate the tight association of vimentin with nuclear grooves.

around three protein filament networks with distinct structural, mechanical and biochemical properties: actin filaments, microtubules, and intermediate filaments (**Figures 1A,B**). All three filaments are reversible polymers that self-assemble from weakly interacting subunits whose local availability is a critical determinant of local cytoskeletal dynamics (Plastino and Blanchoin 2018; Ohi et al., 2021). Both actin filaments and microtubules are structurally polar filaments, respectively composed of actin monomers that hydrolyze ATP, and tubulin dimers that hydrolyze GTP. They both exhibit fast (~ seconds to minutes) turnover rates fueled by ATP/GTP hydrolysis (Theriot and Mitchison 1991; McNally 1996). By contrast, intermediate

filaments are non-polar filaments that lack intrinsic enzymatic activity (Li et al., 2006; Robert et al., 2015). Their remodeling occurs by slow (~ hours) exchange of filamentous tetramers (Çolakoğlu and Brown 2009; Nöding et al., 2014; Robert et al., 2015). It has been proposed that this long-lived intermediate filament network mechanically integrates the cytoskeleton and provides structural memory that helps maintain cell polarity (Gan et al., 2016).

Each of the three cytoskeletal networks has its own set of dedicated regulatory proteins that control their structure, dynamics and mechanics with high spatial and temporal precision (Plastino and Blanchoin 2018; Dutour-Provenzano and Etienne-Manneville 2021; Gudimchuk and McIntosh 2021). Cells are thus able to form different specialized cytoskeletal arrays, such as the branched actin networks at the leading edge of migrating cells, the microtubule spindle in dividing cells, and an intermediate filament cage-like structure that protects the nucleus of cells during confined migration. The posttranslational addition of various chemical groups further enhances the complexity of the cytoskeletal proteome, hence the ability of the cell to fine-tune cytoskeletal functions (MacTaggart and Kashina 2021).

It is increasingly recognized that the functions of the three structural systems are tightly coupled *via* crosslinkers, motors, adhesion complexes and shared signaling factors. Recently, our understanding of the molecular mechanisms of cytoskeletal crosstalk and its consequences for cell shape, mechanics and fundamental processes such as directional migration, has grown (Huber et al., 2015; van Bodegraven and Etienne-Manneville 2020). Still, the role of cytoskeletal crosstalk in cellular mechanosensitivity remains poorly understood. Traditionally actin filaments are considered as the main contributor to mechanosensitivity, since they actively apply contractile (traction) forces to the extracellular matrix and to adjacent cells *via* specialized adhesion complexes and transmit mechanical signals to the nucleus, for instance *via* LINC complexes (Sun et al., 2016; Yap et al., 2018). Microtubules are thought to play mainly a regulatory role through their interactions with the actin cytoskeleton and with cell-matrix and cell-cell adhesions (Dogterom and Koenderink 2019; Rafiq et al., 2019; Pimm and Henty-Ridilla 2021). Intermediate filaments are usually considered as passive cytoskeletal elements that maintain cell/tissue integrity. However, there is a growing appreciation that intermediate filaments play a central role in cellular mechanosensitivity, forming a mechanically strong yet responsive network that links to the actin and microtubule cytoskeleton, cell adhesions, and nuclear complexes (Chang and Goldman 2004). This is especially intriguing because intermediate filaments exhibit much more tissue diversity than the other cytoskeletal subsystems. The actin and microtubule cytoskeleton are differently organized in different cell types, but their molecular composition is relatively conserved, with a limited number of isoforms. By contrast, there are ~ 70 intermediate filament genes in humans, with further diversity arising from alternative splicing. For instance, different types of epithelial cells express different sets of keratins, mesenchymal cells express vimentin, muscle cells express desmin, and neurons express neurofilaments. Intermediate filaments are hence widely used as markers for differentiation (Redmond and Coulombe 2021; Sjöqvist et al., 2021). Herein, we review evidence pointing to the importance of cytoskeletal crosstalk in cellular mechanosensitivity, with a particular focus on the role of intermediate filaments. We demonstrate how intermediate filaments span from cell-cell and cell-matrix adhesion sites, through the cytoplasm and up to the nucleus (see **Figure 1**), thereby orchestrating long-range mechano-chemical crosstalk between the cytoskeleton, cell adhesions, and internal processes.

CONTRIBUTIONS OF CYTOSKELETAL CROSSTALK TO MECHANOSENSING AT THE CELL MEMBRANE

Mechanosensing at Cell/Extracellular Matrix Contacts

Cell-matrix contacts are key players in mechanotransduction as they enable cells to apply forces on the extracellular matrix, in response to its mechanical properties (Sun et al., 2016). These matrix contacts are essential for determining cell polarity, directional migration and the cell's ability to remodel the extracellular matrix (Brabletz et al., 2021). The role of actin-based transmembrane adhesion complexes, including but not limited to focal adhesions, in mechanosensitivity has been extensively reviewed (Kechagia et al., 2019). The role of the other two cytoskeletal filament families in mechanosensitivity of cell-matrix contacts is recently gaining more attention (Leube et al., 2015; Sanghvi-Shah and Weber 2017; van Bodegraven and Etienne-Manneville 2020).

Focal adhesions are mostly identified with actin-based structures; however, multiple intermediate filament proteins have also been identified at focal adhesions (**Figure 1A1**). In epithelial cells, keratin filaments are nucleated at focal adhesions and transported inwards assisted by the actin cytoskeleton (Windoffer et al., 2006; Leube et al., 2015). In fibroblasts and endothelial cells, vimentin filaments are anchored to focal adhesions and regulate their size and adhesion strength (Bhattacharya et al., 2009; Kim et al., 2010; Gregor et al., 2014; Kim et al., 2016; Terriac et al., 2017; Vohnoutka et al., 2019). This involves direct force transmission from cell surface integrins to the cell interior (Maniotis et al., 1997), regulating actin stress fibers (Jiu et al., 2015; Jiu et al., 2017) and the associated mechanosensing machinery (Gregor et al., 2014). Focal adhesion anchoring enables vimentin to promote integrin-mediated activation of the major mechanosensor focal adhesion kinase (FAK) and its downstream tension-dependent signaling cascade (Gregor et al., 2014). Actomyosin-dependent rigidity sensing controls microtubule acetylation, which in turn tunes the mechanosensitivity of focal adhesions (Seetharaman et al., 2021). Since microtubule acetylation also affects the association of intermediate filaments with actin bundles at focal adhesions, this points to a complex three-way feedback mechanism that still remains to be disentangled. Cell adhesion is tightly connected to migration; Vimentin tunes cell migration

through collagen and fibronectin matrices (Ding et al., 2020; Ostrowska-Podhorodecka et al., 2021, Ostrowska-Podhorodecka, Ding et al. 2021). Persistent collective migration of astrocytes was dependent on the size and turnover of focal adhesions, in a cell-specific (leader *vs*. follower) manner. The regulation of focal adhesions and cell-cell contacts requires the intermediate filament network, which is composed mainly of glial fibrillar acidic protein (GFAP), vimentin, and nestin (Moeton et al., 2016; De Pascalis et al., 2018). Intermediate filaments also modulate traction forces; in migrating fibroblasts, the vimentin cytoskeleton was shown to slow down actin retrograde flows, while promoting orientation of actin stress fibers and traction forces (Costigliola et al., 2017). Intermediate filaments modulate also forces oriented perpendicularly to the substrate, through invadopodia (Schoumacher et al., 2010), possibly *via* interacting with actin capping proteins (Lanier et al., 2015).

Intermediate filaments are further anchored to the cell surface by proteins of the plakin family, specifically plectin in hemidesmosomes and desmoplakin in desmosomes (Dowling et al., 1996; Mohammed et al., 2020). Plectin is a major crosslinker connecting the three cytoskeletal filament families (Svitkina et al., 1996; Wiche et al., 2015). Molecular dynamic simulations suggested that plakins act as mechanosensors: pulling forces resulted in plectin and desmoplakin unfolding and exposure of the SH3 domain, which may potentially trigger downstream signaling cascades (Daday et al., 2017). Experimentally, activated plectins were shown to promote microtubule destabilization through their interaction with MAP2, which antagonizes the MAP2-mediated stabilization of MTs (Valencia et al., 2013). Recent studies indicate that FAs and hemidesmosomes are mechanically coupled (Nardone et al., 2017; Wang et al., 2020).

Mechanosignalling at Cell-Cell Contacts

Cell-cell interactions play a crucial role in physiological mechanosensitive processes such as tissue morphogenesis, but also in pathological processes such as inflammatory bowel diseases (Adil et al., 2021). Cells interact through cadherin-based adherens junctions that connect the actin networks of neighboring cells in epithelia and endothelia, and desmosomes that connect the intermediate filaments of neighboring cells and reinforce tissues that experience high mechanical stress such as the epidermis (Rübsam et al., 2018; Broussard et al., 2020) (**Figure 1A2**). Besides providing mechanical coherence, both adhesions are involved in cell and tissue adaptation to mechanical cues (Charras and Yap 2018; Angulo-Urarte et al., 2020; Zuidema et al., 2020). The mechanosensitivity of adherens junctions was shown to rely on force-sensitive conformational changes of α-catenin and vinculin (Yao et al., 2014; Seddiki et al., 2018). Desmosomes are sites of local assembly/reorganization of keratin filaments (Kim et al., 2021), similar to hemidesmosomes. Desmoplakin, one of the core proteins of desmosomes that binds keratin filaments (Bornslaeger et al., 1996), was recently shown to experiences forces in the pN range in stretched epithelial monolayers, suggesting its load-bearing function (Price et al., 2018).

Although previous studies examining adherens junctions (Engl et al., 2014) and desmosomes (Price et al., 2018) considered the different cytoskeletal networks separately, there is evidence that the three cytoskeletal elements interdependently modulate the dynamical properties of cell-cell junctions. Microtubules promote actin recruitment at adherens junctions and intercellular transmission of the contractile forces generated by the actomyosin network (Ko et al., 2019). In migrating astrocytes, intermediate filaments influence actin-driven retrograde flow of adherens junctions (De Pascalis et al., 2018). In migrating epithelial cells, desmosome dynamics was shown to depend on both intermediate filaments and actin (Roberts et al., 2011). Intermediate filaments also appear to be involved in vascular permeability (Bayir and Sendemir 2021) by helping to organize continuous adherens junctions and the underlying actin network *via* plectin crosslinking (Osmanagic-Myers et al., 2015). In epithelia, plectin mechanically couples cortical keratin and actin networks and ensures a uniform distribution of actomyosin-generated forces (Prechova et al., 2022). Finally, growing evidence points to collaboration between intermediate filament-desmosome and actin-adherens junction networks during mechanosensing and force generation (reviewed in (Zuidema et al., 2020)).

CONTRIBUTIONS OF CYTOSKELETAL CROSSTALK TO FORCE TRANSMISSION THROUGH THE CYTOPLASM

Physical interactions between intermediate filaments, actin, and microtubules influence the mechanical properties of the cytoskeleton as a whole, and hence force transmission from the cell surface to the nucleus (**Figure 1B**). The three cytoskeletal filaments strongly differ in their bending rigidity, as quantified by the persistence length, l_p. Intermediate filaments are most flexible, with $l_p \approx 0.5–2$ μm, microtubules are most rigid, with $l_p \approx 1–10$ mm, and actin filaments are intermediate with $l_p \approx 8$ μm (Huber et al., 2015). The filaments also strongly differ in their rupture strain: actin filaments and microtubules only support small tensile strains whereas intermediate filaments support large elongations because their subunits can slide and unfold (Block et al., 2017). Understanding how these single-filament properties translate in cell-scale mechanics is challenging given the molecular and structural complexity of the cytoskeleton. Cell-free reconstitution experiments are hence essential to elucidate the individual and collaborative roles of the different cytoskeletal filaments in cytoskeletal mechanics.

Reconstituted networks of purified actin and intermediate filaments (vimentin or keratin) strain-stiffen when exposed to shear or tensile stresses. These filaments are semiflexible, with a persistence length that is of the same order as the contour length. Experiments and theoretical modelling demonstrated that strain-stiffening occurs because the thermally undulating filaments are straightened out by tensile strains, which reduces the conformational entropy of the fluctuating polymer segments between adjacent crosslinks, and hence opposes further deformation (Gardel et al., 2004; Broedersz and MacKintosh 2014). Depending on the time scale of the imposed mechanical load, reconstituted vimentin networks can additionally dissipate

TABLE 1 | Selected examples of known cytoskeletal crosstalk interactions relevant for environmental mechanosensing that involve intermediate filaments. Interactions are sorted by subcellular localization, noting the structural and crosslinker proteins known to be involved in the crosstalk, as well as the major cellular function.

Localization	Relevant Cytoskeletal Filaments	Interacting Proteins	Cellular Function	References
Ventral membrane (Focal adhesions; epithelial cells)	Keratin Actin	Zyxin Paxillin Talin	Focal adhesions control keratin formation, turnover and transport	(Windoffer et al., 2006; Leube et al., 2015)
Ventral membrane (Focal adhesions; mesenchymal cells)	Vimentin Actin	Plectin Integrins β1, β3 Vinculin FAK Hic-5 Filamin A	Vimentin restricts focal adhesion size and regulates integrin trafficking; focal adhesions control vimentin organization	(Bhattacharya et al., 2009; Kim et al., 2010; Gregor et al., 2014; Kim et al., 2016; Terriac et al., 2017; Vohnoutka et al., 2019)
Lamellipodia (Fibroblasts)	Vimentin Actin	RAC1	Vimentin detachment from membrane sites is essential for lamellipodia formation	Helfand et al. (2011)
Membrane: (hemidesmosomes; epithelial cells)	Keratin Actin Microtubules	Integrin α6β4	Hemidesmosomes control keratin organization, likely important for tissue resilience	(Colburn and Jones 2018; Moch and Leube 2021)
Membrane: (Cell-Cell junctions + leading edge; astrocytes)	Vimentin Actin	Paxillin Plectin N-Cadherin E-Catenin	Vimentin promotes collective directed migration by regulating actomyosin traction force generation	De Pascalis et al. (2018)
Cortex	Vimentin Actin	Plectin	Vimentin interaction maintains cortex tension, required for cell division of confined cells	(Duarte et al., 2019; Serres et al., 2020)
Cytoplasm (mesenchymal cells)	Vimentin Actin Microtubules	Plectin	Plectins crosslink the cytoskeletal networks for cell integrity; vimentin regulates actin stress fibers	(Svitkina et al., 1996; Jiu et al., 2017)
Cytoplasm (mesenchymal cells)	Vimentin Actin	Plectin	Actin arcs drive perinuclear vimentin accumulation; vimentin restrains width of the actin-filled lamellum	(Jiu et al., 2015; Lowery et al., 2015)
Cytoplasm	Actin Keratin14 Lamin A/C	Plectin Paxillin	Matrix rigidity sensing and cell mechanical properties	(Guo et al., 2013; Bonakdar et al., 2015; Laly et al., 2021)
Nucleus	Vimentin Actin Microtubules Lamin A/C	LINC complex formed by sun and nesprin proteins	Nucleo-cytoskeletal force transmission maintains nuclear position under strain and during migration	(Folker et al., 2011; Lombardi et al., 2011; Marks and Petrie 2022)

mechanical stress because crosslinks between filaments can remodel and the filaments themselves lengthen by subunit unfolding and sliding elongations (Aufderhorst-Roberts and Koenderink 2019; Forsting et al., 2019). Combining the different cytoskeletal polymers in composite networks demonstrates intriguing co-dependent mechanical properties. Actin/vimentin and actin/microtubule mixtures were shown to exhibit enhanced stiffness and compressibility compared to the single-component networks (Esue et al., 2006; Pelletier et al., 2009; Lin et al., 2011). Furthermore, microtubules were shown to counteract myosin motor-driven contraction of actin networks through their ability to bear large compressive loads (Lee et al., 2021a). Physical interactions also introduce co-dependent polymerization dynamics of the three cytoskeletal polymers. Branched actin networks reduce the growth rate of microtubules and trigger their depolymerization (Colin et al., 2018), while vimentin filaments bind to microtubules and stabilize them against depolymerization (Schaedel et al., 2021) and also bind to actin filaments (Esue et al., 2006). In the presence of crosslinkers and motors, the three filament systems can additionally co-align and (re-)direct each other's polymerization direction (Preciado López et al., 2014; Gan et al., 2016; Leduc and Etienne-Manneville 2017).

These physical effects identified in simplified reconstituted systems likely contribute to mechanical co-dependencies observed in cells, such as toughening by stress dissipation in the vimentin network (Hu et al., 2019), protection against compressive forces by the vimentin network (Mendez et al., 2014), and vimentin-dependent modulation of actin-myosin contractility (De Pascalis et al., 2018). Raman imaging recently showed that actomyosin forces are transmitted to the intermediate filament cytoskeleton: cells on rigid substrates, where myosin contractility is high (Gupta et al., 2019), contained more unfolded vimentin than on soft substrates, where tension is low (Fleissner et al., 2020). In epithelial monolayers a similar mechanical interplay between the actin and intermediate filament networks was found (Latorre et al., 2018), where cell stretching dilutes the actin cortex and hence decreases tension, while keratin filaments that bear tension re-stiffen the cells. There is evidence that microtubules also contribute to the overall mechanical balance; epithelial folding was for instance shown to emerge from the balance between myosin contractile forces and microtubule-generated pushing forces (Takeda et al., 2018). It would be interesting to evaluate more systematically how mechanical co-dependencies among the three cytoskeletal filament families respond to modified substrate stiffness.

CONTRIBUTIONS OF CYTOSKELETAL CROSSTALK TO MECHANOSENSITIVITY AT THE NUCLEUS

The nucleus plays a key role in mechanotransduction and mechanosensing (reviewed in (Kirby and Lammerding 2018; Janota et al., 2020)). Nuclear chromatin and the cytoskeleton are physically linked through the LINC (Linker of Nucleoskeleton and Cytoskeleton) complex (Bouzid et al., 2019), which is associated with chromatin and nuclear lamins, members of the intermediate filament family (**Figure 1C**). Actin filaments are anchored to the nucleus *via* nesprin-1 and nesprin-2, intermediate filaments *via* nesprin-3, and microtubules *via* nesprin-4 (Zhen et al., 2002; Warren et al., 2005; Wilhelmsen et al., 2005; Roux et al., 2009). Considering the role of intermediate filaments in mechanical stabilization of the nucleus, as shown for vimentin (Patteson et al., 2019) and keratin (Almeida et al., 2015), we propose that future work should focus further on resolving the interactions between the three cytoskeletal components at the nuclear envelope in response to changes in substrate rigidity, for instance by superresolution microscopy and molecular tension sensors (Arsenovic et al., 2016; Leduc and Etienne-Manneville 2017).

The physical links between the nuclear lamins and the cytoskeleton provide continuous feedback between the mechanical properties of the nucleus of the cell and its environment (Buxboim et al., 2014; Lomakin et al., 2020; Venturini et al., 2020). Soft substrates promote phosphorylation and turnover of lamin A/C, resulting in softer and less spread nuclei (Buxboim et al., 2014). Pushing forces on the nuclear envelope exerted by microtubules are balanced by the laminA network for the maintenance of a round nuclear shape (Ramdas and Shivashankar 2015; Tariq et al., 2017). In differentiating Hematopoietic Stem and Progenitor (HSPC) cells, local nuclear invaginations associated with centrosomes and microtubule bundles depend on the laminB density and the activity of dynein (Biedzinski et al., 2020). Such local interactions at the nucleus possibly depend on environmental cues. In MEFs plated on micropatterned substrates with independent control over the overall cell shape and the focal adhesion size, the cell-ECM contact size was shown to have more impact than cell shape on overall cell polarization, in a LaminA dependent manner (Lee et al., 2021b). These results strengthen the notion that cytoskeletal crosstalk affects mechanoresponsiveness all the way from the cell surface to the nucleus.

DISCUSSION

In this mini-review, we gathered recent evidence demonstrating the contribution of cytoskeletal crosstalk in transferring mechanical signals from contact points at the plasma membrane to the nucleus. Intermediate filaments play a central role in this crosstalk, by interacting with the actin and microtubule cytoskeleton, cell-cell and cell-matrix adhesions, and nuclear complexes. We propose to shift focus in cytoskeletal and mechanobiological research towards a more holistic view of the cytoskeleton as a composite structure, examining the responses of *all* three structural families to mechanical cues. The central role of intermediate filaments in mechanosensitivity may render cell/tissue-specific mechanosensitivity. Moreover, during development, aging or pathology, the composition of the intermediate filament cytoskeleton undergoes major changes (Redmond and Coulombe 2021; Sjöqvist et al., 2021). This raises the hypothesis that there may be an "intermediate filament code" that confers cell type-specific mechanosensitive functions.

Elucidating the mechanisms by which intermediate filaments contribute to mechanosensing and mechanotransduction is far from trivial given the molecular complexity of the cytoskeletal proteome together with its cell/tissue specificity. Connecting the manifold molecular-scale interactions to the emergent mechano-biological functions at the cellular level is also challenging. To delineate the functions of different intermediate filament proteins across scales, we believe that it is vital to combine studies in cell culture models and model organisms, where cells can be studied in their native context, with studies of "clean" reconstituted systems, where cytoskeletal crosstalk can be studied under controlled conditions to facilitate combinations with predictive models.

AUTHOR CONTRIBUTIONS

All authors listed have made a substantial, direct, and intellectual contribution to the work and approved it for publication.

FUNDING

This publication is part of the project "How cytoskeletal teamwork makes cells strong" with project number VI.C.182.004 of the NWO Talent Programme which is financed by the Dutch Research Council (NWO).

ACKNOWLEDGMENTS

We thank Pradeep Das for his useful comments on an early version of the manuscipt.

REFERENCES

Adil, M. S., Narayanan, S. P., and Somanath, P. R. (2021). Cell-cell Junctions: Structure and Regulation in Physiology and Pathology. *Tissue Barriers* 9 (1), 1848212. doi:10.1080/21688370.2020.1848212

Almeida, F. V., Walko, G., McMillan, J. R., McGrath, J. A., Wiche, G., Barber, A. H., et al. (2015). The Cytolinker Plectin Regulates Nuclear Mechanotransduction in Keratinocytes. *J. Cel Sci* 128 (24), 4475–4486. doi:10.1242/jcs.173435

Angulo-Urarte, A., van der Wal, T., and Huveneers, S. (2020). Cell-cell Junctions as Sensors and Transducers of Mechanical Forces. *Biochim. Biophys. Acta (Bba) - Biomembranes* 1862 (9), 183316. doi:10.1016/j.bbamem.2020.183316

Arsenovic, P. T., Ramachandran, I., Bathula, K., Zhu, R., Narang, J. D., Noll, N. A., et al. (2016). Nesprin-2G, a Component of the Nuclear LINC Complex, Is Subject to Myosin-dependent Tension. *Biophysical J.* 110 (1), 34–43. doi:10.1016/j.bpj.2015.11.014

Aufderhorst-Roberts, A., and Koenderink, G. H. (2019). Stiffening and Inelastic Fluidization in Vimentin Intermediate Filament Networks. *Soft Matter* 15 (36), 7127–7136. doi:10.1039/c9sm00590k

Bayir, E., and Sendemir, A. (2021). Role of Intermediate Filaments in Blood-Brain Barrier in Health and Disease. *Cells* 10 (6), 1400. doi:10.3390/cells10061400

Bhattacharya, R., Gonzalez, A. M., Debiase, P. J., Trejo, H. E., Goldman, R. D., Flitney, F. W., et al. (2009). Recruitment of Vimentin to the Cell Surface by Beta3 Integrin and Plectin Mediates Adhesion Strength. *J. Cel Sci* 122 (Pt 9), 1390–1400. doi:10.1242/jcs.043042

Biedzinski, S., Agsu, G., Vianay, B., Delord, M., Blanchoin, L., Larghero, J., et al. (2020). Microtubules Control Nuclear Shape and Gene Expression during Early Stages of Hematopoietic Differentiation. *EMBO J.* 39 (23), e103957. doi:10.15252/embj.2019103957

Block, J., Witt, H., Candelli, A., Peterman, E. J., Wuite, G. J., Janshoff, A., et al. (2017). Nonlinear Loading-rate-dependent Force Response of Individual Vimentin Intermediate Filaments to Applied Strain. *Phys. Rev. Lett.* 118 (4), 048101. doi:10.1103/PhysRevLett.118.048101

Bonakdar, N., Schilling, A., Spörrer, M., Lennert, P., Mainka, A., Winter, L., et al. (2015). Determining the Mechanical Properties of Plectin in Mouse Myoblasts and Keratinocytes. *Exp. Cel Res.* 331 (2), 331–337. doi:10.1016/j.yexcr.2014.10.001

Bornslaeger, E. A., Corcoran, C. M., Stappenbeck, T. S., and Green, K. J. (1996). Breaking the Connection: Displacement of the Desmosomal Plaque Protein Desmoplakin from Cell-Cell Interfaces Disrupts anchorage of Intermediate Filament Bundles and Alters Intercellular junction Assembly. *J. Cel Biol.* 134 (4), 985–1001. doi:10.1083/jcb.134.4.985

Bouzid, T., Kim, E., Riehl, B. D., Esfahani, A. M., Rosenbohm, J., Yang, R., et al. (2019). The LINC Complex, Mechanotransduction, and Mesenchymal Stem Cell Function and Fate. *J. Biol. Eng.* 13 (1), 68. doi:10.1186/s13036-019-0197-9

Brabletz, S., Schuhwerk, H., Brabletz, T., and Stemmler, M. P. (2021). Dynamic EMT: a Multi-Tool for Tumor Progression. *EMBO J.* 40 (18), e108647. doi:10.15252/embj.2021108647

Broedersz, C. P., and MacKintosh, F. C. (2014). Modeling Semiflexible Polymer Networks. *Rev. Mod. Phys.* 86 (3), 995–1036. doi:10.1103/revmodphys.86.995

Broussard, J. A., Jaiganesh, A., Zarkoob, H., Conway, D. E., Dunn, A. R., Espinosa, H. D., et al. (2020). Scaling up Single-Cell Mechanics to Multicellular Tissues - the Role of the Intermediate Filament-Desmosome Network. *J. Cel Sci* 133 (6), 228031. doi:10.1242/jcs.228031

Buxboim, A., Swift, J., Irianto, J., Spinler, K. R., Dingal, P. C. D. P., Athirasala, A., et al. (2014). Matrix Elasticity Regulates Lamin-A,C Phosphorylation and Turnover with Feedback to Actomyosin. *Curr. Biol.* 24 (16), 1909–1917. doi:10.1016/j.cub.2014.07.001

Chang, L., and Goldman, R. D. (2004). Intermediate Filaments Mediate Cytoskeletal Crosstalk. *Nat. Rev. Mol. Cel Biol* 5 (8), 601–613. doi:10.1038/nrm1438

Charras, G., and Yap, A. S. (2018). Tensile Forces and Mechanotransduction at Cell-Cell Junctions. *Curr. Biol.* 28 (8), R445–R457. doi:10.1016/j.cub.2018.02.003

Chaudhuri, O., Cooper-White, J., Janmey, P. A., Mooney, D. J., and Shenoy, V. B. (2020). Effects of Extracellular Matrix Viscoelasticity on Cellular Behaviour. *Nature* 584 (7822), 535–546. doi:10.1038/s41586-020-2612-2

Çolakoğlu, G., and Brown, A. (2009). Intermediate Filaments Exchange Subunits along Their Length and Elongate by End-To-End Annealing. *J. Cel Biol.* 185 (5), 769–777. doi:10.1083/jcb.200809166

Colburn, Z. T., and Jones, J. C. R. (2018). Complexes of α6β4 Integrin and Vimentin Act as Signaling Hubs to Regulate Epithelial Cell Migration. *J. Cel Sci* 131 (14), jcs214593. doi:10.1242/jcs.214593

Colin, A., Singaravelu, P., Théry, M., Blanchoin, L., and Gueroui, Z. (2018). Actin-Network Architecture Regulates Microtubule Dynamics. *Curr. Biol.* 28 (16), 2647–2656. e2644. doi:10.1016/j.cub.2018.06.028

Costigliola, N., Ding, L., Burckhardt, C. J., Han, S. J., Gutierrez, E., Mota, A., et al. (2017). Vimentin Fibers orient Traction Stress. *Proc. Natl. Acad. Sci. U.S.A.* 114 (20), 5195–5200. doi:10.1073/pnas.1614610114

Daday, C., Kolšek, K., and Gräter, F. (2017). The Mechano-Sensing Role of the Unique SH3 Insertion in Plakin Domains Revealed by Molecular Dynamics Simulations. *Sci. Rep.* 7 (1), 11669. doi:10.1038/s41598-017-11017-2

De Pascalis, C., Pérez-González, C., Seetharaman, S., Boëda, B., Vianay, B., Burute, M., et al. (2018). Intermediate Filaments Control Collective Migration by Restricting Traction Forces and Sustaining Cell-Cell Contacts. *J. Cel Biol.* 217 (9), 3031–3044. doi:10.1083/jcb.201801162

Ding, I., Ostrowska-Podhorodecka, Z., Lee, W., Liu, R. S. C., Carneiro, K., Janmey, P. A., et al. (2020). Cooperative Roles of PAK1 and Filamin A in Regulation of Vimentin Assembly and Cell Extension Formation. *Biochim. Biophys. Acta (Bba) - Mol. Cel Res.* 1867 (9), 118739. doi:10.1016/j.bbamcr.2020.118739

Dogterom, M., and Koenderink, G. H. (2019). Actin-microtubule Crosstalk in Cell Biology. *Nat. Rev. Mol. Cel Biol* 20 (1), 38–54. doi:10.1038/s41580-018-0067-1

Dowling, J., Yu, Q. C., and Fuchs, E. (1996). Beta4 Integrin Is Required for Hemidesmosome Formation, Cell Adhesion and Cell Survival. *J. Cel Biol.* 134 (2), 559–572. doi:10.1083/jcb.134.2.559

Duarte, S., Viedma-Poyatos, Á., Navarro-Carrasco, E., Martínez, A. E., Pajares, M. A., and Pérez-Sala, D. (2019). Vimentin Filaments Interact with the Actin Cortex in Mitosis Allowing normal Cell Division. *Nat. Commun.* 10 (1), 4200. doi:10.1038/s41467-019-12029-4

Dutour-Provenzano, G., and Etienne-Manneville, S. (2021). Intermediate Filaments. *Curr. Biol.* 31 (10), R522–r529. doi:10.1016/j.cub.2021.04.011

Engl, W., Arasi, B., Yap, L. L., Thiery, J. P., and Viasnoff, V. (2014). Actin Dynamics Modulate Mechanosensitive Immobilization of E-Cadherin at Adherens Junctions. *Nat. Cel Biol* 16 (6), 584–591. doi:10.1038/ncb2973

Esue, O., Carson, A. A., Tseng, Y., and Wirtz, D. (2006). A Direct Interaction between Actin and Vimentin Filaments Mediated by the Tail Domain of Vimentin. *J. Biol. Chem.* 281 (41), 30393–30399. doi:10.1074/jbc.m605452200

Feliksiak, K., Witko, T., Solarz, D., Guzik, M., and Rajfur, Z. (2020). Vimentin Association with Nuclear Grooves in Normal MEF 3T3 Cells. *Int. J. Mol. Sci.* 21 (20), 7478. doi:10.3390/ijms21207478

Feng, D., DuMontier, C., and Pollak, M. R. (2018). Mechanical Challenges and Cytoskeletal Impairments in Focal Segmental Glomerulosclerosis. *Am. J. Physiology-Renal Physiol.* 314 (5), F921–f925. doi:10.1152/ajprenal.00641.2017

Fleissner, F., Kumar, S., Klein, N., Wirth, D., Dhiman, R., Schneider, D., et al. (2020). Tension Causes Unfolding of Intracellular Vimentin Intermediate Filaments. *Adv. Biosyst.* 4 (11), e2000111. doi:10.1002/adbi.202000111

Folker, E. S., Östlund, C., Luxton, G. W. G., Worman, H. J., and Gundersen, G. G. (2011). Lamin A Variants that Cause Striated Muscle Disease Are Defective in Anchoring Transmembrane Actin-Associated Nuclear Lines for Nuclear Movement. *Proc. Natl. Acad. Sci. U.S.A.* 108 (1), 131–136. doi:10.1073/pnas.1000824108

Forsting, J., Kraxner, J., Witt, H., Janshoff, A., and Köster, S. (2019). Vimentin Intermediate Filaments Undergo Irreversible Conformational Changes during Cyclic Loading. *Nano Lett.* 19 (10), 7349–7356. doi:10.1021/acs.nanolett.9b02972

Gan, Z., Ding, L., Burckhardt, C. J., Lowery, J., Zaritsky, A., Sitterley, K., et al. (2016). Vimentin Intermediate Filaments Template Microtubule Networks to Enhance Persistence in Cell Polarity and Directed Migration. *Cel Syst.* 3 (5), 500–501. doi:10.1016/j.cels.2016.11.011

Gardel, M. L., Shin, J. H., MacKintosh, F. C., Mahadevan, L., Matsudaira, P., and Weitz, D. A. (2004). Elastic Behavior of Cross-Linked and Bundled Actin Networks. *Science* 304 (5675), 1301–1305. doi:10.1126/science.1095087

Gregor, M., Osmanagic-Myers, S., Burgstaller, G., Wolfram, M., Fischer, I., Walko, G., et al. (2014). Mechanosensing through Focal Adhesion-anchored Intermediate Filaments. *FASEB J.* 28 (2), 715–729. doi:10.1096/fj.13-231829

Gudimchuk, N. B., and McIntosh, J. R. (2021). Regulation of Microtubule Dynamics, Mechanics and Function through the Growing Tip. *Nat. Rev. Mol. Cel Biol* 22 (12), 777–795. doi:10.1038/s41580-021-00399-x

Guo, M., Ehrlicher, A. J., Mahammad, S., Fabich, H., Jensen, M. H., Moore, J. R., et al. (2013). The Role of Vimentin Intermediate Filaments in Cortical and Cytoplasmic Mechanics. *Biophysical J.* 105 (7), 1562–1568. doi:10.1016/j.bpj.2013.08.037

Gupta, M., Doss, B. L., Kocgozlu, L., Pan, M., Mège, R. M., Callan-Jones, A., et al. (2019). Cell Shape and Substrate Stiffness Drive Actin-Based Cell Polarity. *Phys. Rev. E* 99 (1-1), 012412. doi:10.1103/PhysRevE.99.012412

Haines, R. L., and Lane, E. B. (2012). Keratins and Disease at a Glance. *J. Cel Sci* 125 (Pt 17), 3923–3928. doi:10.1242/jcs.099655

Helfand, B. T., Mendez, M. G., Murthy, S. N. P., Shumaker, D. K., Grin, B., Mahammad, S., et al. (2011). Vimentin Organization Modulates the Formation of Lamellipodia. *Mol. Biol. Cel* 22 (8), 1274–1289. doi:10.1091/mbc.e10-08-0699

Hu, J., Li, Y., Hao, Y., Zheng, T., Gupta, S. K., Parada, G. A., et al. (2019). High Stretchability, Strength, and Toughness of Living Cells Enabled by Hyperelastic Vimentin Intermediate Filaments. *Proc. Natl. Acad. Sci. U.S.A.* 116 (35), 17175–17180. doi:10.1073/pnas.1903890116

Huber, F., Boire, A., López, M. P., and Koenderink, G. H. (2015). Cytoskeletal Crosstalk: when Three Different Personalities Team up. *Curr. Opin. Cel Biol.* 32, 39–47. doi:10.1016/j.ceb.2014.10.005

Janota, C. S., Calero-Cuenca, F. J., and Gomes, E. R. (2020). The Role of the Cell Nucleus in Mechanotransduction. *Curr. Opin. Cel Biol.* 63, 204–211. doi:10.1016/j.ceb.2020.03.001

Jiu, Y., Peränen, J., Schaible, N., Cheng, F., Eriksson, J. E., Krishnan, R., et al. (2017). Vimentin Intermediate Filaments Control Actin Stress Fiber Assembly through GEF-H1 and RhoA. *J. Cel Sci* 130 (5), 892–902. doi:10.1242/jcs.196881

Jiu, Y., Lehtimäki, J., Tojkander, S., Cheng, F., Jäälinoja, H., Liu, X., et al. (2015). Bidirectional Interplay between Vimentin Intermediate Filaments and Contractile Actin Stress Fibers. *Cel Rep.* 11 (10), 1511–1518. doi:10.1016/j.celrep.2015.05.008

Kechagia, J. Z., Ivaska, J., and Roca-Cusachs, P. (2019). Integrins as Biomechanical Sensors of the Microenvironment. *Nat. Rev. Mol. Cel Biol* 20 (8), 457–473. doi:10.1038/s41580-019-0134-2

Kim, H., Nakamura, F., Lee, W., Shifrin, Y., Arora, P., and McCulloch, C. A. (2010). Filamin A Is Required for Vimentin-Mediated Cell Adhesion and Spreading. *Am. J. Physiology-Cell Physiol.* 298 (2), C221–C236. doi:10.1152/ajpcell.00323.2009

Kim, J., Yang, C., Kim, E. J., Jang, J., Kim, S. J., Kang, S. M., et al. (2016). Vimentin Filaments Regulate Integrin-Ligand Interactions by Binding to the Cytoplasmic Tail of Integrin β3. *J. Cel Sci* 129 (10), 2030–2042. doi:10.1242/jcs.180315

Kim, Y.-B., Hlavaty, D., Maycock, J., and Lechler, T. (2021). Roles for Ndel1 in Keratin Organization and Desmosome Function. *Mol. Biol. Cel* 32 (20), ar2. doi:10.1091/mbc.e21-02-0087

Kirby, T. J., and Lammerding, J. (2018). Emerging Views of the Nucleus as a Cellular Mechanosensor. *Nat. Cel Biol* 20 (4), 373–381. doi:10.1038/s41556-018-0038-y

Ko, C. S., Tserunyan, V., and Martin, A. C. (2019). Microtubules Promote Intercellular Contractile Force Transmission during Tissue Folding. *J. Cel Biol.* 218 (8), 2726–2742. doi:10.1083/jcb.201902011

Laly, A. C., Sliogeryte, K., Pundel, O. J., Ross, R., Keeling, M. C., Avisetti, D., et al. (2021). The Keratin Network of Intermediate Filaments Regulates Keratinocyte Rigidity Sensing and Nuclear Mechanotransduction. *Sci. Adv.* 7 (5), 1–12. doi:10.1126/sciadv.abd6187

Lanier, M. H., Kim, T., and Cooper, J. A. (2015). CARMIL2 Is a Novel Molecular Connection between Vimentin and Actin Essential for Cell Migration and Invadopodia Formation. *Mol. Biol. Cel* 26 (25), 4577–4588. doi:10.1091/mbc.e15-08-0552

Latorre, E., Kale, S., Casares, L., Gómez-González, M., Uroz, M., Valon, L., et al. (2018). Active Superelasticity in Three-Dimensional Epithelia of Controlled Shape. *Nature* 563 (7730), 203–208. doi:10.1038/s41586-018-0671-4

Leduc, C., and Etienne-Manneville, S. (2017). Regulation of Microtubule-Associated Motors Drives Intermediate Filament Network Polarization. *J. Cel Biol* 216 (6), 1689–1703. doi:10.1083/jcb.201607045

Lee, G., Han, S.-B., and Kim, D.-H. (2021a). Cell-ECM Contact-Guided Intracellular Polarization Is Mediated via Lamin A/C Dependent Nucleus-Cytoskeletal Connection. *Biomaterials* 268, 120548. doi:10.1016/j.biomaterials.2020.120548

Lee, G., Leech, G., Rust, M. J., Das, M., McGorty, R. J., Ross, J. L., et al. (2021b). Myosin-driven Actin-Microtubule Networks Exhibit Self-Organized Contractile Dynamics. *Sci. Adv.* 7 (6), eabe4334. doi:10.1126/sciadv.abe4334

Leube, R. E., Moch, M., and Windoffer, R. (2015). Intermediate Filaments and the Regulation of Focal Adhesion. *Curr. Opin. Cel Biol.* 32, 13–20. doi:10.1016/j.ceb.2014.09.011

Li, Q.-F., Spinelli, A. M., Wang, R., Anfinogenova, Y., Singer, H. A., and Tang, D. D. (2006). Critical Role of Vimentin Phosphorylation at Ser-56 by P21-Activated Kinase in Vimentin Cytoskeleton Signaling. *J. Biol. Chem.* 281 (45), 34716–34724. doi:10.1074/jbc.m607715200

Lin, Y.-C., Koenderink, G. H., MacKintosh, F. C., and Weitz, D. A. (2011). Control of Non-linear Elasticity in F-Actin Networks with Microtubules. *Soft Matter* 7 (3), 902–906. doi:10.1039/c0sm00478b

Lomakin, A. J., Cattin, C. J., Cuvelier, D., Alraies, Z., Molina, M., Nader, G. P. F., et al. (2020). The Nucleus Acts as a Ruler Tailoring Cell Responses to Spatial Constraints. *Science* 370 (6514), eaba2894. doi:10.1126/science.aba2894

Lombardi, M. L., Jaalouk, D. E., Shanahan, C. M., Burke, B., Roux, K. J., and Lammerding, J. (2011). The Interaction between Nesprins and Sun Proteins at the Nuclear Envelope Is Critical for Force Transmission between the Nucleus and Cytoskeleton. *J. Biol. Chem.* 286 (30), 26743–26753. doi:10.1074/jbc.m111.233700

López, M. P., Huber, F., Grigoriev, I., Steinmetz, M. O., Akhmanova, A., Koenderink, G. H., et al. (2014). Actin-microtubule Coordination at Growing Microtubule Ends. *Nat. Commun.* 5, 4778. doi:10.1038/ncomms5778

Lowery, J., Kuczmarski, E. R., Herrmann, H., and Goldman, R. D. (2015). Intermediate Filaments Play a Pivotal Role in Regulating Cell Architecture and Function. *J. Biol. Chem.* 290 (28), 17145–17153. doi:10.1074/jbc.r115.640359

MacTaggart, B., and Kashina, A. (2021). Posttranslational Modifications of the Cytoskeleton. *Cytoskeleton* 78 (4), 142–173. doi:10.1002/cm.21679

Maniotis, A. J., Chen, C. S., and Ingber, D. E. (1997). Demonstration of Mechanical Connections between Integrins, Cytoskeletal Filaments, and Nucleoplasm that Stabilize Nuclear Structure. *Proc. Natl. Acad. Sci. U.S.A.* 94 (3), 849–854. doi:10.1073/pnas.94.3.849

Marks, P. C., and Petrie, R. J. (2022). Push or Pull: How Cytoskeletal Crosstalk Facilitates Nuclear Movement through 3D Environments. *Phys. Biol.* 19 (2). doi:10.1088/1478-3975/ac45e3

McNally, F. J. (1996). Modulation of Microtubule Dynamics during the Cell Cycle. *Curr. Opin. Cel Biol.* 8 (1), 23–29. doi:10.1016/s0955-0674(96)80044-5

Mendez, M. G., Restle, D., and Janmey, P. A. (2014). Vimentin Enhances Cell Elastic Behavior and Protects against Compressive Stress. *Biophysical J.* 107 (2), 314–323. doi:10.1016/j.bpj.2014.04.050

Moch, M., and Leube, R. E. (2021). Hemidesmosome-Related Keratin Filament Bundling and Nucleation. *Int. J. Mol. Sci.* 22 (4), 2130. doi:10.3390/ijms22042130

Moeton, M., Stassen, O. M. J. A., Sluijs, J. A., van der Meer, V. W. N., Kluivers, L. J., van Hoorn, H., et al. (2016). GFAP Isoforms Control Intermediate Filament Network Dynamics, Cell Morphology, and Focal Adhesions. *Cell. Mol. Life Sci.* 73 (21), 4101–4120. doi:10.1007/s00018-016-2239-5

Mohammed, F., Trieber, C., Overduin, M., and Chidgey, M. (2020). Molecular Mechanism of Intermediate Filament Recognition by Plakin Proteins. *Biochim. Biophys. Acta (Bba) - Mol. Cel Res.* 1867 (11), 118801. doi:10.1016/j.bbamcr.2020.118801

Nardone, G., Oliver-De La Cruz, J., Vrbsky, J., Martini, C., Pribyl, J., Skládal, P., et al. (2017). YAP Regulates Cell Mechanics by Controlling Focal Adhesion Assembly. *Nat. Commun.* 8 (1), 15321. doi:10.1038/ncomms15321

Nöding, B., Herrmann, H., and Köster, S. (2014). Direct Observation of Subunit Exchange along Mature Vimentin Intermediate Filaments. *Biophysical J.* 107 (12), 2923–2931. doi:10.1016/j.bpj.2014.09.050

Ohi, R., Strothman, C., and Zanic, M. (2021). Impact of the 'tubulin Economy' on the Formation and Function of the Microtubule Cytoskeleton. *Curr. Opin. Cel Biol.* 68, 81–89. doi:10.1016/j.ceb.2020.09.005

Osmanagic-Myers, S., Rus, S., Wolfram, M., Brunner, D., Goldmann, W. H., Bonakdar, N., et al. (2015). Plectin Reinforces Vascular Integrity by Mediating Crosstalk between the Vimentin and the Actin Networks. *J. Cel Sci* 128 (22), 4138–4150. doi:10.1242/jcs.172056

Ostrowska-Podhorodecka, Z., Ding, I., Lee, W., Tanic, J., Abbasi, S., Arora, P. D., et al. (2021). Vimentin Tunes Cell Migration on Collagen by Controlling β1 Integrin Activation and Clustering. *J. Cel Sci* 134 (6), jcs254359. doi:10.1242/jcs.254359

Patteson, A. E., Vahabikashi, A., Pogoda, K., Adam, S. A., Mandal, K., Kittisopikul, M., et al. (2019). Vimentin Protects Cells against Nuclear Rupture and DNA Damage during Migration. *J. Cel Biol.* 218 (12), 4079–4092. doi:10.1083/jcb.201902046

Pelletier, V., Gal, N., Fournier, P., and Kilfoil, M. L. (2009). Microrheology of Microtubule Solutions and Actin-Microtubule Composite Networks. *Phys. Rev. Lett.* 102 (18), 188303. doi:10.1103/physrevlett.102.188303

Pimm, M. L., and Henty-Ridilla, J. L. (2021). New Twists in Actin-Microtubule Interactions. *Mol. Biol. Cel* 32 (3), 211–217. doi:10.1091/mbc.e19-09-0491

Plastino, J., and Blanchoin, L. (2018). Dynamic Stability of the Actin Ecosystem. *J. Cel Sci* 132 (4), jcs219832. doi:10.1242/jcs.219832

Prechova, M., Adamova, Z., Schweizer, A. L., Maninova, M., Bauer, A., Kah, D., et al. (2022). Plectin-mediated Cytoskeletal Crosstalk Controls Cell Tension and Cohesion in Epithelial Sheets. *J. Cel Biol* 221 (3), e202105146. doi:10.1083/jcb.202105146

Price, A. J., Cost, A.-L., Ungewiß, H., Waschke, J., Dunn, A. R., and Grashoff, C. (2018). Mechanical Loading of Desmosomes Depends on the Magnitude and Orientation of External Stress. *Nat. Commun.* 9 (1), 5284. doi:10.1038/s41467-018-07523-0

Rafiq, N. B. M., Nishimura, Y., Plotnikov, S. V., Thiagarajan, V., Zhang, Z., Shi, S., et al. (2019). A Mechano-Signalling Network Linking Microtubules, Myosin IIA Filaments and Integrin-Based Adhesions. *Nat. Mater.* 18 (6), 638–649. doi:10.1038/s41563-019-0371-y

Ramdas, N. M., and Shivashankar, G. V. (2015). Cytoskeletal Control of Nuclear Morphology and Chromatin Organization. *J. Mol. Biol.* 427 (3), 695–706. doi:10.1016/j.jmb.2014.09.008

Redmond, C. J., and Coulombe, P. A. (2021). Intermediate Filaments as Effectors of Differentiation. *Curr. Opin. Cel Biol.* 68, 155–162. doi:10.1016/j.ceb.2020.10.009

Robert, A., Rossow, M. J., Hookway, C., Adam, S. A., and Gelfand, V. I. (2015). Vimentin Filament Precursors Exchange Subunits in an ATP-dependent Manner. *Proc. Natl. Acad. Sci. U S A.* 112 (27), E3505–E3514. doi:10.1073/pnas.1505303112

Roberts, B. J., Pashaj, A., Johnson, K. R., and Wahl, J. K. (2011). Desmosome Dynamics in Migrating Epithelial Cells Requires the Actin Cytoskeleton. *Exp. Cel Res.* 317 (20), 2814–2822. doi:10.1016/j.yexcr.2011.09.003

Roux, K. J., Crisp, M. L., Liu, Q., Kim, D., Kozlov, S., Stewart, C. L., et al. (2009). Nesprin 4 Is an Outer Nuclear Membrane Protein that Can Induce Kinesin-Mediated Cell Polarization. *Proc. Natl. Acad. Sci. U.S.A.* 106 (7), 2194–2199. doi:10.1073/pnas.0808602106

Rübsam, M., Broussard, J. A., Wickström, S. A., Nekrasova, O., Green, K. J., and Niessen, C. M. (2018). Adherens Junctions and Desmosomes Coordinate Mechanics and Signaling to Orchestrate Tissue Morphogenesis and Function: An Evolutionary Perspective. *Cold Spring Harb Perspect. Biol.* 10 (11), a029207. doi:10.1101/cshperspect.a029207

Sanghvi-Shah, R., and Weber, G. F. (2017). Intermediate Filaments at the Junction of Mechanotransduction, Migration, and Development. *Front. Cel Dev. Biol.* 5, 1–19. doi:10.3389/fcell.2017.00081

Schaedel, L., Lorenz, C., Schepers, A. V., Klumpp, S., and Köster, S. (2021). Vimentin Intermediate Filaments Stabilize Dynamic Microtubules by Direct Interactions. *Nat. Commun.* 12 (1), 3799. doi:10.1038/s41467-021-23523-z

Schoumacher, M., Goldman, R. D., Louvard, D., and Vignjevic, D. M. (2010). Actin, Microtubules, and Vimentin Intermediate Filaments Cooperate for Elongation of Invadopodia. *J. Cel Biol.* 189 (3), 541–556. doi:10.1083/jcb.200909113

Seddiki, R., Narayana, G. H. N. S., Strale, P.-O., Balcioglu, H. E., Peyret, G., Yao, M., et al. (2018). Force-dependent Binding of Vinculin to α-catenin Regulates Cell-Cell Contact Stability and Collective Cell Behavior. *Mol. Biol. Cel* 29 (4), 380–388. doi:10.1091/mbc.e17-04-0231

Seetharaman, S., Vianay, B., Roca, V., Farrugia, A. J., De Pascalis, C., Boëda, B., et al. (2021). Microtubules Tune Mechanosensitive Cell Responses. *Nat. Mater.* 21, 366–377. doi:10.1038/s41563-021-01108-x

Serres, M. P., Samwer, M., Truong Quang, B. A., Lavoie, G., Perera, U., Görlich, D., et al. (2020). F-actin Interactome Reveals Vimentin as a Key Regulator of Actin Organization and Cell Mechanics in Mitosis. *Dev. Cel* 52 (2), 210–222. e217. doi:10.1016/j.devcel.2019.12.011

Sjöqvist, M., Antfolk, D., Suarez-Rodriguez, F., and Sahlgren, C. (2021). From Structural Resilience to Cell Specification - Intermediate Filaments as Regulators of Cell Fate. *Faseb J.* 35 (1), e21182. doi:10.1096/fj.202001627r

Sun, Z., Guo, S. S., and Fässler, R. (2016). Integrin-mediated Mechanotransduction. *J. Cel Biol.* 215 (4), 445–456. doi:10.1083/jcb.201609037

Svitkina, T. M., Verkhovsky, A. B., and Borisy, G. G. (1996). Plectin Sidearms Mediate Interaction of Intermediate Filaments with Microtubules and Other Components of the Cytoskeleton. *J. Cel Biol.* 135 (4), 991–1007. doi:10.1083/jcb.135.4.991

Takeda, M., Sami, M. M., and Wang, Y.-C. (2018). A Homeostatic Apical Microtubule Network Shortens Cells for Epithelial Folding via a Basal Polarity Shift. *Nat. Cel Biol* 20 (1), 36–45. doi:10.1038/s41556-017-0001-3

Tariq, Z., Zhang, H., Chia-Liu, A., Shen, Y., Gete, Y., Xiong, Z.-M., et al. (2017). Lamin A and Microtubules Collaborate to Maintain Nuclear Morphology. *Nucleus* 8 (4), 433–446. doi:10.1080/19491034.2017.1320460

Terriac, E., Coceano, G., Mavajian, Z., Hageman, T. A., Christ, A. F., Testa, I., et al. (2017). Vimentin Levels and Serine 71 Phosphorylation in the Control of Cell-Matrix Adhesions, Migration Speed, and Shape of Transformed Human Fibroblasts. *Cells* 6 (1), 2. doi:10.3390/cells6010002

Theriot, J. A., and Mitchison, T. J. (1991). Actin Microfilament Dynamics in Locomoting Cells. *Nature* 352 (6331), 126–131. doi:10.1038/352126a0

Valencia, R. G., Walko, G., Janda, L., Novacek, J., Mihailovska, E., Reipert, S., et al. (2013). Intermediate Filament-Associated Cytolinker Plectin 1c Destabilizes Microtubules in Keratinocytes. *Mol. Biol. Cel* 24 (6), 768–784. doi:10.1091/mbc.e12-06-0488

van Bodegraven, E. J., and Etienne-Manneville, S. (2020). Intermediate Filaments against Actomyosin: the David and Goliath of Cell Migration. *Curr. Opin. Cel Biol.* 66, 79–88. doi:10.1016/j.ceb.2020.05.006

Venturini, V., Pezzano, F., Català Castro, F., Häkkinen, H.-M., Jiménez-Delgado, S., Colomer-Rosell, M., et al. (2020). The Nucleus Measures Shape Changes for Cellular Proprioception to Control Dynamic Cell Behavior. *Science* 370 (6514), eaba2644. doi:10.1126/science.aba2644

Vohnoutka, R. B., Gulvady, A. C., Goreczny, G., Alpha, K., Handelman, S. K., Sexton, J. Z., et al. (2019). The Focal Adhesion Scaffold Protein Hic-5 Regulates Vimentin Organization in Fibroblasts. *Mol. Biol. Cel* 30 (25), 3037–3056. doi:10.1091/mbc.e19-08-0442

Wang, W., Zuidema, A., te Molder, L., Nahidiazar, L., Hoekman, L., Schmidt, T., et al. (2020). Hemidesmosomes Modulate Force Generation via Focal Adhesions. *J. Cel Biol* 219 (2), e201904137. doi:10.1083/jcb.201904137

Warren, D. T., Zhang, Q., Weissberg, P. L., and Shanahan, C. M. (2005). Nesprins: Intracellular Scaffolds that Maintain Cell Architecture and Coordinate Cell Function? *Expert Rev. Mol. Med.* 7 (11), 1–15. doi:10.1017/s1462399405009294

Wiche, G., Osmanagic-Myers, S., and Castañón, M. J. (2015). Networking and Anchoring through Plectin: a Key to IF Functionality and Mechanotransduction. *Curr. Opin. Cel Biol.* 32, 21–29. doi:10.1016/j.ceb.2014.10.002

Wilhelmsen, K., Litjens, S. H. M., Kuikman, I., Tshimbalanga, N., Janssen, H., van den Bout, I., et al. (2005). Nesprin-3, a Novel Outer Nuclear Membrane Protein, Associates with the Cytoskeletal Linker Protein Plectin. *J. Cel Biol* 171 (5), 799–810. doi:10.1083/jcb.200506083

Windoffer, R., Kölsch, A., Wöll, S., and Leube, R. E. (2006). Focal Adhesions Are Hotspots for Keratin Filament Precursor Formation. *J. Cel Biol.* 173 (3), 341–348. doi:10.1083/jcb.200511124

Yao, M., Qiu, W., Liu, R., Efremov, A. K., Cong, P., Seddiki, R., et al. (2014). Force-dependent Conformational Switch of α-catenin Controls Vinculin Binding. *Nat. Commun.* 5 (1), 4525. doi:10.1038/ncomms5525

Yap, A. S., Duszyc, K., and Viasnoff, V. (2018). Mechanosensing and Mechanotransduction at Cell-Cell Junctions. *Cold Spring Harb Perspect. Biol.* 10 (8), 1–16. doi:10.1101/cshperspect.a028761

Zhen, Y. Y., Libotte, T., Munck, M., Noegel, A. A., and Korenbaum, E. (2002). NUANCE, a Giant Protein Connecting the Nucleus and Actin Cytoskeleton. *J. Cel Sci* 115 (Pt 15), 3207–3222. doi:10.1242/jcs.115.15.3207

Zuidema, A., Wang, W., and Sonnenberg, A. (2020). Crosstalk between Cell Adhesion Complexes in Regulation of MechanotransductionBioEssays: News and Reviews in Molecular, Cellular and Developmental Biology. *Bioessays* 42 (11), e2000119. doi:10.1002/bies.202000119

Conflict of Interest: The authors declare that the research was conducted in the absence of any commercial or financial relationships that could be construed as a potential conflict of interest.

Publisher's Note: All claims expressed in this article are solely those of the authors and do not necessarily represent those of their affiliated organizations, or those of the publisher, the editors and the reviewers. Any product that may be evaluated in this article, or claim that may be made by its manufacturer, is not guaranteed or endorsed by the publisher.

frontiers | Frontiers in Cell and Developmental Biology

REVIEW
published: 28 April 2022
doi: 10.3389/fcell.2022.872759

Pathophysiological Role of Vimentin Intermediate Filaments in Lung Diseases

*Ranu Surolia and Veena B. Antony**

Division of Pulmonary, Allergy and Critical Care, Department of Medicine, University of Alabama at Birmingham, Birmingham, AL, United States

Vimentin intermediate filaments, a type III intermediate filament, are among the most widely studied IFs and are found abundantly in mesenchymal cells. Vimentin intermediate filaments localize primarily in the cytoplasm but can also be found on the cell surface and extracellular space. The cytoplasmic vimentin is well-recognized for its role in providing mechanical strength and regulating cell migration, adhesion, and division. The post-translationally modified forms of Vimentin intermediate filaments have several implications in host-pathogen interactions, cancers, and non-malignant lung diseases. This review will analyze the role of vimentin beyond just the epithelial to mesenchymal transition (EMT) marker highlighting its role as a regulator of host-pathogen interactions and signaling pathways for the pathophysiology of various lung diseases. In addition, we will also examine the clinically relevant anti-vimentin compounds and antibodies that could potentially interfere with the pathogenic role of Vimentin intermediate filaments in lung disease.

Keywords: vimentin (intermediate filaments), acute lung injury, chronic lung injury, host pathogen interactions, viral infections, bacterial infections, lung cancer, anti-vimentin antibodies

OPEN ACCESS

Edited by:
Dolores Pérez-Sala, Spanish National Research Council (CSIC), Spain

Reviewed by:
Konstantinos Stamatakis, Spanish National Research Council (CSIC), Spain
Tatiana Bogush, Russian Cancer Research Center NN Blokhin, Russia
Karen Ridge, Northwestern University, United States

****Correspondence:***
Veena B. Antony
vantony@uabmc.edu

Specialty section:
This article was submitted to Cell Growth and Division, a section of the journal Frontiers in Cell and Developmental Biology

Received: *09 February 2022*
Accepted: *13 April 2022*
Published: *28 April 2022*

Citation:
Surolia R and Antony VB (2022) Pathophysiological Role of Vimentin Intermediate Filaments in Lung Diseases. Front. Cell Dev. Biol. 10:872759. doi: 10.3389/fcell.2022.872759

INTRODUCTION

Vimentin, a type III intermediate filament, is one of the cell cytoskeleton proteins in mesenchymal cells (Herrmann et al., 1996) and is prominently associated with the maintenance of cell structure, and migration (Ivaska et al., 2007; Eriksson et al., 2009; Herrmann et al., 2009; Battaglia et al., 2018). The $Vim^{-/-}$ mice survive and grow normally (Colucci-Guyon et al., 1994). However, subsequent studies demonstrated that Vimentin intermediate filaments have crucial physiological roles in cell homeostasis (Gurland and Gundersen, 1995; Ivaska et al., 2007; Battaglia et al., 2018; Schaedel et al., 2021), and the $Vim^{-/-}$ mice and cells have altered functions under stress conditions (Henrion et al., 1997; Terzi et al., 1997; Eckes et al., 2000; Nieminen et al., 2006). These studies brought attention to the silent yet crucial role of Vimentin intermediate filaments in the pathophysiological arena. This review will focus on the role of Vimentin intermediate filaments in the pathogenesis of various lung diseases.

VIMENTIN INTERMEDIATE FILAMENTS AND POST-TRANSLATIONAL MODIFICATIONS

Vimentin is a type III intermediate filament named by Frank and Weber in 1978 (Franke et al., 1978). The name vimentin was derived from the Latin word "vimentum," which refers to arrays of flexible rods that can be arranged in both ordered (e.g., lattices, filigrees, and wicker-work) and non-ordered

(e.g., brushwood) forms. As with other types III IFs, vimentin has a central α-helical "rod" domain flanked by the head (N-terminal) and tail (C-terminal) domains on both sides (Chernyatina et al., 2012). Vimentin intermediate filaments, as other intermediate filaments, must rearrange and reorganized during physiological and pathophysiological events that change the physical and functional properties of a cell. These processes are primarily driven by post-translational modifications (PTMs). PTMs of vimentin intermediate filaments change its shape, distribution, and interactions with other signaling molecules for the rapid modulation of its function under different conditions (Kraxner et al., 2021). The intrinsic polyelectrolyte nature of vimentin intermediate filaments (Janmey et al., 2014) is associated with non-enzymatic PTMs during redox imbalances (Perez-Sala et al., 2015; Wilson and Gonzalez-Billault, 2015)and can be mediated through enzymatic or non-enzymatic reactions. The interactions of Vimentin intermediate filaments with Ca^{2+} and Mg^{2+} increase assembly, crosslinking, and stiffness (Lin et al., 2010). Other non-enzymatic modifications are mostly oxidizing, resulting in glutathionylation, nitrosylation, or carbonylation of vimentin (West et al., 2006; Huang et al., 2009; Chavez et al., 2010; Griesser et al., 2021). The cysteine 328 (Cys 328/C328) is targeted by various oxidative modifications (Stamatakis et al., 2006; Gharbi et al., 2007; Perez-Sala et al., 2015). The cells transfected with GFP- tagged C328S vimentin (mutant) demonstrated presence of disassembled short squiggled and dots kind of GFP positive vimentin fragments (Perez-Sala et al., 2015). Hence, oxidation at C328 can cause disassembly of vimentin intermediate filaments.

The most common enzymatic PTM on vimentin intermediate filaments is phosphorylation (Sihag et al., 2007; Snider and Omary, 2014), and is essential for spatio-temporal regulation of its assembly, tissue-specific functions, and in some cases, diseases pathogenesis (Omary et al., 2006; Sihag et al., 2007; Snider and Omary, 2014; Snider et al., 2018). Multiple kinases, various chemical compounds, growth factors, cytokine treatments, viral infections can induce phosphorylation of vimentin intermediate filaments, and the details on these factors and phosphorylation sites is available at (https://www.phosphosite.org/proteinAction.action?id=2622&showAllSites=true). Specifically kinases such as protein kinase A (Inagaki et al., 1987), protein kinase C (Ivaska et al., 2005), cdc2 kinase (Chou et al., 1990; Chou et al., 1991; Chang et al., 2012), p21 activated kinase (Eriksson et al., 2004; Li et al., 2006), Rho-associated kinases (Goto et al., 1998; Sin et al., 1998), Akt1 (Zhu et al., 2011; Wang et al., 2012; Li et al., 2017b), Aurora-B (Goto et al., 2003), and CaMKIIA (Stefanovic et al., 2005) are well-known for phosphorylating vimentin.

PTMs other than oxidation and phosphorylation, include glycosylation (Snider et al., 2018; Tarbet et al., 2018), ubiquitination (Zhu et al., 2017; Cheng et al., 2019), sumoylation (Wang et al., 2010), acetylation (Guo et al., 2018) and citrullination (Inagaki et al., 1989). These PTMs on vimentin intermediate filaments are associated with but are not limited to stress sensing (Perez-Sala et al., 2015; Griesser et al., 2021), regulation of turnover of IF assembly (Herrmann et al., 2009), cell survival (Dinsdale et al., 2004), protein-protein interactions (Wang et al., 2012), and interaction with the nuclear membrane (Neelam et al., 2015). Sumoylation of vimentin by Protein Inhibitor of Activated STAT3 (PIAS3) inhibits glioma cell migration (Wang et al., 2010) while acetylation of vimentin intermediate filaments at K120 b SIRT5 increases metastasis in hepatocellular carcinoma (Guo et al., 2018). Citrullination of vimentin intermediate filaments leads to secretion of citrullinated vimentin (Cit-Vim) as an autoantigen implicated in the pathogenesis of rheumatoid arthritis (RA) (Vossenaar et al., 2004). Cit-Vim interacts with B cells to result autoimmunity in RA (Vossenaar et al., 2004; Valesini et al., 2015). Interestingly, the immunogenic properties of Cit-Vim peptides are being explored to develop an anti-cancer vaccine (Brentville et al., 2020). In recent studies, the pathological role of Cit-Vim in chronic lung diseases like COPD, pulmonary fibrosis, and sarcoidosis have been explored (Vassallo et al., 2014; Lugli et al., 2015; Ytterberg et al., 2015; Musaelyan et al., 2018; Nissen et al., 2019; Li et al., 2021).

VIMENTIN INTERMEDIATE FILAMENTS IN PATHOLOGICAL ROLES IN LUNG DISEASES

With the widespread use of specific antibodies, high-resolution microscopy techniques, and other advanced techniques, it has become evident that the differential amount and forms of vimentin and auto-antibodies to vimentin are present in the bronchoalveolar lavages, cells, and lung tissues from patients with various lung diseases demonstrating the pivotal role of vimentin in their pathogenesis (Rho et al., 2009; Wahlstrom et al., 2009; Li et al., 2017a; Musaelyan et al., 2018; Surolia et al., 2019; Zaccardelli et al., 2019; Li et al., 2021; Zaccardelli et al., 2021). These multiple forms of Vimentin intermediate filaments are comprehensively shown to be involved in inflammation (Benes et al., 2006; Dos Santos et al., 2015; Lam et al., 2018; Yu et al., 2018; Lam et al., 2020), and host-pathogen interactions (Garg et al., 2006; Babrak et al., 2015; Mahesh et al., 2016; Yu et al., 2016; Zhang et al., 2020) in non-malignant acute lung injuries (trauma, viral infections, bacterial infections, etc.) and chronic lung diseases (IPF, autoimmune ILDs, COPD, and asthma) (Li et al., 2017a; Musaelyan et al., 2018; Nissen et al., 2019; Surolia et al., 2019; Li et al., 2021). Additionally, vimentin is a gold-standard marker of epithelial–to-mesenchymal differentiation during malignancies (Satelli and Li, 2011; Bogush et al., 2020), and is also proposed as a diagnostic and prognostic marker in lung cancers (Rho et al., 2009; Dauphin et al., 2013; Rodriguez et al., 2013; Havel et al., 2015; Teocharoen et al., 2021).

Acute Lung Injury/Acute Respiratory Distress Syndrome

ALI is a broad term encompassing the pathophysiology of diffuse alveolar injury by toxin inhalation or as a consequence of systemic diseases, such as sepsis, severe shock, and trauma (Johnson and Matthay, 2010). The activated lymphocytes,

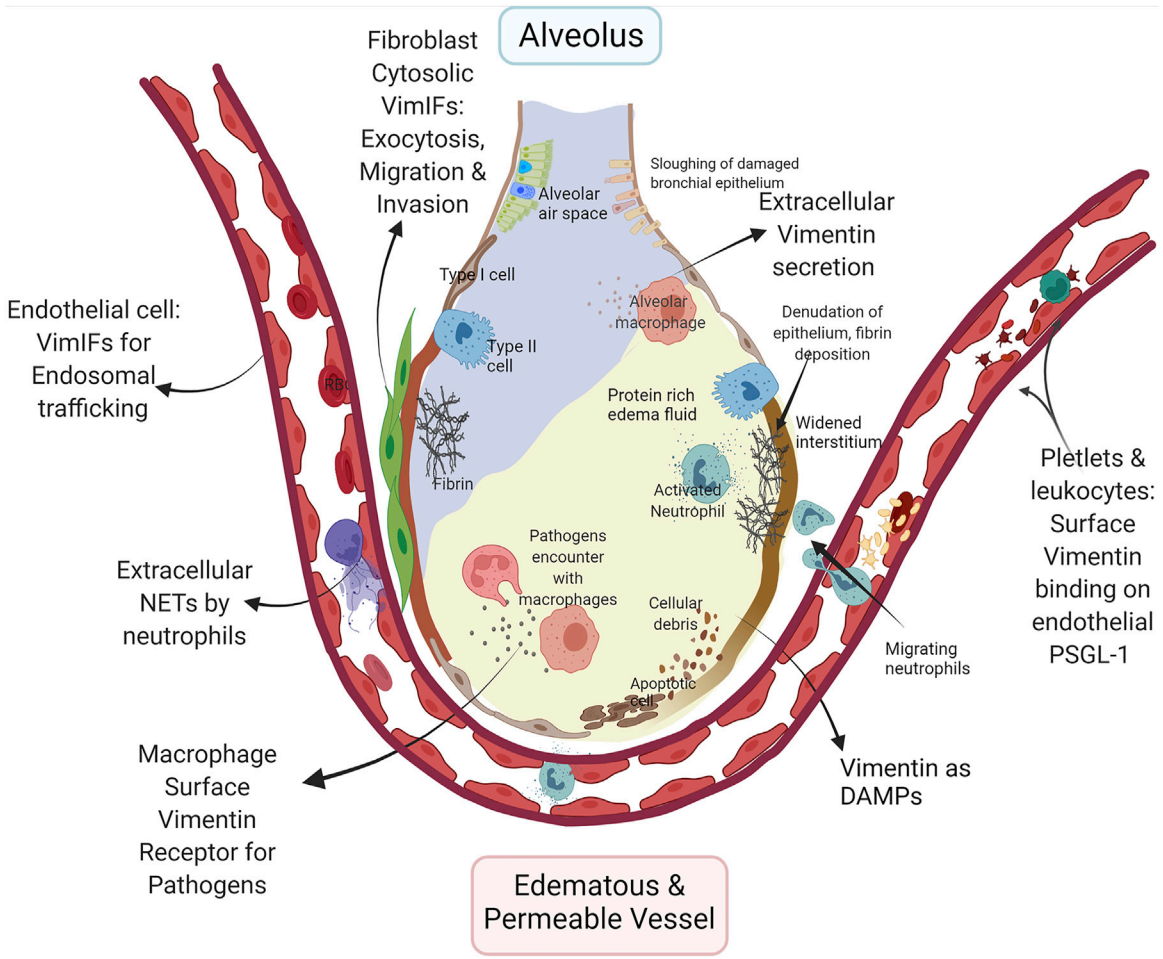

FIGURE 1 | Multifaceted role of vimentin in ARDS/ALI: Increased permeability of the alveolar-capillary membrane and pro-inflammatory conditions are fundamental characteristics of ALI. The schematic demonstrate very few epithelial cells due to increased cell death, and the intra-alveolar space depicted represents the alveolar lining fluid that is in contact with the air. The increased expression of surface vimentin on endothelial cells enhances lymphocyte adhesion and transmigration across endothelial cells through PSGL-1 binding on the lymphocytes, including neutrophils. Expression of vimentin and dynamics of Vimentin intermediate filaments regulate the endosomal signaling through Rab GTPase to transport VE-cadherin to the cell surface in endothelial cells for the maintenance of barrier functions. The PTM on vimentin in neutrophils leads to neutrophil extracellular traps (NETs) *via* netosis. NETs disrupt the microvascular endothelial barrier, increasing edematous and permeable vessels and causing a protein-rich fluid influx in the airspace. The increased expression of vimentin on platelets increases vitronectin and PAI-1 complex formation, which may provide stabilization of thrombi. The fibrins and fibrinolysis-related enzymes cause the dissolution of epithelial surface proteins and denudation of the epithelial barrier layer. Vimentin expression in fibroblasts regulates exocytosis and invasion, contributing to their proliferation in ALI. The surface vimentin on macrophage is essential for several bacteria and viruses for the host cell invasion and phagocytosis. Secreted vimentin from dead cell debris and activated immune cells act as DAMPs. The figure was created with BioRender.com.

cytokines, and Damage-Associated Molecular Patterns (DAMPs) weave a redundant inflammatory network for the development and progression of ALI (Tolle and Standiford, 2013). Various forms of vimentin regulate lymphocyte differentiation, activation, and inflammation through inflammasomes and act as DAMPs, signifying its multipronged role in the development of ALI (Dellagi et al., 1983; Mor-Vaknin et al., 2003; Benes et al., 2006; Nieminen et al., 2006; Dos Santos et al., 2015; Lam et al., 2018; Yu et al., 2018; Su L. et al., 2019; Su L.-X. et al., 2019; Lam et al., 2020) (**Figure 1**).

The differentiation of v-myb-transformed BM2 monoblasts cells to macrophage-like cells is dependent on the expression of vimentin (Benes et al., 2006). The migration and extravasation of monocytes through endothelial cells rely on vimentin intermediate filaments in inflammatory conditions (Nieminen et al., 2006; Lam et al., 2018). Furthermore, anti-vimentin antibodies decrease ROS generation in macrophages, inferring that the surface vimentin is pro-inflammatory (Mor-Vaknin et al., 2003) and are essential for killing bacteria and other pathogens (Forman and Torres, 2001). In addition to improving the anti-bacterial function of macrophages, a recent study demonstrated that the extracellular vimentin modulates the activity of LPS- activated dendritic cells and reduces Th1 differentiation (Yu et al., 2018).

Sepsis is an extreme immune response to an infection, where overactivation of innate immune response and

immunosuppression are responsible for complex immunopathology that causes ARDS. The apoptosis of lymphoid cells after the acute phase sepsis and suppression of lymphoid cell activity contribute to infection-related complications, seen in septic shock (Delano and Ward, 2016) (Su L.-X. et al., 2019). The suppression of vimentin in LPS treated macrophages showed increased inflammatory mediator, TNF-α. In contrast, it decreases the anti-inflammatory cytokine IL-10. Patients with sepsis and septic shock have increased levels of vimentin in serum. The disruption of Vimentin intermediate filaments in lymphocytes results in increased cell death and the release of soluble vimentin into blood circulation, which is related to the worse outcome of sepsis (Su L. et al., 2019). These regulatory responses of vimentin in the LPS injury model demonstrate the role of Vimentin intermediate filaments in immunosuppression during sepsis.

Recombinant extracellular vimentin has been shown to inhibit the infiltration of neutrophils into the lungs of the LPS-ALI mouse model (Lam et al., 2018). Extracellular vimentin itself acts as DAMP (Yu et al., 2018). In a pro-inflammatory environment, vimentin can be secreted by macrophages, monocytes (Mor-Vaknin et al., 2003), neutrophils (Kaplan, 2013), endothelial cells (Li et al., 2017a), apoptotic lymphocytes (Boilard et al., 2003), apoptotic neutrophils (Moisan and Girard, 2006), and injured skeletal muscle cells (Bryant et al., 2006) can secrete extracellular vimentin due to overexpression, traumatic cell injury, or cell death (Mellgren, 2010). As a DAMP, extracellular vimentin suppresses the pro-inflammatory adaptive immune responses by blocking the secretion of pro-inflammatory cytokines IL-12 and IL-6 from LPS stimulated dendritic cells (Yu et al., 2018).

The direct role of Vimentin intermediate filaments in innate immunity was demonstrated in a groundbreaking study showing that the inflammasome activation has obligatory requirements of interaction with vimentin (Dos Santos et al., 2015). Inflammasomes are molecular complexes comprised of basic protein units, including receptors and sensors that regulate the activation of caspase-1 and IL-1β (Guo et al., 2015). In macrophages, vimentin regulates innate immunity by regulating NACHT, LRR, and PYD domains-containing protein 3 (NLRP3) inflammasome pathway (Dos Santos et al., 2015). The inflammasome is a complex made of NLRP3, ASC (apoptosis-associated speck-like protein containing a CARD), and caspase-1. Vimentin intermediate filaments act as scaffolds to form this complex. The interaction of NLRP3 with Vimentin intermediate filaments occurs *via* macrophage inhibitor factor (MIF) (Lang et al., 2018), which activates inflammasomes. This study demonstrated that the vimentin-deficient mice exhibit attenuated ALI after the lipopolysaccharide (LPS) challenge, as represented by reductions in inflammation, IL-1β levels, and endothelial permeability (Dos Santos et al., 2015). Inflammasome complexes and their downstream products are involved in viral infections, bacterial infections, COPD, asthma, and ARDS, which have been reviewed in depth elsewhere (Dos Santos et al., 2012; Howrylak and Nakahira, 2017; Liu et al., 2021; Vora et al., 2021).

Acute lung injuries are associated with neutrophilia, alveolar-capillary membrane destruction, and increased permeability (**Figure 1**), mechanisms of which have been examined in detail (Lin and Fessler, 2021). The exaggerated extravasation and migration of leukocytes through pulmonary blood capillaries are dependent on P-selectins. P-selectin glycoprotein ligand-1 (PSGL-1) on leukocytes binds to P-selectin on platelets and endothelium wherein vimentin can act as an endogenous ligand for P-selectin. The treatment with recombinant vimentin attenuates ALI, plausibly by occupying P-selectin on endothelium which makes it is unavailable for the binding to PSGL-1 of leukocytes and platelets (Lam et al., 2018; Lam et al., 2020). Moreover, Vimentin intermediate filaments indirectly affect neutrophil-mediated ALI by regulating non-apoptotic neutrophil cell death, known as netosis (Brinkmann et al., 2004). During netosis, cellular chromatin is expelled out of the neutrophil, and the expelled chromatins are called neutrophil extracellular traps (NETs) that are decorated with granular proteins and proteases of neutrophils (Papayannopoulos et al., 2010), and these NETs are responsible for increased permeability of microvascular endothelium leading to ALI (Surolia et al., 2021). The NETs themselves can trigger NLRP3 inflammasomes for a sterile inflammation (Allam et al., 2013). The process of netosis is dependent on the citrullination of vimentin intermediate filaments, which leads to their disassembly. The disassembled of vimentin intermediate filaments is essential for the rounding of nucleus in neutrophils, and initiation of decondition of chromatin for netosis (Thiam et al., 2020).

Pulmonary edema in ARDS results from increased microvascular permeability. Vimentin intermediate filaments can indirectly regulate permeability through their functions as endosomal trafficking regulators. Vimentin intermediate filaments interact with endocytosis regulator proteins, namely Rab GTPase family proteins (Cogli et al., 2013; Margiotta et al., 2017; Romano et al., 2021). During edema, the inter-endothelial junctions are maintained by vascular endothelial cadherins (VE-cadherin). Recently, a study demonstrated Rab GTPases, Rab4, -7, and -9 regulate vascular permeability through enhanced VE-cadherin expression at the interendothelial junction (Chichger et al., 2016). Rab7a and Rab9 interactions with vimentin are indispensable for efficient endosome trafficking (Cogli et al., 2013; Margiotta et al., 2017; Romano et al., 2021). It is reasonable to assume that the VE-cadherin exosomes require Rab7 and Rab9 interactions with vimentin intermediate filaments for their successful shuttling to the surface of endothelial cells. Any modulation in the dynamics of PTMs of vimentin intermediate filaments can hamper this endothelial endosomal trafficking to cause edema in ALI.

ARDS/ALI patients have imbalances in coagulation and fibrinolysis pathways, which causes the increased presence of fibrin-rich exudates in the lumen of lung alveoli. Platelets aggregate complexes with fibrin to form stabilized clots in ARDS. Increased expression of vimentin on the surface of platelets polymerizes vitronectin to form a complex with the active form of plasminogen activator inhibitor-1 (PAI-1) (Podor et al., 2002), which stabilizes the thrombus (Konstantinides et al.,

2001). This increased fibrin deposition increases ALI permeability by myriads of pathways (Bastarache, 2009). Additionally, the formation of micro thrombi is also a common coagulation related pathology of ARDS that affects the microvascular endothelium. Vimentin intermediate filaments may have an indirect role in the increased micro thrombosis *via* the regulation of exocytosis (Faigle et al., 2000). *Exocytosis* is a normal process that releases the cell contents to the cell's exterior (Sollner, 2003). The exocytosis of abnormal VWF by endothelial cells causes micothrombosis in ARDS. During microthrmbosis, endothelial cells exocytose von Willebrand Factor (VWF), forming microthrombi complexes with activated platelets.

Moreover, exocytosis is a prerequisite for the migration and invasion of fibroblasts (Bretscher, 2008). Vimentin intermediate filaments act as a reservoir for a vesicle docking and fusion protein regulator, SNAP23 (Faigle et al., 2000). Vimentin intermediate filaments associated with reservoirs has been shown to traffic SNAP23 from the available plasma membrane pool (Faigle et al., 2000). Any PTM or disruption in vimentin intermediate filaments may modulate its availability to form SNARE complexes for exocytosis Specifically, Vimentin intermediate filaments regulated exocytosis may be necessary for the increased migration of fibroblasts and their invasion into fibrinous exudate alveolar spaces (Quesnel et al., 2010). It is not surprising that the BALs from the patient with ALI demonstrate the presence of alveolar fibroblasts, with increased expression of vimentin that is of a persistently activated phenotype with enhanced collagen- 1 producing and migratory capacity (Quesnel et al., 2010). Moreover, FGFs released from fibroblasts attenuate acute lung injury in the LPS model of ALI (Tong et al., 2016). More investigations are required to explore the direct role of fibroblasts in ALI.

Respiratory Viral Infections

Mounting evidence demonstrates the vital role of vimentin intermediate filaments and their soluble forms in virus-host cell interactions (Ramos et al., 2020; Zhang et al., 2020). Vimentin intermediate filaments affect infection, virulence, and replication of viruses in the host cells. For some viral infections, expression of Vimentin intermediate filaments on the cell surface aid at an early stage of infection as a co-receptor for the entry into the host cell (Thomas et al., 1996; Kim et al., 2006; Das et al., 2011; Du et al., 2014). For example, the human immunodeficiency virus (HIV) infects the host cell by making a pre-integration complex with vimentin present on the cell surface. The V3 region of HIV-1 and host surface vimentin interact to form the pre-integration complex after viral binding on the host CD4 receptor. After forming a pre-integration complex, the proteases from HIV-1 cleave vimentin intermediate filaments leading to its collapse towards the nuclear pore, thus bringing the virus into the nuclear entry site (Thomas et al., 1996). Vimentin intermediate filaments can modulate the replication, assembly, and egress of viruses in the host due to their known function of regulating endosomal trafficking *via* Rab7a and Polo-like kinase 1 (Plk1). Rab7a, which is ubiquitously present in early and late endosomes (Aloisi and Bucci, 2013; Guerra and Bucci, 2016), interacts with the insoluble and soluble vimentin (Cogli et al., 2013; Margiotta et al., 2017). Rab7a interacts directly with vimentin, and this interaction modulates vimentin phosphorylation and assembly (Cogli et al., 2013). Rab7a depleted cells have an abundance of insoluble Vimentin intermediate filaments, and defective endosomal trafficking (Romano et al., 2021). Phosphorylation of Vimentin intermediate filaments at Ser459 by Polo-like kinase 1 (Plk1) inhibits the endolytic fusion during mitosis (Ikawa et al., 2014). Altogether these interactions demonstrate vimentin as a critical regulator of late endocytic trafficking and egress of viral particles (Risco et al., 2002; Fay and Pante, 2013; Wu and Pante, 2016; Sabharwal et al., 2019). In another strategy, African swine fever virus, Vaccinia virus, and Enterovirus trigger rearrangement of Vimentin intermediate filaments as cages around the viral replication factories (Risco et al., 2002). These viruses utilize Vimentin intermediate filaments cages to egress and incorporate viral proteins and DNA for its replication (Stefanovic et al., 2005; Turkki et al., 2020). A more comprehensive elaboration on the role of vimentin during host-virus interactions in a wide range of viral infections is described elsewhere (Ramos et al., 2020; Zhang et al., 2020).

Unfortunately, respiratory tract viral infections are a leading cause of morbidity and mortality, where the symptoms can range from mild or asymptomatic upper airway infections to severe pneumonia. The most common respiratory viruses are SARS-CoV-2, influenza, respiratory syncytial virus (RSV), and adenoviruses (**Figure 2**).

Coronaviruses

A coronavirus classified as a member of the Coronaviridae family was identified as SARS-CoV-1 as the causative pathogen of the severe acute respiratory syndrome (SARS) in 2002. Since then, MERS-CoV and SARS-CoV-2 have been identified to cause severe illnesses in humans, such as the Middle East respiratory syndrome (MERS) and COVID-19. Currently, SARS-CoV-2 has precipitated a global public health crisis of our times with more than 25 million infected people up to date worldwide (Nov. 2021), and still continues unabated. The transmembrane spike (S) glycoprotein of SARS-CoV-2 and SARS-CoV have similar affinities to bind on human angiotensin-converting enzyme 2 (ACE2) (Walls et al., 2020). Interestingly, cell surface vimentin is identified as a co-receptor for binding SARS-CoV spike proteins (Yu et al., 2016) and it also acts as a co-receptor for SARS-CoV-2 spike proteins (Suprewicz et al., 2021; Thalla et al., 2021; Amraei et al., 2022). Recent study demonstrated that the coexpression of vimentin with ACE2 increased SARS-CoV-2 entry in HEK-293 cells, and the inhibition of vimentin expression decreased the SARS-CoV-2 infection of human endothelial cells (Amraei et al., 2022). Treatment with anti-vimentin antibodies considerably decreased the virus infection, which shows the direct role of surface vimentin in the binding of virus spike proteins (Yu et al., 2016). These reports do not clarify which domain of vimentin interacts with viral spike protein. Enterovirus 71 (EP71) and Cowpea mosaic virus (CPMV) utilized the tail region of vimentin as a receptor for the entry in host cells (Koudelka et al., 2009; Du et al., 2014); we postulate that the tail region of vimentin interacts

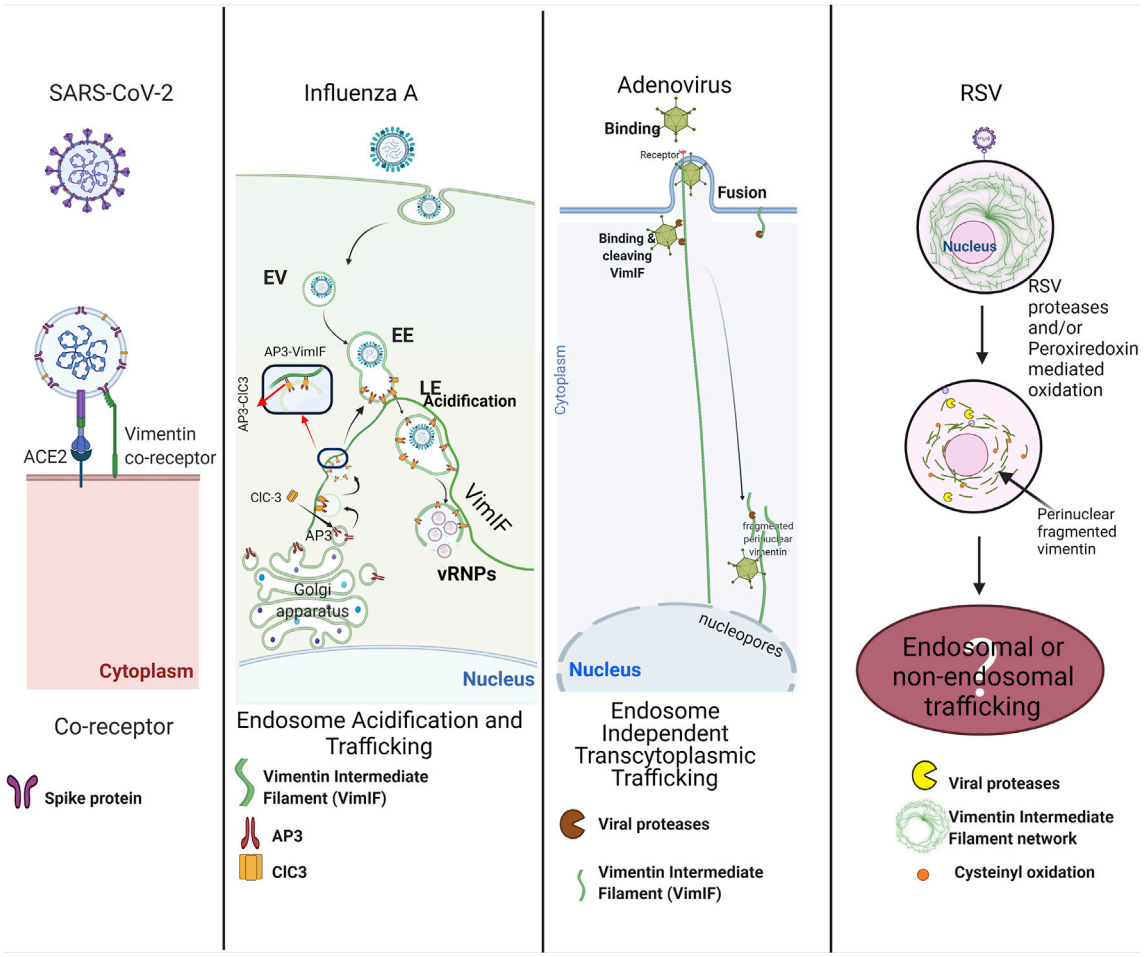

FIGURE 2 | Multiple roles of vimentin in viral respiratory infections: SARS-CoV2 exploits surface vimentin co-receptor for the entry in the host cell. Influenza A virus utilizes vimentin regulated trafficking of late endosomes for the release of vRNPs near the host nucleus. Adenoviruses bind to vimentin intermediate filaments (VimIFs) after host cell invasion, and the viral proteases cleave vimentin intermediate filaments to shuttle viruses in the vicinity of the host nucleus, also called endosome independent transcytoplasmic trafficking. RSV infection causes cleaving of VimIFs and accumulation of VimIF in the peri-nuclear region. Alterations in VimIFs may be associated with endosomal trafficking or non-endosomal trafficking for the shuttling virus next to the nucleus for its replication. The figure was created with BioRender.com.

with the SARS-CoV spike proteins. Overall, vimentin has a role in binding to SARS Co-V and SARS-CoV2 virus (**Figure 2**). Nevertheless, more in depth studies are warranted to consolidate these findings.

Influenza

Influenza A and B infections, commonly known as flu, cause contagious respiratory tract illness by causing upper respiratory tract infections (URTI) and sometimes lower respiratory tract infections (LTRI). An early study showed that disruption of Vimentin intermediate filaments impairs virus production (Arcangeletti et al., 1997), whereas proteomic data support the interaction of vimentin with viral ribonucleoprotein complexes (vRNPs) (Mayer et al., 2007). Later, a detailed study in *vim*$^{-/-}$ cells demonstrated that vimentin regulates endosomal trafficking to release vRNPs in the cytoplasm from the late endosomes, maintaining pH in the endosomes (Wu and Pante, 2016). The regulation of acidification of endosomes can be attributed to the sorting the endosomal chloride channel-3 (ClC-3), a chloride channel and transporter responsible for the endosomal acidification (Hara-Chikuma et al., 2005). The sorting of ClC-3 into the synaptic vesicles is managed by adapter protein-3 (AP-3) (Salazar et al., 2004). Adaptor proteins are protein-binding modules that link protein-binding partners together and facilitate the creation of larger signaling complexes. AP-3 is an essential adapter protein for lyso-endosomal sorting machinery (Odorizzi et al., 1998) that interacts with vimentin intermediate filaments for the sorting of proteins for endosomes formation and their trafficking (Styers et al., 2004). Based on these studies, it is established that vim$^{-/-}$ cells demonstrate decreased acidification of endosomes due to a loss of Vimentin intermediate filaments-AP-3 interactions that would have a negative effect on the sorting and distribution of ClC-3 in the late endosomes (LE). Hence, the decrease in the number and

virulence of virions released by vim$^{-/-}$cells (Wu and Pante, 2016) can be attributed to the decreased endosomal acidification as discussed (**Figure 2**).

Adenoviruses

Adenoviruses are DNA viruses that typically cause mild infections involving the upper or lower respiratory tract (Berk, 1991; Lynch and Kajon, 2016). Studies have shown that the adenoviral serotypes requiring endosome independent trans-cytoplasmic penetration routes have proteases that cleave vimentin intermediate filaments (Belin and Boulanger, 1987; Defer et al., 1990) (**Figure 2**). Although the function of cleaved vimentin is not described in these studies, it is possible that cleaved vimentin could transport the adenovirus directly to the perinuclear region due to collapse of vimentin intermediate filament network similar to HIV-1 infections (Thomas et al., 1996).

Respiratory Syncytial Virus

RSV infects airway mucosa to cause uncomplicated upper respiratory tract infections but can also spread to the lower respiratory tract and are mainly associated with bronchiolitis that can be deadly in children younger than 5 years of age (Shi et al., 2017). Although the direct role of vimentin intermediate filaments in the infection and the life cycle of RSV is not yet explored, RSV infections modulate the activity and expression of host superoxide dismutase (SOD) 1, 2, and 3; catalase, glutathione peroxidase (GPx), and glutathione S-transferase (GST) that leads to increased auto-oxidation of proteins in the cell (Hosakote et al., 2009). It is reported that RSV induces cysteinyl oxidation and decreases the expression of vimentin (Garcia-Barreno et al., 1988; Jamaluddin et al., 2010). Cysteinyl oxidation is an example of oxidative stress-mediated disruption of the vimentin intermediate filaments network and may have pathophysiological implications (Monico et al., 2019). In another study, the RSV mediated modulations in peroxiredoxins 1 and, 4 (Prdx-1 and Prdx-4) were shown to be responsible for the oxidation of nuclear intermediate filament complexes, including vimentin (Jamaluddin et al., 2010). The oxidation of Vimentin intermediate filaments may disturb the nuclear mechanical homeostasis (Neelam et al., 2015) in infected cells, but further studies are required to evaluate the specific role of oxidized Vimentin intermediate filaments in RSV infections (**Figure 2**).

In addition to virus-host interactions and viral life cycle, Vimentin intermediate filaments are associated with the pathogenesis of viral infections mediated ALI. Studies have demonstrated that RSV-induced netosis has a significant role in lung injury (Muraro et al., 2018; Mutua et al., 2021). In the above ALI section, we have discussed the possible role of citrullination of Vimentin intermediate filaments as an initiating step for the decondensation of chromatin and rupturing the nucleus during netosis (Thiam et al., 2020). Hence, Vimentin intermediate filaments have an indirect role in promoting RSV infection mediated acute lung injury.

Of note, the versatile forms and different localization of Vimentin intermediate filaments play a critical role in various stages of viral life cycles and following inflammatory pathways during viral lung infections. Targeting specific forms of vimentin can be utilized as one of the multiple strategies to inhibit viral entry in the host cell.

Respiratory Bacterial Infections

Bacterial infections are severe and prevalent among immunocompromised people (Al-Saad et al., 2008; Ahmed et al., 2011). Macrophages are the first line of defense to phagocytize and kill bacteria (Allard et al., 2018). The host-pathogen interaction mediated by macrophages and lymphocytes is crucial, and any discrepancy leads to serious bacterial infections in the lung and the development of pneumonia and pleurisy (Al-Saad et al., 2008). This section will describe the role of Vimentin intermediate filaments in the host-pathogen interactions and concomitant development of pathological features.

Mycobacterium tuberculosis (*M.tb.*) infections and non-tuberculosis *mycobacterium* infections are common forms of bacterial infections of the lungs in many parts of the world. During *M.tb.* infections, natural killer (NK) cells kill autologously-infected cells without prior sensitization as an innate immune response (Perera Molligoda Arachchige, 2021). The monocytes infected with *M. tb.* H37Ra have upregulated surface expression of vimentin compared to the uninfected monocytes. The NK cells recognize these infected cells by binding the NKp46 ligand to vimentin expressed on *M.tb.* H37Ra infected monocytes (Garg et al., 2006). Furthermore, the same study demonstrated that the neutralization of vimentin reduces the capacity of NK cells to lyse *M.tb.* H37Ra -infected alveolar macrophages. In another study, PKA/PKC mediated phosphorylation of vimentin was demonstrated to differentiate monocyte to macrophage, and these newly differentiated macrophages showed downregulation of expression of vimentin after infection with live *M.tb.* H37Rv infection *via* an ESAT-6 dependent mechanism (Mahesh et al., 2016). The apparent discrepancy of these results can be explained by the differences in the virulence of the mycobacterial strain used for the studies. *M.tb.* H37Ra is an attenuated *Mycobacterium* strain, whereas the *M.tb.* H37Rv is a virulent strain. *M.tb.* H37Ra exhibits significant alterations to either the genome or the expression of virulence genes compared to the virulent variant *M.tb.* H37Rv (Brosch et al., 1999; Li A. H. et al., 2010). The differential response for vimentin expression by these strains points towards the importance of surface vimentin expression in the host immune cell interactions and innate immunity. Virulent *mycobacterium* infection may inhibit the lysis of infected macrophage by NK cells by downregulating vimentin expression. Several mechanisms are altered by virulent strains of *mycobacteria* for the prolonged survival in infected macrophages to increase the intracellular bacterial burden inside the infected macrophages.

The instrumental role of surface vimentin in the host cell invasion has also been demonstrated in infection by *M. avium subsp. Hominissuis*. In order to achieve efficient mucosal invasion, *M. avium* forms microaggregates on the surface of the host cells, facilitating bacterial microaggragate binding

protein 1 (MBP-1) by binding and polymerizing with the host cell surface vimentin.

The interaction of MBP-1 and host cells surface vimentin was shown to be inhibited by anti-vimentin antibody treatment in HEp-2 cells, suggesting that polymerized vimentin expression is vital for *M. avium* adherence to the host cell (Babrak et al., 2015). In addition to host-pathogen interactions, vimentin may also affect the subsequent pathological features of infection in the lung, such as granuloma formation. Granulomas are a compact and organized structure formed by the initial aggregation of infected macrophages and are a salient feature of *tuberculosis* and non-tuberculosis mycobacterial infections (Rubin, 2009). We and others have shown that the necrotic cell death of the infected granulomatous macrophages is associated with the dissipation of the bacteria by breaking the compact structure of granulomas (Russell et al., 2009; Regev et al., 2012; Silva-Gomes et al., 2013; Surolia et al., 2016). The breakdown of granuloma due to necrotic core dissipates bacteria dysregulates the immune response leading to lung tissue destruction and morbidity. Interestingly, the tight and well-formed granuloma are found to be rich in vimentin on their periphery (Kaarteenaho-Wiik et al., 2007). The direct role of vimentin is not understood in these structures and can be related to increased fibroblastic scar formation around the infected macrophages and lymphocytes aggregates (Kaarteenaho-Wiik et al., 2007). Recently, computational experimentation and wet-lab experimental approaches demonstrated the possibility of transforming vimentin-rich macrophages, which can differentiate into the myofibroblasts like cells around the macrophage aggregates in the later stages of granuloma formation (Evans et al., 2020).

Sarcoidosis is an idiopathic lung disease that features granuloma formation (Heinle and Chang, 2014). There is no clinical observation-based evidence for intracellular pathogen inside the sarcoidosis granuloma, yet few studies have demonstrated the plausible presence of dormant *mycobacterium* (Esteves et al., 2016) in vimentin-positive antigen-presenting cells (Wahlstrom et al., 2007; Chen et al., 2008; Wahlstrom et al., 2009). The discovery of the presence of residual *mycobacterium* antigens such as catalase-peroxidase (mKatG), superoxide dismutase A (Sod A), ESAT6, and *M. tuberculosis* heat shock proteins (Mtb-HSP) in the granulomatous lymphocytes roots to the hypothesis for the presence of a dormant form of *mycobacterium*. Vimentin intermediate filaments are well-recognized auto-antigens in sarcoidosis (Kinloch et al., 2018) and are shown to cause clonal expansion of lung-specific Vα2.3 + Vβ22 + CD4 + T lymphocytes in the granuloma (Kinloch et al., 2018). These observations suggest that the presence of surface vimentin on the host cells may be involved in granuloma formation, and future studies are warranted in this understudied area. Overall, these scattered observations namely, the differential expression of vimentin in infected cells, polymerization of vimentin on the cell surface, presence of vimentin as antigen in granuloma presenting lymphocytes, and presence of Vimentin intermediate filaments rich cells in the peripheral fibroblastic case around aggregated lymphocytes, may have an inter-dependent or independent role of vimentin in the granuloma formation and progression of the disease.

Chronic Lung Diseases

Owing to its importance as a mesenchymal marker, the expression of vimentin is extensively demonstrated during lung remodeling as one of the driver for the pathogenesis of chronic lung diseases (Kage and Borok, 2012; Rout-Pitt et al., 2018). Different PTMs on Vimentin intermediate filaments have been explored for their regulatory role in development of chronic lung diseases. The post-translational modification of Vimentin intermediate filaments such as citrullination, carbamylation, and phosphorylation is associated with the pathogenesis of chronic lung diseases namely, idiopathic pulmonary fibrosis (IPF) (Li et al., 2017a; Li et al., 2021), chronic obstructive pulmonary disease (COPD) (Lugli et al., 2015; Nissen et al., 2019), rheumatoid arthritis-associated interstitial lung disease (RA-ILD) (Lugli et al., 2015), and asthma (Zaccardelli et al., 2019; Zaccardelli et al., 2021).

Role of Vimentin in Lung Fibrosis

Interstitial lung diseases (ILD) refer to a collection of disorders characterized by varying degrees of inflammation and fibrosis in the lung interstitium. The most common form of idiopathic ILD is IPF. The firsthand evidence of extracellular and autoimmune forms of vimentin in IPF came from our study showing the presence of anti-vimentin antibodies that were associated with the worse clinical outcomes in the patients with IPF (Li et al., 2017a). We demonstrated that the binding of this anti-vimentin antibodies on HLA-DR was associated with the proliferation of CD4 T cells and enhanced IL-4, IL-17, and TGF-β1 levels (Li et al., 2017a). The transplant-free survival was higher in the patients with lower anti-vimentin autoantibodies. Furthermore, our study also demonstrated that environmental cadmium (Cd) exposures and smoking increased citrullinated vimentin in the bronchoalveolar lavages and serum of patients with IPF (Li et al., 2021) suggesting that citrullinated vimentin acts as a spearhead of inflammatory reactions that over time give rise to fibrotic scar formation of the lung and cause IPF. The peptidyl arginine deiminase 2 (PAD2) mediated citrullination of vimentin solubilizes and secrets vimentin from macrophages in the extracellular space, which in turn acts as DAMPs and activates Toll-like receptors 4 (TLR4)/NF-kB pathway in lung fibroblasts. These fibroblasts secrete pro-fibrotic cytokines TGF-β1, CTGF, and IL-8 (Baran et al., 2007).

The extrinsic risk factors for IPF include smoking, environmental exposures, and air pollution (Zaman and Lee, 2018). Cd, a heavy metal present in cigarette smoke, is found in high levels in the lungs of smokers (Ganguly et al., 2018). The phosphorylated forms of vimentin at Ser 38 and Ser 55 (P-Ser38 and P-Ser55 vim) resulted in Cd mediated peribronchial fibrosis in mice lungs. Our group has demonstrated that Cd-induced AKT and cdc2 activation increase phosphorylation of vimentin intermediate filaments Ser 38 (P-Ser38Vim). The P-Ser38Vim complexes with 14-3-3 for the release of YAP-1 for the translocation in nucleus triggering SMAD2/3 regulated transcription of pro-fibrotic genes in the fibroblasts around the airways (Li et al., 2017b). 14-3-3 is a conserved and regulatory phospho-binding protein with diverse roles in several signaling pathways (Pennington et al., 2018) and utilizes vimentin as a

"sink" that sequester 14-3-3 away from binding partners (Tzivion et al., 2000; Pan et al., 2012; Sluchanko et al., 2017). 14-3-3 regulates autophagy through its interactions with Vimentin intermediate filaments. 14-3-3 forms autophagy-inhibitory Beclin1/14-3-3/vimentin intermediate filament complex for the pathogenesis of cancer (Wang et al., 2012). The dysregulation of autophagy is one of the pathogenic phenomena in IPF (Patel et al., 2012). The increased Vimentin intermediate filaments complexes with Beclin-1 to inhibit the clearance of CollagenI by autophagy in myofibroblasts. Increased ECM deposition and intemperate invasive capacity of myofibroblasts are hallmarks of IPF disease and are related to Vimentin intermediate filaments formation. Vimentin intermediate filaments are essential for invadopodia formation (Helfand et al., 2011). Moreover, we demonstrated that increased Vimentin intermediate filaments in myofibroblasts of fibrotic foci in the lungs of patients with IPF are related to the increased invasiveness of myofibroblasts and disease progression (Surolia et al., 2019). Overall, the ability of Vimentin intermediate filaments for interacting with other signaling molecules to form complexes regulates various pro-fibrotic pathways.

Role of Vimentin in COPD

Chronic inflammation leads to fixed narrowing of small airways (peribronchial fibrosis) and alveolar wall destruction (emphysema) in COPD. The chronic inflammation in COPD is characterized by increased numbers of alveolar macrophages, neutrophils, cytotoxic T-lymphocytes (O'Donnell et al., 2006). The increased activity of PAD2 in the macrophages (Makrygiannakis et al., 2008), likely contribute to the increased levels of citrullinated vimentin in the lungs and serum of COPD patients (Wood et al., 2011; Lugli et al., 2015; Nissen et al., 2019). However, patients with COPD have a specific form of vimentin which is believed to be a metalloproteases cleaved citrullinated form of vimentin (VICM) (Nissen et al., 2019). Neutrophil-specific protease membrane-type 6 matrix metalloproteinase (MT6- MMP) on neutrophil membrane utilizes vimentin as one of their substrate (Starr et al., 2012). Taken together, increased PADs and MMP activity on vimentin in the patients with COPD are the reason for increased levels of VICM. The downstream effects of VICM are not explored yet. In physiological conditions, the cleaved form of extracellular vimentin increases neutrophil and monocyte chemotaxis, generating "eat-me" signals that can potentially increase phagocytic removal of neutrophils to resolve inflammation. On the other hand, lungs from COPD patients are known to have compromised resolution of inflammation (Bozinovski et al., 2014). VICM may have differential responses on neutrophil and monocyte chemotaxis, phagocytosis, and the resolution of inflammation, which in part may be responsible for the frequent acute and chronic bacterial infections. For example, patients with COPD also have a higher prevalence of invasive pulmonary aspergillosis (IPA) (Bulpa et al., 2007; Samarakoon and Soubani, 2008) than those without COPD. Increased VICM levels can be plausible reason for the increased prevalence of *Aspergillus* species colonization in COPD patients. Non-TLR receptor, Dectin-1 has been explored in *Aspergillus* infections in the lungs (Lilly et al., 2012; Dutta et al., 2020). Dectin-1 contributes to respiratory burst, phagocytosis, and TNF-α production (Brown, 2006) and recognizes vimentin as a substrate (Thiagarajan et al., 2013). We think that prevalence of IPA in COPD may be associated with discrepancies in the binding of VICM to Dectin-1. These hypotheses are needed to be further tested.

Role of Vimentin in Autoimmunity Associated Interstitial Lung Diseases

Citrullinated vimentin was first recognized as an antigen for the autoimmunity in RA (Chen et al., 2015), among other citrullinated protein groups that cause anti-citrullinated peptide antibody production (ACPA). It is believed that the production of APCA initiates in the mucosa of the lungs before the onset of RA (Klareskog and Catrina, 2015; Zaccardelli et al., 2019). These observations indicate the possible connection of Cit-Vim antibodies to ILD development in RA patients (Chen et al., 2015; Reid and Guler, 2021). We infer that citrullinated vimentin may have a similar role as DAMP for developing RA-ILD based on the other research in IPF, but further investigation is necessary. One other form of post-translationally modified vimentin is recognized as a carbamylated-vimentin associated with cigarette smoking in patients with RA (Ospelt et al., 2017). Carbamylation is homocitrullination of proteins, where carbamylations are formed by the interaction of isocyanate (HNCO) with α-amino and ε-amino groups of proteins, among them, α-carbamylation, when α-amino groups of amino acids are involved, and ε-carbamylation, which is formed by the interaction of isocyanate with the ε-amino group of lysine (Jaisson et al., 2011). Although carbamylation is well-recognized in patients with RA, it is an APCA-independent process. The direct role of the carbamylated form of vimentin is not known in RA-ILD, IPF, and COPD. Interestingly, a recent study demonstrated that the global carbamylation of proteins by eosinophil peroxidase in the asthmatic airways participates in asthma exacerbations and altered inflammatory responses (Wang Z. et al., 2016). Recent research also has identified that elevated APCA levels were associated with asthma before the onset of RA disease (Zaccardelli et al., 2019). The direct role of citrullinated vimentin antigen and antibody in mucosal inflammation and asthma needs to be explored.

Role of Vimentin in Asthma

Asthmatic lungs have airway narrowing, and obstruction is intricately associated with EMT (Hackett, 2012). Inhaled environmental allergens promote EMT pathways *via* multiple mechanisms in the asthmatic airway. Hence, vimentin has been demonstrated in various airway epithelial cell types upon exposure to various allergens and other stimulants for EMT (Hackett, 2012).

Lung Cancers

Vimentin is crucial for the EMT, metastasis, and invasion of mesenchymal cells (Satelli and Li, 2011; Usman et al., 2021). Hence, no wonder that most studies designated the significance of

vimentin as a biomarker in cancers with clinical relevance in several types of cancers (Ben-Ze'ev and Raz, 1985; Hu et al., 2004; Jin et al., 2010; Li M. et al., 2010; Wei et al., 2008; Bogush et al., 2020) and the more in depth information can be found elsewhere (Satelli and Li, 2011; Zhao et al., 2013; Polioudaki et al., 2015; Mogre et al., 2022). In lung cancers, vimentin has been shown to be the target of various regulating factors that control expression or cause post-translational modification of vimentin. For example, increased activity of PARP-1 on the promoter of the vimentin gene increases the expression levels of vimentin (Rodriguez et al., 2013). In another study, cancer stem cell-derived exosomal miR-210-3p bind and inhibit fibroblast growth factor receptor-like 1 (FGFRL-1) to increase vimentin expression in lung cancer cells (Walls et al., 2020). Increased vimentin provides stability to FAK through VAV2-mediated Rac1 activation that increases the motility and invasiveness in non-small cell lung cancer (Havel et al., 2015). The decreased levels of post-translationally modified glycosylated-vimentin intermediate filaments are associated with the progression of adenocarcinoma (Rho et al., 2009). A recent study demonstrated that reduced glycosylation of vimentin increase the soluble form of vimentin [unit-length filaments (ULFs)] which is crucial for its self-assembly. (Tarbet et al., 2018). Expression of vimentin can also regulate the Slug signaling pathways for the pathogenesis of cancer (Vuoriluoto et al., 2011). These studies signify vimentin as an important driver and biomarker of EMT, increased migration, and metastasis in lung cancers.

In recent years, our understanding of the role of Vimentin intermediate filaments as a crucial player in the development of cancers by regulating non-EMT-dependent pathways has also evolved. Interaction of vimentin intermediate filaments with Beclin-1 inhibits autophagy enhancing tumorigenesis. The Akt1 mediated phosphorylated vimentin interact with 14-3-3 and complexes with Beclin1. The unavailability of Beclin1 for autophagosomal complex results in autophagy inhibition and cell survival in cancer (Wang et al., 2012). Similar work demonstrated that the interaction of Beclin1 with vimentin affects its USP14 mediated de-ubiquitination leading to abrogated degradation which provides an increased ability of cell migration in lung cancer (Cheng et al., 2019). These studies suggested that the formation of protein complexes by vimentin intermediate filaments can regulate new unconventional pro-tumor functions in the cell. Vimentin-associated intergenic cytoplasmic non-coding RNA inhibits Trim16 dependent polyubiquitination and degradation of vimentin intermediate filaments (Tian et al., 2020). These long-lived (unubiquitinated) vimentin intermediate filaments activate AKT-driven metastasis of adenocarcinoma (Tian et al., 2020). Overall, these few studies spotlight the regulatory role of vimentin intermediate filaments in unconventional ways, and more research is warranted to fully understand the role of vimentin in tumor metastasis.

VIMENTIN AS A BIOMARKER AND AS A DRUG TARGET FOR THE LUNG DISEASES

The aforementioned studies present evidence for the crucial role of Vimentin intermediate filaments in the development of lung diseases and prove that vimentin is a potential target for their treatment. Withaferin A and Ajoene are utilized as anti-vimentin strategies to treat *in vitro* and *in vivo* models of lung diseases. Withaferin A and Ajoene, both are plants compounds that inhibit the assembly of Vimentin intermediate filaments (Kaschula et al., 2019). Withaferin A, an alkaloid, is demonstrated to have anti-cancer effects review: Singh et al. (2021). Furthermore, Withaferin A decreased the invasiveness of IPF lung-derived 3D organoid models and mitigated lung fibrosis in the bleomycin mouse model (Surolia et al., 2019). Studies have shown that Withaferin A reduced inflammation in cellular models of cystic fibrosis (Maitra et al., 2009), and an ovalbumin mouse model of allergy and asthma (Zhao et al., 2019). Similarly, Ajoene which is a garlic compound has anti-cancer effects (Taylor et al., 2006; Wang Y. et al., 2016). Overall, these compounds or their derivatives have the potential as anti-vimentin targets for treating various lung diseases.

Although no direct anti-vimentin molecule is approved for the treatment of any lung disease, there are several clinical trials utilizing interventions that decrease the expression of vimentin. The value of amplified expression of vimentin is recognized as a prognostic marker is critical in non-small cell lung cancer (NSCLC) (Al-Saad et al., 2008; Dauphin et al., 2013; Ye et al., 2016; Teocharoen et al., 2021). The expression levels of vimentin were used as a prognostic indicator for the treatment efficacy for patients with NSCLC with erlotinib, erlotinib/bevacizumab (EB) or cisplatin/gemcitabine/bevacizumab (PGB) (Richardson et al., 2012; Villalobos et al., 2019). A phase I trial for FAK inhibitor drugs, namely VS-6063 and RO5126766, will use expression levels of vimentin as a biomarker in patients with NSCLC (NCT03875820).

There are new clinical trials for non-malignant lung diseases using vimentin as a biomarker and/or drug target (NCT03253146, NCT03584802). One of the studies is focused on the clinical value of vimentin and the mechanism of vimentin-mediated immune cell apoptosis during sepsis development. This trial will determine whether the vimentin can be a new target for sepsis diagnosis and treatment (NCT03253146). In an interventional clinical trial study, the autoantibodies to vimentin are being assessed as outcomes for the use of therapeutic plasma exchange, Rituximab, and IV IgG in the patients with severe acute exacerbation of IPF admitted in ICU (NCT03584802).

Simvastatin, a FDA-approved drugs have anti-vimentin effects (Trogden et al., 2018). Statins inhibits the isoprenylation of proteins which activates caspases. Vimentin is a well-known substrate for caspases (Byun et al., 2001). Simvastatin has anti-viral effects for Zika and HIV viruses (Esposito et al., 2016; Espano et al., 2019). Interestingly, vimentin has an important role in the invasion and replication of HIV and Zika viruses in host cells (Thomas et al., 1996; Cortese et al., 2017). As mentioned earlier, of vimentin has a plausible role in the host cell invasion during COVID infections (Ramos et al., 2020; Vora et al., 2021). Currently, the role of Ruxolitinib and Simvastatin therapy are being studied for the prevention and treatment of respiratory failure associated with COVID-19 (NCT04348695). A randomized double-blind placebo-controlled single-center trial

has also demonstrated that Simvastatin significantly prolonged the time to first COPD exacerbation and reduced exacerbation rate (Schenk et al., 2021), NCT00680641).

Pritumumab (Glassy and Hagiwara, 2009; Babic et al., 2018) also known as CLNH11, CLN-IgG, and ACA-11, is the first anti-vimentin monoclonal antibody drug. It is a human IgG1 kappa antibody that binds to tumor cell ectodomain vimentin antigen for its anti-cancer effects. This drug is in clinical trial phase II, and showing beneficial effects against glioma (NCT04396717). Interestingly, testing of Pritumumab as a potential strategy for the anti-COVID 19 effects has been reported recently. Blocking the interaction of SARS-CoV2 spike proteins with surface vimentin co-receptor *via* the Pritumumab reduced the cell surface binding of the virus and cellular infection (Suprewicz et al., 2021).

Concluding remarks

Cytoskeletal filament research areas are expanding to understand the emerging versatile role of intermediate filaments, specifically Vimentin intermediate filaments. Due to technological advancements in the last 30 years, Vimentin intermediate filaments have gained recognition not only as building blocks for the support, compartmentalization, and trafficking in the cells but also as signaling molecules. Blocking/cleavage of extracellular pathological forms, and overexpressing cell surface forms of vimentin by decoy peptides or antibodies can be one of the strategies to target vimentin in lung diseases such as autoimmune diseases, cancer, and infections. Nevertheless, it is challenging to develop explicit strategies to target the pathological forms of vimentin due to its pleiotropic functions and spatiotemporal distribution. A plethora of research studies demonstrate the beneficial effects of anti-vimentin strategies in the treatment of models of various lung diseases. We strongly believe that further in-depth studies are much needed, particularly to understand both the beneficial and deleterious effects of each of the forms of vimentin. These studies will evolve the understanding of the pleotropic effects of all different forms of vimentin, which will aid in the development of novel drug molecules to target vimentin with greater efficiency and without side effects.

AUTHOR CONTRIBUTIONS

RS contributed to acquiring information, writing, and revising the manuscript. VA contributed to writing and revising the manuscript.

FUNDING

Supported by NIEHS, P42 ES027723 (VA), NIH Grant R01 18 ES029981 (VA).

REFERENCES

Ahmed, E. B., Daniels, M., Alegre, M.-L., and Chong, A. S. (2011). Bacterial Infections, Alloimmunity, and Transplantation Tolerance. *Transplant. Rev.* 25, 27–35. doi:10.1016/j.trre.2010.10.003

Al-Saad, S., Al-Shibli, K., Donnem, T., Persson, M., Bremnes, R. M., and Busund, L.-T. (2008). The Prognostic Impact of NF-Kb P105, Vimentin, E-Cadherin and Par6 Expression in Epithelial and Stromal Compartment in Non-small-cell Lung Cancer. *Br. J. Cancer* 99, 1476–1483. doi:10.1038/sj.bjc.6604713

Allam, R., Darisipudi, M. N., Tschopp, J., and Anders, H.-J. (2013). Histones Trigger Sterile Inflammation by Activating the NLRP3 Inflammasome. *Eur. J. Immunol.* 43, 3336–3342. doi:10.1002/eji.201243224

Allard, B., Panariti, A., and Martin, J. G. (2018). Alveolar Macrophages in the Resolution of Inflammation, Tissue Repair, and Tolerance to Infection. *Front. Immunol.* 9, 1777. doi:10.3389/fimmu.2018.01777

Aloisi, A. L., and Bucci, C. (2013). Rab GTPases-Cargo Direct Interactions: fine Modulators of Intracellular Trafficking. *Histol. Histopathol* 28, 839–849. doi:10.14670/HH-28.839

Amraei, R., Xia, C., Olejnik, J., White, M. R., Napoleon, M. A., Lotfollahzadeh, S., et al. (2022). Extracellular Vimentin Is an Attachment Factor that Facilitates SARS-CoV-2 Entry into Human Endothelial Cells. *Proc. Natl. Acad. Sci. U S A.* 119. doi:10.1073/pnas.2113874119

Arcangeletti, M. C., Pinardi, F., Missorini, S., De Conto, F., Conti, G., Portincasa, P., et al. (1997). Modification of Cytoskeleton and Prosome Networks in Relation to Protein Synthesis in Influenza A Virus-Infected LLC-MK2 Cells. *Virus. Res.* 51, 19–34. doi:10.1016/s0168-1702(97)00074-9

Babic, I., Nurmemmedov, E., Yenugonda, V. M., Juarez, T., Nomura, N., Pingle, S. C., et al. (2018). Pritumumab, the First Therapeutic Antibody for Glioma Patients. *Hum. Antibodies* 26, 95–101. doi:10.3233/HAB-170326

Babrak, L., Danelishvili, L., Rose, S. J., Kornberg, T., and Bermudez, L. E. (2015). The Environment of "*Mycobacterium avium* Subsp. Hominissuis" Microaggregates Induces Synthesis of Small Proteins Associated with Efficient Infection of Respiratory Epithelial Cells. *Infect. Immun.* 83, 625–636. doi:10.1128/iai.02699-14

Baran, C. P., Opalek, J. M., Mcmaken, S., Newland, C. A., O'brien, J. M., JR., Hunter, M. G., et al. (2007). Important Roles for Macrophage colony-stimulating Factor, CC Chemokine Ligand 2, and Mononuclear Phagocytes in the Pathogenesis of Pulmonary Fibrosis. *Am. J. Respir. Crit. Care Med.* 176, 78–89. doi:10.1164/rccm.200609-1279oc

Bastarache, J. A. (2009). The Complex Role of Fibrin in Acute Lung Injury. *Am. J. Physiology-Lung Cell Mol. Physiol.* 296, L275–L276. doi:10.1152/ajplung.90633.2008

Battaglia, R. A., Delic, S., Herrmann, H., and Snider, N. T. (2018). Vimentin on the Move: New Developments in Cell Migration. *F1000Res* 7, 7. doi:10.12688/f1000research.15967.1

Belin, M. T., and Boulanger, P. (1987). Processing of Vimentin Occurs during the Early Stages of Adenovirus Infection. *J. Virol.* 61, 2559–2566. doi:10.1128/jvi.61.8.2559-2566.1987

Ben-Ze'ev, A., and Raz, A. (1985). Relationship between the Organization and Synthesis of Vimentin and the Metastatic Capability of B16 Melanoma Cells. *Cancer Res.* 45, 2632–2641.

Benes, P., Maceckova, V., Zdráhal, Z., Konecná, H., Zahradnícková, E., Muzík, J., et al. (2006). Role of Vimentin in Regulation of Monocyte/macrophage Differentiation. *Differentiation* 74, 265–276. doi:10.1111/j.1432-0436.2006.00077.x

Berk, J. E. (1991). Comment on Editorial by Dr. Rogers. *Am. J. Gastroenterol.* 86, 1094.

Bogush, T. A., Basharina, A. A., Eliseeva, B. K., Kaliuzhny, S. A., Bogush, E. A., Kirsanov, V. Y., et al. (2020). A New Approach to Epithelial-Mesenchymal Transition Diagnostics in Epithelial Tumors: Double Immunofluorescent Staining and Flow Cytometry. *Biotechniques* 69, 257–263.

Boilard, E., Bourgoin, S. G., Bernatchez, C., and Surette, M. E. (2003). Identification of an Autoantigen on the Surface of Apoptotic Human T Cells as a New Protein Interacting with Inflammatory Group IIA Phospholipase A2. *Blood* 102, 2901–2909.

Bozinovski, S., Anthony, D., and Vlahos, R. (2014). Targeting Pro-resolution Pathways to Combat Chronic Inflammation in COPD. *J. Thorac. Dis.* 6, 1548–1556. doi:10.3978/j.issn.2072-1439.2014.08.08

Brentville, V. A., Metheringham, R. L., Daniels, I., Atabani, S., Symonds, P., Cook, K. W., et al. (2020). Combination Vaccine Based on Citrullinated Vimentin and

Enolase Peptides Induces Potent CD4-Mediated Anti-tumor Responses. *J. Immunother. Cancer* 8. doi:10.1136/jitc-2020-000560

Bretscher, M. S. (2008). Exocytosis Provides the Membrane for Protrusion, at Least in Migrating Fibroblasts. *Nat. Rev. Mol. Cel Biol* 9, 916. doi:10.1038/nrm2419-c3

Brinkmann, V., Reichard, U., Goosmann, C., Fauler, B., Uhlemann, Y., Weiss, D. S., et al. (2004). Neutrophil Extracellular Traps Kill Bacteria. *Science* 303, 1532–1535. doi:10.1126/science.1092385

Brosch, R., Philipp, W. J., Stavropoulos, E., Colston, M. J., Cole, S. T., and Gordon, S. V. (1999). Genomic Analysis Reveals Variation between *Mycobacterium tuberculosis* H37Rv and the Attenuated *M. tuberculosis* H37Ra Strain. *Infect. Immun.* 67, 5768–5774. doi:10.1128/iai.67.11.5768-5774.1999

Brown, G. D. (2006). Dectin-1: a Signalling Non-TLR Pattern-Recognition Receptor. *Nat. Rev. Immunol.* 6, 33–43. doi:10.1038/nri1745

Bryant, A. E., Bayer, C. R., Huntington, J. D., and Stevens, D. L. (2006). Group A Streptococcal Myonecrosis: Increased Vimentin Expression after Skeletal-Muscle Injury Mediates the Binding ofStreptococcus Pyogenes. *J. Infect. Dis.* 193, 1685–1692. doi:10.1086/504261

Bulpa, P., Dive, A., and Sibille, Y. (2007). Invasive Pulmonary Aspergillosis in Patients with Chronic Obstructive Pulmonary Disease. *Eur. Respir. J.* 30, 782–800. doi:10.1183/09031936.00062206

Byun, Y., Chen, F., Chang, R., Trivedi, M., Green, K. J., and Cryns, V. L. (2001). Caspase Cleavage of Vimentin Disrupts Intermediate Filaments and Promotes Apoptosis. *Cell Death Differ* 8, 443–450. doi:10.1038/sj.cdd.4400840

Chang, I. A., Oh, M. J., Kim, M. H., Park, S. K., Kim, B. G., and Namgung, U. (2012). Vimentin Phosphorylation by Cdc2 in Schwann Cell Controls Axon Growthviaβ1-integrin Activation. *FASEB j.* 26, 2401–2413. doi:10.1096/fj.11-199018

Chavez, J., Chung, W.-G., Miranda, C. L., Singhal, M., Stevens, J. F., and Maier, C. S. (2010). Site-specific Protein Adducts of 4-hydroxy-2(E)-nonenal in Human THP-1 Monocytic Cells: Protein Carbonylation Is Diminished by Ascorbic Acid. *Chem. Res. Toxicol.* 23, 37–47. doi:10.1021/tx9002462

Chen, E. S., Wahlström, J., Song, Z., Willett, M. H., Wikén, M., Yung, R. C., et al. (2008). T Cell Responses to Mycobacterial Catalase-Peroxidase Profile a Pathogenic Antigen in Systemic Sarcoidosis. *J. Immunol.* 181, 8784–8796. doi:10.4049/jimmunol.181.12.8784

Chen, J., Doyle, T. J., Liu, Y., Aggarwal, R., Wang, X., Shi, Y., et al. (2015). Biomarkers of Rheumatoid Arthritis-Associated Interstitial Lung Disease. *Arthritis Rheumatol.* 67, 28–38. doi:10.1002/art.38904

Cheng, Z., Xin, H., and Han, T. (2019). BECN1 Promotes the Migration of NSCLC Cells through Regulating the Ubiquitination of Vimentin. *Cell Adh Migr* 13, 249–259. doi:10.1080/19336918.2019.1638690

Chernyatina, A. A., Nicolet, S., Aebi, U., Herrmann, H., and Strelkov, S. V. (2012). Atomic Structure of the Vimentin central α-helical Domain and its Implications for Intermediate Filament Assembly. *Proc. Natl. Acad. Sci. U.S.A.* 109, 13620–13625. doi:10.1073/pnas.1206836109

Chichger, H., Braza, J., Duong, H., Boni, G., and Harrington, E. O. (2016). Select Rab GTPases Regulate the Pulmonary Endothelium *via* Endosomal Trafficking of Vascular Endothelial-Cadherin. *Am. J. Respir. Cel Mol Biol* 54, 769–781. doi:10.1165/rcmb.2015-0286oc

Chou, Y.-H., Bischoff, J. R., Beach, D., and Goldman, R. D. (1990). Intermediate Filament Reorganization during Mitosis Is Mediated by P34cdc2 Phosphorylation of Vimentin. *Cell* 62, 1063–1071. doi:10.1016/0092-8674(90)90384-q

Chou, Y. H., Ngai, K. L., and Goldman, R. (1991). The Regulation of Intermediate Filament Reorganization in Mitosis. *J. Biol. Chem.* 266, 7325–7328. doi:10.1016/s0021-9258(20)89448-4

Cogli, L., Progida, C., Bramato, R., and Bucci, C. (2013). Vimentin Phosphorylation and Assembly Are Regulated by the Small GTPase Rab7a. *Biochim. Biophys. Acta (Bba) - Mol. Cel Res.* 1833, 1283–1293. doi:10.1016/j.bbamcr.2013.02.024

Colucci-Guyon, E., Portier, M.-M., Dunia, I., Paulin, D., Pournin, S., and Babinet, C. (1994). Mice Lacking Vimentin Develop and Reproduce without an Obvious Phenotype. *Cell* 79, 679–694. doi:10.1016/0092-8674(94)90553-3

Cortese, M., Goellner, S., Acosta, E. G., Neufeldt, C. J., Oleksiuk, O., Lampe, M., et al. (2017). Ultrastructural Characterization of Zika Virus Replication Factories. *Cel Rep.* 18, 2113–2123. doi:10.1016/j.celrep.2017.02.014

Das, S., Ravi, V., and Desai, A. (2011). Japanese Encephalitis Virus Interacts with Vimentin to Facilitate its Entry into Porcine Kidney Cell Line. *Virus. Res.* 160, 404–408. doi:10.1016/j.virusres.2011.06.001

Dauphin, M., Barbe, C., Lemaire, S., Nawrocki-Raby, B., Lagonotte, E., Delepine, G., et al. (2013). Vimentin Expression Predicts the Occurrence of Metastases in Non Small Cell Lung Carcinomas. *Lung Cancer* 81, 117–122. doi:10.1016/j.lungcan.2013.03.011

Defer, C., Belin, M. T., Caillet-Boudin, M. L., and Boulanger, P. (1990). Human Adenovirus-Host Cell Interactions: Comparative Study with Members of Subgroups B and C. *J. Virol.* 64, 3661–3673. doi:10.1128/jvi.64.8.3661-3673.1990

Delano, M. J., and Ward, P. A. (2016). The Immune System's Role in Sepsis Progression, Resolution, and Long-Term Outcome. *Immunol. Rev.* 274, 330–353. doi:10.1111/imr.12499

Dellagi, K., Vainchenker, W., Vinci, G., Paulin, D., and Brouet, J. C. (1983). Alteration of Vimentin Intermediate Filament Expression during Differentiation of Human Hemopoietic Cells. *EMBO J.* 2, 1509–1514. doi:10.1002/j.1460-2075.1983.tb01615.x

Dinsdale, D., Lee, J. C., Dewson, G., Cohen, G. M., and Peter, M. E. (2004). Intermediate Filaments Control the Intracellular Distribution of Caspases during Apoptosis. *Am. J. Pathol.* 164, 395–407. doi:10.1016/s0002-9440(10)63130-6

Dos Santos, G., Kutuzov, M. A., and Ridge, K. M. (2012). The Inflammasome in Lung Diseases. *Am. J. Physiology-Lung Cell Mol. Physiol.* 303, L627–L633. doi:10.1152/ajplung.00225.2012

Dos Santos, G., Rogel, M. R., Baker, M. A., Troken, J. R., Urich, D., Morales-Nebreda, L., et al. (2015). Vimentin Regulates Activation of the NLRP3 Inflammasome. *Nat. Commun.* 6, 6574. doi:10.1038/ncomms7574

Du, N., Cong, H., Tian, H., Zhang, H., Zhang, W., Song, L., et al. (2014). Cell Surface Vimentin Is an Attachment Receptor for Enterovirus 71. *J. Virol.* 88, 5816–5833. doi:10.1128/jvi.03826-13

Dutta, O., Espinosa, V., Wang, K., Avina, S., and Rivera, A. (2020). Dectin-1 Promotes Type I and III Interferon Expression to Support Optimal Antifungal Immunity in the Lung. *Front. Cel. Infect. Microbiol.* 10, 321. doi:10.3389/fcimb.2020.00321

Eckes, B., Colucci-Guyon, E., Smola, H., Nodder, S., Babinet, C., Krieg, T., et al. (2000). Impaired Wound Healing in Embryonic and Adult Mice Lacking Vimentin. *J. Cel Sci* 113 (Pt 13) (Pt 13), 2455–2462. doi:10.1242/jcs.113.13.2455

Eriksson, J. E., Dechat, T., Grin, B., Helfand, B., Mendez, M., Pallari, H.-M., et al. (2009). Introducing Intermediate Filaments: from Discovery to Disease. *J. Clin. Invest.* 119, 1763–1771. doi:10.1172/jci38339

Eriksson, J. E., He, T., Trejo-Skalli, A. V., Härmälä-Braskén, A.-S., Hellman, J., Chou, Y.-H., et al. (2004). Specific *In Vivo* Phosphorylation Sites Determine the Assembly Dynamics of Vimentin Intermediate Filaments. *J. Cel Sci* 117, 919–932. doi:10.1242/jcs.00906

Españo, E., Nam, J.-H., Song, E.-J., Song, D., Lee, C.-K., and Kim, J.-K. (2019). Lipophilic Statins Inhibit Zika Virus Production in Vero Cells. *Sci. Rep.* 9, 11461. doi:10.1038/s41598-019-47956-1

Esposito, A. M., Cheung, P., Swartz, T. H., Li, H., Tsibane, T., Durham, N. D., et al. (2016). A High Throughput Cre-Lox Activated Viral Membrane Fusion Assay Identifies Pharmacological Inhibitors of HIV Entry. *Virology* 490, 6–16. doi:10.1016/j.virol.2015.10.013

Esteves, T., Aparicio, G., and Garcia-Patos, V. (2016). Is There Any Association between Sarcoidosis and Infectious Agents? a Systematic Review and Meta-Analysis. *BMC Pulm. Med.* 16, 165. doi:10.1186/s12890-016-0332-z

Evans, S., Butler, J. R., Mattila, J. T., and Kirschner, D. E. (2020). Systems Biology Predicts that Fibrosis in Tuberculous Granulomas May Arise through Macrophage-To-Myofibroblast Transformation. *Plos Comput. Biol.* 16, e1008520. doi:10.1371/journal.pcbi.1008520

Faigle, W., Colucci-Guyon, E., Louvard, D., Amigorena, S., and Galli, T. (2000). Vimentin Filaments in Fibroblasts Are a Reservoir for SNAP23, a Component of the Membrane Fusion Machinery. *MBoC* 11, 3485–3494. doi:10.1091/mbc.11.10.3485

Fay, N., and Panté, N. (2013). The Intermediate Filament Network Protein, Vimentin, Is Required for Parvoviral Infection. *Virology* 444, 181–190. doi:10.1016/j.virol.2013.06.009

Franke, W. W., Schmid, E., Osborn, M., and Weber, K. (1978). Different Intermediate-Sized Filaments Distinguished by Immunofluorescence Microscopy. *Proc. Natl. Acad. Sci. U.S.A.* 75, 5034–5038. doi:10.1073/pnas.75.10.5034

Ganguly, K., Levänen, B., Palmberg, L., Åkesson, A., and Lindén, A. (2018). Cadmium in Tobacco Smokers: a Neglected Link to Lung Disease? *Eur. Respir. Rev.* 27. doi:10.1183/16000617.0122-2017

Garcia-Barreno, B., Jorcano, J., Aukenbauer, T., López-Galíndez, C., and Melero, J. (1988). Participation of Cytoskeletal Intermediate Filaments in the Infectious Cycle of Human Respiratory Syncytial Virus (RSV). *Virus. Res.* 9, 307–321. doi:10.1016/0168-1702(88)90090-1

Garg, A., Barnes, P. F., Porgador, A., Roy, S., Wu, S., Nanda, J. S., et al. (2006). Vimentin Expressed onMycobacterium Tuberculosis-Infected Human Monocytes Is Involved in Binding to the NKp46 Receptor. *J. Immunol.* 177, 6192–6198. doi:10.4049/jimmunol.177.9.6192

Gharbi, S., Garzón, B., Gayarre, J., Timms, J., and Pérez-Sala, D. (2007). Study of Protein Targets for Covalent Modification by the Antitumoral and Anti-inflammatory Prostaglandin PGA1: Focus on Vimentin. *J. Mass. Spectrom.* 42, 1474–1484. doi:10.1002/jms.1291

Glassy, M. C., and Hagiwara, H. (2009). Summary Analysis of the Pre-clinical and Clinical Results of Brain Tumor Patients Treated with Pritumumab. *Hab* 18, 127–137. doi:10.3233/hab-2009-0209

Goto, H., Kosako, H., Tanabe, K., Yanagida, M., Sakurai, M., Amano, M., et al. (1998). Phosphorylation of Vimentin by Rho-Associated Kinase at a Unique Amino-Terminal Site that Is Specifically Phosphorylated during Cytokinesis. *J. Biol. Chem.* 273, 11728–11736. doi:10.1074/jbc.273.19.11728

Goto, H., Yasui, Y., Kawajiri, A., Nigg, E. A., Terada, Y., Tatsuka, M., et al. (2003). Aurora-B Regulates the Cleavage Furrow-specific Vimentin Phosphorylation in the Cytokinetic Process. *J. Biol. Chem.* 278, 8526–8530. doi:10.1074/jbc.m210892200

Griesser, E., Vemula, V., Mónico, A., Pérez-Sala, D., and Fedorova, M. (2021). Dynamic Posttranslational Modifications of Cytoskeletal Proteins Unveil Hot Spots under Nitroxidative Stress. *Redox Biol.* 44, 102014. doi:10.1016/j.redox.2021.102014

Guerra, F., and Bucci, C. (2016). Multiple Roles of the Small GTPase Rab7. *Cells* 5. doi:10.3390/cells5030034

Guo, D., Song, X., Guo, T., Gu, S., Chang, X., Su, T., et al. (2018). Vimentin Acetylation Is Involved in SIRT5-Mediated Hepatocellular Carcinoma Migration. *Am. J. Cancer Res.* 8, 2453–2466.

Guo, H., Callaway, J. B., and Ting, J. P.-Y. (2015). Inflammasomes: Mechanism of Action, Role in Disease, and Therapeutics. *Nat. Med.* 21, 677–687. doi:10.1038/nm.3893

Gurland, G., and Gundersen, G. G. (1995). Stable, Detyrosinated Microtubules Function to Localize Vimentin Intermediate Filaments in Fibroblasts. *J. Cel Biol* 131, 1275–1290. doi:10.1083/jcb.131.5.1275

Hackett, T.-L. (2012). Epithelial-mesenchymal Transition in the Pathophysiology of Airway Remodelling in Asthma. *Curr. Opin. Allergy Clin. Immunol.* 12, 53–59. doi:10.1097/aci.0b013e32834ec6eb

Hara-Chikuma, M., Yang, B., Sonawane, N. D., Sasaki, S., Uchida, S., and Verkman, A. S. (2005). ClC-3 Chloride Channels Facilitate Endosomal Acidification and Chloride Accumulation. *J. Biol. Chem.* 280, 1241–1247. doi:10.1074/jbc.m407030200

Havel, L. S., Kline, E. R., Salgueiro, A. M., and Marcus, A. I. (2015). Vimentin Regulates Lung Cancer Cell Adhesion through a VAV2-Rac1 Pathway to Control Focal Adhesion Kinase Activity. *Oncogene* 34, 1979–1990. doi:10.1038/onc.2014.123

Heinle, R., and Chang, C. (2014). Diagnostic Criteria for Sarcoidosis. *Autoimmun. Rev.* 13, 383–387. doi:10.1016/j.autrev.2014.01.035

Helfand, B. T., Mendez, M. G., Murthy, S. N. P., Shumaker, D. K., Grin, B., Mahammad, S., et al. (2011). Vimentin Organization Modulates the Formation of Lamellipodia. *MBoC* 22, 1274–1289. doi:10.1091/mbc.e10-08-0699

Henrion, D., Terzi, F., Matrougui, K., Duriez, M., Boulanger, C. M., Colucci-Guyon, E., et al. (1997). Impaired Flow-Induced Dilation in Mesenteric Resistance Arteries from Mice Lacking Vimentin. *J. Clin. Invest.* 100, 2909–2914. doi:10.1172/jci119840

Herrmann, H., Häner, M., Brettel, M., Müller, S. A., Goldie, K. N., Fedtke, B., et al. (1996). Structure and Assembly Properties of the Intermediate Filament Protein Vimentin: the Role of its Head, Rod and Tail Domains. *J. Mol. Biol.* 264, 933–953. doi:10.1006/jmbi.1996.0688

Herrmann, H., Strelkov, S. V., Burkhard, P., and Aebi, U. (2009). Intermediate Filaments: Primary Determinants of Cell Architecture and Plasticity. *J. Clin. Invest.* 119, 1772–1783. doi:10.1172/jci38214

Hosakote, Y. M., Liu, T., Castro, S. M., Garofalo, R. P., and Casola, A. (2009). Respiratory Syncytial Virus Induces Oxidative Stress by Modulating Antioxidant Enzymes. *Am. J. Respir. Cel Mol Biol* 41, 348–357. doi:10.1165/rcmb.2008-0330oc

Howrylak, J. A., and Nakahira, K. (2017). Inflammasomes: Key Mediators of Lung Immunity. *Annu. Rev. Physiol.* 79, 471–494. doi:10.1146/annurev-physiol-021115-105229

Hu, L., Lau, S. H., Tzang, C.-H., Wen, J.-M., Wang, W., Xie, D., et al. (2004). Association of Vimentin Overexpression and Hepatocellular Carcinoma Metastasis. *Oncogene* 23, 298–302. doi:10.1038/sj.onc.1206483

Huang, B., Chen, S. C., and Wang, D. L. (2009). Shear Flow Increases S-Nitrosylation of Proteins in Endothelial Cells. *Cardiovasc. Res.* 83, 536–546. doi:10.1093/cvr/cvp154

Ikawa, K., Satou, A., Fukuhara, M., Matsumura, S., Sugiyama, N., Goto, H., et al. (2014). Inhibition of Endocytic Vesicle Fusion by Plk1-Mediated Phosphorylation of Vimentin during Mitosis. *Cell Cycle* 13, 126–137. doi:10.4161/cc.26866

Inagaki, M., Nishi, Y., Nishizawa, K., Matsuyama, M., and Sato, C. (1987). Site-specific Phosphorylation Induces Disassembly of Vimentin Filaments *In Vitro*. *Nature* 328, 649–652. doi:10.1038/328649a0

Inagaki, M., Takahara, H., Nishi, Y., Sugawara, K., and Sato, C. (1989). Ca2+-dependent Deimination-Induced Disassembly of Intermediate Filaments Involves Specific Modification of the Amino-Terminal Head Domain. *J. Biol. Chem.* 264, 18119–18127. doi:10.1016/s0021-9258(19)84685-9

Ivaska, J., Pallari, H.-M., Nevo, J., and Eriksson, J. E. (2007). Novel Functions of Vimentin in Cell Adhesion, Migration, and Signaling. *Exp. Cel Res.* 313, 2050–2062. doi:10.1016/j.yexcr.2007.03.040

Ivaska, J., Vuoriluoto, K., Huovinen, T., Izawa, I., Inagaki, M., and Parker, P. J. (2005). Pkcε-mediated Phosphorylation of Vimentin Controls Integrin Recycling and Motility. *EMBO J.* 24, 3834–3845. doi:10.1038/sj.emboj.7600847

Jaisson, S., Pietrement, C., and Gillery, P. (2011). Carbamylation-derived Products: Bioactive Compounds and Potential Biomarkers in Chronic Renal Failure and Atherosclerosis. *Clin. Chem.* 57, 1499–1505. doi:10.1373/clinchem.2011.163188

Jamaluddin, M., Wiktorowicz, J. E., Soman, K. V., Boldogh, I., Forbus, J. D., Spratt, H., et al. (2010). Role of Peroxiredoxin 1 and Peroxiredoxin 4 in protection of Respiratory Syncytial Virus-Induced Cysteinyl Oxidation of Nuclear Cytoskeletal Proteins. *J. Virol.* 84, 9533–9545. doi:10.1128/jvi.01005-10

Janmey, P. A., Slochower, D. R., Wang, Y.-H., Wen, Q., and Cēbers, A. (2014). Polyelectrolyte Properties of Filamentous Biopolymers and Their Consequences in Biological Fluids. *Soft Matter* 10, 1439–1449. doi:10.1039/c3sm50854d

Jay Forman, H., and Torres, M. (2001). Redox Signaling in Macrophages. *Mol. Aspects Med.* 22, 189–216. doi:10.1016/s0098-2997(01)00010-3

Jin, H., Morohashi, S., Sato, F., Kudo, Y., Akasaka, H., Tsutsumi, S., et al. (2010). Vimentin Expression of Esophageal Squamous Cell Carcinoma and its Aggressive Potential for Lymph Node Metastasis. *Biomed. Res.* 31, 105–112. doi:10.2220/biomedres.31.105

Johnson, E. R., and Matthay, M. A. (2010). Acute Lung Injury: Epidemiology, Pathogenesis, and Treatment. *J. Aerosol Med. Pulm. Drug Deliv.* 23, 243–252. doi:10.1089/jamp.2009.0775

Kaarteenaho-Wiik, R., Sademies, O., Pääkkö, P., Risteli, J., and Soini, Y. (2007). Extracellular Matrix Proteins and Myofibroblasts in Granulomas of Sarcoidosis, Atypical Mycobacteriosis, and Tuberculosis of the Lung. *Hum. Pathol.* 38, 147–153. doi:10.1016/j.humpath.2006.07.001

Kage, H., and Borok, Z. (2012). EMT and Interstitial Lung Disease: a Mysterious Relationship. *Curr. Opin. Pulm. Med.* 18, 517–523. doi:10.1097/MCP.0b013e3283566721

Kaplan, M. J. (2013). Role of Neutrophils in Systemic Autoimmune Diseases. *Arthritis Res. Ther.* 15, 219. doi:10.1186/ar4325

Kaschula, C. H., Tuveri, R., Ngarande, E., Dzobo, K., Barnett, C., Kusza, D. A., et al. (2019). The Garlic Compound Ajoene Covalently Binds Vimentin, Disrupts the Vimentin Network and Exerts Anti-metastatic Activity in Cancer Cells. *BMC Cancer* 19, 248. doi:10.1186/s12885-019-5388-8

Kim, J.-K., Fahad, A.-M., Shanmukhappa, K., and Kapil, S. (2006). Defining the Cellular Target(s) of Porcine Reproductive and Respiratory Syndrome Virus Blocking Monoclonal Antibody 7G10. *J. Virol.* 80, 689–696. doi:10.1128/jvi.80.2.689-696.2006

Kinloch, A. J., Kaiser, Y., Wolfgeher, D., Ai, J., Eklund, A., Clark, M. R., et al. (2018). *In Situ* Humoral Immunity to Vimentin in HLA-Drb1*03+ Patients with

Pulmonary Sarcoidosis. *Front. Immunol.* 9, 1516. doi:10.3389/fimmu.2018.01516

Klareskog, L., and Catrina, A. I. (2015). Lungs and Citrullination. *Nat. Rev. Rheumatol.* 11, 261–262. doi:10.1038/nrrheum.2015.38

Konstantinides, S., Schäfer, K., Thinnes, T., and Loskutoff, D. J. (2001). Plasminogen Activator Inhibitor-1 and its Cofactor Vitronectin Stabilize Arterial Thrombi after Vascular Injury in Mice. *Circulation* 103, 576–583. doi:10.1161/01.cir.103.4.576

Koudelka, K. J., Destito, G., Plummer, E. M., Trauger, S. A., Siuzdak, G., and Manchester, M. (2009). Endothelial Targeting of Cowpea Mosaic Virus (CPMV) *via* Surface Vimentin. *Plos Pathog.* 5, e1000417. doi:10.1371/journal.ppat.1000417

Kraxner, J., Lorenz, C., Menzel, J., Parfentev, I., Silbern, I., Denz, M., et al. (2021). Post-translational Modifications Soften Vimentin Intermediate Filaments. *Nanoscale* 13, 380–387. doi:10.1039/d0nr07322a

Lam, F. W., Da, Q., Guillory, B., and Cruz, M. A. (2018). Recombinant Human Vimentin Binds to P-Selectin and Blocks Neutrophil Capture and Rolling on Platelets and Endothelium. *J. Immunol.* 200, 1718–1726. doi:10.4049/jimmunol.1700784

Lam, F. W., Brown, C. A., Valladolid, C., Emebo, D. C., Palzkill, T. G., and Cruz, M. A. (2020). The Vimentin Rod Domain Blocks P-Selectin-P-Selectin Glycoprotein Ligand 1 Interactions to Attenuate Leukocyte Adhesion to Inflamed Endothelium. *PLoS One* 15, e0240164. doi:10.1371/journal.pone.0240164

Lang, T., Lee, J. P. W., Elgass, K., Pinar, A. A., Tate, M. D., Aitken, E. H., et al. (2018). Macrophage Migration Inhibitory Factor Is Required for NLRP3 Inflammasome Activation. *Nat. Commun.* 9, 2223. doi:10.1038/s41467-018-04581-2

Li, A. H., Waddell, S. J., Hinds, J., Malloff, C. A., Bains, M., Hancock, R. E., et al. (2010a). Contrasting Transcriptional Responses of a Virulent and an Attenuated Strain of *Mycobacterium tuberculosis* Infecting Macrophages. *PLoS One* 5, e11066. doi:10.1371/journal.pone.0011066

Li, F. J., Surolia, R., Li, H., Wang, Z., Liu, G., Kulkarni, T., et al. (2021). Citrullinated Vimentin Mediates Development and Progression of Lung Fibrosis. *Sci. Transl Med.* 13. doi:10.1126/scitranslmed.aba2927

Li, F. J., Surolia, R., Li, H., Wang, Z., Kulkarni, T., Liu, G., et al. (2017a). Autoimmunity to Vimentin Is Associated with Outcomes of Patients with Idiopathic Pulmonary Fibrosis. *J.I.* 199, 1596–1605. doi:10.4049/jimmunol.1700473

Li, F. J., Surolia, R., Li, H., Wang, Z., Liu, G., Liu, R.-M., et al. (2017b). Low-dose Cadmium Exposure Induces Peribronchiolar Fibrosis through Site-specific Phosphorylation of Vimentin. *Am. J. Physiology-Lung Cell Mol. Physiol.* 313, L80–L91. doi:10.1152/ajplung.00087.2017

Li, M., Zhang, B., Sun, B., Wang, X., Ban, X., Sun, T., et al. (2010b). A Novel Function for Vimentin: the Potential Biomarker for Predicting Melanoma Hematogenous Metastasis. *J. Exp. Clin. Cancer Res.* 29, 109. doi:10.1186/1756-9966-29-109

Li, Q.-F., Spinelli, A. M., Wang, R., Anfinogenova, Y., Singer, H. A., and Tang, D. D. (2006). Critical Role of Vimentin Phosphorylation at Ser-56 by P21-Activated Kinase in Vimentin Cytoskeleton Signaling. *J. Biol. Chem.* 281, 34716–34724. doi:10.1074/jbc.m607715200

Lilly, L. M., Gessner, M. A., Dunaway, C. W., Metz, A. E., Schwiebert, L., Weaver, C. T., et al. (2012). The β-Glucan Receptor Dectin-1 Promotes Lung Immunopathology during Fungal Allergy *via* IL-22. *J.I.* 189, 3653–3660. doi:10.4049/jimmunol.1201797

Lin, W.-C., and Fessler, M. B. (2021). Regulatory Mechanisms of Neutrophil Migration from the Circulation to the Airspace. *Cell. Mol. Life Sci.* 78, 4095–4124. doi:10.1007/s00018-021-03768-z

Lin, Y.-C., Broedersz, C. P., Rowat, A. C., Wedig, T., Herrmann, H., Mackintosh, F. C., et al. (2010). Divalent Cations Crosslink Vimentin Intermediate Filament Tail Domains to Regulate Network Mechanics. *J. Mol. Biol.* 399, 637–644. doi:10.1016/j.jmb.2010.04.054

Liu, B., He, R., Zhang, L., Hao, B., Jiang, W., Wang, W., et al. (2021). Inflammatory Caspases Drive Pyroptosis in Acute Lung Injury. *Front. Pharmacol.* 12, 631256. doi:10.3389/fphar.2021.631256

Lugli, E. B., Correia, R., Fischer, R., Lundberg, K., Bracke, K. R., Montgomery, A. B., et al. (2015). Expression of Citrulline and Homocitrulline Residues in the Lungs of Non-smokers and Smokers: Implications for Autoimmunity in Rheumatoid Arthritis. *Arthritis Res. Ther.* 17, 9. doi:10.1186/s13075-015-0520-x

Lynch, J. P., and Kajon, A. E. (2016). Adenovirus: Epidemiology, Global Spread of Novel Serotypes, and Advances in Treatment and Prevention. *Semin. Respir. Crit. Care Med.* 37, 586–602. doi:10.1055/s-0036-1584923

Mahesh, P. P., Retnakumar, R. J., and Mundayoor, S. (2016). Downregulation of Vimentin in Macrophages Infected with Live *Mycobacterium tuberculosis* Is Mediated by Reactive Oxygen Species. *Sci. Rep.* 6, 21526. doi:10.1038/srep21526

Maitra, R., Porter, M. A., Huang, S., and Gilmour, B. P. (2009). Inhibition of NFκB by the Natural Product Withaferin A in Cellular Models of Cystic Fibrosis Inflammation. *J. Inflamm.* 6, 15. doi:10.1186/1476-9255-6-15

Makrygiannakis, D., Hermansson, M., Ulfgren, A.-K., Nicholas, A. P., Zendman, A. J. W., Eklund, A., et al. (2008). Smoking Increases Peptidylarginine Deiminase 2 Enzyme Expression in Human Lungs and Increases Citrullination in BAL Cells. *Ann. Rheum. Dis.* 67, 1488–1492. doi:10.1136/ard.2007.075192

Margiotta, A., Progida, C., Bakke, O., and Bucci, C. (2017). Rab7a Regulates Cell Migration through Rac1 and Vimentin. *Biochim. Biophys. Acta (Bba) - Mol. Cel Res.* 1864, 367–381. doi:10.1016/j.bbamcr.2016.11.020

Mayer, D., Molawi, K., Martínez-Sobrido, L., Ghanem, A., Thomas, S., Baginsky, S., et al. (2007). Identification of Cellular Interaction Partners of the Influenza Virus Ribonucleoprotein Complex and Polymerase Complex Using Proteomic-Based Approaches. *J. Proteome Res.* 6, 672–682. doi:10.1021/pr060432u

Mellgren, R. L. (2010). A Plasma Membrane Wound Proteome. *J. Biol. Chem.* 285, 36597–36607. doi:10.1074/jbc.m110.110015

Mogre, S., Makani, V., Pradhan, S., Devre, P., More, S., Vaidya, M., et al. (2022). Biomarker Potential of Vimentin in Oral Cancers. *Life (Basel)* 12. doi:10.3390/life12020150

Moisan, E., and Girard, D. (2006). Cell Surface Expression of Intermediate Filament Proteins Vimentin and Lamin B1in Human Neutrophil Spontaneous Apoptosis. *J. Leukoc. Biol.* 79, 489–498. doi:10.1189/jlb.0405190

Mónico, A., Duarte, S., Pajares, M. A., and Pérez-Sala, D. (2019). Vimentin Disruption by Lipoxidation and Electrophiles: Role of the Cysteine Residue and Filament Dynamics. *Redox Biol.* 23, 101098. doi:10.1016/j.redox.2019.101098

Mor-Vaknin, N., Punturieri, A., Sitwala, K., and Markovitz, D. M. (2003). Vimentin Is Secreted by Activated Macrophages. *Nat. Cel Biol* 5, 59–63. doi:10.1038/ncb898

Muraro, S. P., DE Souza, G. F., Gallo, S. W., Da Silva, B. K., DE Oliveira, S. D., Vinolo, M. A. R., et al. (2018). Respiratory Syncytial Virus Induces the Classical ROS-dependent NETosis through PAD-4 and Necroptosis Pathways Activation. *Sci. Rep.* 8, 14166. doi:10.1038/s41598-018-32576-y

Musaelyan, A., Lapin, S., Nazarov, V., Tkachenko, O., Gilburd, B., Mazing, A., et al. (2018). Vimentin as Antigenic Target in Autoimmunity: A Comprehensive Review. *Autoimmun. Rev.* 17, 926–934. doi:10.1016/j.autrev.2018.04.004

Mutua, V., Cavallo, F., and Gershwin, L. J. (2021). Neutrophil Extracellular Traps (NETs) in a Randomized Controlled Trial of a Combination of Antiviral and Nonsteroidal Anti-inflammatory Treatment in a Bovine Model of Respiratory Syncytial Virus Infection. *Vet. Immunol. Immunopathology* 241, 110323. doi:10.1016/j.vetimm.2021.110323

Neelam, S., Chancellor, T. J., Li, Y., Nickerson, J. A., Roux, K. J., Dickinson, R. B., et al. (2015). Direct Force Probe Reveals the Mechanics of Nuclear Homeostasis in the Mammalian Cell. *Proc. Natl. Acad. Sci. U.S.A.* 112, 5720–5725. doi:10.1073/pnas.1502111112

Nieminen, M., Henttinen, T., Merinen, M., Marttila–Ichihara, F., Eriksson, J. E., and Jalkanen, S. (2006). Vimentin Function in Lymphocyte Adhesion and Transcellular Migration. *Nat. Cel Biol* 8, 156–162. doi:10.1038/ncb1355

Nissen, N. I., Karsdal, M., and Willumsen, N. (2019). Post-translational Modifications of Vimentin Reflect Different Pathological Processes Associated with Non-small Cell Lung Cancer and Chronic Obstructive Pulmonary Disease. *Oncotarget* 10, 6829–6841. doi:10.18632/oncotarget.27332

O'donnell, R., Breen, D., Wilson, S., and Djukanovic, R. (2006). Inflammatory Cells in the Airways in COPD. *Thorax* 61, 448–454. doi:10.1136/thx.2004.024463

Odorizzi, G., Cowles, C. R., and Emr, S. D. (1998). The AP-3 Complex: a Coat of many Colours. *Trends Cel Biol.* 8, 282–288. doi:10.1016/s0962-8924(98)01295-1

Omary, M. B., Ku, N.-O., Tao, G.-Z., Toivola, D. M., and Liao, J. (2006). 'Heads and Tails' of Intermediate Filament Phosphorylation: Multiple Sites and Functional Insights. *Trends Biochem. Sci.* 31, 383–394. doi:10.1016/j.tibs.2006.05.008

Ospelt, C., Bang, H., Feist, E., Camici, G., Keller, S., Detert, J., et al. (2017). Carbamylation of Vimentin Is Inducible by Smoking and Represents an

Independent Autoantigen in Rheumatoid Arthritis. *Ann. Rheum. Dis.* 76, 1176–1183. doi:10.1136/annrheumdis-2016-210059

Pan, Y., Zhong, L.-j., Zhou, H., Wang, X., Chen, K., Yang, H.-p., et al. (2012). Roles of Vimentin and 14-3-3 Zeta/delta in the Inhibitory Effects of Heparin on PC-3M Cell Proliferation and B16-F10-Luc-G5 Cells Metastasis. *Acta Pharmacol. Sin* 33, 798–808. doi:10.1038/aps.2012.42

Papayannopoulos, V., Metzler, K. D., Hakkim, A., and Zychlinsky, A. (2010). Neutrophil Elastase and Myeloperoxidase Regulate the Formation of Neutrophil Extracellular Traps. *J. Cel Biol* 191, 677–691. doi:10.1083/jcb.201006052

Patel, A. S., Lin, L., Geyer, A., Haspel, J. A., An, C. H., Cao, J., et al. (2012). Autophagy in Idiopathic Pulmonary Fibrosis. *PLoS One* 7, e41394. doi:10.1371/journal.pone.0041394

Pennington, K., Chan, T., Torres, M., and Andersen, J. (2018). The Dynamic and Stress-Adaptive Signaling Hub of 14-3-3: Emerging Mechanisms of Regulation and Context-dependent Protein-Protein Interactions. *Oncogene* 37, 5587–5604. doi:10.1038/s41388-018-0348-3

Perera Molligoda Arachchige, A. S. (2021). Human NK Cells: From Development to Effector Functions. *Innate Immun.* 27, 212–229. doi:10.1177/17534259211001512

Pérez-Sala, D., Oeste, C. L., Martínez, A. E., Carrasco, M. J., Garzón, B., and Cañada, F. J. (2015). Vimentin Filament Organization and Stress Sensing Depend on its Single Cysteine Residue and Zinc Binding. *Nat. Commun.* 6, 7287. doi:10.1038/ncomms8287

Podor, T. J., Singh, D., Chindemi, P., Foulon, D. M., Mckelvie, R., Weitz, J. I., et al. (2002). Vimentin Exposed on Activated Platelets and Platelet Microparticles Localizes Vitronectin and Plasminogen Activator Inhibitor Complexes on Their Surface. *J. Biol. Chem.* 277, 7529–7539. doi:10.1074/jbc.m109675200

Polioudaki, H., Agelaki, S., Chiotaki, R., Politaki, E., Mavroudis, D., Matikas, A., et al. (2015). Variable Expression Levels of Keratin and Vimentin Reveal Differential EMT Status of Circulating Tumor Cells and Correlation with Clinical Characteristics and Outcome of Patients with Metastatic Breast Cancer. *BMC Cancer* 15, 399. doi:10.1186/s12885-015-1386-7

Quesnel, C., Nardelli, L., Piednoir, P., Lecon, V., Marchal-Somme, J., Lasocki, S., et al. (2010). Alveolar Fibroblasts in Acute Lung Injury: Biological Behaviour and Clinical Relevance. *Eur. Respir. J.* 35, 1312–1321. doi:10.1183/09031936.00074709

Ramos, I., Stamatakis, K., Oeste, C. L., and Pérez-Sala, D. (2020). Vimentin as a Multifaceted Player and Potential Therapeutic Target in Viral Infections. *Int. J. Mol. Sci.* 21. doi:10.3390/ijms21134675

Regev, D., Surolia, R., Karki, S., Zolak, J., Montes- Worboys, A., Oliva, O., et al. (2012). Heme Oxygenase-1 Promotes Granuloma Development and Protects against Dissemination of Mycobacteria. *Lab. Invest.* 92, 1541–1552. doi:10.1038/labinvest.2012.125

Reid, P., and Guler, S. A. (2021). Mortality Trends in Rheumatoid Arthritis: Zooming in on Interstitial Lung Disease. *Ann. ATS* 18, 1953–1954. doi:10.1513/annalsats.202108-899ed

Rho, J.-H., Roehrl, M. H. A., and Wang, J. Y. (2009). Glycoproteomic Analysis of Human Lung Adenocarcinomas Using Glycoarrays and Tandem Mass Spectrometry: Differential Expression and Glycosylation Patterns of Vimentin and Fetuin A Isoforms. *Protein J.* 28, 148–160. doi:10.1007/s10930-009-9177-0

Richardson, F., Young, G. D., Sennello, R., Wolf, J., Argast, G. M., Mercado, P., et al. (2012). The Evaluation of E-Cadherin and Vimentin as Biomarkers of Clinical Outcomes Among Patients with Non-small Cell Lung Cancer Treated with Erlotinib as Second- or Third-Line Therapy. *Anticancer Res.* 32, 537–552.

Risco, C., Rodri´guez, J. R., Lo´pez-Iglesias, C., Carrascosa, J. L., Esteban, M., and Rodri´guez, D. (2002). Endoplasmic Reticulum-Golgi Intermediate Compartment Membranes and Vimentin Filaments Participate in Vaccinia Virus Assembly. *J. Virol.* 76, 1839–1855. doi:10.1128/jvi.76.4.1839-1855.2002

Rodríguez, M. I., Peralta-Leal, A., O'Valle, F., Rodriguez-Vargas, J. M., Gonzalez-Flores, A., Majuelos-Melguizo, J., et al. (2013). PARP-1 Regulates Metastatic Melanoma through Modulation of Vimentin-Induced Malignant Transformation. *Plos Genet.* 9, e1003531. doi:10.1371/journal.pgen.1003531

Romano, R., Calcagnile, M., Margiotta, A., Franci, L., Chiariello, M., Alifano, P., et al. (2021). RAB7A Regulates Vimentin Phosphorylation through AKT and PAK. *Cancers (Basel)* 13. doi:10.3390/cancers13092220

Rout-Pitt, N., Farrow, N., Parsons, D., and Donnelley, M. (2018). Epithelial Mesenchymal Transition (EMT): a Universal Process in Lung Diseases with Implications for Cystic Fibrosis Pathophysiology. *Respir. Res.* 19, 136. doi:10.1186/s12931-018-0834-8

Rubin, E. J. (2009). The Granuloma in Tuberculosis - Friend or Foe? *N. Engl. J. Med.* 360, 2471–2473. doi:10.1056/nejmcibr0902539

Russell, D. G., Cardona, P.-J., Kim, M.-J., Allain, S., and Altare, F. (2009). Foamy Macrophages and the Progression of the Human Tuberculosis Granuloma. *Nat. Immunol.* 10, 943–948. doi:10.1038/ni.1781

Sabharwal, P., Amritha, C. K., Sushmitha, C., Natraj, U., and Savithri, H. S. (2019). Intracellular Trafficking and Endocytic Uptake Pathway of Pepper Vein Banding Virus-like Particles in Epithelial Cells. *Nanomedicine* 14, 1247–1265. doi:10.2217/nnm-2018-0405

Salazar, G., Love, R., Styers, M. L., Werner, E., Peden, A., Rodriguez, S., et al. (2004). AP-3-dependent Mechanisms Control the Targeting of a Chloride Channel (ClC-3) in Neuronal and Non-neuronal Cells. *J. Biol. Chem.* 279, 25430–25439. doi:10.1074/jbc.m402331200

Samarakoon, P., and Soubani, A. (2008). Invasive Pulmonary Aspergillosis in Patients with COPD: a Report of Five Cases and Systematic Review of the Literature. *Chron. Respir. Dis.* 5, 19–27. doi:10.1177/1479972307085637

Satelli, A., and Li, S. (2011). Vimentin in Cancer and its Potential as a Molecular Target for Cancer Therapy. *Cel. Mol. Life Sci.* 68, 3033–3046. doi:10.1007/s00018-011-0735-1

Schaedel, L., Lorenz, C., Schepers, A. V., Klumpp, S., and Köster, S. (2021). Vimentin Intermediate Filaments Stabilize Dynamic Microtubules by Direct Interactions. *Nat. Commun.* 12, 3799. doi:10.1038/s41467-021-23523-z

Schenk, P., Spiel, A. O., Hüttinger, F., Gmeiner, M., Fugger, J., Pichler, M., et al. (2021). Can Simvastatin Reduce COPD Exacerbations? A Randomised Double-Blind Controlled Study. *Eur. Respir. J.* 58. doi:10.1183/13993003.01798-2020

Shi, T., Mcallister, D. A., O'Brien, K. L., Simoes, E. A. F., Madhi, S. A., Gessner, B. D., et al. (2017). Global, Regional, and National Disease burden Estimates of Acute Lower Respiratory Infections Due to Respiratory Syncytial Virus in Young Children in 2015: a Systematic Review and Modelling Study. *The Lancet* 390, 946–958. doi:10.1016/s0140-6736(17)30938-8

Sihag, R. K., Inagaki, M., Yamaguchi, T., Shea, T. B., and Pant, H. C. (2007). Role of Phosphorylation on the Structural Dynamics and Function of Types III and IV Intermediate Filaments. *Exp. Cel Res.* 313, 2098–2109. doi:10.1016/j.yexcr.2007.04.010

Silva-Gomes, S., Appelberg, R., Larsen, R., Soares, M. P., and Gomes, M. S. (2013). Heme Catabolism by Heme Oxygenase-1 Confers Host Resistance to Mycobacterium Infection. *Infect. Immun.* 81, 2536–2545. doi:10.1128/iai.00251-13

Sin, W.-C., Chen, X.-Q., Leung, T., and Lim, L. (1998). RhoA-Binding Kinase α Translocation Is Facilitated by the Collapse of the Vimentin Intermediate Filament Network. *Mol. Cel Biol* 18, 6325–6339. doi:10.1128/mcb.18.11.6325

Singh, N., Yadav, S. S., Rao, A. S., Nandal, A., Kumar, S., Ganaie, S. A., et al. (2021). Review on Anticancerous Therapeutic Potential of Withania Somnifera (L.) Dunal. *J. Ethnopharmacology* 270, 113704. doi:10.1016/j.jep.2020.113704

Sluchanko, N. N., Beelen, S., Kulikova, A. A., Weeks, S. D., Antson, A. A., Gusev, N. B., et al. (2017). Structural Basis for the Interaction of a Human Small Heat Shock Protein with the 14-3-3 Universal Signaling Regulator. *Structure* 25, 305–316. doi:10.1016/j.str.2016.12.005

Snider, N. T., Ku, N. O., and Omary, M. B. (2018). The Sweet Side of Vimentin. *Elife* 7. doi:10.7554/eLife.35336

Snider, N. T., and Omary, M. B. (2014). Post-translational Modifications of Intermediate Filament Proteins: Mechanisms and Functions. *Nat. Rev. Mol. Cel Biol* 15, 163–177. doi:10.1038/nrm3753

Söllner, T. H. (2003). Regulated Exocytosis and SNARE Function (Review). *Mol. Membr. Biol.* 20, 209–220. doi:10.1080/0968768031000104953

Stamatakis, K., Sánchez-Gómez, F. J., and Pérez-Sala, D. (2006). Identification of Novel Protein Targets for Modification by 15-Deoxy-Δ12,14-Prostaglandin J2in Mesangial Cells Reveals Multiple Interactions with the Cytoskeleton. *Jasn* 17, 89–98. doi:10.1681/asn.2005030329

Starr, A. E., Bellac, C. L., Dufour, A., Goebeler, V., and Overall, C. M. (2012). Biochemical Characterization and N-Terminomics Analysis of Leukolysin, the Membrane-type 6 Matrix Metalloprotease (MMP25). *J. Biol. Chem.* 287, 13382–13395. doi:10.1074/jbc.m111.314179

Stefanovic, S., Windsor, M., Nagata, K.-i., Inagaki, M., and Wileman, T. (2005). Vimentin Rearrangement during African Swine Fever Virus Infection Involves Retrograde Transport along Microtubules and Phosphorylation of Vimentin by Calcium Calmodulin Kinase II. *J. Virol.* 79, 11766–11775. doi:10.1128/jvi.79.18.11766-11775.2005

Styers, M. L., Salazar, G., Love, R., Peden, A. A., Kowalczyk, A. P., and Faundez, V. (2004). The Endo-Lysosomal Sorting Machinery Interacts with the Intermediate Filament Cytoskeleton. *MBoC* 15, 5369–5382. doi:10.1091/mbc.e04-03-0272

Su, L.-X., Pan, P., Wang, X.-T., Long, Y., Liu, D.-W., and Zhou, X. (2019b). Vimentin Modulates Apoptosis and Inflammatory Cytokine Release by a Human Monocytic Cell Line (THP-1) in Response to Lipopolysaccharides *In Vitro*. *Chin. Med. J. (Engl)* 132, 1336–1343. doi:10.1097/cm9.0000000000000187

Su, L., Pan, P., Yan, P., Long, Y., Zhou, X., Wang, X., et al. (2019a). Role of Vimentin in Modulating Immune Cell Apoptosis and Inflammatory Responses in Sepsis. *Sci. Rep.* 9, 5747. doi:10.1038/s41598-019-42287-7

Suprewicz, L., Swoger, M., Gupta, S., Piktel, E., Byfield, F. J., Iwamoto, D. V., et al. (2021). *Extracellular Vimentin as a Target against SARS-CoV-2 Host Cell Invasion*. New York: Cold Spring Harbor Laboratory.

Surolia, R., Li, F. J., Wang, Z., Kashyap, M., Srivastava, R. K., Traylor, A. M., et al. (2021). NETosis in the Pathogenesis of Acute Lung Injury Following Cutaneous Chemical burns. *JCI Insight* 6. doi:10.1172/jci.insight.147564

Surolia, R., Li, F. J., Wang, Z., Li, H., Dsouza, K., Thomas, V., et al. (2019). Vimentin Intermediate Filament Assembly Regulates Fibroblast Invasion in Fibrogenic Lung Injury. *JCI Insight* 4. doi:10.1172/jci.insight.123253

Surolia, R., Karki, S., Wang, Z., Kulkarni, T., Li, F. J., Vohra, S., et al. (2016). Attenuated Heme Oxygenase-1 Responses Predispose the Elderly to Pulmonary Nontuberculous Mycobacterial Infections. *Am. J. Physiology-Lung Cell Mol. Physiol.* 311, L928–L940. doi:10.1152/ajplung.00397.2015

Tarbet, H. J., Dolat, L., Smith, T. J., Condon, B. M., O'Brien, E. T3R. D., Valdivia, R. H., et al. (2018). Site-specific Glycosylation Regulates the Form and Function of the Intermediate Filament Cytoskeleton. *Elife* 7. doi:10.7554/eLife.31807

Taylor, P., Noriega, R., Farah, C., Abad, M.-J., Arsenak, M., and Apitz, R. (2006). Ajoene Inhibits Both Primary Tumor Growth and Metastasis of B16/BL6 Melanoma Cells in C57BL/6 Mice. *Cancer Lett.* 239, 298–304. doi:10.1016/j.canlet.2005.08.022

Teocharoen, R., Ruangritchankul, K., Vinayanuwattikun, C., Sriuranpong, V., and Sitthideatphaiboon, P. (2021). Vimentin Expression Status Is a Potential Biomarker for Brain Metastasis Development in EGFR-Mutant NSCLC Patients. *Transl Lung Cancer Res.* 10, 790–801. doi:10.21037/tlcr-20-1020

Terzi, F., Henrion, D., Colucci-Guyon, E., Federici, P., Babinet, C., Levy, B. I., et al. (1997). Reduction of Renal Mass Is Lethal in Mice Lacking Vimentin. Role of Endothelin-Nitric Oxide Imbalance. *J. Clin. Invest.* 100, 1520–1528. doi:10.1172/jci119675

Thalla, D. G., Jung, P., Bischoff, M., and Lautenschläger, F. (2021). Role of Extracellular Vimentin in Cancer-Cell Functionality and its Influence on Cell Monolayer Permeability Changes Induced by SARS-CoV-2 Receptor Binding Domain. *Int. J. Mol. Sci.* 22. doi:10.3390/ijms22147469

Thiagarajan, P. S., Yakubenko, V. P., Elsori, D. H., Yadav, S. P., Willard, B., Tan, C. D., et al. (2013). Vimentin Is an Endogenous Ligand for the Pattern Recognition Receptor Dectin-1. *Cardiovasc. Res.* 99, 494–504. doi:10.1093/cvr/cvt117

Thiam, H. R., Wong, S. L., Qiu, R., Kittisopikul, M., Vahabikashi, A., Goldman, A. E., et al. (2020). NETosis Proceeds by Cytoskeleton and Endomembrane Disassembly and PAD4-Mediated Chromatin Decondensation and Nuclear Envelope Rupture. *Proc. Natl. Acad. Sci. U.S.A.* 117, 7326–7337. doi:10.1073/pnas.1909546117

Thomas, E. K., Connelly, R. J., Pennathur, S., Dubrovsky, L., Haffar, O. K., and Bukrinsky, M. I. (1996). Anti-idiotypic Antibody to the V3 Domain of Gp120 Binds to Vimentin: a Possible Role of Intermediate Filaments in the Early Steps of HIV-1 Infection Cycle. *Viral Immunol.* 9, 73–87. doi:10.1089/vim.1996.9.73

Tian, H., Lian, R., Li, Y., Liu, C., Liang, S., Li, W., et al. (2020). AKT-induced lncRNA VAL Promotes EMT-independent Metastasis through Diminishing Trim16-dependent Vimentin Degradation. *Nat. Commun.* 11, 5127. doi:10.1038/s41467-020-18929-0

Tolle, L. B., and Standiford, T. J. (2013). Danger-associated Molecular Patterns (DAMPs) in Acute Lung Injury. *J. Pathol.* 229, 145–156. doi:10.1002/path.4124

Tong, L., Zhou, J., Rong, L., Seeley, E. J., Pan, J., Zhu, X., et al. (2016). Fibroblast Growth Factor-10 (FGF-10) Mobilizes Lung-Resident Mesenchymal Stem Cells and Protects against Acute Lung Injury. *Sci. Rep.* 6, 21642. doi:10.1038/srep21642

Trogden, K. P., Battaglia, R. A., Kabiraj, P., Madden, V. J., Herrmann, H., and Snider, N. T. (2018). An Image-based Small-molecule Screen Identifies Vimentin as a Pharmacologically Relevant Target of Simvastatin in Cancer Cells. *FASEB j.* 32, 2841–2854. doi:10.1096/fj.201700663r

Turkki, P., Laajala, M., Flodström-Tullberg, M., and Marjomäki, V. (2020). Human Enterovirus Group B Viruses Rely on Vimentin Dynamics for Efficient Processing of Viral Nonstructural Proteins. *J. Virol.* 94. doi:10.1128/JVI.01393-19

Tzivion, G., Luo, Z.-J., and Avruch, J. (2000). Calyculin A-Induced Vimentin Phosphorylation Sequesters 14-3-3 and Displaces Other 14-3-3 Partners *In Vivo*. *J. Biol. Chem.* 275, 29772–29778. doi:10.1074/jbc.m001207200

Usman, S., Waseem, N. H., Nguyen, T. K. N., Mohsin, S., Jamal, A., Teh, M. T., et al. (2021). Vimentin Is at the Heart of Epithelial Mesenchymal Transition (EMT) Mediated Metastasis. *Cancers (Basel)* 13. doi:10.3390/cancers13194985

Valesini, G., Gerardi, M. C., Iannuccelli, C., Pacucci, V. A., Pendolino, M., and Shoenfeld, Y. (2015). Citrullination and Autoimmunity. *Autoimmun. Rev.* 14, 490–497. doi:10.1016/j.autrev.2015.01.013

Vassallo, R., Luckey, D., Behrens, M., Madden, B., Luthra, H., David, C., et al. (2014). Cellular and Humoral Immunity in Arthritis Are Profoundly Influenced by the Interaction between Cigarette Smoke Effects and Host HLA-DR and DQ Genes. *Clin. Immunol.* 152, 25–35. doi:10.1016/j.clim.2014.02.002

Villalobos, M., Czapiewski, P., Reinmuth, N., Fischer, J. R., Andreas, S., Kortsik, C., et al. (2019). Impact of EMT in Stage IIIB/IV NSCLC Treated with Erlotinib and Bevacizumab when Compared with Cisplatin, Gemcitabine and Bevacizumab. *Oncol. Lett.* 17, 4891–4900. doi:10.3892/ol.2019.10153

Vora, S. M., Lieberman, J., and Wu, H. (2021). Inflammasome Activation at the Crux of Severe COVID-19. *Nat. Rev. Immunol.* 21, 694–703. doi:10.1038/s41577-021-00588-x

Vossenaar, E. R., Radstake, T. R., VAN DER Heijden, A., VAN Mansum, M. A., Dieteren, C., DE Rooij, D. J., et al. (2004). Expression and Activity of Citrullinating Peptidylarginine Deiminase Enzymes in Monocytes and Macrophages. *Ann. Rheum. Dis.* 63, 373–381. doi:10.1136/ard.2003.012211

Vuoriluoto, K., Haugen, H., Kiviluoto, S., Mpindi, J.-P., Nevo, J., Gjerdrum, C., et al. (2011). Vimentin Regulates EMT Induction by Slug and Oncogenic H-Ras and Migration by Governing Axl Expression in Breast Cancer. *Oncogene* 30, 1436–1448. doi:10.1038/onc.2010.509

Wahlström, J., Dengjel, J., Persson, B., Duyar, H., Rammensee, H.-G., Stevanoviδc, S., et al. (2007). Identification of HLA-DR-Bound Peptides Presented by Human Bronchoalveolar Lavage Cells in Sarcoidosis. *J. Clin. Invest.* 117, 3576–3582. doi:10.1172/jci32401

Wahlström, J., Dengjel, J., Winqvist, O., Targoff, I., Persson, B., Duyar, H., et al. (2009). Autoimmune T Cell Responses to Antigenic Peptides Presented by Bronchoalveolar Lavage Cell HLA-DR Molecules in Sarcoidosis. *Clin. Immunol.* 133, 353–363. doi:10.1016/j.clim.2009.08.008

Walls, A. C., Park, Y.-J., Tortorici, M. A., Wall, A., Mcguire, A. T., and Veesler, D. (2020). Structure, Function, and Antigenicity of the SARS-CoV-2 Spike Glycoprotein. *Cell* 181, 281–292. doi:10.1016/j.cell.2020.02.058

Wang, L., Zhang, J., Banerjee, S., Barnes, L., Sajja, V., Liu, Y., et al. (2010). Sumoylation of Vimentin354 Is Associated with PIAS3 Inhibition of Glioma Cell Migration. *Oncotarget* 1, 620–627. doi:10.18632/oncotarget.196

Wang, R. C., Wei, Y., An, Z., Zou, Z., Xiao, G., Bhagat, G., et al. (2012). Akt-mediated Regulation of Autophagy and Tumorigenesis through Beclin 1 Phosphorylation. *Science* 338, 956–959. doi:10.1126/science.1225967

Wang, Y., Sun, Z., Chen, S., Jiao, Y., and Bai, C. (2016a). ROS-mediated Activation of JNK/p38 Contributes Partially to the Pro-apoptotic Effect of Ajoene on Cells of Lung Adenocarcinoma. *Tumor Biol.* 37, 3727–3738. doi:10.1007/s13277-015-4181-9

Wang, Z., Didonato, J. A., Buffa, J., Comhair, S. A., Aronica, M. A., Dweik, R. A., et al. (2016b). Eosinophil Peroxidase Catalyzed Protein Carbamylation Participates in Asthma. *J. Biol. Chem.* 291, 22118–22135. doi:10.1074/jbc.m116.750034

Wei, J., Xu, G., Wu, M., Zhang, Y., Li, Q., Liu, P., et al. (2008). Overexpression of Vimentin Contributes to Prostate Cancer Invasion and Metastasis via Src Regulation. *Anticancer Res.* 28, 327–334.

West, M. B., Hill, B. G., Xuan, Y.-T., Bhatnagar, A., West, M. B., Hill, B. G., et al. (2006). Protein Glutathiolation by Nitric Oxide: an Intracellular Mechanism Regulating Redox Protein Modification. *FASEB j.* 20, 1715–1717. doi:10.1096/fj.06-5843fje

Wilson, C., and González-Billault, C. (2015). Regulation of Cytoskeletal Dynamics by Redox Signaling and Oxidative Stress: Implications for Neuronal Development and Trafficking. *Front. Cel. Neurosci.* 9, 381. doi:10.3389/fncel.2015.00381

Wood, A. M., DE Pablo, P., Buckley, C. D., Ahmad, A., and Stockley, R. A. (2011). Smoke Exposure as a Determinant of Autoantibody Titre in 1-antitrypsin Deficiency and COPD. *Eur. Respir. J.* 37, 32–38. doi:10.1183/09031936.00033710

Wu, W., and Panté, N. (2016). Vimentin Plays a Role in the Release of the Influenza A Viral Genome from Endosomes. *Virology* 497, 41–52. doi:10.1016/j.virol.2016.06.021

Ye, Z., Zhang, X., Luo, Y., Li, S., Huang, L., Li, Z., et al. (2016). Prognostic Values of Vimentin Expression and its Clinicopathological Significance in Non-small Cell Lung Cancer: A Meta-Analysis of Observational Studies with 4118 Cases. *PLoS One* 11, e0163162. doi:10.1371/journal.pone.0163162

Ytterberg, A. J., Joshua, V., Reynisdottir, G., Tarasova, N. K., Rutishauser, D., Ossipova, E., et al. (2015). Shared Immunological Targets in the Lungs and Joints of Patients with Rheumatoid Arthritis: Identification and Validation. *Ann. Rheum. Dis.* 74, 1772–1777. doi:10.1136/annrheumdis-2013-204912

Yu, M. B., Guerra, J., Firek, A., and Langridge, W. H. R. (2018). Extracellular Vimentin Modulates Human Dendritic Cell Activation. *Mol. Immunol.* 104, 37–46. doi:10.1016/j.molimm.2018.09.017

Yu, Y. T.-C., Chien, S.-C., Chen, I.-Y., Lai, C.-T., Tsay, Y.-G., Chang, S. C., et al. (2016). Surface Vimentin Is Critical for the Cell Entry of SARS-CoV. *J. Biomed. Sci.* 23, 14. doi:10.1186/s12929-016-0234-7

Zaccardelli, A., Liu, X., Ford, J. A., Cui, J., Lu, B., Chu, S. H., et al. (2019). Asthma and Elevation of Anti-citrullinated Protein Antibodies Prior to the Onset of Rheumatoid Arthritis. *Arthritis Res. Ther.* 21, 246. doi:10.1186/s13075-019-2035-3

Zaccardelli, A., Liu, X., Ford, J. A., Cui, J., Lu, B., Chu, S. H., et al. (2021). Elevated Anti-citrullinated Protein Antibodies Prior to Rheumatoid Arthritis Diagnosis and Risks for Chronic Obstructive Pulmonary Disease or Asthma. *Arthritis Care Res.* 73, 498–509. doi:10.1002/acr.24140

Zaman, T., and Lee, J. S. (2018). Risk Factors for the Development of Idiopathic Pulmonary Fibrosis: A Review. *Curr. Pulmonol Rep.* 7, 118–125. doi:10.1007/s13665-018-0210-7

Zhang, Y., Wen, Z., Shi, X., Liu, Y. J., Eriksson, J. E., and Jiu, Y. (2020). The Diverse Roles and Dynamic Rearrangement of Vimentin during Viral Infection. *J. Cel Sci* 134. doi:10.1242/jcs.250597

Zhao, H. M., Gao, Z. W., Xie, S. X., Han, X., and Sun, Q. S. (2019). Withaferin A Attenuates Ovalbumin Induced Airway Inflammation. *Front. Biosci. (Landmark Ed.* 24, 576–596. doi:10.2741/4737

Zhao, W., Yue, L., Zhou, F., Xu, C., Liang, W., Sui, A., et al. (2013). Clinical Significance of Vimentin Expression and Her-2 Status in Patients with Gastric Carcinoma. *Clin. Translational Sci.* 6, 184–190. doi:10.1111/cts.12043

Zhu, Q.-S., Rosenblatt, K., Huang, K.-L., Lahat, G., Brobey, R., Bolshakov, S., et al. (2011). Vimentin Is a Novel AKT1 Target Mediating Motility and Invasion. *Oncogene* 30, 457–470. doi:10.1038/onc.2010.421

Zhu, Y., Zhang, Y., Sui, Z., Zhang, Y., Liu, M., and Tang, H. (2017). USP14 De-ubiquitinates Vimentin and miR-320a Modulates USP14 and Vimentin to Contribute to Malignancy in Gastric Cancer Cells. *Oncotarget* 8, 48725–48736. doi:10.18632/oncotarget.10706

Conflict of Interest: The authors declare that the research was conducted in the absence of any commercial or financial relationships that could be construed as a potential conflict of interest.

Publisher's Note: All claims expressed in this article are solely those of the authors and do not necessarily represent those of their affiliated organizations, or those of the publisher, the editors and the reviewers. Any product that may be evaluated in this article, or claim that may be made by its manufacturer, is not guaranteed or endorsed by the publisher.

frontiers | Frontiers in Cell and Developmental Biology

ORIGINAL RESEARCH
published: 08 June 2022
doi: 10.3389/fcell.2022.908263

Vimentin Tail Segments Are Differentially Exposed at Distinct Cellular Locations and in Response to Stress

*Irene Lois-Bermejo, Patricia González-Jiménez, Sofia Duarte, María A. Pajares and Dolores Pérez-Sala**

Department of Structural and Chemical Biology, Centro de Investigaciones Biológicas Margarita Salas, CSIC, Madrid, Spain

The intermediate filament protein vimentin plays a key role in cell signaling and stress sensing, as well as an integrator of cytoskeletal dynamics. The vimentin monomer consists of a central rod-like domain and intrinsically disordered head and tail domains. Although the organization of vimentin oligomers in filaments is beginning to be understood, the precise disposition of the tail region remains to be elucidated. Here we observed that electrophilic stress-induced condensation shielded vimentin from recognition by antibodies against specific segments of the tail domain. A detailed characterization revealed that vimentin tail segments are differentially exposed at distinct subcellular locations, both in basal and stress conditions. The 411–423 segment appeared accessible in all cell areas, correlating with vimentin abundance. In contrast, the 419–438 segment was more scantily recognized in perinuclear vimentin and lipoxidative stress-induced bundles, and better detected in peripheral filaments, where it appeared to protrude further from the filament core. These differences persisted in mitotic cells. Interestingly, both tail segments showed closer accessibility in calyculin A-treated cells and phosphomimetic mutants of the C-terminal region. Our results lead us to hypothesize the presence of at least two distinct arrangements of vimentin tail in cells: an "extended" conformation (accessible 419–438 segment), preferentially detected in peripheral areas with looser filaments, and a "packed" conformation (shielded 419–438 segment), preferentially detected at the cell center in robust filaments and lipoxidative stress-induced bundles. These different arrangements could be putatively interconverted by posttranslational modifications, contributing to the versatility of vimentin functions and/or interactions.

Keywords: lipoxidation, posttranslational modifications, vimentin tail, intermediate filament, electrophilic stress, vimentin tail phosphorylation, vimentin reorganization

OPEN ACCESS

Edited by:
Irina Kaverina, Vanderbilt University, United States

Reviewed by:
Alexander Minin, Institute of Protein Research (RAS), Russia
Cecilia Bucci, University of Salento, Italy

****Correspondence:***
Dolores Pérez-Sala
dperezsala@cib.csic.es

Specialty section:
This article was submitted to Cell Growth and Division, a section of the journal Frontiers in Cell and Developmental Biology

Received: *30 March 2022*
Accepted: *17 May 2022*
Published: *08 June 2022*

Citation:
Lois-Bermejo I, González-Jiménez P, Duarte S, Pajares MA and Pérez-Sala D (2022) Vimentin Tail Segments Are Differentially Exposed at Distinct Cellular Locations and in Response to Stress. Front. Cell Dev. Biol. 10:908263. doi: 10.3389/fcell.2022.908263

INTRODUCTION

Vimentin is a type III intermediate filament protein that typically forms an extended network in the cytoplasm of mesenchymal cells, maintaining a close interplay with actin and tubulin structures. Vimentin is involved in numerous functions in physiology, and in the response to stress. Thus, vimentin plays a key role in the positioning and homeostasis of cellular organelles,

cell mechanical properties, cell migration and division (Ivaska et al., 2007; Minin and Moldaver, 2008; Hol and Capetanaki, 2017). Pathophysiological situations associated with vimentin overexpression or dysfunction include cancer, fibrosis, and inflammation (Satelli and Li, 2011; Li et al., 2021; dos Santos et al., 2015). Interestingly, vimentin can also be encountered in the extracellular milieu where it has been involved in cell migration, intercellular communication and pathogen infection (reviewed in Ramos et al., 2020).

Vimentin filaments are extraordinarily versatile and complex structures, which adapt to various cellular situations and stress through a finely tuned regulation (Snider and Omary, 2014; Viedma-Poyatos et al., 2020). Knowledge from *in vitro* experiments has led to propose an assembly sequence consisting in the parallel association of two vimentin monomers into dimers, which then would join in a staggered antiparallel manner to give rise to a tetrameric structure. Several of these tetramers, typically eight in most models, associate laterally to form a unit length filament or "ULF," and end to end connection of many ULF conforms the filaments (Herrmann and Aebi, 2016; Eldirany et al., 2021). As described, this process could result in homogeneous, rope-like structures. However, in cells, filaments coexist with robust bundles, unraveled structures, and oligomeric non-filamentous vimentin, all of which can swiftly arise in response to various stimuli. Moreover, even single filaments are highly polymorphic and several assembly modes, involving different number of tetramers and interactions, have been identified through high resolution cryo-electron microscopy studies of straight sections of cellular filaments (Eibauer et al., 2021).

This versatility is supported by the high diversity of vimentin proteoforms. Nearly 150 modifications of human vimentin appear listed in PhosphoSite v6.6.0.4 (www.phosphosite.org), which could occur in different combinations, giving rise to an extraordinary variety of species differing in their assembly properties. Moreover, vimentin is the target for numerous non-enzymatic modifications by structurally diverse reactive species, which increase its polymorphism (Viedma-Poyatos et al., 2020; Griesser et al., 2021). The structure of the vimentin monomer comprises a central rod domain, which is mainly α-helical and integrated by several coils, and N-terminal (head) and C-terminal (tail) domains of intrinsically disordered structure. The flexible head domain has been reported to fold back onto the rod establishing interactions with coil 1A (Aziz et al., 2009; Aziz et al., 2010). In addition, interactions of the head and coil 1A have been reported to connect adjacent "protofibrils" (octameric strands) within assembled filaments (Eibauer et al., 2021). Moreover, the head domain is a key regulator of filament disassembly since it harbors at least eleven phosphorylation sites that are key for vimentin reorganization in mitosis (Matsuyama et al., 2013).

On the other hand, the structure and functions of the intrinsically disordered tail domain, comprising amino acids 412–466, are less understood. Vimentin tails are thought to protrude out of the rod forming a brush-like structure around the filament core (Kornreich et al., 2015). This seems to be in agreement with immunofluorescence analyses carried out by labeling single filaments with antibodies against the rod and the tail domain, which revealed a "cloud" of C-terminal segments around the compact rod domains (Herrmann and Aebi, 2016). In turn, the disposition of the tails in the brush structure could adopt different conformations due to the interaction between two conserved sequences, i.e. the β-turn formed by residues TRDG and the so-called "epsilon site" on the distal part of the rod comprising residues 364–416 (Kouklis et al., 1991; Hess et al., 2013). These complementary sites appear to associate during filament assembly forming a loop that would prevent filament aggregation and regulate filament thickness (Kouklis et al., 1991). Consistent with this, tailless vimentin can form nearly normal filaments *in vitro*, although wider than wild type filaments and with a higher number of tetramers per cross-section (Eckelt et al., 1992; Brennich et al., 2019). Importantly, the tail domain plays a critical role in vimentin distribution in cells; it acts as a cytoplasmic localization signal and is critical for vimentin intertwining with and modulation of the actin cortex in mitosis (Duarte et al., 2019). Moreover, tailless vimentin forms thick bundles that remain in the proximity of the nucleus causing mitotic alterations (Duarte et al., 2019), and, if present in excess over the full-length form, deeply disrupts the filament network provoking a perinuclear collapse.

In cells, diverse stimuli and types of stress induce fast vimentin remodeling. Vimentin phosphorylation can induce disassembly, for instance, during mitosis (Yamaguchi et al., 2005; Sihag et al., 2007), whereas modifications of its single cysteine residue (C328) in response to oxidative or lipoxidative challenges induce disruption of the network (Pérez-Sala et al., 2015; Mónico et al., 2019). Nevertheless, how these changes affect the tail domain, and *vice versa*, is not completely understood. In contrast to the head domain, fewer studies are available on the consequences of tail domain phosphorylation. Importantly, the tail domain contains several protease cleavage sites, including some for viral proteases (Singh and Arlinghaus, 1989; Shoeman et al., 1990) which cause vimentin perinuclear collapse (Duarte et al., 2019), an effect that has been hypothesized to contribute to the nuclear translocation and import of the viral genome (Thomas et al., 1996; Zhang et al., 2020).

We have previously shown that electrophilic stress induces drastic vimentin remodeling with condensation of filaments in thick juxtanuclear bundles (Pérez-Sala et al., 2015; Mónico et al., 2019). In this work, we attempted to monitor vimentin reorganization by immunofluorescence with antibodies against the tail domain. Given the complexity of the results obtained, additional antibodies with epitopes mapping to consecutive overlapping segments of the vimentin tail were employed to characterize this effect. We have observed that the accessibility of the various tail epitopes varies with the spatial distribution of vimentin in cells under control conditions and with its reorganization in response to stress. Our results are consistent with a dynamic role of the vimentin tail, which could hypothetically influence vimentin assembly and/or interactions in a spatio-temporal manner.

MATERIALS AND METHODS

Reagents

Anti-vimentin antibodies used included mouse monoclonal V9 (Santa Cruz Biotechnology, sc-6260), mouse monoclonal E5 (Santa Cruz Biotechnology, sc-373717), rabbit polyclonal "C-term" (RayBiotech, 102-15110), goat polyclonal "C-end" (Everest Biotech, United Kingdom, EB11207) and "N-term" (Cell Signaling Technology, D21H3), as well as the V9 and E5 conjugates with Alexa Fluor 488 or Alexa Fluor 546, and Alexa Fluor 647 conjugated D21H3, as specified where it corresponds. Anti-actin antibody was from Sigma (A2066). Several secondary antibodies were used: anti-mouse, anti-rabbit and anti-goat immunoglobulins, conjugated with Alexa Fluor 488, 546 or 647, all obtained from Molecular Probes. HRP-conjugated anti-mouse, anti-rabbit and anti-goat antibodies were from Dako. 4,6-diamidino-2-phenylindole (DAPI), Phalloidin-TRITC and acrolein were from Sigma. 4-hydroxynonenal (HNE) was from Cayman Chemical. Calyculin A was from Santa Cruz Biotechnology.

Cell Culture and Treatments

Human adrenal carcinoma cells SW13/cl.2 were a generous gift from Dr. A. Sarriá (University of Zaragoza, Spain). The human primary fibroblasts AG10803 used in this study were from the National Institute of General Medical Sciences (NIGMS) Human Genetic Cell Repository at the Coriell Institute for Medical Research (Candem, NJ, United States). Vero cells, fibroblast-like green monkey kidney cells, were obtained from the collection of Centro de Investigaciones Biológicas Margarita Salas (CIB-CSIC, Madrid). HeLa human cervical carcinoma cells were from the American Type Cell Culture Collection (ATCC). All the cell lines described were cultured in DMEM, supplemented with 10% (v/v) Fetal Bovine Serum (FBS, Biowest), penicillin (100 U/ml) and streptomycin (100 μg/ml) (Invitrogen), except for AG10803 fibroblasts, which were cultured in 20% (v/v) FBS. Cells were kept at 37°C in a humid atmosphere enriched with 5% CO_2. For electrophilic stress studies, cells were treated with vehicle (DMSO) or electrophilic lipids, HNE (10 μM) for 4 h or acrolein (10 μM) for 2 h in serum-free medium. Treatment with calyculin A (20 nM) was performed for 20 min in serum-free medium.

Plasmids and Transfections

Plasmids used in this study include pIRES-DsRed-Express2-vimentin (RFP//vimentin), for expression of untagged vimentin wt, and pEGFP-C1-vimentin wt, described previously (Pérez-Sala et al., 2015), and pmCherry-C1-vimentin wt (Genecopoeia). For cotransfection of plasmids expressing tagged and untagged vimentin constructs a 2:8 DNA ratio was used. Truncated forms of vimentin were expressed from plasmids RFP//vim(1–411), RFP//vim(1–423), RFP//vim(1–448) and RFP//vim(1–459), obtained in our laboratory by introduction of premature stop codons in the original RFP//vimentin plasmid, as previously described (Duarte et al., 2019). Vimentin phosphomimetic constructs, where various serine residues were substituted by aspartic acid (S325D, S412D, S419D), were obtained by mutagenesis of the corresponding RFP//vimentin S➤A mutant plasmids, using the Nzytech mutagenesis kit and the primers specified in **Table 1**. Numbering of vimentin residues in this study considers the initial methionine as position 1. Exogenous expression of vimentin was induced by transfection of the corresponding plasmids into cells in culture. SW12/cl.2 cells at 70% confluency were transfected with 1 μg of DNA, using Lipofectamine 2000 (Invitrogen), following manufacturer's indications. Cells were fixed for further processing 48 h after transfection.

Cell Lysis and Western Blot

Cells were lysed in 50 mM Tris-HCl pH 7.5, 0.1 mM EDTA, 0.1 mM EGTA, 0.1 mM β-mercaptoethanol, 0.5% (w/v) SDS, 50 mM sodium fluoride, 0.1 mM sodium orthovanadate and protease inhibitors: 2 μg/ml leupeptin, 2 μg/ml aprotinin, 2 μg/ml trypsin inhibitor and 1.3 mM Pefablock. Moreover, complete lysis was ensured by passing the cells through a narrow needle ($26^{1/2}$G). The cell lysate was subsequently centrifuged (10,000 g, 4°C, 5 min) and the protein concentration of the supernatant was measured with the bicinchoninic acid (BCA) protein quantification kit (ThermoFischer Scientific). Samples (30 μg of total protein) were denatured in Laemmli buffer (80 mM Tris-HCl pH 6.8, 2% (w/v) SDS, 10% (v/v) glycerol, 5% (v/v) β-mercaptoethanol, 0.15% (w/v) bromophenol blue), during 5 min at 95°C, and loaded onto 12.5% (w/v) SDS-polyacrylamide gels. Proteins were transferred to Immobilon-P membranes (Millipore) using a Transblot semidry transfer unit (Bio-Rad), following a Tris-glycine methanol three-buffer system protocol, as indicated by the manufacturer. Membranes were blocked in 2% (w/v) low-fat powdered milk in 20 mM Tris-HCl pH 7.5, 500 mM NaCl, 0.05% (v/v) Tween 20 (T-TBS), incubated with primary antibodies for 2 h (V9, E5, N-term, anti-actin) or overnight (C-term, C-end), and for 1 h with secondary HRP-conjugated antibodies after washing. Antibodies were diluted in 1% (w/v) bovine serum albumin (BSA) in T-TBS. Signal on membranes was developed with ECL reagents (GE Healthcare) and captured on photographic films (Agfa).

Immunofluorescence

Cells were fixed in 4% (w/v) paraformaldehyde (PFA) for 25 min, and permeabilized with 0.1% (v/v) Triton X-100 in PBS for 20 min prior to being blocked in 1% (w/v) (BSA) in PBS for 1 h. Samples were incubated with either primary and secondary antibodies or with the fluorophore-conjugated primary antibodies for 1 h per antibody, previously diluted (1:200) in 1% (w/v) BSA in PBS. Nuclei were counterstained with DAPI (3 μl/ml) for 15 min, and samples were mounted in Fluorsave (Calbiochem) medium. All incubations were carried out at room temperature. For the V9 and E5 antibodies, controls of their performance in different incubation orders and immunostaining protocols were carried out to verify the results. Fixation with methanol was carried out at −20°C for 10 min and no permeabilization step was required; protocol was continued from the blocking step onwards as described above.

TABLE 1 | Primers used in this study.

Mutant	Primers	
	Forward	Reverse
S325D	GGAGACAGGTGCAGGACCTCACCTGTGAAGTGG	CCACTTCACAGGTGAGGTCCTGCACCTGTCTCC
S412D	GCGAGGAGAGCAGGATTGATCTGCCTCTTCC	GGAAGAGGCAGATCAATCCTGCTCTCCTCGC
S459D	GGTTATCAACGAAACTGATCAGCATCACGATGACC	GGTCATCGTGATGCTGATCAGTTTCGTTGATAACC

Fluorescence Microscopy

Leica TCS SP5 and SP8 confocal microscopes were used to acquire images of fixed samples with a 63× objective. Single confocal sections were taken every 0.5 μm. For comparison of the signals from pairs of antibodies, images were acquired by adjusting the intensity of each channel precisely below the saturation point for each field of view, using the LUT command. Lightning deconvolution module was used together with SP8 confocal imaging, when thus stated. Superresolution microscopy by Stimulated Emission Depletion (STED) was performed in a Leica TCS SP8 microscope, with a 3X STED module. The figures show single z-planes for individual channels, their overlay or z-projections as indicated.

Image Analysis

Images were analyzed with LAS X (Leica Microsystems) or ImageJ software. Surface plots and orthogonal projections were obtained using LAS X software. Plot profiles across individual cells were done in ImageJ for individual channels and the ratio between signals was calculated, when indicated. The recognition pattern of vimentin by the various antibodies tested was assessed through the ratio between the fluorescent intensities of the signals of selected pairs of antibodies, at an area in the vicinity of the plasma membrane. Mean values, normalized per area, allowed to ascertain which antibody signal was most prevalent at the periphery. To assess the coverage of tagged vimentin by E5 and V9 antibodies, the accessibility of E5 and V9 epitopes was determined as the colocalization (Coloc2 plugin, ImageJ) in individual cells between the signal from these antibodies and that from the GFP- or m-Cherry tagged vimentin. Colocalization is expressed as Pearson's R coefficient and colocalization masks were obtained from the colocalization colormap plugin (ImageJ). Filament width in superresolution images was measured as the full width at half maximum (FWHM) distance in filaments with comparable intensity of V9 and E5 signals. The ratio between the width determined by E5 and V9 was calculated for normalization.

Model Building

The hypothetical model was built based on the structure for vimentin available in AlphaFold (alphafold.ebi.ac.uk, structure ID P08670). Such structure was imitated in Inkscape software and was considered as the most compact conformation, according to the structures proposed in this study. Changes in the conformation of vimentin, as presented hereafter, were represented as opening stages from the original one. This model intends to portray the conclusions drawn from this study, but shall not be taken as an exact representation of reality.

Statistical Analysis

All experiments were performed at least three times. Data were analyzed using GraphPad Prism software. Antibody recognition patterns were compared by the mean ratio between pairs of antibodies. Individual ratios were deemed significant by comparison to value 1, corresponding to equal intensities of antibodies, by one sample *t*-test ($\alpha = 0.05$). Ratios were compared among themselves through one-way ANOVA followed by Tukey test ($\alpha = 0.05$). Colocalization was defined by Pearson's R coefficient and mean values were compared through unpaired Student's t-test. Filament width was expressed as the ratio between V9 and E5 FWHM and mean value was compared to value 1, corresponding to equal widths (one sample *t*-test, $\alpha = 0.05$).

RESULTS

Electrophilic Stress-Induced Condensation of Vimentin Hampers Recognition of the Protein by an Anti-C-Terminal Domain Antibody

The cellular vimentin network is highly responsive to electrophilic stress. We have previously reported that the reactive lipid mediator 4-hydroxynonenal (HNE) induces a marked condensation of vimentin filaments at a juxtanuclear location, forming aggresome-like structures (Pérez-Sala et al., 2015). Here, we attempted to monitor this reorganization by transfection with fluorescent fusion constructs, as well as by immunofluorescence with antibodies against different domains of the protein (**Figure 1**). HNE-induced vimentin accumulations were clearly detected in cells cotransfected with RFP//vimentin, for expression of the untagged protein, together with a small proportion of GFP-vimentin fusion construct to light up the vimentin network (**Figure 1A**), as well as by immunofluorescence with an antibody against the vimentin N-terminus (**Figure 1B**). Unexpectedly, aggresome-like accumulations could not be properly detected with an antibody against the vimentin segment spanning residues 430–457, located in the tail domain (C-term antibody) (**Figure 1C**). This lack of recognition was not due to vimentin degradation with loss of the C-terminal epitope as indicated by western blot (**Figure 1D**), which showed the same

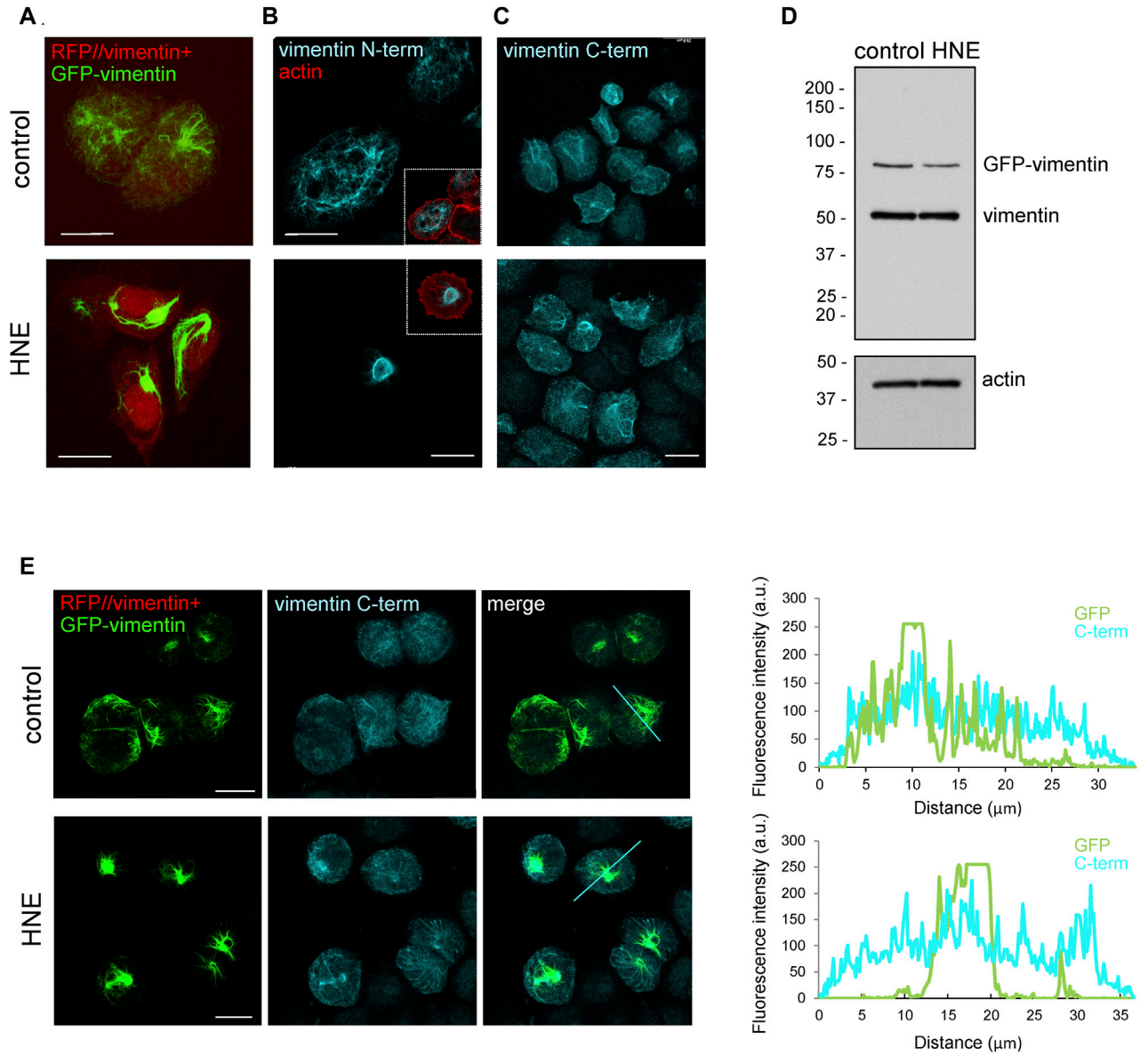

FIGURE 1 | Vimentin juxtanuclear accumulations induced by treatment with HNE are poorly recognized by an anti-C-terminal antibody. SW13/cl.2 cells stably transfected with RFP//vimentin wt, coding for untagged vimentin and RFP as separate products, plus GFP-vimentin wt were treated with vehicle or 10 μM HNE for 4 h. Formation of HNE-induced vimentin accumulations was assessed by **(A)** direct fluorescence microscopy (green, GFP-vimentin; red, RFP background indicative of transfection), **(B)** immunofluorescence with an anti-N-terminal vimentin antibody, and **(C)** immunofluorescence with an anti-C-terminal vimentin antibody (C-term). In **(B)**, the cell contour is marked by staining of cortical actin with phalloidin. **(D)** Cells expressing RFP//vimentin wt plus GFP-vimentin wt were treated with vehicle or HNE and cell lysates were analyzed by western blot with V9 anti-vimentin antibody. The position of the molecular weight standards (in kDa) is shown at the left of the blots. **(E)** Cells stably transfected as in **(A)** were treated with vehicle or HNE and subjected to immunofluorescence with anti-C-terminal antibody (C-term). Vimentin distribution was monitored by confocal fluorescence microscopy. Maximal z-projections are shown. Right panels show the fluorescence intensity profiles for vimentin detected by GFP fluorescence and by immunofluorescence with the C-term antibody along the lines marked in the merged image. Scale bars, 20 μm.

construct size in lysates from control and HNE-treated cells. The poor detection of HNE-induced vimentin condensations by immunofluorescence with the C-term antibody was confirmed by simultaneously monitoring the GFP-vimentin construct (**Figure 1E**). This revealed that the C-term antibody displayed a poor recognition, not only of vimentin accumulations in HNE-treated cells, but also of vimentin present in robust filaments or bundles in control cells, while detecting more scattered vimentin structures, as reflected in the plots of the intensity profiles (**Figure 1E**, right panels). Thus, these observations indicate that in certain vimentin structures the tail domain is shielded from recognition by the C-term antibody. To get further insight into this effect we next assessed the performance of additional antibodies directed against the tail domain.

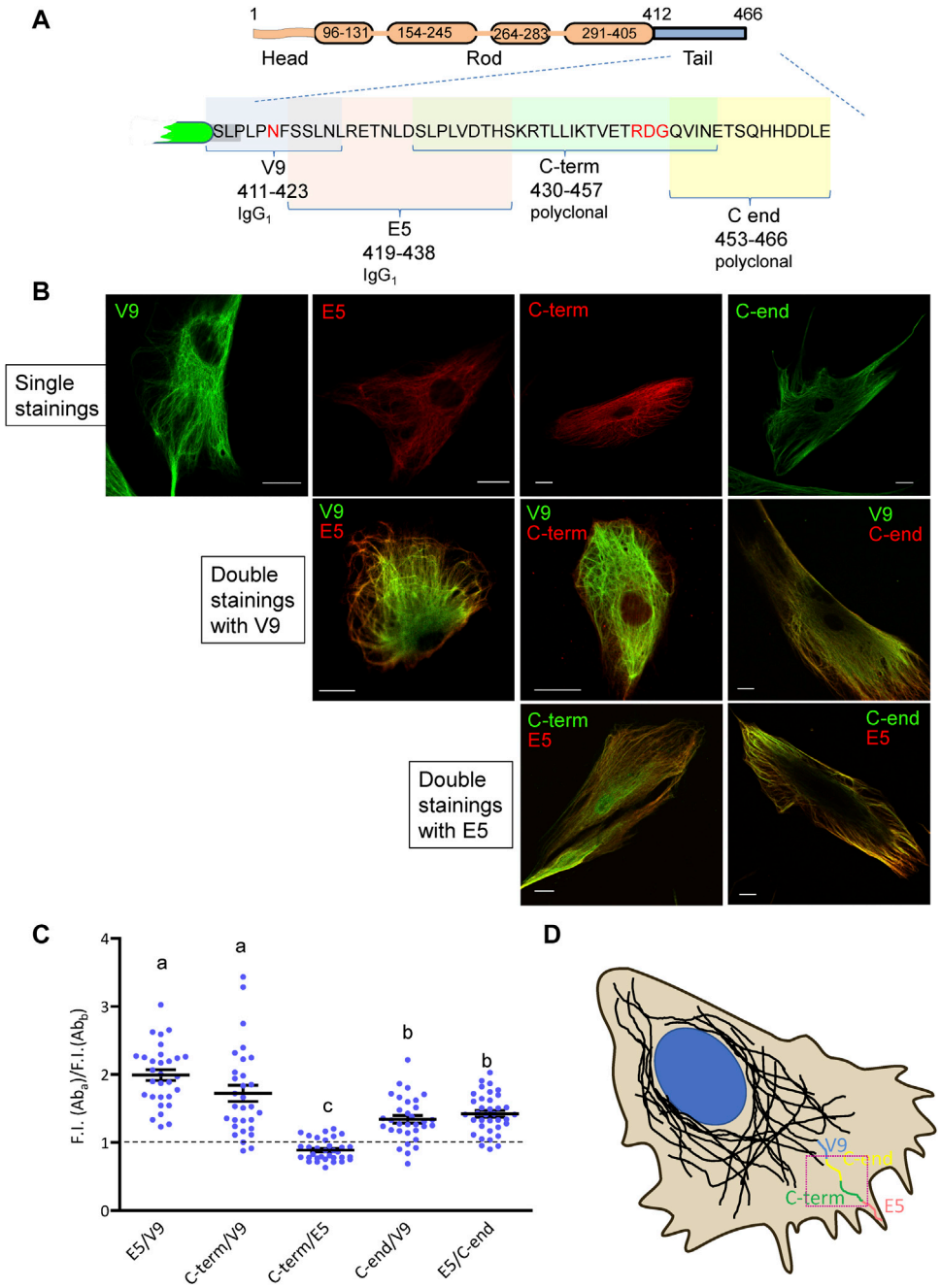

FIGURE 2 | Recognition of vimentin by several antibodies with epitopes mapping at the tail domain. **(A)** Schematic representation of vimentin structure and the tail domain showing the epitopes of the antibodies used for detection. **(B)** Primary human dermal fibroblasts were subjected to immunofluorescence with the indicated antibodies, alone or in combinations, as indicated. Overlays of single z sections are shown. **(C)** Quantification of the ratio between the fluorescence intensity of pairs of antibodies at the cell periphery. For selected ROIs close to the plasma membrane, as illustrated by the red square in **(D),** fluorescence intensity was measured for both channels, and the ratio, calculated ($n \geq 30$ for each pair). All results proved significant when means were compared to a theoretical value of 1 (corresponding to the same fluorescent intensity for both channels) through one sample *t*-test ($\alpha = 0.05$). Significance among all ratios is shown in a letter-code; non-significant differences, indicated with the same letter, were only registered between pairs E5/V9—"C-term"/V9 and "C-end"/V9—E5/"C-end." Statistical analysis was performed through 1-way ANOVA ($\alpha = 0.05$), followed by Tukey test. **(D)** Schematic representation of the recognition pattern for each antibody at the periphery of cells, arranged according to their maximum reach, under non-saturation fluorescent intensity conditions. Scale bars, 20 μm.

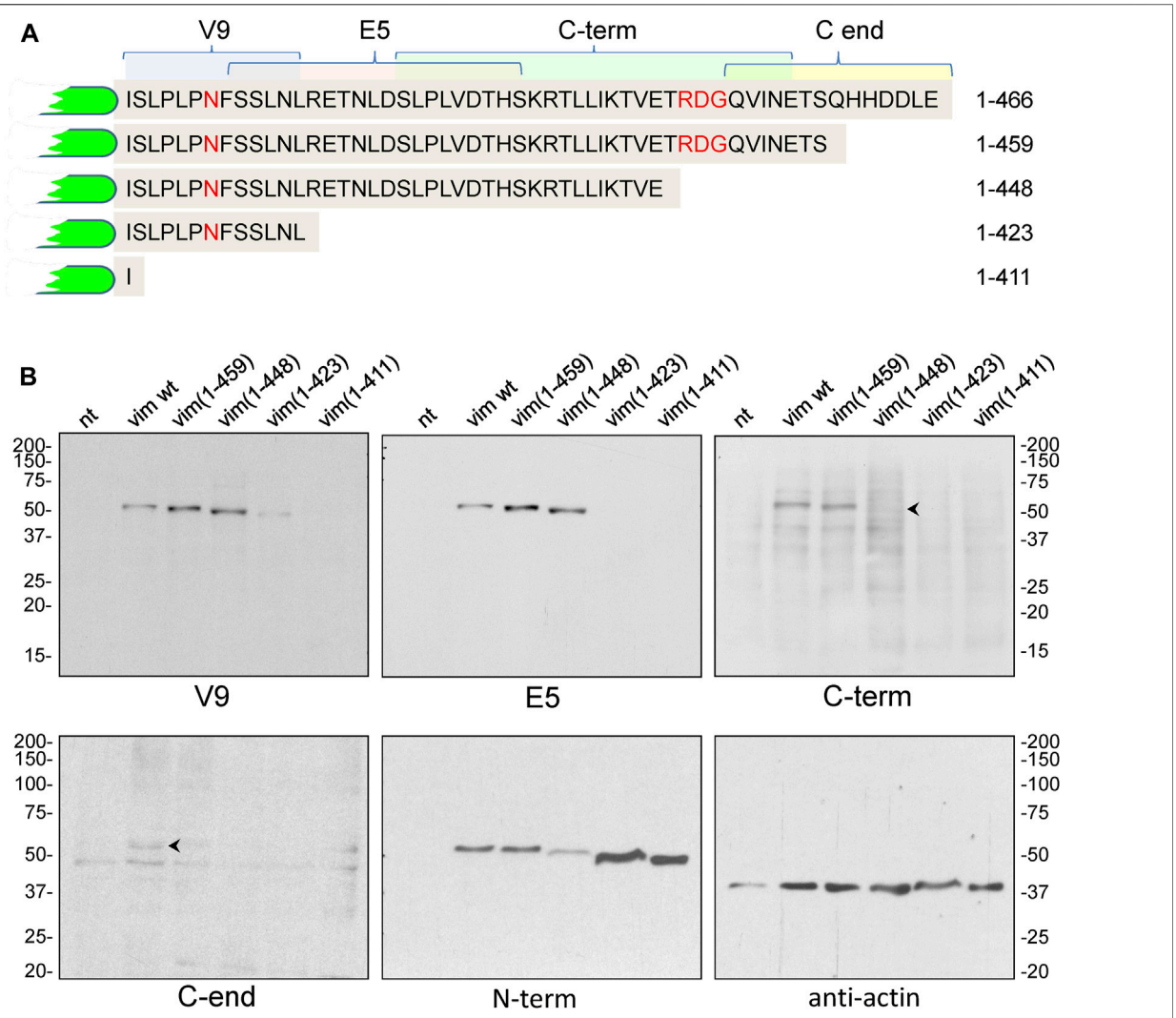

FIGURE 3 | Analysis of the recognition of vimentin full length and C-terminal truncated mutants by antibodies against different epitopes of the tail domain. **(A)** Schematic of the tail sequences of the truncated vimentin mutants, indicating the epitopes recognized by the antibodies used in this study. **(B)** SW13/cl.2 cells were transfected with vimentin full length or the indicated truncated mutants. Cell lysates were analyzed by SDS-PAGE and western blot with the antibodies specified. Antibodies against vimentin N-terminus (N-term) and anti-actin were used as controls. The position of the molecular weight standards (in kDa) is shown at the left and right of the blots.

Vimentin Tail Epitopes Show Variable Accessibility Across the Cytoplasm

In order to understand the variable accessibility of vimentin tail segments in wild-type cells, we analyzed its detection by antibodies recognizing consecutive segments of the tail sequence. The scheme in **Figure 2A** depicts a simplified view of the vimentin monomer with its head, rod and tail domains, the sequence of the latter displayed in full to show the location of the epitopes of the various antibodies used. All antibodies detected vimentin by immunofluorescence in human primary dermal fibroblasts when used individually (**Figure 2B**). The recognition of vimentin by different combinations of these antibodies was then studied by adjusting the signals from all antibodies to obtain maximal, though non-saturated intensities. Remarkably, we observed that the V9 antibody (epitope 411–423) yielded an intense signal throughout most of the cytoplasm and above all in the robust filaments located near the perinuclear area (**Figure 2B**). In contrast, both the E5 (419–438) and the C-term (430–457) antibodies appeared to preferentially recognize vimentin located at the cell periphery (**Figure 2B**). Interestingly, signals from E5 and C-term antibodies gave a high degree of overlap, with a slightly more frequent preferential E5 staining in peripheral filaments. Lastly, the C-end antibody yielded a signal that was proportionally higher than that of V9 at peripheral filaments but lower than that of E5. To quantify these observations, the ratios between the fluorescence intensities obtained with the different pairs of antibodies at peripheral areas of the cell (see defined ROI in

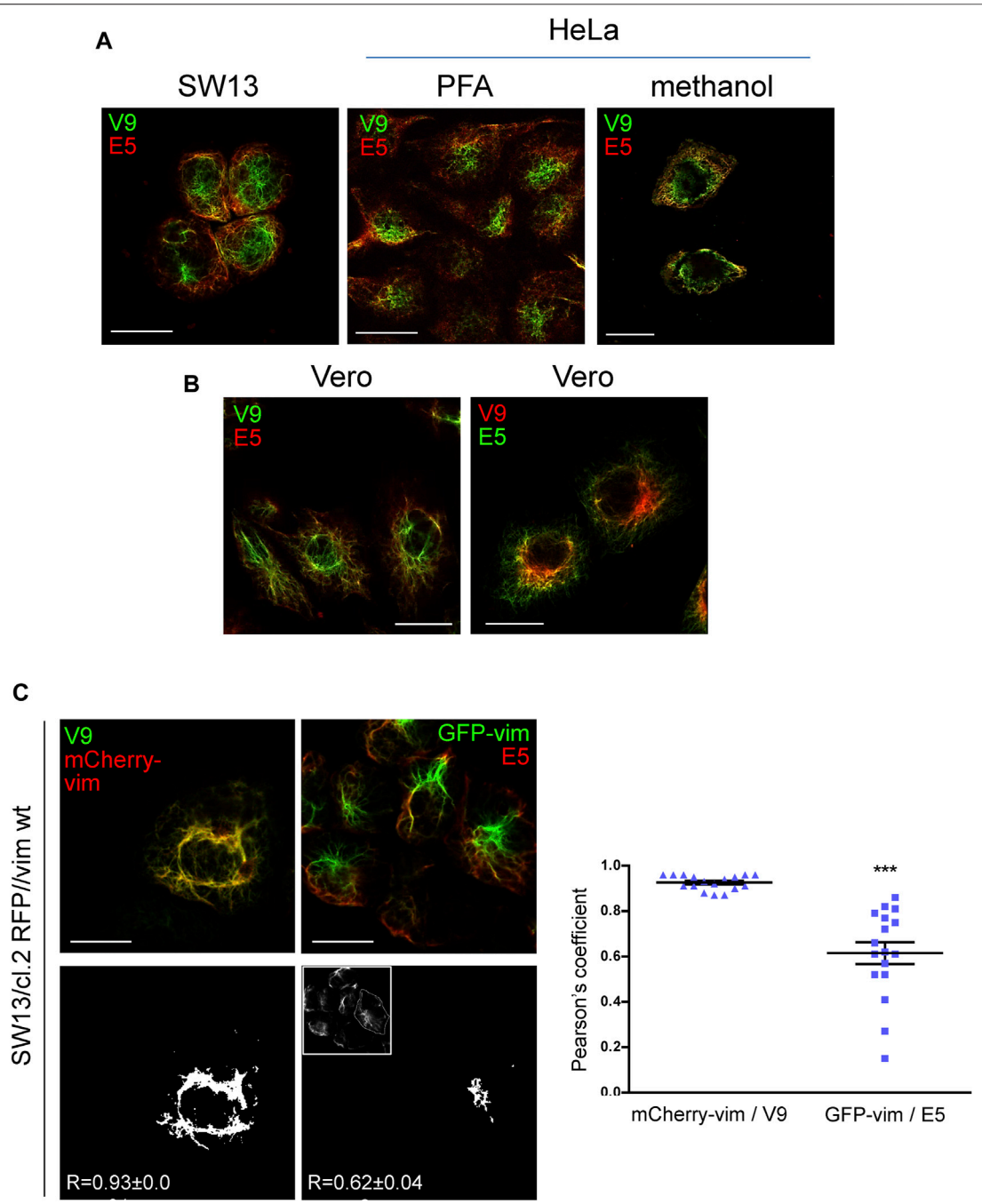

FIGURE 4 | Differential recognition of vimentin C-terminal epitopes in several cell types. **(A)** Vimentin in SW13/cl.2 cells stably expressing RFP//vimentin wt fixed with PFA and in HeLa cells fixed with PFA or methanol, as indicated, was observed by immunofluorescence with anti-vimentin V9-Alexa488 and anti-vimentin E5-Alexa546, followed by confocal microscopy. Single sections at 1–2 microns from the basal plane are shown. **(B)** Vero cells fixed with PFA as above were immunostained with the indicated antibodies, namely: left panel, anti-vimentin V9-Alexa488 plus anti-vimentin E5-Alexa546; right panel, anti-vimentin V9-Alexa568 plus anti-vimentin E5-Alexa488, and observed by confocal microscopy. **(C)** SW13/cl.2 RFP//vimentin wt cells, expressing untagged vimentin, were cotransfected with a small amount of mCherry-vimentin (mCherry-vim) or GFP-vimentin (GFP-vim), as indicated, to highlight the full vimentin network. Subsequently, they were subjected to immunofluorescence with V9-Alexa488 and E5-Alexa546, respectively. The overlap between the total vimentin signal and that of the corresponding antibodies was calculated as the Pearson coefficient from 17 cells per experimental condition. The adjacent graph depicts all values obtained along with the mean values ± SEM. Differences between experiments were significant (***$p < 0.0001$), as determined by unpaired Student's t-test. Scale bars, 20 μm.

Figure 2D) were calculated (**Figure 2C**). These results clearly showed that the C-term, E5 and C-end antibodies selectively recognized peripheral filaments with respect to V9, i.e., showed a poorer recognition of filaments at the central region of the cell. These data led us to propose a scheme according to which, the antibodies against the different segments of the tail domain would preferentially recognize vimentin at different distances from the cell center to the cell periphery in the following order: V9 (411–423), C-end (453–466), C-term (430–457) and E5 (419–438), in this cell type (**Figure 2D**).

As a control for the specificity of these antibodies, we explored their ability to recognize several truncated vimentin mutants, spanning the indicated segments of the tail domain (**Figure 3A**), by western blot. The V9 monoclonal antibody recognized all constructs except vim(1–411), that lacks the whole tail and therefore, the V9 epitope (**Figure 3B**). In turn, E5 (epitope spanning the 419–438 segment), recognized all constructs except vim(1–411) and vim(1–423). The C-term antibody, raised against the 430–457 peptide, showed marginal or no recognition of the vim(1–448) construct, which indicates that the distal sequence of this peptide is necessary for antibody binding. Finally, an antibody against the last fourteen residues (C-end antibody) only recognized full-length vimentin. Nevertheless, the performance of the last two antibodies in western blot was not optimal. As expected, an antibody against the N-terminus of vimentin recognized all constructs. An anti-actin antibody was used as a control (**Figure 3B**).

The Differential Exposure of Vimentin Tail Regions Occurs in Several Cell Types

The results shown above suggest a differential exposure of vimentin epitopes at distinct subcellular locations. For subsequent experiments, we decided to compare signals from the V9 and E5 antibodies because they belong to the same immunoglobulin subtype (IgG_1, Kappa light chain) and are available as direct fluorescent conjugates. First, we explored whether the differential spatial distribution of V9 and E5-immunoreactivity occurred in several cell types (**Figure 4**). Vimentin-deficient SW13/cl.2 cells stably transfected with vimentin wt showed a juxtanuclear enrichment of V9-positive vimentin, whereas the recognition by E5 was more defined at the cell periphery (**Figure 4A**). A preferential detection of central vimentin by V9 and peripheral vimentin by E5 was also observed in HeLa cells, independently of the fixation method (**Figure 4A**), as well as in Vero cells (**Figure 4B**). In the latter cell type, a control inverting the conjugated fluorophores, i.e., employing V9-Alexa Fluor 546 and E5-Alexa Fluor 488, confirmed the selective detection of the epitopes at different cellular locations (**Figure 4B**).

In order to assess this differential distribution by methods not relying only on antibody binding, we combined immunofluorescence with the transfection of a small proportion of fluorescent vimentin constructs to directly light up the vimentin network (**Figure 4C**), as previously reported (Ho et al., 1998; Yoon et al., 1998; Pérez-Sala et al., 2015). Interestingly, V9-Alexa488 fluorescence markedly colocalized with mCherry-vimentin, thus reflecting protein abundance, whereas E5-Alexa546 fluorescence showed scarce colocalization with GFP-vimentin at the center of the cell, but detected the peripheral areas where the GFP-vimentin signal was less intense. This limited correlation between E5 signal and total vimentin highlights again the restricted accessibility of the 419–438 segment (E5 epitope) in vimentin at the robust central filaments, compared to peripheral regions, where the density of the network is lower.

High Resolution Analysis of the Differential Immunoreactivity of Vimentin Tail Segments

Next, the differential recognition of the V9 and E5 epitopes was assessed by high resolution microscopy strategies (**Figure 5**). Analysis of single filaments in fibroblasts by confocal microscopy clearly showed a different proportion of the fluorescence intensities along the filament length, with immunoreactivity changing gradually from a V9-prevalent to an E5-predominant signal towards the distal portion of filaments (**Figure 5A**). Moreover, a surface plot of the filament confirmed a better accessibility of the E5 epitope towards the filaments tip. A lower accessibility of the E5 epitope in perinuclear filaments was also observed by STED (**Figure 5B**). Further characterization of vimentin immunoreactivity using the Leica Lightning module allowed visualization of V9 and E5 signals on single filaments in SW13/cl.2 cells expressing vimentin wt, and revealed an alternate dotted pattern with a higher abundance of V9 positive spots towards the center of the cell, and of E5 towards the cell periphery (**Figure 5C**).

Next, STED microscopy was performed on thin filaments close to the cell periphery (**Figure 5D**), and the distribution of antibodies on the filament was assessed determining the width of each signal through FWHM (full width at half maximum) measurements, as described in the methods section. Filaments alike in size, at a similar distance from the plasma membrane and with comparable E5 and V9 signal intensities were chosen for quantification. Compared to the width of the V9 signal, the amplitude of E5 staining was 1.42 times larger (1.42 ± 0.10) (**Figure 5E**), as represented in **Figure 5F**. Although further confirmation is required, these results could suggest that the E5 epitope is accessible at points farther from the center of the filament, thus, in a more open tail conformation.

Exposure of Vimentin Tail Segments in a Truncated Protein

The vimentin tail has been proposed to form a hairpin structure due to the interaction of the β-turn comprising the RDG motif with the epsilon-site on the distal portion of the rod (Kouklis et al., 1991; Hess et al., 2013). Indeed, a model of the C-terminal segment of the vimentin monomer obtained from AI-based AlphaFold shows that the β-turn-rod interaction could impose a bend of the tail forming a loop that would project from the filament (**Figure 6A**). The V9

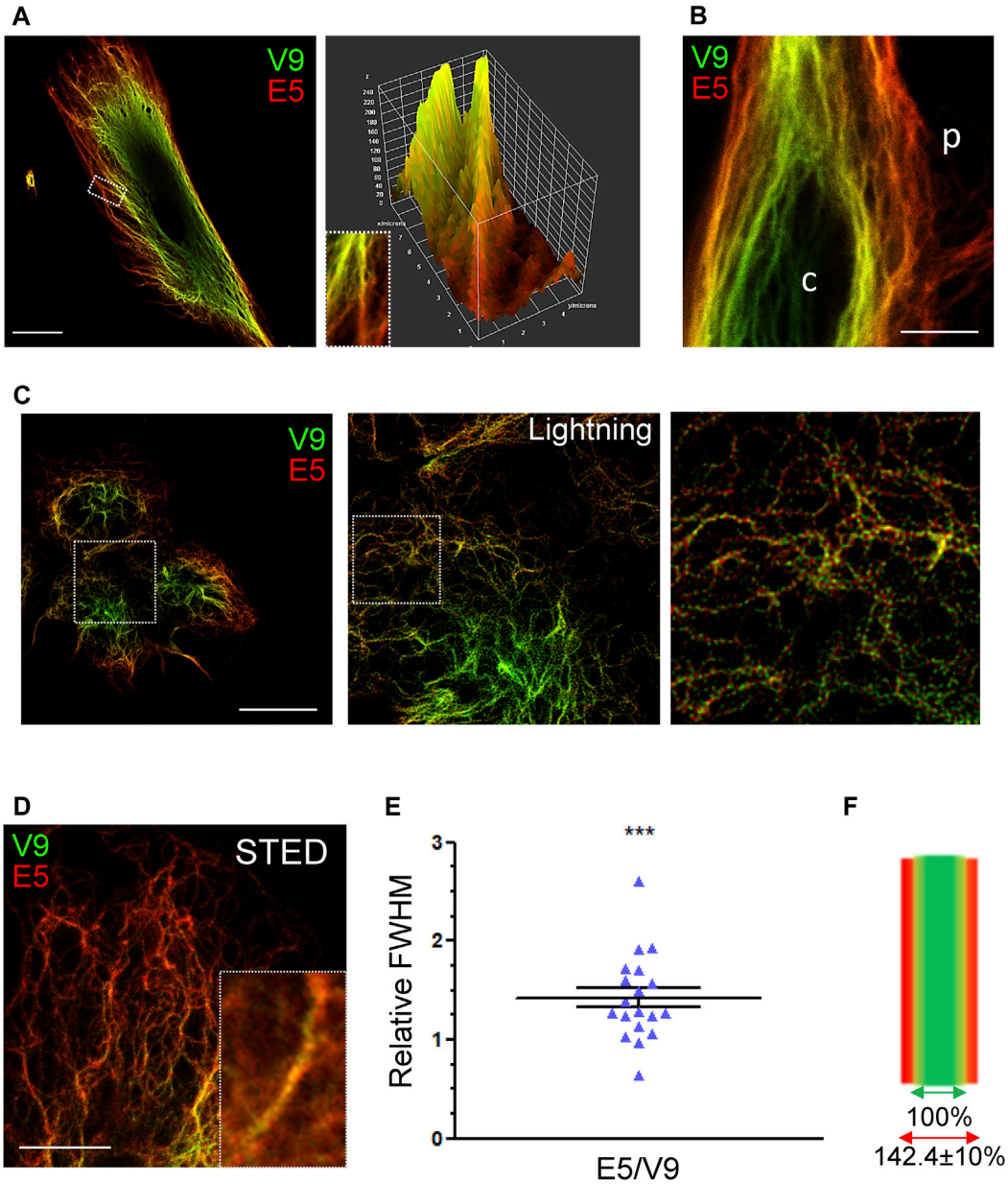

FIGURE 5 | Analysis of the differential accessibility of vimentin tail domain epitopes by high resolution microscopy. **(A)** Human fibroblasts were stained with V9-Alexa488 and E5-Alexa546 antibodies. A single confocal section is shown. The area delimited by the rectangle in the left panel is enlarged in the right panel (inset) and the corresponding surface plot illustrating the graded change in immunoreactivity of the vimentin filaments is shown. Scale bar, 20 μm. **(B)** Human fibroblasts stained as in **(A)** were visualized by STED superresolution microscopy. The peripheral (p) and central regions (c) of the cell are indicated. Scale bar, 5 μm. **(C)** SW13/cl.2 cells stably expressing RFP//vimentin wt were stained with V9-Alexa488 and E5-Alexa546 and visualized by confocal microscopy using an SP8 confocal microscope; the middle and right panels show enlarged areas of images acquired with the lightning module and processed with the lightning deconvolution tool afterwards. Scale bar, 20 μm. **(D)** Insight into vimentin filaments at the cell edge using STED super-resolution microscopy obtained from SW13/cl.2 cells expressing RFP//vimentin wt. Inset depicts a representative filament. Scale bar, 5 μm. **(E)** Scatter plot depicting the relative width of filaments as estimated from the signals of the E5 and V9 antibodies. Width was calculated, for each channel, as full width at half maximum (FWHM) in filaments from STED images ($n = 19$). Results proved significant when mean value was compared to theoretical value (1) through one sample t-test (***$p < 0.001$). **(F)** Graphical representation of vimentin filaments width, as recorded by each antibody, according to data presented in **(E)**. Values are indicated as mean ± SEM.

epitope could occupy the apex of the loop, therefore, being accessible in spite of filament compaction or bundling, whereas the E5 epitope could be shielded from recognition in the folded conformation. To explore this possibility we performed immunostaining of a vimentin (1–448) truncated construct, which lacks the RDG motif (Duarte et al., 2019) (**Figure 6B**). As previously characterized, vim(1–448) yielded a mixed assembly pattern consisting of both extended filaments and curly bundles (Duarte et al., 2019). Vim(1–448)

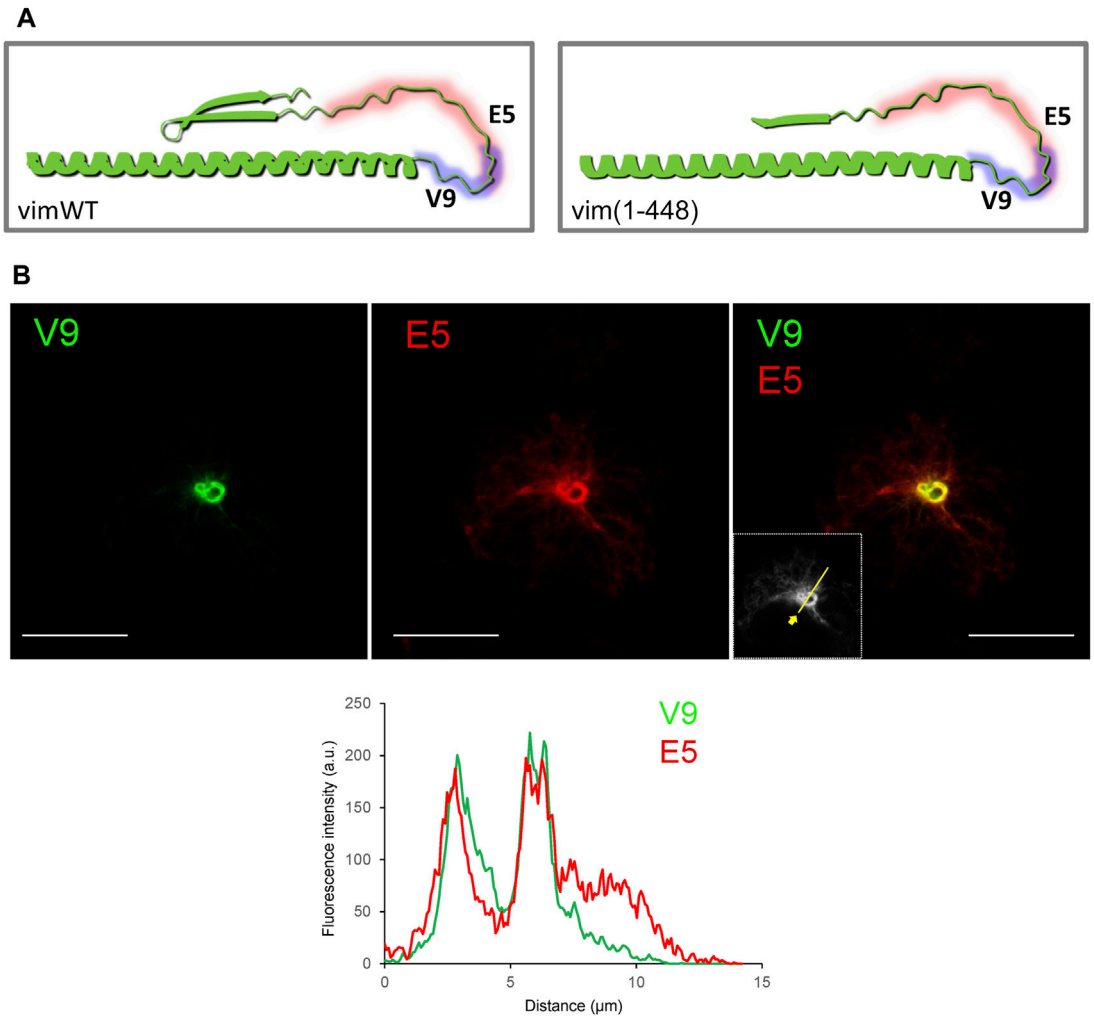

FIGURE 6 | Recognition of a C-terminal truncated vimentin mutant by the V9 and E5 antibodies. **(A)** Models of the vimentin C-terminus, according to AlphaFold predicted structure. Left panel, vimentin residues 350 to 466 are presented illustrating the predicted interaction between the β-turn and the epsilon site, and the resulting loop of the tail domain, potentially masking certain epitopes. Right panel, model for the truncated vimentin (1–448) mutant, lacking the constriction of the interaction, thus potentially allowing exposure of additional segments of the tail. **(B)** Immunoreactivity of a vimentin (1–448) mutant towards V9 and E5 antibodies was assessed by immunofluorescence in SW13/cl.2 transfected with this construct. Results are representative from three experiments with similar results. The fluorescence intensity profiles along the line depicted in the inset are shown in the lower panel. Scale bars, 20 µm.

could be detected with both V9 and E5 antibodies. Interestingly, equilibration of maximal intensities showed that the dense swirls were similarly detected by both antibodies. Nevertheless, under these conditions, peripheral filaments were still preferentially detected by E5. This indicates that removal of the RDG motif appears to improve the relative accessibility of the E5 epitope in dense bundles, although its exposure continues to be greater in peripheral filaments.

Accessibility of Vimentin Tail Segments in Different Cellular Contexts

The results shown above suggest the coexistence of several populations of vimentin in cells, differing in the accessibility of the tail domain under standard cell culture conditions. Therefore, we aimed to explore whether this phenomenon occurred in different cellular situations, where a higher dynamicity of the vimentin network could be expected.

The vimentin network suffers a drastic reorganization in response to stress, as already illustrated in **Figure 1**. Therefore, we first explored whether the formation of aggresome-like structures elicited by electrophilic compounds implied changes in the recognition of vimentin tail segments by the V9 and E5 antibodies. Treatment of Vero cells with the electrophilic compound acrolein induced intense vimentin remodeling with formation of thick bundles and aggresome-like structures that could be detected with both V9 and E5 antibodies in a significant proportion of cells (**Figure 7A**). Interestingly, imaging signals from both antibodies below saturation point revealed the predominance of the V9 signal at the center of aggresomes,

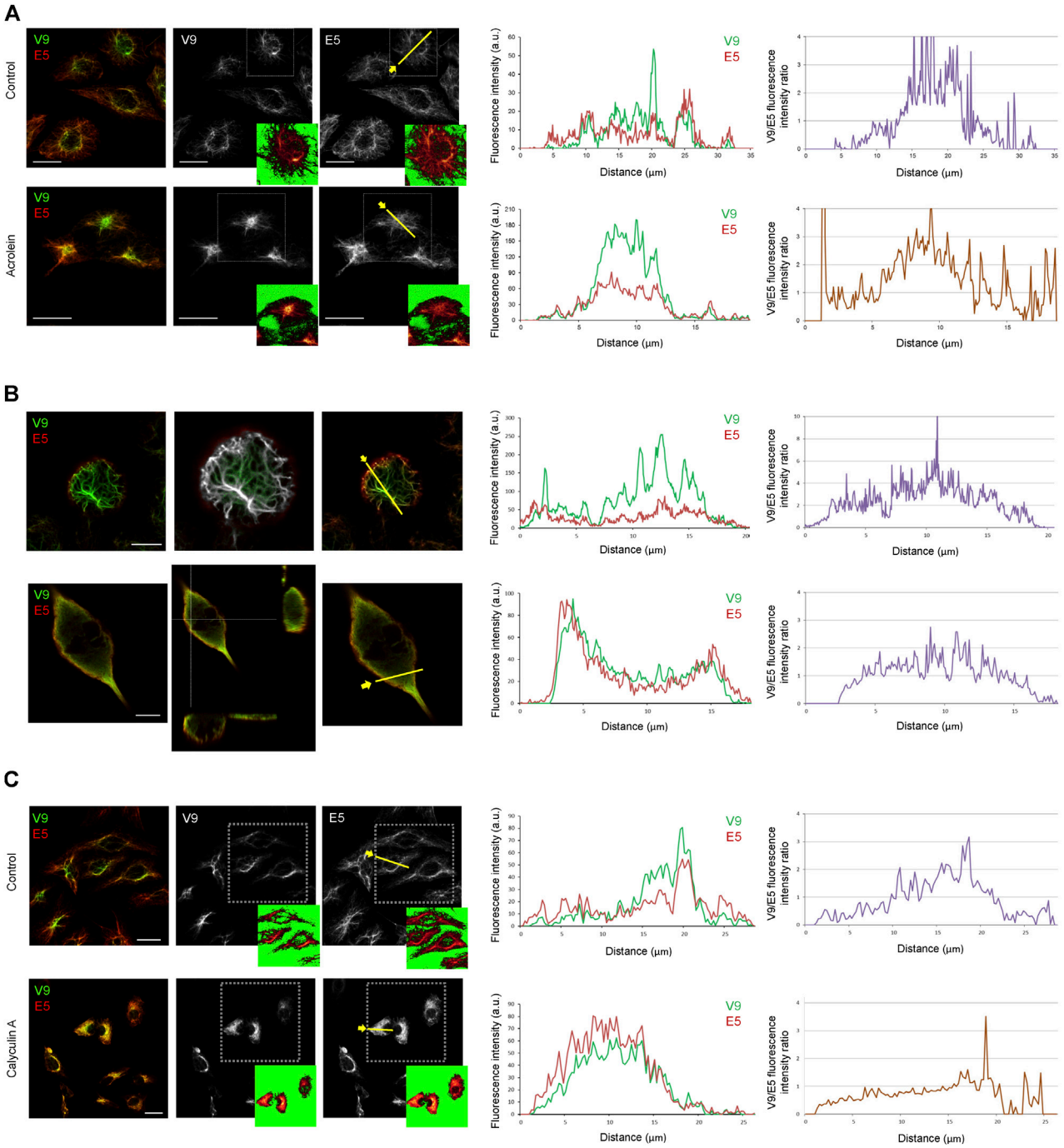

FIGURE 7 | Differential accessibility of vimentin C-terminal epitopes under various experimental conditions affecting vimentin assembly. **(A)** Effect of electrophilic stress on the exposure of V9 and E5 epitopes. Vero cells were treated with vehicle (control) or 10 μM acrolein for 2 h, as indicated, and processed for immunodetection with V9-Alexa488 and E5-Alexa546. Single confocal images of merged and individual channels are shown. Regions of interest, delimited by dotted squares are shown in insets as visualized with the LUT command to illustrate the cell contours and the levels of saturation of the signals. Fluorescence intensity profiles along the yellow line were obtained for each channel and shown at the right. The far right panel shows the intensity ratio of V9 and E5 fluorescence intensities. **(B)** Immunoreactivity of vimentin tail segments in mitotic cells. Upper panels, SW13/cl.2 cells expressing vimentin wt undergoing mitosis were imaged as above and a single confocal section at a basal z-plane is shown. The middle image shows the colocalization mask highlighting the points of coincidence between the signals of both antibodies (in white). Lower panels, human fibroblasts undergoing mitosis were immunostained as above. A single confocal section is shown in the left image and orthogonal projections are depicted in the middle panel to illustrate the peripheral disposition of the E5 signal. Fluorescence intensity profiles along the yellow lines drawn in the right images and the V9/E5 intensity ratio are plotted at the right for both cell types. **(C)** Effect of calyculin A on vimentin tail immunoreactivity. Vero cells treated with vehicle (control) or 20 nM calyculin A for 20 min and stained with V9 and E5 antibodies. Regions of interest, delimited by dotted squares are shown in insets visualized with the LUT command. Fluorescence intensity profiles along the yellow line and V9/E5 fluorescence intensity ratio are plotted at the right. Scale bars, 20 μm.

and of E5 in peripheral filaments. This is illustrated by the fluorescence intensity profiles as well as by the ratio of V9/E5 fluorescence intensities in the aggresome vs. peripheral filaments, which reaches 3–4 in the aggresomes but is lower in the surrounding cytoplasm (**Figure 7A**). Since, as shown above, the V9 signal appears to correlate with vimentin abundance, these observations clearly show that V9, but not E5, efficiently detects the accumulation of vimentin in the aggresome.

During mitosis, vimentin is phosphorylated by a series of kinases (Yamaguchi et al., 2005; Izawa and Inagaki, 2006), which results in a cell type-dependent reorganization, characterized by different degrees of disassembly, ranging from filament preservation to nearly complete solubilization (Duarte et al., 2019; Chou et al., 1989). In SW13/cl.2 cells stably expressing vimentin, filaments are preserved in mitosis and translocate to the cell periphery, where they interact with the actin cortex (Duarte et al., 2019). Monitoring the V9 epitope showed its accessibility in the robust filaments that line the cell cortex at the basal layers of mitotic cells (**Figure 7B**, upper images), as previously reported by us (Duarte et al., 2019). In contrast, the E5 epitope was less accessible in these structures and was more clearly detected at a peripheral cell layer, as illustrated in the fluorescence intensity profiles and the plot of V9/E5 intensity ratios, where values at the cell periphery are below 1. Nevertheless, points of coincidence of the two signals could be spotted (**Figure 7B**, colocalization mask). In sharp contrast, in mitotic human fibroblasts, vimentin distributed in bundles with a loose appearance or as a diffuse background indicative of disassembly or solubilization, respectively (**Figure 7B**, lower images). Interestingly, the V9 and E5 signals also displayed obvious differences under these conditions. Both the loose bundles and the internal diffuse background showed slightly predominant V9 immunoreactivity, whereas the E5 epitope was preferentially detected at the most peripheral region. These differences were obvious in orthogonal projections of these images, which showed an external layer with more intense E5 reactivity and the internal volume, positive for both signals, but with areas of preferential V9 staining, as illustrated in the fluorescence intensity profiles and the corresponding fluorescence ratios. These observations indicate that differences in the accessibility of both vimentin tail epitopes persist, in spite of the disassembly occurring in mitosis in this cell type.

Phosphatase inhibitors, like calyculin A, an inhibitor of protein phosphatase 1 (PP1) and 2A (PP2A), have been shown to induce vimentin hyperphosphorylation and solubilization (Quintanar, 2000; Eriksson et al., 2004). Therefore, we explored the effect of calyculin A on the recognition of vimentin by V9 and E5 antibodies (**Figure 7C**). Incubation with calyculin A elicited diverse morphological alterations of the vimentin network in Vero cells, including filament coalescence into thick bundles and accumulations that displayed a similar recognition by E5 and V9 antibodies, indicating a more similar accessibility of epitopes. These results, illustrated in the fluorescence intensity profiles and the V9/E5 fluorescence ratios shown in **Figure 7C** suggest that vimentin phosphorylation, as a consequence of phosphatase inhibition, could improve the accessibility of the E5 epitope.

Exposure of Vimentin Tail Segments in Phosphomimetic Mutants

Interestingly, the vimentin tail displays several phosphorylation sites, although their function is not well understood. As an initial approach to investigate a potential role of phosphorylation in the accessibility of vimentin tail segments we studied several mutants introducing phosphomimetic residues at sites close to the V9 and E5 epitopes, namely, vimentin S419D and vimentin S412D. In addition, a phosphomimetic mutant in segment 2B of the rod, vimentin S325D, was studied for comparison. The impact of these mutations on vimentin network distribution was assessed first by immunofluorescence with an antibody against the N-terminal end of vimentin, in order to avoid potential interferences of the mutations with the binding of antibodies against the tail domain (**Figure 8**). Vimentin S419D and S412D formed extended filament networks similar to that formed by vimentin wt, although filaments frequently appeared less robust and with a reticular disposition. In contrast, vimentin S325D formed apparently shorter filaments of irregular orientation. Immunofluorescence of these mutant networks with the V9 and E5 antibodies showed an attenuation of the differences in the recognition patterns. In vimentin S419D, the central area of the cell was still preferentially recognized by V9. In contrast, vimentin S412D showed a higher overlap of V9 and E5 signals, indicating a more similar accessibility of the corresponding epitopes. Remarkably, vimentin S325D filaments appeared to be comparably stained by V9 or E5, irrespectively of the cell region. These observations, which are illustrated in the surface plots (**Figure 8**, bottom panels), suggest that introducing phosphomimetic residues at several sites of the vimentin C-terminus, impacts its assembly and/or the disposition of the tail domain, thus influencing exposure of different segments. Nevertheless, other explanations are possible as it will be discussed below.

DISCUSSION

The intermediate filament protein vimentin can form an amazing variety of dynamic interchangeable structures, which are involved in a plethora of cellular functions. Vimentin assembly, location and interaction can be finely tuned by posttranslational modifications (PTM), which can occur throughout the sequence of the protein giving rise to a wide variety of proteoforms (Snider and Omary, 2014; Griesser et al., 2021). The disordered tail of vimentin, which can harbor a variety of PTM (Griesser et al., 2021), has been reported to modulate the assembly of filaments and to support interactions with other cytoskeletal structures (Kouklis et al., 1993; Duarte et al., 2019). Nevertheless, the conformation of this segment is not known and could be affected by several factors including PTM, binding of divalent cations and/or protein-protein interactions (Lin et al., 2010). Here, we have observed that the accessibility of various segments of vimentin C-terminus displays defined spatial patterns in cells, which suggests the presence of distinct

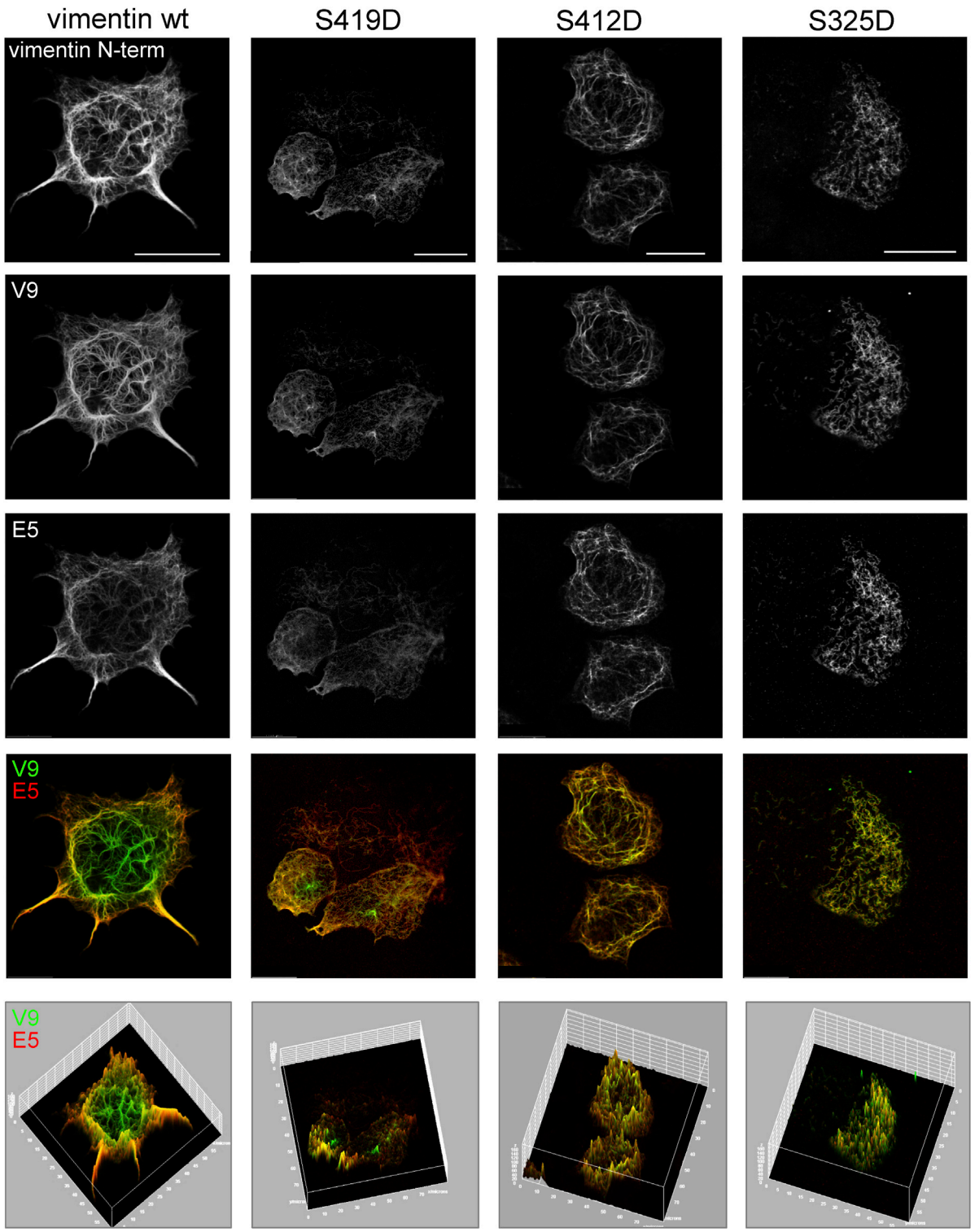

FIGURE 8 | Assembly and C-terminal epitope recognition of vimentin phosphomimetic mutants. SW13/cl.2 cells were transfected with plasmids for expression of vimentin wt or the indicated phosphomimetic mutants. The distribution of the vimentin network was assessed by immunofluorescence with the N-term antibody (N-term-Alexa647), and the immunoreactivity of the tail domain monitored by staining with V9-Alexa488 and E5-Alexa546, as indicated. Single channels and merged V9/E5 images are shown. The bottom panels depict the surface plots for every condition in order to better illustrate the intensity and distribution of V9 and E5 signals. Scale bars, 20 μm.

vimentin populations differing in the conformation of the tail domain, with a selective subcellular distribution.

The first indication of a differential exposure of tail segments was obtained when comparing the signals from GFP-vimentin and from vimentin detected by immunofluorescence with antibodies against the N- or C-terminus of the protein upon treatment with HNE, an electrophilic lipid which causes filament retraction towards the nucleus. Unexpectedly, whereas, apparently, GFP-vimentin and the anti-N-terminus antibody did not reveal vimentin filaments at the periphery of HNE-treated cells, the C-term antibody did (**Figure 1**). Interestingly, approaches combining immunological detection and fluorescent vimentin constructs (**Figure 1E**) clarified that these differences arose from the fact that the intense GFP-vimentin and anti-N-terminus signals at the HNE-induced bundles became saturated before the scarce peripheral filaments became detectable. Conversely, as the C-term antibody poorly recognized vimentin bundles and accumulations, the signal of peripheral vimentin could be detected without reaching saturation.

Interestingly, detailed characterization of vimentin tail immunoreactivity has unveiled a differential accessibility of two close vimentin tail segments, namely, the V9 and E5 epitopes, at distinct cell regions. The V9 epitope, located in segment 411–423, is accessible throughout the filament network, whereas the E5 epitope, located between residues 419 and 438, is shielded from recognition in bundles at the cell center and in aggresome-like structures, but is preferentially detected in sparse filaments. In this case, combination of immunological detection and fluorescent vimentin constructs clearly showed that the V9 signal keeps a better correlation with the overall distribution and abundance of vimentin throughout the cell, and therefore, reflects more accurately the morphology of the network, whereas E5 immunodetection poorly recognizes robust filaments under resting conditions. This reduced accessibility of the E5 epitope could be due to several reasons including the density of filament packing, a differential conformation of the vimentin tail, presence of PTM and/or protein interactions, without disregarding intramolecular or intrafilament interactions, for instance with the head domain.

Earlier works have described the distinct subcellular localization of vimentin proteoforms. Phosphorylated disassembled vimentin has been located at leading lamelipodia (Helfand et al., 2011) and vimentin phosphorylated at S459 has been reported to be mostly located at cell protrusions (Kotula et al., 2013). In turn, vimentin bearing certain oxidative PTM has been described to be destined for secretion to the extracellular medium or exposure at the plasma membrane (Frescas et al., 2017). In this work, we observe a subpopulation of vimentin forming robust filaments at the center on the cells, mainly underneath the nucleus in resting cells and at the center of basal planes in mitotic cells that are selectively stained with the V9 antibody, with poor accessibility of the E5 epitope.

Although the structure of the vimentin tail is not known, detailed *in vitro* work indicates the existence of "points of order" in this intrinsically disordered domain (Hess et al., 2013). As mentioned before, studies with anti-idiotypic antibodies (Kouklis et al., 1991) have defined the so-called "beta" and "epsilon" sites, located in the tail, residues 444–452, and at the C-terminal end of the rod, residues 364–416, respectively, the beta site being important for vimentin filament assembly and architecture (Kouklis et al., 1993; Makarova et al., 1994). Moreover, the beta site has been proposed to fold over the epsilon site in assembled vimentin, which would lead to the formation of a loop, hypothetically protruding from filaments.

Together with these previous works, our results could propose a model in which the V9 epitope, centered in N417, would protrude from assembled filaments, therefore being accessible in compact filaments and even bundles, whereas the E5 epitope, closer to the beta-turn, could be shielded in robust filaments due to the β-turn-epsilon site interaction and/or to the apposition of vimentin tail pairs occurring during polymerization. This would be particularly important under certain stress conditions causing further filament condensation, which could mask the C-terminal epitopes to make them virtually undetectable as shown in **Figure 1**. A schematic representation of hypothetical conformations of the vimentin tail, as suggested from the exposure of the various epitopes, and assisted by AlphaFold, is presented in **Figure 9**. Interestingly, it is well known that tail domains of other intermediate filaments, for instance neurofilaments, are involved in regulation of their assembly or crossbridging, in a process that is modulated by phosphorylation occurring selectively at distinct cellular locations (Yuan et al., 2012). In addition, the conformation of tail domains can be differentially involved in protein-protein interactions. The tail domain of desmin, which is 71% homologous to that of vimentin, bears important sites for interaction with the chaperone αB-crystallin (Sharma et al., 2017). In reconstituted systems, αB-crystallin has been shown to bind to desmin oligomers and coassemble with them, but to scarcely bind to preformed filaments. Thus, αB-crystallin has been proposed as a sensor for different assembly states of desmin (Sharma et al., 2017). In an analogous way, the results shown here could indicate that certain antibodies against the C-terminal domain, mainly E5 and C-term, may serve as "sensors" or indicators of vimentin assembly. In line with our results, early studies on desmin also described a differential accessibility of a C-terminal segment. In particular, the region containing the RDG motif, residues 442–450 in chicken desmin, was accessible to site-specific antibodies in disassembled subunits and loosely packed filamentous structures, but not in desmin mature filaments, neither *in vitro* nor in muscle cells (Birkenberger and Ip, 1990). Therefore, these findings support our interpretation regarding the different immunoreactivity of vimentin tail segments depending on the assembly state of the protein.

Importantly, epitope exposure, and therefore tail conformation, could be regulated by PTM either by affecting the tail per se or indirectly by modulating the assembly state of vimentin. Indeed, it has been previously noted that the beta site is flanked by phosphorylation sites, including S430, S458 and S459 (Hess et al., 2013; Kornreich et al., 2015) that influence vimentin assembly (Eriksson et al., 2004).

Notably, EPR studies of *in vitro* PKA phosphorylated vimentin showed an important impact of phosphorylation on the C-terminal region of the rod (Pittenger et al., 2008). S412,

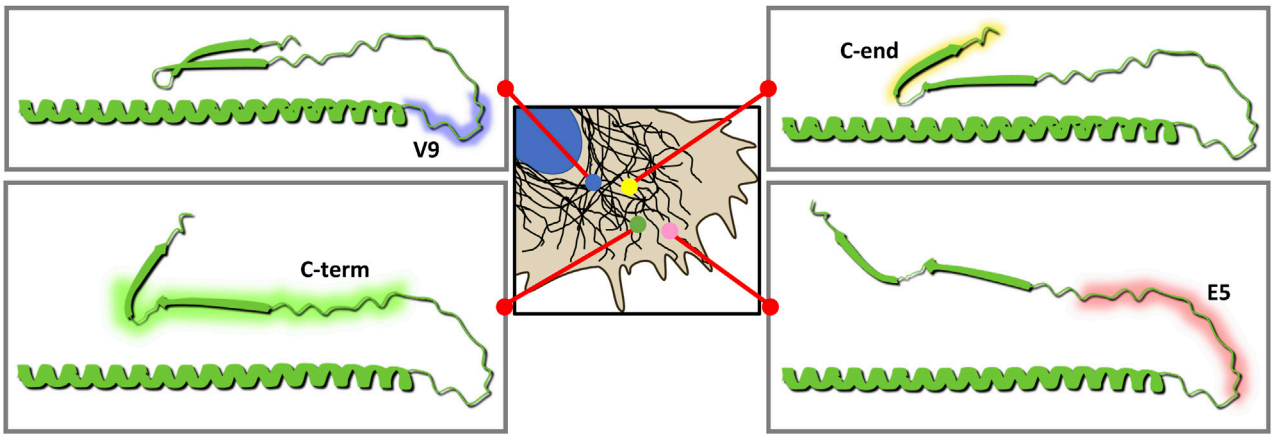

FIGURE. 9 | Model of the potential conformations of vimentin tail based on the differential exposure of epitopes observed. Vimentin is represented from the residue 350 to the C-terminus. The structure depicted here is based on the predictions of vimentin structure available in AlphaFold. Antibody epitopes are indicated in a color code as in **Figure 2**: V9 in blue, E5 in pink, "C-term" in green and "C-end" in yellow. The areas of the cell where epitopes are preferentially detected in each case are indicated, similar to **Figure 2**. Closer to the cell periphery, where vimentin would adopt the most extended conformation, all antibodies would be putatively capable of binding their epitopes. The E5 epitope is the first one to be less recognizable when approaching the cell center, followed by "C-term." In areas closer to the nucleus, V9 antibody would be the antibody to preferentially bind vimentin, putatively in its most compact conformation.

S419 and S420 were found to be phosphorylated in this study, although the precise impact of these sites was not assessed. Indeed, although vimentin phosphorylation is widely recognized to control vimentin assembly, modifications at the head domain are much better characterized both from the mechanistic and functional points of view. The vimentin head is also known to fold over the rod forming a loop-like structure. Interestingly, EPR studies have shown that the phosphorylation of the head domain laterally separates the heads but does not necessarily disrupts the head-rod association (Aziz et al., 2009). Our observations do not allow discerning whether shielding of the E5 epitope is due to lateral apposition or to the tail-rod interaction. Nevertheless, our results with the 1–448 truncated vimentin mutant and high resolution microscopy indicate that likely both the beta-epsilon interaction and lateral apposition of the tails are involved in shielding the E5 (and/or C-term) epitopes in cells, since removal of the β-site partially improves the detection of the E5 epitope in bundles.

In contrast, differences in the exposure of the V9 and E5 epitopes persist in mitotic cells, even in spite of the apparent disassembly of vimentin in mitotic fibroblasts. This may indicate that disassembly in mitosis does not necessarily imply marked changes in tail conformation. Conversely, we have observed that calyculin A, which is known to increase the phosphorylation state of vimentin by precluding dephosphorylation, induces the formation of cellular vimentin assemblies with a more comparable exposure of V9 and E5 epitopes. Interestingly, calyculin A has been reported to increase phosphorylation at sites already modified in interphase cells, including some present in the C-terminal domain, and different from those that are phosphorylated in mitosis (Eriksson et al., 1992; Eriksson et al., 2004). Several tail domain residues have been found phosphorylated in mitosis, although to a lower extent and apparently exerting a weaker functional impact than those present in the head domain (Chou et al., 2003). Thus, the importance of phosphorylation on vimentin tail conformation could be site-dependent.

In fact, our observations with single phosphomimetic mutants suggest a variable impact of the phosphorylation of certain sites on network organization, which appears to be more intense when the mutated sites are closer to or within the rod domain. Under these conditions, parallel changes in the degree of assembly and vimentin tail epitope exposure appear to take place, with mutations at the beginning of the tail (S412D), and above all, at the C-terminal region of the rod domain (S325D), leading to sparser filaments with a similar exposure of epitopes and loss of the cell region dependence of the tail conformation. In contrast, the pattern of the S419D mutant is closer to the wt. Therefore, it could be hypothesized that charged residues and/or phosphorylation at certain positions could impact the conformation of the tail domain. Whether this potential conformational change implies unfolding or unpairing of tail segments remains to be elucidated.

According to the PhosphoSite database, both S412 and S419 have been found phosphorylated in ischemic tumors (Mertins et al., 2014) and in HeLa cells after treatment with gambogic acid (Yue et al., 2016). In addition, phosphorylation of S419 has been found in BHK21 fibroblasts treated with calyculin A (Eriksson et al., 2004), whereas phosphorylation of S412 was shown in cells arrested in mitosis by nocodazole treatment (Olsen et al., 2010). In turn, phosphorylation of S325 has been described in multiple cell types and experimental conditions (https://www.phosphosite.org/siteAction.action?id=4148959). Interestingly, the proximity of S325 to C328, a hot spot for modification by oxidants and electrophiles and a key regulator of vimentin assembly and reorganization in response to oxidative stress, raises the possibility of cross-talk between S325 phosphorylation and

C328 modification in the regulation of vimentin organization, which deserves further study.

In summary, our results point to the existence of diverse vimentin populations with different tail conformations in cells. These populations can be distinguished by the exposure of precise epitopes and likely reflect distinct states of assembly, potentially regulated by PTM, including phosphorylation. These different populations could also be involved in distinct interactions or functions which deserve further investigation.

DATA AVAILABILITY STATEMENT

The raw data supporting the conclusion of this article will be made available by the authors, without undue reservation.

AUTHOR CONTRIBUTIONS

IL-B, PG-J, and DP-S performed experiments, analyzed data and prepared illustrations. SD performed experiments. MP designed mutagenesis primers, provided feedback and critically reviewed the manuscript. IL-B and DP-S designed experiments and wrote the manuscript. DP-S designed and coordinated the study. All authors contributed to manuscript revision, read, and approved the submitted version.

FUNDING

This work was supported by the European Union's Horizon 2020 research and innovation program under the Marie Sklodowska-Curie Grant agreement no. 675132 "Masstrplan" and Grant RTI2018-097624-B-I00 from Agencia Estatal de Investigación, Micinn/FEDER, Spain to DP-S. PG-J is supported by PRE2019-088194 from Micinn/FEDER.

ACKNOWLEDGMENTS

Feedback from COST Actions CA15214 "EuroCellNet" and CA19105 "EpiLipidNet" is gratefully acknowledged. We wish to thank the personnel of the Laser Confocal and Multidimensional in vivo Microscopy Facility at CIB Margarita Salas. Partial support of the publication fee by the CSIC Open Access Publication Support Initiative through its Unit of Information Resources for Research (URICI) is acknowledged.

REFERENCES

Aziz, A., Hess, J. F., Budamagunta, M. S., FitzGerald, P. G., and Voss, J. C. (2009). Head and Rod 1 Interactions in Vimentin. *J. Biol. Chem.* 284, 7330–7338. doi:10.1074/jbc.m809029200

Aziz, A., Hess, J. F., Budamagunta, M. S., Voss, J. C., and Fitzgerald, P. G. (2010). Site-directed Spin Labeling and Electron Paramagnetic Resonance Determination of Vimentin Head Domain Structure. *J. Biol. Chem.* 285, 15278–15285. doi:10.1074/jbc.m109.075598

Birkenberger, L., and Ip, W. (1990). Properties of the Desmin Tail Domain: Studies Using Synthetic Peptides and Antipeptide Antibodies. *J. Cell. Biol.* 111, 2063–2075. doi:10.1083/jcb.111.5.2063

Brennich, M. E., Vainio, U., Wedig, T., Bauch, S., Herrmann, H., and Koster, S. (2019). Mutation-induced Alterations of Intra-filament Subunit Organization in Vimentin Filaments Revealed by SAXS. *Soft Matter.* 15(9):1999-2008. doi:10.1039/c8sm02281j

Chou, Y.-H., Khuon, S., Herrmann, H., and Goldman, R. D. (2003). Nestin Promotes the Phosphorylation-dependent Disassembly of Vimentin Intermediate Filaments during Mitosis. *MBoC* 14, 1468–1478. doi:10.1091/mbc.e02-08-0545

Chou, Y. H., Rosevear, E., and Goldman, R. D. (1989). Phosphorylation and Disassembly of Intermediate Filaments in Mitotic Cells. *Proc. Natl. Acad. Sci. U.S.A.* 86, 1885–1889. doi:10.1073/pnas.86.6.1885

dos Santos, G., Rogel, M. R., Baker, M. A., Troken, J. R., Urich, D., Morales-Nebreda, L., et al. (2015). Vimentin Regulates Activation of the NLRP3 Inflammasome. *Nat. Commun.* 6, 6574. doi:10.1038/ncomms7574

Duarte, S., Viedma-Poyatos, Á., Navarro-Carrasco, E., Martínez, A. E., Pajares, M. A., and Pérez-Sala, D. (2019). Vimentin Filaments Interact with the Actin Cortex in Mitosis Allowing Normal Cell Division. *Nat. Commun.* 10, 4200. doi:10.1038/s41467-019-12029-4

Eckelt, A., Herrmann, H., and Franke, W. W. (1992). Assembly of a Tail-Less Mutant of the Intermediate Filament Protein, Vimentin, *In Vitro* and *In Vivo*. *Eur. J. Cell. Biol.* 58, 319–330.

Eibauer, M., Weber, M. S., Turgay, Y., Sivagurunathan, S., Goldman, R. D., and Medalia, O. (2021). *The Molecular Architecture of Vimentin Filaments*. BioRxiv. doi:10.1101/2021.07.15.452584

Eldirany, S. A., Lomakin, I. B., Ho, M., and Bunick, C. G. (2021). Recent Insight into Intermediate Filament Structure. *Curr. Opin. Cell. Biol.* 68, 132–143. doi:10.1016/j.ceb.2020.10.001

Eriksson, J. E., Brautigan, D. L., Vallee, R., Olmsted, J., Fujiki, H., and Goldman, R. D. (1992). Cytoskeletal Integrity in Interphase Cells Requires Protein Phosphatase Activity. *Proc. Natl. Acad. Sci. U.S.A.* 89, 11093–11097. doi:10.1073/pnas.89.22.11093

Eriksson, J. E., He, T., Trejo-Skalli, A. V., Härmälä-Braskén, A.-S., Hellman, J., Chou, Y.-H., et al. (2004). Specific *In Vivo* Phosphorylation Sites Determine the Assembly Dynamics of Vimentin Intermediate Filaments. *J. Cell. Sci.* 117, 919–932. doi:10.1242/jcs.00906

Frescas, D., Roux, C. M., Aygun-Sunar, S., Gleiberman, A. S., Krasnov, P., Kurnasov, O. V., et al. (2017). Senescent Cells Expose and Secrete an Oxidized Form of Membrane-Bound Vimentin as Revealed by a Natural Polyreactive Antibody. *Proc. Natl. Acad. Sci. U. S. A.* 114, E1668–E1677. doi:10.1073/pnas.1614661114

Griesser, E., Vemula, V., Mónico, A., Pérez-Sala, D., and Fedorova, M. (2021). Dynamic Posttranslational Modifications of Cytoskeletal Proteins Unveil Hot Spots under Nitroxidative Stress. *Redox Biol.* 44, 102014. doi:10.1016/j.redox.2021.102014

Helfand, B. T., Mendez, M. G., Murthy, S. N. P., Shumaker, D. K., Grin, B., Mahammad, S., et al. (2011). Vimentin Organization Modulates the Formation of Lamellipodia. *MBoC* 22, 1274–1289. doi:10.1091/mbc.e10-08-0699

Herrmann, H., and Aebi, U. (2016). Intermediate Filaments: Structure and Assembly. *Cold Spring Harb. Perspect. Biol.* 8, a018242. doi:10.1101/cshperspect.a018242

Hess, J. F., Budamagunta, M. S., Aziz, A., FitzGerald, P. G., and Voss, J. C. (2013). Electron Paramagnetic Resonance Analysis of the Vimentin Tail Domain Reveals Points of Order in a Largely Disordered Region and Conformational Adaptation upon Filament Assembly. *Protein Sci.* 22, 47–55. doi:10.1002/pro.2182

Ho, C. L., Martys, J. L., Mikhailov, A., Gundersen, G. G., and Liem, R. K. (1998). Novel Features of Intermediate Filament Dynamics Revealed by Green Fluorescent Protein Chimeras. *J. Cell. Sci.* 111 (Pt 13) (Pt 13), 1767–1778. doi:10.1242/jcs.111.13.1767

Hol, E. M., and Capetanaki, Y. (2017). Type III Intermediate Filaments Desmin, Glial Fibrillary Acidic Protein (GFAP), Vimentin, and Peripherin. *Cold Spring Harb. Perspect. Biol.* 9, a021642. doi:10.1101/cshperspect.a021642

Ivaska, J., Pallari, H.-M., Nevo, J., and Eriksson, J. E. (2007). Novel Functions of Vimentin in Cell Adhesion, Migration, and Signaling. *Exp. Cell. Res.* 313, 2050–2062. doi:10.1016/j.yexcr.2007.03.040

Izawa, I., and Inagaki, M. (2006). Regulatory Mechanisms and Functions of Intermediate Filaments: a Study Using Site- and Phosphorylation State-specific Antibodies. *Cancer Sci.* 97, 167–174. doi:10.1111/j.1349-7006.2006.00161.x

Kornreich, M., Avinery, R., Malka-Gibor, E., Laser-Azogui, A., and Beck, R. (2015). Order and Disorder in Intermediate Filament Proteins. *FEBS Lett.* 589, 2464–2476. doi:10.1016/j.febslet.2015.07.024

Kotula, E., Faigle, W., Berthault, N., Dingli, F., Loew, D., Sun, J.-S., et al. (2013). DNA-PK Target Identification Reveals Novel Links between DNA Repair Signaling and Cytoskeletal Regulation. *PLoS One* 8, e80313. doi:10.1371/journal.pone.0080313

Kouklis, P. D., Hatzfeld, M., Brunkener, M., Weber, K., and Georgatos, S. D. (1993). *In Vitro* assembly Properties of Vimentin Mutagenized at the Beta-Site Tail Motif. *J. Cell. Sci.* 106 (Pt 3) (Pt 3), 919–928. doi:10.1242/jcs.106.3.919

Kouklis, P. D., Papamarcaki, T., Merdes, A., and Georgatos, S. D. (1991). A Potential Role for the COOH-Terminal Domain in the Lateral Packing of Type III Intermediate Filaments. *J. Cell. Biol.* 114, 773–786. doi:10.1083/jcb.114.4.773

Li, F. J., Surolia, R., Li, H., Wang, Z., Liu, G., Kulkarni, T., et al. (2021). Citrullinated Vimentin Mediates Development and Progression of Lung Fibrosis. *Sci. Transl. Med.* 13. doi:10.1126/scitranslmed.aba2927

Lin, Y.-C., Broedersz, C. P., Rowat, A. C., Wedig, T., Herrmann, H., Mackintosh, F. C., et al. (2010). Divalent Cations Crosslink Vimentin Intermediate Filament Tail Domains to Regulate Network Mechanics. *J. Mol. Biol.* 399, 637–644. doi:10.1016/j.jmb.2010.04.054

Makarova, I., Carpenter, D., Khan, S., and Ip, W. (1994). A Conserved Region in the Tail Domain of Vimentin Is Involved in its Assembly into Intermediate Filaments. *Cell. Motil. Cytoskelet.* 28, 265–277. doi:10.1002/cm.970280309

Matsuyama, M., Tanaka, H., Inoko, A., Goto, H., Yonemura, S., Kobori, K., et al. (2013). Defect of Mitotic Vimentin Phosphorylation Causes Microophthalmia and Cataract via Aneuploidy and Senescence in Lens Epithelial Cells. *J. Biol. Chem.* 288, 35626–35635. doi:10.1074/jbc.m113.514737

Mertins, P., Yang, F., Liu, T., Mani, D. R., Petyuk, V. A., Gillette, M. A., et al. (2014). Ischemia in Tumors Induces Early and Sustained Phosphorylation Changes in Stress Kinase Pathways but Does Not Affect Global Protein Levels. *Mol. Cell. Proteomics* 13, 1690–1704. doi:10.1074/mcp.m113.036392

Minin, A. A., and Moldaver, M. V. (2008). Intermediate Vimentin Filaments and Their Role in Intracellular Organelle Distribution. *Biochem. Mosc.* 73, 1453–1466. doi:10.1134/s0006297908130063

Mónico, A., Duarte, S., Pajares, M. A., and Pérez-Sala, D. (2019). Vimentin Disruption by Lipoxidation and Electrophiles: Role of the Cysteine Residue and Filament Dynamics. *Redox Biol.* 23, 101098. doi:10.1016/j.redox.2019.101098

Olsen, J. V., Vermeulen, M., Santamaria, A., Kumar, C., Miller, M. L., Jensen, L. J., et al. (2010). Quantitative Phosphoproteomics Reveals Widespread Full Phosphorylation Site Occupancy during Mitosis. *Sci. Signal* 3, ra3. doi:10.1126/scisignal.2000475

Pérez-Sala, D., Oeste, C. L., Martínez, A. E., Garzón, B., Carrasco, M. J., and Cañada, F. J. (2015). Vimentin Filament Organization and Stress Sensing Depend on its Single Cysteine Residue and Zinc Binding. *Nat. Commun.* 6, 7287. doi:10.1038/ncomms8287

Pittenger, J. T., Hess, J. F., Budamagunta, M. S., Voss, J. C., and Fitzgerald, P. G. (2008). Identification of Phosphorylation-Induced Changes in Vimentin Intermediate Filaments by Site-Directed Spin Labeling and Electron Paramagnetic Resonance. *Biochemistry* 47, 10863–10870. doi:10.1021/bi801137m

Quintanar, J. L. (2000). Vimentin in Cultured Chromaffin Cells: an Immunofluorescent, Biochemical and Functional Study. *Cell. Physiol. Biochem.* 10, 91–98. doi:10.1159/000016338

Ramos, I., Stamatakis, K., Oeste, C. L., and Pérez-Sala, D. (2020). Vimentin as a Multifaceted Player and Potential Therapeutic Target in Viral Infections. *Ijms* 21, 4675. doi:10.3390/ijms21134675

Satelli, A., and Li, S. (2011). Vimentin in Cancer and its Potential as a Molecular Target for Cancer Therapy. *Cell. Mol. Life Sci.* 68, 3033–3046. doi:10.1007/s00018-011-0735-1

Sharma, S., Conover, G. M., Elliott, J. L., Der Perng, M., Herrmann, H., and Quinlan, R. A. (2017). αB-crystallin Is a Sensor for Assembly Intermediates and for the Subunit Topology of Desmin Intermediate Filaments. *Cell. Stress Chaperones* 22, 613–626. doi:10.1007/s12192-017-0788-7

Shoeman, R. L., Höner, B., Stoller, T. J., Kesselmeier, C., Miedel, M. C., Traub, P., et al. (1990). Human Immunodeficiency Virus Type 1 Protease Cleaves the Intermediate Filament Proteins Vimentin, Desmin, and Glial Fibrillary Acidic Protein. *Proc. Natl. Acad. Sci. U.S.A.* 87, 6336–6340. doi:10.1073/pnas.87.16.6336

Sihag, R. K., Inagaki, M., Yamaguchi, T., Shea, T. B., and Pant, H. C. (2007). Role of Phosphorylation on the Structural Dynamics and Function of Types III and IV Intermediate Filaments. *Exp. Cell. Res.* 313, 2098–2109. doi:10.1016/j.yexcr.2007.04.010

Singh, B., and Arlinghaus, R. B. (1989). Vimentin Phosphorylation by P37mos Protein Kinase *In Vitro* and Generation of a 50-kDa Cleavage Product in V-Mos-Transformed Cells. *Virology* 173, 144–156. doi:10.1016/0042-6822(89)90230-4

Snider, N. T., and Omary, M. B. (2014). Post-translational Modifications of Intermediate Filament Proteins: Mechanisms and Functions. *Nat. Rev. Mol. Cell. Biol.* 15, 163–177. doi:10.1038/nrm3753

Thomas, E. K., Connelly, R. J., Pennathur, S., Dubrovsky, L., Haffar, O. K., and Bukrinsky, M. I. (1996). Anti-idiotypic Antibody to the V3 Domain of Gp120 Binds to Vimentin: a Possible Role of Intermediate Filaments in the Early Steps of HIV-1 Infection Cycle. *Viral Immunol.* 9, 73–87. doi:10.1089/vim.1996.9.73

Viedma-Poyatos, Á., Pajares, M. A., and Pérez-Sala, D. (2020). Type III Intermediate Filaments as Targets and Effectors of Electrophiles and Oxidants. *Redox Biol.* 36, 101582. doi:10.1016/j.redox.2020.101582

Yamaguchi, T., Goto, H., Yokoyama, T., Sillje´, H., Hanisch, A., Uldschmid, A., et al. (2005). Phosphorylation by Cdk1 Induces Plk1-Mediated Vimentin Phosphorylation during Mitosis. *J. Cell. Biol.* 171, 431–436. doi:10.1083/jcb.200504091

Yoon, M., Moir, R. D., Prahlad, V., and Goldman, R. D. (1998). Motile Properties of Vimentin Intermediate Filament Networks in Living Cells. *J. Cell. Biol.* 143, 147–157. doi:10.1083/jcb.143.1.147

Yuan, A., Rao, M. V., Veeranna and Nixon, R. A. (2012). Neurofilaments at a Glance. *J. Cell. Sci.* 125, 3257–3263. doi:10.1242/jcs.104729

Yue, Q., Feng, L., Cao, B., Liu, M., Zhang, D., Wu, W., et al. (2016). Proteomic Analysis Revealed the Important Role of Vimentin in Human Cervical Carcinoma HeLa Cells Treated with Gambogic Acid. *Mol. Cell. Proteomics* 15, 26–44. doi:10.1074/mcp.m115.053272

Zhang, Y., Wen, Z., Shi, X., Liu, Y. J., Eriksson, J. E., and Jiu, Y. (2020). The Diverse Roles and Dynamic Rearrangement of Vimentin during Viral Infection. *J. Cell. Sci.* 134. doi:10.1242/jcs.250597

Conflict of Interest: The authors declare that the research was conducted in the absence of any commercial or financial relationships that could be construed as a potential conflict of interest.

Publisher's Note: All claims expressed in this article are solely those of the authors and do not necessarily represent those of their affiliated organizations, or those of the publisher, the editors and the reviewers. Any product that may be evaluated in this article, or claim that may be made by its manufacturer, is not guaranteed or endorsed by the publisher.

frontiers | Frontiers in Cell and Developmental Biology

TYPE Original Research
PUBLISHED 18 July 2022
DOI 10.3389/fcell.2022.891281

OPEN ACCESS

EDITED BY
Dolores Pérez-Sala,
Spanish National Research Council (CSIC), Spain

REVIEWED BY
Inmaculada Navarro-Lérida,
Autonomous University of Madrid, Spain
Chungho Kim,
Korea University, South Korea
José Luis Rodríguez-Fernández,
Spanish National Research Council (CSIC), Spain

*CORRESPONDENCE
Franziska Lautenschläger,
f.lautenschlaeger@physik.uni-saarland.de

SPECIALTY SECTION
This article was submitted to Cell Growth and Division, a section of the journal Frontiers in Cell and Developmental Biology

RECEIVED 07 March 2022
ACCEPTED 27 June 2022
PUBLISHED 18 July 2022

CITATION
Thalla DG, Rajwar AC, Laurent AM, Becher JE, Kainka L and Lautenschläger F (2022), Extracellular vimentin is expressed at the rear of activated macrophage-like cells: Potential role in enhancement of migration and phagocytosis. *Front. Cell Dev. Biol.* 10:891281. doi: 10.3389/fcell.2022.891281

Extracellular vimentin is expressed at the rear of activated macrophage-like cells: Potential role in enhancement of migration and phagocytosis

Divyendu Goud Thalla[1], Ashish Chand Rajwar[1], Annalena Maria Laurent[1], Johanna Elisabeth Becher[2], Lucina Kainka[1] and Franziska Lautenschläger[1,3]*

[1]Experimental Physics, Saarland University, Saarbrücken, Germany, [2]Centre for Bioinformatics, Saarland University, Saarbrücken, Germany, [3]Centre for Biophysics, Saarland University, Saarbrücken, Germany

Macrophages have a vital role in the immune system through elimination of cell debris and microorganisms by phagocytosis. The activation of macrophages by tumour necrosis factor-α induces expression of extracellular cell-surface vimentin and promotes release of this vimentin into the extracellular environment. Vimentin is a cytoskeletal protein that is primarily located in the cytoplasm of cells. However, under circumstances like injury, stress, senescence and activation, vimentin can be expressed on the extracellular cell surface, or it can be released into the extracellular space. The characteristics of this extracellular vimentin, and its implications for the functional role of macrophages and the mechanism of secretion remain unclear. Here, we demonstrate that vimentin is released mainly from the back of macrophage-like cells. This polarisation is strongly enhanced upon macrophage activation. One-dimensional patterned lines showed that extracellular cell-surface vimentin is localised primarily at the back of activated macrophage-like cells. Through two-dimensional migration and phagocytosis assays, we show that this extracellular vimentin enhances migration and phagocytosis of macrophage-like cells. We further show that this extracellular vimentin forms agglomerates on the cell surface, in contrast to its intracellular filamentous form, and that it is released into the extracellular space in the form of small fragments. Taken together, we provide new insights into the release of extracellular cell-surface vimentin and its implications for macrophage functionality.

KEYWORDS

extracellular vimentin, macrophages, activation, migration, polarisation, phagocytosis, vimentin secretion

Introduction

Macrophages are immune cells that have multiple roles in physiological processes, which range from removal of cellular waste and tissue regeneration and remodelling, to protection against pathogen invasion (Krzyszczyk et al., 2018; Herzog et al., 2019; Zhang et al., 2021). Due to their heterogeneous functions, macrophages have a crucial role in the immune system (Viola et al., 2019).

An earlier study revealed that activation of macrophages by tumour necrosis factor (TNF)-α leads to extracellular cell-surface expression and release of vimentin into the surrounding medium (Mor-Vaknin et al., 2003). Similarly, in atherosclerosis, monocyte chemoattractant protein-1 (CCL2) and oxidised low-density lipoproteins stimulate secretion of vimentin from macrophages (Kim et al., 2020). Vimentin is a type III intermediate filament that is primarily located inside cells of mesenchymal origin. However, vimentin can also be expressed on the outside of cells under conditions such as inflammation, stress and senescence (Mor-Vaknin et al., 2003; Frescas et al., 2017; Patteson et al., 2020). Previous studies have shown that astrocytes, neutrophils, monocytes, apoptotic lymphocytes and endothelial cells can also secrete vimentin (Boilard et al., 2003; Mor-Vaknin et al., 2003; Moisan and Girard, 2006; Greco et al., 2010; Kaplan, 2013; Patteson et al., 2020). Within the cell, vimentin is involved in cellular functions such as adhesion, migration and signalling (Ivaska et al., 2007), while recent studies have indicated its functions as a dynamic extracellular protein in cancers (Satelli and Li., 2011; Satelli et al., 2014; Satelli et al., 2015), viral infections (Yang et al., 2016; Ghosh et al., 2018; Bryant et al., 2006; Schäfer et al., 2017; Suprewicz et al., 2022) and general cellular functions (Thalla et al., 2021). Despite the many functional roles now defined for extracellular vimentin, the characteristics and the circumstances of its secretion remain unclear.

Vimentin that is secreted by activated macrophages is also involved in bacterial elimination (Mor-Vaknin et al., 2003) and the immune response (Ramos et al., 2020). Therefore, we questioned the role of secreted vimentin in macrophage activity, and particularly in phagocytosis. It is already known that activation of macrophages enhances phagocytic activity and improves pathogen clearance (Leopold Wager and Wormley, 2014; Jaggi et al., 2020). It is also known that activation of macrophages by TNF-α results in enhanced phagocytosis of the fungal pathogen *Cryptococcus neoformans* (Collins and Bancroft, 1992), with the same is seen for glial macrophages in response to TNF-α in glial–neuronal cell co-cultures (Neniskyte et al., 2014). However, the role of extracellular vimentin for macrophage activity and functionality is not known.

In this study, we investigated the location and form of this extracellular vimentin. We further examined the influence of extracellular vimentin on macrophage functionality. Using fluorescence microscopy techniques and one-dimensional (1D) patterned lines, we show that vimentin is not equally distributed on the surface of activated macrophages, but is located at the 'back' of the cells. We also show that vimentin is released into the extracellular environment in the form of small fragments. Using 2D migration and phagocytosis assays, we further show that addition of recombinant vimentin to macrophages has a similar effect on phagocytic activity and migration as for activated macrophages.

This study thus characterises extracellular vimentin and describes its influence on macrophage functionality. On the basis of these data, we propose a secretion pathway for vimentin. Collectively, these findings are crucial to understand how the immune system is regulated, and they offer new ways to interfere with it.

Materials and methods

Cell culture

HL60 cells were cultured in cell culture flasks (Grenier) in RPMI 1640 medium (Gibco) supplemented with 10% foetal bovine serum (Fischer Scientific), 1% 1:1 penicillin-streptomycin (Fischer Scientific) and 1% Glutamax (Gibco). The cells were passaged at a concentration of 10^6 cells/mL. HL60 cells were differentiated into a macrophage lineage by treatment with 10 nM TPA (Sigma) for 24 h (referred to as macrophages). Post-differentiation, the cells were treated with 5 ng/ml TNF-α (Gibco) for up to 6 days, to induce macrophage activation. Media containing TNF-α was changed every second day for the 3 and 6 days activation.

For confirmation of extracellular vimentin expression, HL60 cells that expressed GFP-tagged vimentin (GFP-Vimentin HL60 cells) were used. These were gifted by Dr. Monika Zwerger, DFG, Germany. These GFP-HL60 cells were cultured as indicated above, with the addition of 0.1 μg/ml puromycin (Gibco) to the growth medium.

Immunostaining

Immunostaining of extracellular vimentin was carried out using the Alexa 647 fluorophore conjugated to the anti-vimentin V9 antibody (Santa Cruz Biotechnology). The cells were prepared by washing with phosphate-buffered saline (PBS) once to remove traces of the growth medium, and were fixed with 4% paraformaldehyde (Science Service) for 10 min. The samples were then blocked for 1 h with 3% bovine serum albumin (BSA) in phosphate-buffered saline. Finally, the cells were incubated with 1:200 V9 anti-vimentin antibody for 1 h, and then viewed under a fluorescence microscope.

The cell membrane was stained using a WGA CF 488A (Biotium) or Alexa Fluor 549 conjugated wheatgerm agglutinin (WGA) conjugate (W11262, Invitrogen). Cell membrane

staining using WGA was performed in conjunction with the V9 anti-vimentin antibody, with WGA staining by incubation with 1:200 anti-WGA antibody for 10 min, followed by fixing of the cells.

For M1 marker, activated macrophages were incubated with 1:100 anti CD68 antibody Alexa 488 (Santa Cruz Biotechnology) for 1 h.

Live-cell imaging was performed using the CSV anti-cell-surface vimentin antibody (Abnova). For this purpose, the cells were incubated with 1:100 CSV for 1 h prior to microscopy.

For permeabilised and non permeabilised comparison, cells were treated with or without triton x-100 0.2% (v/v) for 10 min prior to blocking with 3% (w/v) BSA and cells were incubated with 1:200 beta actin antibody (Proteintech) for 1 h. After washing with PBS, cells were incubated with 1:500 anti-rabbit 488 secondary antibody. Then samples were incubated with 1: 200 V9 anti-vimentin antibody for 1 h.

Quantification of extracellular vimentin

For confirmation and characterisation of the pattern of extracellular vimentin expression on macrophage activation, activation of GFP-vimentin HL60 cells was used. The macrophages were plated on a micro porous transwell membrane (0.4 µm, Corning). The upper and lower compartments were filled with growth medium supplemented with or without TNF-α. Differentiated, inactivated macrophages were used as the control. The medium was collected from the bottom wells after 1 day and 3 days of activation with TNF-α. The collected medium plated into 96-well plates, and the fluorescence intensities were determined using a plate reader (Tecan M200 Pro), with measurement at 488 nm.

1D pattern

To produce 1D patterns we prepared PDMS microchips with channels of 5 µm width and attached them to glass bottom dishes using plasma activation. At the next step, the channels were filled with fibronectin (25 µg/ml, Sigma). The PDMS part of the chips were then pulled off and the glass bottom dishes were washed twice with PBS. Afterwards, cells were placed on these patterns (4,000 cells/µl, working volume 500 µL) and stored in the incubator for 1 h. The patterns were washed once with PBS before cells were fixed and stained for vimentin with the V9 antibody.

Imaging

Fluorescence images were acquired using inverted microscopes. For polarization experiments, the images were acquired using a Ti-Eclipse (Nikon) equipped with Yokagawa spinning disk. For 1D pattern experiments and phagocytosis experiments, the images were acquired using an Epi-fluorescence microscope (Ti-Eclipse, Nikon). For GFP-Vimentin HL60 cells, confocal images were acquired using a LSM900 with Airyscan 2 (Zeiss). The TIRF images were acquired using a Ti-Eclipse with TIRF (Nikon).

Scanning electron microscopy

For scanning electron microscopy cells were placed on gridded coverslips and treated for activation and differentiation as described before. Cells were fixed in solution containing 2% (v/v) glutaraldehyde (Merck) and 2% (v/v) PFA (Science Service) diluted in 0.2 M sodium cacodylate buffer (Merck) for 120 min.

The samples were incubated three times with 0.1 g sodium borohydride (Merck) in 10 ml PBS for 10 min before they were stained for vimentin as described before. The images were acquired using a spinning disc as described before. After imaging the cell were again incubated in the fixation solution overnight. Next, the samples were incubated in 0.1% tannic acid (Merck). Cell drying was performed by successively replacing water with ethanol (>99.8%, Fisher Scientific) and ethanol with hexamethyldisilizane (98%, Carl Roth and >99%, Sigma Aldrich). Eventually, the samples were sputtered with 4–6 nm platinum. Images were acquired at 5 kV under high vacuum using FEI Quanta 400 electron microscope. Secondary electrons were detected using an Everhart-Thornley detector.

Migration assay

To investigate the 2D migration of macrophages after activation and stimulation with 100 ng/ml recombinant vimentin (Prospec), fluorescent images of cell nuclei, which were stained using 250 ng/ml Hoechst for 20 min, and bright-field images were recorded over 30 min with a frame rate of 1 min. The cells were kept at 37°C and 5% CO_2 during the experiment. Cell trajectories were analysed using the ImageJ plugin Trackmate. For blocking the effect of vimentin in activated macrophages, live cell stain of cell surface vimentin antibody (Abnova) was added for 2 h prior to acquisition of migration data. For each cell, the mean migration speed was calculated as the mean value of the instantaneous speeds in between two successive recorded positions.

Phagocytosis assay

To investigate the phagocytic activity of macrophages under stimulation with extracellular recombinant vimentin, fluorescently-labelled latex beads were used in phagocytosis assays. The assay protocol was developed following the

manufacturer instructions (Phagocytosis Assay kits; IgG FITC; Item No. 500290; Cayman Chemicals). For vimentin treatment, differentiated cells were treated with human recombinant vimentin 100 ng/ml (Prospec) for 24 h and activated macrophages were preincubated with V9 anti-vimentin antibody (Santa Cruz) for 2 h prior to phagocytosis experiment.

For quantification of phagocytosis, the microscopy images obtained were analysed using the ImageJ software (Fiji). The analysis consisted of two steps: first, the cell shape was determined by manually outlining the cell on the bright-field image using the Polygon selections tool. The cell 'mask' obtained was then saved in the ROI Manager and layered over the fluorescent image. The mean fluorescent intensity of the beads within the cell area can be measured. Additionally, the background fluorescence in an area without cells was then measured for each image. With this data, the "phagocytic index" was calculated for each condition, as $PI = I_{beads}/I_{background}$. The average measurement of bead fluorescence corresponded to the number of fluorescently labelled beads that had been phagocytized by the macrophages, and was thus used to quantify their phagocytic activity.

Results

Activated macrophages express cell-surface vimentin in a polarised manner

First, we asked whether vimentin is expressed isotopically on the surface of cells. For this, we differentiated HL-60 cells into macrophages by treating them with 12-O-tetradecanoylphorbol-13-acetate (TPA). After 24 h, these macrophages were activated with TNF-α. Interestingly, TNF-α also induces HL-60 macrophage differentiation (Squinto et al., 1989). However, we used TPA to differentiate our cells.

With permeabilisation of the cell membrane during immunofluorescence staining omitted, this ensured that the images acquired using the fluorescently labelled V9 anti-vimentin antibody only showed vimentin on the surface of the cells.

Upon treatment of the HL-60 cells with TPA for 24 h, they were seen to differentiate into macrophages (Figure 1A). TNF-α treatment of these macrophages triggered the appearance of cell-surface vimentin in a polarised manner, as seen using the V9 anti-vimentin antibody; i.e., the vimentin expressed was not equally distributed over the cell surface. The vimentin expressed on the extracellular surface of these macrophages was instead polarised, as it was predominantly seen over particular areas of the cell surface (Figure 1B). The proportion of the cells that expressed vimentin in this polarised manner was determined by cell counting. There was a >2-fold increase in the polarisation of extracellular cell-surface vimentin in these TNF-α–activated macrophages compared to the non-activated macrophages. During TNF-α activation for up to 6 days, greater proportions macrophages with polarised surface vimentin were seen after 1 day and 2 days (Figure 1C). These data thus show that extracellular cell-surface vimentin is expressed in a polarised manner on these TNF-α–activated macrophages.

We further confirm the extracellular localization of vimentin by using CSV antibody which specifically binds to the extracelllular vimentin in live activated macrophages (Figure 2A). This was complemented with comparing the permebalized and non permebalized cells where beta actin was labelled along with vimentin in activated macrophages. Neverthless, some fluorescent signal can be obsereved around the nucleus which could be from the antibody that has been endocytosed. In Figure 2B, it can be clearly seen that fluroscence signal from permeablized activated macrophages is more prominent. However, only unpsecific signal can be observed in non-permeabized activated macrophages. We also classify the macrophages into M1 macrophages upon activation by TNF- α by using CD68 activation marker (Figure 2C).

Extracellular cell-surface vimentin is predominantly expressed at the back of activated macrophages and secreted in the form small fragments

Although the vimentin was polarised on the surface of these TNF-α–activated macrophages, as the "front" and "back" of these cells were not easily differentiable in these 2D fixed samples, its exact positioning was unknown (Figure 3A). To solve this problem, patterned migration lines on glass coverslips were used, whereby the front and back of the cells can be distinguished by recording time-lapse movies. By following the macrophage migration on patterned lines coated with fibronectin, a simplified cell shape can be defined that allows visualisation of the position on the extracellular cell surface of the vimentin upon TNF-α activation (Figure 3B).

Here, the nucleus was always at the front end of these macrophages during migration. The position of the nucleus was then used as the reference to define the front of the fixed cells. Using this method, the surface vimentin was seen to be polarised at the back of the activated macrophages, allowing us to conclude that vimentin was secreted from the back of these TNF-α–activated macrophages. In contrast, prior to TNF-α activation, the differentiated macrophages were seen to secrete vimentin at a site close to the nucleus (Figure 3C). As, 1 and 3 days activation showed comparable vimentin polarization (Figure 1C), here we used 3 days activation in 1D pattern experiment (Figure 3C).

To further resolve the structure of the polarized vimentin on the cell surface, we used confocal microscopy for imaging. For this, genetically transformed HL-60 cells with vimentin tagged with green fluorescent protein (GFP-vimentin HL60 cells) were differentiated and activated. Here, images of elongated macrophages were acquired in order to evaluate the structure as well as the position of the surface vimentin. We observed small fragments of vimentin at the secretion sites of both differentiated

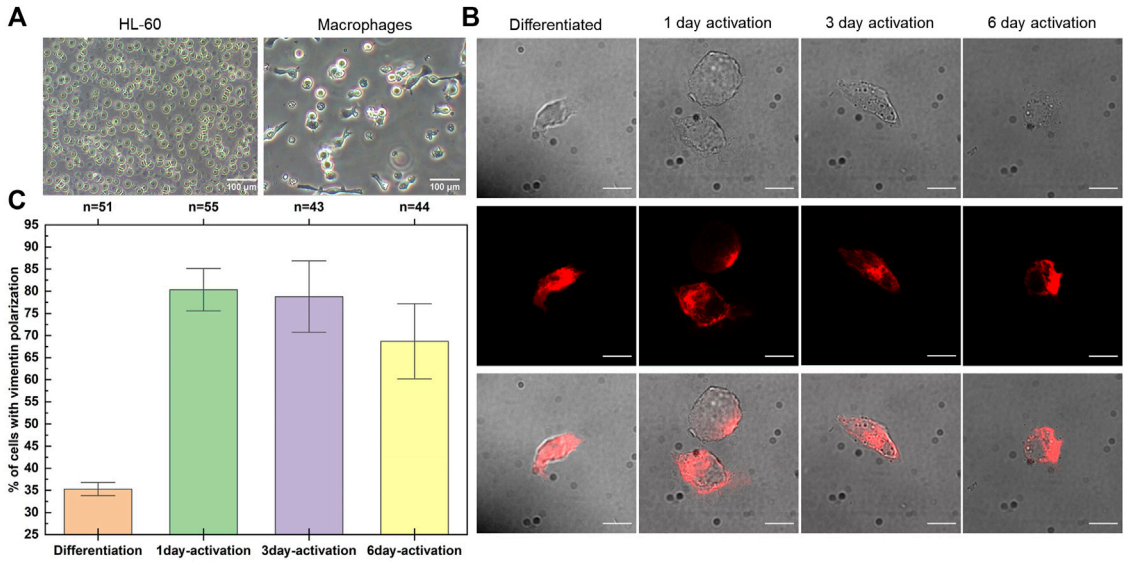

FIGURE 1
Polarised expression of extracellular vimentin on the surface of TNF-α–activated macrophages. **(A)** Representative HL-60 cells before (left) and after (right) differentiation with TPA. **(B)** Representative non-permeabilised fixed samples of macrophages (Differentiated) stained with the V9 anti-vimentin antibody, showing expression of vimentin on their surface after 1, 3, and 6 days of TNF-α activation. Top row: Phase contrast images. Middle row: Fluorescent images for vimentin (red). Bottom row: Overlay of phase contrast and fluorescent images. Scale bar, 10 μm. **(C)** Quantification of the proportion of macrophages expressing extracellular cell-surface vimentin in a polarised manner over the 6 days of TNF-α activation. n denotes the total number of cells analyzed, error bars correspond to standard deviation.

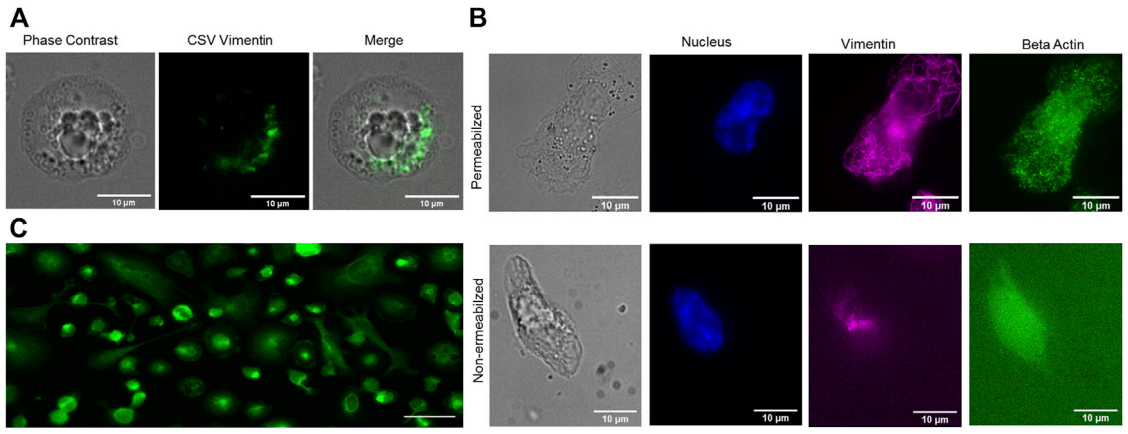

FIGURE 2
(A) Live cell imaging of activated macrophages using CSV antibody. **(B)** Comparison of permeablized vs. non permeablized activated macrophages labelled using beta actin antibody and anti vimentin V9 antibody (Nucleus, blue:actin, green: vimentin, magenta). **(C)** M1 macrophage classification using CD68 macrophage activation marker after TNF- α activation. Scale bar 10 μm.

and TNF-α–activated macrophages (Figure 4A). In order to confirm the small fragments are on the outside of the cell, images of differentiated and TNF-α–activated macrophages were acquired using scanning electron microscopy (SEM) (Figure 4B). Further, we confirmed the presence of vimentin on the dot like structure by visualizing the same cell in both confocal and SEM by using coverslip with grid (Figure 4C).

Quantification of vimentin secretion upon activation

It is known that as well as being expressed on the extracellular cell surface, vimentin can then be released into the extracellular surroundings of the cell (Danielsson et al., 2018). We thus asked whether, and in what way, the vimentin secreted by these TNF-

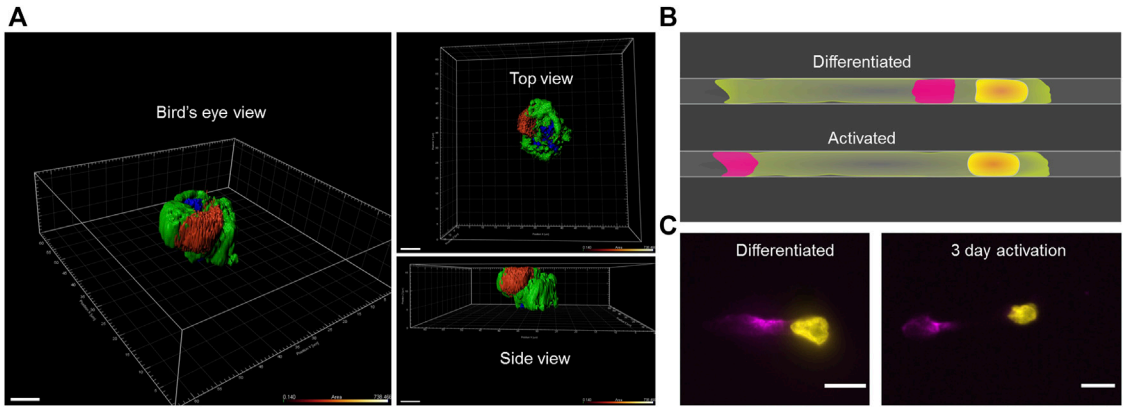

FIGURE 3
Visualisation of surface vimentin on macrophages patterned on one-dimensional lines. **(A)** Representative three-dimensional projections of a TNF-α–activated macrophage (red, surface vimentin: green, cell membrane), demonstrated using IMARIS. Scale bar, 7 μm. **(B)** Illustration of the vimentin secretion sites (red) for the differentiated and TNF-α–activated macrophages using patterned lines. Yellow, nucleus; green, cell membrane. **(C)** Representative differentiated and TNF-α–activated macrophage attached and elongated along the pattern on a glass coverslip, revealing the site of vimentin secretion (yellow, nucleus; magenta, extracellular cell-surface vimentin). Scale bar, 10 μm.

α–activated macrophages is functional. Here, we imaged the contact region between the activated macrophages and the glass bottom of the dish to visualise the vimentin released into the medium from the extracellular surface of the activated macrophages, using total internal reflection fluorescence (TIRF) microscopy. Fixed non-permeabilised 3-days-activated macrophages were fluorescently labelled using the V9 antibody. This revealed vimentin agglomerates in the vicinity of the activated macrophages (Figure 5A). These vimentin agglomerates appeared to be in a non-filamentous and fragmented form.

To quantify the vimentin released from these activated macrophages, 0.4-μm transwell insert assays were used with genetically transformed HL-60 cells in which vimentin was tagged with green fluorescent protein (GFP-vimentin HL60 cells). These GFP-vimentin HL60 cells were differentiated using TPA and placed inside the upper chambers of transwell inserts. They were then activated with TNF-α, and left for 1 day and 3 days. The vimentin released into the cell medium passed through the pores of the membrane and was collected in the bottom chamber along with the culture medium. The medium in the bottom chamber was transferred to 96-well plates, and the fluorescence intensity was measured using a plate reader. These data showed that the amount of vimentin released into the medium depended on the time of TNF-α activation of these macrophages (Figure 5B).

Extracellular vimentin enhances migration and phagocytosis of macrophages

Macrophages are known to have a vital role in the immune system through phagocytosis of cellular debris and elimination of bacterial pathogens. We thus next investigated this extracellular cell-surface vimentin on the functionality of macrophages, in terms of their migration and phagocytosis.

The migration speeds of the macrophages were measured using a 2D migration assay (Figure 6A). As the media from the TNF-α–activated macrophages that contained secreted vimentin is expected to have some residual TNF-α, recombinant vimentin was used here. Addition of recombinant vimentin to the differentiated macrophages significantly increased their migration speed. Further, the migration speed of the TNF-α–activated macrophages was significantly reduced when they were pre-incubated with the CSV antibody (Figure 6B).

To investigate the phagocytic activity of macrophages under the influence of extracellular vimentin, phagocytosis assays using fluorescently-labeled latex beads were carried out to measure the phagocytic process *in vitro*. With phagocytosis analysed according to the phagocytotic index defined by the intracellular fluorescence intensities following phagocytosis of fluorescent beads (Figure 6C), this was seen to be significantly increased in the TNF-α–activated macrophages compared to the differentiated macrophages (Figure 6D). Further, this effect was mimicked by addition of 100 ng/ml recombinant vimentin to the differentiated macrophages, while it was blocked by the V9 anti-vimentin antibody in the TNF-α–activated macrophages (Figure 6D). As for the migration effect, this enhanced phagocytosis might be due to the high expression levels of vimentin in the TNF-α–activated macrophages. Thus, from these data, we can conclude that extracellular addition of recombinant vimentin enhances both the migration and phagocytosis of these macrophages.

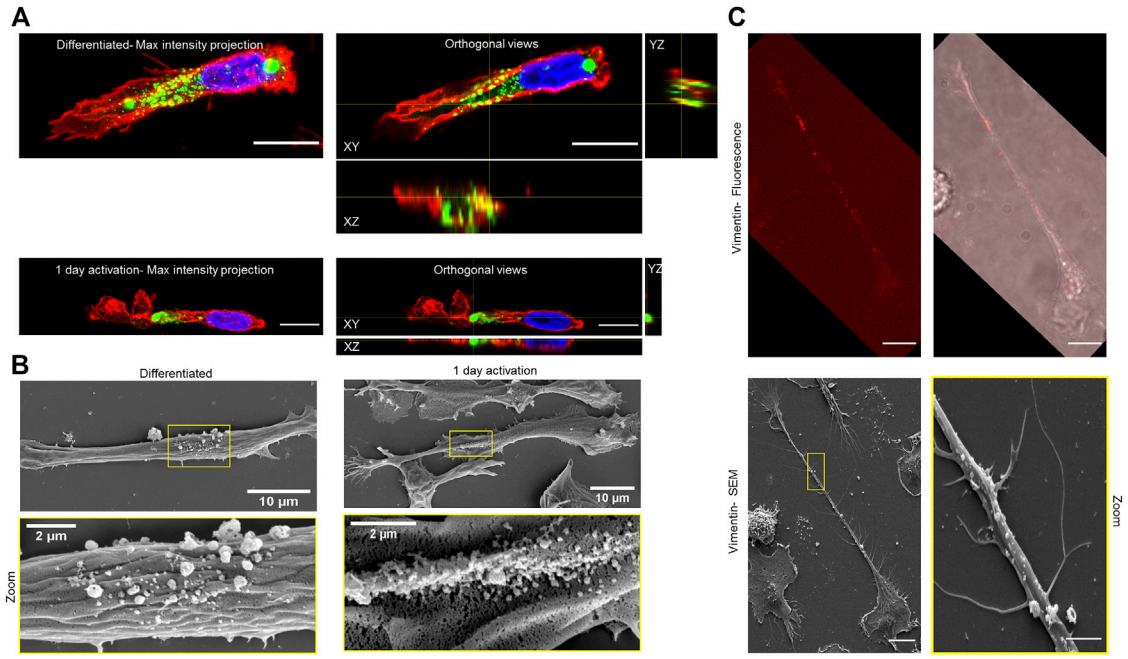

FIGURE 4
Visualisation of surface vimentin on macrophages differentiated from GFP-vimentin HL60. **(A)** Maximum intensity projection and orthogonal views of differentiated and TNF-α–activated macrophage (red, membrane; green, surface vimentin; blue, nucleus), acquired with confocal microscopy. Scale bar, 10 µm. **(B)** Scanning electron microscopy images of vimentin secretion sites for the differentiated and TNF-α–activated macrophages. Bottom row: higher magnification of vimentin secretion site marked with yellow rectangle. This study was performed on 2D (glass coverslips) not on fibronectin coated 1D patterns. In order to have more residual cells after differentiation and activation, we used 1 day activation of both confocal LSM900 **(A)** and SEM imaging **(B)**. **(C)** Confocal and SEM imaging using coverslips with grid. Top: Fluorescence images of vimentin (red; V9 antibody) stained in non-permeablized activated macropahges. Scale bar 10 µm. Bottom: SEM images of the same cell where the dot like structure can be seen at the same site of vimentin staining. Bottom (Right): magnified image of area marked in yellow of left. Scale bar 2 µm.

Discussion

The detection of vimentin in the extracellular space then promoted the question as to how it is secreted from inside these TNF-α–activated macrophages. Previously this extracellular vimentin was thought to have been released from necrotic cells, although it has also been suggested that it might be secreted. Previous studies have shown exosomes as a source of vimentin, and demonstrated that these can transport and release vimentin into the extracellular space (Chen et al., 2016; Adolf et al., 2018; Parvanian et al., 2020). Exosomes are packaged with membranes in the Golgi apparatus, and in activated macrophages, block of transport through the Golgi apparatus inhibits the release of extracellular vimentin (Mor-Vaknin et al., 2003). This has thus strengthened the idea that vimentin is secreted with the help of exosomes. However, it has remained unclear what the characteristics of this secreted vimentin are.

In the present study, we show that vimentin is released from the back of these TNF-α–activated macrophages, and that this polarised release is enhanced by the macrophage activation. Moreover, using confocal, TIRF and SEM, we have confirmed that the structure of the secreted vimentin is not filamentous, as is its intracellular counterpart, but is in form of fragments, as indicated in recent studies (Suprewicz et al., Lalioti et al., 2021). Nevertheless, further confirmation of data from GFP-vimentin HL60 is needed as it may not behave identical to endogenous vimentin.

It is believed that post-translational modifications are a prerequisite for vimentin secretion from macrophages and endothelial cells (Noh et al., 2016; Liu et al., 2020; Patteson et al., 2020), which would appear necessary to break down the long vimentin filaments to smaller fragments (Mónico et al., 2019). In the case activated macrophages, the extracellular vimentin was shown to be phosphorylated (Mor-Vaknin et al., 2003). A recent study showed that vimentin is recruited to the cell membrane via an alteration in the filamentous form to an oligomeric form that consists of 4–12 monomers (Hwang and Ise, 2020). This multimeric form of vimentin showed a higher binding affinity to lipid bilayers compared to that of filamentous vimentin. However, the mechanism by which the intracellular vimentin is secreted into the extracellular space is not well characterised. Here, by combining data from the literature and

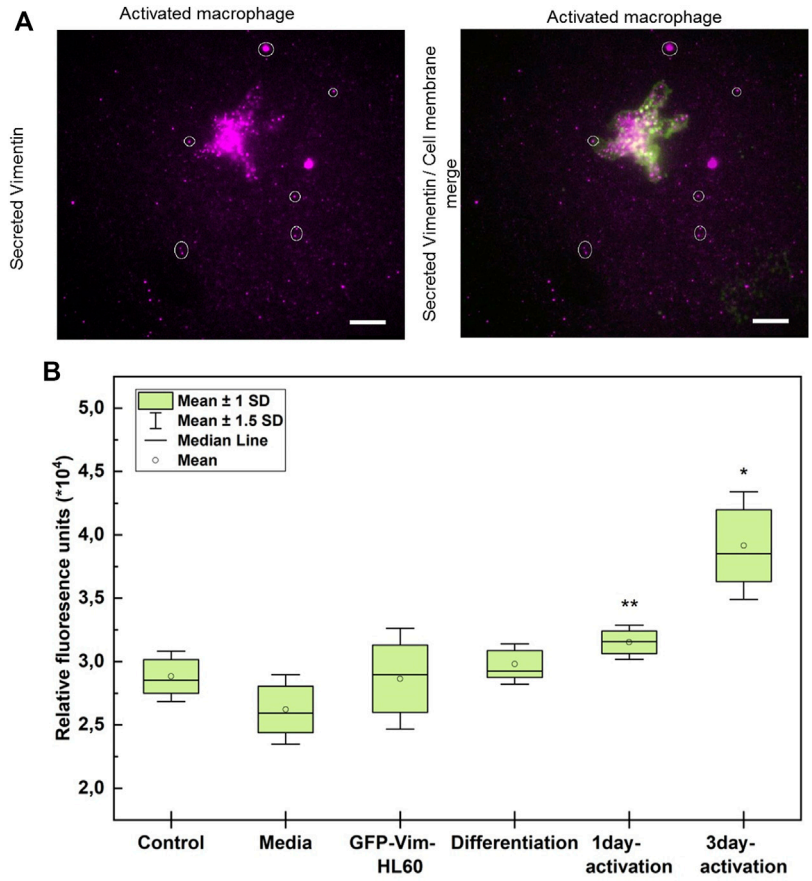

FIGURE 5
TNF-α–activated macrophages secrete vimentin into the extracellular space. **(A)** Representative total internal reflection fluorescence microscopy of secreted vimentin (magenta) around a TNF-α–activated macrophage (green, cell membrane). Scale bar is 10 μm. **(B)** Quantification of the relative fluorescence of vimentin in the media from activated macrophages expressing GFP-tagged vimentin (repeated 2 times with six replicates of each condition). Conditions: Control, blank; media, RMPI; Differentiation, media from differentiated macrophages; 1 day activation TNF-α; 3 days activation, media from macrophages activated for 3 days with TNF-α. * $p < 0.05$; ** $p < 0.01$ (Student's t-tests).

the findings from the present study, we can predict a secretion mechanism as we illustrated in Figure 6. As seen from the present study, extracellular cell-surface vimentin is polarised at the back of TNF-α–activated macrophages, and the images from TIRF shows that small fragments of vimentin either from exosomes or filaments are released close to a large agglomerate of vimentin on the cell surface. Therefore, we propose that at the membrane surface of these TNF-α–activated macrophages, vimentin filaments disassemble into small fragments, to form agglomerates, which can then be released into cell medium or into blood serum (Figure 7B).

Vimentin expression in the extracellular space of cells has been attributed to circumstances such as cell activation, senescence, injury and stress (Mor-Vaknin et al., 2003; Frescas et al., 2017; Walker et al., 2018). In most of these scenarios, the secretion of vimentin is related to immune activity (Ramos et al., 2020). For example, the vimentin secreted by activated macrophages has been suggested to be involved in immune functions via generation of oxidative metabolites and elimination of bacteria (Mor-Vaknin et al., 2003). Another example is shown in patients with rheumatic arthritis, where neutrophils secrete citrullinated vimentin during the release of neutrophil extracellular traps that are produced to immobilise pathogens and promote immune responses (Carmona-Rivera et al., 2013; Kaplan, 2013). Further, in the *Mycobacterium tuberculosis*, vimentin binds to the natural killer cell surface receptor NKp46 and contributes to lysis of infected cells (Garg et al., 2006). Finally, extracellular vimentin blocks pro-inflammatory secretion by activated dendritic cells, which promotes inhibition of adaptive immune responses. This mechanism prevents tissue damage and promotes bacteria elimination (Yu et al., 2018).

On the basis of this evidence that extracellular vimentin partially regulates inflammatory processes, we investigated the role of extracellular vimentin on macrophage function. Using migration assays, we show that elevated levels of extracellular

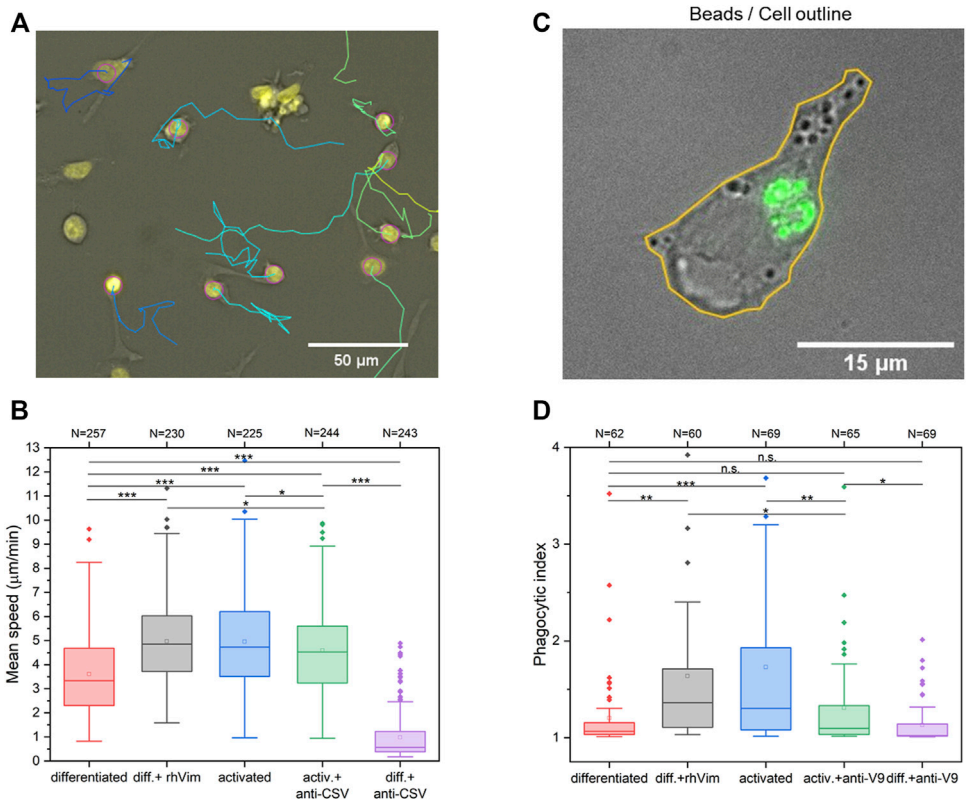

FIGURE 6
Stimulation of migration and phagocytosis of macrophages by addition of recombinant (rh)Vimentin. **(A)** Migration tracks of TNF-α–activated macrophages visualised using TrackMate ImageJ plugin.**(B)** Quantification of migration speeds of differentiated macrophages without and with addition to the medium of 100 ng/ml rhVimentin and anti-cell-surface vimentin antibody, and of TNF-α–activated macrophages without and with addition of the anti-cell-surface vimentin antibody (CSV). **(C)** Visualisation of fluorescent beads (green) phagocytosed by a TNF-α–activated macrophage using fluorescence microscopy. Cell outline (yellow) defined from phase contrast image. **(D)** Phagocytic index determined by the fluorescence intensity within the differentiated macrophages without and with addition of 100 ng/ml rhVimentin and anti-vimentin antibody (V9), and of TNF-α–activated macrophages without and with addition of the anti-vimentin antibody (V9). *, $p < 0.05$; **, $p < 0.01$; ***, $p < 0.001$. n.s. not significant (Student's t-tests). All experiments were repeated three times. The data is presented as box plots with whiskers drawn within the 1.5 IQR value. N indicates the total number of cells analyzed.All experiments were done three times.

cell-surface vimentin enhance the migration speed of macrophages. Here, it was not relevant if the extracellular vimentin was added as recombinant vimentin or if it was from secretion of activated macrophages. This increase in macrophage migration by addition of recombinant vimentin complements our recent study where we showed similar effects in MCF-7 cells (Thalla et al., 2021).

Earlier studies have demonstrated that increases in phagocytic activity by macrophages involves extracellular vimentin. However, in these previous studies, the vimentin was expressed on the surface of apoptotic neutrophils and T cells and acted as a signalling agent to attract macrophages and further facilitate the elimination process (Boilard et al., 2003; Moisan and Girard, 2006; Ise et al., 2012; Starr et al., 2012). On the surface of phagocytes, vimentin interacts with O-Glc-NAc-modified proteins expressed on apoptotic cells, which generates an "eat me" signal for elimination by macrophages (Ise et al., 2012). To date, surface vimentin has been believed to be a mediator that helps to attract macrophages towards the cells that need to be phagocytosed. However, one study that investigated extracellular vimentin directly expressed on activated macrophages demonstrated enhanced bacteria elimination (Mor-Vaknin et al., 2003). In the present study, we further explored the effects of extracellular vimentin expressed on the surface of macrophages in terms of macrophage function. We show that recombinant vimentin treatment of HL-60 differentiated macrophages has a similar effect as TNF-α–activated macrophages in terms of enhanced phagocytic activity. Interestingly, in a recent study it was shown that extracellular addition of vimentin lead to TNF- α secretion in macrophages (Kim et al., 2020). Consequently, this could be a possible mechanism behind the enhanced migration and phagocytic activity in macrophages.

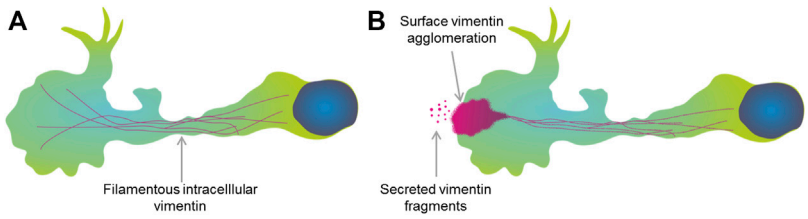

FIGURE 7
Proposed model of vimentin secretion. **(A)** A macrophage with intracellular vimentin in the filamentous form. **(B)** Dissociation of filamentous vimentin at the cell membrane in the activated macrophage might lead to agglomeration at the surface of the macrophage. Then, the vimentin can be released into the extracellular space in the form of small fragments.

Taken together, we demonstrate that vimentin is expressed in a polarised form on the surface of activated macrophages, and that it is released in a fragmented form. We also show that extracellular vimentin influences the functionality of macrophages by enhancing their migration and phagocytosis.

Altogether, these data suggests that extracellular vimentin is used to regulate macrophages in the immune system through effective elimination of bacterial pathogens.

Data availability statement

The raw data supporting the conclusions of this article will be made available by the authors, without undue reservation.

Author contributions

DT was involved in conceptualization of the project; supervision; data analysis and visualization; and writing original draft. AR performed polarization and secretion experiments; data analysis and visualization; contributed in writing. AL performed the migration and phagocytosis experiments; data analysis and visualization. JB performed 1D pattern experiments; data analysis and visualization. LK performed scanning electron microscopy experiments; visualization. FL was involved in the conceptualisation of the project, contributed in writing/review and editing the manuscript; supervision; project administration; and funding acquisition. All authors have read and agreed to the published version of the manuscript.

Funding

This research was funded with the support of the DFG (SFB 1027, project A10).

Conflict of interest

The authors declare that the research was conducted in the absence of any commercial or financial relationships that could be construed as a potential conflict of interest.

Publisher's note

All claims expressed in this article are solely those of the authors and do not necessarily represent those of their affiliated organizations, or those of the publisher, the editors and the reviewers. Any product that may be evaluated in this article, or claim that may be made by its manufacturer, is not guaranteed or endorsed by the publisher.

Acknowledgments

We are thankful to Monika Zwerger for transfecting the GFP-HL60 cells. Additionally, we would like to thank Alexandra K. Kiemer for her active participation in discussions and suggestions.

References

Adolf, A., Rohrbeck, A., Münster-Wandowski, A., Johansson, M., Kuhn, H. G., Kopp, M. A., et al. (2018). Release of astroglial vimentin by extracellular vesicles: Modulation of binding and internalization of C3 transferase in astrocytes and neurons. *Glia* 67, 703–717. doi:10.1002/glia.23566

Boilard, E., Bourgoin, S. G., Bernatchez, C., and Surette, M. E. (2003). Identification of an autoantigen on the surface of apoptotic human T cells as a new protein interacting with inflammatory group IIA phospholipase A2. *Blood* 102, 2901–2909. doi:10.1182/blood-2002-12-3702

Bryant, A. E., Bayer, C. R., Huntington, J. D., and Stevens, D. L. (2006). Group A streptococcal myonecrosis: Increased vimentin expression after skeletal-muscle injury mediates the binding ofStreptococcus pyogenes. *J. Infect. Dis.* 193, 1685–1692. doi:10.1086/504261

Chen, Z., Yang, L., Cui, Y., Zhou, Y., Yin, X., Guo, J., et al. (2016). Cytoskeleton-centric protein transportation by exosomes transforms tumor-favorable macrophages. *Oncotarget* 7, 767387–767402. doi:10.18632/oncotarget.11794

Collins, H. L., and Bancroft, G. J. (1992). Cytokine enhancement of complement-dependent phagocytosis by macrophages: Synergy of tumor necrosis factor-α and granulocyte-macrophage colony-stimulating factor for phagocytosis of Cryptococcus neoformans. *Eur. J. Immunol.* 22, 1447–1454. doi:10.1002/eji.1830220617

Danielsson, F., Peterson, M. K., Caldeira Araújo, H., Lautenschläger, F., and Gad, A. K. B. (2018). Vimentin diversity in health and disease. *Cells* 7. doi:10.3390/cells7100147

Frescas, D., Roux, C. M., Aygun-Sunar, S., Gleiberman, A. S., Krasnov, P., Kurnasov, O. V., et al. (2017). Senescent cells expose and secrete an oxidized form of membrane-bound vimentin as revealed by a natural polyreactive antibody. *Proc. Natl. Acad. Sci.* 114, E1668–E1677. doi:10.1073/pnas.1614661114

Garg, A., Barnes, P. F., Porgador, A., Roy, S., Wu, S., Nanda, J. S., et al. (2006). Vimentin expressed on *Mycobacterium tuberculosis*-Infected human monocytes is involved in binding to the NKp46 receptor. *J. Immunol.* 177, 6192–6198. doi:10.4049/jimmunol.177.9.6192

Ghosh, P., Halvorsen, E. M., Ammendolia, D. A., Mor-Vaknin, N., O'riordan, M. X. D., Brumell, J. H., et al. (2018). Invasion of the brain by Listeria monocytogenes is mediated by InlF and host cell vimentin. *mBio* 9, e00160–18. doi:10.1128/mBio.00160-18

Greco, T. M., Seeholzer, S. H., Mak, A., Spruce, L., and Ischiropoulos, H. (2010). Quantitative mass spectrometry-based proteomics reveals the dynamic range of primary mouse astrocyte protein secretion. *J. Proteome Res.* 9, 2764–2774. doi:10.1021/pr100134n

Herzog, C., Pons Garcia, L., Keatinge, M., Greenald, D., Moritz, C., Peri, F., et al. (2019). Rapid clearance of cellular debris by microglia limits secondary neuronal cell death after brain injury *in vivo*. *Development* 146, dev174698. doi:10.1242/dev.174698

Hwang, B., and Ise, H. (2020). Multimeric conformation of type III intermediate filaments but not the filamentous conformation exhibits high affinity to lipid bilayers. *Genes Cells* 25, 413–426. doi:10.1111/gtc.12768

Ise, H., Goto, M., Komura, K., and Akaike, T. (2012). Engulfment and clearance of apoptotic cells based on a GlcNAc-binding lectin-like property of surface vimentin. *Glycobiology* 22, 788–805. doi:10.1093/glycob/cws052

Ivaska, J., Pallari, H. M., Nevo, J., and Eriksson, J. E. (2007). Novel functions of vimentin in cell adhesion, migration, and signaling. *Exp. Cell Res.* 313, 2050–2062. doi:10.1016/j.yexcr.2007.03.040

Jaggi, U., Yang, M., Matundan, H. H., Hirose, S., Shah, P. K., Sharifi, B. G., et al. (2020). Increased phagocytosis in the presence of enhanced M2-like macrophage responses correlates with increased primary and latent HSV-1 infection. *PLoS Pathog.* 16, e1008971. doi:10.1371/journal.ppat.1008971

Kaplan, M. J. (2013). Role of neutrophils in systemic autoimmune diseases. *Arthritis Res. Ther.* 15, 219. doi:10.1186/ar4325

Khandpur, C., Carmona-Rivera, R., Vivekanandan-Giri, A., Gizinski, A., Yalavarthi, S., Knight, J., et al. (2013). Neutrophil extracellular traps are a source of citrullinated autoantigens and stimulate inflammatory responses in rheumatoid arthritis (P4061). *J. Immunol.* 190, 127.2. doi:10.1126/scitranslmed.3005580

Kim, S., Cho, W., Kim, I., Lee, S.-H., Oh, G. T., and Park, Y. M. (2020). Oxidized LDL induces vimentin secretion by macrophages and contributes to atherosclerotic inflammation. *J. Mol. Med.* 98, 973–983. doi:10.1007/s00109-020-01923-w

Krzyszczyk, P., Schloss, R., Palmer, A., and Berthiaume, F. (2018). The role of macrophages in acute and chronic wound healing and interventions to promote pro-wound healing phenotypes. *Front. Physiology* 9. doi:10.3389/fphys.2018.00419

Lalioti, V., González-Sanz, S., Lois-Bermejo, I., González-Jiménez, P., Viedma-Poyatos, Á., Merino, A., et al. (2021). Immunolocalization studies of vimentin and ACE2 on the surface of cells exposed to SARS-CoV-2 Spike proteins. *bioRxiv* 2021, 442648. doi:10.1101/2021.05.04.442648

Leopold Wager, C. M., and Wormley, F. L. (2014). Classical versus alternative macrophage activation: The ying and the yang in host defense against pulmonary fungal infections. *Mucosal Immunol.* 7, 1023–1035. doi:10.1038/mi.2014.65

Liu, M., Wang, R., Sun, X., Liu, Y., Wang, Z., Yan, J., et al. (2020). Prognostic significance of PD-L1 expression on cell-surface vimentin-positive circulating tumor cells in gastric cancer patients. *Mol. Oncol.* 14, 865–881. doi:10.1002/1878-0261.12643

Moisan, E., and Girard, D. (2006). Cell surface expression of intermediate filament proteins vimentin and lamin B1 in human neutrophil spontaneous apoptosis. *J. Leukoc. Biol.* 79, 489–498. doi:10.1189/jlb.0405190

Mónico, A., Duarte, S., Pajares, M. A., and Pérez-Sala, D. (2019). Vimentin disruption by lipoxidation and electrophiles: Role of the cysteine residue and filament dynamics. *Redox Biol.* 23, 101098.

Mor-Vaknin, N., Punturieri, A., Sitwala, K., and Markovitz, D. M. (2003). Vimentin is secreted by activated macrophages. *Nat. Cell Biol.* 5, 59–63. doi:10.1038/ncb898

Neniskyte, U., Vilalta, A., and Brown, G. C. (2014). Tumour necrosis factor alpha-induced neuronal loss is mediated by microglial phagocytosis. *FEBS Lett.* 588, 2952–2956. doi:10.1016/j.febslet.2014.05.046

Noh, H., Yan, J., Hong, S., Kong, L.-Y., Gabrusiewicz, K., Xia, X., et al. (2016). Discovery of cell surface vimentin targeting mAb for direct disruption of GBM tumor initiating cells. *Oncotarget* 7. doi:10.18632/oncotarget.12458

Parvanian, S., Yan, F., Su, D., Coelho-Rato, L. S., Venu, A. P., Yang, P., et al. (2020). Exosomal vimentin from adipocyte progenitors accelerates wound healing. *Cytoskeleton* 77, 399–413. doi:10.1002/cm.21634

Patteson, A. E., Vahabikashi, A., Goldman, R. D., and Janmey, P. A. (2020). Mechanical and non-mechanical functions of filamentous and non-filamentous vimentin. *BioEssays* 42, 2000078. doi:10.1002/bies.202000078

Ramos, I., Stamatakis, K., Oeste, C. L., and Pérez-Sala, D. (2020). Vimentin as a multifaceted player and potential therapeutic target in viral infections. *Int. J. Mol. Sci.* 21, 4675. doi:10.3390/ijms21134675

Satelli, A., and Li, S. (2011). Vimentin in cancer and its potential as a molecular target for cancer therapy. *Cell Mol. Life Sci.* 68, 3033–3046. doi:10.1007/s00018-011-0735-1

Satelli, A., Mitra, A., Brownlee, Z., Xia, X., Bellister, S., Overman, M. J., et al. (2015). Epithelial–mesenchymal transitioned circulating tumor cells capture for detecting tumor progression. *Clin. Cancer Res.* 21, 899–906. doi:10.1158/1078-0432.ccr-14-0894

Satelli, A., Mitra, A., Cutrera, J. J., Devarie, M., Xia, X., Ingram, D. R., et al. (2014). Universal marker and detection tool for human sarcoma circulating tumor cells. *Cancer Res.* 74, 1645–1650. doi:10.1158/0008-5472.can-13-1739

Schäfer, G., Graham, L. M., Lang, D. M., Blumenthal, M. J., Bergant Marušič, M., and Katz, A. A. (2017). Vimentin modulates infectious internalization of human papillomavirus 16 pseudovirions. *J. Virology* 91, e00307–17. doi:10.1128/JVI.00307-17

Squinto, S. P., Doucet, J. P., Block, A. L., Morrow, S. L., and Davenport, W. D., Jr. (1989). Induction of macrophage-like differentiation of HL-60 leukemia cells by tumor necrosis factor-α: Potential role of fos expression. *Mol. Endocrinol.* 3, 409–419. doi:10.1210/mend-3-2-409

Starr, A. E., Bellac, C. L., Dufour, A., Goebeler, V., and Overall, C. M. (2012). Biochemical characterization and N-terminomics analysis of leukolysin, the membrane-type 6 matrix metalloprotease (MMP25): Chemokine and vimentin cleavages enhance cell migration and macrophage phagocytic activities. *J. Biol. Chem.* 287, 13382–13395. doi:10.1074/jbc.m111.314179

Suprewicz, Ł., Swoger, M., Gupta, S., Piktel, E., Byfield, F. J., Iwamoto, D. V., et al. (2022). Extracellular vimentin as a target against SARS-CoV-2 host cell invasion. *Small* 18, e2105640. doi:10.1002/smll.202105640

Thalla, D. G., Jung, P., Bischoff, M., and Lautenschläger, F. (2021). Role of extracellular vimentin in cancer-cell functionality and its influence on cell monolayer permeability changes induced by SARS-CoV-2 receptor binding domain. *Int. J. Mol. Sci.* 22, 7469. doi:10.3390/ijms22147469

Viola, A., Munari, F., Sánchez-Rodríguez, R., Scolaro, T., and Castegna, A. (2019). The metabolic signature of macrophage responses. *Front. Immunol.* 10. doi:10.3389/fimmu.2019.01462

Walker, J. L., Bleaken, B. M., Romisher, A. R., Alnwibit, A. A., and Menko, A. S. (2018). In wound repair vimentin mediates the transition of mesenchymal leader cells to a myofibroblast phenotype. *Mol. Biol. Cell* 29, 1555–1570. doi:10.1091/mbc.e17-06-0364

Yang, J., Zou, L., Yang, Y., Yuan, J., Hu, Z., Liu, H., et al. (2016). Superficial vimentin mediates DENV-2 infection of vascular endothelial cells. *Sci. Rep.* 6, 38372. doi:10.1038/srep38372

Yu, M. B., Guerra, J., Firek, A., and Langridge, W. H. R. (2018). Extracellular vimentin modulates human dendritic cell activation. *Mol. Immunol.* 104, 37–46. doi:10.1016/j.molimm.2018.09.017

Zhang, C., Yang, M., and Ericsson, A. C. (2021). Function of macrophages in disease: Current understanding on molecular mechanisms. *Front. Immunol.* 12. doi:10.3389/fimmu.2021.620510

frontiers | Frontiers in Cell and Developmental Biology

TYPE Original Research
PUBLISHED 30 August 2022
DOI 10.3389/fcell.2022.932983

OPEN ACCESS

EDITED BY
Dolores Pérez-Sala,
Spanish National Research Council (CSIC), Spain

REVIEWED BY
Satoshi Kametaka,
Nagoya University, Japan
Christof Taxis,
University of Marburg, Germany

*CORRESPONDENCE
Pekka Taimen,
pepeta@utu.fi

†**Present address:**
Song-Ping Li,
Faculty of Life Sciences and Biopharmaceuticals, Shenyang Pharmaceutical University China, Shenyang, China

SPECIALTY SECTION
This article was submitted to Cell Growth and Division, a section of the journal Frontiers in Cell and Developmental Biology

RECEIVED 30 April 2022
ACCEPTED 27 July 2022
PUBLISHED 30 August 2022

CITATION
West G, Turunen M, Aalto A, Virtanen L, Li S-P, Heliö T, Meinander A and Taimen P (2022), A heterozygous p.S143P mutation in LMNA associates with proteasome dysfunction and enhanced autophagy-mediated degradation of mutant lamins A and C. *Front. Cell Dev. Biol.* 10:932983. doi: 10.3389/fcell.2022.932983

A heterozygous p.S143P mutation in *LMNA* associates with proteasome dysfunction and enhanced autophagy-mediated degradation of mutant lamins A and C

Gun West[1,2], Minttu Turunen[1,2], Anna Aalto[2,3], Laura Virtanen[1,2], Song-Ping Li[1,2†], Tiina Heliö[4], Annika Meinander[2,3] and Pekka Taimen[1,2,5*]

[1]Institute of Biomedicine and FICAN West Cancer Centre, University of Turku, Turku, Finland, [2]InFLAMES Research Flagship Center, University of Turku and Åbo Akademi University, Turku, Finland, [3]Faculty of Science and Engineering, Åbo Akademi University, Turku, Finland, [4]Heart and Lung Center Helsinki University Hospital and University of Helsinki, Helsinki, Finland, [5]Department of Pathology, Laboratory Division, Turku University Hospital, Turku, Finland

Lamins A and C are nuclear intermediate filament proteins that form a proteinaceous meshwork called lamina beneath the inner nuclear membrane. Mutations in the *LMNA* gene encoding lamins A and C cause a heterogenous group of inherited degenerative diseases known as laminopathies. Previous studies have revealed altered cell signaling pathways in lamin-mutant patient cells, but little is known about the fate of mutant lamins A and C within the cells. Here, we analyzed the turnover of lamins A and C in cells derived from a dilated cardiomyopathy patient with a heterozygous p.S143P mutation in *LMNA*. We found that transcriptional activation and mRNA levels of *LMNA* are increased in the primary patient fibroblasts, but the protein levels of lamins A and C remain equal in control and patient cells because of a meticulous interplay between autophagy and the ubiquitin-proteasome system (UPS). Both endogenous and ectopic expression of p.S143P lamins A and C cause significantly reduced activity of UPS and an accumulation of K48-ubiquitin chains in the nucleus. Furthermore, K48-ubiquitinated lamins A and C are degraded by compensatory enhanced autophagy, as shown by increased autophagosome formation and binding of lamins A and C to microtubule-associated protein 1A/1B-light chain 3. Finally, chaperone 4-PBA augmented protein degradation by restoring UPS activity as well as autophagy in the patient cells. In summary, our results suggest that the p.S143P-mutant lamins A and C have overloading and deleterious effects on protein degradation machinery and pharmacological interventions with compounds enhancing protein degradation may be beneficial for cell homeostasis.

KEYWORDS

lamin A/C (LMNA), ubiquitin (Ub), autophagy, degradation, disease mutations, ubiquitin-proteasome degradation system

Introduction

Eukaryotic cells are continuously dealing with misfolded proteins, compromising cellular homeostasis. To maintain functional protein homeostasis, these misfolded proteins are modulated by the cellular protein quality control (PQC) systems that promote refolding, degradation, or sequestering of proteins into compartments (Arrasate et al., 2004; Powers et al., 2009). Molecular chaperones are important components of PQC and the first defense mechanism against proteotoxicity by recognizing misfolded proteins and promoting refolding (Tiroli-Cepeda and Ramos, 2011). However, if the misfolded proteins cannot be repaired, they are marked for degradation.

In eukaryotic cells, the ubiquitin-proteasome system (UPS) and the autophagy-lysosome systems are two major intracellular machineries that regulate the amount of proteins by degrading misfolded, damaged, and aggregated proteins. Under normal conditions, up to 80–90% of proteins are degraded by proteasomes that are found not only in the cytoplasm both free and attached to the endoplasmic reticulum (ER) but also throughout the nucleoplasm (Lee and Goldberg, 1998; Wójcik and DeMartino, 2003; Collins and Goldberg, 2017). Short-lived proteins are degraded through the UPS, which is initiated by sequential addition of ubiquitin chains to target proteins by the E1-E2-E3 enzyme cascade (Bachmair and Varshavsky, 1989; Hershko and Ciechanover, 1998). The 26S proteasomes are composed of the 19S regulatory particle that recognizes and unfolds the ubiquitin chains as well as the 20S core particle that hydrolyses the protein into short peptides or amino acids (Voges et al., 1999). Dysregulation of the PQC leading to aggregation of misfolded proteins is characteristic for different human diseases such as neurodegenerative diseases, cancer, diabetes, lysosomal storage diseases and cardiovascular diseases (Amm et al., 2014; Maejima, 2020).

Macroautophagy (hereafter called autophagy) is a conserved molecular pathway that accounts for 10–20% of protein degradation (Gronostajski et al., 1985). Under cellular stress conditions such as hypoxia, starvation, or DNA damage, accumulated protein aggregates and damaged organelles are increasingly eradicated through autophagy. Autophagy is mediated by double-membrane vesicles called autophagosomes that engulf cellular material to be fused with the endosomes and lysosomes for degradation (Gatica et al., 2018). Autophagy can be divided into non-selective that is a bulk degradation pathway for cytoplasmic components, and selective that specifically removes protein aggregates and damaged organelles (Glick et al., 2010). In selective autophagy, target proteins are ubiquitinated and recognized by carrier proteins such as sequestosome 1 (SQSTM1/p62), optineurin, neighbor of BRCA1, nuclear dot protein 52 kDa, Tax1-binding protein 1, and Toll-interacting protein that bring them to the autophagosomes (Lippai and Lőw, 2014). UPS and autophagy are interconnected, and inhibition of UPS has been shown to activate autophagy in a compensatory manner (Wang and Wang, 2015; Pohl and Dikic, 2019).

The nuclear lamina, a meshwork of proteins underlying the inner nuclear membrane, is primarily composed of nuclear intermediate filament proteins called lamins and their associated proteins. A-type lamins (lamins A and C) are encoded by the *LMNA* gene through alternative splicing (Lin and Worman, 1993). Lamin C is transcribed directly from the *LMNA* gene, while lamin A is expressed as a precursor (pre-lamin A) that undergoes posttranslational modification steps to become the mature lamin A (Dechat et al., 2010). The nuclear lamina provides the nucleus with mechanical strength and regulates chromatin organization and gene expression (Dahl et al., 2006; Dechat et al., 2010; Osmanagic-Myers et al., 2015; Briand and Collas, 2020). Mutations in the *LMNA* gene or alterations in its expression levels have been linked to a variety of diseases called laminopathies, and to some extent, cancer progression (Burke and Stewart, 2013; Sakthivel and Sehgal, 2016).

Previous studies have shown that a selective autophagy known as nucleophagy degrades various nuclear proteins, including lamins, during different cellular stresses (Papandreou and Tavernarakis, 2019). In support, lamins A, C and B1 have been shown to interact with microtubule-associated protein 1A/1B-light chain 3 (LC3-I/II), an autophagy-linked protein, upon DNA damage (Dou et al., 2015; Li et al., 2019). Also, cells with the p.H222P *Lmna* mutation have been shown to increasingly form autophagosomes that contain nuclear components (Park et al., 2009).

How UPS and autophagy are involved in the degradation of lamins A and C still remains poorly understood. In the current study, we investigated whether disease-associated mutations in lamins A and C alter their turnover and how functionally defective mutant lamins are processed within cells. We found that mRNA levels of lamins A and C are increased in fibroblasts obtained from a dilated cardiomyopathy patient with a heterozygous p.S143P *LMNA* mutation. However, the mutant lamins A and C are more unstable and increasingly tagged for degradation by K48-linked ubiquitination, which in turn leads to saturation of UPS. Although K48-linked ubiquitin chains are compensatorily degraded by autophagy, they still accumulate in the nucleus. A chaperone, 4-PBA, restored degradation through UPS and augmented protein degradation by further activation of autophagy. These results suggest that pharmacological

intervention with compounds that enhance clearance of mutant lamin might be beneficial in some of the laminopathies.

Materials and methods

Cell culture

Primary fibroblasts from a healthy donor and from a patient carrying the p.S143P mutation in the *LMNA* gene were cultured in Minimum Essential Medium containing 15% fetal bovine serum, 1x penicillin/streptomycin/glutamine, 1x non-essential amino acids, and 1x vitamins (all from Invitrogen, Waltham, Massachusetts, United States) as previously described (West et al., 2016; Shah et al., 2019). HeLa cells transduced with a pFLAG-FLRU-vector expressing *LMNA* shRNA and either wild-type or p.S143P mutant lamin A insert were cultured in Dulbecco's Modified Eagle Medium supplied with 10% fetal bovine serum and 1x penicillin/streptomycin/glutamine (all from Invitrogen) as described earlier (West et al., 2016). The use of patient derived cells was approved by the Ethics Committees of the Hospital District of Helsinki and Uusimaa (HUS 387/13/03/2009 and HUS/1187/2019). All procedures were undertaken with informed consent and according to the principles expressed in the Declaration of Helsinki.

Chemicals and antibodies

Cells were treated with 300 μg/ml cycloheximide (CHX) (Sigma-Aldrich, St. Louis, Missouri, United States), 50 μM leptomycin B (LMB) (Santa Cruz Biotechnology, Dallas, Texas, United States), 20 mM ammonium chloride (NH_4Cl), 1 μM MG132 (Sigma-Aldrich) and/or 5 mM 4-Phenylbutyric acid (4-PBA) (Selleck Chemicals, Houston, Texas, United States). The primary antibodies included mouse monoclonal anti-lamins A and C (1:10,000, a kind gift from Professor Robert Goldman, Northwestern University), mouse monoclonal anti-actin (1:500, clone AC-40, Sigma-Aldrich), rabbit monoclonal anti-Atg5 (1:100, clone D5F5U, #12994, Cell Signaling Technology, Danvers, Massachusetts, United States), rabbit monoclonal anti-Atg7 (1:100, clone D12B11, #8558, Cell Signaling Technology), rabbit polyclonal anti-LC3-I/II (IF:1:100, WB:1:1000, #4108, Cell Signaling Technology), mouse monoclonal anti-p62 (IF:1:100, WB:1:1000, clone 2C11, ab56416, Abcam Cambridge, United Kingdom), mouse monoclonal HRP-conjugated anti-GAPDH (1:10,000, clone 1E6D9, #HRP-60004, Proteintech, Rosemont, Illinois, United States), rabbit monoclonal anti-ubiquitin-K48 (1:400, clone Apu2, #ZRB2150, Sigma-Aldrich) and mouse monoclonal vimentin (1:100, clone V6, #V6630, Sigma-Aldrich). Secondary antibodies for western blotting were HRP-conjugated donkey anti-rabbit-IgG and sheep anti-mouse-IgG (both from Thermo Fischer Scientific, Waltham, Massachusetts, United States). Secondary antibodies for immunofluorescence were Alexa 488/555 goat-anti-mouse and goat-anti-rabbit antibodies (all from Thermo Fischer Scientific). Pan-ubiquitin chains were purified using a protein consisting of four ubiquitin-associated domains in tandem fused to GST and His (referred to as pan-TUBE), kindly provided by Professor Mads Gyrd Hansen, University of Copenhagen, Denmark.

Reverse transcription quantitative polymerase chain reaction (RT-qPCR)

RNA was extracted using the NucleoSpin RNA kit (Macherey-Nagel, Düren, Germany) and 1 μg of high-quality RNA was converted to cDNA using the SensiFAST cDNA synthesis kit (Bioline, Toronto, Ontario, Canada). Amplification was performed using a SensiFAST SYBR Lo-ROX PCR kit (Bioline) for 3 min at 95°C followed by 40 cycles of 5 s at 95°C, 10 s at 60°C and 15 s at 72°C. The fold change was calculated using the 2−ΔΔCt method and normalized to GAPDH. The primers used were for GAPDH 5′-TAAATTGAGCCCGCAGCCTCCC-3′ and 5′-ATGTGGCTC GGCTGGCGACG-3'; *LMNA* total 5′-GGGATGCCCGCAAGA CCCTT-3′ and 5′-GGTATTGCGCGCTTTCAGCTCC-3'; *LMNA* WT 5′-GCTCTGCTGAACTCCAAGGAGG-3′ and 5′-GCCTCA AGCTTGGCCACCTG-3'; *LMNA* S143P 5′-GCTCTGCTGAAC CCCAAGGAGG-3′ and 5′-GCCTCAAGCTTGGCCACCTG-3'.

Mass spectrometry

The mass spectrometry analyses were performed at the Turku Proteomics Facility as follows: proteins separated on an SDS-PAGE gel were digested with peptides dissolved in 15 μL of 0.1% formic acid. The Liquid Chromatography Electrospray Ionization Tandem Mass Spectrometric (LC-ESI-MS/MS) analyses were performed on a nanoflow HPLC system (Easy-nLC1200, Thermo Fisher Scientific) coupled to the Orbitrap Fusion Lumos Tribrid mass spectrometer (Thermo Fisher Scientific) equipped with a nano-electrospray ionization source. Peptides were first loaded on a trapping column and subsequently separated inline on a 15 cm C18 column (75 μm × 15 cm, ReproSil- Pur 5 μm 200 A C18-AQ, Dr. Maisch HPLC GmbH, Ammerbuch-Entringen, Germany). The mobile phase consisted of water with 0.1% formic acid (solvent A) or acetonitrile/water (80:20 (v/v)) with 0.1% formic acid (solvent B). A 30 min gradient from 8 to 37% B was used to elute peptides. Mass spectrometry data were acquired automatically by using Thermo Xcalibur 4.1 software (Thermo Fisher Scientific). An information-dependent acquisition method consisted of an Orbitrap MS survey scan of the mass range 300–1300 m/z followed by HCD fragmentation in a top speed mode with a 3 s cycle time for precursor selection. An inclusion list including possible tryptic

peptides containing the mutation p.S143P site was created and added to the LC-MS/MS method.

Luciferase assay of *LMNA* promoter activity

The human promoter region of *LMNA* was recognized from the earlier published rat *LMNA* promoter sequence (Tiwari et al., 1998). The promoter sequence was chosen to include the TATA box, GC box, and activator protein 1 (AP1) binding site. The upstream -1.3 kB promoter region (sequence -1334 to-16) was synthesized and subcloned into a pNLCoI1 [luc2-P2A-NlucP/Hygro] vector (Promega, Madison, Wisconsin, United States) at GenScript, Netherlands. The vector (50 ng/ml) was transfected into fibroblasts using Lipofectamine (Thermo Fischer Scientific) and, after 72 h, Dual Glo luciferase assay reagent was added. After an incubation time of 15 min at RT, the firefly luciferase was measured on a luminometer. Then Dual Glo Stop and Go reagent was added, incubated for 15 min, and renilla fluorescence was measured on a luminometer. The background was subtracted and the values were normalized to renilla (firefly/renilla).

Western blot analysis

Cells were pelleted, washed twice with 1xPBS at 4°C, and solubilized in M-PER mammalian protein extraction reagent (Thermo Fisher Scientific) supplemented with 1x protease and 1x phosphatase inhibitors. Whole cell extract was boiled in Laemmli buffer and separated on a 4–10% gradient gel (BioRad, Hercules, California, United States), transferred to a nitrocellulose membrane (BioRad) and incubated for 1 h in RT or overnight at 4°C with primary antibody. The membrane was incubated with horseradish peroxidase (HRP)-conjugated secondary antibody (1:10,000) for 1 h at RT. The chemiluminescent signal was detected with an Enhanced Chemiluminescence kit (Thermo Fischer Scientific) using a ChemiDoc MP (BioRad). The blots were quantified with ImageJ and their values normalized by dividing them with GAPDH values. The western blots were repeated independently at least two times.

Immunofluorescence and confocal microscopy

Cells grown on glass plates were fixed with 10% formalin for 10 min, followed by permeabilization with 0.1% Triton-X for 10 min. Samples were incubated with primary antibodies for 1 h at RT followed by secondary antibodies (1:400) for 1 h at RT. LysoTracker Red DND-99 (Thermo Fischer) was added to cells at a concentration of 100 nM and incubated for 30 min. Acridine orange (Invitrogen, 3568) was diluted in PBS and used at a final concentration of 10 µg/ml on fixed and permeabilized cells for 15 min. All immunofluorescence glass plates were mounted with ProLong Diamond Antifade Mountant, including DAPI (Thermo Fischer Scientific). Confocal images were taken on a Marianas 3i Yokogawa CSU-W1 spinning disk confocal microscope attached to an inverted Zeiss AxioObserver Z1 microscope (Intelligent Imaging Innovations GmbH, Göttingen, Germany). The microscope was controlled by SlideBook six software (Intelligent Imaging Innovations GmbH) and a 63x/1.4 Zeiss Plan-Apochromat oil objective was used. The mean fluorescence intensities were analyzed with ImageJ (National Institutes of Health) or Fiji software (Schindelin et al., 2012) using 20x mid-plane sections of confocal images or images taken with a Nikon Eclipse Ni microscope with a 20x/0.5 Plan-Apochromat objective. The Pearson's correlation coefficients were determined from 10 confocal images (60–100 individual cells) taken with 63× objective and analyzed with the coloc2 plugin in Fiji.

Proximity ligation assay

Cells grown on glass plates were fixed with 10% formalin for 10 min and permeabilized with 0.1% Triton X-100 in 1xPBS for 10 min. Duolink PLA kit (DUO92105, Millipore Sigma, Burlington, Massachusetts, United States) was used according to the manufacturer's protocol. After blocking, the samples were incubated with primary antibodies in a humified chamber at 37°C for 1 h, followed by incubation with secondary antibodies (anti-rabbit PLUS and anti-mouse MINUS PLA-probes). Following the ligation and amplification steps, the coverslips were mounted with ProLong Diamond with DAPI. The number of PLA signals per cell was determined visually, and the cells with more than three PLA signals were considered positive.

Proteasome purification and activity assay

A proteasome 20S activity assay kit (MAK172, Millipore Sigma) was used for live-cell measurements of proteasome activity in patient and control fibroblasts (80.000 cells per well on a 96-well plate). Any inhibitors were added 24 h prior to measurements, and the proteasome assay loading solution 1 h before measurements. A plate reader at 490/525 nm (excitation/emission) was used for detection.

To isolate 20S proteasomes from control and patient fibroblasts or from lentivirally transduced HeLa cells expressing either FLAG-tagged WT-lamin A or p.S143P lamin A, the cells were first washed three times with cold 1xPBS and further lysed with a buffer containing 50 mM HEPES pH 7.5, 5 mM EDTA, 150 mM NaCl, and 1% Triton-X100 for 30 min on ice. The cell lysates were centrifuged at 15,000 rpm for 15 min at 4°C, and the supernatants were analyzed with a 20S proteasome assay kit (Bio-Techne Ltd, Abingdon, United Kingdom)

according to the manufacturer's protocol. Briefly, the proteasomes were activated in a 1x reaction buffer containing sodium dodecyl sulfate (SDS) and incubated for 20 min at 37°C before being mixed with the fluorogenic peptide suc-LLVY-AMC. The amount of cleaved AMC fragment was measured using a plate reader at 345/445 nm (excitation/emission). Any inhibitors were added 24 h prior to harvesting the cells, and the same inhibitors were used when adding the fluorogenic substrate. The background was subtracted and the values from control cells were used to normalize the results.

Purification of ubiquitin conjugates from cells under denaturing conditions

An equal number of cells were washed twice with 1xPBS and pelleted before lysing using a buffer containing 50 mM Tris pH 7.5, 150 mM NaCl, 1% Triton X-100, 1 mM EDTA, 10% glycerol supplemented with 1 mM DTT, 5 mM NEM, 1x protease and phosphatase inhibitors, 5 mM chloroacetamide, and 1% SDS. Lysates were sonicated, diluted to 0.1% SDS, and cleared before incubation with Glutathione Sepharose™ 4B (BioRad). For purification with the recombinant protein GST-TUBE (30–100 mg/ml), the lysate was incubated with the beads for a minimum of 2 h under rotation at 4°C. The beads were washed three times with ice cold wash buffer containing 10 mM Tris pH 7.5, 150 mM NaCl, 0.1% Triton X-100, 5% glycerol, and eluted using Laemmli sample buffer. The samples were boiled for 10 min and separated on a 4–10% gel.

For purification with antibody, the beads were first incubated with the lysate under rotation at 4°C overnight. After adding 1 µg of antibody and 1 h of incubation, the beads were washed twice with 1xPBS and the samples were dissolved in Laemmli buffer. The samples were boiled for 10 min and separated on a 4–10% gel.

Results

Lamins A and C are upregulated at mRNA, but not at protein level in *LMNA*-mutant patient cells

To study whether a disease-related point mutation in lamins A and C affect their turnover, we took advantage of primary fibroblasts obtained from a patient carrying a heterozygous p.S143P (c.427C) missense mutation in *LMNA*. Based on RT-qPCR, equal amounts of *LMNA* mRNAs with both c.427T and c.427C sequences were produced in the patient fibroblasts, indicating that both the wild-type (WT) and the mutant allele are transcribed in a similar manner (Figure 1A). Similarly, mass spectrometry analysis detected both WT and p.S143P specific protein fragments of lamins A and C in the patient cells, suggesting that both transcripts are translated into proteins (Figure 1B). However, total *LMNA* mRNA levels were significantly higher in the patient cells when compared to control cells from a healthy individual (Figure 1C). This was supported by a luciferase assay that showed higher *LMNA* promotor activity in the patient cells compared to controls (Figure 1D). Despite the increased transcription, the protein levels of lamins A and C in the patient cells were similar to controls under normal culture conditions (Figure 1E). This prompted us to analyze the stability of the lamins A and C upon inhibition of protein synthesis with cycloheximide. After 16- and 24-h treatments with cycloheximide, we noted an accelerated reduction of lamin A and C protein levels in the patient cells, indicating that they are more unstable and potentially increasingly degraded (Figure 1E).

We further asked whether lamins A and C in the patient cells are properly transported into the nucleus and treated the cells with leptomycin B, which inhibits nuclear export by blocking binding of chromosomal regional maintenance protein (CRM1) to leucine-rich nuclear export signals (Kudo et al., 1999). Calculated mean fluorescence intensity after 16-h leptomycin B treatment showed increased accumulation of lamins A and C in the nucleus of patient cells, suggesting that they are transported into nuclei and that nuclear export by CRM1 is required for their turnover (Figures 1F,G). Taken together, the results indicate that lamins A and C are increasingly produced in the patient cells, accumulate in the nucleus, and are further transported into the cytoplasm for degradation.

Lamins A and C are increasingly ubiquitinated by K48-linked chains in *LMNA*-mutant patient cells

We next asked if lamins A and C were increasingly K48-ubiquitinated in the patient cells compared to control cells. Ubiquitin contains seven lysine residues (K6, K11, K27, K29, K33, K48, K63) and one methionine (M1) that can attach to other ubiquitin chains, forming linear or branched linkages (Pohl and Dikic, 2019). Ubiquitination is mediated by the attachment of ubiquitin chains of different linkages and sizes to the lysine residues of target proteins. Among the eight different ubiquitin linkages, the lysine 48 (K48)-linkage is the most studied and is a canonical signal for protein degradation (Chau et al., 1989). Other ubiquitin linkages such as K6, K11, K27, and K29 have also been shown to mediate proteasomal degradation, whereas K48 and K63 are also involved in lysosomal degradation (Dammer et al., 2011). The K48-ubiquitin staining was predominantly nuclear in the patient fibroblasts, whereas a predominantly cytoplasmic staining pattern was observed in the control cells (Figure 2A). To analyze if lamins A and C were modified by ubiquitination, we used a GST-tagged recombinant pan-tandem ubiquitin-binding entity (pan-

10.3389/fcell.2022.932983

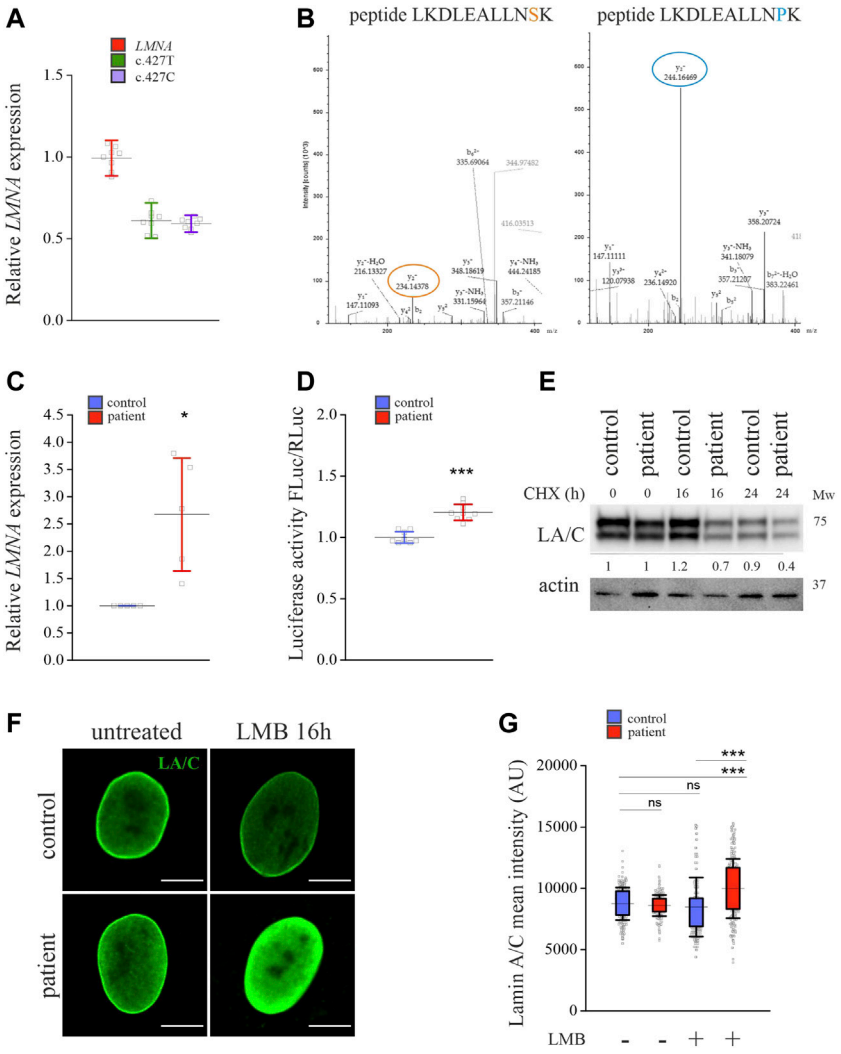

FIGURE 1
Expression and degradation of lamins A and C are enhanced in *LMNA* mutant patient cells. **(A)** RT-qPCR analysis of *LMNA* expression in the patient fibroblasts carrying a heterozygous p.S143P *LMNA* mutation. Allele-specific primers detecting either wild-type (c.427T) or mutant (c.427C) alleles, or primers detecting both (*LMNA*) were used. N = 3 individual experiments. **(B)** LC-ESI-MS/MS analysis of peptide fragments covering both wild-type and mutant lamins A and C in the patient cells. The sequences specific to the p.143S and p.143P lamin A and C peptide fragments are shown on the top, and the corresponding peaks in the mass spectra are encircled. **(C)** RT-qPCR analysis of relative overall *LMNA* expression in the control and patient fibroblasts (N = 3). **(D)** Luciferase assay measuring activity of an upstream −1.3 kb *LMNA* promotor sequence in the control and patient fibroblasts (N = 3). **(E)** Western blot analysis shows protein levels of lamins A and C (LA/C) in the patient and control fibroblasts treated with 300 µg/ml cycloheximide (CHX) for given time points. Numerical values show levels of lamins A and C normalized to actin, which was used as a loading control. **(F)** Confocal microscopy images from control and patient cells stained for lamins A and C before or after 16-h treatment with 50 µM leptomycin B (LMB). Mid-plane confocal sections are shown. Scale bar 10 µm. **(G)** Mean fluorescence intensities (AU) were measured from confocal images and plotted (N = 300). Note upregulation of lamins A and C after 16-h treatment with 50 µM LMB in the patient fibroblasts. The whiskers show the mean values ±s.d. and boxplots show the 75th and 25th percentiles of the calculated intensities, $*p < 0.05$, $**p < 0.01$, $***p < 0.001$.

TUBE) to pull down ubiquitinated substrates under denatured conditions. Coherent with the K48-staining, there was more overall K48-ubiquitin in the patient cells compared to control cells (Figure 2B). The pulldown showed that lamins A and C were ubiquitinated in both cell cultures, but increasingly in the patient cells (Figure 2B). Additionally, a smear denoting ubiquitinated lamins A and C with higher molecular weight was noted in the patient cells. Likewise, immunoprecipitation with the lamin A antibody verified that lamins A and C are increasingly K48-ubiquitinated in the patient cells compared to controls

10.3389/fcell.2022.932983

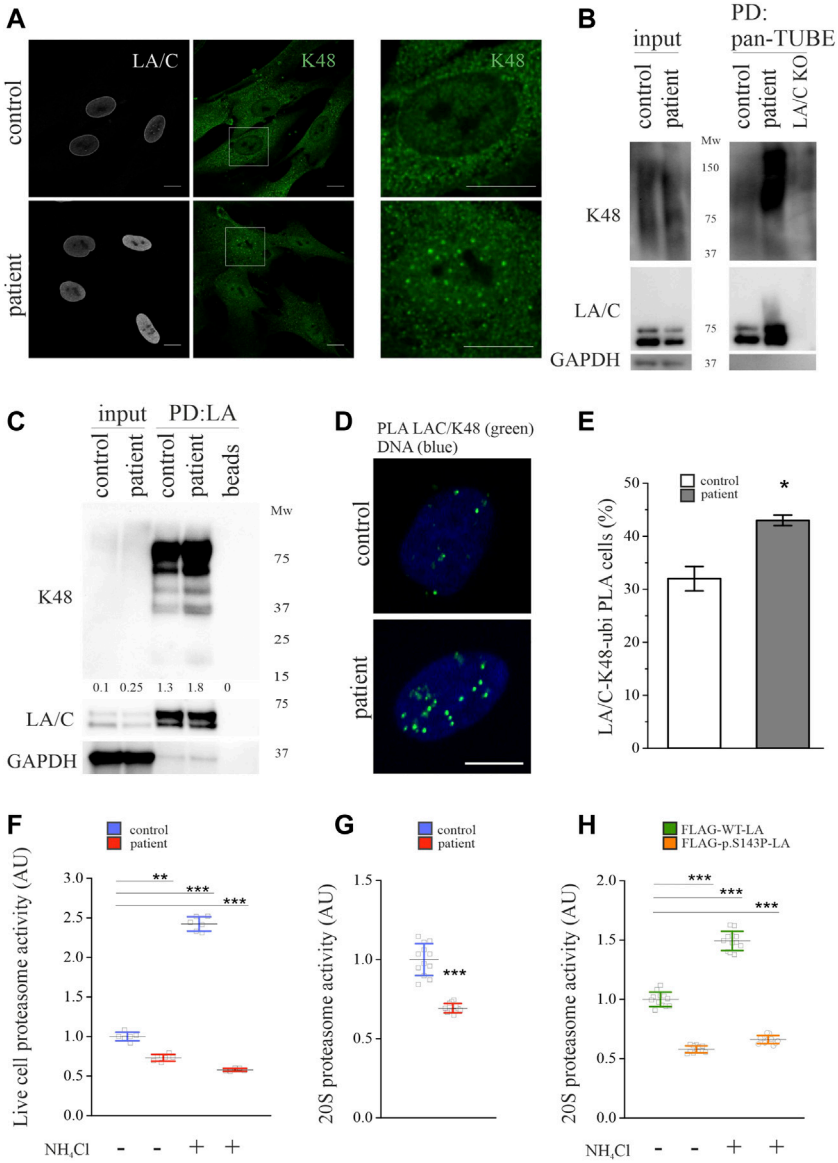

FIGURE 2
Lamins A and C are ubiquitinated by K48-linked chains in *LMNA* mutant patient fibroblasts. **(A)** Representative confocal microscopy images from control and patient fibroblasts stained for lamins A and C and K48-linked ubiquitin chains. Scale bar 10 μm. **(B)** Pulldown with GST-tagged recombinant pan-tandem ubiquitin-binding entity (pan-TUBE) under denatured conditions. **(C)** Pulldown with lamin A antibody under denatured conditions. K48-ubiquitin levels were normalized to GAPDH, which was used as a loading control. **(D-E)** Proximity ligation assay (PLA) of lamins A and C and K48-ubiquitin in the control and patient fibroblasts as calculated from >300 individual cells. Cells with more than three PLA signals were considered positive. Data are expressed as mean ± s.e.m, $*p < 0.05$. **(F)** Proteasome activity of control and patient fibroblasts treated with or without 20 mM NH_4Cl for 24 h. N = 3 individual experiments. **(G)** Chymotrypsin-like activity of 20S proteasomes isolated from control and patient fibroblasts (N = 3). **(H)** Chymotrypsin-like activity of 20S proteasomes isolated from Hela cells expressing either FLAG-tagged WT-LA or p.S143P-LA and treated with or without 20 mM NH_4Cl for 24 h (N = 3). The whiskers show mean values ±s.d $**p < 0.01$, $***p < 0.001$.

(Figure 2C). The association between lamins A and C and K48-ubiquitin was further studied with PLA, which detected a statistically significantly increased number of PLA signals in the patient cells relative to controls (Figures 2D,E). These results strongly argue that lamins A and C are increasingly ubiquitinated with K48-linked chains in the patient cells.

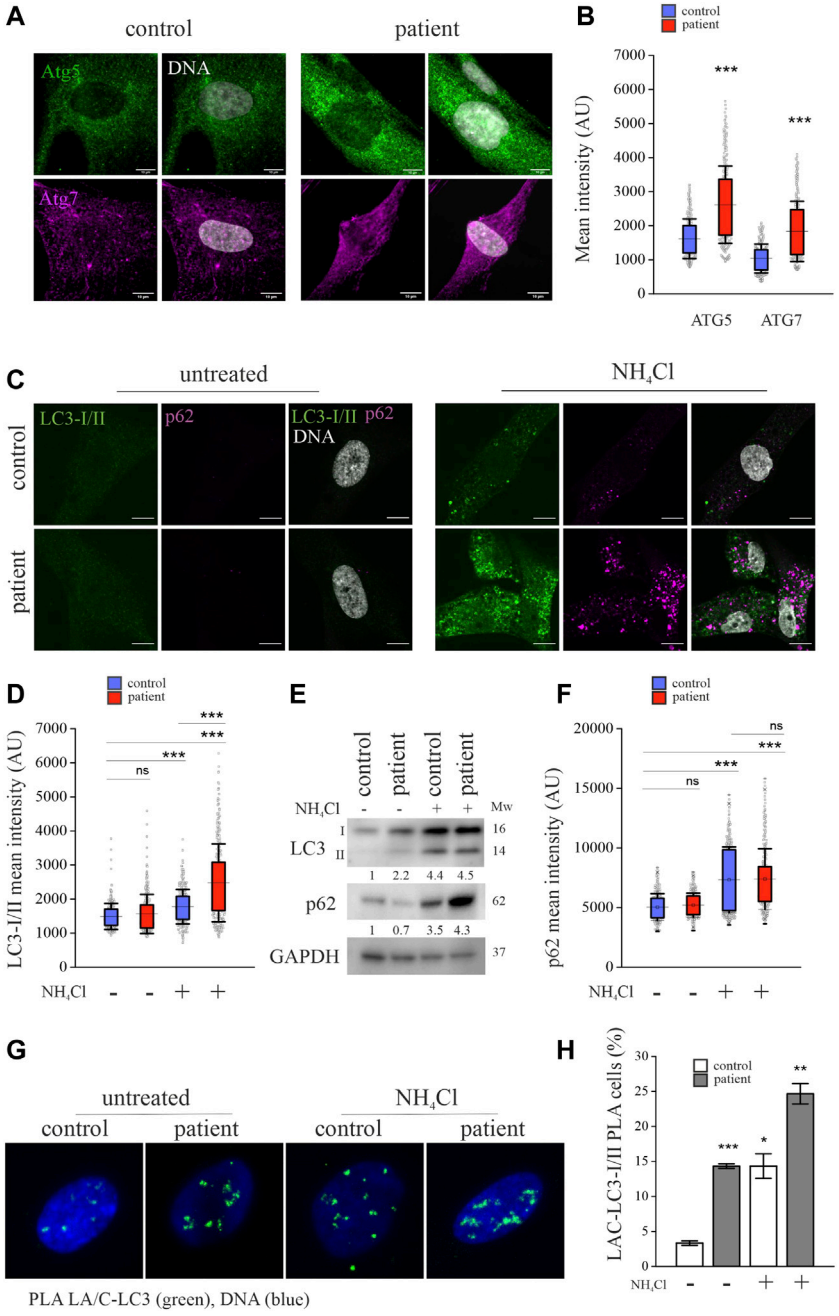

FIGURE 3
Lamins A and C are increasingly committed to autophagy in *LMNA* mutant patient fibroblasts. **(A)** Confocal microscopy images from the patient and control fibroblasts stained for autophagy-related proteins Atg5 and Atg7. Scale bar 10 μm. **(B)** Calculated mean fluorescence intensity values from Atg5 and Atg7 stainings. The whiskers show mean values ± s.d and boxplots show the 75th and 25th percentiles (N = 300), *** $p < 0.001$. **(C)** Confocal microscopy images from the patient and control fibroblasts treated with or without 20 mM NH_4Cl for 24h and stained for Atg8/LC3-I/II and SQSTM1/p62. Note the accumulation of LC3-I/II or p62 after NH_4Cl treatment especially in the patient cells. Scale bar 10 μm. **(D)** Calculated mean fluorescence intensity values from LC3-I/II staining. The whiskers show mean values ± s.d and boxplots show the 75th and 25th percentiles (N = 300), *** $p < 0.001$ (compared to untreated control cells). **(E)** Western blot analysis from control and patient fibroblasts treated with 20 mM NH_4Cl for 24 h. Pooled LC3-I/II and p62 levels were normalized to GAPDH, which was used as a loading control. Note the increase of LC3-II after NH_4Cl treatment. **(F)** Calculated mean fluorescence intensity values from p62 staining. (N = 300), *** $p < 0.001$ **(G–H)** Proximity ligation assay (PLA) detecting association of lamins A and C with LC3-I/II in the control and patient fibroblasts. The percentage of cells with PLA signals was determined from >300 cells and the cells with more than three PLA signals were considered positive. Data is expressed as mean ± s.e.m, * $p < 0.05$, ** $p < 0.01$, *** $p < 0.001$.

10.3389/fcell.2022.932983

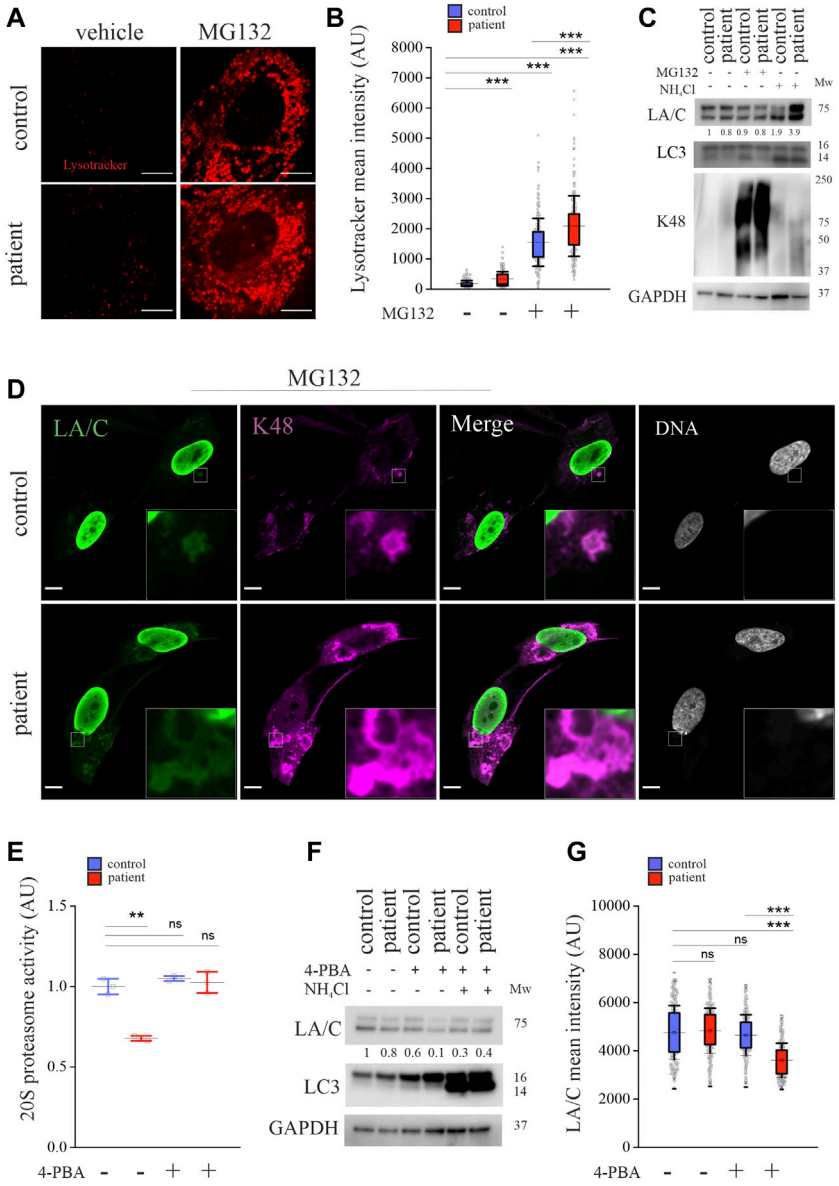

FIGURE 4
Crosstalk between autophagy and UPS is impaired in *LMNA* mutant patient cells. **(A)** LysoTracker Red DND-99 staining from untreated and MG132-treated control and patient cells. **(B)** Calculated mean fluorescence intensity values show more LysoTracker positive lysosomes in the patient cells and their number is further increased after 24-h treatment with 1 μM MG132. **(C)** Western blot analysis from control and patient cells treated with 1 μM MG132 or 20 mM NH_4Cl for 24 h. Protein levels of lamins A and C (LA/C) were normalized to GAPDH, which was used as a loading control. All the proteins were detected on the same membrane. **(D)** Confocal microscopy images from control and patient cells treated with MG132 and stained for lamins A and C and K48-ubiquitin. Insets show cytosolic structures that co-stain with lamins A and C and K48 antibodies. Scale bar 10 μm. **(E)** Chymotrypsin-like activity as measured in control and patient cells treated with 5 mM 4-PBA for 24 h (N = 3 individual experiments) $^{**}p < 0.01$. **(F)** Western blot analysis of control and patient cells treated with or without 5 mM 4-PBA. Autophagy was inhibited with 20 mM NH_4Cl and GAPDH was used as a loading control. **(G)** Calculated mean fluorescence intensity values (AU) from control and patient fibroblasts treated with or without 5 mM 4-PBA for 24 h and stained for lamins A and C (N = 300). The whiskers show mean values ±s.d and boxplots show the 75th and 25th percentiles, $^{*}p < 0.05$, $^{***}p < 0.001$.

Degradation through the ubiquitin-proteasome system is impaired in the patient cells

The ubiquitin-proteasome system (UPS) and autophagy are the two major degradation pathways in eukaryotic cells. To find out which mechanisms are responsible for the degradation of lamins A and C in the patient and control cells, we first analyzed the rate of UPS-mediated degradation in the patient cells compared to control cells. The 20S proteasome has seven β-subunits connected to the proteolytic activity of UPS. The β-subunits possess three different enzyme specificities, namely caspase-like, trypsin-like and chymotrypsin-like activity, whereof the chymotrypsin-like activity is widely assumed to reflect the degree of protein degradation (Kisselev et al., 2003). Therefore, the proteasome activity was analyzed on live cells (Figure 2F) and on isolated 20S proteasomes (Figure 2G) by using a fluorogenic substrate specific for chymotrypsin-like activity. Interestingly, we detected only a ~70% overall chymotrypsin-like activity in the patient cells compared to controls (Figure 2F). In an analogue, the chymotrypsin-like activity of isolated 20S proteasomes was decreased in the patient cells compared to controls (Figure 2G). Since inhibition or impairment of UPS or autophagy leads to compensatory activation of the other system, we treated the cells with ammonium chloride (NH_4Cl) to shut down lysosomal degradation and therefore the autophagy pathway. The chymotrypsin-like activity increased in control cells after 24-h NH_4Cl treatment, while it had no positive effect on the patient cells, indicating dysfunctional proteasome activity (Figure 2F). The impact of the p.S143P mutant lamin was further verified by measuring chymotrypsin-like activity in lentivirally transduced HeLa cells expressing either FLAG-tagged wild-type lamin A (WT-LA) or p.S143P mutant lamin A (p.S143P-LA) (Figure 2H). Correspondingly, the chymotrypsin-like activity was 50% lower in FLAG-p.S143P-LA expressing cells compared to FLAG-WT-LA expressing cells, indicating that the expression of mutant lamin leads to reduced proteasome activity (Figure 2H). Furthermore, 24-h NH_4Cl treatment increased the chymotrypsin-like activity of FLAG-WT-LA expressing cells but had no significant effect on FLAG-p.S143P-LA expressing cells (Figure 2H). In conclusion, the results show that UPS activity is decreased in the patient cells and unresponsive to inhibition of autophagy.

Degradation of lamins A and C through autophagy is enhanced in *LMNA*-mutant patient cells

To find out whether lamins A and C are degraded by autophagy, we focused on ATG5, ATG7, ATG8/LC3-I/II and SQSTM1/p62, which are critical in turnover by autophagy (Komatsu and Ichimura, 2010; Martens and Fracchiolla, 2020; Collier et al., 2021). Confocal microscopy showed increased ATG5 and ATG7 staining intensity in the perinuclear area of the patient cells and this finding was verified with calculated mean fluorescence intensity values from microscopy images, indicating increased nascent autophagosome formation in these cells (Figures 3A,B). Conversion of LC3-1 to LC3-II is generated by the conjugation of cytosolic LC3-I to phosphatidylethanolamine on the surface of nascent autophagosomes. Staining for LC3-I/II showed very little or no difference between the patient and control cells under normal culture conditions (Figure 3C). However, cytoplasmic LC3-I/II accumulation was pronounced in the patient cells after inhibiting autophagosome fusion to lysosomes by NH_4Cl treatment (Kawai et al., 2007; Yu et al., 2013; Teves et al., 2017) (Figure 3C). Similarly, calculated mean fluorescence intensities of LC3-I/II were higher in the patient cells after NH_4Cl treatment (Figure 3D). Western blot analysis confirmed that NH_4Cl treatment increased LC3 levels due to accumulation of LC3-II and also indicated that the autophagy flux is upregulated in patient cells (Figure 3E). SQSTM1/p62, an autophagic transport protein, binds ubiquitinated proteins and mediates their degradation by directly binding to LC3-II (Lippai and Lőw, 2014). Confocal images visualized elevated levels of p62 after inhibiting autophagy with NH_4Cl in both the control and patient cells (Figure 3C), showing that p62 is an autophagy substrate, as previously shown by others (Pankiv et al., 2007). Similar to LC3, calculated mean fluorescence intensities and western blot analysis confirmed increased levels of p62, especially in the patient cells after autophagy inhibition (Figures 3E,F). Correlation analysis showed co-localization of p62 and LC3-I/II in control and patient cells under normal cell culture conditions, and NH_4Cl treatment further increased the co-localization, indicating spatial accumulation of both proteins due to autophagy inhibition (Supplementary Figures S1A). NH_4Cl treatment, however, had no detectable effect on co-localization of p62 and lamins A and C (Supplementary Figures S1B-C).

To further examine the role of autophagy in the degradation of lamins A and C, we used a proximity ligation assay (PLA) to confirm the association between lamins A and C and LC3-I/II. PLA signals were seen in 15% of patient cells compared to 4% of control cells under normal culture conditions, and their prevalence further increased after NH_4Cl treatment (Figures 3G,H). These results suggest that lamins A and C bind to LC3 and are degraded through autophagy in both cell cultures, but the autophagic flux is increased in the patient cells.

Crosstalk between autophagy and UPS is impaired in *LMNA*-mutant patient cells

Previous studies have shown that UPS inhibition can activate autophagy (Albornoz et al., 2019). To test this, we stained the cells with LysoTracker Red, which is a marker for acidic

organelles, including lysosomes. The confocal images and calculated mean fluorescence intensities showed more LysoTracker Red positive acidic organelles in the patient cells and their number further increased upon MG132 treatment (Figures 4A,B). We also stained the cells with another marker, acridine orange (AO), which is a stain that fluoresces green in the cytoplasm or when bound to DNA, whereas AO trapped in acidic vesicular organelles or bound to RNA fluoresces red. We noticed more AO-positive red vesicular structures in the patient cells' cytoplasm and their number further increased upon MG132 treatment, indicating either elevated formation or slowed processing of acidic organelles in these cells (Supplementary Figures S2A). Autophagy flux was further analyzed with western blot analysis showing increased LC3-II after NH_4Cl treatment in both cell cultures, indicating inhibition of autophagy (Figure 4C). MG132 treatment showed a slight increase in LC3-II in the control cells but no change in the patient cells. Taken together, the results indicate that autophagy is activated in the patient cells after MG132 treatment. As expected, K48-ubiquitin chains were enriched after MG132 treatment in both cell cultures, but there was also a detectable increase in the patient cells after NH_4Cl treatment (Figure 4C). MG132 treatment had no effect on protein levels of lamins A and C in either of the cell cultures (Figure 4C). However, NH_4Cl treatment increased lamin A and C levels, especially in the patient cells, verifying our results that lamins A and C are continuously degraded through an autophagy/lysosomal pathway in these cells (Figure 4C). To analyze the fate of K48-linked lamins A and C, the cells were stained for K48-ubiquitin, and lamins A and C after MG132 treatment. Interestingly, we noticed an accumulation of cytoplasmic lamin A and C positive particles that co-stained with K48-ubiquitin especially in the patient cells (Figure 4D). This structure was rarely found in the control cells and was negative in DNA staining, excluding the possibility of nuclear leakage. The Pearson's correlation coefficients of K48-ubiquitin and lamin A and C stainings were 0.41 and 0.44 for control and patient cells, respectively. Further staining for vimentin showed that K48 accumulations in the cytoplasm were surrounded by vimentin cages (Supplementary Figures S2B), as previously reported for aggresomes (Johnston et al., 1998). Taken together, the results suggest that K48-tagged lamins A and C are degraded by UPS but in the patient cells also through autophagy in a compensatory manner upon UPS dysfunction.

4-Phenylbutyric acid (4-PBA) is a chaperone that binds to hydrophobic parts of unfolded proteins and protects cells from protein aggregation, promotes proteins folding and reduces ER stress (Iannitti and Palmieri, 2011). Similarly, we have previously shown that 4-PBA alleviates aggregation of mutant lamins A and C and ER stress in p.S143P primary cells (West et al., 2016). To study whether 4-PBA could be used to restore the UPS activity in the patient cells, the cells were treated with 4-PBA for 24 h. Chymotrypsin-like activity was rescued in the patient cells while no additive effect was noted in the control cells (Figure 4E). Previous studies have shown that 4-PBA also enhances autophagy (Nissar et al., 2017; Gadallah et al., 2021), and correspondingly, we detected increased LC3-I levels in the patient and control cells after 4-PBA treatment (Figure 4F). When 4-PBA was combined with NH_4Cl, LC3-II levels increased significantly, verifying that autophagy flux is enhanced under these circumstances (Figure 4F). Protein levels of lamins A and C slightly decreased after 4-PBA treatment in the patient cells, as seen by western blot and calculated mean fluorescence intensity values from cells stained for lamins A and C (Figures 4F,G). Furthermore, lamin A and C protein levels remained low when patient cells were treated with both 4-PBA and NH_4Cl, suggesting that UPS-mediated degradation of lamins A and C was restored. Taken together, the results show that UPS dysfunction in the patient cells can be reversed by 4-PBA treatment.

Discussion

Mutations in the *LMNA* gene cause disorders with a wide variety of clinical phenotypes. The most common laminopathy is dilated cardiomyopathy, which is almost exclusively due to heterozygous missense mutations of the *LMNA*. In the current study, we asked whether the dilated cardiomyopathy-associated p.S143P mutation in *LMNA* affects turnover and processing of lamins A and C. We found that transcriptional activity and mRNA levels of lamins A and C are increased in patient fibroblasts while their protein levels remain similar to controls. This finding in particular raised the question about the fate of mutant lamins and prompted us to focus on UPS and autophagy, the main systems upholding cellular homeostasis by protein degradation.

We show that a fraction of lamins A and C in the patient cells are short-lived, increasingly K48-ubiquitinated and targeted for degradation by UPS. However, the function of UPS, as measured by chymotrypsin-like activity, is reduced in the patient cells, which leads to an accumulation of K48-linked ubiquitin chains within the nucleus. UPS has a critical role in removing misfolded, damaged and mutated proteins, and several studies have reported accumulation of ubiquitinated protein targets, protein aggregates, and UPS impairment in different heart diseases (Gilda and Gomes, 2017). Previously, Cattin et al. showed that heterozygous $Lmna^{\Delta K32/+}$ mice develop dilated cardiomyopathy and have increased degradation of ΔK32-lamins A and C. This further leads to UPS impairment and accumulation of toxic ΔK32-lamins A and C (Cattin et al., 2013). UPS impairment has also been demonstrated in cardiomyopathy caused by mutations in desmin or αB-crystallin (CryAB) leading to accumulation of desmin in skeletal and cardiac muscle (Bence et al., 2001; McLendon and Robbins, 2011). A missense mutation of

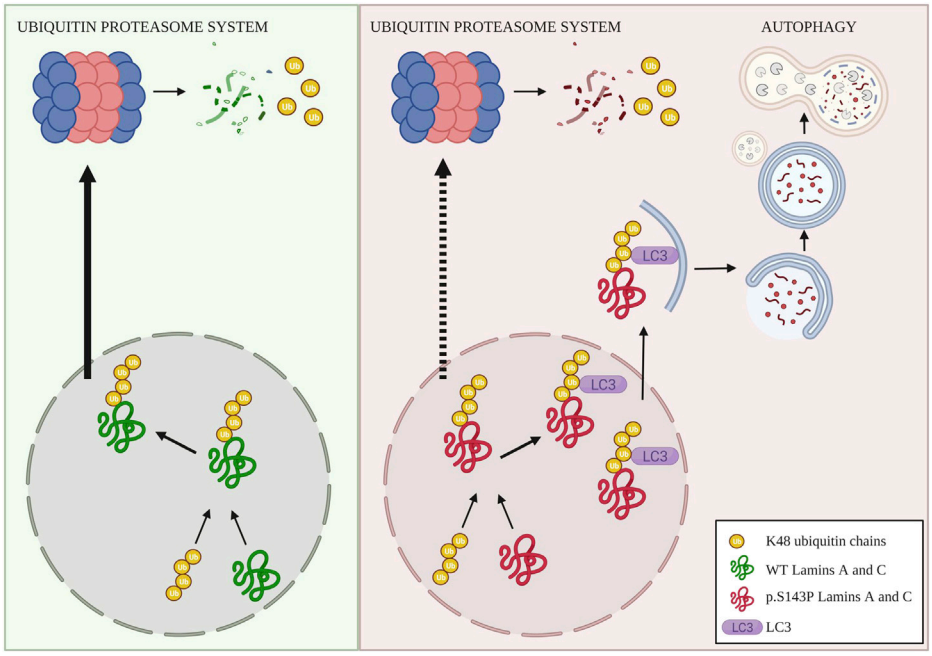

FIGURE 5
Illustrative picture of degradation of K48-ubiquitinated lamins A and C. In normal cells, wild-type lamins A and C are partially ubiquitinated with K48-linked chains that lead to UPS-mediated degradation of lamins A and C. In the patient cells, lamins A and C are increasingly K48-ubiquitinated, presumably due to increased turnover and production, as well as proteasomal dysfunction. This leads to saturation of UPS and an accumulation of K48-linked ubiquitin chains within the nucleus. Saturation and dysfunction of UPS further lead to compensatory degradation of K48-lamins A and C through autophagy, created with BioRender.com.

CryAB showed UPS impairment prior to heart hypertrophy and was associated with delivery of ubiquitinated proteins into the 20S proteasome (Chen et al., 2005). Similarly, a mutation in the transcription factor NKX2-5 leads to adult-onset dilated cardiomyopathy and expression of such a specific mutant form of NKX2 in COS-7 cells or HL-1 cardiomyocytes causes UPS impairment (Costa et al., 2013).

Compensatory activation of autophagy might have a role in alleviating the disease pathology after UPS impairment. Our results show that autophagy is enhanced in patient cells in general, as seen by the increased perinuclear accumulation of Atg5 and Atg7, indicating autophagosome formation. Furthermore, lamins A and C were increasingly associated with LC3 in patient cells, suggesting that the enhanced rate of autophagy is, at least partially, due to degradation of lamins A and C. In consistent with our results, others have also shown autophagic degradation of lamins A and C. For example, in Hutchinson-Gilford progeria syndrome (HGPS), the E3 ubiquitin ligase SMURF2 was shown to oligo-ubiquitinate lamins A and C and multi-monoubiquitinate progerin for degradation through autophagy (Borroni et al., 2018; Blank, 2020). Park et al. also showed that in embryonic fibroblasts obtained from the *Lmna*$^{H222P/H222P}$ mice, a model for Emery-Dreifuss muscular dystrophy, lamins A and C were degraded through autophagy (Park et al., 2009). Interestingly, in a transgenic *Drosophila melanogaster* model mimicking human cardiomyopathy, overexpression of Atg1 eliminated aggregates of mutant lamin C and reduced cardiac arrhythmia, suggesting that enhanced autophagy activity and processing of lamins A and C are beneficial for cell and tissue homeostasis (Bhide et al., 2018).

We further show that lentiviral expression of FLAG-tagged p.S143P lamin A in HeLa cells leads to dysfunctional UPS, indicating that the defect found in patient cells is likely due to mutant lamin. The exact mechanism has yet to be elucidated, but we have previously shown that p.S143P lamins A and C are more nucleoplasmic compared to wild-type lamins A and C, are incapable of forming normal filaments, and occasionally assemble into disorganized aggregates (West et al., 2016) that may be more prone to degradation. Whether it is only the mutant forms of lamins A and C that are K48-ubiquitinated in the heterozygote patient cells and choke up UPS would be of interest to analyze in future studies. For this purpose, a mutant-specific antibody against lamins A and C would be highly beneficial. In agreement with this hypothesis, we have earlier shown that inhibition of UPS using MG132 increases aggregation of lamins A and C in the nucleoplasm of lentivirally transduced fibroblasts expressing p.S143P-LA

(West et al., 2016). In the present study, we also show that UPS dysfunction can be reversed by treatment with a chaperone, 4-PBA. The reversibility of UPS activity indicates that the decrease in activity is due to the buildup of degradation products. We found that 4-PBA also enhanced autophagy in both control and patient cells, which further augmented the degradation of proteins. A similar strategy, i.e., activation of autophagy, has also been used in other models of laminopathies, e.g. in the $Lmna^{H222P/H222P}$ mice, where the mTOR pathway inhibitor temsirolimus enhanced autophagy and improved cardiac function (Choi et al., 2012). UPS and autophagy are highly dynamic and quickly adapting systems that preserve cellular homeostasis through interplay. Still, a default in one of the systems can cause severe disease, especially in the long run. Accumulation of misfolded proteins is linked to a variety of different diseases such as neurodegenerative diseases, cancer, diabetes, lysosomal storage diseases and cardiovascular diseases (Amm et al., 2014; Maejima, 2020). Damaged, misfolded, or non-functional proteins are removed through UPS, but impairment or inhibition of UPS leads to protein accumulation within the cell. Aggregated proteins that cannot unfold to pass through the proteolytic barrel in the proteasomes can inhibit UPS and are instead degraded through autophagy (Verhoef et al., 2002). To protect the cells from toxic buildup, the aggregated proteins are transported towards the microtubule-organizing center (MTOC) where the aggresomes are formed (Johnston et al., 1998; Kopito, 2000). Cytoplasmic aggresomes are enriched in chaperones, ubiquitin and proteasomal subunits with a cage of vimentin (Wójcik et al., 1996). In the patient cells, cytoplasmic accumulations of lamins A and C co-localizing with ubiquitin were detected after inhibition of UPS with MG132. These accumulations were surrounded by vimentin such as the aggresomes. Whether they are equal to the aggresomes is unclear; however, similar cytoplasmic accumulations were not detected in untreated cells. Instead, the patient cells showed accumulated K48-linked lamins A and C in the nucleus, which could represent sequestration within the nucleus. Reported sequestration within the nucleus includes cajal bodies, PML bodies, nuclear speckles, and nucleoli (Fu et al., 2005; Park et al., 2011). It is possible that the p.S143P mutant forms of lamins A and C are misfolded, unable to pass through the proteolytic barrel of UPS and further "choking" it up, which leads to sequestration of lamins A and C into compartments for further degradation. Activation of autophagy in patient cells might be an early step in the disease mechanism to eliminate misfolded and damaged proteins. External stresses that burden autophagy could increase misfolded lamins A and C above a critical level that leads to the formation of visible nuclear aggregates. However, the results of the current study were limited to cell cultures derived from one patient and an age-matched control. Whether the UPS is equally dysfunctional in cell cultures obtained from patients with other *LMNA* mutations remains to be analyzed in future studies.

In summary, we suggest that in normal cells a small portion of lamins A and C is K48-ubiquitinated and degraded by UPS while in the lamin mutant cells, lamins A and C are increasingly expressed, K48-ubiquitinated and targeted for degradation through UPS (Figure 5). This leads to a dysfunction of UPS and a buildup of K48-ubiquitin chains within the nucleus. Toxic accumulation of ubiquitinated targets could be part of the disease mechanism within the patient tissues, and the ongoing burden of UPS degradation and/or external stresses may eventually increase the impairment of UPS. In the patient cells lamins A and C are degraded by compensatory enhanced autophagy (Figure 5). Whether the patient cells, can uphold enhanced autophagy still remains to be answered. Additionally, autophagy activity has been reported to decrease with age, which would have a tremendous effect on cell homeostasis. Promisingly, a chaperone used in this study, 4-PBA, restored UPS activity and further enhanced autophagy and normalized protein levels of lamins A and C in the patient cells. Such small molecular drugs may eventually turn out to be beneficial for the treatment of laminopathies with similar molecular etiology.

Data availability statement

The mass spectrometry proteomics data have been deposited to the ProteomeXchange Consortium via the PRIDE (Perez-Riverol et al., 2022) partner repository with the dataset identifier PXD033937.

Ethics statement

The studies involving human participants were reviewed and approved by the Ethics Committees of the Hospital District of Helsinki and Uusimaa (HUS 387/13/03/2009 and HUS/1187/2019). The patients/participants provided their written informed consent to participate in this study.

Author contributions

GW designed and performed research and wrote the manuscript. MT performed computational image analysis and cell experiments. AA designed and performed ubiquitin-related analysis. LV carried out confocal microscopy imaging. S-PL designed promoter region analysis. TH recruited patients and provided material. AM edited the manuscript, and PT wrote the manuscript and supervised the study. All co-authors approved the final version of the manuscript.

Funding

This project was supported by grants received from the Academy of Finland, the Sigrid Jusélius Foundation, and the Finnish Foundation for Cardiovascular Research.

Acknowledgments

The Turku Proteomics Facility at the University of Turku and Abo Akademi University is supported by Biocenter Finland and is acknowledged for expertise in mass spectrometry analysis. Cell Imaging and Cytometry Core at the Turku Bioscience Centre, Turku, Finland, is acknowledged for help with imaging studies, Robert D. Goldman (Feinberg School of Medicine at Northwestern University, United States) for providing lamin A and C antibodies, Kaisa Huhtinen (University of Turku, Finland) for providing autophagy-related antibodies, and Mads Gyrd Hansen (University of Copenhagen, Denmark) for providing pan-TUBE construct. All patients and healthy donors are acknowledged for donating biopsies for this research.

Conflict of interest

The authors declare that the research was conducted in the absence of any commercial or financial relationships that could be construed as a potential conflict of interest.

Publisher's note

Supplementary material

The Supplementary Material for this article can be found online at: https://www.frontiersin.org/articles/10.3389/fcell.2022.932983/full#supplementary-material

SUPPLEMENTARY FIGURE S1
Lamin A and C staining after NH_4Cl treatment. **(A)** Pearson's correlation coefficients of p62 and LC3-I/II stainings as determined from untreated and NH_4Cl-treated control and patient cells. The data was retrieved from 10 randomly selected confocal images including 60-100 individual cells per sample. Note an increased correlation upon NH_4Cl treatment. **(B)** Pearson's correlation coefficients of p62 and lamin A/C stainings as determined from untreated and NH_4Cl-treated control and patient cells. **(C)** Control and patient cells stained with antibodies against p62 and lamins A and C show slightly increased lamin A and C intensities after treatment with 20 mM NH_4Cl for 24 h. Scale bar 10 µm. The whiskers show mean values ± s.d $*p < 0.05$.

SUPPLEMENTARY FIGURE S2
Cytoplasmic changes after proteasome inhibition with MG132. **(A)** Acridine orange staining from untreated and MG132-treated control and patient cells showing acidic vesicular organelles (AVO) in red and cell nucleus and membranes in green. **(B)** Treatment of control and patient cells with 1 µM MG132 for 24 h leads to accumulation of cytoplasmic K48 ubiquitin which is surrounded by perinuclear vimentin cage (shown with arrows). Scale bar 10 µm.

References

Albornoz, N., Bustamante, H., Soza, A., and Burgos, P. (2019). Cellular responses to proteasome inhibition: molecular mechanisms and beyond. *Int. J. Mol. Sci.* 20 (14), 3379. doi:10.3390/ijms20143379

Amm, I., Sommer, T., and Wolf, D. H. (2014). Protein quality control and elimination of protein waste: the role of the ubiquitin-proteasome system. *Biochim. Biophys. Acta* 1843, 182–196. doi:10.1016/j.bbamcr.2013.06.031

Arrasate, M., Mitra, S., Schweitzer, E. S., Segal, M. R., and Finkbeiner, S. (2004). Inclusion body formation reduces levels of mutant huntingtin and the risk of neuronal death. *Nature* 431, 805–810. doi:10.1038/nature02998

Bachmair, A., and Varshavsky, A. (1989). The degradation signal in a short-lived protein. *Cell* 56, 1019–1032. doi:10.1016/0092-8674(89)90635-1

Bence, N. F., Sampat, R. M., and Kopito, R. R. (2001). Impairment of the ubiquitin-proteasome system by protein aggregation. *Science* 292, 1552–1555. doi:10.1126/science.292.5521.1552

Bhide, S., Trujillo, A. S., O'Connor, M. T., Young, G. H., Cryderman, D. E., Chandran, S., et al. (2018). Increasing autophagy and blocking Nrf2 suppress laminopathy-induced age-dependent cardiac dysfunction and shortened lifespan. *Aging Cell* 17, e12747. doi:10.1111/acel.12747

Blank, M. (2020). Targeted regulation of nuclear lamins by ubiquitin and ubiquitin-like modifiers. *Cells* 9 (6), 1340. doi:10.3390/cells9061340

Borroni, A. P., Emanuelli, A., Shah, P. A., Ilić, N., Apel-Sarid, L., Paolini, B., et al. (2018). Smurf2 regulates stability and the autophagic-lysosomal turnover of lamin a and its disease-associated form progerin. *Aging Cell* 17, e12732. doi:10.1111/acel.12732

Briand, N., and Collas, P. (2020). Lamina-associated domains: peripheral matters and internal affairs. *Genome Biol.* 21, 85. doi:10.1186/s13059-020-02003-5

Burke, B., and Stewart, C. L. (2013). The nuclear lamins: flexibility in function. *Nat. Rev. Mol. Cell Biol.* 14, 13–24. doi:10.1038/nrm3488

Cattin, M. E., Bertrand, A. T., Schlossarek, S., Le Bihan, M. C., Skov Jensen, S., Neuber, C., et al. (2013). Heterozygous LmnadelK32 mice develop dilated cardiomyopathy through a combined pathomechanism of haploinsufficiency and peptide toxicity. *Hum. Mol. Genet.* 22, 3152–3164. doi:10.1093/hmg/ddt172

Chau, V., Tobias, J. W., Bachmair, A., Marriott, D., Ecker, D. J., Gonda, D. K., et al. (1989). A multiubiquitin chain is confined to specific lysine in a targeted short-lived protein. *Science* 243, 1576–1583. doi:10.1126/science.2538923

Chen, Q., Liu, J. B., Horak, K. M., Zheng, H., Kumarapeli, A. R., Li, J., et al. (2005). Intrasarcoplasmic amyloidosis impairs proteolytic function of proteasomes in cardiomyocytes by compromising substrate uptake. *Circ. Res.* 97, 1018–1026. doi:10.1161/01.RES.0000189262.92896.0b

Choi, J. C., Muchir, A., Wu, W., Iwata, S., Homma, S., Morrow, J. P., et al. (2012). Temsirolimus activates autophagy and ameliorates cardiomyopathy caused by lamin A/C gene mutation. *Sci. Transl. Med.* 4, 144ra102. doi:10.1126/scitranslmed.3003875

Collier, J. J., Suomi, F., Oláhová, M., McWilliams, T. G., and Taylor, R. W. (2021). Emerging roles of ATG7 in human health and disease. *EMBO Mol. Med.* 13, e14824. doi:10.15252/emmm.202114824

Collins, G. A., and Goldberg, A. L. (2017). The logic of the 26S proteasome. *Cell* 169, 792–806. doi:10.1016/j.cell.2017.04.023

Costa, M. W., Guo, G., Wolstein, O., Vale, M., Castro, M. L., Wang, L., et al. (2013). Functional characterization of a novel mutation in NKX2-5 associated with

congenital heart disease and adult-onset cardiomyopathy. *Circ. Cardiovasc. Genet.* 6, 238–247. doi:10.1161/CIRCGENETICS.113.000057

Dahl, K. N., Scaffidi, P., Islam, M. F., Yodh, A. G., Wilson, K. L., and Misteli, T. (2006). Distinct structural and mechanical properties of the nuclear lamina in Hutchinson-Gilford progeria syndrome. *Proc. Natl. Acad. Sci. U. S. A.* 103, 10271–10276. doi:10.1073/pnas.0601058103

Dammer, E. B., Na, C. H., Xu, P., Seyfried, N. T., Duong, D. M., Cheng, D., et al. (2011). Polyubiquitin linkage profiles in three models of proteolytic stress suggest the etiology of alzheimer disease. *J. Biol. Chem.* 286, 10457–10465. doi:10.1074/jbc.M110.149633

Dechat, T., Adam, S. A., Taimen, P., Shimi, T., and Goldman, R. D. (2010). Nuclear lamins. *Cold Spring Harb. Perspect. Biol.* 2, a000547. doi:10.1101/cshperspect.a000547

Dou, Z., Xu, C., Donahue, G., Shimi, T., Pan, J. A., Zhu, J., et al. (2015). Autophagy mediates degradation of nuclear lamina. *Nature* 527, 105–109. doi:10.1038/nature15548

Fu, L., Gao, Y. S., Tousson, A., Shah, A., Chen, T. L., Vertel, B. M., et al. (2005). Nuclear aggresomes form by fusion of PML-associated aggregates. *Mol. Biol. Cell* 16, 4905–4917. doi:10.1091/mbc.e05-01-0019

Gadallah, S. H., Ghanem, H. M., Abdel-Ghaffar, A., Metwaly, F. G., Hanafy, L. K., and Ahmed, E. K. (2021). 4-Phenylbutyric acid and rapamycin improved diabetic status in high fat diet/streptozotocin-induced type 2 diabetes through activation of autophagy. *Arch. Physiol. Biochem.* 127, 235–244. doi:10.1080/13813455.2019.1628069

Gatica, D., Lahiri, V., and Klionsky, D. J. (2018). Cargo recognition and degradation by selective autophagy. *Nat. Cell Biol.* 20, 233–242. doi:10.1038/s41556-018-0037-z

Gilda, J. E., and Gomes, A. V. (2017). Proteasome dysfunction in cardiomyopathies. *J. Physiol.* 595, 4051–4071. doi:10.1113/JP273607

Glick, D., Barth, S., and Macleod, K. F. (2010). Autophagy: Cellular and molecular mechanisms. *J. Pathol.* 221, 3–12. doi:10.1002/path.2697

Gronostajski, R. M., Pardee, A. B., and Goldberg, A. L. (1985). The ATP dependence of the degradation of short- and long-lived proteins in growing fibroblasts. *J. Biol. Chem.* 260, 3344–3349. doi:10.1016/S0021-9258(19)83626-8

Hershko, A., and Ciechanover, A. (1998). The ubiquitin system. *Annu. Rev. Biochem.* 67, 425–479. doi:10.1146/annurev.biochem.67.1.425

Iannitti, T., and Palmieri, B. (2011). Clinical and experimental applications of sodium phenylbutyrate. *Drugs R. D.* 11, 227–249. doi:10.2165/11591280-000000000-00000

Johnston, J. A., Ward, C. L., and Kopito, R. R. (1998). Aggresomes: a cellular response to misfolded proteins. *J. Cell Biol.* 143, 1883–1898. doi:10.1083/jcb.143.7.1883

Kawai, A., Uchiyama, H., Takano, S., Nakamura, N., and Ohkuma, S. (2007). Autophagosome-lysosome fusion depends on the pH in acidic compartments in CHO cells. *Autophagy* 3, 154–157. doi:10.4161/auto.3634

Kisselev, A. F., Garcia-Calvo, M., Overkleeft, H. S., Peterson, E., Pennington, M. W., Ploegh, H. L., et al. (2003). The caspase-like sites of proteasomes, their substrate specificity, new inhibitors and substrates, and allosteric interactions with the trypsin-like sites. *J. Biol. Chem.* 278, 35869–35877. doi:10.1074/jbc.M303725200

Komatsu, M., and Ichimura, Y. (2010). Physiological significance of selective degradation of p62 by autophagy. *FEBS Lett.* 584, 1374–1378. doi:10.1016/j.febslet.2010.02.017

Kopito, R. R. (2000). Aggresomes, inclusion bodies and protein aggregation. *Trends Cell Biol.* 10, 524–530. doi:10.1016/s0962-8924(00)01852-3

Kudo, N., Matsumori, N., Taoka, H., Fujiwara, D., Schreiner, E. P., Wolff, B., et al. (1999). Leptomycin B inactivates CRM1/exportin 1 by covalent modification at a cysteine residue in the central conserved region. *Proc. Natl. Acad. Sci. U. S. A.* 96, 9112–9117. doi:10.1073/pnas.96.16.9112

Lee, D. H., and Goldberg, A. L. (1998). Proteasome inhibitors: valuable new tools for cell biologists. *Trends Cell Biol.* 8, 397–403. doi:10.1016/s0962-8924(98)01346-4

Li, Y., Jiang, X., Zhang, Y., Gao, Z., Liu, Y., Hu, J., et al. (2019). Nuclear accumulation of UBC9 contributes to SUMOylation of lamin A/C and nucleophagy in response to DNA damage. *J. Exp. Clin. Cancer Res.* 38, 67. doi:10.1186/s13046-019-1048-8

Lin, F., and Worman, H. J. (1993). Structural organization of the human gene encoding nuclear lamin a and nuclear lamin C. *J. Biol. Chem.* 268, 16321–16326. doi:10.1016/S0021-9258(19)85424-8

Lippai, M., and Lőw, P. (2014). The role of the selective adaptor p62 and ubiquitin-like proteins in autophagy. *Biomed. Res. Int.* 2014, 832704. doi:10.1155/2014/832704

Maejima, Y. (2020). The critical roles of protein quality control systems in the pathogenesis of heart failure. *J. Cardiol.* 75, 219–227. doi:10.1016/j.jjcc.2019.09.019

Martens, S., and Fracchiolla, D. (2020). Activation and targeting of ATG8 protein lipidation. *Cell Discov.* 6, 23. doi:10.1038/s41421-020-0155-1

McLendon, P. M., and Robbins, J. (2011). Desmin-related cardiomyopathy: an unfolding story. *Am. J. Physiol. Heart Circ. Physiol.* 301, H1220–H1228. doi:10.1152/ajpheart.00601.2011

Nissar, A. U., Sharma, L., Mudasir, M. A., Nazir, L. A., Umar, S. A., Sharma, P. R., et al. (2017). Chemical chaperone 4-phenyl butyric acid (4-PBA) reduces hepatocellular lipid accumulation and lipotoxicity through induction of autophagy. *J. Lipid Res.* 58, 1855–1868. doi:10.1194/jlr.M077537

Osmanagic-Myers, S., Dechat, T., and Foisner, R. (2015). Lamins at the crossroads of mechanosignaling. *Genes Dev.* 29, 225–237. doi:10.1101/gad.255968.114

Pankiv, S., Clausen, T. H., Lamark, T., Brech, A., Bruun, J. A., Outzen, H., et al. (2007). p62/SQSTM1 binds directly to Atg8/LC3 to facilitate degradation of ubiquitinated protein aggregates by autophagy. *J. Biol. Chem.* 282, 24131–24145. doi:10.1074/jbc.M702824200

Papandreou, M. E., and Tavernarakis, N. (2019). Nucleophagy: from homeostasis to disease. *Cell Death Differ.* 26, 630–639. doi:10.1038/s41418-018-0266-5

Park, R., Wang'ondu, R., Heston, L., Shedd, D., and Miller, G. (2011). Efficient induction of nuclear aggresomes by specific single missense mutations in the DNA-binding domain of a viral AP-1 homolog. *J. Biol. Chem.* 286, 9748–9762. doi:10.1074/jbc.M110.198325

Park, Y. E., Hayashi, Y. K., Bonne, G., Arimura, T., Noguchi, S., Nonaka, I., et al. (2009). Autophagic degradation of nuclear components in mammalian cells. *Autophagy* 5, 795–804. doi:10.4161/auto.8901

Perez-Riverol, Y., Bai, J., Bandla, C., Hewapathirana, S., García-Seisdedos, D., Kamatchinathan, S., et al. (2022). The PRIDE database resources in 2022: A Hub for mass spectrometry-based proteomics evidences. *Nucleic Acids Res.* 50 (D1), D543–D552. doi:10.1093/nar/gkab1038

Pohl, C., and Dikic, I. (2019). Cellular quality control by the ubiquitin-proteasome system and autophagy. *Science* 366, 818–822. doi:10.1126/science.aax3769

Powers, E. T., Morimoto, R. I., Dillin, A., Kelly, J. W., and Balch, W. E. (2009). Biological and chemical approaches to diseases of proteostasis deficiency. *Annu. Rev. Biochem.* 78, 959–991. doi:10.1146/annurev.biochem.052308.114844

Sakthivel, K. M., and Sehgal, P. (2016). A novel role of lamins from genetic disease to cancer biomarkers. *Oncol. Rev.* 10, 309. doi:10.4081/oncol.2016.309

Shah, D., Virtanen, L., Prajapati, C., Kiamehr, M., Gullmets, J., West, G., et al. (2019). Modeling of LMNA-related dilated cardiomyopathy using human induced pluripotent stem cells. *Cells* 8, 594. doi:10.3390/cells8060594

Teves, J. M. Y., Bhargava, V., Kirwan, K. R., Corenblum, M. J., Justiniano, R., Wondrak, G. T., et al. (2017). Parkinson's disease skin fibroblasts display signature alterations in growth, redox homeostasis, mitochondrial function, and autophagy. *Front. Neurosci.* 11, 737. doi:10.3389/fnins.2017.00737

Tiroli-Cepeda, A. O., and Ramos, C. H. (2011). An overview of the role of molecular chaperones in protein homeostasis. *Protein Pept. Lett.* 18, 101–109. doi:10.2174/092986611794475093

Tiwari, B., Muralikrishna, B., and Parnaik, V. K. (1998). Functional analysis of the 5' promoter region of the rat lamin a gene. *DNA Cell Biol.* 17, 957–965. doi:10.1089/dna.1998.17.957

Verhoef, L. G., Lindsten, K., Masucci, M. G., and Dantuma, N. P. (2002). Aggregate formation inhibits proteasomal degradation of polyglutamine proteins. *Hum. Mol. Genet.* 11, 2689–2700. doi:10.1093/hmg/11.22.2689

Voges, D., Zwickl, P., and Baumeister, W. (1999). The 26S proteasome: a molecular machine designed for controlled proteolysis. *Annu. Rev. Biochem.* 68, 1015–1068. doi:10.1146/annurev.biochem.68.1.1015

Wang, C., and Wang, X. (2015). The interplay between autophagy and the ubiquitin-proteasome system in cardiac proteotoxicity. *Biochim. Biophys. Acta* 1852, 188–194. doi:10.1016/j.bbadis.2014.07.028

West, G., Gullmets, J., Virtanen, L., Li, S. P., Keinänen, A., Shimi, T., et al. (2016). Deleterious assembly of the lamin A/C mutant p.S143P causes ER stress in familial dilated cardiomyopathy. *J. Cell Sci.* 129, 2732–2743. doi:10.1242/jcs.184150

Wójcik, C., and DeMartino, G. N. (2003). Intracellular localization of proteasomes. *Int. J. Biochem. Cell Biol.* 35, 579–589. doi:10.1016/s1357-2725(02)00380-1

Wójcik, C., Schroeter, D., Wilk, S., Lamprecht, J., and Paweletz, N. (1996). Ubiquitin-mediated proteolysis centers in HeLa cells:indication from studies of an inhibitor of the chymotrypsin-like activity of the proteasome. *Eur. J. Cell Biol.* 71, 311–318. https://www.researchgate.net/publication/14276742

Yu, C., Huang, X., Xu, Y., Li, H., Su, J., Zhong, J., et al. (2013). Lysosome dysfunction enhances oxidative stress-induced apoptosis through ubiquitinated protein accumulation in hela cells. *Anat. Rec.* 296, 31–39. doi:10.1002/ar.22612

frontiers | Frontiers in Cell and Developmental Biology

TYPE Original Research
PUBLISHED 31 August 2022
DOI 10.3389/fcell.2022.934586

OPEN ACCESS

EDITED BY
Ming Guo,
Massachusetts Institute of Technology, United States

REVIEWED BY
Alexei Arnaoutov,
Eunice Kennedy Shriver National Institute of Child Health and Human Development (NIH), United States
Jeremy T. Smyth,
Uniformed Services University of the Health Sciences, United States

*CORRESPONDENCE
Lori L. Wallrath,
Lori-wallrath@uiowa.edu

SPECIALTY SECTION
This article was submitted to Cell Growth and Division, a section of the journal Frontiers in Cell and Developmental Biology

RECEIVED 02 May 2022
ACCEPTED 20 July 2022
PUBLISHED 31 August 2022

CITATION
Shaw NM, Rios-Monterrosa JL, Fedorchak GR, Ketterer MR, Coombs GS, Lammerding J and Wallrath LL (2022), Effects of mutant lamins on nucleo-cytoskeletal coupling in Drosophila models of LMNA muscular dystrophy.
Front. Cell Dev. Biol. 10:934586.
doi: 10.3389/fcell.2022.934586

Effects of mutant lamins on nucleo-cytoskeletal coupling in *Drosophila* models of *LMNA* muscular dystrophy

Nicholas M. Shaw[1], Jose L. Rios-Monterrosa[1], Gregory R. Fedorchak[2], Margaret R. Ketterer[1], Gary S. Coombs[3], Jan Lammerding[2] and Lori L. Wallrath[1]*

[1]Department of Biochemistry, Carver College of Medicine, University of Iowa, Iowa City, IA, United States, [2]The Nancy E. and Peter C. Meinig School of Biomedical Engineering, Weill Institute for Cell and Molecular Biology, Cornell University, Ithaca, NY, United States, [3]Biology Department, Waldorf University, Forest City, IA, United States

The nuclei of multinucleated skeletal muscles experience substantial external force during development and muscle contraction. Protection from such forces is partly provided by lamins, intermediate filaments that form a scaffold lining the inner nuclear membrane. Lamins play a myriad of roles, including maintenance of nuclear shape and stability, mediation of nuclear mechanoresponses, and nucleo-cytoskeletal coupling. Herein, we investigate how disease-causing mutant lamins alter myonuclear properties in response to mechanical force. This was accomplished *via* a novel application of a micropipette harpooning assay applied to larval body wall muscles of *Drosophila* models of lamin-associated muscular dystrophy. The assay enables the measurement of both nuclear deformability and intracellular force transmission between the cytoskeleton and nuclear interior in intact muscle fibers. Our studies revealed that specific mutant lamins increase nuclear deformability while other mutant lamins cause nucleo-cytoskeletal coupling defects, which were associated with loss of microtubular nuclear caging. We found that microtubule caging of the nucleus depended on Msp300, a KASH domain protein that is a component of the linker of nucleoskeleton and cytoskeleton (LINC) complex. Taken together, these findings identified residues in lamins required for connecting the nucleus to the cytoskeleton and suggest that not all muscle disease-causing mutant lamins produce similar defects in subcellular mechanics.

KEYWORDS

myonuclei, muscular dystrophies, *Drosophila*, lamins, LINC complex, microtubules, muscle

Introduction

The nuclei of skeletal muscles experience high levels of mechanical force during muscle development and contraction of muscle fibers during work (Rosen & Baylies, 2017; Sweeney & Hammers, 2018). Muscle cells possess structural components to withstand such force, including high expression levels of A-type lamins, lamins A and C (Swift et al., 2013; Cho et al., 2017). Lamins, intermediate filaments that line the inner nuclear membrane, provide structural support for the nucleus, determine the nuclear shape, and organize genomic DNA for proper gene expression (Goldman et al., 2004; Burke & Stewart, 2006; Swift et al., 2013; Zwerger et al., 2013; Camozzi et al., 2014; Dialynas et al., 2015; Kim et al., 2017; Wong et al., 2022). Dominant mutations in the *LMNA* gene encoding the A-type lamins, A and C, cause Emery-Dreifuss muscular dystrophy, limb-girdle muscular dystrophy type 1B, and congenital muscular dystrophy (Bonne et al., 1999; Rankin & Ellard, 2006; Astejada et al., 2007; Worman & Bonne, 2007; Lu et al., 2011; Maggi et al., 2016). Lamins have a conserved domain structure consisting of a head domain, a central coiled-coil rod domain, and a tail domain possessing an Ig-like fold (Dhe-Paganon et al., 2002; Krimm et al., 2002; Mounkes et al., 2003; Herrmann et al., 2007). Lamins dimerize through their rod domain, form filaments through head-to-tail interactions and antiparallel lateral assembly, through lateral contacts that are not well understood to form a meshwork underlying the inner nuclear membrane (Kapinos et al., 2010; Dittmer & Misteli, 2011; Turgay & Medalia, 2017; Eldirany et al., 2021).

The mechanisms by which mutations in the *LMNA* gene cause muscular dystrophy remain incompletely understood and are a topic of intense investigation. Studies in cultured cells and model organisms of muscular dystrophy-associated *LMNA* mutations have revealed insights into potential pathomechanisms (Stewart et al., 2007; Zwerger et al., 2013; Rzepecki & Gruenbaum, 2018; Earle et al., 2020; Coombs et al., 2021). These studies have shown that mutant lamins cause nuclear chromatin protrusions, transient nuclear envelope rupture, increased DNA damage, and abnormal intracellular signaling (Goldman et al., 2004; Dialynas et al., 2015; Hatch & Hetzer, 2016; Earle et al., 2020; Coombs et al., 2021). A potential mechanism to explain these defects is that *LMNA* mutations impair nuclear stability and disrupt nucleo-cytoskeletal connections, which may be particularly devastating in mechanically active tissues such as skeletal and cardiac muscles (Folker et al., 2011; Zwerger et al., 2013; Shin & Worman, 2022).

Cytoskeletal forces are transmitted to the nucleus through the linker of nucleoskeleton and cytoskeleton (LINC) complex (Crisp et al., 2006; Wang et al., 2009; Cain et al., 2018; Hieda, 2019). The LINC complex is comprised of nesprins, proteins that span the outer nuclear membrane and possess a Klarsicht-ANC1-Syne-homology (KASH) domain (Sosa et al., 2012; Wang et al., 2012; Horn, 2014; Kim et al., 2015), and Sad1 and UNC-84 (SUN) domain proteins that span the inner nuclear membrane (Crisp et al., 2006; Wang et al., 2009; Cain et al., 2018; Hieda, 2019). Mammals have six genes encoding a variety of KASH domain proteins, with further complexity generated by alternative splicing (Zhang et al., 2001; Potter & Hodzic, 2018). Mutations in *SYNE1* and *SYNE2*, encoding nesprin 1 and 2, respectively, cause Emery-Dreifuss muscular dystrophy (Zhang et al., 2007; Heller et al., 2020). The nesprin KASH domain connects to the SUN domain proteins across the nuclear lumen. Mammals have two genes encoding SUN proteins, *SUN1* and *SUN2* (Dreger et al., 2001; Hodzic et al., 2004). SUN domain proteins interact with lamins, thereby linking the nucleoskeleton to the cytoskeleton. DNA sequence variation in *SUN1* and *SUN2* might modify muscular dystrophy severity (Meinke et al., 2014).

The goal of this study was to determine the effects of specific mutant lamins on the nuclear shape and nucleo-cytoskeletal coupling in muscle. To achieve this goal, we generated *Drosophila* models of *LMNA* muscular dystrophy possessing either wild-type or mutant *Lamin C* (*LamC*) transgenes. The *LamC* transgenic lines have similar genetic backgrounds, with the exception of the site of insertion of the P-element. *LamC* is an orthologue of human *LMNA* and the only A-type lamin encoded by the *Drosophila* genome. The *Drosophila* LamC protein shares a domain structure that includes 35% amino acid identity and 54% similarity with human lamin A/C. Like human *LMNA*, the expression of endogenous *LamC* is initiated upon cellular differentiation (Riemer et al., 1995). The transcriptional regulators that drive muscle cell differentiation are similar between *Drosophila* and humans (Tapscott et al., 1988; Maire et al., 2020). In both species, differentiated myoblasts fuse to form multinucleated muscle fibers that attach to tendon cells (Ovalle, 1987; Krimm et al., 2002; Schulman et al., 2015; Lemke & Schnorrer, 2018; Richier et al., 2018; Balakrishnan et al., 2021). Thus, much of muscle development and physiology is shared between the two species. Herein, we use the *Drosophila* larval body wall muscles as a proxy for human skeletal muscles. Larval body wall muscles are represented by over 300 individual muscle fibers that can easily be prepared as a muscle fillet (Ramachandran & Budnik, 2010). The use of larval body wall muscles allows for whole organism muscle function assays, cytological analyses, and fillets for *in situ* microharpooning assays to measure nuclear-cytoskeletal coupling and nuclear deformability.

Muscle-specific expression of mutant lamins in an otherwise wild-type *Drosophila* background caused dominant effects on muscle physiology and/or function. These *Drosophila* models of lamin-associated muscle disease revealed vast differences among the mutant lamins tested. Specific mutant lamins altered nuclear shape and succumbed to nuclear envelope deformation under force application. By contrast, other mutant lamins partially uncoupled the nucleus from the cytoskeleton. Interestingly, the domain of lamin affected did not correlate with the loss of

a particular nuclear defect, suggesting a complex structure/function relationship, potentially involving additional binding partners. Muscles expressing mutant lamins that caused uncoupling of the nucleus from the cytoskeleton showed a lack of microtubule nuclear caging. A lack of microtubule caging was also observed upon RNAi knockdown of *Msp300*, a *Drosophila* KASH domain protein. Taken together, these data suggest that specific residues within lamin alter nucleo-cytoskeletal coupling that is supported by Msp300. Furthermore, mutation-specific cellular defects suggest that different pathological mechanisms might lead to the common muscle atrophy associated with *LMNA* skeletal muscle disease.

Materials and methods

Drosophila stocks

Drosophila stocks were cultured in cornmeal/sucrose media at 25°C (Shaffer et al., 1994). To generate the *Lamin C* (*LamC*) transgenic lines, full length *LamC* (Gold Clone, accession number AY095046, Berkeley *Drosophila* Genome Project, available from the *Drosophila* Genomics Resource Center, Bloomington, IN) was cloned into the pUAST P-element transformation vector (Brand & Perrimon, 1993). This vector contains a minimal promoter downstream of five upstream activating sequences (UAS) that bind the yeast Gal4 transcriptional activator. Standard embryo injection procedures were used to generate the transgenic stocks in which the P-element was relatively randomly inserted within the genome (BestGene, Chino Hills). Eight to ten independent transgenic lines were established for each *LamC* construct. The site of insertion was mapped to a specific chromosome, and the transgenes were made homozygous. Insertions that were not homozygous viable were discarded. Western analysis was performed, and transgenes that expressed levels of LamC relative to that of the endogenous *LamC* gene were used for analysis. Muscle-specific expression was achieved by crossing the transgenic lines to the *C57* Gal4 driver stock that expresses the yeast Gal4 specifically in larval body wall muscles (Brand and Perrimon, 1993; Gorczyca et al., 2007). The resulting progeny express either wild-type or mutant *LamC* in their larval body wall muscles.

Viability assays

Genetic crosses were performed in plastic vials with standard medium, cultured at 25°C. Parental flies were removed after larvae were observed in the vials. Dead pupae and live flies were counted for approximately one and a half weeks after the parental adults were removed. Percent viability was calculated by dividing the number of live flies by the total number of live flies plus dead pupae. The total number of living adults plus dead pupae counted for each genotype ranged from 43 to 555. An ANOVA analysis was performed to determine statistical significance. Error bars shown represent 95% confidence interval analyses in GraphPad Prism using the Wilson/Brown method.

Microharpoon assay and analysis

Microharpoons were generated from borosilicate glass rods (Sutter; OD: 1.0 mm, ID: 0.78, 10 cm length) using a Sutter P-97 micropipette puller. The following parameters were used to achieve tip diameters of ≈1 μm and a suitable taper length: HEAT = 500; PULL = 250; VEL = 220; TIME = 200. *Drosophila* third instar larvae were dissected to expose their body wall muscles. Muscle fillets were secured with magnets on a custom-built, microscope-compatible dissection apparatus and submerged in muscle dissection buffer (128 mM NaCl; 5 mM Hepes, pH 7.4; 2 mM KCl; 35 mM sucrose) supplemented with the fluorescent DNA-binding dye Hoechst 33342 (2 μg/ml) to allow visualization of myonuclei.

The microharpoon assay was performed as previously described (Fedorchak & Lammerding, 2016; Lombardi et al., 2011b), with slight modifications to the pull parameters to accommodate the technique's use on semi-intact muscle preparations. The microharpoon was inserted into the cytoskeleton ~10–15 μm from the edge of the nucleus (based on crosshairs in the objective) and pulled 30 μm in the direction away from the nucleus at a rate of 2 μm/s using custom MATLAB software to control the motorized micromanipulator (Eppendorf InjectMan NI2). The pull direction was along the long axis of the myofiber and away from the nucleus. Images were acquired at ×32 magnification (×20 objective with ×1.6 Optivar) every five seconds.

Nucleo-cytoskeletal connectivity was assessed using a custom MATLAB program (MATLAB 2010, Natick, MA) available upon request. For each nucleus, the user first selected a binary threshold value from a histogram of "pixel count versus intensity" to account for heterogeneity in the Hoechst 33342 signal, which the program thresholds to provide an accurate trace of the nucleus during deformation. After applying erosion and dilation processing steps to smooth the thresholded nucleus, the program uses the MATLAB "regionprops" function to track the centroid of the nucleus, generate a nuclear bounding box, and extract the necessary parameters to fit an ellipse to the nucleus. Changes in nuclear strain, centroid displacement, and additional parameters were computed. For most calculations, the frame prior to micropipette harpoon removal (frame of maximum pull) was compared with the first frame before the initiation of the pull. Myonuclei were excluded from analysis if 1) the myofiber was at an angle > ±30° from the vertical axis, 2) the micropipette harpoon was not inserted at the proper distance (≈10–15 μm) from the nuclear envelope, 3) the microharpoon failed to enter the cytoplasm and instead brushed over the top of the fiber, and

4) the myofiber retracted during or after the micropipette harpoon pull.

Immunohistochemistry

Third instar larval body wall muscle dissections were performed according to published procedures (Budnik et al., 1990). After fixation in 4% paraformaldehyde, preparations were stored in 1X PBS. Muscle fillets were washed three times in 1X PBS for five minutes each wash. Muscle fillets were then washed three times in permeabilization buffer (1X PBS, 0.5% Triton-X-100, and 5 mM $MgCl_2$) for five minutes each wash. Preparations were stained with Texas Red®-X Phalloidin (1:400 dilution) in permeabilization buffer containing 0.5% boiled/filtered fish skin gelatin (G-7765, Sigma-Aldrich, St. Louis) and stained with either guinea pig anti-Msp300 antibodies (kind gift from T. Volk; 1:100 dilution), mouse anti-Klar-C (#9C10, Developmental Studies Hybridoma Bank University of Iowa, Iowa City 1:25 dilution), rat anti-Koi (kind gift from J.A. Fischer; either 1:20 or 1:50 dilution), mouse anti-α-tubulin (#12G10, Developmental Studies Hybridoma Bank University of Iowa, Iowa City; 1:200 dilution), and mouse anti-lamin C (1:200 dilution) or mouse anti-lamin Dm_0 (#ADL84.12; Developmental Studies Hybridoma Bank University of Iowa, Iowa City; 1:400 dilution). Nuclear pores were stained with MAb414 (ab24609, Abcam, Cambridge, United Kingdom; mouse monoclonal antibody, 1:2,000 dilution). Microscopy was performed using either a Leica DMLB phase contrast fluorescence microscope and a Zeiss 710 confocal microscope or a Leica Thunder fluorescence microscope. Three channel images were merged to produce composite images using ImageJ.

Quantification of the cytoplasmic and nuclear immunofluorescent signal was performed using the integration intensity feature of Fiji (Schindelin et al., 2012). Briefly, nuclei were selected as regions of interest (ROI) using the cell counting function. Muscle fibers were visualized by phalloidin staining and outlined using the trace tool. Nuclear staining was quantified using the integrative intensity feature. A cytoplasmic signal was quantified by subtracting the integrative intensity of the nuclei from the total signal intensity. The correction factor was calculated by drawing a circle in an area lacking muscle and measuring the integrated intensity. This measurement was divided by the area of the circle to yield the correction factor. The background signal was determined by multiplying the area of the ROI by the correction factor, then subtracting this value from the raw integrated intensity values.

Quantification of perinuclear microtubular staining was performed visually by three individuals blinded to the genotype of the larvae. The final number of nuclei assigned to each phenotype represents the average of the three measurements. Each phenotype is represented as a percent of the total nucleus score.

Larval motility assays

Quantitative measurements of larval velocity (mm/min) were made for the host stock (w^{1118}) and larvae expressing either wild-type or mutant *LamC* in larval body wall muscles *via* the *C57* Gal4 driver (Gorczyca, 2007; Brand, 1993). Motility was also quantified for larvae with body wall muscle-specific expression of either *luciferase* RNAi or an RNAi transgene against a LINC complex component. For motility assays, third instar larvae were placed on a room temperature 1.8% agarose-filled 15-cm Petri dish for ten minutes to allow adjustment to a new substrate. Following, five larvae were placed in the center of a second 1.8% agarose-filled Petri dish marked with concentric circles. Their crawling was videotaped for 2 minutes using a cell phone. Also, the videos were analyzed using wrMTack, a plug-in for ImageJ (Brooks et al., 2016). A calibration line was drawn from the first concentric circle to the second using the "line tool" to produce the calibration length value. The path crawled by each larva was traced by generating a Z-project using the max intensity function in ImageJ. Distances traveled were measured by tracing larval paths with the segmented line drawing tool. Distances were divided by the calibration length value, resulting in the distance in millimeters. Velocities were calculated by dividing the distance traveled by the recording time (120 s). Two groups of five larvae were measured per genotype. The resulting values were plotted using GraphPad Prism (GraphPad Prism version 8.0.0 for Mac, GraphPad Software, San Diego, California, United States), and velocities were compared to those of the wild type using a one-way ANOVA with Holm-Sidak's correction.

Statistics

Groups of datasets were analyzed using a one-way analysis of variance (ANOVA). Comparisons between two datasets that showed a normal distribution were analyzed using the Student's *t*-test. Excel (16051.14931.20132.0, Microsoft, Seattle) and GraphPad Prism (v.8.0.0 for Mac, GraphPad Software, San Diego) were used to generate graphs and perform statistical analyses. Error bars in graphs represent means ± standard deviation (SD) unless otherwise noted. All results reported were derived from a minimum of three independent biological samples.

Results

Drosophila larval body wall muscle-specific expression of mutant lamins caused premature death

We modeled eight *LMNA* mutations in *Drosophila LamC* that were selected based on their causality in human disease (Figure 1A; Table 1). These mutations altered amino acids in all three lamin

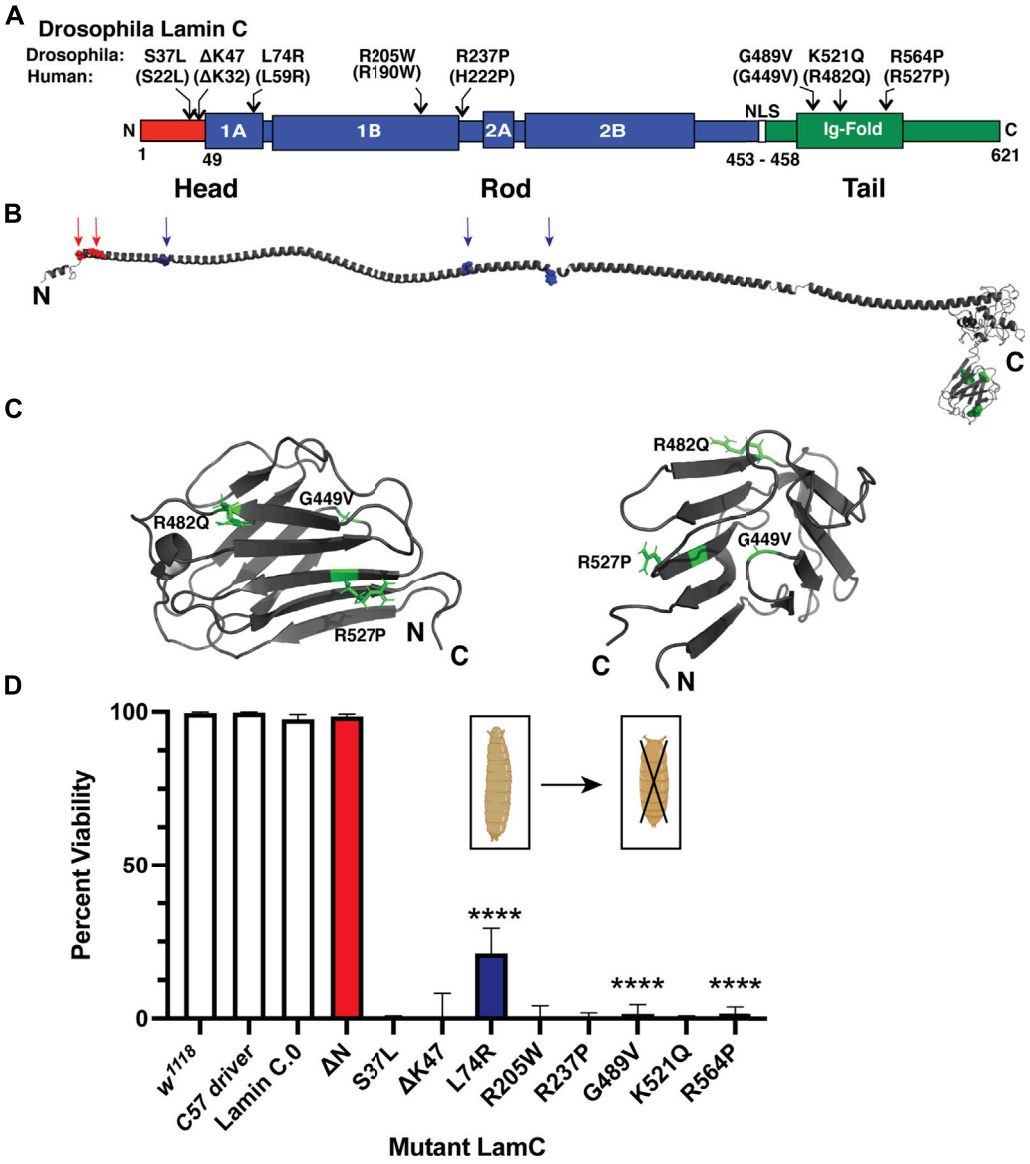

FIGURE 1
Muscle-specific expression of mutant *LamC* causes premature death. **(A)** Diagram of the *Drosophila* LamC domain structure with the head (red), rod (blue), and tail (green) domains indicated. The positions of the amino acid changes examined in this study are shown with the corresponding human amino acid changes in parentheses. **(B)** Three-dimensional model of full-length human lamin A (Hinz et al., 2021) with the position of the amino acid changes in the head and rod domain indicated by arrows. The positions of amino acid changes in the Ig fold are indicated in the magnified view (panel C). **(C)** Enlarged views of the three-dimensional lamin A/C Ig-fold domain based on an NMR structure (PBD 1IVT) (Krimm et al., 2002) with the amino acid substitutions examined here labeled. **(D)** Larvae with body wall muscle-specific expression of wild-type and mutant *LamC* were allowed to develop and scored for adult viability. Percent viability was calculated by dividing the number of live adults by the total number of offspring (adult flies plus dead pupae). The X-axis shows the genotype, and the Y-axis shows the percent viability. Larvae expressing *LamC* S37L, ΔK47, R205W, R237P, and K521Q yielded no surviving adults. Larvae expressing *LamC* L74R, G489V, and R564P had a significant reduction in survivability to adulthood. Colors correspond to the protein domain where the amino acid change is located: head (red), rod (blue), and tail (green). Fisher's exact test was used to compare values for the mutants versus the wild-type control. Total progeny scored per genotype ranged from 43 to 555. Error bars represent 95% confidence intervals. ****, $p \leq 0.0001$. Bio-icons in panel D were created with BioRender.com.

protein domains. Some of the amino acid changes affected amino acids that are identical between human lamin A/C and *Drosophila* LamC (S37L, K47, L74, R205, and R237), while others are represented by conservative substitutions (R237 and K521).

The amino acid changes under investigation were mapped onto the three-dimensional structure of lamin A/C that is based on a combination of experimental data and *in silico* predictions (Figure 1B) (Krimm et al., 2002; Strelkov et al., 2004; Lilina et al.,

TABLE 1 Lamin A/C amino acid changes examined in this study.

Human a.a. change	Drosophila a.a. change	Domain	Muscular phenotype	Reference
ΔN	ΔN	Head	AD-EDMD	Walter et al. (2005)
S22L	S37L	Head	DCM	Pethig et al. (2005)
ΔK32	ΔK47	Head	AD-EDMD and dropped head syndrome	Muchir et al. (2004) and D'Amico et al. (2005)
L59R	K74R	Rod	DCM	McPherson (2009)
R190W	R205W	Rod	DCM	Pethig et al. (2005), Arbustini et al. (2002), Hermida-Prieto et al. (2004), Sylvius et al. (2005), and Song et al. (2007)
H222P	R237P	Rod	EDMD	Bonne et al. (2000)
G449V	G489V	Tail	Striated muscle laminopathy	Dialynas et al. (2010)
R482Q	K521Q	Tail	AR-EDMD	Wiltshire et al. (2013)
R527P	R564P	Tail	AD-EDMD	Bonne et al. (1999) and Brown et al. (2001)

2020; Hinz et al., 2021). The amino acid residues S22 and K32 map within a short-predicted alpha-helical region of the head domain (Figure 1B). The amino acid residues L59, R190, and H22 map within the long alpha-helical regions of the rod domain ("coiled coil"). The amino acid residue G449V maps to a loop region within the Ig fold (Figure 1C). By contrast, amino acid residues R482 and R527 map to β-sheets in the Ig fold (Figure 1C). Thus, by testing this set of amino acid changes, we are surveying all three conserved lamin domains.

To determine the effects of these mutant lamins on the physical properties of myonuclei, we expressed the mutant lamins in *Drosophila* larval body wall muscles using the tissue-specific Gal4/UAS system (Caygill & Brand, 2016). The *C57* Gal4 driver stock expresses the Gal4 transcription factor in larval body wall muscles throughout larval development (Brand & Perrimon, 1993; Gorczyca et al., 2007). These flies were crossed with flies expressing either wild-type or mutant *LamC* transgenes. Larvae with body wall muscle-specific expression of wild-type *LamC* developed normally; they crawled up the vial wall, underwent metamorphosis to pupae, and emerged as adults with no apparent defects. By contrast, larvae with body wall-specific expression of mutant *LamC* exhibited difficulties crawling up the vial wall and died during the late pupal stage. Death at this stage is consistent with loss of larval body wall muscle function, which is required for morphogenesis (Fortier et al., 2003; Dialynas et al., 2010). To quantify the effects of the mutant lamins on viability, the fraction of viable adults was calculated by dividing the number of live adult flies by the number of total progeny (live plus dead pupae). A small percentage of viable adults resulted from the expression of LamC L74R, G489V, and R564P (Figure 1D). However, no adult progeny resulted upon expression of LamC S37L, ΔK47, R205W, R237P, and K521Q (Figure 1D). Western analysis of protein extracted from larval carcasses (mostly body wall muscle) revealed that the lethality was caused by the mutant LamC, not by general over-expression of LamC. LamC levels were similar in all genotypes, except for R564P, which had high variable expression among biological replicates (Supplementary Figures S1A, B). Thus, amino acid substitutions in all three lamin domains cause lethality at the pupal stage.

Specific mutant lamins cause nuclear envelope protein mislocalization

To investigate the cause of lethality due to mutant versions of LamC at the cellular level, immunohistochemistry was performed on larval body wall muscles. Muscles expressing either wild-type or mutant *LamC* transgenes were stained with antibodies against LamC, lamin Dm_0 (the only B-type lamin in *Drosophila*), and FG-repeat containing nuclear pore proteins. Antibody staining showed that wild-type LamC localization was confined to the nucleus, particularly the nuclear envelope, as observed for the host stock w^{1118} (Figure 2; Supplementary Figure S2). Myonuclei expressing LamC R205W were abnormally shaped, with LamC confined to the nucleus; however, nuclear aggregates were also apparent (Figure 2; Supplementary Figure S2). By contrast, myonuclei expressing LamC S37L, L74R, G489V, K521Q, and R564P had a spherical nuclear shape and showed cytoplasmic aggregation of LamC. Thus, the mutant lamins exhibited a range of abnormal cellular localization patterns that did not correlate with the domain of lamin affected.

In humans, A- and B-type lamins form independent networks underlying the inner nuclear envelope (Shimi et al., 2015). To determine if the mutant LamC proteins perturbed the distribution of the *Drosophila* B-type lamin, lamin Dm_0, larval body wall muscles expressing either wild-type or mutant *LamC* transgenes were stained with antibodies specific to lamin Dm_0. Neither expression of wild-type LamC nor mutant LamC perturbed the localization of lamin Dm_0 at the nuclear envelope (Supplementary Figure S3). These data strongly

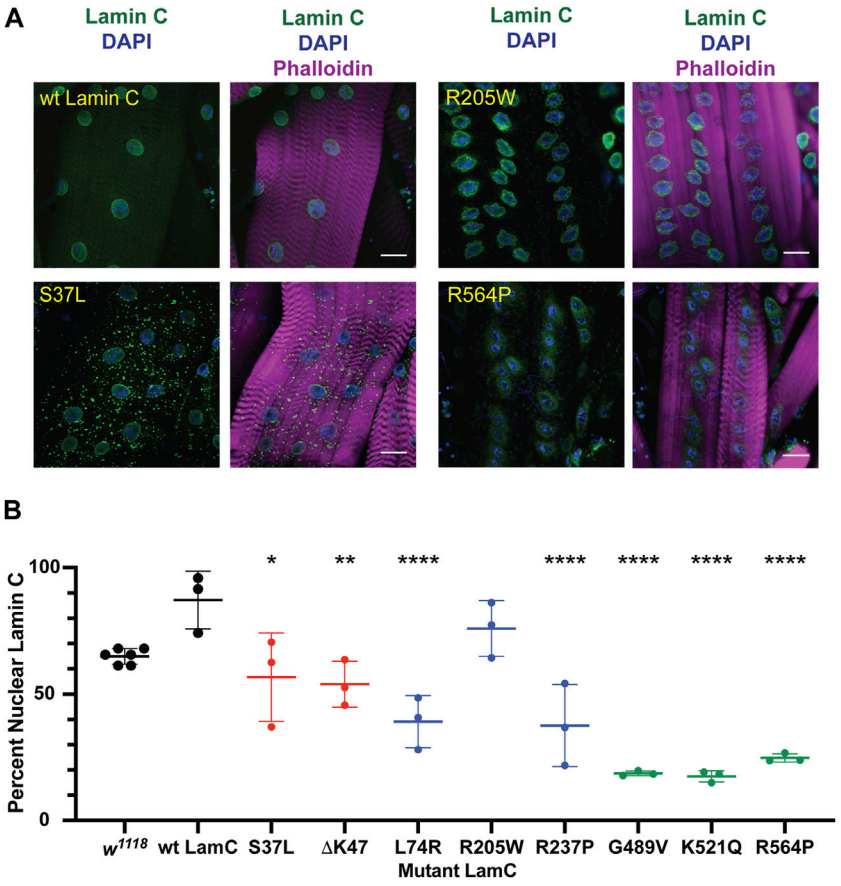

FIGURE 2
Muscle-specific expression of mutant *LamC* causes cytoplasmic lamin aggregation. (**A**) Third instar larval body wall muscles expressing either wild-type or mutant LamC were dissected and stained with antibodies to LamC (green), phalloidin (magenta), and DAPI (blue). Representative images for an amino acid substitution in each of the three LamC domains are shown. Images of muscle expressing all of the amino acid changes examined here are shown in Supplementary Figure S2. Scale bar: 30 μm. (**B**) Percentage of nuclear LamC was quantified by measuring the intensity of nuclear LamC antibody staining divided by the total amount of staining in the muscle cell (i.e., nuclear plus cytoplasmic LamC) and multiplying by 100. Three to six muscle fibers containing five to 29 nuclei from two to three larvae were analyzed. Each data point represents the average percent nuclear signal in a muscle fiber. The mean and standard deviation of the values obtained for muscle fibers of each genotype are shown. A one-way ANOVA analysis was used to determine statistical significance. *, $p \leq 0.05$; **, $p \leq 0.01$; ***, ≤0.001; ****, $p \leq 0.0001$.

suggest that the two lamin types form independent networks in *Drosophila*, like in humans, and that mutant LamC does not overtly interfere with lamin Dm_0 organization.

Lamins interact with many different proteins in the nucleus, including those that make up nuclear pores (NUPs) (Wilson & Foisner, 2010; Kittisopikul et al., 2021). To determine if the mutant lamins altered the localization of nuclear pore proteins, larval body wall muscles expressing either wild-type or mutant *LamC* transgenes were stained with antibodies to FG-repeat-containing NUPs. As anticipated, muscles expressing wild-type *LamC* showed punctate anti-NUP staining at the nuclear envelope (Figure 3; Supplementary Figure S4). In contrast, in muscles expressing LamC ΔK47, the anti-NUP staining was distributed unevenly around the nuclear envelope (Supplementary Figure S4). Perhaps this reflects the involvement of lamins in the proper spacing of nuclear pores (Furukawa et al., 2009; Kittisopikul et al., 2021). Intriguingly, in muscles expressing LamC R205W, R237P, G489V, K521Q, and R564P, the NUPs mislocalized to the cytoplasm (Figure 3; Supplementary Figure S4). Mislocalization may cause depletion of the NUPs in the envelope, affecting nuclear–cytoplasmic transport. In addition, cytoplasmic aggregation of NUPs could be toxic to cytoplasmic events such as intracellular signaling and maintenance of redox homeostasis (Rajasekaran et al., 2007; Chivet et al., 2020; Bobylev et al., 2021; Coombs et al., 2021; Potulska-Chromik et al., 2021). Thus, the mutant lamins had differing effects on NUP localization with several residues in the rod and Ig-like fold domains implicated in proper NUP formation. Substitution at these residues caused NUP cytoplasmic aggregation, suggesting

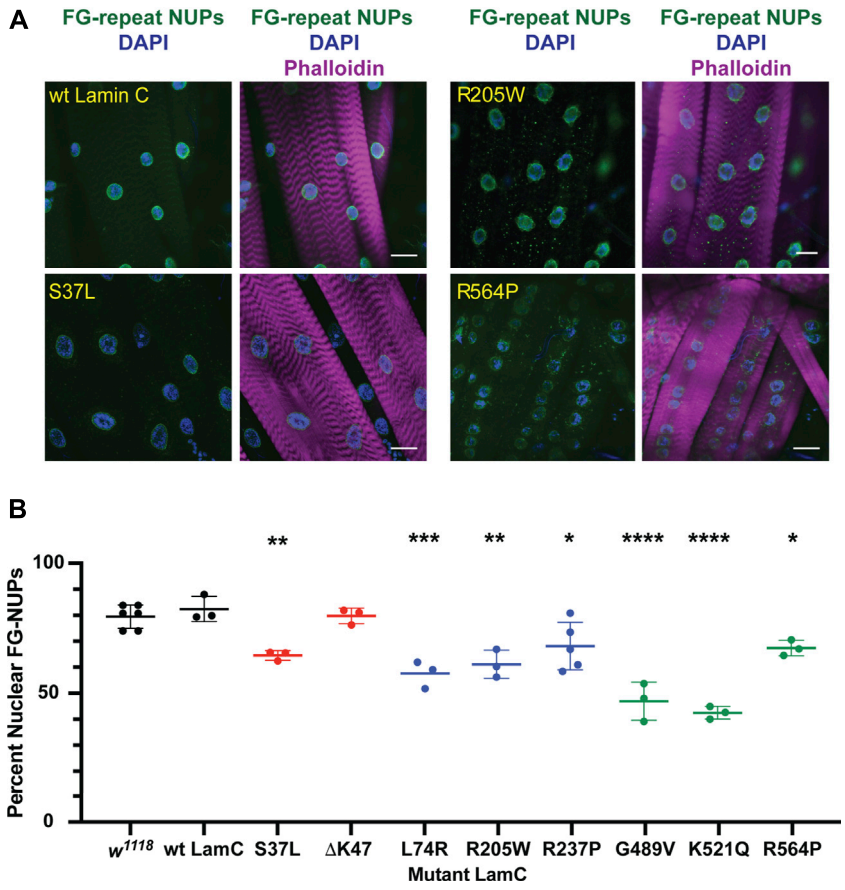

FIGURE 3
Mutant *LamC* alters the localization of FG-containing nuclear pore proteins. **(A)** Third instar larval body wall muscles expressing wild-type or mutant LamC were dissected and stained with antibodies to FG-repeat-containing nuclear pore proteins (NUPs) (green), phalloidin (magenta), and DAPI (blue). Representative images for an amino acid substitution in each of the three LamC domains are shown. Results from all amino acid changes studied in this manuscript are shown in Supplementary Figure S4. Scale bar: 30 μm. **(B)** Percent of nuclear NUP staining was quantified by measuring the intensity of the nuclear FG-repeat antibody staining divided by the total amount of staining (nuclear plus cytoplasmic), then multiplying by 100. Three to six muscle fibers containing three to 28 nuclei from two to three larvae were analyzed. Each data point represents the average percent nuclear signal in a muscle fiber. The mean and standard deviation of the values obtained for muscle fibers of each genotype are shown. A one-way ANOVA analysis was used to determine statistical significance. *, $p \leq 0.05$; **, $p \leq 0.01$; ***, ≤0.001; ****, $p \leq 0.0001$.

the formation of an abnormal A-type lamin meshwork does not support proper assembly or maintenance of the NUPs.

Specific mutant lamins cause nucleo-cytoskeletal uncoupling and nuclear deformation

To understand the functional consequences of the mutant lamins on the mechanical properties of myonuclei, we employed a novel application of a microharpooning assay. This assay allows for quantitative assessment of nucleo-cytoskeletal coupling and nuclear deformation under local force application to the perinuclear cytoskeleton (Maniotis et al., 1997; Lombardi et al., 2011a; Fedorchak & Lammerding, 2016). The assay uses a fine-tipped glass needle to "harpoon" the cytoskeleton at a defined position near the nucleus and then applies a precisely defined displacement while monitoring induced nuclear displacement and deformation *via* real-time fluorescence microscopy imaging. The application described here was the first use of this technique on living, multinucleated muscle fibers *in situ*. For standard preparation of the larval body wall muscle, a longitudinal cut is made at the ventral midline of the larvae, organs are removed, and the remaining tissue, termed a muscle fillet, represents body wall muscles, attached to tendon cells adhered to the hypodermis (Carayon et al., 2020).

For our studies, larval body wall muscles were dissected, immobilized on a glass slide (Figure 4A), and harpooned in a physiological buffer while mounted on a microscope. A fine-tipped glass needle attached to a computer-controlled

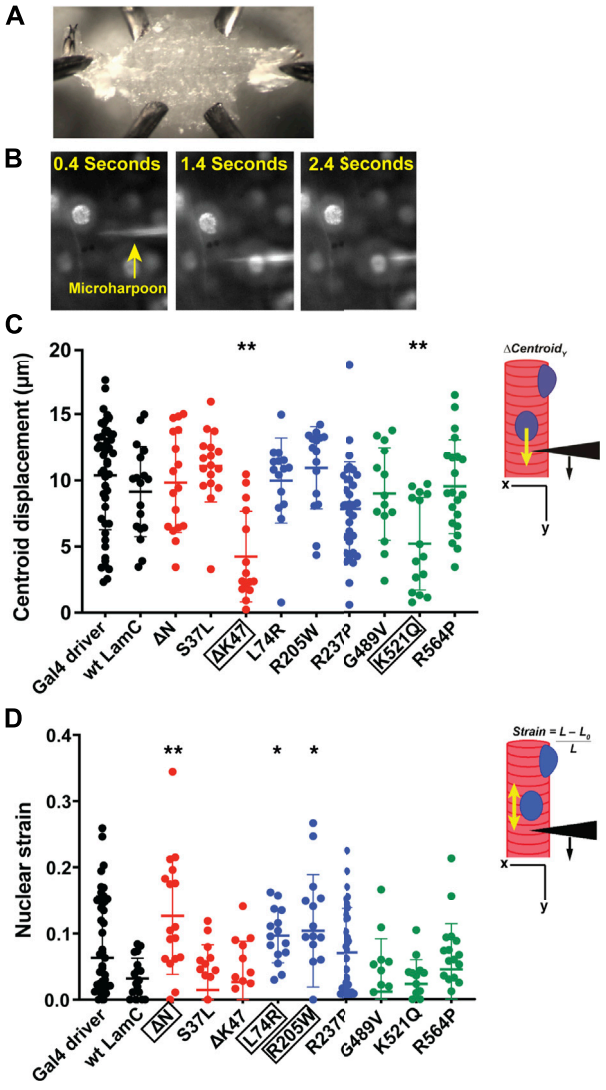

FIGURE 4
Specific mutant lamins reduce nucleoskeletal-cytoskeletal coupling and increase nuclear deformation. Body wall muscles from larvae expressing either wild-type or mutant LamC were dissected and maintained in a physiological buffer. **(A)** Representative semi-intact larval body wall muscle fillet is shown. Such muscle fillets were used for micropipette harpooning assays to measure physical coupling between the nucleus and cytoplasm and nuclear strain. **(B)** Representative time-lapse images from a video of microharpooning wild-type muscles. Images shown were taken at 0.4, 1.4, and 2.4 s from the video recording. **(C)** Inset diagram shows the experimental approach with the black arrowhead representing a micropipette, the black arrow indicating the direction of force application, and the yellow arrow representing the movement of the center point of the nucleus, centroid displacement, which is a change in position in the y-direction. Expression of wild-type LamC did not alter centroid displacement compared to that of the Gal4 driver control. In contrast, centroid displacement was reduced for larvae expressing LamC ΔK47 and K521Q, indicating a loss of nucleoskeleton-cytoskeleton coupling. Colors correspond to the domains in which each amino acid change is located: head (red), rod (blue), and tail (green). An ANOVA analysis was used to determine statistical significance among the genotypes. Boxed amino acids

(*Continued*)

FIGURE 4
are those with statistical differences; 15–48 nuclei were analyzed per genotype. *, $p \leq 0.05$; **; $p \leq 0.01$. **(D)** Inset diagram shows the experimental approach with the black arrowhead representing a micropipette needle, the black arrow indicating the direction of force application, and the yellow double-headed arrow representing the measured change in nuclear deformation. Nuclear strain is measured as the length of the nucleus at the end of the force application minus the length of the nucleus upon initial force application divided by the initial length of the nucleus. Expression of wild-type LamC did not alter nuclear strain compared to that of the Gal4 driver-only control. In contrast, muscles expressing LamC ΔN, L74R, and R205W showed increased nuclear strain compared to the controls. An ANOVA analysis was used to determine statistical significance. Boxed amino acids are those with statistical differences; 15–48 nuclei were analyzed per genotype. *, $p \leq 0.05$; **, $p \leq 0.01$.

micromanipulator was inserted 10–15 µm from the edge of a nucleus and pulled 30 µm at a rate of 2 µm/s. The direction of pull was along the long axis of the muscle fiber and away from the nucleus. Images were captured by time-lapse microscopy for five seconds (Figure 4B; Supplementary Videos S1–S4). From the recorded videos, two types of subcellular mechanical measurements were taken. First, the distance the center of the nucleus was displaced from its original position upon force application by the microharpoon ("nuclear centroid displacement") served as a quantitative measurement of nucleo-cytoskeletal coupling (Figure 4C). Defects in nucleo-cytoskeletal coupling are expected to result in reduced nuclear centroid displacement (Lombardi et al., 2011b). Second, the extent of nuclear elongation upon force application, normalized to the initial length of the nucleus ("nuclear strain"), served as a quantitative measurement of nuclear deformability (Figure 4D). Relative to the controls, only muscles expressing LamC ΔK47 and K521Q showed a significant decrease in nuclear centroid displacement (Figure 4C), suggesting that these mutant lamins partially uncoupled the nucleus from the cytoskeleton. Compared to controls, only LamC ΔN, L74R, and R205W showed significantly increased nuclear deformation (Figure 4D), suggesting reduced nuclear mechanical stability. We recognize that nuclear deformation in the microharpoon assay can also be influenced by the transmitted force, so an increase in nuclear deformation could also result from increased force transmission to the nucleus, but the more likely explanation appears to be an increase in nuclear deformability. Surprisingly, some mutant lamins (S37L, R237P, G489V, and R564P) had no apparent effect on either nuclear-cytoskeletal coupling or nuclear deformability (Figure 4D). Such findings suggest that these mutants might cause defects unrelated to the mechanical properties of the nucleus such as genome organization. Collectively, these data show that mutant lamins have distinct effects on the physical properties of the nucleus regardless of the lamin domain affected.

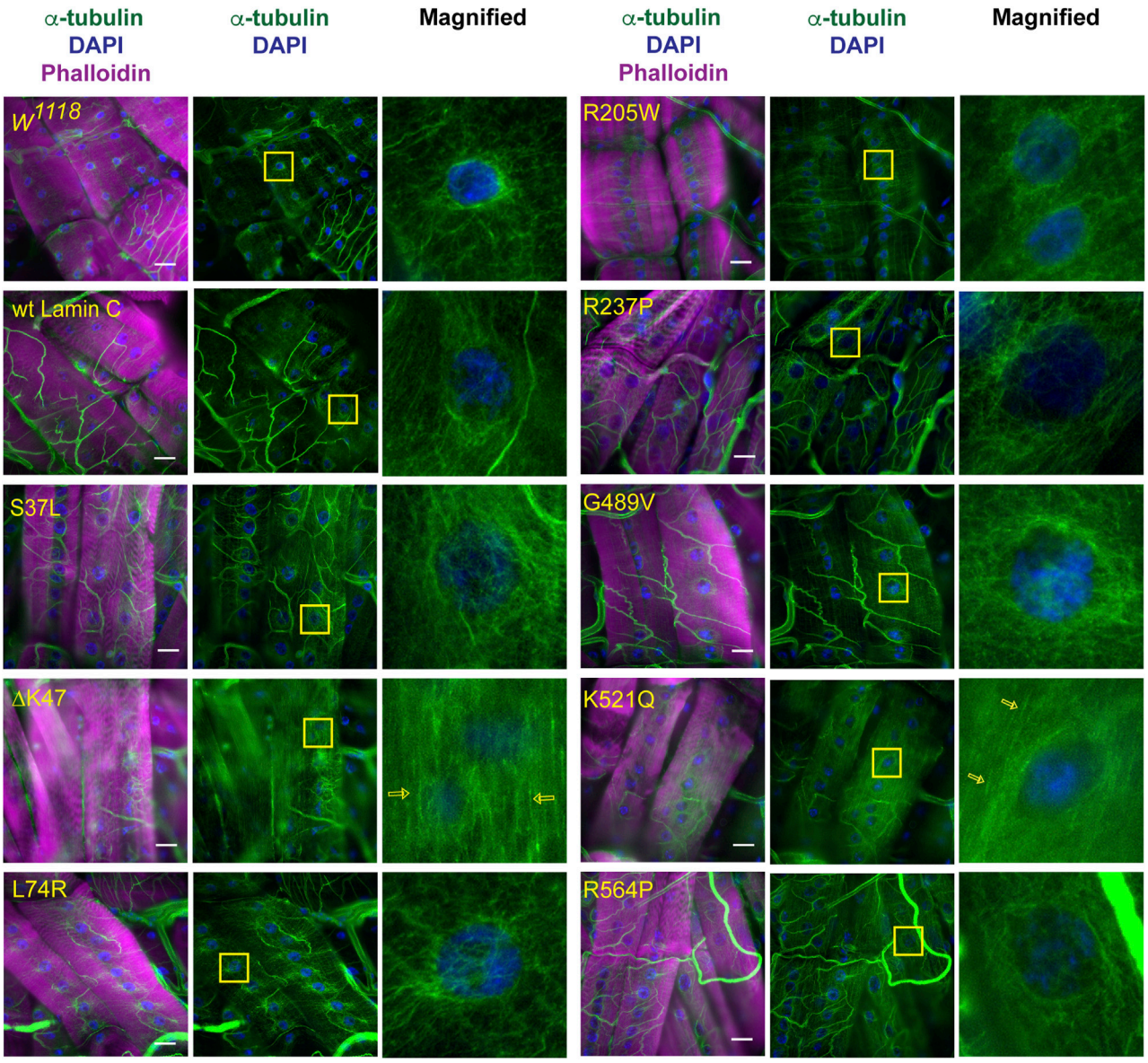

FIGURE 5
Specific mutant lamins cause loss of microtubular caging around the nucleus. Third instar larval body wall muscles expressing either wild-type or mutant LamC were stained with antibodies to α-tubulin (green and white in magnified images), phalloidin (magenta), and DAPI (blue). In wild-type muscle, α-tubulin forms a cage around the nucleus as observed for the host stock w^{1118} and muscles expressing wild-type LamC. Expression of the majority of mutant lamins did not alter the α-tubulin nuclear cage. However, the cage was not apparent in muscles expressing mutant LamC ΔK47 and K521Q. In these cases, the microtubules were arrayed parallel to the length of the muscle fiber (open yellow arrows). Yellow boxes indicate the area magnified in the right panels. Scale Bar: 30 μm.

Mutant lamins that reduce nucleo-cytoskeletal coupling exhibit loss of myonuclear microtubule caging

Given the lack of an apparent correlation between nuclear mechanical defects and nuclear envelope protein localization, we examined perinuclear cytoskeletal organization as a potential factor. Based on the muscle staining of phalloidin, which binds actin (Supplementary Figures S2–S4), and anti-alpha-actinin, which crosslinks actin (Supplementary Figure S5), no overt muscle-wide defects in actin organization were apparent in the muscles expressing mutant LamC at the light microscope level; however, they could be present. Other typical components of the cytoskeleton include cytoplasmic intermediate filaments

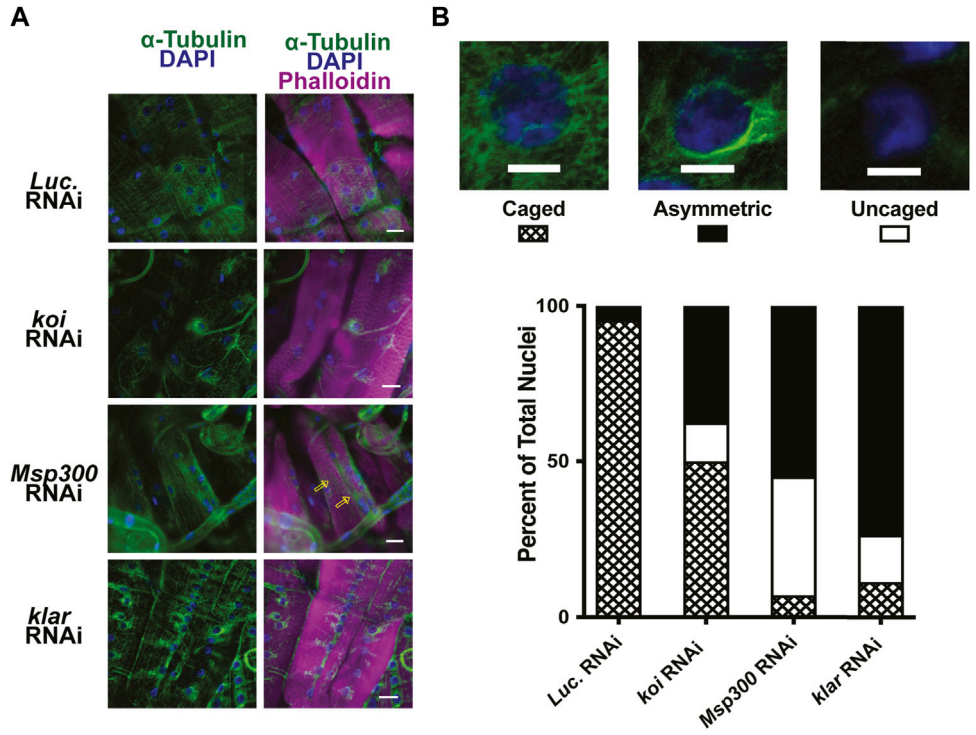

FIGURE 6
RNAi against LINC complex components disrupts perinuclear microtubule organization. **(A)** Immunohistochemistry was performed on third instar larval body wall muscles expressing either RNAi against *Luciferase* (control) or LINC complex components using antibodies to α-tubulin (green), phalloidin (magenta), and DAPI (blue). Open yellow arrows indicate microtubules that run parallel with the long axis of the muscle fiber, giving rise to uncaged nuclei. **(B)** Representative patterns of microtubule organization around the nucleus are shown at the top. Scale Bar: 10 mm. The graph represents the percentage of nuclei showing each pattern of localization per genotype. Muscles expressing an RNAi against *Luciferase* (*luc*) show nearly 100% caged nuclei. In contrast, RNAi knockdown of each of the LINC complex members shows increased numbers of asymmetric and uncaged nuclei. A range of 32–79 nuclei were scored per genotype. Scale Bar: 30 μm.

and microtubules. However, the *Drosophila* genome does not contain genes encoding the standard cytoplasmic intermediate filaments such as desmin and vimentin (Herrmann & Strelkov, 2011; Cho et al., 2016). Therefore, we stained with antibodies to α-tubulin, which revealed striking differences among the mutant lamins in perinuclear microtubule organization. In larval body wall muscles expressing wild-type *LamC*, microtubules form a cage around the nucleus like that observed for the host stock (Figure 5). Similar microtubule cages have also been observed in mammalian cells (Bruusgaard et al., 2006; Earle et al., 2020). The α-tubulin staining pattern of muscles expressing LamC S37L, L74R, R205W, R237P, G489V, and R564P gave similar results to that of the wild type (Figure 5). By contrast, α-tubulin staining of muscles expressing LamC ΔK47 and K521Q showed a loss of microtubule caging around the nucleus. Instead, the microtubules were aligned orthogonal to the long axis of the muscle fiber and did not show any enrichment at the nucleus (Figure 5). Interestingly, the lack of myonuclear microtubule caging was only observed for the two mutants that eliminated nucleo-cytoskeletal coupling and not in the other mutants that had normal nucleo-cytoskeletal force transmission. This suggests that microtubules are critical components for the nucleo-cytoskeletal coupling in *Drosophila* larval body wall muscles. This idea is supported by the fact that the mutant versions of LamC that cause loss of nuclear microtubule caging also exhibit larval motility defects (Supplementary Figure S6).

RNAi knockdown of the LINC complex component Msp300 recapitulates the loss of nuclear microtubule caging

Nesprins are components of the LINC complex and have been shown in some cases to interact with microtubules (Chang et al., 2015; Starr, 2017; Maurer & Lammerding, 2019). The *Drosophila* LINC complex consists of a single SUN domain protein Klaroid (Koi), encoding the SUN domain protein, and either Msp300 or Klarischt (Klar) as the KASH domain proteins (Yu et al., 2006; Kracklauer et al., 2007; Technau & Roth, 2008; Xie & Fischer, 2008). To assay

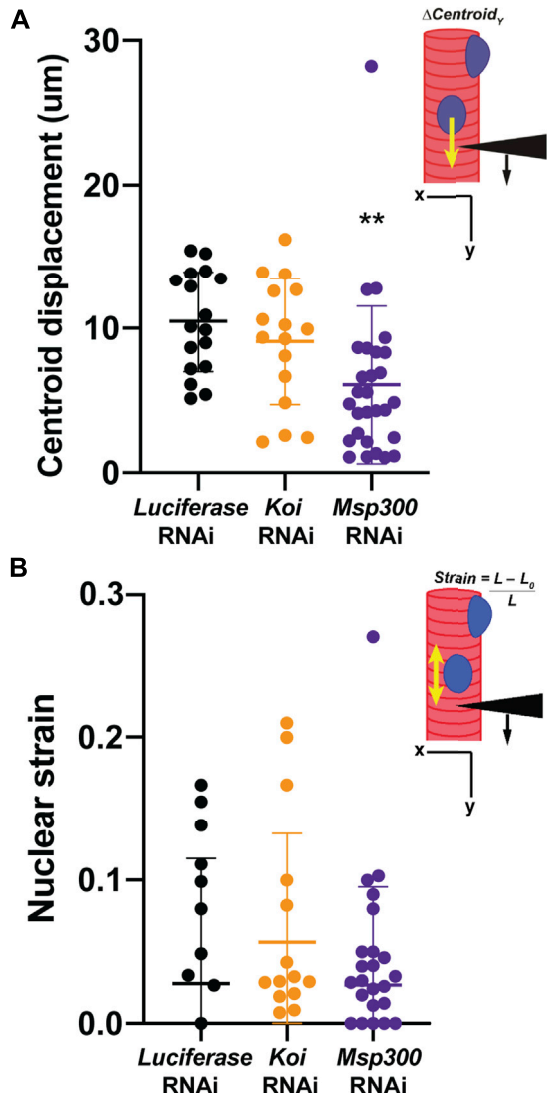

FIGURE 7
Muscle-specific RNAi against *Msp300* causes loss of nucleoskeletal-cytoskeletal coupling. The micropipette harpooning assay was performed on larval body wall muscles expressing an RNAi transgene against either *Luciferase* (as a control) or a LINC complex component. **(A)** Inset diagram shows the experimental approach with the black arrowhead representing a micropipette, the black arrow indicating the direction of force application, and the yellow arrow representing the movement of the center point of the nucleus, centroid displacement, which is a change in position in the Y-direction. RNAi against *Msp300* reduced centroid displacement relative to the *Luciferase* RNAi control, suggesting impaired force transmission between the cytoskeleton and nucleus. In contrast, RNAi against *Koi* produced no change in nuclear centroid displacement relative to the control. A one-way ANOVA was used to determine statistical significance; 16–28 nuclei were analyzed per genotype. **, $p \leq 0.01$ **(B)** Inset diagram shows the experimental approach with the black arrowhead representing a micropipette needle, the black arrow indicating the direction of force application, and the yellow double-headed arrow representing the measured change in nuclear deformation. Nuclear strain is measured as the length of the nucleus at the end of the force application minus the length of the nucleus upon the initial force application divided by the length
(*Continued*)

FIGURE 7
at the end of the force application. RNAi knockdown of the LINC complex components did not alter nuclear strain, indicating that LINC complex disruption did not change nuclear stiffness. A one-way ANOVA was used to determine statistical significance. No statistically significant changes among genotypes were observed; 16–28 nuclei were analyzed per genotype.

for the involvement of the LINC complex in perinuclear microtubule organization in *Drosophila* larval body wall muscles, we used RNAi transgenes to deplete each of the LINC complex components separately in larval body wall muscles. Effective depletion of each protein was confirmed by immunofluorescence, with RNAi targeting *luciferase* as a negative control (Supplementary Figure S7). Larval body wall muscles typically show nuclear microtubule caging (Figure 5). In muscles expressing the *luciferase* RNAi control, more than 90% of the myonuclei had the expected microtubule caging (Figures 6A, B). By contrast, larval body wall muscles with depletion of LINC complex components showed a range of myonuclear phenotypes (Figure 6B). Some myonuclei displayed an asymmetrical arrangement of microtubules, with enrichment of microtubules on one side of the nucleus. Other myonuclei completely lacked microtubule caging. Msp300 depletion produced the greatest number of myonuclei that lacked microtubule caging compared to the other genotypes. In the Msp300 depleted cells, the microtubules were aligned orthogonal to the long axis of the muscle fiber, remarkably like the microtubule arrangement in muscles expressing LamC ΔK47 and K521Q (Figure 5). These findings suggest that Msp300 is a crucial link between lamins and perinuclear microtubules.

Given that depletion of Msp300 caused loss of microtubule caging, we hypothesized that this would lead to an uncoupling of the nucleus from the cytoskeleton like that observed in the LamC ΔK47 and K521Q. To test this hypothesis, we performed microharpooning on muscle fibers expressing either *luciferase*, *Klar*, or *Msp300* RNAi transgenes. The centroid displacement values obtained for muscles depleted for Klar were similar to those of the *luciferase* RNAi control (Figure 7A; Supplementary Videos S5–S7) and consistent with the normal nuclear microtubule caging observed in the Klar depleted muscle. By contrast, depletion of Msp300 caused a significant reduction in centroid displacement relative to that of the control, indicative of a partial loss of nucleo-cytoskeletal coupling (Figure 7A). Motility assays showed that depletion of Msp300 caused reduced larval motility, suggesting a functional significance for coupling between the nucleoskeleton and the cytoskeleton (Supplementary Figure S8). The *Msp300* RNAi transgene is predicted to reduce levels of all known Msp300 isoforms. Given recent findings on isoform-specific functions of Msp300, it is possible that loss of muscle function is due to

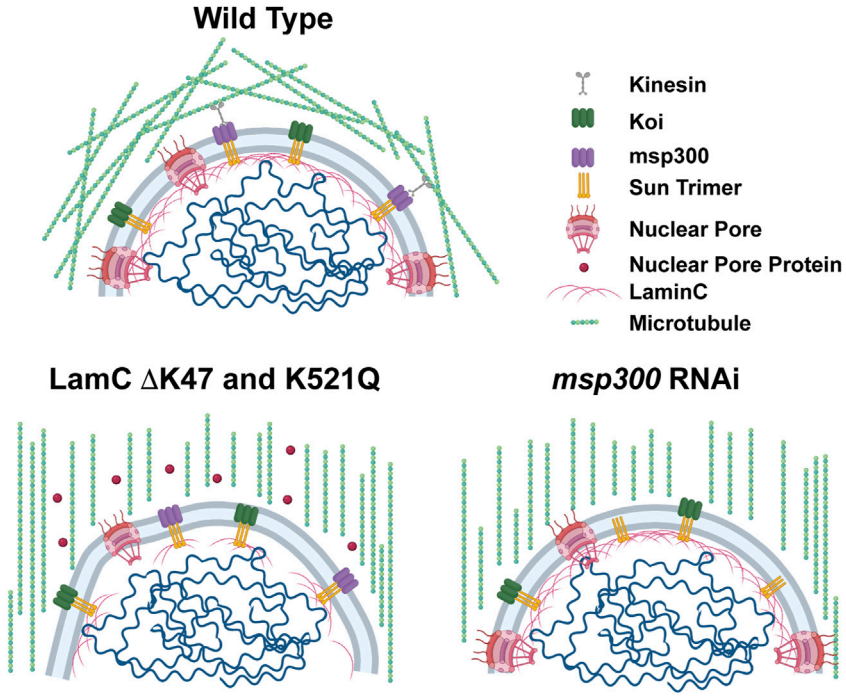

FIGURE 8
Models show microtubular organization in lamin mutant muscles with impaired nuclear-cytoskeletal connections. Diagram of wild-type muscles in which microtubules form a cage around the nucleus (top). The microtubule cage around the nucleus is reduced in larval body wall muscles expressing either LamC ΔK47 or K521Q (bottom). In these cases, the microtubules run parallel with the long axis of the muscle fiber. In addition, these two mutant lamins cause cytoplasmic mislocalization of nuclear pore proteins (red circles). The microtubule cage around the nucleus is also reduced upon RNAi knockdown of *Msp300*, a KASH-domain LINC complex component, and the microtubules run parallel to the long axis of the muscle fiber. Bio-icons in the model were created with BioRender.com.

altered Z disc structure and/or abnormal nuclear positioning (Rey et al., 2021).

Results from the microharpooning assays suggested that Msp300 depletion did not alter nuclear deformation similar to LamC ΔK47 and K521Q, the two mutant lamins that caused uncoupling of the nucleus and cytoskeleton (Figure 7B). Thus, the microharpooning assay functionally distinguished mutants that alter nuclear mechanics from those that do not. Taken together, our experiments indicate that depletion of Msp300 or expression of LamC ΔK47 and K521Q mutants causes impaired nucleo-cytoskeletal force transmission in *Drosophila* body wall muscles by disrupting the nuclear microtubule cage (Figures 5, 6 and 8), establishing an important role of the perinuclear microtubule network organized by Msp300 in transmitting cytoskeletal forces to the myonuclei.

Discussion

Mutations in *LMNA* cause a plethora of disease phenotypes including skeletal muscular dystrophy and dilated cardiomyopathy (Bonne et al., 1999; Bonne et al., 2000; Hermida-Prieto et al., 2004; Pethig et al., 2005) (Table 1). Individuals with the same *LMNA* mutation can exhibit dramatically different disease presentations and have clinically distinct diagnoses (Muchir et al., 2004; Porcu et al., 2021). This variability can even be observed in closely related family members, strongly implying that phenotypic variability is due to modifier genes. Herein, our goal was to examine muscle defects resulting from specific mutant lamins in a defined genetic background that allows for a direct comparison without the complication of genetic background modifiers. To accomplish this goal, we generated *Drosophila* models of *LMNA*-associated muscular dystrophy. In these models, the mutant lamins display dominant defects, as in human diseases (Worman, 2012). Our studies revealed that specific amino acid changes alter the mechanical functions of myonuclei (Figure 4). Some mutant lamins dramatically affected nuclear deformation, while others impaired nucleo-cytoskeletal coupling. Furthermore, some mutant lamins mislocalized and altered nuclear pore protein localization, while others did not. Collectively, these data demonstrate that the altered

phenotypes do not correlate with the domain of lamin affected and that different cellular defects can lead to common premature death in these *Drosophila* models.

Among our observations, we noted that five of the eight amino acid changes in lamin resulted in LamC cytoplasmic aggregation (Figure 2). It is interesting to note that mutant lamins that caused minimal cytoplasmic aggregation altered nuclear shape, a property largely determined by the lamin meshwork (Horn, 2014; Maurer & Lammerding, 2019). Cytoplasmic aggregation of proteins can lead to deleterious consequences for muscle function. Consistent with this idea, increasing rates of autophagy, which reduces cytoplasmic aggregates, suppressed muscle defects caused by mutant lamins in multiple model organisms (Park et al., 2009; Choi et al., 2012; Ramos et al., 2012; Liao et al., 2016; Chiarini et al., 2019; Coombs et al., 2021). In fact, *in silico* studies suggest that lamin aggregation might serve as a predictor of pathogenicity for *LMNA* variants of uncertain significance (Anderson et al., 2021). Seven of the eight amino acid changes in LamC resulted in cytoplasmic aggregation of FG-repeat NUPs (Figure 3). It is unclear if the NUPs are improperly inserted or ineffectively anchored in the nuclear envelope. Regardless, a reduction in functional NUPs is likely to affect nuclear–cytoplasmic transport of biomolecules, causing a myriad of defects. Consistent with the results presented here, FG-repeat NUPs were observed in the cytoplasm of human muscle biopsy tissue from *LMNA* skeletal muscular dystrophy patients, demonstrating clinical relevance (Dialynas et al., 2015).

Herein, we were able to directly assay the functional consequences of mutant lamins on nuclear deformability and nucleo-cytoskeletal coupling *via* a novel application of a microharpooning assay. Three of the mutant lamins (LamC ΔN, L74R, and R205W) showed increased nuclear deformation under force application (Figure 4). In prior studies using a different means of applying nuclear deformation, LamC ΔN was also found to be highly deformable, validating this novel application (Zwerger et al., 2013). Only two mutant lamins (LamC ΔK47 and K521Q) caused a loss of nucleo-cytoskeletal coupling (Figure 4). Surprisingly, these two mutants do not cause overt mislocalization of Koi and Msp300; however, protein–protein interactions could be perturbed by the mutant lamins without gross mislocalization (Supplementary Figure S9). Additionally, these two mutants did not appear to alter nuclear deformation, demonstrating that loss of physical properties needed for coupling is not necessarily required for maintaining nuclear shape upon force application. However, we cannot rule out that these mutations did not increase nuclear deformability, since it is possible that reduced force transmission from the cytoskeleton to the nucleus counteracted this effect.

A particularly noteworthy finding was that nucleo-cytoskeletal uncoupling by specific mutant lamins and depletion of Msp300 were associated with loss of myonuclear microtubule caging (Figures 5, 7 and Figure 8). Our findings are consistent with those of others showing that a network of microtubules around the nucleus in larval body wall muscles is dependent on Msp300 (Volk, 2013). The mechanisms by which microtubules are recruited to the nuclear envelope in differentiated muscle are incompletely understood (Bugnard et al., 2005; Bartolini & Gundersen, 2006; Rogers et al., 2008; Tillery et al., 2018; Becker et al., 2020). In mouse myoblasts undergoing differentiation, centrosomal protein PCM-1 relocalizes to the nuclear envelope by a mechanism that requires Nesprin 1 (Espigat-Georger et al., 2016). Furthermore, the centrosomal protein AKAP450 is required for microtubule nucleation at the nuclear envelope in differentiated myotubes (Gimpel et al., 2017). Consistent with the role of centrosomal proteins in microtubule recruitment, the large scaffold protein AKAP6 links centrosomal protein AKAP9 and nesprin-1α to nucleate microtubules at the nuclear envelope in rat cardiomyocytes (Vergarajauregui et al., 2020). This process is dependent on the induction of muscle-specific isoforms of AKAP6 and nesprin-1α by the transcriptional regulator myogenin (Becker et al., 2020). Similarly, in the *Drosophila* fat body, a network of microtubules around the nucleus is stabilized by several centrosomal proteins and a spectraplakin (Shot) that localize at the nuclear envelope (Wang et al., 2015; Sun et al., 2019; Zheng et al., 2020). It will be of interest to identify the proteins that nucleate microtubules at the nuclear envelope in *Drosophila* larval body wall muscles and investigate how specific mutant lamins alter such interactions.

The functional consequences of the impaired nucleo-cytoskeletal coupling in muscles expressing LamC ΔK47 and K521Q are not known. It is possible that the loss of nuclear microtubule caging reduces larval motility because the non-caged longitudinal microtubules interfere with the actin-myosin contractile apparatus. A dense microtubule network led to increased myocyte stiffness that impaired contractility in failing hearts (Bajpai et al., 2018). In this case, pharmacological treatments leading to the detyrosination of microtubules lowered cytoplasmic viscosity and restored cardiac contractile function. It is also possible that loss of the microtubule nuclear caging in the larval body wall muscle increases nuclear envelope damage, resulting in the loss of muscle function. During muscle contraction, myonuclei move in coordination with the sarcoplasm *via* connections with the cytoskeleton (Lorber et al., 2020). Uncoupling the nucleus from the cytoskeleton can result in asynchronous movements, which generate variable drag forces on myonuclei during muscle contraction (Lorber et al., 2020). Such drag forces might impact normal nuclear mechanosensing and/or lead to nuclear envelope rupture and DNA damage. Consistent with this idea, increased DNA damage has been observed in *LMNA* disease models and human muscle biopsy tissue (Earle et al., 2020). Activation of DNA damage response pathways might signal to block muscle contractions to prevent further DNA damage. In these instances, the microtubule nuclear cage is predicted to serve as a shock

absorber, providing protection from mechanical force during muscle contraction. Paradoxically, uncoupling the nucleus from the cytoskeleton *via* disruption of the LINC complex suppresses muscle defects in mouse models of laminopathies (Earle et al., 2020; Chai et al., 2021). In such cases, an altered nuclear lamina might cause nuclei to be especially vulnerable to forces applied from the cytoskeleton; uncoupling the nucleus and cytoskeleton proved beneficial, possibly by reducing forces across the nuclear envelope. Future studies are needed to assess the complex relationship between microtubules and myonuclear integrity.

Only five of the eight mutant lamins studied here showed changes in the physical properties or nucleo-cytoskeletal coupling of myonuclei, as measured by the microharpooning assay, yet all eight caused premature death (Figure 1). The mutant lamins that did not alter nuclear mechanics might play a role in gene expression. Genomes are rich with lamin-associated domains (LADs) in which sections of chromosomes are in close opposition with the lamin meshwork (Mohanta et al., 2021; Wong et al., 2021). In fact, in some cell types, LADs represent up to half of the genome (Briand & Collas, 2020; Mohanta et al., 2021; Rullens & Kind, 2021). In general, LADs are relatively gene poor and lack active transcription. Therefore, the mutant lamins studied here might form an abnormal lamin meshwork that alters contacts with the genome, resulting in altered gene expression.

Collectively, our studies highlight the vast heterogeneity in muscle defects caused by mutant lamins while keeping the genetic background constant. As with other studies of lamins, specific cellular defects do not correlate with alterations in specific protein domains of lamin. Therefore, predictions of how *LMNA* variants of uncertain significance alter lamin function are challenging. Studies such as these will allow for the grouping of mutant lamins that share similar defective properties, which ultimately will guide treatments.

Data availability statement

The original contributions presented in the study are included in the article/Supplementary Material; further inquiries can be directed to the corresponding author.

Author contributions

NS, GF, MK, GC, JL, and LW contributed to the experimental design. NS, GF, MK, GC, and LW performed experiments. Data were analyzed by NS, JR-M, GF, MK, GC, JL, and LW. The manuscript was prepared by NS, JR-M, JL, and LW. The manuscript was reviewed and edited by NS, JR-M, GF, MK, GC, JL, and LW.

Funding

This research was supported by funds from a Burroughs Welcome Fund Collaborative Research Travel Grant (1017502), the Muscular Dystrophy Association (Development Award MDA603238), the National Institutes of Health (NIH, R21AR075193) to LW; NIH R01 (HL082792) to JL, the National Science Foundation (awards #1715606 and URoL 2022048) to JL, the Volkswagen Foundation Life program (award A130142) to JL, a University of Iowa ICRU Fellowship to NS, and the University of Iowa Carver College of Medicine FUTURE Program support of GC. Bio-icons in Figure 1D and Figure 8 were created with BioRender.com.

Acknowledgments

We thank N. P. Mohar for technical assistance. We are grateful for the gift of antibodies from T. Volk and J. A. Fischer.

Conflict of interest

The authors declare that the research was conducted in the absence of any commercial or financial relationships that could be construed as a potential conflict of interest.

Publisher's note

Supplementary material

The Supplementary Material for this article can be found online at: https://www.frontiersin.org/articles/10.3389/fcell.2022.934586/full#supplementary-material

References

Anderson, C. L., Langer, E. R., Routes, T. C., McWilliams, S. F., Bereslavskyy, I., Kamp, T. J., et al. (2021). Most myopathic lamin variants aggregate: A functional genomics approach for assessing variants of uncertain significance. *NPJ Genom. Med.* 6 (1), 103. doi:10.1038/s41525-021-00265-x

Arbustini, E., Pilotto, A., Repetto, A., Grasso, M., Negri, A., Diegoli, M., et al. (2002). Autosomal dominant dilated cardiomyopathy with atrioventricular block: a lamin A/C defect-related disease. *J. Am. Coll. Cardiol.* 39 (6), 981–990. doi:10.1016/s0735-1097(02)01724-2

Astejada, M. N., Goto, K., Nagano, A., Ura, S., Noguchi, S., Nonaka, I., et al. (2007). Emerinopathy and laminopathy clinical, pathological and molecular features of muscular dystrophy with nuclear envelopathy in Japan. *Acta Myol.* 26 (3), 159–164.

Bajpai, G., Schneider, C., Wong, N., Bredemeyer, A., Hulsmans, M., Nahrendorf, M., et al. (2018). The human heart contains distinct macrophage subsets with divergent origins and functions. *Nat. Med.* 24 (8), 1234–1245. doi:10.1038/s41591-018-0059-x

Balakrishnan, M., Sisso, W. J., and Baylies, M. K. (2021). Analyzing muscle structure and function throughout the larval instars in live Drosophila. *Star. Protoc.* 2 (1), 100291. doi:10.1016/j.xpro.2020.100291

Bartolini, F., and Gundersen, G. G. (2006). Generation of noncentrosomal microtubule arrays. *J. Cell Sci.* 119 (20), 4155–4163. doi:10.1242/jcs.03227

Becker, R., Leone, M., and Engel, F. B. (2020). Microtubule organization in striated muscle cells. *Cells* 9 (6), E1395. doi:10.3390/cells9061395

Bobylev, A. G., Fadeev, R. S., Bobyleva, L. G., Kobyakova, M. I., Shlyapnikov, Y. M., Popov, D. V., et al. (2021). Amyloid aggregates of smooth-muscle Titin impair cell adhesion. *Int. J. Mol. Sci.* 22 (9), 4579. doi:10.3390/ijms22094579

Bonne, G., Di Barletta, M. R., Varnous, S., Becane, H. M., Hammouda, E. H., Merlini, L., et al. (1999). Mutations in the gene encoding lamin A/C cause autosomal dominant Emery-Dreifuss muscular dystrophy. *Nat. Genet.* 21 (3), 285–288. doi:10.1038/6799

Bonne, G., Mercuri, E., Muchir, A., Urtizberea, A., Becane, H. M., Recan, D., et al. (2000). Clinical and molecular genetic spectrum of autosomal dominant Emery-Dreifuss muscular dystrophy due to mutations of the lamin A/C gene. *Ann. Neurol.* 48 (2), 170–180. doi:10.1002/1531-8249(200008)48:2<170::aid-ana6>3.0.co;2-j

Brand, A. H., and Perrimon, N. (1993). Targeted gene expression as a means of altering cell fates and generating dominant phenotypes. *Development* 118 (2), 401–415. doi:10.1242/dev.118.2.401

Briand, N., and Collas, P. (2020). Lamina-associated domains: Peripheral matters and internal affairs. *Genome Biol.* 21 (1), 85. doi:10.1186/s13059-020-02003-5

Brooks, D. S., Vishal, K., Kawakami, J., Bouyain, S., and Geisbrecht, E. R. (2016). Optimization of wrMTrck to monitor Drosophila larval locomotor activity. *J. Insect Physiol.* 93-94, 11–17. doi:10.1016/j.jinsphys.2016.07.007

Brown, C. A., Lanning, R. W., McKinney, K. Q., Salvino, A. R., Cherniske, E., Crowe, C. A., et al. (2001). Novel and recurrent mutations in lamin A/C in patients with Emery-Dreifuss muscular dystrophy. *Am. J. Med. Genet.* 102 (4), 359–367. doi:10.1002/ajmg.1463

Bruusgaard, J. C., Liestol, K., and Gundersen, K. (2006). Distribution of myonuclei and microtubules in live muscle fibers of young, middle-aged, and old mice. *J. Appl. Physiol.* 100 (6), 2024–2030. doi:10.1152/japplphysiol.00913.2005

Budnik, V., Zhong, Y., and Wu, C. F. (1990). Morphological plasticity of motor axons in Drosophila mutants with altered excitability. *J. Neurosci.* 10 (11), 3754–3768.

Bugnard, E., Zaal, K. J., and Ralston, E. (2005). Reorganization of microtubule nucleation during muscle differentiation. *Cell Motil. Cytoskelet.* 60 (1), 1–13. doi:10.1002/cm.20042

Burke, B., and Stewart, C. L. (2006). The laminopathies: The functional architecture of the nucleus and its contribution to disease. *Annu. Rev. Genomics Hum. Genet.* 7, 369–405. doi:10.1146/annurev.genom.7.080505.115732

Cain, N. E., Jahed, Z., Schoenhofen, A., Valdez, V. A., Elkin, B., Hao, H., et al. (2018). Conserved SUN-KASH interfaces mediate LINC complex-dependent nuclear movement and positioning. *Curr. Biol.* 28 (19), 3086–3097. e3084. doi:10.1016/j.cub.2018.08.001

Camozzi, D., Capanni, C., Cenni, V., Mattioli, E., Columbaro, M., Squarzoni, S., et al. (2014). Diverse lamin-dependent mechanisms interact to control chromatin dynamics. Focus on laminopathies. *Nucleus* 5 (5), 427–440. doi:10.4161/nucl.36289

Carayon, A., Bataille, L., Lebreton, G., Dubois, L., Pelletier, A., Carrier, Y., et al. (2020). Intrinsic control of muscle attachment sites matching. *Elife* 9, e57547. doi:10.7554/eLife.57547

Caygill, E. E., and Brand, A. H. (2016). The GAL4 system: A versatile system for the manipulation and analysis of gene expression. *Methods Mol. Biol.* 1478, 33–52. doi:10.1007/978-1-4939-6371-3_2

Chai, R. J., Werner, H., Li, P. Y., Lee, Y. L., Nyein, K. T., Solovei, I., et al. (2021). Disrupting the LINC complex by AAV mediated gene transduction prevents progression of Lamin induced cardiomyopathy. *Nat. Commun.* 12 (1), 4722. doi:10.1038/s41467-021-24849-4

Chang, W., Worman, H. J., and Gundersen, G. G. (2015). Accessorizing and anchoring the LINC complex for multifunctionality. *J. Cell Biol.* 208 (1), 11–22. doi:10.1083/jcb.201409047

Chiarini, F., Evangelisti, C., Cenni, V., Fazio, A., Paganelli, F., Martelli, A. M., et al. (2019). The cutting edge: The role of mTOR signaling in laminopathies. *Int. J. Mol. Sci.* 20 (4), E847. doi:10.3390/ijms20040847

Chivet, M., Marchioretti, C., Pirazzini, M., Piol, D., Scaramuzzino, C., Polanco, M. J., et al. (2020). Polyglutamine-expanded androgen receptor alteration of skeletal muscle homeostasis and myonuclear aggregation are affected by Sex, Age and muscle metabolism. *Cells* 9 (2), E325. doi:10.3390/cells9020325

Cho, A., Kato, M., Whitwam, T., Kim, J. H., and Montell, D. J. (2016). An atypical tropomyosin in Drosophila with intermediate filament-like properties. *Cell Rep.* 16 (4), 928–938. doi:10.1016/j.celrep.2016.06.054

Cho, S., Irianto, J., and Discher, D. E. (2017). Mechanosensing by the nucleus: From pathways to scaling relationships. *J. Cell Biol.* 216 (2), 305–315. doi:10.1083/jcb.201610042

Choi, J. C., Muchir, A., Wu, W., Iwata, S., Homma, S., Morrow, J. P., et al. (2012). Temsirolimus activates autophagy and ameliorates cardiomyopathy caused by lamin A/C gene mutation. *Sci. Transl. Med.* 4 (144), 144ra102. 144ra102. doi:10.1126/scitranslmed.3003875

Coombs, G. S., Rios-Monterrosa, J. L., Lai, S., Dai, Q., Goll, A. C., Ketterer, M. R., et al. (2021). Modulation of muscle redox and protein aggregation rescues lethality caused by mutant lamins. *Redox Biol.* 48, 102196. doi:10.1016/j.redox.2021.102196

Crisp, M., Liu, Q., Roux, K., Rattner, J. B., Shanahan, C., Burke, B., et al. (2006). Coupling of the nucleus and cytoplasm: Role of the LINC complex. *J. Cell Biol.* 172 (1), 41–53. doi:10.1083/jcb.200509124

Dhe-Paganon, S., Werner, E. D., Chi, Y. I., and Shoelson, S. E. (2002). Structure of the globular tail of nuclear lamin. *J. Biol. Chem.* 277 (20), 17381–17384. doi:10.1074/jbc.C200038200

Dialynas, G., Shrestha, O. K., Ponce, J. M., Zwerger, M., Thiemann, D. A., Young, G. H., et al. (2015). Myopathic lamin mutations cause reductive stress and activate the nrf2/keap-1 pathway. *PLoS Genet.* 11 (5), e1005231. doi:10.1371/journal.pgen.1005231

Dialynas, G., Speese, S., Budnik, V., Geyer, P. K., and Wallrath, L. L. (2010). The role of Drosophila Lamin C in muscle function and gene expression. *Development* 137 (18), 3067–3077. doi:10.1242/dev.048231

Dittmer, T. A., and Misteli, T. (2011). The lamin protein family. *Genome Biol.* 12 (5), 222. doi:10.1186/gb-2011-12-5-222

Dreger, M., Bengtsson, L., Schoneberg, T., Otto, H., and Hucho, F. (2001). Nuclear envelope proteomics: Novel integral membrane proteins of the inner nuclear membrane. *Proc. Natl. Acad. Sci. U. S. A.* 98 (21), 11943–11948. doi:10.1073/pnas.211201898

D'Amico, A., Haliloglu, G., Richard, P., Talim, B., Maugenre, S., Ferreiro, A., et al. (2005). Two patients with "Dropped head syndrome" due to mutations in LMNA or SEPN1 genes. *Neuromuscul. Disord.* 15 (8), 521–524. doi:10.1016/j.nmd.2005.03.006

Earle, A. J., Kirby, T. J., Fedorchak, G. R., Isermann, P., Patel, J., Iruvanti, S., et al. (2020). Mutant lamins cause nuclear envelope rupture and DNA damage in skeletal muscle cells. *Nat. Mat.* 19 (4), 464–473. doi:10.1038/s41563-019-0563-5

Eldirany, S. A., Lomakin, I. B., Ho, M., and Bunick, C. G. (2021). Recent insight into intermediate filament structure. *Curr. Opin. Cell Biol.* 68, 132–143. doi:10.1016/j.ceb.2020.10.001

Espigat-Georger, A., Dyachuk, V., Chemin, C., Emorine, L., and Merdes, A. (2016). Nuclear alignment in myotubes requires centrosome proteins recruited by nesprin-1. *J. Cell Sci.* 129 (22), 4227–4237. doi:10.1242/jcs.191767

Fedorchak, G., and Lammerding, J. (2016). Cell microharpooning to study nucleo-cytoskeletal coupling. *Methods Mol. Biol.* 1411, 241–254. doi:10.1007/978-1-4939-3530-7_16

Folker, E. S., Ostlund, C., Luxton, G. W., Worman, H. J., and Gundersen, G. G. (2011). Lamin A variants that cause striated muscle disease are defective in anchoring transmembrane actin-associated nuclear lines for nuclear movement. *Proc. Natl. Acad. Sci. U. S. A.* 108 (1), 131–136. doi:10.1073/pnas.1000824108

Fortier, T. M., Vasa, P. P., and Woodard, C. T. (2003). Orphan nuclear receptor betaFTZ-F1 is required for muscle-driven morphogenetic events at the prepupal-pupal transition in *Drosophila melanogaster*. *Dev. Biol.* 257 (1), 153–165. doi:10.1016/s0012-1606(03)00036-8

Furukawa, K., Ishida, K., Tsunoyama, T. A., Toda, S., Osoda, S., Horigome, T., et al. (2009). A-type and B-type lamins initiate layer assembly at distinct areas of the nuclear envelope in living cells. *Exp. Cell Res.* 315 (7), 1181–1189. doi:10.1016/j.yexcr.2008.12.024

Gimpel, P., Lee, Y. L., Sobota, R. M., Calvi, A., Koullourou, V., Patel, R., et al. (2017). Nesprin-1α-Dependent microtubule nucleation from the nuclear envelope via Akap450 is necessary for nuclear positioning in muscle cells. *Curr. Biol.* 27 (19), 2999–3009. e2999. doi:10.1016/j.cub.2017.08.031

Goldman, R. D., Shumaker, D. K., Erdos, M. R., Eriksson, M., Goldman, A. E., Gordon, L. B., et al. (2004). Accumulation of mutant lamin A causes progressive changes in nuclear architecture in Hutchinson-Gilford progeria syndrome. *Proc. Natl. Acad. Sci. U. S. A.* 101 (24), 8963–8968. doi:10.1073/pnas.0402943101

Gorczyca, D., Ashley, J., Speese, S., Gherbesi, N., Thomas, U., Gundelfinger, E., et al. (2007). Postsynaptic membrane addition depends on the Discs-Large-interacting t-SNARE Gtaxin. *J. Neurosci.* 27 (5), 1033–1044. doi:10.1523/JNEUROSCI.3160-06.2007

Hatch, E. M., and Hetzer, M. W. (2016). Nuclear envelope rupture is induced by actin-based nucleus confinement. *J. Cell Biol.* 215 (1), 27–36. doi:10.1083/jcb.201603053

Heller, S. A., Shih, R., Kalra, R., and Kang, P. B. (2020). Emery-Dreifuss muscular dystrophy. *Muscle Nerve* 61 (4), 436–448. doi:10.1002/mus.26782

Hermida-Prieto, M., Monserrat, L., Castro-Beiras, A., Laredo, R., Soler, R., Peteiro, J., et al. (2004). Familial dilated cardiomyopathy and isolated left ventricular noncompaction associated with lamin A/C gene mutations. *Am. J. Cardiol.* 94 (1), 50–54. doi:10.1016/j.amjcard.2004.03.029

Herrmann, H., Bar, H., Kreplak, L., Strelkov, S. V., and Aebi, U. (2007). Intermediate filaments: From cell architecture to nanomechanics. *Nat. Rev. Mol. Cell Biol.* 8 (7), 562–573. doi:10.1038/nrm2197

Herrmann, H., and Strelkov, S. V. (2011). History and phylogeny of intermediate filaments: Now in insects. *BMC Biol.* 9, 16. doi:10.1186/1741-7007-9-16

Hieda, M. (2019). Signal transduction across the nuclear envelope: Role of the LINC complex in bidirectional signaling. *Cells* 8 (2), E124. doi:10.3390/cells8020124

Hinz, B. E., Walker, S. G., Xiong, A., Gogal, R. A., Schnieders, M. J., and Wallrath, L. L. (2021). *In silico* and *in Vivo* analysis of amino acid substitutions that cause laminopathies. *Int. J. Mol. Sci.* 22 (20), 11226. doi:10.3390/ijms222011226

Hodzic, D. M., Yeater, D. B., Bengtsson, L., Otto, H., and Stahl, P. D. (2004). Sun2 is a novel mammalian inner nuclear membrane protein. *J. Biol. Chem.* 279 (24), 25805–25812. doi:10.1074/jbc.M313157200

Horn, H. F. (2014). LINC complex proteins in development and disease. *Curr. Top. Dev. Biol.* 109, 287–321. doi:10.1016/b978-0-12-397920-9.00004-4

Kapinos, L. E., Schumacher, J., Mucke, N., Machaidze, G., Burkhard, P., Aebi, U., et al. (2010). Characterization of the head-to-tail overlap complexes formed by human lamin A, B1 and B2 "half-minilamin" dimers. *J. Mol. Biol.* 396 (3), 719–731. doi:10.1016/j.jmb.2009.12.001

Kim, D. I., Birendra, K. C., and Roux, K. J. (2015). Making the LINC: SUN and KASH protein interactions. *Biol. Chem.* 396 (4), 295–310. doi:10.1515/hsz-2014-0267

Kim, J. K., Louhghalam, A., Lee, G., Schafer, B. W., Wirtz, D., and Kim, D. H. (2017). Nuclear lamin A/C harnesses the perinuclear apical actin cables to protect nuclear morphology. *Nat. Commun.* 8 (1), 2123. doi:10.1038/s41467-017-02217-5

Kittisopikul, M., Shimi, T., Tatli, M., Tran, J. R., Zheng, Y., Medalia, O., et al. (2021). Computational analyses reveal spatial relationships between nuclear pore complexes and specific lamins. *J. Cell Biol.* 220 (4), e202007082. doi:10.1083/jcb.202007082

Kracklauer, M. P., Banks, S. M., Xie, X., Wu, Y., and Fischer, J. A. (2007). Drosophila klaroid encodes a SUN domain protein required for Klarsicht localization to the nuclear envelope and nuclear migration in the eye. *Fly. (Austin)* 1 (2), 75–85. doi:10.4161/fly.4254

Krimm, I., Ostlund, C., Gilquin, B., Couprie, J., Hossenlopp, P., Mornon, J. P., et al. (2002). The Ig-like structure of the C-terminal domain of lamin A/C, mutated in muscular dystrophies, cardiomyopathy, and partial lipodystrophy. *Structure* 10 (6), 811–823. doi:10.1016/s0969-2126(02)00777-3

Lemke, S. B., and Schnorrer, F. (2018). *In vivo* imaging of muscle-tendon morphogenesis in Drosophila pupae. *J. Vis. Exp.* 132, 57312. doi:10.3791/57312

Liao, C. Y., Anderson, S. S., Chicoine, N. H., Mayfield, J. R., Academia, E. C., Wilson, J. A., et al. (2016). Rapamycin reverses metabolic Deficits in lamin A/C-deficient mice. *Cell Rep.* 17 (10), 2542–2552. doi:10.1016/j.celrep.2016.10.040

Lilina, A. V., Chernyatina, A. A., Guzenko, D., and Strelkov, S. V. (2020). Lateral A11 type tetramerization in lamins. *J. Struct. Biol.* 209 (1), 107404. doi:10.1016/j.jsb.2019.10.006

Lombardi, M. L., Jaalouk, D. E., Shanahan, C. M., Burke, B., Roux, K. J., and Lammerding, J. (2011a). The interaction between nesprins and sun proteins at the nuclear envelope is critical for force transmission between the nucleus and cytoskeleton. *J. Biol. Chem.* 286 (30), 26743–26753. doi:10.1074/jbc.M111.233700

Lombardi, M. L., Zwerger, M., and Lammerding, J. (2011b). Biophysical assays to probe the mechanical properties of the interphase cell nucleus: Substrate strain application and microneedle manipulation. *J. Vis. Exp.* 55, 3087. doi:10.3791/3087

Lorber, D., Rotkopf, R., and Volk, T. (2020). A minimal constraint device for imaging nuclei in live Drosophila contractile larval muscles reveals novel nuclear mechanical dynamics. *Lab. Chip* 20 (12), 2100–2112. doi:10.1039/d0lc00214c

Lu, J. T., Muchir, A., Nagy, P. L., and Worman, H. J. (2011). LMNA cardiomyopathy: Cell biology and genetics meet clinical medicine. *Dis. Model. Mech.* 4 (5), 562–568. doi:10.1242/dmm.006346

Maggi, L., Carboni, N., and Bernasconi, P. (2016). Skeletal muscle laminopathies: A review of clinical and molecular features. *Cells* 5 (3), E33. doi:10.3390/cells5030033

Maire, P., Dos Santos, M., Madani, R., Sakakibara, I., Viaut, C., and Wurmser, M. (2020). Myogenesis control by SIX transcriptional complexes. *Semin. Cell Dev. Biol.* 104, 51–64. doi:10.1016/j.semcdb.2020.03.003

Maniotis, A. J., Chen, C. S., and Ingber, D. E. (1997). Demonstration of mechanical connections between integrins, cytoskeletal filaments, and nucleoplasm that stabilize nuclear structure. *Proc. Natl. Acad. Sci. U. S. A.* 94 (3), 849–854. doi:10.1073/pnas.94.3.849

Maurer, M., and Lammerding, J. (2019). The driving force: Nuclear mechanotransduction in cellular function, fate, and disease. *Annu. Rev. Biomed. Eng.* 21, 443–468. doi:10.1146/annurev-bioeng-060418-052139

Meinke, P., Mattioli, E., Haque, F., Antoku, S., Columbaro, M., Straatman, K. R., et al. (2014). Muscular dystrophy-associated SUN1 and SUN2 variants disrupt nuclear-cytoskeletal connections and myonuclear organization. *PLoS Genet.* 10 (9), e1004605. doi:10.1371/journal.pgen.1004605

Mohanta, T. K., Mishra, A. K., and Al-Harrasi, A. (2021). The 3D genome: From structure to function. *Int. J. Mol. Sci.* 22 (21), 11585. doi:10.3390/ijms222111585

Mounkes, L., Kozlov, S., Burke, B., and Stewart, C. L. (2003). The laminopathies: Nuclear structure meets disease. *Curr. Opin. Genet. Dev.* 13 (3), 223–230. doi:10.1016/s0959-437x(03)00058-3

Muchir, A., Medioni, J., Laluc, M., Massart, C., Arimura, T., van der Kooi, A. J., et al. (2004). Nuclear envelope alterations in fibroblasts from patients with muscular dystrophy, cardiomyopathy, and partial lipodystrophy carrying lamin A/C gene mutations. *Muscle Nerve* 30 (4), 444–450. doi:10.1002/mus.20122

Ovalle, W. K. (1987). The human muscle-tendon junction. A morphological study during normal growth and at maturity. *Anat. Embryol.* 176 (3), 281–294. doi:10.1007/BF00310184

Park, Y. E., Hayashi, Y. K., Bonne, G., Arimura, T., Noguchi, S., Nonaka, I., et al. (2009). Autophagic degradation of nuclear components in mammalian cells. *Autophagy* 5 (6), 795–804. doi:10.4161/auto.8901

Pethig, K., Genschel, J., Peters, T., Wilhelmi, M., Flemming, P., Lochs, H., et al. (2005). LMNA mutations in cardiac transplant recipients. *Cardiology* 103 (2), 57–62. doi:10.1159/000082048

Porcu, M., Corda, M., Pasqualucci, D., Binaghi, G., Sanna, N., Matta, G., et al. (2021). A very long-term observation of a family with dilated cardiomyopathy and overlapping phenotype from lamin A/C mutation. *J. Cardiovasc. Med.* 22 (1), 53–58. doi:10.2459/JCM.0000000000001060

Potter, C., and Hodzic, D. (2018). Analysis of high molecular Weight isoforms of nesprin-1 and nesprin-2 with vertical agarose Gel electrophoresis. *Methods Mol. Biol.* 1840, 25–33. doi:10.1007/978-1-4939-8691-0_3

Potulska-Chromik, A., Jedrzejowska, M., Gos, M., Rosiak, E., Kierdaszuk, B., Maruszak, A., et al. (2021). Pathogenic mutations and putative phenotype-affecting variants in polish myofibrillar Myopathy patients. *J. Clin. Med.* 10 (5), 914. doi:10.3390/jcm10050914

Rajasekaran, N. S., Connell, P., Christians, E. S., Yan, L. J., Taylor, R. P., Orosz, A., et al. (2007). Human alpha B-crystallin mutation causes oxido-reductive stress and protein aggregation cardiomyopathy in mice. *Cell* 130 (3), 427–439. doi:10.1016/j.cell.2007.06.044

Ramachandran, P., and Budnik, V. (2010). Dissection of Drosophila larval body-wall muscles. *Cold Spring Harb. Protoc.* 2010 (8), pdb.prot5469. pdb prot5469. doi:10.1101/pdb.prot5469

Ramos, F. J., Chen, S. C., Garelick, M. G., Dai, D. F., Liao, C. Y., Schreiber, K. H., et al. (2012). Rapamycin reverses elevated mTORC1 signaling in lamin

A/C-deficient mice, rescues cardiac and skeletal muscle function, and extends survival. *Sci. Transl. Med.* 4 (144), 144ra103. doi:10.1126/scitranslmed.3003802

Rankin, J., and Ellard, S. (2006). The laminopathies: A clinical review. *Clin. Genet.* 70 (4), 261–274. doi:10.1111/j.1399-0004.2006.00677.x

Rey, A., Schaeffer, L., Durand, B., and Morel, V. (2021). Drosophila nesprin-1 isoforms differentially contribute to muscle function. *Cells* 10 (11), 3061. doi:10.3390/cells10113061

Richier, B., Inoue, Y., Dobramysl, U., Friedlander, J., Brown, N. H., and Gallop, J. L. (2018). Integrin signaling downregulates filopodia during muscle-tendon attachment. *J. Cell Sci.* 131 (16), jcs217133. doi:10.1242/jcs.217133

Riemer, D., Stuurman, N., Berrios, M., Hunter, C., Fisher, P. A., and Weber, K. (1995). Expression of Drosophila lamin C is developmentally regulated: Analogies with vertebrate A-type lamins. *J. Cell Sci.* 108 (10), 3189–3198. doi:10.1242/jcs.108.10.3189

Rogers, G. C., Rusan, N. M., Peifer, M., and Rogers, S. L. (2008). A multicomponent assembly pathway contributes to the formation of acentrosomal microtubule arrays in interphase Drosophila cells. *Mol. Biol. Cell* 19 (7), 3163–3178. doi:10.1091/mbc.E07-10-1069

Rosen, J. N., and Baylies, M. K. (2017). Myofibrils put the squeeze on nuclei. *Nat. Cell Biol.* 19 (10), 1148–1150. doi:10.1038/ncb3618

Rullens, P. M. J., and Kind, J. (2021). Attach and stretch: Emerging roles for genome-lamina contacts in shaping the 3D genome. *Curr. Opin. Cell Biol.* 70, 51–57. doi:10.1016/j.ceb.2020.11.006

Rzepecki, R., and Gruenbaum, Y. (2018). Invertebrate models of lamin diseases. *Nucleus* 9 (1), 227–234. doi:10.1080/19491034.2018.1454166

Schindelin, J., Arganda-Carreras, I., Frise, E., Kaynig, V., Longair, M., Pietzsch, T., et al. (2012). Fiji: An open-source platform for biological-image analysis. *Nat. Methods* 9 (7), 676–682. doi:10.1038/nmeth.2019

Schulman, V. K., Dobi, K. C., and Baylies, M. K. (2015). Morphogenesis of the somatic musculature in *Drosophila melanogaster*. *Wiley Interdiscip. Rev. Dev. Biol.* 4 (4), 313–334. doi:10.1002/wdev.180

Shaffer, C. D., Wuller, J. M., and Elgin, S. C. (1994). Raising large quantities of Drosophila for biochemical experiments. *Methods Cell Biol.* 44, 99–108. doi:10.1016/s0091-679x(08)60908-5

Shimi, T., Kittisopikul, M., Tran, J., Goldman, A. E., Adam, S. A., Zheng, Y., et al. (2015). Structural organization of nuclear lamins A, C, B1, and B2 revealed by superresolution microscopy. *Mol. Biol. Cell* 26 (22), 4075–4086. doi:10.1091/mbc.E15-07-0461

Shin, J. Y., and Worman, H. J. (2022). Molecular Pathology of laminopathies. *Annu. Rev. Pathol.* 17, 159–180. doi:10.1146/annurev-pathol-042220-034240

Song, K., Dube, M. P., Lim, J., Hwang, I., Lee, I., and Kim, J. J. (2007). Lamin A/C mutations associated with familial and sporadic cases of dilated cardiomyopathy in Koreans. *Exp. Mol. Med.* 39 (1), 114–120. doi:10.1038/emm.2007.13

Sosa, B. A., Rothballer, A., Kutay, U., and Schwartz, T. U. (2012). LINC complexes form by binding of three KASH peptides to domain interfaces of trimeric SUN proteins. *Cell* 149 (5), 1035–1047. doi:10.1016/j.cell.2012.03.046

Starr, D. A. (2017). Muscle development: Nucleating microtubules at the nuclear envelope. *Curr. Biol.* 27 (19), R1071–r1073. doi:10.1016/j.cub.2017.08.030

Stewart, C. L., Kozlov, S., Fong, L. G., and Young, S. G. (2007). Mouse models of the laminopathies. *Exp. Cell Res.* 313 (10), 2144–2156. doi:10.1016/j.yexcr.2007.03.026

Strelkov, S. V., Kreplak, L., Herrmann, H., and Aebi, U. (2004). Intermediate filament protein structure determination. *Methods Cell Biol.* 78, 25–43. doi:10.1016/s0091-679x(04)78002-4

Sun, T., Song, Y., Dai, J., Mao, D., Ma, M., Ni, J. Q., et al. (2019). Spectraplakin shot Maintains perinuclear microtubule organization in Drosophila polyploid cells. *Dev. Cell* 49 (5), 731–747. doi:10.1016/j.devcel.2019.03.027

Sweeney, H. L., and Hammers, D. W. (2018). Motor proteins. *Cold Spring Harb. Perspect. Biol.* 10 (2), a021931. doi:10.1101/cshperspect.a021931

Swift, J., Ivanovska, I. L., Buxboim, A., Harada, T., Dingal, P. C., Pinter, J., et al. (2013). Nuclear lamin-A scales with tissue stiffness and enhances matrix-directed differentiation. *Science* 341 (6149), 1240104. doi:10.1126/science.1240104

Sylvius, N., Bilinska, Z. T., Veinot, J. P., Fidzianska, A., Bolongo, P. M., Poon, S., et al. (2005). *In vivo* and *in vitro* examination of the functional significances of novel lamin gene mutations in heart failure patients. *J. Med. Genet.* 42 (8), 639–647. doi:10.1136/jmg.2004.023283

Tapscott, S. J., Davis, R. L., Thayer, M. J., Cheng, P. F., Weintraub, H., and Lassar, A. B. (1988). MyoD1: A nuclear phosphoprotein requiring a Myc homology region to convert fibroblasts to myoblasts. *Science* 242 (4877), 405–411. doi:10.1126/science.3175662

Technau, M., and Roth, S. (2008). The Drosophila KASH domain proteins Msp-300 and Klarsicht and the SUN domain protein Klaroid have no essential function during oogenesis. *Fly. (Austin)* 2 (2), 82–91. doi:10.4161/fly.6288

Tillery, M. M. L., Blake-Hedges, C., Zheng, Y., Buchwalter, R. A., and Megraw, T. L. (2018). Centrosomal and non-centrosomal microtubule-organizing centers (MTOCs) in *Drosophila melanogaster*. *Cells* 7 (9), E121. doi:10.3390/cells7090121

Turgay, Y., and Medalia, O. (2017). The structure of lamin filaments in somatic cells as revealed by cryo-electron tomography. *Nucleus* 8 (5), 475–481. doi:10.1080/19491034.2017.1337622

Vergarajauregui, S., Becker, R., Steffen, U., Sharkova, M., Esser, T., Petzold, J., et al. (2020). AKAP6 orchestrates the nuclear envelope microtubule-organizing center by linking golgi and nucleus via AKAP9. *Elife* 9, e61669. doi:10.7554/eLife.61669

Volk, T. (2013). Positioning nuclei within the cytoplasm of striated muscle fiber: Cooperation between microtubules and KASH proteins. *Nucleus* 4 (1), 18–22. doi:10.4161/nucl.23086

Walter, M. C., Witt, T. N., Weigel, B. S., Reilich, P., Richard, P., Pongratz, D., et al. (2005). Deletion of the LMNA initiator codon leading to a neurogenic variant of autosomal dominant Emery-Dreifuss muscular dystrophy. *Neuromuscul. Disord.* 15 (1), 40–44. doi:10.1016/j.nmd.2004.09.007

Wang, N., Tytell, J. D., and Ingber, D. E. (2009). Mechanotransduction at a distance: Mechanically coupling the extracellular matrix with the nucleus. *Nat. Rev. Mol. Cell Biol.* 10 (1), 75–82. doi:10.1038/nrm2594

Wang, S., Reuveny, A., and Volk, T. (2015). Nesprin provides elastic properties to muscle nuclei by cooperating with spectraplakin and EB1. *J. Cell Biol.* 209 (4), 529–538. doi:10.1083/jcb.201408098

Wang, W., Shi, Z., Jiao, S., Chen, C., Wang, H., Liu, G., et al. (2012). Structural insights into SUN-KASH complexes across the nuclear envelope. *Cell Res.* 22 (10), 1440–1452. doi:10.1038/cr.2012.126

Wilson, K. L., and Foisner, R. (2010). Lamin-binding proteins. *Cold Spring Harb. Perspect. Biol.* 2 (4), a000554. doi:10.1101/cshperspect.a000554

Wiltshire, K. M., Hegele, R. A., Innes, A. M., and Brownell, A. K. (2013). Homozygous lamin A/C familial lipodystrophy R482Q mutation in autosomal recessive Emery Dreifuss muscular dystrophy. *Neuromuscul. Disord.* 23 (3), 265–268. doi:10.1016/j.nmd.2012.11.011

Wong, X., Hoskins, V. E., Melendez-Perez, A. J., Harr, J. C., Gordon, M., and Reddy, K. L. (2021). Lamin C is required to establish genome organization after mitosis. *Genome Biol.* 22 (1), 305. doi:10.1186/s13059-021-02516-7

Wong, X., Melendez-Perez, A. J., and Reddy, K. L. (2022). The nuclear lamina. *Cold Spring Harb. Perspect. Biol.* 14 (2), a040113. doi:10.1101/cshperspect.a040113

Worman, H. J., and Bonne, G. (2007). Laminopathies": A wide spectrum of human diseases. *Exp. Cell Res.* 313 (10), 2121–2133. doi:10.1016/j.yexcr.2007.03.028

Worman, H. J. (2012). Nuclear lamins and laminopathies. *J. Pathol.* 226 (2), 316–325. doi:10.1002/path.2999

Xie, X., and Fischer, J. A. (2008). On the roles of the Drosophila KASH domain proteins Msp-300 and Klarsicht. *Fly. (Austin)* 2 (2), 74–81. doi:10.4161/fly.6108

Yu, J., Starr, D. A., Wu, X., Parkhurst, S. M., Zhuang, Y., Xu, T., et al. (2006). The KASH domain protein MSP-300 plays an essential role in nuclear anchoring during Drosophila oogenesis. *Dev. Biol.* 289 (2), 336–345. doi:10.1016/j.ydbio.2005.10.027

Zhang, Q., Bethmann, C., Worth, N. F., Davies, J. D., Wasner, C., Feuer, A., et al. (2007). Nesprin-1 and -2 are involved in the pathogenesis of Emery Dreifuss muscular dystrophy and are critical for nuclear envelope integrity. *Hum. Mol. Genet.* 16 (23), 2816–2833. doi:10.1093/hmg/ddm238

Zhang, Q., Skepper, J. N., Yang, F., Davies, J. D., Hegyi, L., Roberts, R. G., et al. (2001). Nesprins: A novel family of spectrin-repeat-containing proteins that localize to the nuclear membrane in multiple tissues. *J. Cell Sci.* 114 (24), 4485–4498. doi:10.1242/jcs.114.24.4485

Zheng, Y., Buchwalter, R. A., Zheng, C., Wight, E. M., Chen, J. V., and Megraw, T. L. (2020). A perinuclear microtubule-organizing centre controls nuclear positioning and basement membrane secretion. *Nat. Cell Biol.* 22 (3), 297–309. doi:10.1038/s41556-020-0470-7

Zwerger, M., Jaalouk, D. E., Lombardi, M. L., Isermann, P., Mauermann, M., Dialynas, G., et al. (2013). Myopathic lamin mutations impair nuclear stability in cells and tissue and disrupt nucleo-cytoskeletal coupling. *Hum. Mol. Genet.* 22 (12), 2335–2349. doi:10.1093/hmg/ddt079

frontiers | Frontiers in Cell and Developmental Biology

TYPE Original Research
PUBLISHED 19 September 2022
DOI 10.3389/fcell.2022.929495

OPEN ACCESS

EDITED BY
Weimin Li,
Washington State University,
United States

REVIEWED BY
Thomas Magin,
Leipzig University, Germany
Gregory F. Weber,
University of Indianapolis, United States

*CORRESPONDENCE
Robert D. Goldman,
r-goldman@northwestern.edu

SPECIALTY SECTION
This article was submitted to Cell Growth and Division, a section of the journal Frontiers in Cell and Developmental Biology

RECEIVED 26 April 2022
ACCEPTED 18 August 2022
PUBLISHED 19 September 2022

CITATION
Sivagurunathan S, Vahabikashi A, Yang H, Zhang J, Vazquez K, Rajasundaram D, Politanska Y, Abdala-Valencia H, Notbohm J, Guo M, Adam SA and Goldman RD (2022), Expression of vimentin alters cell mechanics, cell-cell adhesion, and gene expression profiles suggesting the induction of a hybrid EMT in human mammary epithelial cells.
Front. Cell Dev. Biol. 10:929495.
doi: 10.3389/fcell.2022.929495

Expression of vimentin alters cell mechanics, cell-cell adhesion, and gene expression profiles suggesting the induction of a hybrid EMT in human mammary epithelial cells

Suganya Sivagurunathan[1], Amir Vahabikashi[1], Haiqian Yang[2], Jun Zhang[3,4], Kelly Vazquez[4,5], Dhivyaa Rajasundaram[6], Yuliya Politanska[7], Hiam Abdala-Valencia[7], Jacob Notbohm[3,4,5], Ming Guo[2], Stephen A. Adam[1] and Robert D. Goldman[1]*

[1]Department of Cell and Developmental Biology, Feinberg School of Medicine, Northwestern University, Chicago, IL, United States, [2]Department of Mechanical Engineering, Massachusetts Institute of Technology, Cambridge, MA, United States, [3]Biophysics Program, University of Wisconsin-Madison, Madison, WI, United States, [4]Department of Engineering Physics, University of Wisconsin-Madison, Madison, WI, United States, [5]Department of Mechanical Engineering, University of Wisconsin-Madison, Madison, WI, United States, [6]Department of Pediatrics, University of Pittsburgh School of Medicine, Pittsburgh, PA, United States, [7]Department of Medicine, Feinberg School of Medicine, Northwestern University, Chicago, IL, United States

Vimentin is a Type III intermediate filament (VIF) cytoskeletal protein that regulates the mechanical and migratory behavior of cells. Its expression is considered to be a marker for the epithelial to mesenchymal transition (EMT) that takes place in tumor metastasis. However, the molecular mechanisms regulated by the expression of vimentin in the EMT remain largely unexplored. We created MCF7 epithelial cell lines expressing vimentin from a cumate-inducible promoter to address this question. When vimentin expression was induced in these cells, extensive cytoplasmic VIF networks were assembled accompanied by changes in the organization of the endogenous keratin intermediate filament networks and disruption of desmosomes. Significant reductions in intercellular forces by the cells expressing VIFs were measured by quantitative monolayer traction force and stress microscopy. In contrast, laser trapping micro-rheology revealed that the cytoplasm of MCF7 cells expressing VIFs was stiffer than the uninduced cells. Vimentin expression activated transcription of genes involved in pathways responsible for cell migration and locomotion. Importantly, the EMT related transcription factor *TWIST1* was upregulated only in wild type vimentin expressing cells and not in cells expressing a mutant non-polymerized form of vimentin, which only formed unit length filaments (ULF). Taken together, our results suggest that vimentin expression induces a hybrid EMT correlated with the upregulation of genes involved in cell migration.

KEYWORDS

vimentin, Twist1, desmoplakin, hybrid/partial EMT, intracellular mechanics, intercellular forces, cell-cell adhesion

Introduction

Intermediate filaments (IFs) are a large family of cytoskeletal proteins that are a feature of metazoans. They are encoded by 70 different genes subdivided into six classes (types I to VI) (Herrmann and Aebi, 2016) based on the homology of their conserved rod domains. The expression of IF proteins is cell type-specific and regulated based on the stages of differentiation of tissues and organs (Eriksson et al., 2009; Lowery et al., 2015). Vimentin, a type III IF protein is specific to mesenchymal and endothelial cells. In fully polymerized form, vimentin intermediate filaments (VIFs) are involved in cell motility (Mendez et al., 2010) and in protecting cells against mechanical stresses (Guo et al., 2013; Mendez et al., 2014; Patteson et al., 2019; Vahabikashi et al., 2019). Vimentin forms a homopolymer where two dimers associate laterally in anti-parallel fashion to form a tetramer and there is evidence that eight of these tetramers form a Unit Length Filament (ULF). ULFs anneal end to end and undergo a process of radial compaction to form ~10 nm filaments (Herrmann et al., 1996; Herrmann and Aebi, 2016).

Vimentin has been associated with cell migration in numerous studies. For example, the expression of vimentin is initiated in human breast epithelial cells induced to migrate following the wounding of monolayer cultures. This expression ceases following the closure of the wound (Gilles et al., 1999). In addition, mice lacking vimentin have impaired wound healing and fibroblasts from vimentin knock out mice have reduced cell motility and lack directionality (Eckes et al., 2000, 1998). Further, disrupting the VIF network in fibroblasts with a dominant-negative vimentin$_{(1–138)}$ reduces cell motility (Helfand et al., 2011) and a reduction in vimentin expression affects breast carcinoma cell migration (Messica et al., 2017). The transient expression of vimentin and its assembly into VIFs in MCF7 epithelial cells alters cell shape, motility and adhesion (Mendez et al., 2010).

Apart from the established roles of VIFs in cell migration and in protecting the mechanical integrity of cells, the expression of vimentin is considered to be an important marker of the epithelial-to-mesenchymal transition (EMT) (Zeisberg and Neilson, 2009). The EMT is a process whereby an epithelial cell transitions into a mesenchymal phenotype through a series of changes such as a loss of epithelial markers, a loss of apical-basal polarity, disruptions of cell-cell adhesions, alteration of cell-basement membrane attachments, rearrangements of cytoskeletal systems and increased motility and invasiveness (Kalluri and Weinberg, 2009). Vimentin expression appears to be indispensable for Slug or H-Ras-V12G-induced-EMT-associated cell migration mediated by its role in inducing the receptor tyrosine kinase Axl (Vuoriluoto et al., 2011). Indeed, VIFs act as a scaffold to recruit Slug to ERK, thereby increasing the phosphorylation of Slug (Virtakoivu et al., 2015).

Although there are numerous reports correlating the expression of vimentin with cell migration during a wide range of processes including wound repair and cancer metastasis (Ridge et al., 2022), little is known regarding the specific molecular and cellular changes brought about by vimentin expression. With the aim of investigating the changes that are caused by vimentin expression, we have established inducible MCF7 cell lines expressing either wild type (WT) vimentin, which polymerizes into mature VIFs, or a ULF mutant (Y117L) (Meier et al., 2009) form of vimentin, which can be expressed but cannot polymerize into mature VIFs. We have used these cell lines to identify potential alterations in gene expression and mechanical properties of MCF7 cells upon vimentin expression. The induction of vimentin expression and its assembly into polymerized VIFs alters cell mechanics, disrupts cell-cell adhesion, modifies cell-substrate and cell-cell forces and activates cell migratory pathways. Interestingly, the EMT specific transcription factor, *TWIST1* is upregulated only in WT vimentin expressing cells, but not in cells expressing the ULF form of vimentin.

Materials and methods

Cell culture

MCF7 cells obtained from the American Type Culture Collection (#ATCC HTB-22) were cultured in MEM (11095-080, Thermo Fisher Scientific, United States) supplemented with fetal bovine serum (Cytiva Hyclone, Fisher Scientific, United States), 50U/ml of Penicillin and 0.05 mg/ml of Streptomycin (P4333, Sigma-Aldrich, St. Louis, United States), MEM non-essential amino acids (25-025-CI, Corning, United States), sodium pyruvate (25-000-CI) and 0.01 mg/ml bovine insulin (I6634, Sigma-Aldrich, St. Louis, United States). The cells were maintained at 37 °C with 5% CO_2.

Constructs

WT and ULF mutant vimentin were cloned in the cumate inducible vector–pCDH-CuO-MCS-IRES-GFP-EF1α-CymR-T2A-Neo (QM812B-1, System Biosciences, United States) and transfected into 293FT packaging cells with psPAX2 (Addgene plasmid #12260) and pVSV-G (Clontech, United States) using Xfect transfection reagent (Takara Bio, United States).

psPAX2 was a gift from Didier Trono (Addgene plasmid # 12260; http://n2t.net/addgene:12260; RRID:Addgene_12260) MCF7 cells were transduced with the viral particles packaged by the 293FT cells following collection of the culture medium 48 h and 72 h post transfection. Polybrene (8 μg/ml) was added to the viral particles before transducing the MCF7 cells. The transduced cells were selected with 1,400 μg/ml G418 for 14 days. Cells expressing WT vimentin that formed networks of VIFs as assessed by epifluorescence imaging, were selected by limited dilution to establish structurally homogenous populations. Cells expressing either WT or ULF mutant vimentin were induced for 5 days with 5X cumate, sorted for GFP expression and made into a homogeneous population (Supplementary Figure S1A). The sorted and selected MCF7 cells were grown with or without 5X cumate (inducer) (QM150A-1, System Biosciences, United States) and used in all experiments.

Immunofluorescence

Cells were seeded on #1.5 coverslips and allowed to grow for at least 24 h. Subsequently the cells were fixed with 4% paraformaldehyde in PBS for 10 min at room temperature (RT) and were permeabilized for 10 min with 0.1% Triton-X 100 (Sigma-Aldrich, St. Louis, United States). After washing with 1X PBS, the coverslips were incubated for 30 min with specific antibodies diluted in 1X PBS containing 5% goat serum. The antibodies used were chicken anti-vimentin (1:200, CPCA-Vim, EnCor Biotechnology, United States), mouse anti-cytokeratin18 (1:200, PRO-61028, RDI), rabbit anti-desmoplakin (1:20, in house antibody (Jones and Goldman, 1985)), tubulin (1:500, in house antibody (DM1α)), vinculin (1:200, V4505, Sigma-Aldrich, St. Louis, United States), E-cadherin1 (1:200, M106, Takara, United States, kind gift from Cara Gottardi, Northwestern University). The coverslips were washed twice with 0.05% Tween 20 for 5 min each and further incubated with their respective secondary antibodies conjugated with Alexa Fluor dyes in 1X PBS (1:400, A-21202, A-21206, A-11041, ThermoFisher Scientific, United States). For staining actin, phalloidin (1:400, A12380, ThermoFisher Scientific, United States) was added along with the secondary antibody. The coverslips were washed twice with 0.05% Tween 20 in 1X PBS before mounting with ProLong Glass antifade mountant (P36980, Thermo Fisher Scientific, United States).

Microscopy

Confocal images were captured with a laser scanning confocal microscope (Nikon A1R confocal microscope, Nikon, Tokyo, Japan) using an oil immersion objective lens (Plan Apo 60X Oil objective, 1.4NA, Nikon). Maximum intensity projections of the Z stacks are presented. 3D Structured Illumination Microscopy (SIM) was carried out with a Nikon N-SIM Structured Illumination Super-resolution microscope system (Nikon N-SIM, Nikon, Tokyo, Japan) using an oil immersion objective lens (CFI SR Apochromat 100X, 1.49 NA, Nikon). Raw SIM images were reconstructed with the N-SIM module of Nikon Elements Advanced Research using the following parameters: Illumination contrast:1.00; high-resolution noise suppression:0.75; out-of-focus blur suppression:0.25. Brightness and contrast were adjusted for image presentation.

Images of keratin intermediate filament (KIF) networks were analyzed for the number of junctions and keratin bundle thickness using the BoneJ plugin in ImageJ as used previously by Laly et al (Laly et al., 2021). Regions of interest with an area of approximately 85 μm^2 were analyzed for keratin bundle thickness using the thickness option in the BoneJ plugin. The images were then binarized using the Shanbag threshold method and skeletonized. Skeletonized images were analyzed for the number of junctions detected in the KIF networks prior to and following the induction of vimentin expression.

Cells stained with phalloidin were thresholded using the 'Huang white' method for analyzing the aspect ratio, circularity, cell height and cell area.

Confocal images of desmoplakin across cell groups were used for the quantification of cells with disrupted desmosomes. The cells in each field were counted and considered as the total number of cells and the number of cells lacking the peripheral localization of desmoplakin were counted as cells with disrupted desmosomes. Cells with mislocalized desmoplakin even on one side of the periphery were still counted as cells with disrupted desmosomes. Percentages were calculated for the images across different cell groups.

Western blot analyses

Cells grown in culture dishes were trypsinized and centrifuged at 1,500 rpm for 3 min. Cell pellets were lysed with Radio-Immunoprecipitation Assay buffer and sonicated. The lysates were centrifuged at 9300xg for 5 min to remove debris. The protein concentration in the supernatant was determined with the Pierce BCA protein assay kit (23225, ThermoFisher Scientific, United States). 30–50 μg protein was boiled for 10 min with the addition of 4X Laemmli buffer. The boiled lysates were electrophoresed in 10% SDS-PAGE gels and transferred to nitrocellulose membranes. The blots were blocked with 5% non-fat dry milk in 1X TBST before incubating overnight with respective antibodies–vimentin (1:1,000, CPCA-Vim, EnCor Biotechnology), Keratin8 (1:1,000, 1,432-1, Epitomics, United States) and GAPDH (1:1,000, sc-365062, Santa Cruz Biotechnology, United States). After washing the blots three times for 5 min each with 1X TBST, they were incubated for 1 h with fluorescent secondary antibodies in 1X

TBST (1:10,000, IRDye 800CW, 680RD, LI-COR Biosciences, United States). The blots were then imaged with an Odyssey Fc Imaging System (LI-COR Biosciences, United States) after washing for 3X (5 min) with 1X TBST.

RNA sequencing library preparation

RNA from cell lines was isolated using the RNAeasy Plus mini kit (Qiagen, Germany). RNA quality and quantity were measured using Agilent 4,200 Tapestation with the high Sensitivity RNA ScreenTape System (Agilent Technologies). Briefly, mRNA was isolated from 80 ng of purified total RNA using oligo-dT beads (New England Biolabs, Inc). An NEBNext Ultra™ RNA kit (New England Biolabs, United States) was used for full-length cDNA synthesis and library preparation. Libraries were pooled, denatured and diluted, resulting in a 2.0 p.m. DNA solution. PhiX control was spiked at 1%. Libraries were sequenced on an Illumina NextSeq 500 instrument (Illumina Inc) using NextSeq 500 High Output reagent kit (Illumina Inc) (1x75 cycles) with a target read depth of approximate (5–10) million aligned reads per sample.

RNA analysis

Quality controlled FASTQ files were aligned to the Ensembl *Homo sapiens* genome (GRCh38) using STAR aligner (version 2.6.1). We then used featureCounts (Liao et al., 2014) to generate counts of reads uniquely mapped to annotated genes using the GRCh38 annotation gtf file (Anders et al., 2015). Differential gene expression analysis between the different conditions was estimated using DESeq2 (Love et al., 2014) based on the negative binomial distribution. The resulting *p*-values were adjusted using the Benjamini and Hochberg's approach for controlling the false discovery rate, and differentially expressed genes were determined at the 5% threshold. Gene set enrichment analysis was used to assess the statistical enrichment of gene ontologies, and pathways (Subramanian et al., 2005), and visualized using Clusterprofiler (v3.16.1) (Yu et al., 2012). All statistical analyses were performed using R software 4.0.1 (R Core Team (2020)).

Real time PCR

RNA from the various cell lines was isolated using the RNAeasy Plus mini kit (Qiagen, Germany) and converted to cDNA using an iScript cDNA synthesis kit (1708891, Bio-Rad Laboratories, United States). Primers against *SNAI1* (Forward primer (FP) - GCGAGCTGCAGGACTCTAAT; Reverse primer (RP)–GGACAGAGTCCCAGATGAGC), *TCF7* (FP–ACATGCAGCTATACCCAGGC; RP- CTTGGTGCTTTT CCCTCGAC), *TWIST1* (FP-CTCGGACAAGCTGAGCAAGA; RP- GCTCTGGAGGACCTGGTAGA), *CDH11* (FP–CCCAGTACACGTTGATGGCT; RP - AATGAATTC CGACGGTGGCT) and MMP16 (FP–TCAGCACTGGAAGACGGTTG; RP - AAATACTGC TCCGTTCCGCA) (Integrated DNA Technologies, United States) were used to amplify the respective genes with Light cycler 480 SYBR Green I master (04 887 352 001, Applied Biosystems, United States) in a CFX96 Real Time System (Bio-Rad Laboratories, United States). 18S rRNA was used as the internal control and the fold change values were calculated according to the $2^{-}\Delta\Delta Cq$ method (Livak and Schmittgen, 2001).

Polyacrylamide substrates and micropatterning

Polyacrylamide gels were used as substrates for traction force microscopy as reported previously (Saraswathibhatla and Notbohm, 2020). The gels were made with a Young's modulus of 6 kPa and thickness of 100 µm embedded with 0.008% (weight/volume) fluorescent particles (diameter 0.2 µm, carboxylate modified; Life Technologies). The fluorescent particles were localized to the top surface of the gels by centrifuging upside down during polymerization at 700 rpm for 10 min. Polydimethylsiloxane sheets with 1.0 mm diameter holes were placed on top of the gels, enabling functionalization of 1-mm circular islands of collagen I (1 ml of 0.1 mg/ml) using sulfo-SANPAH. For each dish, 500 µL of cell solution (0.6 million cells per mL of medium) was pipetted onto the masks and incubated at 37°C for 2 h. After the sheets were removed, confluent cell islands formed within 10–12 h and were subsequently imaged.

Imaging for traction force microscopy and monolayer stress microscopy

An Eclipse Ti microscope (Nikon, Melville, NY) with a 10× numerical aperture 0.5 objective (Nikon) and an Orca Flash 4.0 camera (Hamamatsu, Bridgewater, NJ) running Elements Ar software (Nikon) was used for imaging. Images were captured of both the cells (by phase contrast) (1 frame) and the fluorescent particles (50 frames). During imaging, the cells were maintained at 37°C and 5% CO_2. After imaging, cells were removed by treating with 0.05% trypsin for 1 h at 37°C, and reference images of the fluorescent particles were collected.

Fluctuation based super resolution processing

FBSR processing was performed using NanoJ-LiveSRRF (Gustafsson et al., 2016; Stubb et al., 2020). Each set of images

of fluorescent particles (50 frames at a resolution of 2048 × 2044 pixels with 0.65 μm/pixel) was used for reconstruction to increase the spatial resolution by a factor of two (4,096 × 4,088 pixels with 0.325 μm/pixel). The optimal reconstruction parameters were defined by resolution-scaled error (RSE) and resolution-scaled Pearson coefficient (RSP), computed by LiveSRRF.

Traction force microscopy and monolayer stress microscopy

Traction refers to the vector field of in-plane force per area applied by the cells to the substrate. To quantify tractions, cell-induced displacements of the fluorescent particles were measured using Fast Iterative Digital Image Correlation (FIDIC) (Bar-Kochba et al., 2015) using 128 × 128 pixel (41.6 × 41.6 μm^2) subsets centered on a grid with a spacing of 32 pixels (10.4 μm). The large subset size used reduced the noise floor substantially, which was essential for the experiments, as the cells produced small tractions. Tractions and intercellular stresses were computed using unconstrained Fourier-transform traction microscopy (Butler et al., 2002) accounting for the finite substrate thickness (del Álamo et al., 2007; Trepat et al., 2009) and monolayer stress microscopy (Tambe et al., 2013, 2011), which is based on the two-dimensional balance of forces. The root mean square of the traction vector was computed for each cell island. The two normal stresses computed from monolayer stress microscopy were averaged to quantify the tension; the mean tension was computed for each cell island.

Measurement of intracellular motion

All samples were imaged on a Leica SP8 confocal microscope with a resonant scanner at 37°C. Carboxylate-modified latex beads with a diameter of 0.5 um (Sigma-Aldrich, L3280) were added to the culture media (1:3000) 24 h prior to the measurement. Motions of endocytosed particles inside cells were recorded every 12 ms for 20 s. Particles in 10 different cells in each group were measured. All tested ULF mutant vimentin expressing cells and WT vimentin expressing cells had visible GFP. The whole experiment was repeated with a new batch of cells. Particle tracking was performed with TrackMate (Tinevez et al., 2017).

Calculation of cytoplasmic shear modulus from intracellular motion

The complex modulus of cytoplasm follows a weak power law (Gupta and Guo, 2017).

$$G(\omega) = G_0(-i\omega)^{\beta}$$

$$\beta \sim 0$$

For a tracer particle embedded in three-dimensional matrix, the complex shear modulus of matrix and N-dimensional mean square displacement (MSD) of trace particles inside are related by (Mason and Weitz, 1995; Squires and Mason, 2009).

$$\langle \Delta r^2(\omega) \rangle = \frac{2Nk_BT}{3i\omega\pi dG(\omega)}$$

Combining these two relationships we get

$$\langle \Delta r^2(\omega) \rangle_{2D} = \frac{4k_BT}{3\pi dG_0}(-i\omega)^{-1}$$

In the time domain

$$\langle \Delta r^2(\tau) \rangle_{2D} = \frac{4k_BT}{3\pi dG_0}$$

Thus, the compliance $(1/G_0)$ can be estimated from the high frequency MSD of intracellular motion by

$$\frac{1}{G_0} = \frac{3\pi d\langle \Delta \rangle r^2(\tau)_{2D}}{4k_BT}$$

This relation quantifies the high-frequency equilibrium mechanics of cytoplasm and can be applied to the plateau of intracellular MSD (Gupta and Guo, 2017). In the calculation, we used MSD of the minimal time interval $\Delta r^2(\tau = 12\,ms)$ to reflect the level of plateau. Outliers are removed. Outliers are defined as elements more than three scaled mean absolute deviation from the median.

Statistical Analyses. One-way ANOVA was used to compare the differences between uninduced cells, induced cells expressing WT vimentin and induced cells expressing ULF mutant vimentin. The Dunnett test was used for corrections of multiple comparisons.

Data availability statement

The sequencing data has been deposited in Gene Expression Omnibus (Accession number – GSE206724).

Results

The different stages of vimentin assembly in MCF7 cells

The microinjection or transient transfection of vimentin into epithelial cells null for this type III IF protein results in rapid changes in cell shape, motility and cell-cell adhesion (Mendez et al., 2010). With the aim of understanding some of the mechanistic changes brought about by vimentin expression in tumor-derived human breast epithelial cells null for vimentin expression, MCF7 cell lines with inducible vimentin expression

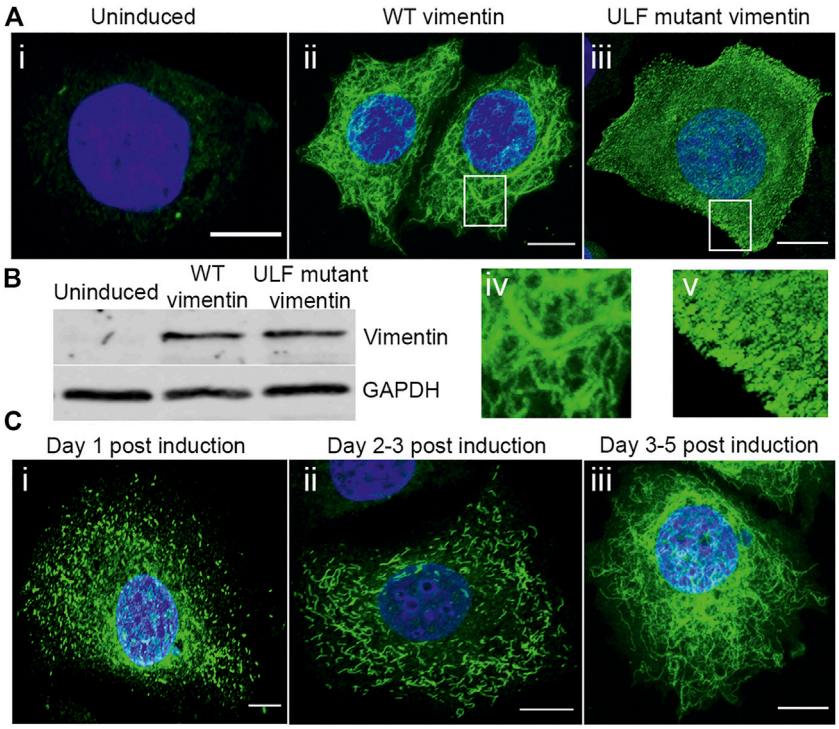

FIGURE 1
Expression and assembly stages of vimentin in inducible MCF7. **(A)** Immunofluorescence images of vimentin expression in **(A)** (i) uninduced MCF7 and (ii) cumate-induced MCF7 cells expressing WT vimentin and (iii) ULF mutant vimentin. Magnified images of WT vimentin or ULF mutant expressing cells are shown in (iv) and (v) respectively. **(B)** Western blot showing the expression levels of vimentin in uninduced MCF7 cells, WT vimentin in MCF7 cells following induction and ULF mutant vimentin in MCF7 cells, run along with an internal control, GAPDH. **(C)** Immunofluorescence images of vimentin in cumate-induced MCF7 cells expressing WT vimentin. C (i) and C (ii) show the vimentin on day 1 (C-i) and day 2 (C-ii) post cumate induction as particles and squiggles respectively, indicating the assembly stages of vimentin. c-iii is observed on day 5 post cumate induction where vimentin is observed as an extensive filamentous network. Scale bar is 10 μm.

were established. MCF7 was chosen as the cell of choice since it expresses only an endogenous keratin IF (KIF) network and is null for vimentin. MCF7 cells were transduced with a cumate inducible vector expressing either wild type (WT) vimentin or the Y117L mutant of vimentin (Herrmann and Aebi, 2016). The Y117L mutant vimentin halts assembly at the Unit Length Filament (ULF) stage and thus provides the opportunity to express vimentin but not mature VIF networks. Addition of inducer to the cells expressing WT vimentin resulted in the assembly of a complex VIF network after 4–5 days (Figure 1 A-ii, A-iv), whereas cells expressing the ULF mutant produced only non-filamentous particles and occasional short VIFs (squiggles) (Prahlad et al., 1998) after this time period (Figures 1 A-iii, A-v). We also followed the assembly of VIFs at earlier times after the induction of vimentin expression. At 1–2 days post induction, vimentin was present primarily as particles and squiggles of short IFs (Figures 1 C-i & C-ii) and by day 5, most cells had an extensive VIF network (Figure 1C-iii), demonstrating that the WT vimentin assembled according to previously defined steps in VIF polymerization *in situ* (Prahlad et al., 1998). Immunoblotting revealed that WT and ULF mutant vimentin cells expressed similar levels of vimentin after induction (Figure 1B), while uninduced cells lacked vimentin expression (Figures 1A-i,B). After the introduction of vimentin in the MCF7 cells, we examined the cell groups for changes in the cell height, area and shape, all of which were not altered significantly between the cell groups (Supplementary Figure S1B–E).

Expression of vimentin and the assembly of VIFs does not alter keratin expression levels but does alter the organization of keratin intermediate filaments (KIFs) in MCF7 cells

Cells undergoing an EMT lose their epithelial markers, including the types I and II keratins, K8/18, as they start acquiring mesenchymal features such as the initiation of vimentin expression (Zeisberg and Neilson, 2009). Therefore, we determined whether the expression levels of K8/K18 were altered after inducing vimentin expression in MCF7 cells. The results of

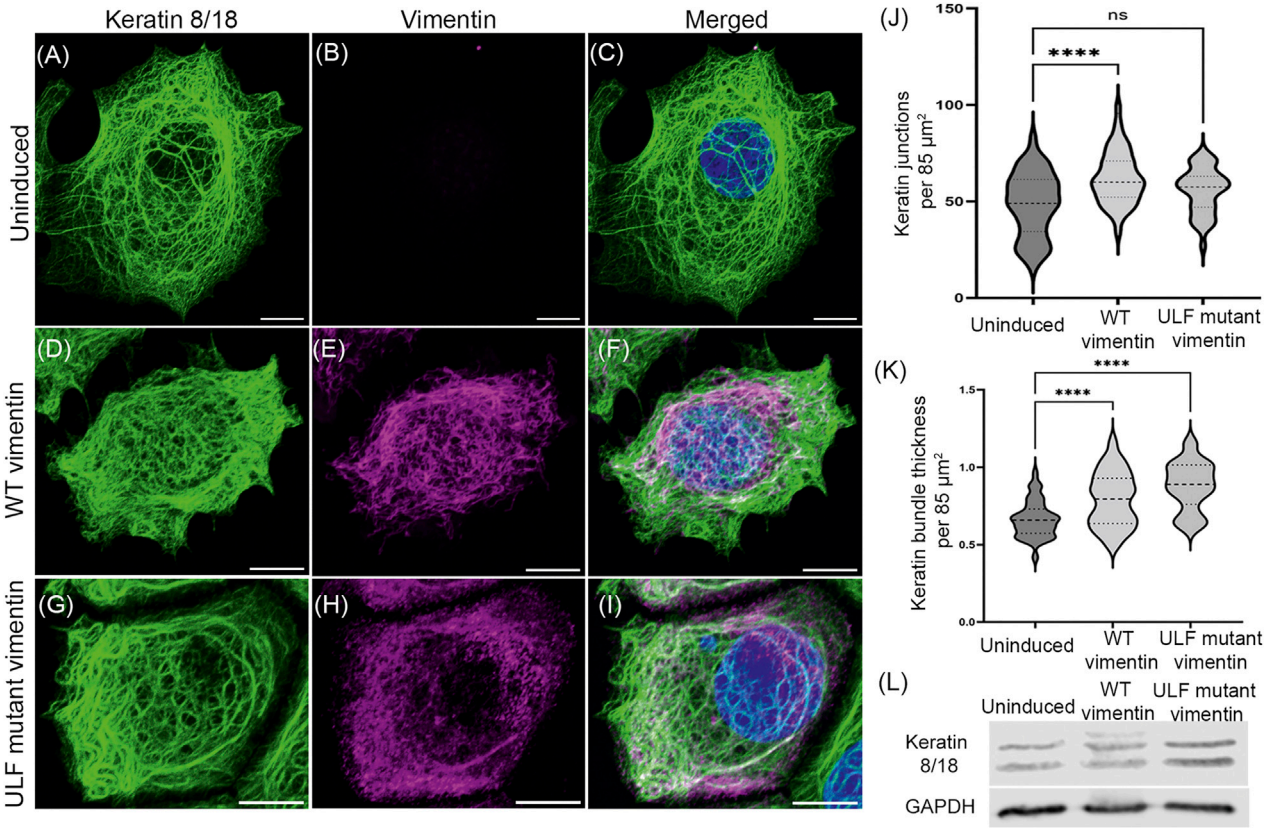

FIGURE 2
Vimentin expression does not alter the endogenous expression of keratin in MCF7. Immunofluorescence images of keratin 18 (A, D and G) and vimentin (B, E and H) in uninduced MCF7 cells **(A–C)**, WT vimentin in induced MCF7 cells **(D–F)** and ULF mutant vimentin in MCF7 cells **(G–I)**. Figures C, F and I show the overlay of keratin 18 and vimentin in the respective cells. Scale bar is 10 µm. **(J)** Graph showing the number of keratin junctions in uninduced MCF7 and in cells expressing either WT vimentin or ULF mutant vimentin. **(K)** Graph showing the keratin bundle thickness in uninduced MCF7 cells and following the induction of WT vimentin or ULF mutant vimentin. **(L)** Western blot showing the expression levels of keratin 8/18 in uninduced MCF7, MCF7 cells expressing WT vimentin or ULF mutant vimentin. GAPDH is used as loading control. One-way ANOVA was used to compare the differences between the groups. ****$p < 0.0001$. All the experiments were done on cells sorted for GFP expression 5 days post induction with cumate.

Western blot analyses showed that the amounts of K8/K18 did not change when either WT or ULF mutant vimentin were expressed. However, we could observe an additional keratin band only in the lysates from cells expressing WT vimentin. This could possibly be attributable to a post-translational modification (Figure 2L).

The organization of K8/18 KIF networks was affected in the cells expressing WT or ULF mutant vimentin (Figures 2A–J). Specifically, morphometric analysis revealed that WT vimentin expressing cells showed a significant increase in the number of overlaps or junctions of the bundles (tonofibrils) comprising the KIF networks resulting in tighter meshworks. The tonofibrils in these cells were significantly thicker (Figures 2J,K). In contrast the number of KIF junctions was not altered in ULF mutant vimentin expressing cells but the tonofibrils were thicker when compared with uninduced cells (Figures 2J,K).

Since reorganization of cytoskeletal proteins is considered as one of the molecular processes associated with initiation of EMT (Kalluri and Weinberg, 2009), we examined the organization of actin and microtubules upon vimentin expression. Interestingly, the cortical actin was more prominent in the uninduced cells which is not the case with the cells expressing vimentin. Moreover, the cells with either form of vimentin (WT or ULF mutant) were observed to have small protrusions unlike the uninduced cells (Supplementary Figure S2). We did not observe major changes in the organization of microtubules among the cell groups (Supplementary Figure S3).

Vimentin expression disrupts the organization of desmosomes involved in cell-cell adhesion in MCF7 cells

Loss of cell-cell adhesion is one of the hallmarks of epithelial cells undergoing the EMT. Desmoplakin is a major component of

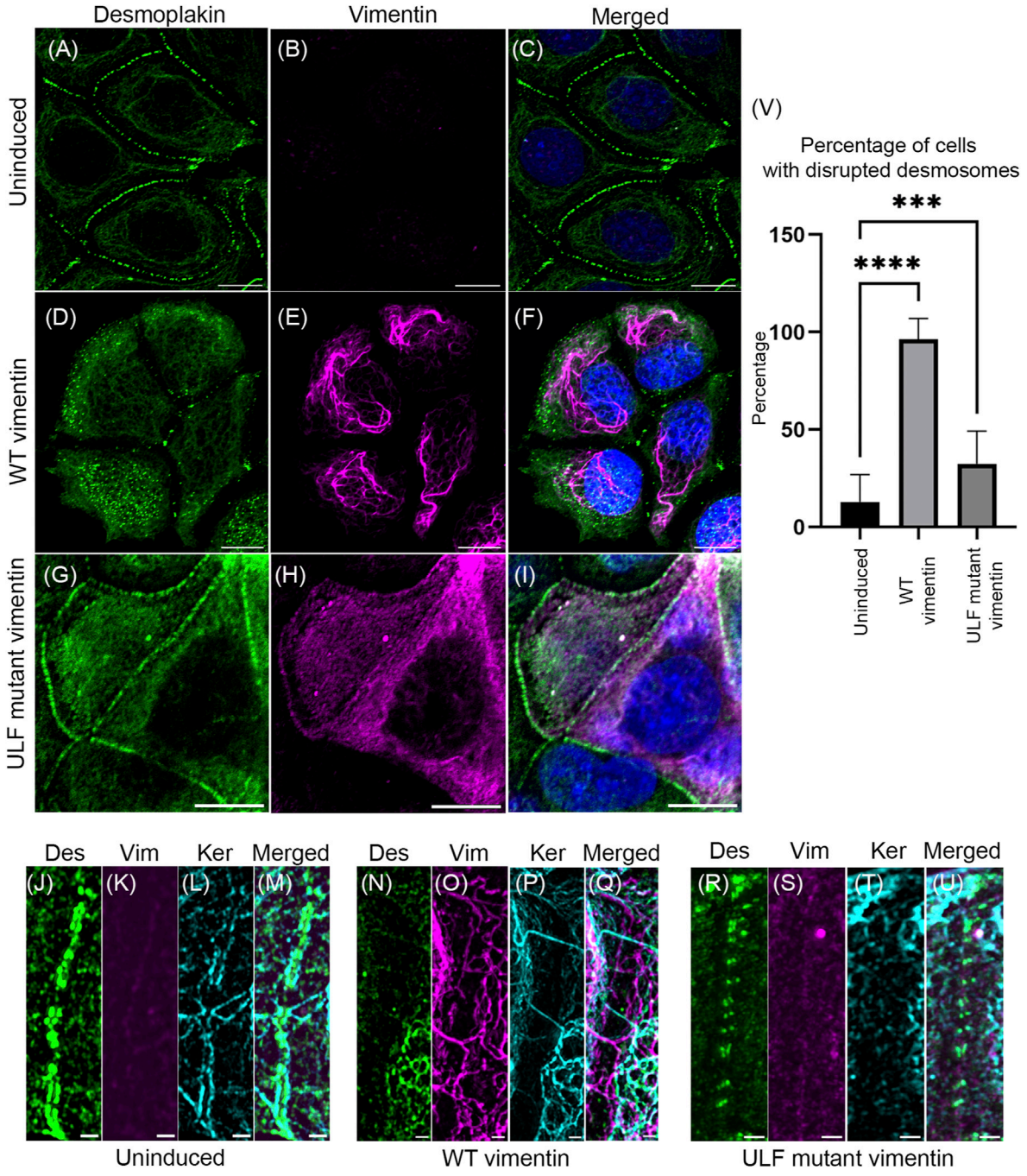

FIGURE 3
Expression of vimentin in MCF7 disrupts desmosomes. Immunofluorescence images of desmoplakin **(A,D,G)** and vimentin **(B,E,H)** in uninduced MCF7 **(A,B,C)**, cumate-induced MCF7 expressing WT vimentin **(D,E,F)** or ULF mutant vimentin **(G,H,I)**. Figures C, F and I show the overlay of desmoplakin and vimentin in the respective cells. Scale bar is 10 μm. Structured Illumination Microscopy (SIM) images of desmoplakin (J, N, R), vimentin (K, O, S), and keratin (L, P, T) in uninduced MCF7 cells **(J–M)**, cumate-induced MCF7 cells expressing WT vimentin **(N–Q)** and cumate-induced MCF7 cells expressing ULF mutant vimentin **(R–U)**. Figure M, Q and U show the respective overlays. Scale bar is 1 μm. **(V)** Graph showing the percentage of cells having disrupted desmoplakin in uninduced MCF7 cells (N = 205) and in MCF7 cells induced to express either WT (N = 101) or ULF mutant vimentin (N = 191). One way ANOVA was used to compare the differences between the groups.****$p < 0.0001$; ***$p < 0.001$. All the experiments were done on cells sorted for GFP expression 5 days post induction with cumate (Des–desmoplakin; Vim–vimentin; Ker–keratin).

the cytoplasmic face of the desmosomes involved in connecting KIFs to sites of cell-cell adhesion (Green et al., 1987; Smith and Fuchs, 1998). We have previously shown that introducing vimentin into MCF7 cells by transient transfection leads to loss of desmosomal structure and internalization of desmoplakin (Mendez et al., 2010). In the vimentin inducible MCF7 cells, desmoplakin was aligned in the periphery of uninduced contacting cells (Figures 3A–C). Following induction of vimentin expression, the desmosomes were disrupted and desmoplakin was displaced from the cell surfaces (Figures 3D–F). In contrast, the number of cells with disrupted desmosomes was reduced in ULF mutant vimentin expressing cells when compared to cells expressing WT vimentin (Figures 3G–I). The changes in desmosomes were revealed at higher resolution using Structured Illumination Microscopy (SIM). This demonstrated the parallel alignment of desmoplakin on either side of the surface of contacting uninduced cells (Figure 3J–M). SIM images of WT vimentin expressing cells clearly demonstrated that the desmoplakin was no longer aligned in the periphery of the majority of cells (Figure 3N–Q). Most of the mislocalized desmoplakin was associated with KIFs with a few associated with VIFs in the induced cells expressing WT vimentin (Supplementary Figure S4). In contrast, cells expressing ULF mutant vimentin largely retained desmoplakin localization in regions of cell-cell contact. However, we observed fewer linkages of keratin to desmoplakin compared to the uninduced cells (Figure 3R–U). Morphometric analysis demonstrated that desmosomes were disrupted in ~96% of the cells expressing WT vimentin whereas only ~32% were disrupted in cells expressing ULF mutant vimentin (Figure 3V). Overall, the results show that the expression of vimentin disrupts desmoplakin positioning at cell-cell adhesive junctions thereby causing the loss of desmosomal structures in MCF7 cells.

An important marker of the loss of cell-cell adhesion during the EMT is E-cadherin (Kalluri and Weinberg, 2009). Therefore, we determined the localization of E-cadherin in the cells with and without vimentin. Our results showed that the localization of E-cadherin appeared the same in uninduced and induced cells expressing either WT vimentin or ULF mutant vimentin (Supplementary Figure S5).

Vimentin expression reduces both cell-substrate traction force and intercellular tension in MCF7 cells

The loss of desmosomal structures following vimentin induction should lead to a weakening of the adhesive forces between adjacent cells in an epithelial sheet (Broussard et al., 2017). Since desmosomes are disrupted in the vimentin expressing cells (Figure 3), we measured the intercellular tension between uninduced and induced cells expressing WT or ULF mutant vimentin. Cells were seeded in islands of 1 mm diameter onto 3 kPa polyacrylamide gels containing fluorescent beads. The tractions and stresses were calculated using monolayer traction force and monolayer stress microscopy respectively (Figures 4A–C). The overall traction was significantly reduced in the cells expressing ULF mutant vimentin, however the reduction of traction observed in WT vimentin expressing cells did not have statistical significance compared to the uninduced cells (Figure 4D). In addition, monolayer stress microscopy indicated that the mean tension between cells expressing either WT or ULF mutant vimentin was significantly reduced compared to the uninduced cells with no significant difference between the two groups (Figure 4 C and E). It is interesting to note that although uninduced cells and the WT vimentin expressing cells exerted traction on the substrate that is not statistically different, the force was not transmitted to the neighboring cells upon vimentin expression (Figure 4 D and E). Further, we also analyzed the distribution of intercellular forces within the cell island. This was done by averaging the tension for all data points at different distances R from the center of the island. The results indicated that the intercellular tension sometimes appeared to increase with increasing radial position, but the increase was relatively small, ~10 Pa (Figure 4F), which was smaller than the differences between uninduced cells and cells expressing either WT or ULF mutant vimentin (~50 Pa, Figure 4E). Overall, expression of either form of vimentin reduces the cell-substrate and cell-cell forces in epithelial cells.

As indicated above, the reduction in cell-cell adhesive forces can be attributed to a loss of the structural integrity of desmosomes (Figure 3). To understand if the decreases in cell-substrate forces might be due to the alterations in cell-matrix junctions/focal adhesions, we stained the cells with vinculin and β1 integrin antibodies. Surprisingly, we did not observe significant changes in the organization of either focal adhesions or β1 integrin (Supplementary Figure S6,S7).

Vimentin expression increases intracellular stiffness in MCF7 cells

Vimentin regulates cell mechanics by altering cytoplasmic stiffness (Guo et al., 2013; Vahabikashi et al., 2019). To quantify the changes in the cytoplasmic mechanics of cells expressing WT or ULF mutant vimentin, we probed the intracellular dynamics and mechanics of endocytosed 0.5 μm diameter tracer particles in the cytoplasm by recording spontaneous fluctuations of the particles in living cells. We found that particles inside ULF mutant vimentin cells were less mobile than in the uninduced cells null for vimentin, while particles in the cells expressing WT vimentin were even less mobile (Figure 5A). As expected, the ensemble average of mean square displacement (MSD) of all the particles in different cells exhibited two distinct scaling regimes (Figure 5B): While the low frequency, apparently diffusive

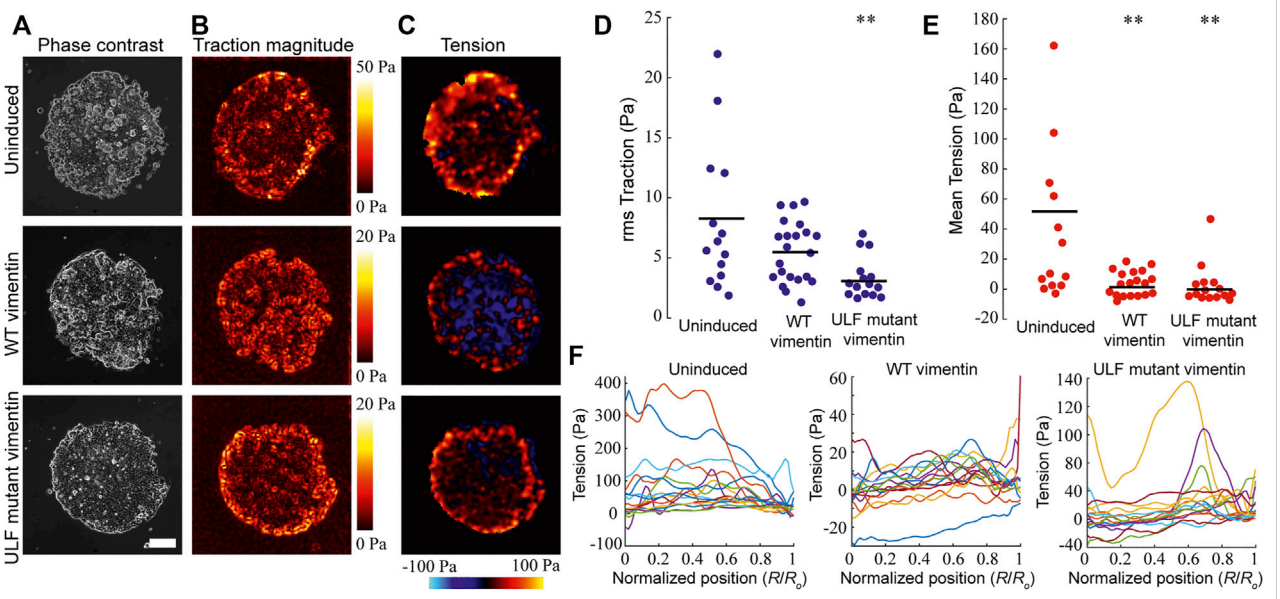

FIGURE 4
Vimentin expression reduced traction and intercellular forces in MCF7. **(A)** Representative phase contrast images of individual islands of uninduced MCF7 cells, and cumate-induced MCF7 cells expressing either WT vimentin or ULF mutant vimentin (scale bar 200 μm). **(B)** Color maps of magnitude of cell-substrate traction of cell islands corresponding to the images in column **(A)**. **(C)** Color maps of intercellular tension of the cell islands **(D)** Root-mean-square (rms) traction among uninduced MCF7 cells (n = 14) and MCF7 cells expressing either WT vimentin (n = 21) or ULF mutant vimentin (n = 15). **(E)** Average of intercellular stress comparison among uninduced MCF7 cells (n = 14), cumate-induced MCF7 cells expressing WT vimentin (n = 21) or ULF mutant vimentin (n = 15). In panels D and E, each dot represents an independent cell island, horizontal lines indicate means, and ** indicates $p < 0.01$ compared to uninduced (ANOVA with Bonferroni correction). **(F)** Intercellular stress plotted against normalized radial position, where 0 indicates the center of the cell island and R_0 is the radius of the cell island. Each line represents a different cell island.

regime, is governed by active enzymatic activities, the high frequency regime is dominated by thermal fluctuations (Gupta and Guo, 2017). As shown in Figure 5B, we found that high-frequency (>20 Hz) intracellular dynamics became weaker as vimentin expression was increased, indicating that the cytoplasm was stiffer. At high frequencies spontaneous motion is mainly thermally driven, in which case the modulus is inversely proportional to the average MSD (Mason and Weitz, 1995; Squires and Mason, 2009). Although distinguishable, the relative increase in modulus by expressing vimentin is limited to ~50% (Figure 5C). Thus, expression of WT or ULF mutant forms of vimentin make the cytoplasm stiffer with WT vimentin having the maximum effect on cytoplasmic stiffness.

Alterations in gene expression accompany the induction of vimentin expression: *TWIST1* is uniquely upregulated in WT vimentin expressing cells

To determine if the overall pattern of gene expression changes following the introduction of vimentin into MCF7 epithelial cells during the EMT, we sequenced RNA isolated from MCF7 cells with and without vimentin expression. Differential gene expression analyses identified the increased expression of 481 genes (>2 fold) in WT vimentin expressing cells in comparison with uninduced cells and 159 genes (>2 fold) in ULF mutant vimentin expressing cells. Interestingly, gene set enrichment analysis of the differentially expressed genes indicated that both WT and ULF mutant vimentin activated genes known to be involved in regulating cell locomotion/cell motility and cell junction organization (Figure 6 A and B). To understand how the expression of WT or ULF mutant vimentin impacts these molecular changes, differential gene expression analysis was performed comparing MCF7 cells expressing WT vimentin and those expressing ULF mutant vimentin. There were 78 genes in this category. Strikingly, bHLH transcription factors and E box binding factors were upregulated in cells expressing WT vimentin but not in cells expressing ULF mutant vimentin (Figure 6C). More specifically, *TWIST1*, a major EMT related transcription factor was upregulated in cells expressing WT vimentin, but not in cells expressing ULF mutant vimentin (Figure 6 C and D). Upregulation of *TWIST1* in cells expressing WT vimentin was also confirmed by real time PCR (Figure 6E). Along with the EMT specific transcription factor, *TWIST1*, we also observed an

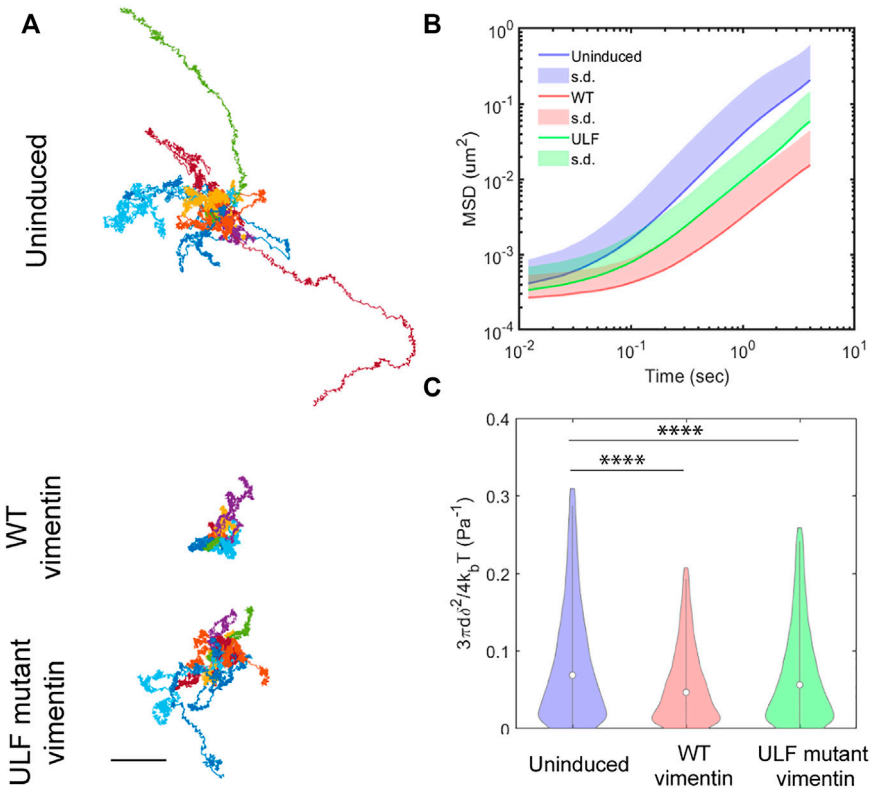

FIGURE 5
Vimentin expression reduces intracellular motion. **(A)** Trajectories of particles measured in 10 different cells in each group, from videos taken every 12 ms over 20 s time intervals. Scale bar, 0.5 μm. **(B)** Mean Square Displacement (MSD) of particles. **(C)** Compliance of cytoplasm. δ^2 is the MSD over 12 ms, k_b is Boltzmann constant, $T = 310$ K is temperature, $d = 0.5$ μm is the diameter of the particles. One way ANOVA was used to compare the differences between the groups. ****$p < 0.0001$.

increase in the expression levels of several mesenchymal specific genes such as *CDH11, MMP16, Col12A1* (Figure 6D) some of which are expressed during early hybrid EMT stages (Aiello et al., 2018; Pastushenko and Blanpain, 2019). Hence, our transcriptome analyses suggest that the expression of WT vimentin can induce the expression of the transcription factors necessary for cell migration.

Discussion

When vimentin expression is induced in MCF7 cells, it first forms particles and then short VIFs or squiggles, which then associate in tandem to form complete VIF networks (Herrmann and Aebi, 2016; Prahlad et al., 1998). We found similar assembly steps in the formation of VIF networks in MCF7 cells following the induction of vimentin expression. With the induction of vimentin expression, we observed that the organization of KIFs is altered with a significant increase in the number of keratin junctions in the cells expressing WT vimentin, indicating a tighter meshwork of KIF. A similar reduction in mesh size or "tightening" of KIF meshworks has been detected in lung alveolar epithelial cells placed under shear stress. This is accompanied by an increase in KIF meshwork stiffness as measured by particle tracking microrheology (Sivaramakrishnan et al., 2008). Based on these findings, we speculate that the organization of KIFs is rearranged in a way to facilitate the stress-enduring capacity of the cells encountered during cell migration following the expression of vimentin and the full transition to a mesenchymal cell phenotype. Based on these considerations, it is possible that the tighter meshworks formed by the bundles of KIFs (tonofibrils) work synergistically with the induction of vimentin to increase the stiffness of MCF7 cells.

Coincident with the changes in vimentin expression and assembly, desmosomes are disrupted in the MCF7 cells. The importance of desmosomes in cancer progression has been shown in the conditional knock-out of the *Dsp* gene in mouse pancreatic β cells where loss of desmosomes increased local invasion, even though the cells retained intact E-cadherin expression (Chun and Hanahan, 2010). Similarly, the loss of the desmosomal protein *Perp* has been suggested to be involved in epithelial cancer progression, under conditions where

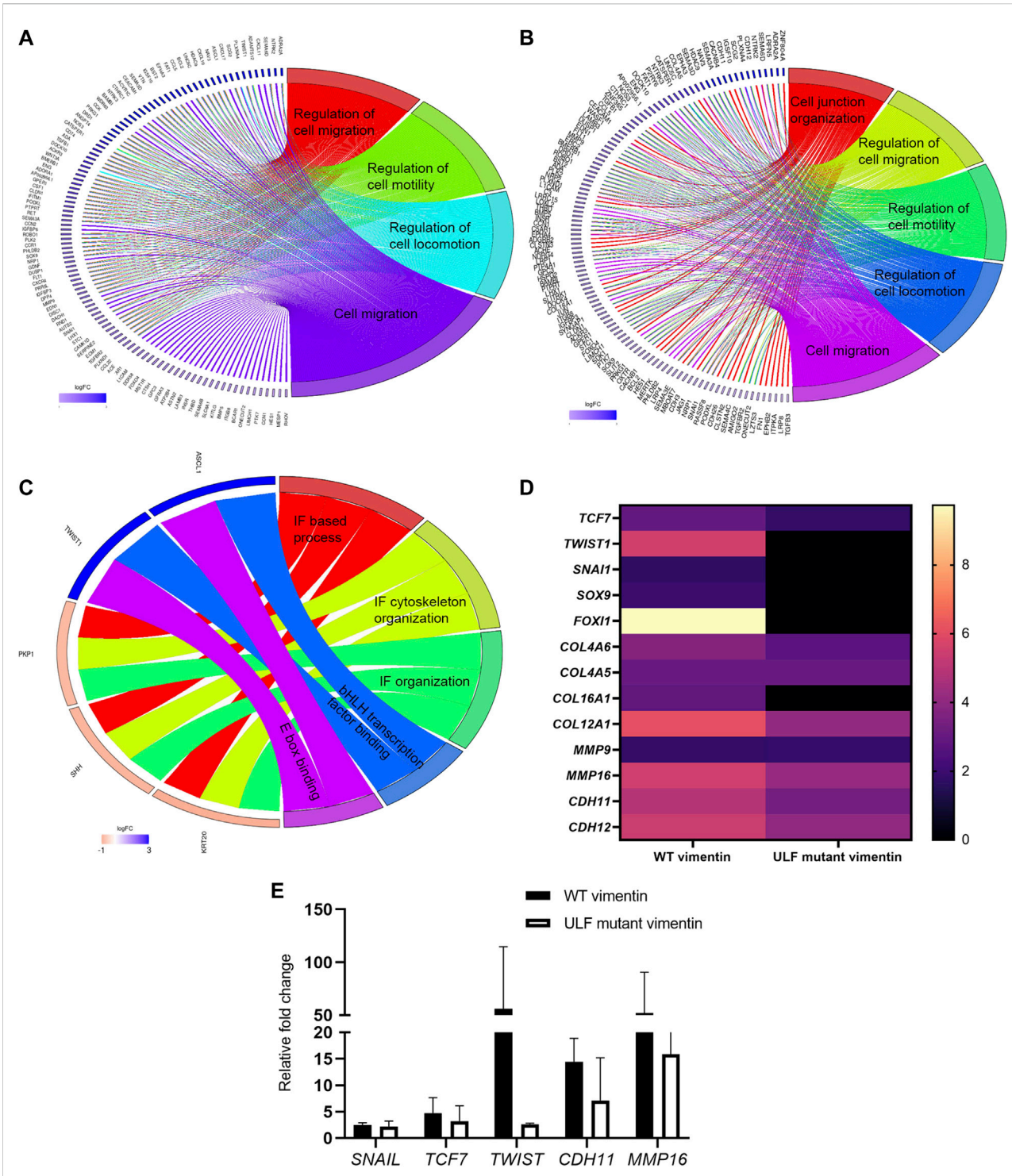

FIGURE 6
Upregulation of *TWIST1* requires WT vimentin. Circos plot representation of significantly enriched pathways linked with **(A)** WT vimentin vs. uninduced; **(B)** ULF mutant vimentin vs. uninduced; **(C)** WT vimentin vs. ULF mutant vimentin. The ribbon/arc that originates from different genes and terminates at associated pathways demonstrates the connectivity of genes and overrepresented pathways; **(D)** Heatmap shows the fold change values of transcription factors and few of the mesenchymal markers in cells expressing WT or ULF mutant vimentin. **(E)** Graph depicts the relative fold change values of genes obtained by real time PCR (n = 3). 18S rRNA was used as the internal control.

adherens junctions are not affected (Beaudry et al., 2010). Based on these studies, it has been suggested that epithelial cancer progression occurs in two steps; with desmosomal loss being the initial step followed by the loss of adherens junctions (Dusek and Attardi, 2011). In our study, we have observed the mislocalization of desmoplakin and disruption of desmosomes in cells expressing WT vimentin and to a lesser extent by ULF mutant vimentin. However, our transcriptome analysis indicates that the expression of the adherens junction marker, *E-cadherin,* is not altered upon expression of vimentin. This is supported by our analysis of the localization of E-cadherin in uninduced and in WT vimentin or ULF mutant vimentin expressing MCF7 cells (Supplementary Figure S5). With these observations, we can speculate that the expression of vimentin regulates the initial steps of the EMT associated with cancer metastasis/progression.

Our results also demonstrate that the expression of both WT and ULF mutant vimentin reduce traction and intercellular forces. In support of this finding, osteosarcoma cells expressing KIFs but lacking VIFs exert increased traction forces compared to these cells when vimentin is expressed (Jiu et al., 2017). In addition, the disruption of desmosome-KIF interactions by the expression of a dominant negative mutant of desmoplakin decreases both cell-cell and cell-substrate forces in epithelial carcinoma cells. There is also an increase in the cell-cell and cell-substrate forces when the desmosome-KIF interaction is strengthened (Broussard et al., 2017). Based upon these findings, it is possible that the induction of vimentin expression and its polymerization into VIFs or ULFs in MCF7 cells, may act to displace desmoplakin-KIF interactions and thereby reduce the intercellular and cell-substrate forces that we detected in our study. Other possible reasons for the ULF mutant vimentin exerting lesser traction force on the substrate could be due to changes in focal adhesion composition and organization (see Supplementary Figure S6) including reduced linkages of KIFs to the desmoplakin in the cells expressing ULF vimentin.

The impact of the expression of VIFs on cortical and cytoplasmic stiffness has been shown in mesenchymal cells (Guo et al., 2013; Vahabikashi et al., 2019). Cells expressing vimentin are twice as stiff as vimentin null cells which contain no cytoskeletal IFs (Guo et al., 2013). In further support of this we find that in MCF7 cells expressing either the WT or ULF mutant forms of vimentin have reduced intracellular dynamics assayed by the movements of endocytosed particles, indicating an increase cytoplasmic stiffness. It has been shown that the expression of vimentin and the metastatic potential of cancerous cells are correlated (Wei et al.,2008). Therefore, it is possible that our findings showing an increased cytoplasmic stiffness in cells expressing vimentin may be involved in the induction of cell migration and metastasis. Magnetic resonance elastography performed on breast and liver tumors to evaluate the stiffness of the tumors has revealed that malignant tumors are stiffer than benign tumors and normal tissues (Lorenzen et al., 2002; Venkatesh et al., 2012). In addition, cell stiffness increases with an increase in invasive potential in human breast carcinoma and glioblastoma cells (Kim et al., 2016; Monzo et al., 2021). In contrast, there is a widespread notion that cells with higher metastatic potential are more deformable and compliant (Holenstein et al., 2019; Plodinec et al., 2012; Swaminathan et al., 2011). In order to explain these differences, it may be that the relationships between cell stiffness and metastatic potential are cell type specific and/or vary based on the methods used for measuring stiffness. Another factor in these differences may be related to the "tuning" of the mechanical properties of cancerous cells at different stages of metastasis (Gensbittel et al., 2021).

Expression of WT and ULF mutant vimentin in MCF7 cells activates pathways involved in cell migration and cell junction organization. Interestingly, upregulation of *TWIST1*, an EMT specific transcription factor is seen only in cells which express WT vimentin, and not ULF mutant vimentin. *TWIST1* is involved in all the stages of cancer metastasis and its expression contributes to metastasis and invasion by inducing the EMT (Yang et al., 2004). Moreover, TWIST1 regulates the expression of vimentin during the EMT by increasing the expression of Cul2 circular RNA (Meng et al., 2018). Since the upregulation of *TWIST1* was observed only in WT vimentin expressing cells, we speculate that fully polymerized VIFs, but not partially assembled ULF could influence the regulation of *TWIST1*. This latter finding may be related to the role of polymerized VIF networks in signal transduction (Chang and Goldman, 2004; Helfand et al., 2005). In further support of this possibility, vimentin is known to act as a scaffold for kinases such as ERK and it recruits proteins for phosphorylation (Perlson et al., 2006; Virtakoivu et al., 2015). In addition, it has been shown that TWIST1 is regulated by ERK kinase (Weiss et al., 2012) which in turn is regulated by vimentin (Perlson et al., 2006; Virtakoivu et al., 2015). In the future it will be interesting to determine if VIFs, but not ULFs, act as a scaffold for certain kinases such as ERK, which might result in the upregulation of *TWIST1*.

Although we have observed an upregulation of *TWIST1* and several other mesenchymal markers such as *CDH11, MMP16, MME* and collagens upon the induction of vimentin expression, we did not see changes in the expression of E-*cadherin*, an important marker for the EMT transition. Recently, a partial or hybrid EMT has been identified in which E-cadherin and the expression of epithelial markers such as *Epcam*, *Cldn2* and *Cldn4* are retained but cells still undergo a successful metastasis (Aiello et al., 2018). Cells undergoing a partial EMT possess both epithelial and mesenchymal characteristics, which have been related to collective migration (Aiello et al., 2018; Pastushenko and Blanpain, 2019). Also, whether the cells undergo a partial or complete EMT seems to depend on the subtype of tumors. Interestingly, MCF7 cells are predicted to go through a partial

EMT process for cancer dissemination (Aiello et al., 2018). In agreement with this observation, our results in MCF7 cells show no changes in the expression levels of *E-cadherin,* but do appear to show an upregulation of other mesenchymal markers associated with a hybrid EMT. Based on these results, we hypothesize that the expression of WT vimentin drives the MCF7 cells into early/late partial EMT stages.

ULF–Unit Length Filament; VIF–Vimentin Intermediate Filament; KIF–Keratin Intermediate Filament; EMT–Epithelial to Mesenchymal Transition; SIM–Structured Illumination Microscopy; MSD–Mean Square Displacement.

Data availability statement

The datasets presented in this study can be found in online repositories. The names of the repository/repositories and accession number(s) can be found below: Gene Expression Omnibus accession number: GSE206724.

Author contributions

SS, AV, JN, MG, SA, RG designed research; SS, HY, JZ, KV, YP, HV performed research; SS, HY, JZ, KV, DR, analyzed data; SS, HY, JZ, DR, SA, RG wrote the paper.

Funding

This work was supported by NIH P01GM096971 awarded to RG and 1R01 GM140108 awarded to MG, Ian Wong (Brown University) and RG. Imaging work was performed at the Northwestern University Center for Advanced Microscopy generously supported by CCSG P30 CA060553 awarded to the Robert H Lurie Comprehensive Cancer Center. Structured illumination microscopy was performed on a Nikon N-SIM system, purchased through the support of NIH 1S10OD016342-01. Flow cytometry work was supported by the Northwestern University RHLCCC Flow Cytometry Facility and a Cancer Center Support Grant (NCI CA060553). Flow Cytometry Cell Sorting was performed on a BD FACSAria SORP system and BD FACSymphony S6 SORP system, purchased through the support of NIH 1S10OD011996-01 and 1S10OD026814-01. RNA sequencing was carried out in the Metabolomics Core -"Integrative Genomics" at the Robert H. Lurie Comprehensive Cancer Center.

Conflict of interest

The authors declare that the research was conducted in the absence of any commercial or financial relationships that could be construed as a potential conflict of interest.

Publisher's note

Supplementary material

The Supplementary Material for this article can be found online at: https://www.frontiersin.org/articles/10.3389/fcell.2022.929495/full#supplementary-material

References

Aiello, N. M., Maddipati, R., Norgard, R. J., Balli, D., Li, J., Yuan, S., et al. (2018). EMT subtype influences epithelial plasticity and mode of cell migration. *Dev. Cell.* 45, 681–695. e4. doi:10.1016/j.devcel.2018.05.027

Anders, S., Pyl, P. T., and Huber, W. (2015). HTSeq-A Python framework to work with high-throughput sequencing data. *Bioinformatics* 31, 166–169. doi:10.1093/bioinformatics/btu638

Bar-Kochba, E., Toyjanova, J., Andrews, E., Kim, K. S., and Franck, C. (2015). A fast iterative digital volume correlation algorithm for large deformations. *Exp. Mech.* 55, 261–274. doi:10.1007/s11340-014-9874-2

Beaudry, V. G., Jiang, D., Dusek, R. L., Park, E. J., Knezevich, S., Ridd, K., et al. (2010). Loss of the p53/p63 regulated desmosomal protein perp promotes tumorigenesis. *PLoS Genet.* 6, e1001168–16. doi:10.1371/journal.pgen.1001168

Broussard, J. A., Yang, R., Huang, C., Nathamgari, S. S. P., Beese, A. M., Godsel, L. M., et al. (2017). The desmoplakin-intermediate filament linkage regulates cell mechanics. *Mol. Biol. Cell.* 28, 3156–3164. doi:10.1091/mbc.E16-07-0520

Butler, J. P., Toli-Nørrelykke, I. M., Fabry, B., and Fredberg, J. J. (2002). Traction fields, moments, and strain energy that cells exert on their surroundings. *Am. J. Physiol. Cell. Physiol.* 282, C595–C605. doi:10.1152/AJPCELL.00270.2001

Chang, L., and Goldman, R. D. (2004). Intermediate filaments mediate cytoskeletal crosstalk. *Nat. Rev. Mol. Cell. Biol.* 5, 601–613. doi:10.1038/NRM1438

Chun, M. G. H., and Hanahan, D. (2010). Genetic deletion of the desmosomal component Desmoplakin promotes tumor microinvasion in a mouse model of pancreatic neuroendocrine carcinogenesis. *PLoS Genet.* 6, e1001120. doi:10.1371/journal.pgen.1001120

del Álamo, J. C., Meili, R., Alonso-Latorre, B., Rodríguez-Rodríguez, J., Aliseda, A., Firtel, R. A., et al. (2007). Spatio-temporal analysis of eukaryotic cell motility by improved force cytometry. *Proc. Natl. Acad. Sci. U. S. A.* 104, 13343–13348. doi:10.1073/PNAS.0705815104

Dusek, R. L., and Attardi, L. D. (2011). Desmosomes: New perpetrators in tumour suppression. *Nat. Rev. Cancer* 11, 317–323. doi:10.1038/nrc3051

Eckes, B., Colucci-Guyon, E., Smola, H., Nodder, S., Babinet, C., Krieg, T., et al. (2000). Impaired wound healing in embryonic and adult mice lacking vimentin. *J. Cell. Sci.* 113, 2455–2462. doi:10.1242/JCS.113.13.2455

Eckes, B., Dogic, D., Colucci-Guyon, E., Wang, N., Maniotis, A., Ingber, D., et al. (1998). Impaired mechanical stability, migration and contractile capacity in vimentin-deficient fibroblasts. *J. Cell. Sci.* 111, 1897–1907. doi:10.1242/JCS.111.13.1897

Eriksson, J. E., Dechat, T., Grin, B., Helfand, B., Mendez, M., Pallari, H. M., et al. (2009). Introducing intermediate filaments: From discovery to disease. *J. Clin. Investig.* 119, 1763–1771. doi:10.1172/JCI38339

Gensbittel, V., Kräter, M., Harlepp, S., Busnelli, I., Guck, J., and Goetz, J. G. (2021). Mechanical adaptability of tumor cells in metastasis. *Dev. Cell.* 56, 164–179. doi:10.1016/j.devcel.2020.10.011

Gilles, C., Polette, M., Zahm, J. M., Tournier, J. M., Volders, L., Foidart, J. M., et al. (1999). Vimentin contributes to human mammary epithelial cell migration. *J. Cell. Sci.* 112, 4615–4625. doi:10.1242/JCS.112.24.4615

Green, K. J., Geiger, B., Jones, J. C. R., Talian, J. C., and Goldman, R. D. (1987). The relationship between intermediate filaments and microfilaments before and during the formation of desmosomes and adherens-type junctions in mouse epidermal keratinocytes. *J. Cell. Biol.* 104, 1389–1402. doi:10.1083/JCB.104.5.1389

Guo, M., Ehrlicher, A. J., Mahammad, S., Fabich, H., Jensen, M. H., Moore, J. R., et al. (2013). The role of vimentin intermediate filaments in cortical and cytoplasmic mechanics. *Biophys. J.* 105, 1562–1568. doi:10.1016/j.bpj.2013.08.037

Gupta, S. K., and Guo, M. (2017). Equilibrium and out-of-equilibrium mechanics of living mammalian cytoplasm. *J. Mech. Phys. Solids* 107, 284–293. doi:10.1016/J.JMPS.2017.07.007

Gustafsson, N., Culley, S., Ashdown, G., Owen, D. M., Pereira, P. M., and Henriques, R. (2016). Fast live-cell conventional fluorophore nanoscopy with ImageJ through super-resolution radial fluctuations. *Nat. Commun.* 7, 12471. doi:10.1038/ncomms12471

Helfand, B. T., Chou, Y. H., Shumaker, D. K., and Goldman, R. D. (2005). Intermediate filament proteins participate in signal transduction. *Trends Cell. Biol.* 15, 568–570. doi:10.1016/j.tcb.2005.09.009

Helfand, B. T., Mendez, M. G., Murthy, S. N. P., Shumaker, D. K., Grin, B., Mahammad, S., et al. (2011). Vimentin organization modulates the formation of lamellipodia. *Mol. Biol. Cell.* 22, 1274–1289. doi:10.1091/mbc.E10-08-0699

Herrmann, H., and Aebi, U. (2016). Intermediate filaments: Structure and assembly. *Cold Spring Harb. Perspect. Biol.* 8, a018242. doi:10.1101/cshperspect.a018242

Herrmann, H., Häner, M., Brettel, M., Müller, S. A., Goldie, K. N., Fedtke, B., et al. (1996). Structure and assembly properties of the intermediate filament protein vimentin: The role of its head, rod and tail domains. *J. Mol. Biol.* 264, 933–953. doi:10.1006/JMBI.1996.0688

Holenstein, C. N., Horvath, A., Schär, B., Schoenenberger, A. D., Bollhalder, M., Goedecke, N., et al. (2019). The relationship between metastatic potential and *in vitro* mechanical properties of osteosarcoma cells. *Mol. Biol. Cell.* 30, 887–898. doi:10.1091/mbc.E18-08-0545

Jiu, Y., Peränen, J., Schaible, N., Cheng, F., Eriksson, J. E., Krishnan, R., et al. (2017). Vimentin intermediate filaments control actin stress fiber assembly through GEF-H1 and RhoA. *J. Cell. Sci.* 130, 892–902. doi:10.1242/jcs.196881

Jones, J. C. R., and Goldman, R. D. (1985). Intermediate filaments and the initiation of desmosome assembly. *J. Cell. Biol.* 101, 506–517. doi:10.1083/JCB.101.2.506

Kalluri, R., and Weinberg, R. A. (2009). The basics of epithelial-mesenchymal transition. *J. Clin. Investig.* 119, 1420–1428. doi:10.1172/JCI39104

Kim, T. H., Gill, N. K., Nyberg, K. D., Nguyen, A. v., Hohlbauch, S. v., Geisse, N. A., et al. (2016). Cancer cells become less deformable and more invasive with activation of β-adrenergic signaling. *J. Cell. Sci.* 129, 4563–4575. doi:10.1242/jcs.194803

Laly, A. C., Sliogeryte, K., Pundel, O. J., Ross, R., Keeling, M. C., Avisetti, D., et al. (2021). The keratin network of intermediate filaments regulates keratinocyte rigidity sensing and nuclear mechanotransduction. *Sci. Adv.* 7, 6187–6214. doi:10.1126/SCIADV.ABD6187/SUPPL_FILE/ABD6187_SM

Liao, Y., Smyth, G. K., and Shi, W. (2014). FeatureCounts: An efficient general purpose program for assigning sequence reads to genomic features. *Bioinformatics* 30, 923–930. doi:10.1093/bioinformatics/btt656

Livak, K. J., and Schmittgen, T. D. (2001). Analysis of relative gene expression data using real-time quantitative PCR and the 2(-Delta Delta C(T)) Method. *Methods* 25, 402–408. doi:10.1006/METH.2001.1262

Lorenzen, J., Sinkus, R., Lorenzen, M., Dargatz, M., Leussler, C., Röschmann, P., et al. (2002). MR elastography of the breast:preliminary clinical results. *Rofo* 174, 830–834. doi:10.1055/S-2002-32690

Love, M. I., Huber, W., and Anders, S. (2014). Moderated estimation of fold change and dispersion for RNA-seq data with DESeq2. *Genome Biol.* 15, 550. doi:10.1186/s13059-014-0550-8

Lowery, J., Kuczmarski, E. R., Herrmann, H., and Goldma, R. D. (2015). Intermediate filaments play a pivotal role in regulating cell architecture and function. *J. Biol. Chem.* 290, 17145–17153. doi:10.1074/jbc.R115.640359

Mason, T. G., and Weitz, D. A. (1995). Optical measurements of frequency-dependent linear viscoelastic moduli of complex fluids. *Phys. Rev. Lett.* 74, 1250–1253. doi:10.1103/PhysRevLett.74.1250

Meier, M., Padilla, G. P., Herrmann, H., Wedig, T., Hergt, M., Patel, T. R., et al. (2009). Vimentin coil 1A—a molecular switch involved in the initiation of filament elongation. *J. Mol. Biol.* 390, 245–261. doi:10.1016/J.JMB.2009.04.067

Mendez, M. G., Kojima, S., and Goldman, R. D. (2010). Vimentin induces changes in cell shape, motility, and adhesion during the epithelial to mesenchymal transition. *FASEB J.* 24, 1838–1851. doi:10.1096/fj.09-151639

Mendez, M. G., Restle, D., and Janmey, P. A. (2014). Vimentin enhances cell elastic behavior and protects against compressive stress. *Biophys. J.* 107, 314–323. doi:10.1016/j.bpj.2014.04.050

Meng, J., Chen, S., Han, J. X., Qian, B., Wang, X. R., Zhong, W. L., et al. (2018). Twist1 regulates vimentin through Cul2 circular RNA to promote EMT in hepatocellular carcinoma. *Cancer Res.* 78, 4150–4162. doi:10.1158/0008-5472.CAN-17-3009

Messica, Y., Laser-Azogui, A., Volberg, T., Elisha, Y., Lysakovskaia, K., Eils, R., et al. (2017). The role of vimentin in regulating cell invasive migration in dense cultures of breast carcinoma cells. *Nano Lett.* 17, 6941–6948. doi:10.1021/acs.nanolett.7b03358

Monzo, P., Crestani, M., Chong, Y. K., Ghisleni, A., Hennig, K., Li, Q., et al. (2021). Adaptive mechanoproperties mediated by the formin FMN1 characterize glioblastoma fitness for invasion. *Dev. Cell.* 56, 2841–2855.e8. doi:10.1016/J.DEVCEL.2021.09.007

Pastushenko, I., and Blanpain, C. (2019). EMT transition states during tumor progression and metastasis. *Trends Cell. Biol.* 29, 212–226. doi:10.1016/j.tcb.2018.12.001

Patteson, A. E., Vahabikashi, A., Pogoda, K., Adam, S. A., Mandal, K., Kittisopikul, M., et al. (2019). Vimentin protects cells against nuclear rupture and DNA damage during migration. *J. Cell. Biol.* 218, 4079–4092. doi:10.1083/JCB.201902046

Perlson, E., Michaelevski, I., Kowalsman, N., Ben-Yaakov, K., Shaked, M., Seger, R., et al. (2006). Vimentin binding to phosphorylated Erk sterically hinders enzymatic dephosphorylation of the kinase. *J. Mol. Biol.* 364, 938–944. doi:10.1016/J.JMB.2006.09.056

Plodinec, M., Loparic, M., Monnier, C. A., Obermann, E. C., Zanetti-Dallenbach, R., Oertle, P., et al. (2012). The nanomechanical signature of breast cancer. *Nat. Nanotechnol.* 7, 757–765. doi:10.1038/NNANO.2012.167

Prahlad, V., Yoon, M., Moir, R. D., Vale, R. D., and Goldman, R. D. (1998). Rapid movements of vimentin on microtubule tracks: Kinesin-dependent assembly of intermediate filament networks. *J. Cell. Biol.* 143, 159–170. doi:10.1083/JCB.143.1.159

R Core Team (2020). *R: A language and environment for statistical computing R foundation for statistical computing*. Vienna, Austria. Available at: http://www.r-project.org/index.html (accessed February 23, 2022).

Ridge, K. M., Eriksson, J. E., Pekny, M., and Goldman, R. D. (2022). Roles of vimentin in health and disease. *Genes. Dev.* 36, 391–407. doi:10.1101/GAD.349358.122

Saraswathibhatla, A., and Notbohm, J. (2020). Tractions and stress fibers control cell shape and rearrangements in collective cell migration. *Phys. Rev. X* 10, 011016. doi:10.1103/PhysRevX.10.011016

Sivaramakrishnan, S., DeGiulio, J. v., Lorand, L., Goldman, R. D., and Ridge, K. M. (2008). Micromechanical properties of keratin intermediate filament networks. *Proc. Natl. Acad. Sci. U. S. A.* 105, 889–894. doi:10.1073/pnas.0710728105

Smith, E. A., and Fuchs, E. (1998). Defining the interactions between intermediate filaments and desmosomes. *J. Cell. Biol.* 141, 1229–1241. doi:10.1083/JCB.141.5.1229

Squires, T. M., and Mason, T. G. (2009). Fluid mechanics of microrheology. *Annu. Rev.*. 42, 413–438. doi:10.1146/ANNUREV-FLUID-121108-145608

Stubb, A., Laine, R. F., Miihkinen, M., Hamidi, H., Guzmán, C., Henriques, R., et al. (2020). Fluctuation-Based super-resolution traction force microscopy. *Nano Lett.* 20, 2230–2245. doi:10.1021/acs.nanolett.9b04083

Subramanian, A., Tamayo, P., Mootha, V. K., Mukherjee, S., Ebert, B. L., Gillette, M. A., et al. (2005). Gene set enrichment analysis: A knowledge-based approach for interpreting genome-wide expression profiles. *Proc. Natl. Acad. Sci. U. S. A.* 102, 15545–15550. doi:10.1073/PNAS.0506580102/SUPPL_FILE/06580FIG7

Swaminathan, V., Mythreye, K., Tim O'Brien, E., Berchuck, A., Blobe, G. C., and Superfine, R. (2011). Mechanical Stiffness grades metastatic potential in patient tumor cells and in cancer cell lines. *Cancer Res.* 71, 5075–5080. doi:10.1158/0008-5472.CAN-11-0247

Tambe, D. T., Corey Hardin, C., Angelini, T. E., Rajendran, K., Park, C. Y., Serra-Picamal, X., et al. (2011). Collective cell guidance by cooperative intercellular forces. *Nat. Mat.* 10, 469–475. doi:10.1038/NMAT3025

Tambe, D. T., Croutelle, U., Trepat, X., Park, C. Y., Kim, J. H., Millet, E., et al. (2013). Monolayer stress microscopy: Limitations, artifacts, and accuracy of recovered intercellular stresses. *PLOS ONE* 8, e55172. doi:10.1371/JOURNAL.PONE.0055172

Tinevez, J. Y., Perry, N., Schindelin, J., Hoopes, G. M., Reynolds, G. D., Laplantine, E., et al. (2017). TrackMate: An open and extensible platform for single-particle tracking. *Methods* 115, 80–90. doi:10.1016/J.YMETH.2016.09.016

Trepat, X., Wasserman, M. R., Angelini, T. E., Millet, E., Weitz, D. A., Butler, J. P., et al. (2009). Physical forces during collective cell migration. *Nat. Phys.* 5, 426–430. doi:10.1038/nphys1269

Vahabikashi, A., Park, C. Y., Perkumas, K., Zhang, Z., Deurloo, E. K., Wu, H., et al. (2019). Probe sensitivity to cortical versus intracellular cytoskeletal network stiffness. *Biophys. J.* 116, 518–529. doi:10.1016/j.bpj.2018.12.021

Venkatesh, S. K., Yin, M., Glockner, J. F., Takahashi, N., Araoz, P. A., Talwalkar, J. A., et al. (2012). *MR elastography of liver tumors: Preliminary results*, 190, 1534. doi:10.2214/AJR.07.3123

Virtakoivu, R., Mai, A., Mattila, E., de Franceschi, N., Imanishi, S. Y., Corthals, G., et al. (2015). Vimentin-ERK signaling uncouples slug gene regulatory function. *Cancer Res.* 75, 2349–2362. doi:10.1158/0008-5472.CAN-14-2842

Vuoriluoto, K., Haugen, H., Kiviluoto, S., Mpindi, J. P., Nevo, J., Gjerdrum, C., et al. (2011). Vimentin regulates EMT induction by Slug and oncogenic H-Ras and migration by governing Axl expression in breast cancer. *Oncogene* 30, 1436–1448. doi:10.1038/onc.2010.509

Wei, J., Xu, G., Wu, M., Zhang, Y., Li, Q., Liu, P., et al. (2008). Overexpression of vimentin contributes to prostate cancer invasion and metastasis via src regulation. *Anticancer Res.* 28 (1A), 327–334.

Weiss, M. B., Abel, E. v., Mayberry, M. M., Basile, K. J., Berger, A. C., and Aplin, A. E. (2012). TWIST1 is an ERK1/2 effector that promotes invasion and regulates MMP-1 expression in human melanoma cells. *Cancer Res.* 72, 6382–6392. doi:10.1158/0008-5472.CAN-12-1033

Yang, J., Mani, S. A., Donaher, J. L., Ramaswamy, S., Itzykson, R. A., Come, C., et al. (2004). Twist, a master regulator of morphogenesis, plays an essential role in tumor metastasis. *Cell.* 117, 927–939. doi:10.1016/J.CELL.2004.06.006

Yu, G., Wang, L. G., Han, Y., and He, Q. Y. (2012). ClusterProfiler: An R package for comparing biological themes among gene clusters. *OMICS A J. Integr. Biol.* 16, 284–287. doi:10.1089/omi.2011.0118

Zeisberg, M., and Neilson, E. G. (2009). Biomarkers for epithelial-mesenchymal transitions. *J. Clin. Investig.* 119, 1429–1437. doi:10.1172/JCI36183

frontiers | Frontiers in Cell and Developmental Biology

TYPE Original Research
PUBLISHED 04 October 2022
DOI 10.3389/fcell.2022.946190

OPEN ACCESS

EDITED BY
Dolores Pérez-Sala,
Spanish National Research Council (CSIC), Spain

REVIEWED BY
Marta Llimargas,
Spanish National Research Council (CSIC), Spain
Joaquin de Navascues,
University of Essex, United Kingdom
Martin Gregor,
IMG CAS, Czechia

*CORRESPONDENCE
Rudolf E. Leube,
rleube@ukaachen.de

SPECIALTY SECTION
This article was submitted to Cell Growth and Division, a section of the journal Frontiers in Cell and Developmental Biology

RECEIVED 17 May 2022
ACCEPTED 14 September 2022
PUBLISHED 04 October 2022

CITATION
Moch M, Schieren J and Leube RE (2022), Cortical tension regulates desmosomal morphogenesis. *Front. Cell Dev. Biol.* 10:946190. doi: 10.3389/fcell.2022.946190

Cortical tension regulates desmosomal morphogenesis

Marcin Moch, Jana Schieren and Rudolf E. Leube*

Institute of Molecular and Cellular Anatomy, RWTH Aachen University, Aachen, Germany

Mechanical stability is a fundamental and essential property of epithelial cell sheets. It is in large part determined by cell-cell adhesion sites that are tightly integrated by the cortical cytoskeleton. An intimate crosstalk between the adherens junction-associated contractile actomyosin system and the desmosome-anchored keratin intermediate filament system is decisive for dynamic regulation of epithelial mechanics. A major question in the field is whether and in which way mechanical stress affects junctional plasticity. This is especially true for the desmosome-keratin scaffold whose role in force-sensing is virtually unknown. To examine this question, we inactivated the actomyosin system in human keratinocytes (HaCaT) and canine kidney cells (MDCK) and monitored changes in desmosomal protein turnover.

Partial inhibition of myosin II by para-nitro-blebbistatin led to a decrease of the cells' elastic modulus and to reduced desmosomal protein turnover in regions where nascent desmosomes are formed and, to a lower degree, in regions where larger, more mature desmosomes are present. Interestingly, desmosomal proteins are affected differently: a significant decrease in turnover was observed for the desmosomal plaque protein desmoplakin I (DspI), which links keratin filaments to the desmosomal core, and the transmembrane cadherin desmoglein 2 (Dsg2). On the other hand, the turnover of another type of desmosomal cadherin, desmocollin 2 (Dsc2), was not significantly altered under the tested conditions. Similarly, the turnover of the adherens junction-associated E-cadherin was not affected by the low doses of para-nitro-blebbistatin. Inhibition of actin polymerization by low dose latrunculin B treatment and of ROCK-driven actomyosin contractility by Y-27632 treatment also induced a significant decrease in desmosomal DspI turnover. Taken together, we conclude that changes in the cortical force balance affect desmosome formation and growth. Furthermore, they differentially modulate desmosomal protein turnover resulting in changes of desmosome composition. We take the observations as evidence for a hitherto unknown desmosomal mechanosensing and mechanoresponse pathway responding to an altered force balance.

Abbreviations: BSA, bovine serum albumin; DAPI, 4′,6-diamidino-2-phenylindole; DMSO, dimethyl sulfoxideDsc2—desmocollin two Dsg2—desmoglein two; DspI, desmoplakin one; F-actin, filamentous actin; FBS, fetal bovine serum; FRAP, fluorescence recovery after photobleaching; GFP, green fluorescent protein; max. int. projection, maximum intensity projection; MDCK, Madin-Darby canine kidney (cell line); mW, milli watt; min, minute; nm, nano meter; n.s, not significant; PBS, phosphate-buffered saline; PFA, paraformaldehyde; μM, micro molar; μm, micro meter.

KEYWORDS

Keratin, myosin II, desmosome, desmoplakin, desmoglein, desmocollin, actin, adhesion

Introduction

Barrier-forming epithelia are characterized by the high degree of mechanical cohesiveness and stability. These properties rely on tight cell-cell adhesion and associated cytoskeletal networks, which form a resilient yet highly adaptable transcellular scaffold. An important architectural feature is the integration of cell-cell adhesion sites by the submembraneous cell cortex.

Two major systems can be distinguished in epithelial cells:

i) A dense layer of actomyosin is situated directly below the plasma membrane. It consists of filamentous actin and non-muscle myosin II. The myosin motor activity supports actin-dependent cortical tension (Ananthakrishnan & Ehrlicher, 2007; Chugh & Paluch, 2018). It cooperates with other components of the actin cytoskeleton, including prominent stress fibers. The actomyosin system is associated with adherens junctions (Priya & Yap, 2015), which include the classical cadherins as transmembrane receptors. They are linked to the actin system *via* linker molecules including catenins (recent review in (Rubsam et al., 2018)).
ii) A less investigated layer can be distinguished below the actomyosin layer. It consists of keratin intermediate filaments, which are anchored to desmosomal adhesions and form a web-like network structure with important mechanobiological functions (Quinlan et al., 2017; Prechova et al., 2022). A fundamental difference to the actomyosin cortex is the inability of the keratin intermediate filament network to actively generate force. But keratin filaments exhibit unique mechanical properties, notably a very high degree of flexibility and extensibility which they share with other intermediate filament types (Block et al., 2015; Yoon & Leube, 2019). Keratin intermediate filaments are attached to desmosomal cadherins of the desmoglein (Dsg) and desmocollin (Dsc) type *via* desmoplakin (Dsp). In addition, several linker molecules, including plakophilins and plakoglobin (also referred to as *γ*-catenin), connect the desmosomal components forming an electron dense plaque (recent review in (Mohammed & Chidgey, 2021; Muller et al., 2021; Hegazy et al., 2022)). The cortical keratin intermediate filaments are part of a rim and spokes system consisting of radial spokes in the cytoplasm that are connected to the submembraneous cortical rim, which interconnects desmosomes (Quinlan et al., 2017). Rim and spoke components can be generated from nascent desmosomes (Moch et al., 2019).

Evidence for a crosstalk between both the actomyosin-adherens junction and keratin-desmosome systems has accumulated over the years (Green et al., 1987; Godsel et al., 2010; Rubsam et al., 2018). Recent work has furthermore provided evidence for the functional relevance of the crosstalk to achieve mechanical homeostasis and responsiveness (Broussard et al., 2017; Prechova et al., 2022). Exactly, how changes in the mechanical environment are sensed and translated into cellular responses is less well understood. This is particularly true for the keratin-desmosome scaffold. To address this question, we decreased the intrinsic actomyosin-dependent tension by low dose treatment with the myosin II inhibitor para-nitro-blebbistatin and examined changes in desmosomal protein turnover. We observe a desmosomal protein-specific response and take this as evidence for a mechanosensing pathway that determines desmosomal protein composition and may thereby affect the mechanical tissue properties.

Materials and methods

Cell culture and drugs

Immortalized human HaCaT keratinocytes were kindly provided by Dr. Petra Boukamp (Boukamp et al., 1988). They were used to generate the keratin 5-YFP-expressing cell clone B10 (Moch et al., 2013). Madin-Darby canine kidney MDCK cells were obtained from the German Cancer Research Center (DKFZ; Heidelberg; *cf.* (Windoffer et al., 2022)). The cells were grown at 37 °C in a 5% CO_2 humidified atmosphere and Dulbecco's Modified Eagle's Medium (DMEM) with l-alanyl-glutamine (Sigma-Aldrich, St. Louis, MO, United States of America) and 10% (v/v) fetal bovine serum (FBS; SeraPlus from PAN Biotech, Aidenbach, Germany). For passaging, cells were washed and incubated for 15 min at 37 °C in phosphate-buffered saline (PBS) without Ca^{2+}/Mg^{2+} (Sigma-Aldrich). Thereafter, the cells were treated for 5–10 min with 0.05% trypsin (Genaxxon bioscience, Ulm, Germany) at 37 °C. Confluent cells were passaged once a week and were seeded at a concentration of 40,000–60,000 cells/cm^2 in 6 ml cell culture medium in 25 cm^2 cell culture flasks (Greiner Bio-One, Frickenhausen, Germany). For experiments, cells were grown in 35-mm diameter dishes at a concentration of ≈100,000 cells/cm^2 (HaCaT) and 35,000 cells/cm^2 (MDCK) with 2 ml cell culture medium. For HaCaT cells, surfaces were pre-coated with laminin 332-rich matrix from 804G rat cells as described

(Langhofer et al., 1993; Moch et al., 2013). For MDCK cells, surfaces were pre-coated with 5 μg/cm^2 human fibronectin (Sigma-Aldrich). Cells were transfected 1 day prior to experiments with 4–5 μg of plasmid DNA and 1.5 μl Xfect in a total volume of 100 μl Xfect reaction buffer (Takara Bio, Kusatsu, Shiga, Japan) per 2 ml of cell culture medium. Latrunculin B (AdipoGen, Liestal, Switzerland) and para-nitro-blebbistatin (Optopharma, Budapest, Hungary) were dissolved in pure dimethyl sulfoxide (DMSO; Sigma-Aldrich) at a concentration of 1 and 2 mM, respectively. Y-27632 (Stemcell Technologies, Vancouver, Canada) was dissolved in PBS at a concentration of 20 mM. Aliquots were stored at −20°C, and thawed aliquots were used within 1 day. When not stated otherwise, the final DMSO concentration after addition of para-nitro-blebbistatin, latrunculin B or in corresponding controls was 0.5% (v/v). Experiments were performed in 25 mM 4-(2-hydroxyethyl)-1-piperazineethanesulfonic acid-buffered DMEM without phenol red (Life Technologies, Carlsbad, CA, United States) supplemented with 2% (v/v) FBS. When not otherwise stated, cells were preincubated for 30–120 min with drug-containing or control medium prior to experiments.

Plasmids

Plasmid DspI-GFP (p928) coding for human desmoplakin I fused to GFP was a kind gift from Kathy Green (Godsel et al., 2005). The generation of Dsc2-GFP and Dsc2-mCerulean coding for human Dsc2 (GenBank id: BC063291.1) fused to GFP or mCerulean, respectively, has been described (Windoffer et al., 2002; Moch et al., 2019). Cloning of Dsg2-GFP coding for human Dsg2 (gift from Stephan Schäfer) fused to GFP was also described previously (Moch et al., 2019). This plasmid contains the human Dsg2 cDNA (GenBank id: BC099655.3) but lacks the codons for the carboxyterminal amino acids QHSYS. E-cadherin-GFP plasmid encodes the human version of E-cadherin (GenBank id: NM_004360.5) with GFP at its C-terminus and 5′-CCGCGG-3′ nucleotides in the linker region. The N-terminus of GFP, that is encoded by 5′-ATGGTG-3′, is not present. mApple-Actin was a gift from James Nelson (Stanford University, Stanford, CA, United States).

Measurement of elastic modulus

Elastic material properties at the cell border were measured with a Chiaro Nanoindenter equipped with an OP1550 interferometer (Optics11 Life, Amsterdam, Netherlands). The set-up was mounted on an inverted Axio Observer seven microscope (Carl Zeiss, Jena, Germany). All experiments were performed at 37°C in an incubation chamber within 30–90 min after addition of para-nitro-blebbistatin or control medium. Ferrule-top force sensors with cantilever stiffness between 0.18 and 0.29 N/m and spherical tip radius between 9.0 and 9.5 μm were used for the experiments. The cantilever was placed on the border between two flat cells at the edge of a given cell colony, as determined by bright-field microscopy. The automated "find surface" setting was chosen to approach the cell surface, followed by an indentation-controlled measurement profile of 2 s approach time to reach the final depth of 350 nm, a holding time of 1 and 2 s of retraction. In this mode, the indentation depth was controlled in real-time by refreshing the piezo stroke accordingly to feedback from the cantilever. Measurements were analyzed with DataViewer V2.4.0 software from Optics11. Since the indentation depth was considerably smaller than the indenter tip size, the Hertzian model was chosen to process the data and fit the load-indentation curve:

$$F = \frac{4}{3} E_{eff} \sqrt{R} h^{\frac{3}{2}}$$

with F being the load exerted by the cantilever, E_{eff} the effective Young's Modulus (assuming cells to be incompressible, Poisson ratio pre-configured to 0.5), R the radius of the indenter tip and h the depth of indentation. The percentage of the maximal load (Pmax %) for contact point fitting was adjusted to the true contact point. Values for effective Young's modulus were considered with $R^2 \geq 0.9$.

Immunocytochemistry and cell fixation

For immunocytochemistry, cells were grown on 18-mm diameter high-precision glass cover slips with a thickness of 170 μm (Paul Marienfeld, Lauda-Königshofen, Germany) in six-well dishes (CytoOne®; Starlab International, Hamburg, Germany) for 2 days (MDCK) or 3 days (HaCaT). Fixation was performed by incubation in fresh 99.9% (v/v) methanol (Alfa Aesar, Heysham, United Kingdom) for 3 min at −20°C followed by washing in PBS (Biochrom, Schaffhausen, Switzerland) at room temperature for 5 min and optional storage over night at 4°C. Alternatively, cells were fixed in pre-warmed (37°C) 4% (v/v) paraformaldehyde (Merck, Darmstadt, Germany) in PBS (pH 7.2–7.4; adjusted with NaOH at up to 60°C) for 15 min at 37°C, then washed with PBS, and permeabilized for 3 min with 0.2% (v/v) Triton-X100 (Sigma-Aldrich) in PBS at room temperature. Primary and secondary antibodies were diluted with 1% (w/v) bovine serum albumin (BSA; SERVA, Heidelberg, Germany) in PBS. The samples were incubated with primary antibodies for 1 h, washed with PBS for 5–15 min, and incubated with secondary antibodies and 0.2 μg/ml 40,6-diamidino-2-phenylindole (DAPI; Hoffmann La Roche, Basel,

Switzerland) for 40 min. Finally, cells were washed with PBS for 20 min and mono-deionized H_2O for 30 s before mounting with Mowiol (Carl Roth, Karlsruhe, Germany) on glass slides (R. Langenbrinck, Emmendingen, Germany). The prepared samples were dried over night at 4°C and stored at the same temperature until recording within 2 weeks. Guinea pig polyclonal antibodies against DspI (DP-1) were from Progen Biotechnik (Heidelberg, Germany). Phalloidin coupled to Alexa Fluor 488 or 647 and highly cross absorbed secondary goat antibodies coupled to Alexa Fluor 488 were from Thermo Fisher Scientific (Waltham, MA, United States).

Microscopy

Microscopical recordings were performed with a laser scanning confocal microscope (LSM 710) using Zen black 2.1 SP3 software (Carl Zeiss, Jena, Germany). The microscope was equipped with an Airyscan detector, oil immersion objective (×63/1.40-N.A, DIC M27), and a focus-shift correction system (DefiniteFocus; all from Carl Zeiss). For live-cell imaging, the microscope was pre-warmed to 37°C in an incubation chamber with 5% CO_2. Living cells were imaged in glass-bottom dishes (12 mm glass-diameter, thickness 1.5#; MatTek, Bratislava, Slovakia) in 25 mM 4-(2-hydroxyethyl)-1-piperazineethanesulfonic acid-buffered DMEM without phenol red (Life Technologies) supplemented with 2% (v/v) FBS.

Fluorescence recovery after photobleaching (FRAP) experiments were recorded at 60 s time intervals before and after bleaching with the Airyscan detector set to standard confocal mode. The images (x = y = 33.74 µm = 512 pixel) were acquired at a pixel dwell speed of 6.27 µs, gain 850, and 16 bit-depth in three dimensions at a z-resolution of 0.65 µm. The pinhole was set to 100 µm which corresponds to two airy units for the used 460–480 and 495–550 nm emission range dual filter. For excitation of GFP the argon-ion laser (module LGK 7872 ML8) was used at 488 nm and 0.2–0.5% power. In addition, the photon multiplier was increased to the limit of safe operation. Bleaching was triggered automatically 60 s after the first z-stack within an area of 13.2 × 13.2 µm (200 × 200 pixel) for HaCaT cells or 8.45 × 16.9 µm (128 × 256 pixel) for MDCK cells. For bleaching, the laser was set to 100% power and the target area was scanned 10 times. Note that the bleaching took approximately 7–10 s resulting in a small inaccuracy between time points 0 and 1 min.

Non-FRAP experiments were recorded with all 32 PMTs of the Airyscan in the "super resolution" mode at z = 0.25 µm for immunostainings and the second-best resolution mode "resolution vs sensitivity" at z = 0.5 µm for living cells. The argon-ion laser was used at 458 nm for excitation of mCerulean, at 488 nm for GFP or Alexa488, and the photon multiplier was used at lowest setting. For excitation of mApple, a 543 nm HeNe-laser (module LGK 7786 P) was used. For excitation of DAPI, a 405 nm diode laser (laser cassette 405 cw) was used, and for excitation of Alexa 647, a 633 nm HeNe-laser (module LGK 7628-1F) was used. In immunostainings, DAPI was recorded at 420–480 nm, Alexa 488 at 460–480 nm and 495–550 nm. Live cell recordings of mApple were performed at 460–480 and 495–620 nm. In general, the detector gain was set to 850–900 for living cells and 700–850 for fixed samples. The digital gain was only increased for super resolution of living samples when necessary to a max value of 2.0. Immunostainings were scanned at second fastest speed at automatically calculated optimal resolution in unidirectional mode. Living cells for super resolution were scanned at fastest possible speed in bidirectional mode and custom resolution. Finally, the signal was processed for static samples with automatic 3D settings (including deconvolution) and for living samples with automatic 2D settings (without deconvolution). Multispectral images were acquired with a 34-channel QUASAR detector.

Image analysis and statistical analysis

Microscopy images were processed and analyzed in the Fiji distribution of ImageJ software package (Schindelin et al., 2012; Rueden et al., 2017). The subsequent translocation of fluorescence from the unbleached cell part to the bleached region was measured as described previously (Moch et al., 2013) with two modifications. (i) The fluorescence intensity before bleaching was defined as $I^{unbleached} = I_{t=unbleached} - I_{t=0} = 1 = 100\%$ (t = 0 corresponding to 1 min after bleaching) and the fluorescence for all subsequent time points as $I_{t=n}^{bleached} = (I_{t=n} - I_{t=0})/I^{unbleached}$. (ii) The measured FRAP area was smaller than the bleached area to avoid movement of unbleached desmosomes into the region of interest (see also microscopy section for parameters).

For statistical analysis, experiments were performed at least three times independently on different days except for the 10 and 20 µM para-nitro-blebbistatin treatments, which were performed on 2 days. The results for every time point and condition were combined into single datasets for each experiment. These results were tested for outliers (alpha = 0.05) with GraphPad online outlier calculator (GraphPad, San Diego, CA, United States), and, when applicable, the farthest outlier was removed. In a next step, time points were tested for Gaussian distribution with the D'Agostino and Pearson omnibus normality test and with the Shapiro-Wilk normality test using GraphPad 5.01 software (GraphPad). For FRAP experiments, we concentrated only on the last time

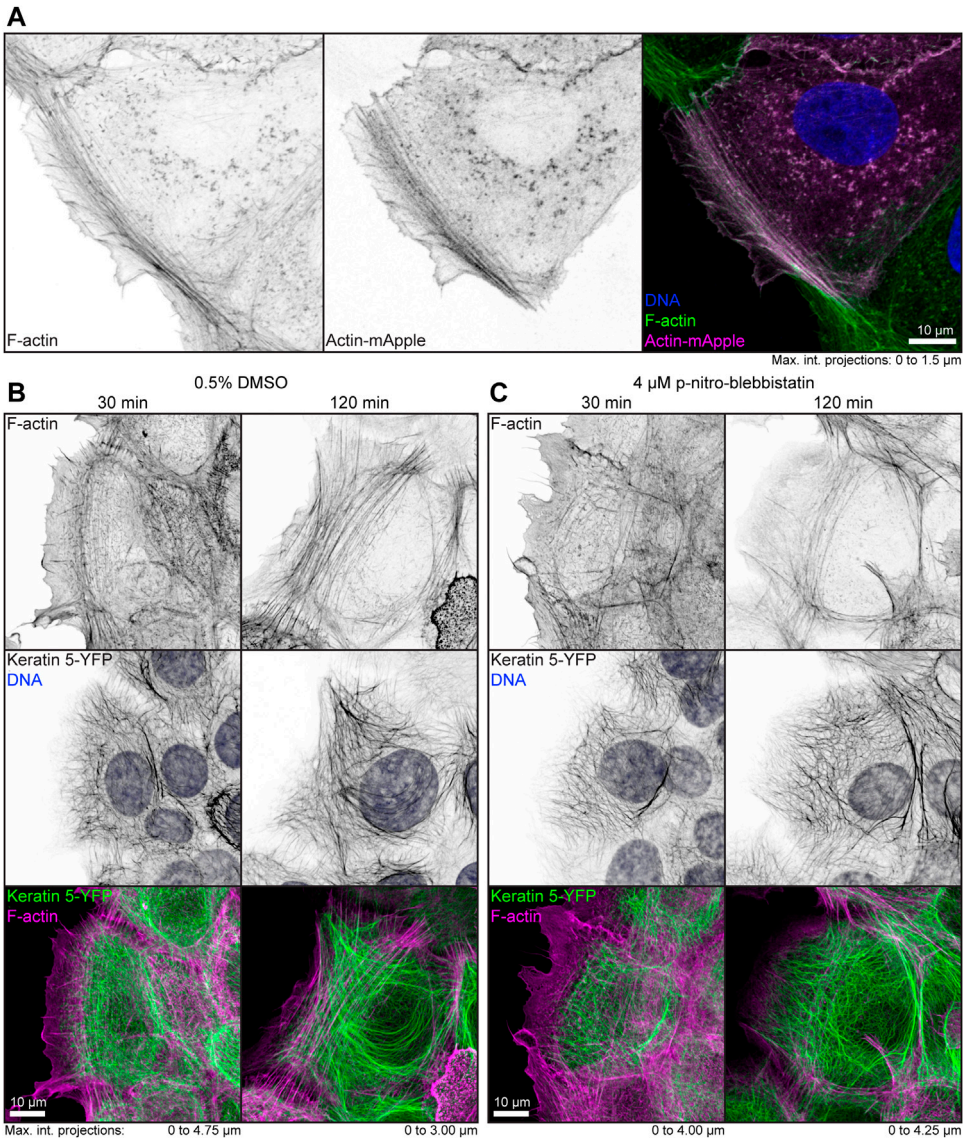

FIGURE 1
Low dose para-nitro-blebbistatin treatment does not affect the overall organization of the actin and keratin cytoskeleton. The fluorescence micrographs show maximum intensity projections of fixed HaCaT keratinocytes. **(A)** illustrates co-localization of Alexa-488-tagged phalloidin (F-Actin; left) and Actin-mApple fluorescence (middle). The overlay of both (right) reveals overlapping distribution of filamentous actin but not of cytoplasmic non-filamentous actin that is only detectable with Actin-mApple. **(B,C)** The images show the distribution of Alexa-647-tagged phalloidin (F-Actin; top) together with keratin 5-YFP and DAPI (DNA; middle; co-localization of actin and keratin in lower panel) in HaCaT B10 cells. Note that the actin and keratin cytoskeleton are not significantly affected by a 30–120 min treatment with 0.5% DMSO **(B)** and that cells remained flat and well spread even after addition of para-nitro-blebbistatin (4 µM) presenting a normal-appearing actin and keratin cytoskeleton **(C).**

point per condition (15 min post bleaching, t = 14) and compared it with the control. Therefore, a nonparametric (Mann-Whitney) test in GraphPad was used because not all data sets were normally distributed and the data were unpaired. Results with $p < 0.05$ were considered significant. Graphs and fitting curves (exponential rise to maximum) were made with SigmaPlot 12.0 (Inpixon, Düsseldorf, Germany). For nanoindentation experiments, all conditions were tested with the Kruskal–Wallis test before Dunn's multiple comparison post-test was applied. Figures were prepared with Adobe Photoshop and Illustrator CS 6 (Adobe, San Jose, CA, United States of America). Movies were encoded in h.264 video format using Handbrake 1.3.3 software (https://handbrake.fr/).

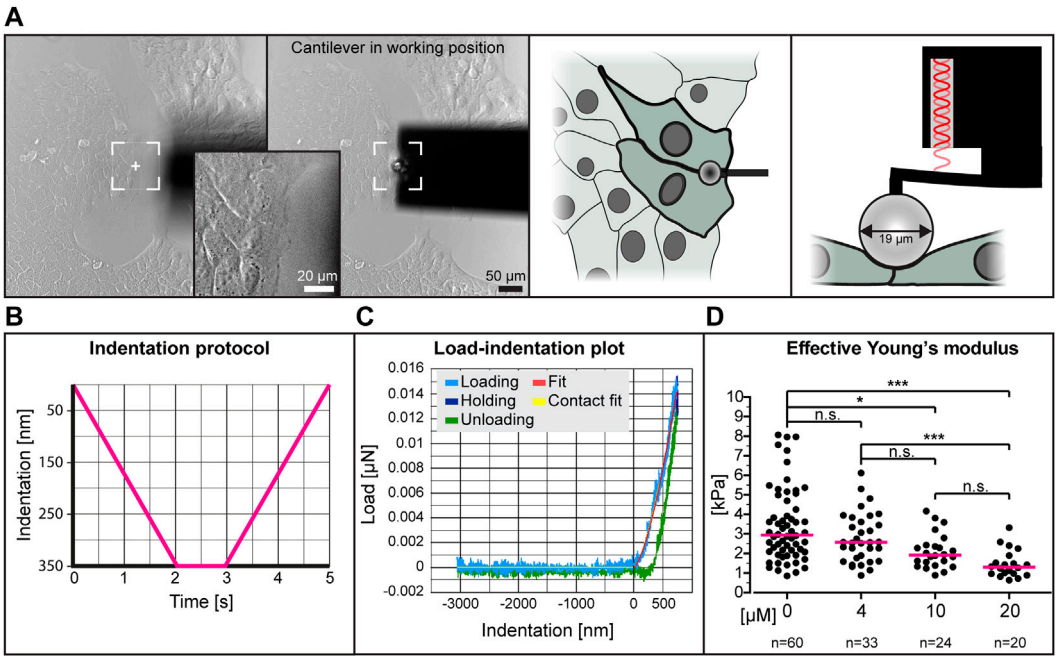

FIGURE 2
The effective Young's modulus of HaCaT cells decreases with increased dose of para-nitro-blebbistatin. The Young's modulus was measured with the help of a nanoindenter. **(A)** presents bright-field images at left depicting the cantilever in relation to the cells before positioning and during indentation. Note that the cantilever is placed at the border between 2 cells at the periphery of a cell colony. The schemes at right further illustrate the positioning of the cantilever from the top and the side, respectively. **(B)** The graph illustrates the indentation protocol consisting of a 2 s 350 nm indentation, 1 s holding and 2 s retraction. **(C)** The graph shows an exemplary load-indentation curve encompassing a loading (light blue), holding (dark blue) and unloading part (green). To calculate the Young's modulus, the Hertzian model uses the fitted loading curve (red) and the contact point (yellow). **(D)** The scatter dot plot shows the effective Young's moduli for cells treated with 0, 4, 10 and 20 µM para-nitro-blebbistatin for 30–90 min. The plot was generated by combining the medians per condition. Kruskal–Wallis test is significant with a $p < 0.0001$ and Dunn's multiple comparison post-test shows significant differences as indicated in the graph (*$p < 0.05$, ***$p < 0.0001$).

Results

The overall organization of the actin and keratin cytoskeleton is maintained in the presence of low para-nitro-blebbistatin levels

Para-nitro-blebbistatin has been described as a non-cytotoxic and photostable alternative to blebbistatin (Kepiro et al., 2014) that can be used without noticeable side-effects at a concentration of up to 20 µM according to the manufacturer (Optopharma). However, as already reported for blebbistatin (Swift et al., 2012), we noted that para-nitro-blebbistatin has considerable autofluorescence (Supplementary Figure S1). This autofluorescence interfered with the fluorescence recordings of fluorescent desmosomal protein reporters. Thus, we observed a very strong autofluorescence of 20 µM para-nitro-blebbistatin in the detection spectrum of Dsg2-mCerulean (excitation with 456 nm light). This precluded reliable evaluation of the Dsg2-mCerulean signal (Supplementary Movie S1). On the other hand, DspI-mApple that was excited with 543 nm light in parallel did not show this problem (Supplementary Movie S1). Another serious problem that we encountered was that para-nitro-blebbistatin fluorescence increased over time reaching a peak by 15 min, which appeared to be stable (Supplementary Figure S1A). To reduce para-nitro-blebbistatin autofluorescence to acceptable levels, we lowered the drug concentration to 3 or 4 µM. In addition, we used the Argon-ion laser at 488 nm instead of 456 nm and employed GFP- instead of mCerulean-based fluorescence reporters. The emission was recorded below 550 nm, because most autofluorescence was detectable in a second peak above 547 nm (Supplementary Figure S1B).

To examine the effect of low-dose para-nitro-blebbistatin on the actin system, HaCaT cells were either labeled with fluorophore-coupled phalloidin or mApple-actin. Both labels detected F-actin reliably (Figure 1A). In a first set of experiments, HaCaT B10 cells were incubated with 0.5% (v/v) DMSO alone or together with 4 µM para-nitro-blebbistatin. Cells were fixed after 30 and 120 min and were subsequently stained with Alexa647 labelled phalloidin. The DMSO control presented well-developed actin stress fibers that were anchored at cell borders (Figure 1B). Cells that were treated with 4 µM para-nitro-blebbistatin retained an F-actin distribution with overall

resemblance to control cells but with a slightly reduced number of actin fibers (Figure 1C). Similarly, the drug treatment had no major effect on the keratin network organization as assessed by keratin 5-YFP distribution (Figures 1B,C). We therefore concluded that the changes in the actin and keratin networks are not dramatic during 30–120 min of para-nitro-blebbistatin treatment at 4 μM and that global network rearrangement would therefore not interfere with effects of myosin inhibition.

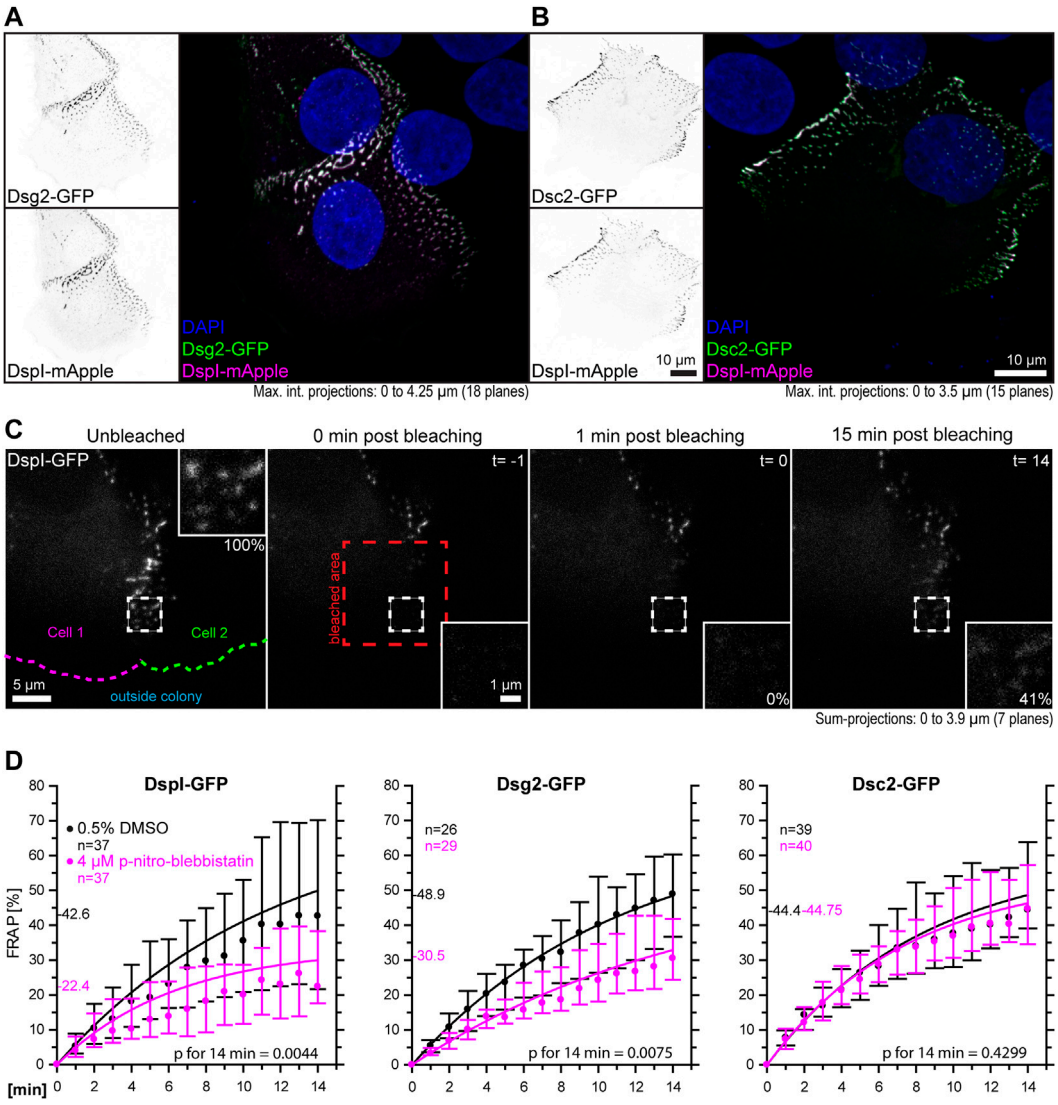

FIGURE 3
Myosin II inhibition decreases the desmosomal turnover of Dspl and Dsg2 but not of Dsc2 in HaCaT keratinocytes. HaCaT cells were transfected with plasmids encoding fluorescently tagged Dspl (Dspl-GFP or Dspl-mApple), Dsg2 (Dsg2-GFP) or Dsc2 (Dsc2-GFP). **(A,B)** presents fluorescence micrographs of cells doubly transfected to express either Dsg2-GFP or Dsc2-GFP together with Dspl-mApple. Note that the fluorescent molecules co-localize in punctate structures, i. e. desmosomes that are located at borders of partially overlapping cells. **(C)** shows aspects of the workflow. It presents fluorescence images from a FRAP experiment in which cells were treated with 0.5% DMSO. The sum-projection overviews show from left to right the Dspl-GFP signal in a cell just prior to bleaching, immediately, 1 and 15 min after bleaching with insets depicting the bleached region at high magnification. Fluorescence recovery measurements were started 1 minute after bleaching at which time fluorescence intensity was set as 0% and the corresponding time point was defined as t = 0. In this way, diffusion-related rapid fluorescence recovery was not taken into account for the quantitative measurements depicted in the graphs below. Aspects of this procedure are illustrated in Supplementary Movie S2 comparing solvent-treated to para-nitro-blebbistatin-treated cells. **(D)** The diagrams show time-dependent fluorescence recovery curves of Dspl-GFP, Dsg2-GFP, and Dsc2-GFP that were started 1 min after bleaching (= time point 0). The experiments were performed as illustrated in **(C)**. Dots represent medians, whiskers correspond to the 25–75th percentiles, and statistical analysis was performed with a Mann-Whitney test 14 min after the measurements were started.

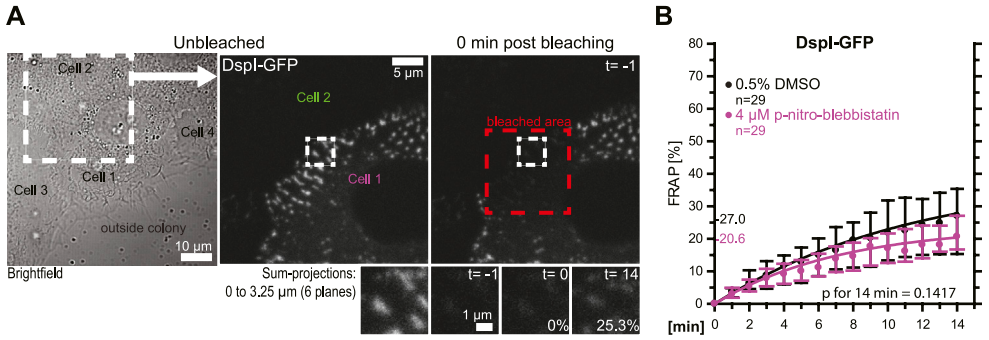

FIGURE 4
Desmosomes within a cell colony are only mildly affected by low dose myosin II inhibition. HaCaT cells were transfected with plasmids encoding fluorescently tagged DspI (DspI-GFP). **(A,B)** The micrographs and graph show results of FRAP experiments, in which DspI was bleached in desmosomes that were located toward the center of the cell colony. The microscopy pictures present from left to right an overview bright-field image and fluorescence images corresponding to the marked area before and immediately after bleaching. The region of interest prior to, immediately after, 1 and 15 min after bleaching is depicted below. The graph shows the results of multiple measurements (same denotations as in Figure 3D).

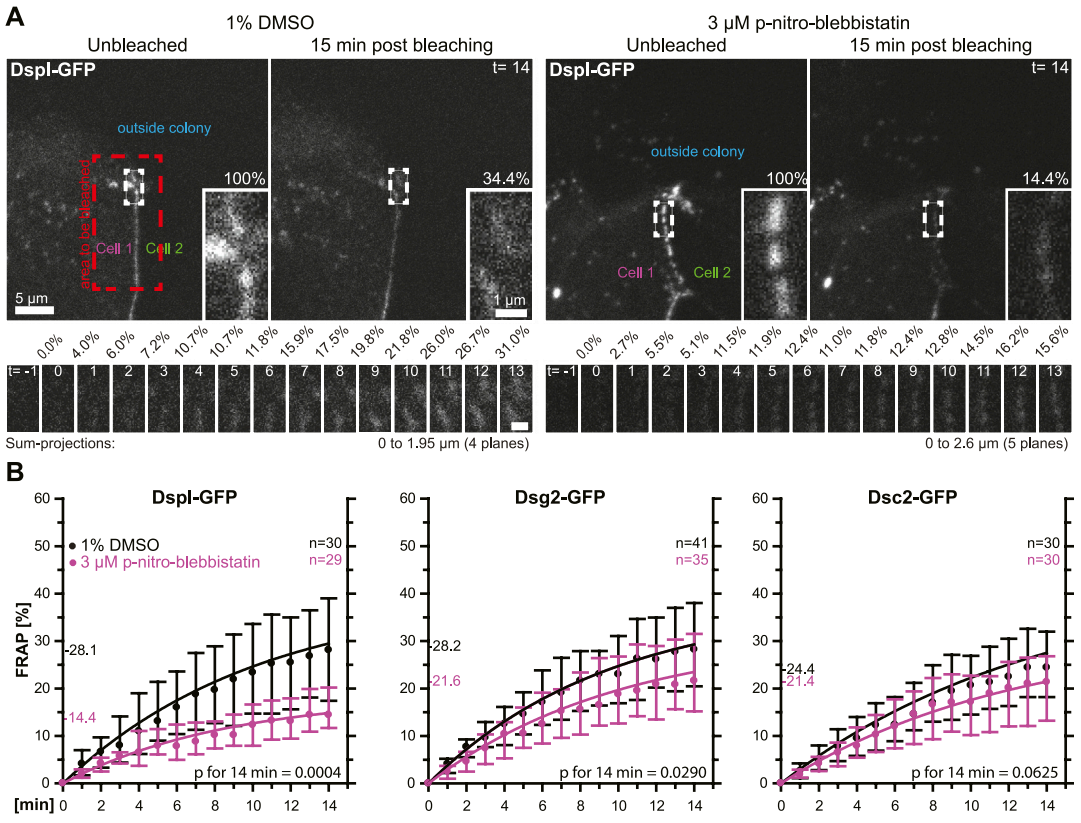

FIGURE 5
Myosin II inhibition decreases the desmosomal turnover of DspI and Dsg2 but not of Dsc2 in simple epithelial MDCK cells. MDCK cells were transfected with fluorescently tagged desmosomal proteins and fluorescence was recorded in cells at the border of colonies. **(A)** shows examples of fluorescence recordings (sum-projections) in cells incubated with control medium (left) or with 3 µM para-nitro-blebbistatin (right) just prior to bleaching and 15 min after bleaching. Note that every fluorescent cell is next to a non-transfected cell. The bleached regions of interest are presented as insets at higher magnification. Below are images of the measured regions at the intermediate time points. **(B)** The diagrams show fluorescence recovery curves of DspI-GFP, Dsg2-GFP and Dsc2-GFP that were started 1 min after bleaching. The experiments were performed as described in Figure 3C. Dots represent medians, whiskers correspond to the 25–75th percentiles, and statistical analysis was performed with a Mann-Whitney test at 14 min after the measurements were started.

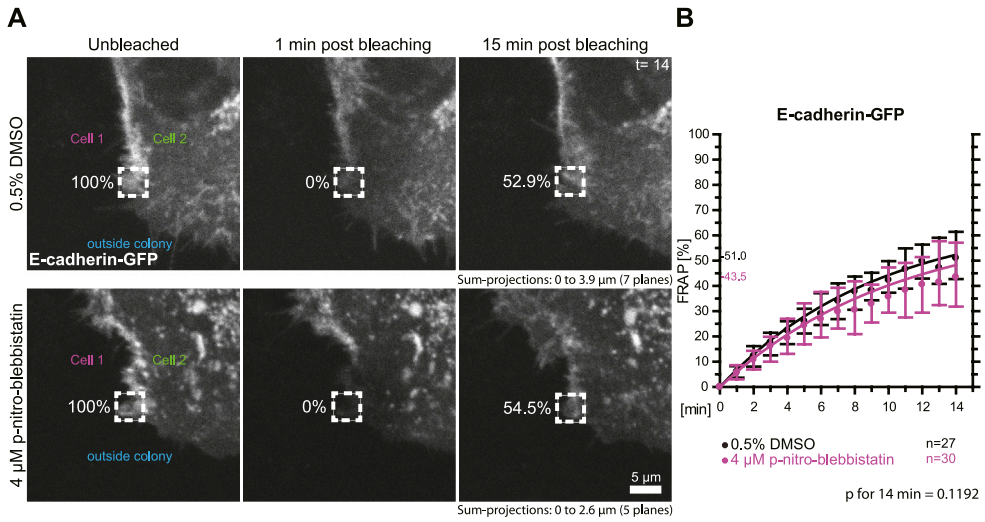

FIGURE 6
Myosin II inhibition does not significantly affect the turnover of E-cadherin at cell borders. HaCaT keratinocytes were transfected with a plasmid encoding human E-cadherin-GFP. **(A)** Regions at cell colony borders were selected for FRAP. Sum-projections of fluorescence were generated and are shown from left to right prior to, 1 and 15 min after photobleaching. The relative fluorescence measured in the regions of interest are given in %. Cells were either incubated with control medium (top) or with 4 µM para-nitro-blebbistatin (bottom). The first sum-projection shows complete E-cadherin-GFP signal in a peripheral cell that is next to a non-transfected cell directly before bleaching. **(B)** The diagram depicts the fluorescence recovery curves of E-cadherin-GFP from 1 to 15 min after photobleaching. Dots represent medians, whiskers correspond to the 25–75th percentiles, and statistical analysis was performed with a Mann-Whitney test for the last time-point.

Myosin II inhibition decreases the elastic Young's modulus at cell-cell contact regions

To determine whether low dose para-nitro-blebbistatin treatment affects the elasticity of HaCaT cells, we performed nanoindentation experiments. We probed cell-cell contact regions at the edge of cell colonies (Figures 2A,B). Setting the indentation depth at 350 nm generated load-indentation plots such as that shown in Figure 2C. The effective Young's modulus was then calculated according to the Hertzian model.

The collated data from five different experiments using different concentrations of para-nitro-blebbistatin are shown in Figure 2D. The resulting median effective Young's modulus of untreated cells was 2.95 kPa, 1.3 kPa for 20 µM para-nitro-blebbistatin, 1.93 kPa for 10 µM para-nitro-blebbistatin and 2.57 kPa for 4 µM para-nitro-blebbistatin revealing a concentration-dependent reduction of the Young's modulus.

Myosin II inhibition decreases the turnover of desmoplakin I and desmoglein 2 but not of desmocollin 2 at adhering cell borders

The goal of this study was to examine the influence of cortical tension on desmosomal polypeptide turnover. We focused on polypeptide components that are known to represent the stable moiety of desmosomes, i.e., desmosomal cadherins and desmoplakin (Fulle et al., 2021). To make sure that the dotted structures at cell-cell borders were desmosomes, we performed double-transfection experiments of different desmosomal polypeptides. As predicted, Dsg2-GFP and Dsc2-GFP localized to the same puncta as DspI-mApple (Figures 3A,B). Furthermore, we did not see any obvious differences in the distribution of the GFP- and mApple-tagged versions of DspI, both of which localized to puncta that were also labeled by anti-Dsp polyclonal antibodies, which reacted with the endogenous and exogenous Dsp versions in methanol-fixed cells (Supplementary Figure S2). Confluent, desmosome-connected HaCaT cells typically overlap. As a result, the maximum intensity projections of multiple focal planes capture not only cross-sectional views of desmosomes but also en-face views.

For desmosome turnover analyses we decided to perform FRAP analyses. To this end, cells were considered that were localized at the periphery of cell colonies. New desmosomes are formed in these regions and observations can be standardized (Moch et al., 2019). The turnover determined in this way reflects incorporation and removal of proteins into desmosomes. For simplicity's sake, we assumed that it is mainly independent of degradation and protein synthesis. In the experiments cells were incubated with control medium or 4 µM para-nitro-blebbistatin for 30–120 min. Single transfected cells with untransfected

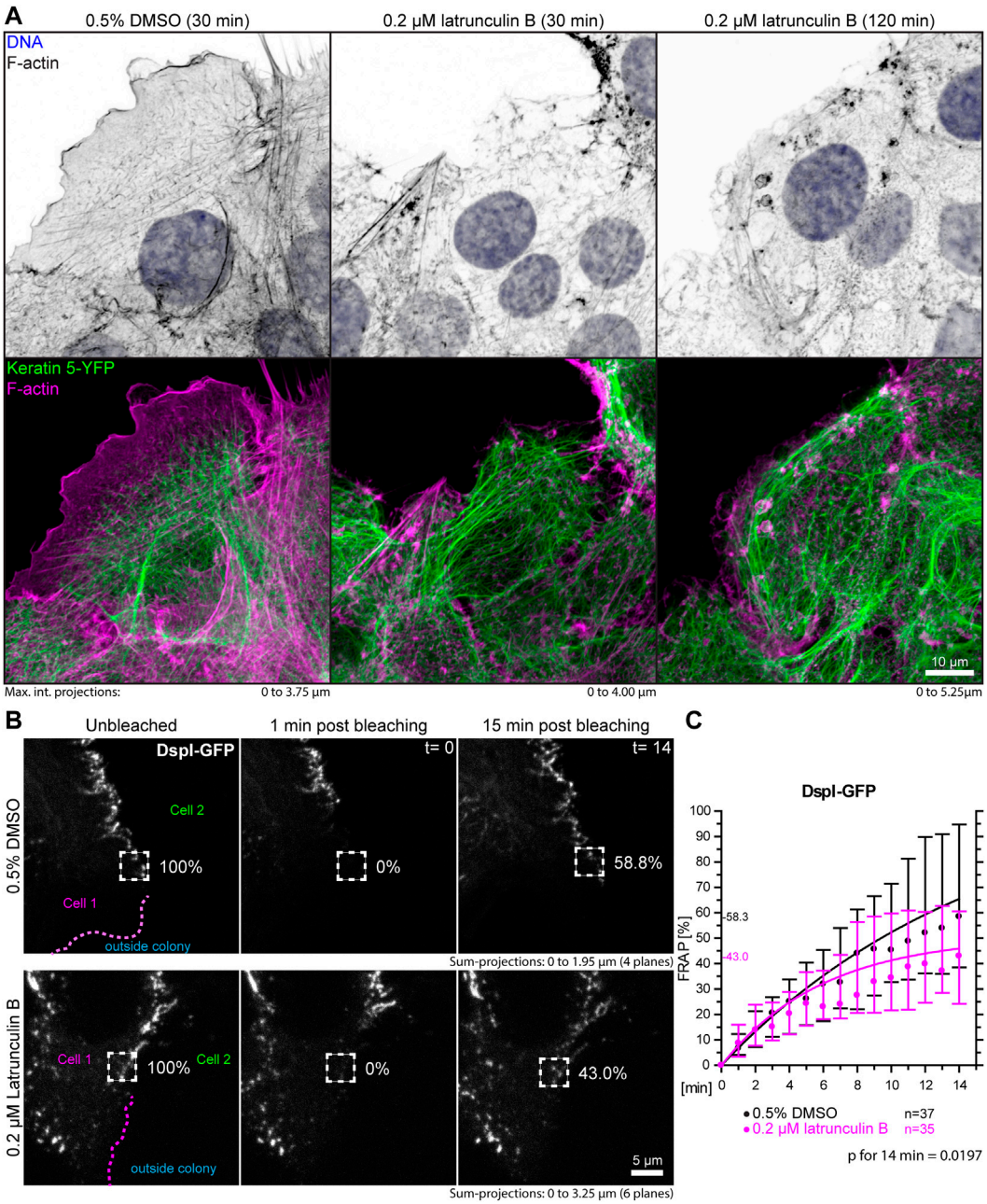

FIGURE 7
Partial depolymerization of F-actin reduces desmosomal DspI turnover. **(A)** The images show maximum intensity projections of fluorescence in fixed HaCaT keratinocytes. Actin filaments were stained with Alexa-647 tagged phalloidin (top panels) in HaCaT B10 cells that stably express keratin 5-YFP (composite images in bottom panel). The cells were incubated with control medium (0.5% DMSO; left) or 0.2 µM latrunculin B (middle and right). Note that the latrunculin B treatment leads to significant yet incomplete actin filament depletion. **(B)** shows the results of FRAP analyses. Sum-projections of confocal DspI-GFP fluorescence recordings are shown from left to right just prior to bleaching, 1 min afterwards and after 15 min in control cells (0.5% DMSO; top) and cells treated with 0.2% latrunculin B in addition (bottom). The regions of interest are demarcated by broken lines and the relative fluorescence measured in these regions are given in %. **(C)** The graph depicts the fluorescence recovery curves of DspI-GFP from 1 to 15 min after photobleaching. Dots represent medians, whiskers correspond to the 25–75th percentiles, and statistical analysis was performed with a Mann-Whitney test for the last time point.

neighbors were chosen and areas encompassing the outermost desmosomal clusters were selected for FRAP analysis. They were typically located within 10 µm of the periphery of the colonies. Larger regions of interest were bleached that contained these areas to avoid that unbleached desmosomes moved into the region that was analyzed. To capture the fluorescence of entire desmosomes,

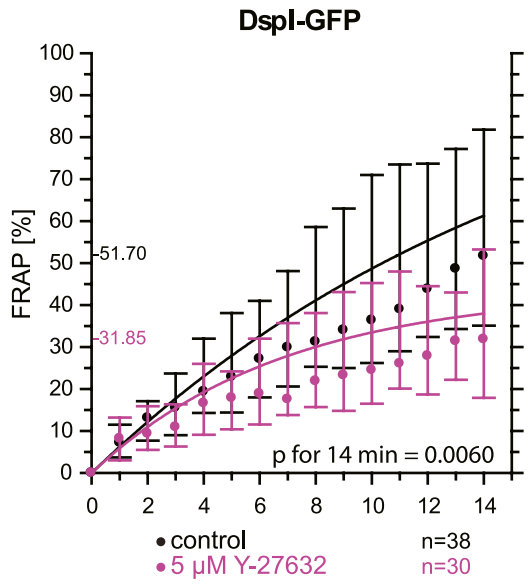

FIGURE 8
Inhibition of Rho-associated protein kinases decreases desmosomal protein turnover in HaCaT keratinocytes. The graph depicts the fluorescence recovery curves of DspI-GFP from 1 to 15 min after photobleaching in cells that were untreated (only medium change prior to experiment) or treated with 5 µM Y-27632. Dots represent medians, whiskers correspond to the 25–75th percentiles, and statistical analysis was performed with a Mann-Whitney test for the last time point.

the regions of interest were scanned in three dimensions and sum-projections were prepared for analysis. Furthermore, fluorescence recovery measurements were started 1 minute after bleaching, at which time (defined as t = 0) fluorescence intensity was set as 0%. In this way, diffusion-dependent rapid fluorescence recovery, which may have occurred during the first minute after bleaching, was not taken into account. The amount of fluorescence recovery was then quantified once a minute for 14 min and compared to fluorescence recorded just prior to bleaching (Figure 3C, Supplementary Movie S2). DspI-GFP turnover was significantly reduced in para-nitro-blebbistatin-treated cells. It decreased from a median of 42.6% to a median of 22.4% after 14 min ($p = 0.0044$) (Figure 3D). A similar reduction of turnover was also observed for Dsg2-GFP. It was reduced to a median of 30.5% in para-nitro-blebbistatin-treated cells in comparison to a median of 48.9% in un-treated control cells ($p = 0.0075$) (Figure 3D). In contrast, the turnover of Dsc2-GFP was not significantly reduced after 14 min in para-nitro-blebbistatin treated cells ($p = 0.4299$) and remained nearly unaffected with 44.8 vs 44.4% (Figure 3D). Time-lapse images furthermore showed that desmosomal clusters still assembled in the presence of 4 µM para-nitro-blebbistatin (Supplementary Movie S3, Supplementary Figure S3).

In the following experiments, turnover analyses were carried out for desmosomes that were not localized at the colony periphery (Figures 4A,B). The results revealed that these desmosomes had an overall reduced DspI-GFP turnover (median of 27.0 vs 42.6%). Treatment with 4 µM para-nitro-blebbistatin reduced the turnover further to a median of 20.6%, which was not statistically significant. Reduced baseline tension at these tightly coupled cell-cell borders may have contributed to the reduced desmosomal protein turnover and its reduced sensitivity to myosin II inhibition.

In a next set of experiments, we tested whether the observed phenomena were cell type-specific. To this end, we selected simple epithelium-derived canine MDCK cells that have been used as a model to examine desmosome dynamics (Windoffer et al., 2002; Gloushankova et al., 2003). The experimental setup was identical to that used for the analysis of desmosomal protein turnover in HaCaT cells with only minor modifications. Cells were analyzed 2 days after seeding instead of 3 days after seeding, the concentration of para-nitro-blebbistatin was reduced to 3 µM and the shape of bleached regions was changed to account for the more linear arrangement of desmosomes due to the columnar cell shape of MDCK cells (Figure 5A). The results were overall confirmatory (Figure 5B). The turnover of DspI-GFP and Dsg2-GFP were significantly reduced by para-nitro-blebbistatin ($p = 0.0004$ and $p = 0.029$, respectively), whereas the turnover of Dsc2-GFP was only mildly affected ($p = 0.0625$). The base turnover of the analyzed desmosomal proteins was, however, considerably lower in MDCK cells than in HaCaT cells.

E-cadherin turnover is not significantly affected by partial myosin II inhibition

To test whether the turnover of the adherens junction and actin-associated classical E-cadherin is affected by myosin II activity we transfected HaCaT cells with a plasmid encoding E-cadherin-GFP and performed FRAP analyses in these cells (Figure 6A). Measurements were as described for the desmosomal proteins in the preceding section. The median turnover of E-cadherin-GFP decreased slightly from a median of 51.0% in untreated control cells to a median of 43.5% in 4 µM para-nitro-blebbistatin treated HaCaT cells when measured for 14 min (Figure 6B). This decrease, however, was not significant ($p = 0.1192$). We therefore conclude that any effect on E-cadherin turnover must be weaker than that on DspI and Dsg2 and would require more sensitive or alternative detection methods.

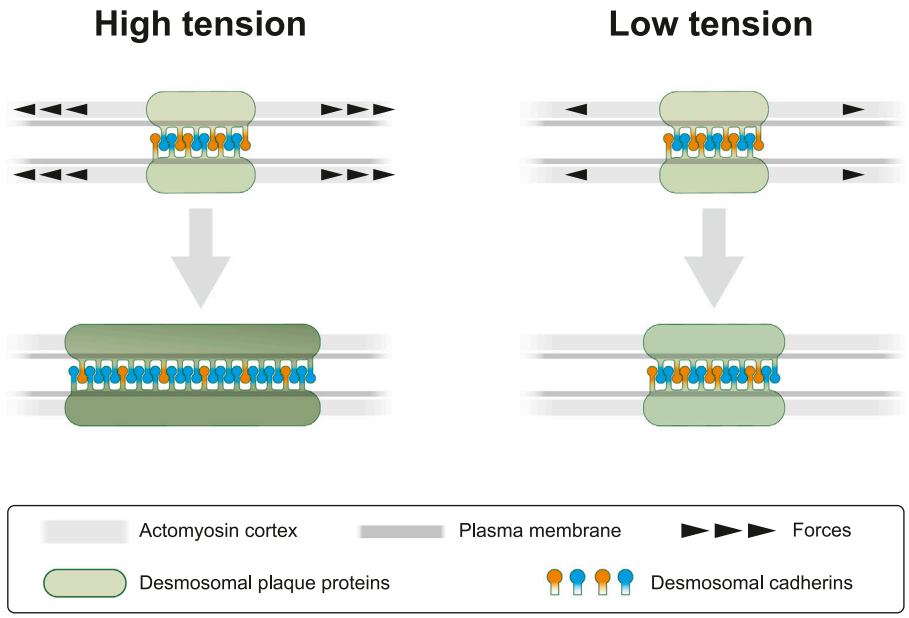

FIGURE 9
Cortical actomyosin tension regulates desmosomal morphogenesis affecting desmosome size and composition. In the present study we modulate cortical actomyosin-dependent tension by pharmacological interference. At high lateral tension desmosomal growth is supported by recruitment of desmosomal plaque proteins (green) and transmembrane proteins (orange and blue). Reduced tension negatively regulates desmosomal growth by selectively decreasing recruitment of desmosomal components. This results not only in smaller desmosomal size but also in different desmosomal composition, which is depicted as a brighter green color of the desmosomal plaque and an altered balance of desmosomal cadherins. The latter is reflected by a relative increase of "orange" cadherins (e.g., Dsc2) at low tension *versus* an increased number of "blue" cadherins (e.g., Dsg2) at high tension. We take these observations as an indication of the capacity of desmosomes to sense and respond to mechanical signals.

Depolymerization of F-actin and ROCK inhibition reduce desmoplakin I turnover in desmosomes

A prediction of the blebbistatin inhibition experiments is that reduction of cortical actin would also affect desmosomal protein turnover. To test this, HaCaT cells were treated with 0.2 µM latrunculin B, which reduced cortical actin and actin stress fibers (Figure 7A, Supplementary Movie S4). At this low latrunculin concentration, the cells did not retract strongly as we previously observed for 3 µM latrunculin in HaCaT cells (Moch and Leube, 2021). Thus, we were able to minimize cell shape changes that make analyses unreliable and did not have to deal with highly mobile desmosomes, which we observed in cells with completely depolymerized F-actin. Figure 7A shows that latrunculin treatment resulted in minor changes such as a slight retraction from the cell periphery, keratin filament straightening and filament compaction, which was to be expected from previous experiments using higher latrunculin concentrations (Moch and Leube, 2021). FRAP analysis of DspI-GFP in low dose latrunculin B-treated HaCaT cells showed that desmosomal turnover is significantly reduced in comparison to control cells when measured for 14 min (43.0 *versus* 58.3%, $p = 0.0197$, Figures 7B,C).

As an alternative to actin depolymerization, we tested whether a reduction of actin-tension by inhibition of Rho-associated protein kinases ROCK1 and ROCK2 would also decrease desmosomal turnover. To this end, cells were treated with a low dose of the ROCK inhibitor Y-27632. FRAP analysis of DspI-GFP in HaCaT cells treated with 5 µM Y-27632 showed that desmosomal turnover is also significantly reduced in comparison to control cells when measured for 14 min (31.9 *versus* 51.7%, $p = 0.006$, Figure 8).

Discussion

Desmosomes are prominent and abundant cell-cell junctions in epithelial tissues. They form, together with the associated keratin cytoskeleton, a transcellular scaffold, which is essential for epithelial tissue cohesion and mechanical stress dissipation. Yet, desmosomes are not just static structures but are subject to continuous turnover affecting all its components, albeit to different degrees (Windoffer et al., 2002; Gloushankova et al.,

2003; Moch et al., 2019; Fulle et al., 2021). It is not known how this turnover is regulated and why it occurs. But it is reasonable to assume that the regulation of desmosomal protein turnover helps to adjust desmosomal size and composition to the local force balance. To test this idea, we inhibited endogenous actomyosin contractility, which is known to confer cortical tension (Ananthakrishnan & Ehrlicher, 2007; Chugh & Paluch, 2018). Our experimental results show that myosin II inhibition decreases the turnover of the desmosomal plaque protein DspI and the desmosomal cadherin Dsg2 but not the turnover of the desmosomal cadherin Dsc2 in human HaCaT keratinocytes and canine kidney epithelium derived MDCK cells. These results reveal a hitherto unknown mechanosensing response of desmosomes as summarized schematically in Figure 9. It is fully in line with the previous observation that Dsg2 experiences mechanical tension (Baddam et al., 2018) and that increased load-bearing is perceived by Dsp (Price et al., 2018).

Desmosomal protein turnover is affected by multiple pathways including (i) delivery of newly synthesized polypeptides, (ii) exchange with non-desmosomal pools and (iii) removal by endocytosis. Each of these mechanisms appears to regulate the different desmosomal components in different ways. Thus, polypeptide delivery is dependent on myosin for desmoplakin (Godsel et al., 2005; Green et al., 2010) and dependent on kinesin-1 for desmoglein 2 and kinesin-2 for desmocollin 2, respectively (Nekrasova et al., 2011). The functional importance of exchange between desmosomal and non-desmosomal pools of plasma membrane-bound desmosomal cadherins has been emphasized (Waschke & Spindler, 2014; Hiermaier et al., 2022) and likely involves lipid rafts (Resnik et al., 2011; Stahley et al., 2014). Endocytosis may affect individual desmosomal components (Delva et al., 2008; Green et al., 2010; Resnik et al., 2011; Brennan et al., 2012), desmosomal halves (Demlehner et al., 1995) or even entire desmosomes (Fulle et al., 2021). It is controlled by keratins (Kroger et al., 2013). The examples illustrate the complexity of desmosomal protein turnover and the multiple factors, which may either increase or decrease it. Detailed quantitative analyses are needed to determine the contribution of each mechanism and the involved signalling pathways to the overall context-dependent regulation of desmosomal plasticity in order to link it to desmosomal mechanosensation and mechanoresponse. Be it as it may, the observed complexity is at the root of cell type-specific and function-related desmosomal adaptation.

Tension-dependent mechanisms are attractive pathways to support desmosome formation. These pulling forces could be generated from nearby actin stress fibres that are anchored to adjacent adherens junctions or focal adhesions. In support, adherens junction formation has been shown to precede desmosome formation (Gosavi et al., 2011; Shafraz et al., 2018). These punctate contacts may exert more local tension than the closely spaced cell contacts that are encountered toward the centre of the cell colonies. There, load is shared by multiple cell-cell contacts. This force dissipation may result in smaller forces and tensional loads per desmosome. The decreased stress would then go along with decreased turnover and consequently reduced desmosome formation. Conversely, wounding would result in increased local tension through, e.g., focal adhesion-anchored actin stress fibres, creating a scenario similar to that encountered in the periphery of cell colonies, where desmosome formation is needed to mechanically couple the expanding epithelial cell layer.

A prediction of our current study is that increased changes in the force load affect desmosomal protein turnover. This hypothesis can be tested by controlled force application, e.g., in a tissue stretcher (Faust et al., 2011; Pullen et al., 2021). A precedence for load-dependent bond formation and stabilization has been provided by analyses of E-cadherin (Rakshit et al., 2012; Sivasankar, 2013). The proposed mechanobiological feedback loop of desmosomes is likely relevant for epithelial tissue morphogenesis, epithelial wound repair and tumour metastasis.

Data availability statement

The raw data supporting the conclusion of this article will be made available by the authors, without undue reservation.

Author contributions

Conceptualization, MM and RL; methodology, MM and JS; validation, MM; formal analysis, MM, JS. and RL; investigation, MM and JS; data curation, MM and JS; writing—original draft preparation, MM, JS, and RL; writing—review and editing, MM and RL; visualization, MM and JS; project administration, RL; funding acquisition, RL.

Funding

This research was funded by the Deutsche Forschungsgemeinschaft (LE566/18-2; LE566/22- 2/SPP 1782; 363055819/GRK2415).

Acknowledgments

We thank Kathleen Green, James Nelson, and Stephan Schäfer for valuable plasmid constructs. We thank Petra Boukamp for HaCaT keratinocytes and Monika Borchert-Stuhlträger for cloning of Dsg2-GFP. We thank Adam Breitscheidel for design of Figure 9.

Conflict of interest

The authors declare that the research was conducted in the absence of any commercial or financial relationships that could be construed as a potential conflict of interest.

Publisher's note

All claims expressed in this article are solely those of the authors and do not necessarily represent those of their affiliated organizations, or those of the publisher, the editors and the reviewers. Any product that may be evaluated in this article, or claim that may be made by its manufacturer, is not guaranteed or endorsed by the publisher.

Supplementary material

The Supplementary Material for this article can be found online at: https://www.frontiersin.org/articles/10.3389/fcell.2022.946190/full#supplementary-material

References

Ananthakrishnan, R., and Ehrlicher, A. (2007). The forces behind cell movement. *Int. J. Biol. Sci.* 3 (5), 303–317. doi:10.7150/ijbs.3.303

Baddam, S. R., Arsenovic, P. T., Narayanan, V., Duggan, N. R., Mayer, C. R., Newman, S. T., et al. (2018). The desmosomal cadherin desmoglein-2 experiences mechanical tension as demonstrated by a FRET-based tension biosensor expressed in living cells. *Cells* 7 (7), E66. doi:10.3390/cells7070066

Block, J., Schroeder, V., Pawelzyk, P., Willenbacher, N., and Koster, S. (2015). Physical properties of cytoplasmic intermediate filaments. *Biochim. Biophys. Acta* 1853, 3053–3064. doi:10.1016/j.bbamcr.2015.05.009

Boukamp, P., Petrussevska, R. T., Breitkreutz, D., Hornung, J., Markham, A., and Fusenig, N. E. (1988). Normal keratinization in a spontaneously immortalized aneuploid human keratinocyte cell line. *J. Cell Biol.* 106 (3), 761–771. doi:10.1083/jcb.106.3.761

Brennan, D., Peltonen, S., Dowling, A., Medhat, W., Green, K. J., Wahl, J. K., 3rd, et al. (2012). A role for caveolin-1 in desmoglein binding and desmosome dynamics. *Oncogene* 31 (13), 1636–1648. doi:10.1038/onc.2011.346

Broussard, J. A., Yang, R., Huang, C., Nathamgari, S. S. P., Beese, A. M., Godsel, L. M., et al. (2017). The desmoplakin-intermediate filament linkage regulates cell mechanics. *Mol. Biol. Cell* 28 (23), 3156–3164. doi:10.1091/mbc.E16-07-0520

Chugh, P., and Paluch, E. K. (2018). The actin cortex at a glance. *J. Cell Sci.* 131 (14), jcs186254. doi:10.1242/jcs.186254

Delva, E., Jennings, J. M., Calkins, C. C., Kottke, M. D., Faundez, V., and Kowalczyk, A. P. (2008). Pemphigus vulgaris IgG-induced desmoglein-3 endocytosis and desmosomal disassembly are mediated by a clathrin- and dynamin-independent mechanism. *J. Biol. Chem.* 283 (26), 18303–18313. doi:10.1074/jbc.M710046200

Demlehner, M. P., Schafer, S., Grund, C., and Franke, W. W. (1995). Continual assembly of half-desmosomal structures in the absence of cell contacts and their frustrated endocytosis: A coordinated sisyphus cycle. *J. Cell Biol.* 131 (3), 745–760. doi:10.1083/jcb.131.3.745

Faust, U., Hampe, N., Rubner, W., Kirchgessner, N., Safran, S., Hoffmann, B., et al. (2011). Cyclic stress at mHz frequencies aligns fibroblasts in direction of zero strain. *PLoS One* 6 (12), e28963. doi:10.1371/journal.pone.0028963

Fulle, J. B., Huppert, H., Liebl, D., Liu, J., Alves de Almeida, R., Yanes, B., et al. (2021). Desmosome dualism - most of the junction is stable, but a plakophilin moiety is persistently dynamic. *J. Cell Sci.* 134 (21), jcs258906. doi:10.1242/jcs.258906

Gloushankova, N. A., Wakatsuki, T., Troyanovsky, R. B., Elson, E., and Troyanovsky, S. M. (2003). Continual assembly of desmosomes within stable intercellular contacts of epithelial A-431 cells. *Cell Tissue Res.* 314 (3), 399–410. doi:10.1007/s00441-003-0812-3

Godsel, L. M., Dubash, A. D., Bass-Zubek, A. E., Amargo, E. V., Klessner, J. L., Hobbs, R. P., et al. (2010). Plakophilin 2 couples actomyosin remodeling to desmosomal plaque assembly via RhoA. *Mol. Biol. Cell* 21 (16), 2844–2859. doi:10.1091/mbc.E10-02-0131

Godsel, L. M., Hsieh, S. N., Amargo, E. V., Bass, A. E., Pascoe-McGillicuddy, L. T., Huen, A. C., et al. (2005). Desmoplakin assembly dynamics in four dimensions: Multiple phases differentially regulated by intermediate filaments and actin. *J. Cell Biol.* 171 (6), 1045–1059. doi:10.1083/jcb.200510038

Gosavi, P., Kundu, S. T., Khapare, N., Sehgal, L., Karkhanis, M. S., and Dalal, S. N. (2011). E-cadherin and plakoglobin recruit plakophilin3 to the cell border to initiate desmosome assembly. *Cell. Mol. Life Sci.* 68 (8), 1439–1454. doi:10.1007/s00018-010-0531-3

Green, K. J., Geiger, B., Jones, J. C., Talian, J. C., and Goldman, R. D. (1987). The relationship between intermediate filaments and microfilaments before and during the formation of desmosomes and adherens-type junctions in mouse epidermal keratinocytes. *J. Cell Biol.* 104 (5), 1389–1402. doi:10.1083/jcb.104.5.1389

Green, K. J., Getsios, S., Troyanovsky, S., and Godsel, L. M. (2010). Intercellular junction assembly, dynamics, and homeostasis. *Cold Spring Harb. Perspect. Biol.* 2 (2), a000125. doi:10.1101/cshperspect.a000125

Hegazy, M., Perl, A. L., Svoboda, S. A., and Green, K. J. (2022). Desmosomal cadherins in health and disease. *Annu. Rev. Pathol.* 17, 47–72. doi:10.1146/annurev-pathol-042320-092912

Hiermaier, M., Kugelmann, D., Radeva, M., Didona, D., Ghoreschi, K., Farzan, S., et al. (2022). Pemphigus foliaceus autoantibodies induce redistribution primarily of extradesmosomal desmoglein 1 in the cell membrane. *Front. Immunol.* 13, 882116. doi:10.3389/fimmu.2022.882116

Kepiro, M., Varkuti, B. H., Vegner, L., Voros, G., Hegyi, G., Varga, M., et al. (2014). para-Nitroblebbistatin, the non-cytotoxic and photostable myosin II inhibitor. *Angew. Chem. Int. Ed. Engl.* 53 (31), 8211–8215. doi:10.1002/anie.201403540

Kroger, C., Loschke, F., Schwarz, N., Windoffer, R., Leube, R. E., and Magin, T. M. (2013). Keratins control intercellular adhesion involving PKC-alpha-mediated desmoplakin phosphorylation. *J. Cell Biol.* 201 (5), 681–692. doi:10.1083/jcb.201208162

Langhofer, M., Hopkinson, S. B., and Jones, J. C. (1993). The matrix secreted by 804G cells contains laminin-related components that participate in hemidesmosome assembly *in vitro*. *J. Cell Sci.* 105 (3), 753–764. doi:10.1242/jcs.105.3.753

Moch, M., Herberich, G., Aach, T., Leube, R. E., and Windoffer, R. (2013). Measuring the regulation of keratin filament network dynamics. *Proc. Natl. Acad. Sci. U. S. A.* 110 (26), 10664–10669. doi:10.1073/pnas.1306020110

Moch, M., and Leube, R. E. (2021). Hemidesmosome-related keratin filament bundling and nucleation. *Int. J. Mol. Sci.* 22 (4), 2130. doi:10.3390/ijms22042130

Moch, M., Schwarz, N., Windoffer, R., and Leube, R. E. (2019). The keratin-desmosome scaffold: Pivotal role of desmosomes for keratin network morphogenesis. *Cell. Mol. Life Sci.* 77, 543–558. doi:10.1007/s00018-019-03198-y

Mohammed, F., and Chidgey, M. (2021). Desmosomal protein structure and function and the impact of disease-causing mutations. *J. Struct. Biol.* 213 (3), 107749. doi:10.1016/j.jsb.2021.107749

Muller, L., Hatzfeld, M., and Keil, R. (2021). Desmosomes as signaling hubs in the regulation of cell behavior. *Front. Cell Dev. Biol.* 9, 745670. doi:10.3389/fcell.2021.745670

Nekrasova, O. E., Amargo, E. V., Smith, W. O., Chen, J., Kreitzer, G. E., and Green, K. J. (2011). Desmosomal cadherins utilize distinct kinesins for assembly into desmosomes. *J. Cell Biol.* 195 (7), 1185–1203. doi:10.1083/jcb.201106057

Prechova, M., Adamova, Z., Schweizer, A. L., Maninova, M., Bauer, A., Kah, D., et al. (2022). Plectin-mediated cytoskeletal crosstalk controls cell tension and cohesion in epithelial sheets. *J. Cell Biol.* 221 (3), e202105146. doi:10.1083/jcb.202105146

Price, A. J., Cost, A. L., Ungewiss, H., Waschke, J., Dunn, A. R., and Grashoff, C. (2018). Mechanical loading of desmosomes depends on the magnitude and orientation of external stress. *Nat. Commun.* 9 (1), 5284. doi:10.1038/s41467-018-07523-0

Priya, R., and Yap, A. S. (2015). Active tension: The role of cadherin adhesion and signaling in generating junctional contractility. *Curr. Top. Dev. Biol.* 112, 65–102. doi:10.1016/bs.ctdb.2014.11.016

Pullen, R., Konrad, J., Merkel, R., and Hoffmann, B. (2021). Skin under strain: From epithelial model tissues to adult epithelia. *Cells* 10 (7), 1834. doi:10.3390/cells10071834

Quinlan, R. A., Schwarz, N., Windoffer, R., Richardson, C., Hawkins, T., Broussard, J. A., et al. (2017). A rim-and-spoke hypothesis to explain the biomechanical roles for cytoplasmic intermediate filament networks. *J. Cell Sci.* 130 (20), 3437–3445. doi:10.1242/jcs.202168

Rakshit, S., Zhang, Y., Manibog, K., Shafraz, O., and Sivasankar, S. (2012). Ideal, catch, and slip bonds in cadherin adhesion. *Proc. Natl. Acad. Sci. U. S. A.* 109 (46), 18815–18820. doi:10.1073/pnas.1208349109

Resnik, N., Sepcic, K., Plemenitas, A., Windoffer, R., Leube, R., and Veranic, P. (2011). Desmosome assembly and cell-cell adhesion are membrane raft-dependent processes. *J. Biol. Chem.* 286 (2), 1499–1507. doi:10.1074/jbc.M110.189464

Rubsam, M., Broussard, J. A., Wickstrom, S. A., Nekrasova, O., Green, K. J., and Niessen, C. M. (2018). Adherens junctions and desmosomes coordinate mechanics and signaling to orchestrate tissue morphogenesis and function: An evolutionary perspective. *Cold Spring Harb. Perspect. Biol.* 10 (11), a029207. doi:10.1101/cshperspect.a029207

Rueden, C. T., Schindelin, J., Hiner, M. C., DeZonia, B. E., Walter, A. E., Arena, E. T., et al. (2017). ImageJ2: ImageJ for the next generation of scientific image data. *BMC Bioinforma.* 18 (1), 529. doi:10.1186/s12859-017-1934-z

Schindelin, J., Arganda-Carreras, I., Frise, E., Kaynig, V., Longair, M., Pietzsch, T., et al. (2012). Fiji: An open-source platform for biological-image analysis. *Nat. Methods* 9 (7), 676–682. doi:10.1038/nmeth.2019

Shafraz, O., Rubsam, M., Stahley, S. N., Caldara, A. L., Kowalczyk, A. P., Niessen, C. M., et al. (2018). E-cadherin binds to desmoglein to facilitate desmosome assembly. *Elife* 7, e37629. doi:10.7554/eLife.37629

Sivasankar, S. (2013). Tuning the kinetics of cadherin adhesion. *J. Invest. Dermatol.* 133 (10), 2318–2323. doi:10.1038/jid.2013.229

Stahley, S. N., Saito, M., Faundez, V., Koval, M., Mattheyses, A. L., and Kowalczyk, A. P. (2014). Desmosome assembly and disassembly are membrane raft-dependent. *PLoS One* 9 (1), e87809. doi:10.1371/journal.pone.0087809

Swift, L. M., Asfour, H., Posnack, N. G., Arutunyan, A., Kay, M. W., and Sarvazyan, N. (2012). Properties of blebbistatin for cardiac optical mapping and other imaging applications. *Pflugers Arch.* 464 (5), 503–512. doi:10.1007/s00424-012-1147-2

Waschke, J., and Spindler, V. (2014). Desmosomes and extradesmosomal adhesive signaling contacts in pemphigus. *Med. Res. Rev.* 34 (6), 1127–1145. doi:10.1002/med.21310

Windoffer, R., Borchert-Stuhltrager, M., and Leube, R. E. (2002). Desmosomes: Interconnected calcium-dependent structures of remarkable stability with significant integral membrane protein turnover. *J. Cell Sci.* 115 (8), 1717–1732. doi:10.1242/jcs.115.8.1717

Windoffer, R., Schwarz, N., Yoon, S., Piskova, T., Scholkemper, M., Stegmaier, J., et al. (2022). Quantitative mapping of keratin networks in 3D. *Elife* 11, e75894. doi:10.7554/eLife.75894

Yoon, S., and Leube, R. E. (2019). Keratin intermediate filaments: Intermediaries of epithelial cell migration. *Essays Biochem.* 63 (5), 521–533. doi:10.1042/EBC20190017

Frontiers in
Cell and Developmental Biology

Explores the fundamental biological processes of life, covering intracellular and extracellular dynamics.

The world's most cited developmental biology journal, advancing our understanding of the fundamental processes of life. It explores a wide spectrum of cell and developmental biology, covering intracellular and extracellular dynamics.

Discover the latest Research Topics

See more →

Frontiers

Avenue du Tribunal-Fédéral 34
1005 Lausanne, Switzerland
frontiersin.org

Contact us

+41 (0)21 510 17 00
frontiersin.org/about/contact